Advances in Planar Lipid Bilayers and Liposomes

Volume 3

Advances in
Planar Lipid Bilayers and Liposomes

EDITORIAL BOARD

Advances in Planar Lipid Bilayers and Liposomes

Volume 3

Editor

A. Leitmannova Liu
Department of Physiology
Michigan State University
East Lansing, Michigan
USA
and
Centre for Interface Sciences
Microelectronics Department
Faculty of Engineering & Information
Slovak Technical University, Bratislava
Slovak Republic

Founding Editor

H.T. Tien†
Department of Physiology
Michigan State University
East Lansing, Michigan
USA

Amsterdam ● Boston ● Heidelberg ● London ● New York ● Oxford
Paris ● San Diego ● San Francisco ● Singapore ● Sydney ● Tokyo
An imprint of Academic Press

Academic Press is an imprint of Elsevier
84 Theobald's Road, London WC1X 8RR, UK
Radarweg 29, PO Box 211, 1000 AE Amsterdam, The Netherlands
The Boulevard, Langford Lane, Kidlington, Oxford OX5 1GB, UK
30 Corporate Drive, Suite 400, Burlington, MA 01803, USA
525 B Street, Suite 1900, San Diego, CA 92101-4495, USA

First edition 2006

ISBN-13: 978-0-12-370622-5
ISBN-10: 0-12-370622-X
ISSN: 1554-4516

Printed and bound in USA

06 07 08 09 10 10 9 8 7 6 5 4 3 2 1

CONTENTS

CONTRIBUTORS

This page intentionally left blank

PREFACE

Volume 3 presents recent research on Bilayer Lipid Membranes (BLMs) based on a historic perspective of the lipid bilayer concept and its experimental realization. Many of the contributing authors were in close collaboration with late Prof. H. Ti Tien, the funding editor of this book series, on the use of supported BLMs for biosensors and molecular devices development.

In 1961 at the Symposium on the Plasma Membrane, when a group of researchers (Rudin, Mueller, Tien and Wescott) reported the reconstitution of a bimolecular lipid membrane *in vitro*, the report was met with skepticism. Those present included some of the foremost proponents of the lipid bilayer concept, such as Davson, Danielli, Stoeckenius, Adrian, Mauro, Finean and many others.

The research group began the report with a description of mundane soap bubbles, followed by 'black holes' in soap films, … ending with an invisible 'black' lipid membrane, made from lipid extracts of cow's brains. The reconstituted structure (6–9 nm thick) was created just like a cell membrane separating two aqueous solutions. As one of the members of the amused audience remarked, ''… the report sounded like … cooking in the kitchen, rather than a scientific experiment!'' That was in 1961, and the first report by the group was published a year later. In reaction to that report, Bangham, the originator of liposomes, in an article written in 1996 entitled 'Surrogate cells or Trojan horses': ''… a preprint of a paper was lent to me by Richard Keynes, then Head of the Department of Physiology (Cambridge), and my boss. This paper was a bombshell … . They (Rudin, Mueller, Tien and Wescott) described methods for preparing a membrane … not too dissimilar to that of a node of Ranvier … . The physiologists went mad over the model, referred to as a 'BLM,' an acronym for Bilayer or by some for Black Lipid Membrane. They were as irresistible to play with as soap bubbles''

Indeed, the group under the leadership of D.O. Rudin, then working in Philadelphia, PA, on the 9th floor, at Eastern Pennsylvania Psychiatric Institute (now defunct), was playing with soap bubbles with the 'equipment' purchased from the local toyshop! While nothing unusual for the researchers at work, it must have been a curious and mysterious sight for the occasional visitors who happened to pass through the laboratories there!

Today, after four decades of research and development, BLMs (also referred to nowadays as planar lipid bilayers), along with liposomes, have become established disciplines in certain areas of membrane biophysics and cell biology and in biotechnology. The lipid bilayer, existing in all cell membranes, is most unique in that it serves not merely as a physical barrier among cells, but functions as a two-dimensional matrix for all sorts of reactions. Also, the lipid bilayer, after suitable modification, acts as a conduit for ion transport, as a framework for antigen–antibody binding, as a bipolar electrode for redox reactions, and as a reactor for energy conversion (e.g. practical AIDS research, and 'microchips' study. In reactions involving light, BLMs have provided insights into the conversion of solar energy *via*, water photolysis, and to photobiology comprising apoptosis and

photodynamic therapy. Supported bilayer lipid membranes (s-BLMs) are being used in biosensor development. In addition, this volume reviews the studies of others in collaboration with our laboratory and also recent research of others on the use of BLMs as models of certain biomembranes.

With this background in mind, the present volume of *Advances* series on planar lipid membranesand liposomes continues to include invited chapters on a broad range of topics, ranging fromtheoretical research to specific studies and experimental methods, but also refers to practical applications in many areas. The author of each chapter presents the results of his/her laboratory. We continue in our endeavor to focus in this series on newcomers in this interdisciplinary field, but we also wish to attract experienced scientists. We also try to show the importance of BLMs applications for further development of this scientific research worldwide. The contributed chapters are separate entities to themselves, but they have one common feature. They are based on lipid bilayer concept of biomembranes, and have a significant impact to further development of the lipid bilayer research. We are thankful to all contributor(s) for their expert knowledge in BLM research area, for the shared information about their work and also for their patience in preparation of this volume after the unexpected death of the funding editor Prof. H. Ti Tien. Their willingness to write these chapters in his memory is much appreciated by the whole scientific community.

The first stage of editorial work on this volume is still based on a joint effort of late Prof. H.T. Tien and me. I would like to express my gratitude once more to everybody who contributed a chapter to this volume. I highly value the support and help of Dr. Kostas Marinakis, Publisher of Chemistry and Chemical Engineering Department in Elsevier and all his coworkers, especially Deirdre Clark in different stages of preparation of this book series. We will try our best to keep these *Advances* series alive and to pay our tribute to the scientific works of Prof. H. Ti Tien.

Angelica Leitmannova Liu
(Editor)

CHAPTER 1

Supported Lipid Bilayers for the Detection of Hormone-Receptor Interactions

Vered Sacks-Granek and Judith Rishpon*

Department of Molecular Microbiology and Biotechnology, Tel-Aviv University, Ramat-Aviv 69978, Israel

Contents

*Corresponding author. Tel: +972-3-6409366; Fax: +972-3-6409407;
E-mail: Judithri@tauex.tau.ac.il

ADVANCES IN PLANAR LIPID BILAYERS AND LIPOSOMES, VOLUME 3
ISSN 1554-4516 DOI: 10.1016/S1554-4516(05)03001-2

PROLOGUE

Hormone–receptor interactions play a key role in controlling balanced homeostasis. A hormone is a naturally occurring substance secreted by specialized cells that affect the metabolism or behavior of other cells possessing functional receptors for the hormone. The interaction between a hormone and its complementary receptor stimulates a physiological response in the target cell.

Cell membranes are composed of lipids, proteins, carbohydrates, and cholesterol in the form of a phospholipid double (bilayer) containing phospholipid molecules with a long hydrophobic tail and a hydrophilic head group embedded in the membrane proteins. As the structure of the lipid bilayer prevents the free passage of hormones into and out of the cell, specific receptors are required to mediate the interaction between the extracellular membrane phase and the intracellular volume. Receptors belong to a special class of transmembrane proteins that bind signaling molecules. Following binding, the receptor acts as a signal transducer that converts an extracellular ligand-binding event into an intracellular signal, thereby altering the activity of the target cell.

The universally studied model system for the cell membrane is a synthetic phospholipid bilayer that serves as a physical barrier between liquid compartments. Furthermore, the bilayer can function as two-dimensional (2D) matrix for biological reactions. Biological activity is accomplished by suitable modification of the bilayer, such as embedding biologically active molecules like receptors, ion-channels, antigen, antibody, and signal transduction proteins.

This chapter describes the contribution of a biologically modified supported bilayer in the field of endocrinology and its importance to pharmacology, epidemiology, virology, medicine, and environmental sciences. The binding of hormone to its receptor activates a cascade of reactions within the cell that affect physiological and biological function.

1. HORMONES

Cells communicate through chemical signals. A hormone is defined as a complex signal molecule produced in a specialized cell that elicits a physiologic response in another cell bearing a receptor for the hormone. Thus, hormone systems can be described as a broadcast of long-lasting chemical messengers. Hormones can be hydrophilic, in which case the receptors are on the cell surface, or lipophilic, in which the receptor can be intracellular. Although certain hormones can circulate dissolved in the blood, most are bound to plasma proteins.

Hormones produced by the endocrine glands are secreted by cells directly into the general circulation, exerting a physiologic effect on target cells located at distant sites. The endocrine chemical communication system comprises the pituitary gland, pineal body, thyroid and parathyroid glands, adrenals, pancreas,

Table 1. Human hormones produced by the endocrine system

Hormone	Principal source
Thyroid-stimulating hormone (TSH)	Pituitary gland
Follicle-stimulating hormone (FSH)	Pituitary gland
Luteinizing hormone (LH)	Pituitary gland
Growth hormone (GH)	Pituitary gland
Adrenocorticotropic hormone (ACTH)	Pituitary gland
Gonadotropin-releasing hormone (GnRH)	Pituitary gland
Dopamine	Pituitary gland
Melatonin	Pineal body
Throxin (T4)	Thyroid Gland
Parathyroid hormone (PTH)	Parathyroid glands
Glucocorticoids (e.g., cortisol)	Adrenal cortex
Mineralocorticoids (e.g., aldosterone)	Adrenal cortex
Androgens (e.g., testosterone)	Adrenal cortex
Adrenaline (epinephrine)	Adrenal medulla
Noradrenaline (norepinephrine)	Adrenal medulla
Estrogens (e.g., estradiol)	Ovarian follicle
Progesterone	Corpus luteum and placenta
Human chorionic gonadotropin (HCG)	Trophoblast and placenta
Androgens (e.g., testosterone)	Testes
Insulin	Pancreas (Islets of Langerhans)
Insulin-like growth factor (IGF-1)	Liver

and gonads (testes and ovaries). A partial list of human hormones produced by the endocrine glands is presented in Table 1.

1.1. Classification of hormones

Hormones are derived from amino acids, cholesterol, or phospholipids (Fig. 1). Chemically, hormones are classified as (1) proteins or peptides, (2) modified amino acids, or (3) steroids.

1.1.1. Proteins and peptides

The size of protein or peptide hormones ranges from as few as 3 amino acids to over 200 residues. One group of peptide hormones, represented by insulin, consists of two subunits attached by disulfide bonds between two cysteine molecules. The more complicated structures are the glycoprotein hormones. For example, the anterior pituitary gland hormone comprises two protein subunits attached by complex sugar moieties [1].

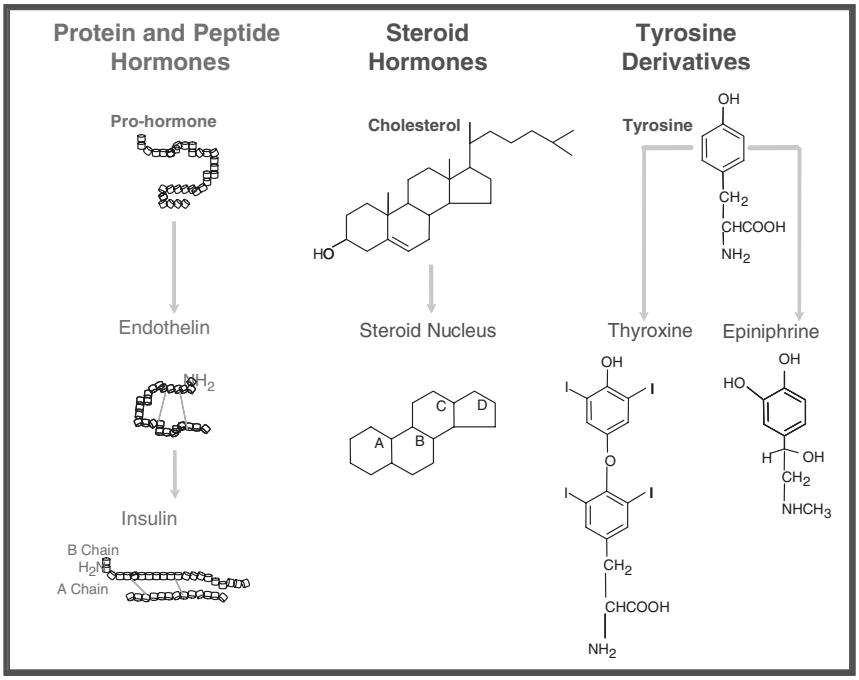

Fig. 1. Schematic demonstration of hormone classification.

1.1.2. Modified amino acids

Amine hormones are derived from amino acids – for example, the catecholamines (epinephrine (EP) (adrenalin) and norepinephrine), thyroxine from tyrosine, histamine from histidine, and serotonin from tryptophan. The activity of norepinephrine as both neurotransmitter and hormone is just one example of the complexity of endocrine balance and control. The catecholamine hormones are secreted by the adrenal medulla and are rapidly broken down once released into the circulation. Tryptophan is the precursor of serotonin (5-hydroxytryptamine) and melatonin synthesis. Thyroid hormones are formed by the conjugation of two tyrosine molecules.

1.1.3. Steroids

Steroid hormones are derived from cholesterol except for retinoic acid, which is derived from vitamin A. All adrenal and gonadal steroids (sex hormones), including vitamin D, have the same basic ring skeleton structure (Fig. 2). The specificity of steroid hormones derives from side chains, residues, and spatial orientation. Steroid hormones are transported bound to plasma proteins and typically react with receptor sites inside a cell. Thyroid hormones resemble steroid hormones in their binding to serum proteins and mechanism of action.

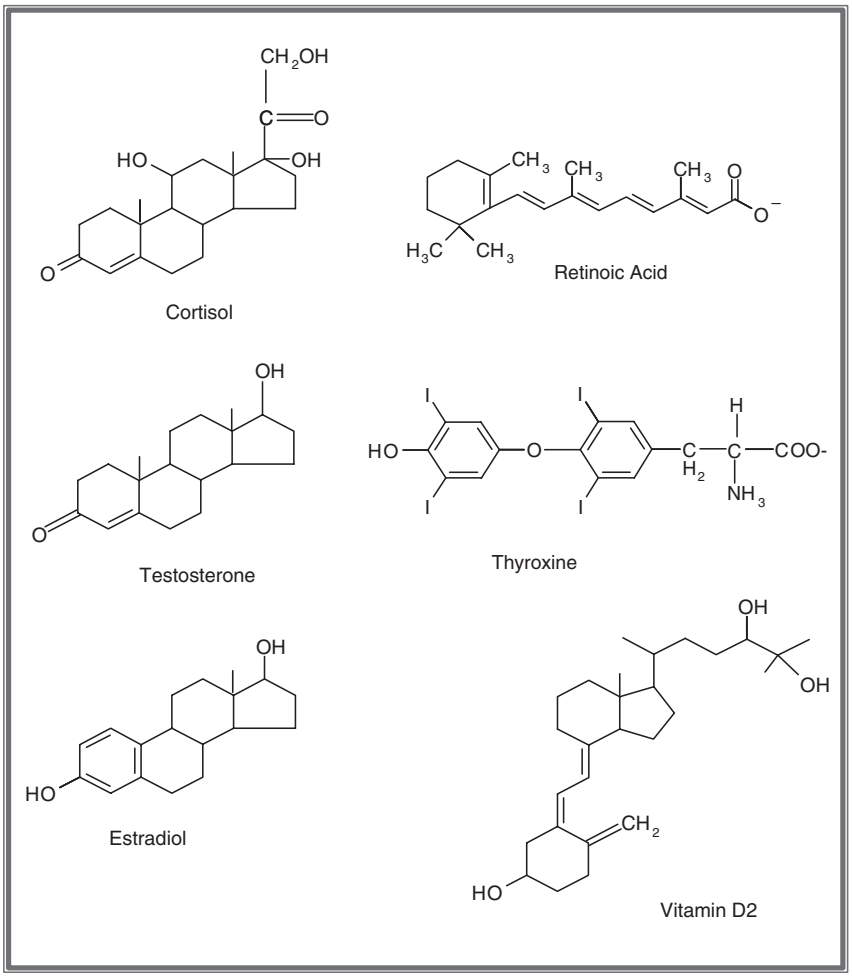

Fig. 2. Schematic ring skeleton structure of steroid hormones.

1.1.4. Phospholipids

Another group that should be mentioned includes hormones derived from lipids and phospholipids. This group includes the major classes of eicosanoids, including prostaglandins, prostacyclins, thromboxanes, and leukotrienes (Fig. 3).

1.2. Mechanism of action

A hormone elicits a response in its target cells following recognition by a cell-surface receptor protein specific for that particular hormone. This unique receptor molecule is the only receiver that can accept the message, recognize the specific hormone, and mediate the biological pathway to activate the intracellular response to the signal. The binding of hormones to their complementary receptors

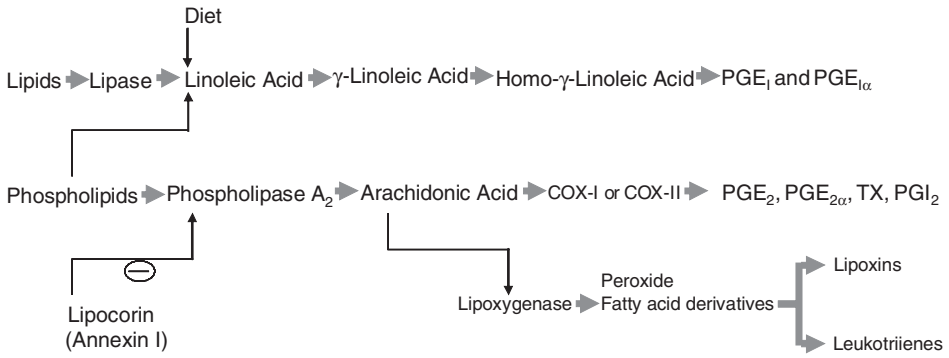

Fig. 3. Schematic description of hormones derived from lipids and phospholipids synthesis pathway. The described pathway products, prostaglandins (PGE), prostacyclins (PGI), thromboxanes (TX), and leukotrienes release to the cytoplasm direct membrane action for cellular response.

can either activate or inhibit various cellular functions. The diversity of receptor structures and functions is exceptionally broad.

1.2.1. Regulation

The absolute hormone concentration in plasma is of great importance in health balance. Any deviation from the physiological hormone concentrations is crucial and can result in acute disease. The parameters for achieving the precise local hormone concentration are hormone reproduction *versus* hormone degradation, hormone delivery rate, and the equilibrium between bound and free hormone.

The secretion of hormones is regulated by feedback loops that control the hormone concentration in the blood. Figure 4 schematically describes a simple feedback loop.

One example of the feedback mechanism in the human body is male sperm production in which the release of follicle-stimulating hormone (FSH) and luteinizing hormone (LH) from the brain is followed by the production of testosterone, the main androgen (male sex hormone) produced by the testes. Sperm production, as well as several secondary male sex characteristics (deepening voice, beard growth, appearance of body hair), is derived from the amount of testosterone in the blood. When the testosterone concentration achieves the optimal concentration, sperm production is stimulated, whereas the production of the brain hormones (FSH, LH) is inhibited when testosterone is increased. This feedback loop is summarized in Fig. 5.

2. RECEPTORS

Cell-surface receptors are integral membrane proteins that interact with the hormone and stimulate direct or indirect response of the cell organelles, including the

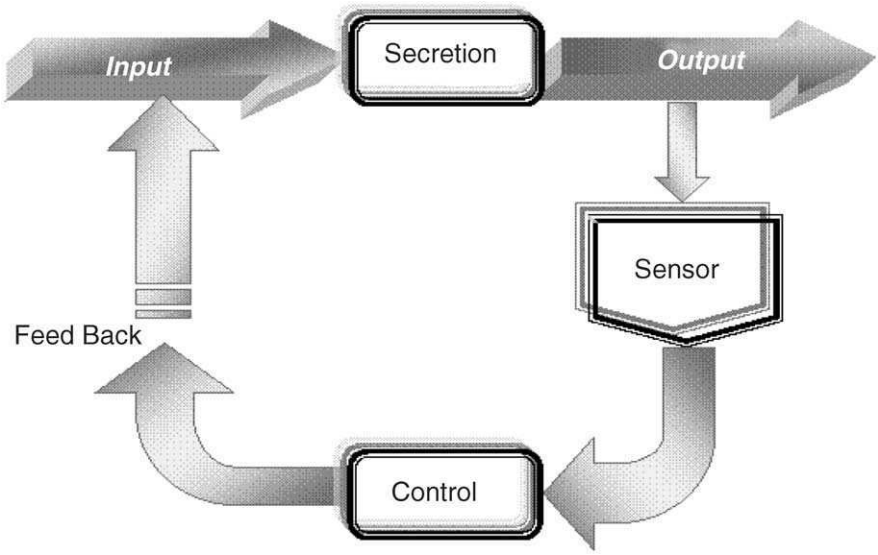

Fig. 4. Scheme of a simple feedback loop of a biological secretion system. The output of the secretion process is detected by a biological 'sensor'. The sensing mechanism is delivering the signal to a control system. The control system sends a signal to the input process, actually it is the feedback for the input.

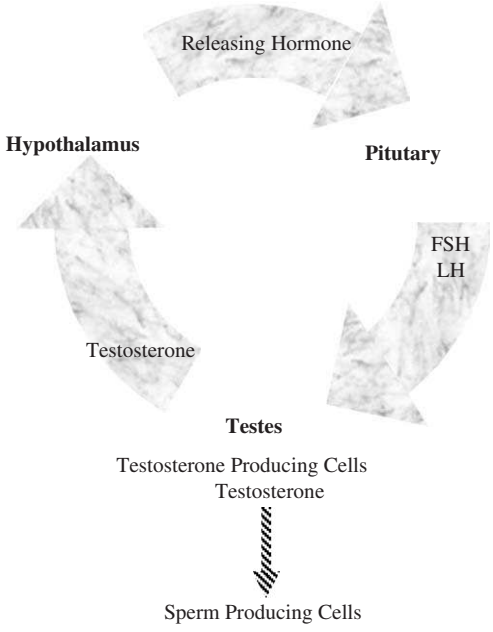

Fig. 5. Example of feedback loop balanced male sperm production.

nucleus. As a mediator between the cell interior and the outer environment, a receptor interacts with the cell membrane. Receptors anchored to the cell membrane are transmembrane receptors that pass through the plasma membrane with their N-terminal exposed at the exterior of the cell and their C-terminal projecting into the cytoplasm. Nuclear receptors diffuse between the cell organelles by interacting with the cell membranes.

2.1. Receptor superfamilies

Most cell-surface receptors fall into five structurally related types called superfamilies: G-protein-linked (or secondary messenger), ligand-gated (or ion channel), tyrosine kinase, growth factor, and hormone, which characterize hormone–receptor structure and the biochemical pathway.

The binding site of the receptor is a unique region of the protein that interacts solely with the hormone. The selectivity of the receptor is based on three-dimensional (3D) structure recognition. Furthermore, the fine specificity of the receptor to a hormone from a given superfamily is based on the relative amounts of different hormone concentrations. The driving force for delivering the message from the extracellular volume to the intracellular phase is called the gradient of hormone concentration.

As mentioned, the receptor is the cell component that delivers a signal from the extracellular surrounding volume to the cell interior. As the cell membrane is a hydrophobic matrix, water-soluble proteins and peptide hormones such as EP, gonadotropin-releasing hormone (GnRH), thyroid-stimulating hormone (TSH), LH, and parathyroid hormone (PTH) do not diffuse across the cell membranes. Conversely, the mediation between the hydrophobic molecules and the intracellular volume is achieved by the transmembrane receptor. This superfamily of receptors is characterized by an extracellular region, which allows hormone–receptor interactions, and an intracellular part, which activates a specific protein cascade, thereby initiating various physiologic phenomena. Hydrophobic molecules diffuse directly across the phospholipid plasma membrane of target cells and bind to the intracellular receptor proteins. These signal molecules include steroid hormones, thyroid hormones, retinoids, and vitamin D. Although they differ greatly from one another in both chemical structure (Fig. 2) and function, all act by a similar mechanism.

This very large super family also includes several receptor proteins that are activated by intracellular metabolites rather than by secreted signal molecules. Many family members have been identified only by DNA sequencing and their ligand is not yet known, such proteins are therefore referred to as orphan nuclear receptors.

3. HORMONE–RECEPTOR INTERACTIONS

Hormone interaction with the cell receptor depends on the chemical type of hormone, and recognition of the ligand by the receptor is based on 3D structure identification. Polypeptide/protein hormones act on a receptor located in the cell membrane, thereby exposing receptor-binding sites on the intracellular side of the membrane, which in turn elicit a response to the signal. The interaction between protein and peptide hormones with the receptor initiates the production of a second messenger (the hormone is the first messenger). The most common of these are cyclic adenosine monophosphate (c-AMP) AMP and protein kinase, which trigger a series of molecular interactions that alter the physiologic state of the cell. This entire process is often referred to as signal transduction.

As lipids, steroid hormones passively diffuse across the plasma membrane to bind to cytoplasmic and/or nuclear proteins that serve as receptors of the hormone. Steroid hormones bind to the receptor and the complex binds to hormone response elements – stretches of DNA responsive to the hormone – thereby turning target genes 'on' or 'off'. The intracellular receptors for the steroid and thyroid hormones, retinoids, and vitamin D all bind to specific DNA sequences adjacent to the genes regulated by the ligand. The binding of inactive receptors to the ligand alters the conformation of the receptor protein, which causes inhibitory complexes to dissociate or activates the receptor to allow the entrance of the signal into the nucleus. Ligand binding also causes the receptor to bind to co-activator proteins that induce altered rates of transcription in the associated genes. To summarize, the combination between specific gene regulatory proteins and the existence of specific intracellular receptors activates the gene transcription process.

3.1. Agonists and antagonists

In general, molecules that bind to the hormone-binding sites of receptors are divided into two classes: (a) agonists that mimic the natural hormone activity by binding to the receptor and inducing all the postreceptor events that lead to a biologic effect; and (b) antagonists that bind the receptor and block binding of the agonist, hence preventing the trigger of intracellular signaling events. Because the receptor recognizes the 3D structure of the hormone, molecules different from the hormone have the potential to interact with the receptor.

3.2. Transduction mechanisms

Cell-surface receptor proteins, defined by their transduction mechanism of activation, can be divided into four main groups as discussed below.

Ion-channel-linked receptors are involved in rapid synaptic signaling between electrically excitable cells. This type of signaling is mediated by a small number of neurotransmitters that transiently open or close an ion channel formed by the protein to which they bind, briefly changing the ion permeability of the plasma membrane and thereby the excitability of the postsynaptic cell.

G-protein-linked receptors act indirectly to regulate the activity of a separate plasma-membrane-bound target protein, which can be either an enzyme or an ion channel. A specific protein called a trimeric guanosine triphosphate (GTP)-binding protein (G-protein) is mediated between the receptor and the target protein, initiating the production of a second messenger. If the target protein is an enzyme, then activation can change the concentration of one or more intracellular mediators (second messengers). If the target protein is an ion channel, then the G-protein changes the ion permeability of the plasma membrane.

Enzyme-linked receptors are single-pass transmembrane proteins. The ligand-binding domain directed outside the cell and the active site (catalytic or enzyme-binding site) is positioned inside the cell. This group of signal transduction proteins is heterogeneous in structure compared with the other two classes. The vast majority, however, are protein kinases, or are associated with protein kinases, and ligand binding causes the phosphorylation of specific sets of proteins in the target cell.

Several smaller groups of receptors include (a) cell-surface receptors activated by intracellular proteolytic events, (b) two-subunit transmembrane cell-surface receptors such as insulin, growth hormone, prolactin, most growth factors, and cytokines. Binding of the hormone or growth factor at the extracellular domain results in receptor dimerization, thereby turning on the activation of the biochemical pathway.

Because steroid and thyroid hormones are lipophilic and spontaneously diffuse across cell membranes (Fig. 2), mediation between the hormone and the physiologic cell activation occurs *via* an intracellular receptor. Interaction between the hormone and the receptor is followed by dimerization and activation of the biochemical cascade [2]. This super family is unique because the activated dimer reacts directly with the cell nucleus. Binding of the activated receptor to DNA activates transcription, which in the presence of other transcription factors initiates RNA synthesis. Steroid membrane receptors can initiate the opening of ion channels or activate classical second messenger systems [1]. Certain steroids and thyroid hormones can stimulate nongenomic rapid responses in target cells by initiating a signal-transduction enzyme cascade.

4. PHYSIOLOGIC EFFECTS

The endocrine system provides the means to control a multitude of physiologic processes. In principle, all physiologic effects are mediated by multiple hormones

acting in concert. Normal growth, from birth to adulthood for example, is certainly dependent on growth hormone, but thyroid hormone, insulin-like growth factor-1, glucocorticoids, and several other hormones are critically involved in this process as well. Reproductive system maturity is controlled by the pituitary-derived hormones (FSH and LH), as well as by steroid hormones derived from cholesterol, including testosterone, estrogen, 17-b-estradiol, and di-hydro-testosterone, among others.

4.1. Steroids

Steroid hormone binding to the steroid receptor is followed by a series of events that include dissociation from heat shock proteins [3–5], dimerization [6–8], and binding to DNA at the estrogen response element [9,10]. Although research on the structure of the steroid receptor is of great importance, its unique mechanism precludes the possibility of crystallizing the whole molecule. The structure of the active site of several receptors has been solved by ligand-binding domains and/or DNA-binding domains such as the estrogen ligand-binding domain [11,12], the estrogen DNA-binding domain [13], the retinoic acid receptor–ligand-binding domain [14], and others [15–21].

4.2. Protein and peptides

The hormonal products of neuroendocrine cells in the animal nervous system are usually proteins or peptides. Protein and peptide hormones can be large molecules and are generally hydrophilic in their chemical properties. The hydrophilic nature of the peptide hormones means that they do not readily pass through the hydrophobic phospholipids that comprise the cell membrane. Hence, peptide hormones do not enter their target cells to convey their signal message to the cell. Peptide hormones interact with a cell-surface receptor protein, which transduces the message to the cell *via* intracellular second messengers. The specific pathway of the hormone to deliver the signal from the cell environment within the nucleus is varied.

The regulation of whole-body energy metabolism hormones, for example, is controlled by the pancreatic hormones (insulin, glucagon, and somatostatin). These hormones are involved in adjustment of the concentration and activities of numerous enzymes required in catabolism and anabolism of the major cell energy supplies.

Insulin essentially maintains low blood glucose levels by counter of the concerted action of hyperglycemia-generating hormones. Untreated disorders associated with insulin generally lead to severe hyperglycemia and shortened life span.

Insulin, insulin-like growth factors (IGF-1 and IGF-2), and relaxin are members of a family of structurally and functionally similar molecules. The common of this

family is the tertiary structure and their involvement in growth-promoting. The insulin's dominant role is metabolism while IGFs' and relaxin's dominant roles are in the regulation of cell growth and differentiation.

Insulin is synthesized as a prohormone in the pancreas. The synthesised molecule is altered and packed in the Golgy system and the endoplasmic reticulum. Insulin secretion to the blood is principally regulated by plasma glucose levels.

Insulin generates its intracellular effects by binding to a plasma membrane receptor. In addition to its role in regulating glucose metabolism, insulin stimulates lipogenesis, diminishes lipolysis, and increases amino acid transport into cells. Insulin also modulates transcription, altering the cell content of numerous mRNAs. It stimulates growth, DNA synthesis, and cell replication; effects that it holds in common with the IGFs and relaxin.

Glucagon is a 29 amino acid hormone synthesized also in islets of Langerhans of the pancreas as a very large proglucagon molecule. Glucagon lacks a plasma carrier protein and its circulating half-life is about 5 min.Glucagon is secreted and immediately delivered to the liver that is the main principal effect site of glucagons. The role of glucagon is well established. It binds to plasma membrane receptors and is coupled through G-proteins to adenylate cyclase. The resultant increases in cAMP and PKA reverse all of the effects described above that insulin has on the liver. The increases also lead to a marked elevation of circulating glucose, with the glucose being derived from liver gluconeogenesis and liver glycogenolysis.

Somatostatin is a 14-amino acid peptide secreted either by other cells type of the pancreas or by the hypothalamus. In neural tissue, somatostatin inhibits GH secretion and thus has systemic effects. In the pancreas, somatostatin acts as a paracrine inhibitor of other pancreatic hormones and thus also has systemic effects. It has been speculated that somatostatin secretion responds principally to blood glucose levels, increasing as blood glucose levels rise and thus leading to down-regulation of glucagon secretion.

4.3. Xenohormones

Because the endocrine system is one of the major control systems, the interaction between the receptor and any foreign molecule that mimics the hormone is potentially hazardous. Exposure to such residues can be followed by uncontrolled physiological phenomena that could lead to hormone-dependent adverse health effects. Substances (pollutants) originating outside the body that have hormone- and estrogen-like activities and interact with the endocrine cascade are called 'xenohormones' (XNHs) [22]. Compounds that interfere with any step of the chain of events induced by hormone binding have the potential to block the adverse effects of excess exposure to hormone.

For example, steroid hormones control fundamental events in embryonic development and sex differentiation and profoundly affect the nervous system, the

reproductive system, and the immune system through their actions as ligand-inducible transcription factors [23]. Epidemiologic investigations in males over the past few decades have documented an increase in testicular cancer [24]. Clinical oncologists have long recognized a group of cancers that respond to hormonal manipulation, e.g., tumors of the breast, endothelium, thyroid, and prostate. Tumors of the ovary and testis are likewise hormone related, although they do not usually respond to hormone therapy [25]. The common clinical and epidemiologic features of some of these tumors seem to be closely linked at the molecular level. That all of these effects are related to increased exposure to environmental endocrine disrupters have been widely hypothesized [26] but remain a matter of controversy [27–30].

The harmful effect of such chemicals on wildlife has been reported [31,32]; for example, the reproductive failure of several seal species from PCBs pollution [33]. In relation to organochlorine chemicals, reproductive alteration and gender behavioral changes in birds, decreased reproductive capacity and the feminization of fish, and thyroid alterations of Great Lakes salmon have been reported [34]. In Florida's Lake Apopka, organochlorine pesticide contamination has led to reproductive failure in alligators, with severe alterations of the sexual organs of male alligators [35].

Steroid hormones influence the growth, differentiation, secondary sex signs, and function of many target tissues. The steroid receptor can be activated either by hormone or by hormone-like, 3D-structured chemicals that exist in water, soil, and air. The accumulation of such chemicals in the human body, especially in fat tissue, is followed by an uncontrolled stimulation of a natural biological cascade, leading to appearance of physiological phenomena, which under uncontrolled conditions concern homeostasis. The interaction of steroid or steroid-like compounds with the steroid production proteins cascade is of key importance in hormone-dependent cancer development. The XNHs are a diverse group of substances that do not necessarily share any structural resemblance to the prototypical steroid but can interfere with the action of the hormone [36]. Such chemicals include natural and synthetic hormones, phytohormones derived from plants, and a wide variety of man-made industrial compounds [37]. On the other hand, the potential of molecules to mimic the natural hormone activity or to block the receptor active site is widely used in pharmacology and drug development for therapeutic purposes.

5. MEMBRANES

The cells of all living organisms contain specialized structures surrounded by a limiting, selectively permeable plasma membrane composed of phospholipids and proteins. The fundamental structure of the biomembrane is a lipid bilayer. The lipid bilayer is unique because it serves not merely as a physical barrier

among cells but also functions as a 2D matrix for different reactions. Biochemical composition data have shown that typically more than 30 phospholipid molecules are present for every protein molecule, but the proportion can vary from membrane to membrane.

The cell membrane is characterized by its fundamental construction unit – the specific phospholipids. Lipids present in membranes are diverse in structural details but have a common structural feature. All lipids are amphipathic, that is, they have a polar head group separated from nonpolar acyl chains. Many of the characteristic properties of amphipaths are the direct consequence of the segregation between polar and nonpolar regions.

In general, fluidity decreases (or viscosity increases) with (a) increasing cholesterol content by preventing the tight packing of the long hydrocarbon tails, (b) higher chain length, which affects the melting temperature, or (c) multivalent ion concentration in the medium. Microviscosity appears to decrease with increasing nonsaturation, temperature, and the presence of lipid-soluble agents, such as organic solvents, detergents, and anaesthetics. Other molecules like functional proteins, construction proteins, and derivatives like cholesterol determine membrane characteristics.

The most valuable model system for membrane research is the phospholipid bilayer. The formation of a synthetic bilayer lipid membrane (BLM) as a model of biomembranes has contributed greatly to experimental methods used in the studies of membrane phenomena. This discipline has been extensively characterized over the last four decades. The first report in 1961 proposed the model of a BML that described mundane ‘soap bubbles’, followed by ‘black holes’ in soap films, ending with an invisible ‘black’ or BLM constructed by blowing a soap bubble from the lipids extracted from cow’s brains. The thickness of the reconstructed structure was 60–90 Å and, similar to a cell membrane, could separate two aqueous solutions [38].

This multidisciplinary research involves progress in several disciplines: developing techniques for BLM formation [39,40]; understanding the measured signals obtained from constructed membranes by physical and mathematical models; embedding biological compounds such as enzymes, antibodies, receptors, ion-channels, etc. into the phospholipid bilayers; assembling bilayers to different substrates; and applying the combined pure research results to developing a practical device.

Embedding highly selective biomolecules (antibodies, enzymes, nucleic acids, receptors) or biological systems (organelles, whole cells) in a synthetic bilayer combines the advantages of membrane technology with analytical detection. Because bilayer immobilization strategies allow the mimicking of the natural environment of a biological compound and preserve its biological activity and natural reactions, the conditions for biological recognition are optimal. If a concentration proportional signal is generated, then the system has the potential for analytical determination.

5.1. Supported lipid bilayers

Assembling a phospholipid bilayer onto a solid substrate is a wide research topic that has had great use in imitating cell membranes [41–45]. A variety of surfaces can be equipped with functionalized layers that possess a required specific electrical, optical, acoustical, or chemical property. Consequently, the supported lipid bilayer attached to an appropriate surface has not only made a progressive contribution to scientific research but also served as an attractive building block for biotechnology applications [41,46–50].

5.2. Techniques for lipid layer immobilization

An ideal monolayer is depicted as perfectly aligned, closely packed alkane chains attached to a smooth surface (Fig. 6). Two methods can be used to deposit molecular layers on solid substrates (e.g., glass or metal): Langmuir–Blodgett transfer [51] and self-assembly [51–53].

The use of self-assembly of lipid layers in various fields of research is rapidly growing. In particular, many biomedical fields apply self assemble monolayer (SAMs) as an interface layer between a solid surface and a solution or vapor. An essential attitude in this discipline is monolayer assembly and the addition of the following layers. Monolayers are divided into uniform, mixed, and functionalized categories. Immobilizing biological components, including (oligo-) nucleotides,

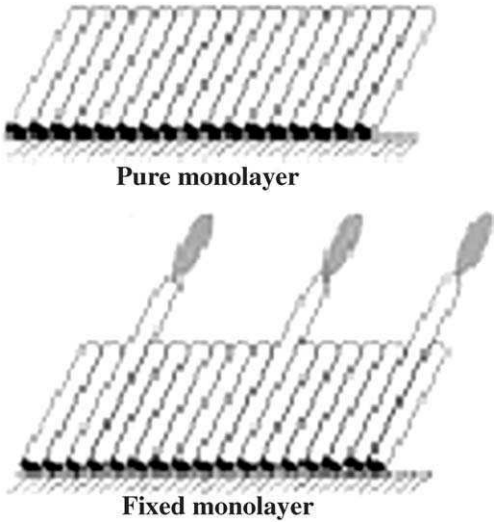

Fig. 6. Schematic drawing of a pure and mixed monolayer. Sulfur (black) is attached to a gold surface. Functional groups (shaded) are elevated into the solution or gaseous phase (Copyright: Royal Society of Chemistry; Analyst 122 (1997) 43r–50r. With permission).

proteins, antibodies receptors, and polymers, within the monolayer allows their natural-specific activity.

In addition, the preparation and structural characterization of supported monolayer assemblies of oriented organic molecules have been of great interest in a variety of interface studies. Examples involve lubrication [54], electrochemistry [55,56], electronic and vibration spectroscopy [57–59], photochemical mechanism [58,60], electrical conduction [58,61–63], catalysis [64], and biological membranes [65–67].

An essential class of self-assembled monolayers is based on the strong adsorption of disulfides (R–S–S–R), sulfides (R–S–R), and thiols (R–SH) on a metal surface (gold, silver, or mercury). Furthermore, the sulfo monolayers are highly oriented, and dialkane sulfides form highly ordered monolayers on metal [68]. Sulfur donor atoms coordinate strongly on a gold substrate, and van der Waals forces between the methylene groups orient and stabilize the monolayer. The alkane chain length affects the order of the assembled layer; long-chain (number of methylene groups $n > 10$) alkanethiols assemble in a crystalline-like way [69]. A shorter chain length is followed by less ordered layer structures.

A well-defined orientation of membrane structures is important, particularly in interaction biosensors. Techniques based on surface plasmon resonance (SPR) or monomode dielectric waveguides [70], as well as microtiter plate immunoassays [71], require more sophisticated approaches.

5.3. Langmuir–Blodgett assembly technique

The Langmuir–Blodgett assembly demonstrated that monolayers of amphiphilic molecules could be ordered on the surface of water by applying pressure undergoing phase changes from a gaseous state of noninteracting molecules to a ‘solid state’ in which the molecules interact in a rigid film. Langmuir and Blodgett realized the transfer of such monolayers from the water surface to a solid substrate by slowly passing an appropriately treated substrate through the air/water interface. Films can be picked up (a) only on passing from air into water and vice versa (*Y*-type deposition), (b) only on passing from water to air (*Z*-type), and (c) on immersion from air into water only (*X*-type) [72]. The forming of film characteristics is affected by the following factors: temperature, pH, solution purity, and stabilized ion concentration. The films are vector ordered so that when transferred to the substrate, multilayers having the desired electro/optical properties can be assembled.

5.4. Properties of supported bilayer lipid membranes

The electrical properties of supported BLMs are well defined. An equivalent circuit consisting of resistors and capacitors is the basis for quantitative measurements

and presents a physical model for the layer's electrical response. The exact electrical circuit depends on the specific conditions, including the layer's structure and the potential/current applied.

The general equations are:

The charging current (i_c) is determined by the capacitance. Equation (1) describes the correlation between charging current (i_c) and the capacitance.

$$i_c = C_m \frac{dV}{dt} = C_m A \tag{1}$$

In certain cases, the capacitance current capacitance is constant.

From Ohm's law, the current i_r through the membrane depends on the membrane resistance

$$i_r = \frac{V}{R_m} \tag{2}$$

Equation (2) describes the correlation between the resistance current (i_r) and the membrane resistance.

5.5. Supported bilayer lipid membrane biosensors

The formation of BLMs on various substrates with long-term stability opened the way for basic research and development work in biotechnology [73,74]. Understanding the physical properties of supported layers under changing biological conditions made a great contribution to the biosensors field [75–77]. Biosensors are molecular sensors that combine a biological recognition mechanism with a physical transduction technique. Biosensors provide a class of inexpensive, portable instruments that permit sophisticated analytical measurements to be undertaken rapidly at decentralized locations [78].

In the late 1990s, a pioneer study described the development of a biosensing technique, in which the conductance of a population of molecular ion channels is switched on by the recognition event [79]. This approach mimics biological sensory functions and can be used with most receptor types, including antibodies and nucleotides. The technique is very flexible and even in its simplest form is sensitive to Pico molar concentrations of proteins. The sensor is an impedance element whose dimensions can readily be reduced to become an integral component of a microelectronic circuit. The system can be used in a wide range of applications and in complex media, including blood. Such uses might include cell typing and the detection of large proteins, viruses, antibodies, DNA, electrolytes, drugs, pesticides, hormones, and low-molecular-weight compounds.

The active elements of the ion-channel switch (ICS) comprise a gold electrode tethered to a lipid membrane containing gramicidin ion channels linked to antibodies. The molecular structure of the tethered membrane, based on previous studies [52,71,80–86], results in the formation of an ionic reservoir between the

gold electrode and the membrane. The ionic reservoir can be accessed electrically through connection to the gold electrode (Fig. 7).

In the presence of an applied potential, ions flow between the reservoir and the external solution when the channels are conductive. The ion current is switched off when mobile channels diffusing within the outer half of the membrane become cross-linked to the antibodies immobilized at the membrane surface. This action prevents the protein from forming dimers with channels immobilized within the inner half of the membrane. The number of dimers is measured from the electrical conduction of the membrane. The switch has a high gain; a single channel facilitates the flux of up to a million ions per second. A quantitative model of the biosensor has been verified experimentally.

The membrane consists of lipids and channels, some immobilized on the gold surface and others diffusing laterally within the plane of the membrane. With a low density of channels and a high density of immobilized antibodies, each channel can access up to 103 more capture antibodies than if the gating mechanism were triggered by a directing binding of analyte to the channels. The speed and sensitivity of the biosensor response can be adjusted in direct proportion to the number of binding sites that are accessible to each mobile channel, allowing for the quantitative detection of analyte from subpicomolar to micromolar concentrations in less than 10 min (Fig. 8).

The similarity to a natural cell membrane accelerated this research field and has led to mimicking cell communication and signal transduction pathways in particular. Fukuda *et al*. [87] described the dynamic behavior of a transmembrane molecular switch as an artificial cell-surface receptor. A study that attempted simulation and simplified the signal transduction system [88–91] involving ligand–receptor interaction and the G-protein-linked pathway was published in 2001 [87] (Fig. 9).

Wang *et al*. [92] described a BLM study for which the main goal was to develop a simple method for reconstituting membrane receptors in BLMs without prior purification of the receptor. The receptor indeed retained its ligand activity after reconstitution in the BLM. Furthermore, the group studied the relation between receptor–ligand interactions and the electrical properties of the reconstituted BLMs, such as membrane capacitance (C_m) and membrane resistance (R_m) (Fig. 10).

Focusing on glycophorin in erythrocytes and asialoglycoprotein in hepatocytes as examples, the authors found that the resistance of reconstituted BLMs decreased when adding blood-type monoclonal antibody and solutions of galactose, respectively. The decrease was ligand-concentration dependent, but the membrane capacitance was not influenced. This system provides a simple, practical approach to determining the interactions between a receptor and its ligand. Wang's group applied the easily measured membrane electrical properties to provide a sensitive and rapid tool for monitoring the interactions of membrane lipids with other species. The similarity to natural biological membranes that contain proteins enables the lipid–protein–glycan complexes to act as signal

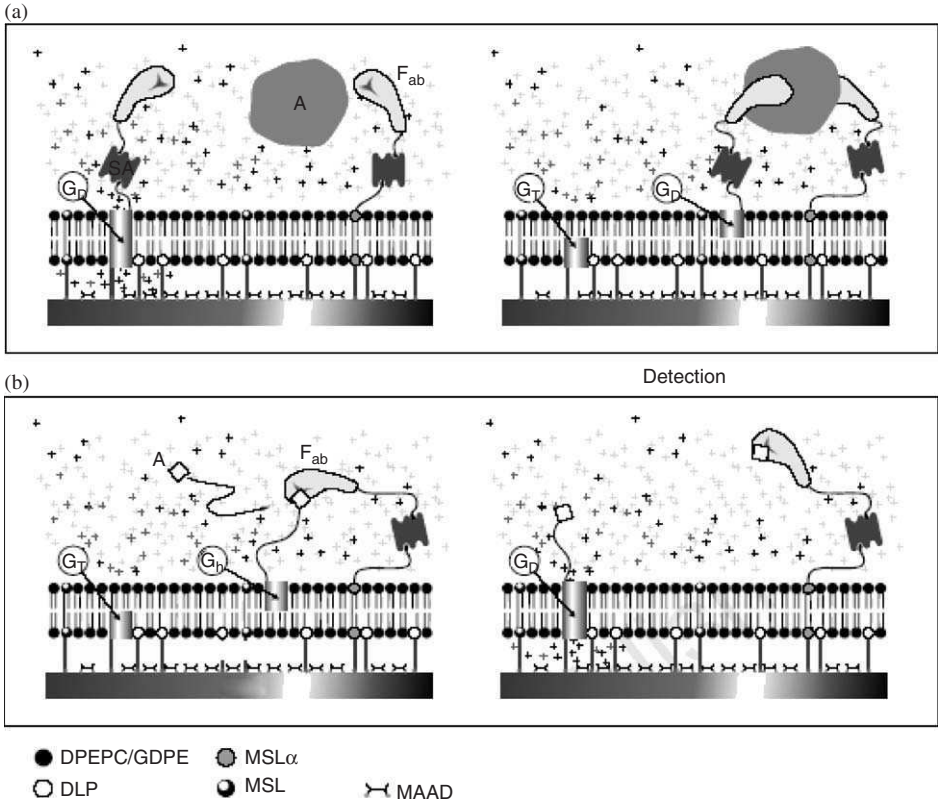

Fig. 7. Schematic ion-channel switch (ICS) biosensor. (a) Two-site sandwich assay. Immobilized ion channels (GT), synthetic archaebacterial membrane-spanning lipids (MSL), and half-membrane-spanning tethered lipids (DLP) are attached to a gold surface *via* polar linkers and sulfur–gold bonds. Polar spacer molecules (MAAD) are directly attached to the gold surface using the same chemistry. Mobile half-membrane-spanning lipids (DPEPC/GDPE) and mobile ion channels gramicidin (Ga) complete the membrane. The mobile ion channels are biotinylated and coupled to biotinylated antibody fragments (Fab9) using streptavidin (SA) intermediates. Some of the membrane-spanning lipids (MSLa) possess biotin-tethered Fab9. In the absence of analyte (A), the mobile ion channels diffuse within the outer monolayer of the tethered membrane, intermittently forming conducting dimers (GD). The addition of the targeted analyte cross-links the Fabs on the MSLa and Ga and forms complexes that tether the Ga distant from their immobilized inner-layer partners. This prevents the formation of channel dimers and lowers the electrical conductivity of the membrane. (b) Competitive assay. Here a similar membrane is formed except that it contains hapten-linked gramicidin (Gh). The membrane is rinsed with a streptavidin solution after which an appropriate biotinylated, haptenspecific Fab′ is added, forming complexes between the MSLa and the Gh. The Gh is thus tethered distant from its immobilized inner-layer partners, GT, preventing the formation of dimers and lowering the electrical conductance of the membrane. The sensor is stored in this state until the addition of analyte competes with the hapten for the Fab′, liberating the channel and resulting in an increase in the membrane conductance (Copyright: Nature 1997 (387) 580–583 with permission).

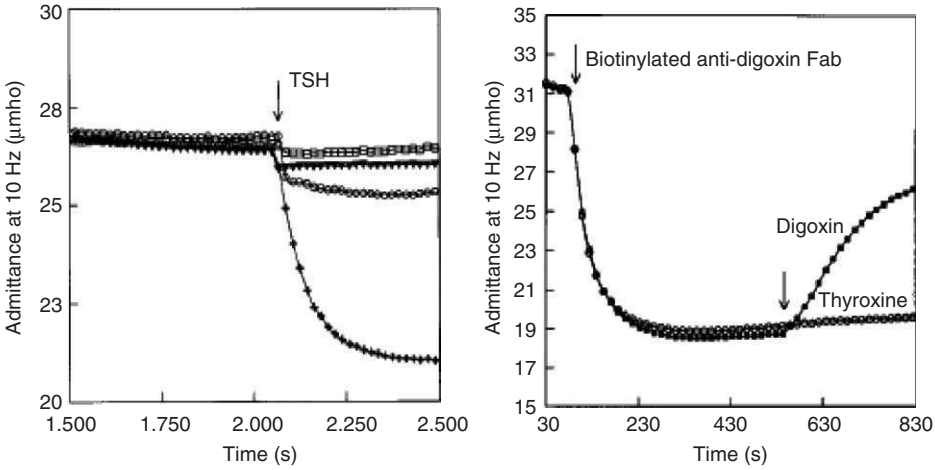

Fig. 8. Left frame: Response of ICS biosensor to TSH. (a) Assembly procedures. First, a tethered membrane 0.16 mm^2 in area is formed on a freshly evaporated gold film. The gold film is 100 nm thick and is bonded to a clean glass microscope slide using a 5-nm layer of chromium. The slide is then immersed in an ethanol solution of the immobile lipid-layer mixture for 1 h 20 °C. The mixture comprises 59 mM DLP, 4.4 MSL-4XB, 4.4 mM MSLOH, 7.5 nM gAYYSSB*n*, and 35 mM EDS. The slide is then removed and rinsed thoroughly in ethanol, air-dried, and clamped to a series of teflon cylinders, each 4 mm internal diameter, 5 mm long, each defining a well volume of 200 ml above the coated gold surface. A further 5 ml of mobile-layer mixture in ethanol solution is added, which contains 350 nM gA-5XB and a 14 mM (30:70) mix of GDPE:DPEPC, after which the slide is rinsed with 500 ml of phosphate buffered saline (PBS). This induces the spontaneous formation of a bilayer membrane. Care is taken not to introduce air bubbles or to take the newly formed membrane surface through an air–water interface. Having rinsed thrice with PBS to eliminate any residual excess membrane lipid, 5 ml of 1.6 mM streptavidin in PBS is added. Following incubation for 10 min, the supernatant is thoroughly rinsed with PBS and a further 20 ml of 0.2 mM b-Fab9 is added. This is then incubated for a further 10 min and thoroughly rinsed with PBS to remove residual material. The sensor is now stored ready to use. (b) Measurement procedure. The admittance is measured at 10 Hz using an excitation amplitude of 50 mV and an offset potential of 2300 at the gold electrode relative to the test solution. Traces are shown using different specificities of biotinylated Fab9: open squares, b-antiferritin; filled triangles, -anti-a-TSH; circles, b-anti-b-TSH; and crosses, a 50:50 mix of b-anti-a-TSH and b-anti-b-TSH. 2 nM of TSH is added at the arrow. The mixed population of biotinylated anti-a and biotinylated anti-b Fab9 elicited a substantial response when the TSH was added. However, the other three biotinylated-Fab9 populations only elicited a small or negligible response when used in isolation. Right Frame: Response to digoxin. A similar membrane is prepared to that described in left frame legend. The principal difference is that the concentration of MSLa is increased tenfold and Ga is replaced by Gh. The total concentration of MSL is maintained. Following the formation of the membrane, it is incubated with 40 nM streptavidin for 10 min and rinsed again. The addition of 5 ml of 50 nM biotinylatedantidigoxin (first arrow) results in a decrease in the admittance. The

transduction proteins, in addition to the more common construction of the bimolecular lipid layer. In favor of easy measurement of the electrical properties of BLMs, the authors determined the receptor–ligand interaction by monitoring the change in electrical properties of the reconstituted BLM system and further studied the relation between the receptor–ligand interaction and the change in electrical properties.

In addition, blood-type-B erythrocyte receptors were reconstructed to the BLM system. The addition of anti-B monoclonal antibody was followed by a decrease in R_m, whereas no change of C_m was measured. In this case, the BLM ruptured after period of time.

The results of that study point out that additional amount of antibody positively related to the magnitude of R_m decrease and negatively related to membrane stability duration (time from adding antibody to membrane rupture). Following the addition of bathing solution or anti-A antibody, both C_m and R_m showed no obvious change.

In a hepatocyte receptors reconstituting the BLM system, adding galactose solution caused an R_m decrease but no C_m change. Similar to erythrocyte receptors reconstituting the BLM system, the decrease in hepatocyte R_m was positively related to the amount of galactose (see Table 2). The hepatocyte receptor reconstituting the BLM system is different from the erythrocyte receptors system because after adding galactose solution, the hepatocyte receptors reconstituting BLM did not rupture during the experiment. For plain BLM consisting only of EPC-Chol, galactose did not affect C_m, R_m, or membrane stability. We should mention, however, one shortcoming of the conventional BLM system, namely, its stability, which rarely lasts more than 8 h. This shortcoming has been overcome by forming the BLM on either a metallic substrate or a hydro-gel support with long-term stability, as reported in Refs. [75,77,93,94]. The reconstituted receptors retain biological activity. The interactions between receptor and ligand correlate well with the change in electrical properties, especially the R_m of the membrane.

In this case, the BLM acts as a model system for signal transduction proteins and can therefore determine the interaction between receptor and ligand. Furthermore, this system has the potential to be widely used in finding drugs that act on membrane receptors and to research the drug delivery system that targets membrane receptors.

---

membrane is then thoroughly rinsed with PBS and stored ready for use. The addition of 3 (5 ml) digoxin (second arrow) causes the admittance to increase (filled squares). The rate and size of this increase is related to the concentration of digoxin. The process may be repeated many times following rinsing with PBS solution. A control is shown in which thyroxine was used in place of digoxin, eliciting no response (circles) (Copyright: Nature 387 (1997) 580–583 with permission).

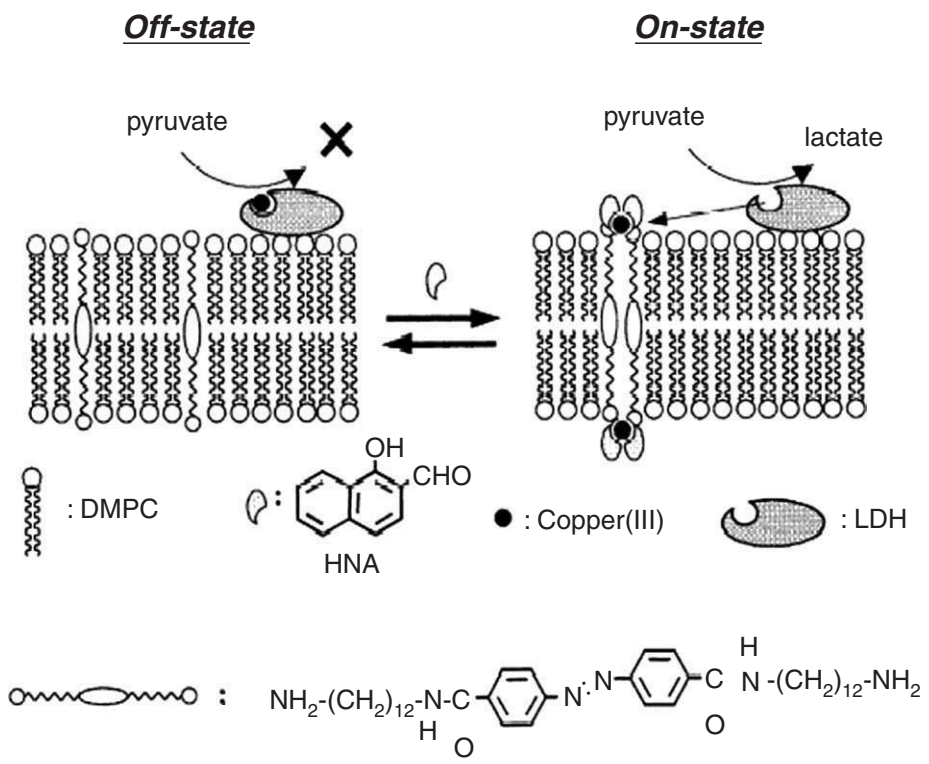

Fig. 9. Schematic representation of dynamic regulation of reversible signaling by azobenzen-containing artificial cell-surface receptor (Copyrights: Journal of Molec. Catal.: B: Enzymatic 11 (2201) 971–976 with permission).

The effect of the amount of antibody on the magnitude of R_m decrease and the membrane stability duration is summarized in Table 2.

5.6. Hormone–receptor interaction within supported phospholipid bilayer membranes

Supported membranes on solid surfaces are of practical and scientific interest for several reasons. Besides the natural environment for the immobilization of proteins under nondenaturing conditions and in well-defined orientations, the supported BLM allows the preparation of ultrathin layers, characterized by high electric resistance on the conductors. The incorporation of receptors into these insulating layers results in a change in electrical and optical parameters, as well as the interaction between a hormone and the embedded receptor [95]. Therefore, using such receptors as the recognition element in electrochemical biosensing facilitates the quantification of minute amounts of a hormone or XNH in real time. Moreover, the supported BLM provides the possibility of studying

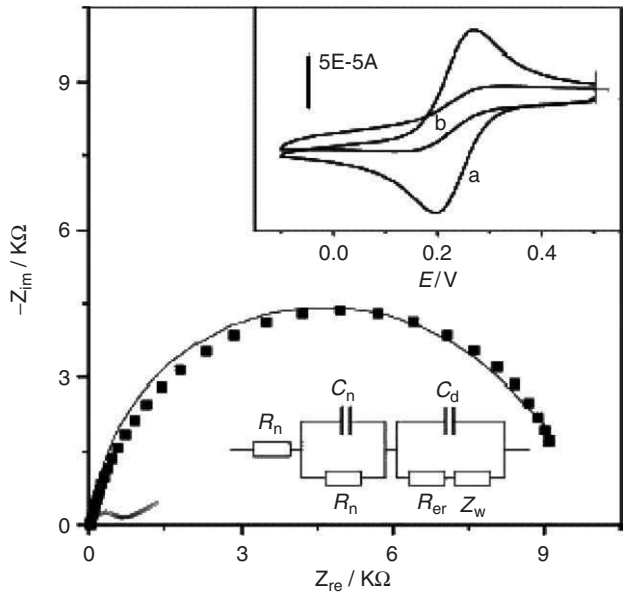

Fig. 10. Impedance spectra at the bare GCE (△), DTDB–BLM/GCE (■), and fitted data (solid line) according to the modified Randle's equivalent circuit in10 mM $K_3Fe(CN)_6/K_4Fe(CN)_6$ (1:1 mixture); and CVs (insert) of 5 mM $K_3[Fe(CN)_6]$ at the bare GCE (a), and DTDB–BLM/GCE (b) at 50 mV/s in 0.1 M KCl (Copyrights: Anal. Chim. Acta 507 (2004) 259–265 with permission).

Table 2. Summary of the effect of the amount of antibody on the magnitude of R_m and the membrane stability duration

Volume of antibody (μl)	$\Delta R_m/R_m,0$	t (s)	$(\Delta R_m/R_m,0)/t$
50	0.77	626	1.23×10^{-3}
100	0.93	636	1.46×10^{-3}
200	0.93	196	4.74×10^{-3}

Notes: ΔR_m is the decrease in R_m after the addition of antibody, $R_m,0$ is the membrane resistance before the addition of antibody, and t is the membrane stability duration after the addition of antibody.

molecular mechanisms of membrane functions, such as ion sensing, material transport, excitability, gated channels, antigen–antibody binding, signal transduction, energy conversion, and hormone–receptor interactions [39,93,96–103].

The amine hormone dopamine (DA) is an important neurotransmitter and extracellular messenger in biological systems. The determination of DA and related catecholamine compounds is significant for neurochemistry and brain-science studies. Since its discovery in the 1950s, DA has been of interest to neuroscientists and chemists. A loss of DA-containing neurons can result in serious diseases like Parkinsonism. Because DA and other catecholamines are easily oxidizable

compounds, they were once thought to be detectable by electrochemical methods based on anodic oxidation. Traditional electrochemical measurements are not specific, however, and could not be used for DA determination because of the interference from ascorbic acid (AA), which usually exists in real systems in large amounts. Nafion and correlated cation exchange polymer film coating [104–106] were considered a robust method to increase the specificity of the measurement system.

Self-assembled phospholipid and lipid-like s-BLMs have been widely studied as a nano-thickness film unit to mimic the complicated functions of biomembranes. The incorporation of DA in an s-BLM of dimyristoylphosphatidylcholine (DMPC) was reported, describing the mediator effect of DA in the film for AA and NADH oxidations. The s-BLM was constructed with 5,5-ditetradecyl-2-(2-trimethyl-ammonioethyl)-1,3-dioxane bromide (DTDB) on a glassy carbon electrode (GCE). The assembled BLM film forms electron-enriched sandwich centers as a result of the functional dioxane group. This milieu should be favorable for the electrochemical reactions of cationic species like DA and related catecholamines. In that study, a drastic change in the electrochemical characteristics of the s-BLM was achieved. The DTDB–BLM/GCE provided a significant accumulation and catalytic effect for DA determination with a high sensitivity and wide linear response range, which could be used for DA determination when the AA concentration is high. The DTDB–BLM/GCE exhibits high electrocatalytic activity toward the oxidation of DA and AA, and the catalytic potential of AA oxidation is 160 mV more negative than that of DA. The homogeneous catalytic effect of AA by the oxidized DA was effectively eliminated at the DTDB–BLM/GCE. A significant adsorption accumulation effect toward cationic species like DA was achieved due to the existence of the electronegative 1,3-dioxane group in DTDB–BLM, which resulted in a highly sensitive and selective determination of DA even in the presence of a 1000-fold higher concentration of AA. The DTDB–BLM/GCE also responded rapidly.

Another type of hormone detection is based on a DTDB self-assembled bilayer for EP determination in the presence of AA. EP (adrenaline), a hormone secreted from the adrenal glands, is an important catecholamine neurotransmitter for the mammalian central nervous system. The electrochemical behavior of EP and its analogs is interesting for understanding the physiological functions and has been studied extensively under normal experimental conditions [40,107–112].

This modified electrode (DTDB/GCE) has strong membrane adsorption accumulation and electro-catalytic ability toward EP and AA. The oxidation of EP is controlled by a double-step adsorption accumulation process of the DTDB–BLM. The parameters of fitted Langmuir isotherm Γ_{max}, B_{ADS}, and ΔG_{ADS} values are summarized in Table 3.

The differential pulse voltammogram (DPV) peaks for EP and AA oxidations appeared at 0.220 and 0.085 V *versus* saturated calomel electrode (SCE), respectively, allowing the determination of EP in the presence of a high AA concentration (Fig. 11).

Table 3. Calculated parameters for Langmuir model

Epinephrine concentration	Γ_{max}	B_{ADS}	ΔG_{ADS}
Step 1			
Less than 1 mM	1.0×10^{-11} mol/cm^2	2.04×106 dm^3/mol^1	-45.17 kJ/mol^1
Step 2			
Higher than1 μM	4.92×10^{-11} mol/cm^2	7.35×104 dm^3/mol^1	-37.1 kJ/mol^1

Notes: B_{ADS} reflects the affinity of the adsobate molecules toward adsorption sites, ΔG_{ADS} stands for Gibbs energy adsorption, and Γ_{max} is the surface coverage.

The advantage of DTDB–BLM was demonstrated experimentally in comparison with the other three BLMs and attributed to the dioxane group, as well as to the suitable length of the carbon chain of DTDB molecule. The current response of the DTDB/GCE was fast and reproducible, and suitable for electrochemical sensing in flow-injection systems, with a linear range of 1×10^{-8} to 1×10^{-4} M.

Estrogen, a hormone produced in the ovaries, adrenal glands, and fat tissues, is essential for the normal development, maturation, and function of the female reproductive tract. Additional small amounts are secreted by the male testes. Both endogenous estrogen and environmental xenoestrogens initiate their physiological actions in target tissue *via* interactions with a nuclear receptor system that functions as a ligand-inducible transcription factor. Receptor overactivation, followed by overexpression of the target gene, has been associated with the feminization of male fish [113], alligators [35], rats, and turtles [114].

Deriving the toxic potential from xenoestrogens structures is difficult because of the wide variety of such compounds. The structural diversity of the xenoestrogens has confounded attempts to measure the estrogenic potential of samples of estrogenic and xenoestrogenic compounds using conventional chemical analyses. Most applied techniques are based on a cloned receptor in yeast and a reporter gene. Such general screening for estrogenic activity was described and applied in sewage treatment water effluents [115]. The bioassays are performed under sterile laboratory conditions and quantitatively detect estrogens as well as xenoestrogens within 4–10 days.

The first study to describe the embedding of a natural isolated steroid hormone receptor in an assembled phospholipid bilayer was published in 2002 [116]. In this study, two stages of assembly yielded a hybrid bilayer: (1) spontaneous self-assembly of decanthiol on gold surface as a hydrophobic monolayer and (2) adhesion of phospholipid molecules to a hydrophobic monolayer. The modification of the electrode did not damage the receptor's ability to react with physiological concentrations of the hormone, and its selectivity was proved as well.

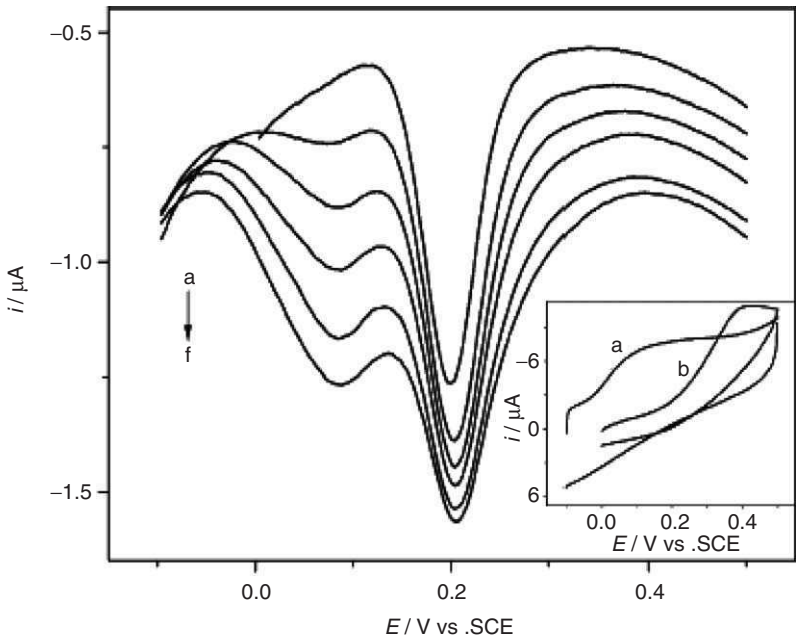

Fig. 11. Differential pulse voltammograms (DPVs) for 1.0×10.5 M EP mixed with different concentration of AA at DTDB/GCE: (a) 0 M, (b) 1.0×10.4 M, (c) 2.5×10.4 M, (d) 5×10.4 M, (e) 6.5×10.4 M, and (f) 1.0×10.3 M in 0.1 M pH 6.0 PBS. Pulse height: 25.0 mV; pulse width: 60.0 ms; and pulse period: 0.5 s. Inset: cyclic voltammograms for 6.26×10.4 M AA in 0.1 M pH 6.0 PBS at DTDB/GCE (a) and bare GCE (b). Scan rate: 50 mV/s (Copyrights: Electrochim. Acta 49 (2004) 4351–4357 with permission).

5.7. Application of impedance spectroscopy to supported bilayer lipid membranes

Impedance spectroscopy (IS) has been used to reveal information on structural parameters of examined layers on modified electrodes. Employing fast impedance techniques based on a short galvanostatic pulse and following the resulting changes in the potential provided extremely fast electrochemical measurements (0.2–1 s). This approach allows the resolution of slow and fast charging processes occurring at the electrode and leads to the resolution of the capacitances and resistances values of the layers [117]. An electrochemical description of the interface is achieved by measuring the impedance as a function of frequency and by representing the data in a complex plane plot (Nuiquist plot) [118]. Impedance studies of self-assembled lipid monolayers have been described in detail [53,119,120].

Applying the impedance technique to study events following the binding of estrogen or xenoestrogen to a native estrogen receptor embedded within a synthetic lipid bilayer membrane, self-assembled onto a gold electrode, yielded a

rapid, physiological concentration-sensitive detection [116]. Estrogen or xenoestrogen binding to the receptor-modified electrode was immediately followed by conformational changes in the lipid layer, resulting in alterations of its electrical properties (Fig. 12).

As expected for a thicker layer, the formation of the bilayer increases R and decreases C as compared with the monolayer. Penetration of the receptor into the lipid layer further increased the value of R and decreased the value of C (Fig. 13).

Fast impedance measurements result in a significantly shorter measurement time and detection under conditions that are comparable to the natural environment of the hormone and its receptor. The experiments were conducted in phosphate buffered solutions in the absence of a redox couple. The signals obtained were fitted to calculate signals that attributed the equivalent circuit according to the following equation

$$E(t) = IR_s + R_{p1}(1 - e^{t-\tau_1}) + R_{p2}(1 - e^{t-\tau_2}) \quad (3)$$

where E is the measured potential, I the applied current, and τ the characteristic lifetime.

The effects of estrogen, bisphenol A, and genistein on the electrical properties of the bilayer-receptor-modified electrode show that the responses to the natural hormone and the xenoestrogen are similar. In general, the R_s values increased, the R_{p1} values decreased, the lifetime τ_1 values decreased, and accordingly the calculated C_1 values decreased (Fig. 14).

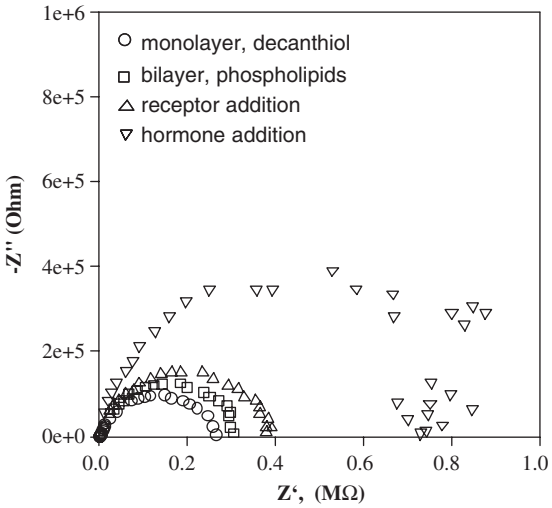

Fig. 12. Nyquist plots for biolayer constructions as measured by AC impedance techniques: monolayer, bilayer, receptor, and 0.5 μg/ml estrogen (Copyrights: Environ. Sci. Technol. 36 (2002) 1574–1578 with permission).

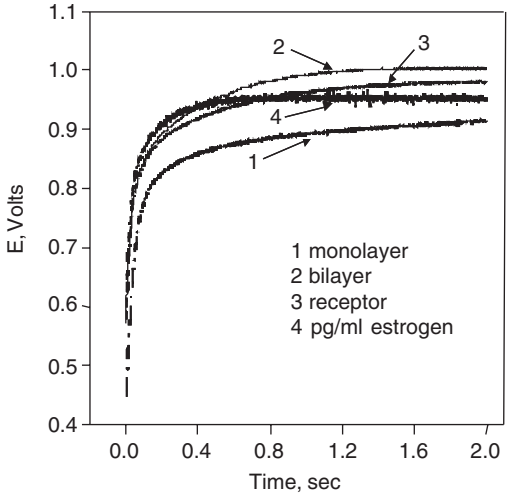

Fig. 13. Changes in electrode potentials during a galvanostatic pulse as obtained for (1) monolayer, (2) bilayer, (3) embedded receptor, and (4) 1 pg/ml (0.1 pM) estrogen (Copyrights: Environ. Sci. Technol. 36 (2002) 1574–1578 with permission).

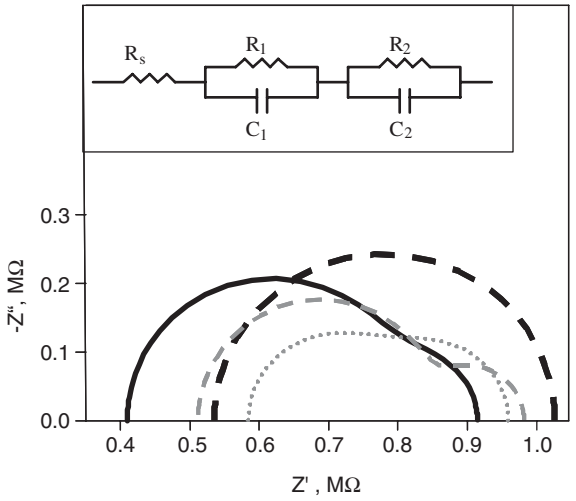

Fig. 14. Nyquist plot for biolayer construction as drawn using the calculated capacitance and resistance values measured by galvanostatic pulses: (_) monolayer, (– –) bilayer, (- -) receptor, and (…) 1 pg/ml estrogen. Inset: Equivalent circuit (Copyrights: Environ. Sci. Technol. 36 (2002) 1574–1578 with permission).

These alterations can be attributed to dimerization and conformational changes of the receptor, which increase its hydrophobic behavior and allow it to enter into the lipid layer. Atomic force microscopy and quartz crystal microbalance experiments validated the electrochemical findings. The responses to the xenoestrogens

Table 4. Summary of the effects of exposure to different estrogen and xenoestrogen concentrations on the electrical properties of the bilayer-receptor modified electrodes

	$\Delta\%R_s$ (MΩ)	$\Delta\%\tau$ (s)	$\Delta\%R_s$ (MΩ)	$\Delta\%C$ (μF)
Estrogen 0.015 pg/ml	No change	No change	No change	No change
Estrogen 44 pg/ml	74.28	−19.96	−45.74	−28.98
Bisphenol-A 30 ng/ml	24.43	−56.63	−16.4	−47.34
Bisphenol-A 3 μg/ml	33.84	−63.26	−26.54	−48.69
Genistein 1 ng/ml	56.28	−21.71	−30.18	−9.78

bisphenol A, and genistein correlated with those of traditional biological assays reported in the literature. We should note that this method does not distinguish between antagonists and agonists (Table 4).

The feasibility of the IS method to detect other steroid hormones was examined. An androgen receptor was embedded in the same platform and the effects of testosterone and xenotestosterone residues were followed (Rishpon, unpublished data). The sensor response to testosterone as well as to testosterone-like molecules agreed with literature data. The technique presented here has the potential to serve as a platform for the study of universal receptor–hormone interactions.

6. CONCLUSIONS

This review describes the advantages of using supported BLMs in the field of hormone–receptor interactions. The incorporation of receptor-based electrodes as the recognition element in supported lipid bilayers for electrochemical biosensing allows the rapid quantification of minute amounts of analyte in real time. The unique s-BLM tool is a robust method for developing such biosensors because it represents a perfect connection between a physical transducer and a biological layer. Electrochemical technology provides an analytical, quantitative tool that can adjust to rapid measurements, with the s-BLM providing a natural environment for the receptor – the living cell.

Combining the natural receptor environment and the receptor's specific ability to detect the analyte with the ability to detect quantitatively small changes following hormone–receptor interactions is useful for preventing the exposure of populations to endocrine-disrupting chemicals. The information gained from this system is applicable not only to researching and understanding hormone–receptor interactions but also to monitoring environmental pollution, health risk, drug delivery, and drug development. The study of hormone–receptor system and the intracellular signaling pathways thus invoked will advance the fields of medicine, endocrinology, biochemistry, and pharmacology.

The outcome of the research reported in this chapter will lead to the development of economical and easy-to-use sensors aimed at the routine and continuous monitoring of endocrine disrupters in suspect environmental locations. Such systems are the key to identifying and defining potent chemicals or pollutants and provide a highly sensitive monitoring method by eliciting an immediate response to a wide range of known or unknown chemicals. The electrochemical detection of hormone–receptor interactions is an ideal technology for the rapid in situ identification and definition of pollutants as XNHs that can serve as an economical and easy-to-use sensor in the field.

REFERENCES

[1] S. Nussey, S. Whitehead, Endocrinology: An Integrated Approach, BIOS Scientific Publisher, Ltd, Oxford, 2001.
[2] P. Germain, L. Altucci, W. Bourguet, C. Rochette-Egly, H. Gronemeyer, Nuclear receptor superfamily: principles of signaling, Pure Appl. Chem. 75 (2003) 1619–1664.
[3] E.R. Sanchez, L.E. Faber, I.W.J. Henze, W.B. Prat, The 56–59 kilodalton protein identified in untransformed steroid receptor complexes is a unique protein that exists in cytosol in a complex with both the 70 and 90 kilodalton heat shock proteins, Biochemistry 29 (1990) 5145–5152.
[4] I. Joab, C. Radanyi, M. Renior, T. Buchou, M.G. Catelli, N. Binart, J. Mester, E. E. Baulieu, Common non hormone binding component in non-transformed chick oviduct receptors of four steroid hormones, Nature 308 (1984) 850–853.
[5] E.R. Sanchez, Hsp56: a novel heat shock protein associated with untransformed steroid receptor complexes, J. Biol. Chem. 265 (1990) 22067–22070.
[6] M.S. Gordon, A.C. Notides, Computer modeling of estradiol interaction with the estrogen receptor, J. Steroid Biochem. 25 (1986) 177–181.
[7] V. Kumar, P. Chambon, The estrogen receptor binds tightly to its responsive element as a ligand induced homodimer, Cell 55 (1988) 145–156.
[8] A.D. Linstedt, N.B. West, R.M. Brenner, Analysis of monomeric-dimeric states of the estrogen receptor with monoclonal antiestrophilins, J. Steroid Biochem. 24 (1986) 677–686.
[9] J.M. Beekman, G.F. Allan, S.Y. Tsai, M.-J. Tsai, B.W. O'Malley, Transcriptional activation by the estrogen receptor requires a conformational change in the ligand binding domain, Mol. Endocrinol. 7 (1993) 1266–1274.
[10] N.H. Ing, J.M. Beekman, S.Y. Tsai, M.-J. Tsai, B.W. O'Malley, Members of the steroid hormone receptor superfamily interact with TFIIB(S300-II), J. Biol. Chem. 267 (1992) 17617–17623.
[11] A. Mueller-Fahrnow, U. Enger, Ligand binding domain of estrogen receptors, Curr. Opin. Biotechnol. 10 (1999) 550–556.
[12] P.B. Sigler, S.P. Williams, Hormone-bound human progesterone receptor ligand-binding domain, Nature 393 (1998) 392.
[13] J.W. Schwabe, L. Chapman, J.T. Finch, D. Rhodes, The crystal structure of the oestrogen receptor DNA-binding domain bound to DNA: how receptors discriminate between their response elements, Cell 75 (1993) 567–578.
[14] J.P. Renaud, N. Rochel, M. Ruff, V. Vivat, P. Chambon, H. Gronemeyer, D. Moras, Crystal structure of the RAR-σ ligand-binding domain bound to all-trans retinoic acid, Nature 378 (1995) 681–689.
[15] W. Bourguet, M. Ruff, P. Chambon, H. Gronemeyer, D. Moras, Crystal structure of the ligand-binding domain of the human nuclear receptor RXR-α, Nature 375 (1995) 377–382.

[16] B.D. Darimont, R.L. Wagner, J.W. Apriletti, M.R. Stallcup, P.J. Kushner, J.D. Baxter, R.J. Fletterick, K.R. Yamamoto, Structure and specificity of nuclear receptor-coactivator interactions, Genes Dev 12 (1998) 3343–3356.
[17] M.S. Lee, S.A. Kliewer, J. Provencal, P.E. Wright, R.M. Evans, Structure of the retinoid X receptor alpha DNA binding domain: a helix required for homodimeric DNA binding, Science 249 (1993) 157–160.
[18] P.M. Matias, P. Donner, R. Coelho, M. Thomaz, C. Peixoto, S. Macedo, N. Otto, S. Joschko, P. Scholz, A. Wegg, S. Basler, M. Schafer, U. Egner, M.A. Carrondo, Structural evidence for ligand specificity in the binding domain of the human androgen receptor. Implications for pathogenic gene mutations, J. Biol. Chem. 275 (2000) 26164–26171.
[19] R.L. Wagner, J.W. Apriletti, M.E. McGrath, B.L. West, J.D. Baxter, R.J. Fletterick, A structural role for hormone in the thyroid hormone receptor, Nature 378 (1995) 690–697.
[20] S.P. Williams, P.B. Sigler, Atomic structure of progesterone complexed with its receptor, Nature 393 (1998) 392–396.
[21] J.M. Wurtz, W. Bourguet, J.P. Renaud, P. Chambon, D. Moras, H. Gronemeyer, A canonical structure for the ligand-binding domain of nuclear receptors, Nature Struct. Biol. 3 (1996) 87–94.
[22] R.L. Cooper, R.J. Kavlock, Endocrine disruptors and reproductive development: a weight-of-evidence overview, J. Endocrinol. 152 (1997) 159–166.
[23] R.M. Evans, The steroid and thyroid hormone receptor superfamily, Science 240 (1988) 889–895.
[24] J. Toppari, J. Larsen Chr., P. Christiansen, A. Giwercman, L.J. Grandjean, B. J'gou, T.K. Jansen, P. Jouannet, N. Keiding, H. Leffers, J.A. McLachlan, O. Meyer, J. Miller, E. Rajpert-De Meyts, T. Scheike, R. Sharpe, J. Sumpter, N.E. Skakkebruk, Male reproductive health and environmental xenoestrogens, Environ. Health. Prespect. 104 (1996) 741–803.
[25] S. Lowry, Oncology – molecular-basis for hormone-related cancer, Lancet 341 (1993) .
[26] T. Colborn, F. vom Saal, Environmental Endocrine-Disrupting Chemicals: Neural, Endocrine, and Behavioral Effects – Preface, Toxicology and Industrial Health St, NW, Washington, DC 20037, USA; World Wildlife Fund, Wildlife & Contaminants Program, Washington, DC 20037, USA; Univ Missouri, Div. Biol. Sci., Columbia, MO 65211, USA, 14 (1998) 9–23.
[27] S. Safe, Environmental estrogens: roles in male reproductive tract problems and in breast cancer, Rev. Environ. Health 17 (2002) 253–262.
[28] S. Safe, E.d.a.h.h.i.t.a. problem, Endocrine disruptors and human health: is there a problem, Toxicology 205 (2004) 3–10.
[29] K.B. Moysich, R.J. Menezes, J.A. Baker, L. Falkner, Environmental exposure to polychlorinated biphenyls and breast cancer risk, Rev. Environ. Health 17 (2002) 263–277.
[30] C. Charlier, J.M. Foidart, F. Pitance, P. Herman, U. Gaspard, M. Meurisse, G. Plomteux, Environmental dichlorodiphenyltrichlorethane or hexachlorobenzene exposure and breast cancer: is there a risk? Clin. Chem. Lab. Med. 42 (2004) 222–227.
[31] R.J. Kavlock, G.T. Ankley, A perspective on the risk assessment process for endocrine-disruptive effects on wildlife and human health, Risk Anal 16 (1996) 731–739.
[32] R. Bigsby, R.E. Chapin, G.P. Daston, B.J. Davis, J. Gorski, L.E. Gray, K.L. Howdeshell, R.T. Zoeller, F.S. vom Saal, Evaluating the effects of endocrine disrupters on endocrine function during development, Eviron. Health. Perspect. 65211 USA Univ. Missouri, Div. Biol. Sci., Columbia, MO 65211, USA, Indiana Univ. Sch. Med., Indianapolis, IN, USA Natl. Inst. Environ. Hlth. Sci. Res. Triangle Pk, NC USA Procter & Gamble Co, Cincinnati, OH, USA, Univ. Wisconsin, Madison, WI, USA, US EPA, Res. Triangle Pk, NC 27711 USA 107 (1999) 613–618.

[33] P.J. Reijnders, Reproductive failure in common seals feeding on fish from polluted coastal waters, Nature 324 (1986) 456–457.
[34] G.A. Fox, Wildlife as sentinels of human health effects in the great lakes – St. Lawrence Basin, Environ. Health Perspect. 109 (2001).
[35] L.J. Guillette, T.S. Gross, D.A. Gross, A.A. Rooney, H.F. Percival, Gonadal Steroidogenesis *in-vitro* from juvenile alligators obtained from contaminated or control lakes, Environ. Health Prespect. 103 (1995) 31–36.
[36] M. Seifert, G. Brenner-Weiss, S. Haindl, M. Nusser, U. Obst, B. Hock, A new concept for the bioeffects-related analysis of xenoestrogens: hyphenation of receptor assays with LC-MS, Fresen. J. Anal. Chem. 363 (1999) 767–770.
[37] S.M. Singh, S. Gauthier, F. Labrie, Androgen receptor antagonists (antiandrogens): structure–activity relationships, Curr. Med. Chem. 7 (2000) 211–247.
[38] P. Mueller, D.O. Rudin, H.T. Tien, W.C. Wescott, Reconstitution of cell membrane structure in vitro and its transformation into an excitable system, Nature 194 (1962) 979–980.
[39] J. Barber, Photosynthesis in Relation to Model Systems, Vol. 3, Elsevier/North Holland, New York, 1979, pp. 115–173.
[40] J.E. Baur, E.W. Kristensen, L.J. May, D.J. Wiedemann, R.M. Wightman, Fast-scan voltammetry of biogenic-amines, Anal. Chem. 60 (1988) 1268–1272.
[41] E. Sackman, Supported membranes: scientific and practical applications, Science 271 (1996) 43–48.
[42] J.G. Salafsky, J.S.G. Boxer, Architecture and function of membrane proteins in planar supported bilayers: a study with photosynthetic reaction centers, Biochemistry 35 (1996) 14773–14781.
[43] I. Reviakine, W. Bergsma-Schutter, A. Brisson, Growth of protein 2-D crystals on supported planar lipid bilayers imaged in situ by AFM, J. Struct. Biol. 121 (1998) 356–362.
[44] P.E. Milhiet, M.C. Giocondi, O. Baghdadi, F. Ronzon, B. Roux, C. Le Grimellec, Spontaneous insertion and partitioning of alkaline phosphatase into model lipid rafts, EMBO Rep 3 (2002) 485–490.
[45] C.M. Yip, J. McLaurin, Amyloid-beta peptide assembly: a critical step in fibrillogenesis and membrane disruption, Biophys. J. 80 (2001) 1359–1371.
[46] S.G. Boxer, Molecular transport and organization in supported lipid membranes, Curr. Opin. Chem. Biol. 4 (2000) 704–709.
[47] I. Reviakine, A. Brisson, Streptavidin 2D crystals on supported phospholipid bilayers: towards constructing anchored phospholipid bilayers, Langmuir 17 (2001) 8293–8299.
[48] L. Kam, S.G. Boxer, Spatially selective manipulation of supported lipid bilayers by laminar flow: steps toward biomembrane microfluidics, Langmuir 19 (2003) 1624–1631.
[49] C. Larsson, M. Rodahl, F. Hook, Characterization of DNA immobilization and subsequent hybridization on a 2D arrangement of streptavidin on a biotin-modified lipid bilayer supported on SiO_2, Anal. Chem. 75 (2003) 5080–5087.
[50] R.P. Richter, A.R. Brisson, Following the formation of supported lipid bilayers on mica – a study combining AFM, QCM-D and ellipsometry, Biophys. J. 88 (2005) 3422–3433.
[51] G.G. Roberts, C.W. Pitt, Langmuir-Blodgett Films, Elsevier, Amsterdam, 1983.
[52] E.L. Florin, H.E. Gaub, Painted supported lipid-membranes, Biophys. J. 64 (1993) 375–383.
[53] R.P. Janke, R.W. Fawcett, A. Ulman, Impedance spectroscopy of self-assembled monolayers on Au111: sodium ferrocyanide charge transfer at modified electrodes, Langmuir 14 (1998) 3011–3018.
[54] A.W. Adamson, Physical Chemistry of Surfaces, Wiley, New York, 1976.
[55] R.W. Murray, Chemically modified electrodes, Acc. Chem. Res. 13 (1980) 135–141.
[56] M.P. Soriaga, A.T. Hubbard, J. Am. Chem. Soc. 104 (1982) 3937–3945.

[57] W. Knoll, M.R. Philpott, W.G. Golden, Surface infrared and surface enhanced raman vibrational spectra of monolayer assemblies in contact with rough metal surfaces, J. Chem. Phys. 77 (1982) 219–225.
[58] H. Kuhn, D. Mobius, Techniques of Organic Chemistry, Vol. 1, Wiley, New York, 1972.
[59] J.F. Rabolt, R. Santo, J.D. Swalen, Appl. Spectrosc. 34 (1980) 517–521.
[60] D.G. Whitten, Angew. Chem. Int. Ed. Engl. 18 (1979) 440–450.
[61] J.-P. Furtlehner, J. Messier, Conduction in MIM structures with an organic monomolecular layer at high electric fields, Thin Solid Films 68 (1980) 233–239.
[62] E.E. Polymeropoulos, J. Sagiv, Electrical conduction through adsorbed monolayers, J. Chem. Phys. 69 (1978) 1836–1847.
[63] M. Sugi, T. Fukui, Phys. Rev. B. 18 (1978) 725–732.
[64] M.A. Richard, J. Deutsch, G.M. Whitesides, Hydrogenation of oriented monolayers of ω-unsaturated fatty acids supported on platinum, J. Am. Chem. Soc. 100 (1979) 6613–6625.
[65] R.D. Kornberg, H.M. McConnell, Inside–outside transitions of phospholipids in vesicle membranes, Biochemistry 10 (1971) 1111–1118.
[66] T.J. McIntosh, R.C. Waldbilling, J.D. Robertson, Lipid bilayer ultrastructure. Electron density profiles and chain tilt angles as determined by X-ray diffraction, Biochim. Biophys. Acta 448 (1976) 15–33.
[67] R.C. Waldbillig, J.D. Robertson, T.J. McIntosh, Biochim. Biophys. Acta 448 (1976) 1–14.
[68] R.G. Nuzzo, D.L. Allara, Adsorption of bifunctional organic disulfides on gold surfaces, J. Am. Chem. Soc 105 (1983) 4481–4483.
[69] M.D. Porter, T.B. Bright, D.L. Allara, C.E.D. Chidsey, Spontaneously organized molecular Assemblies. 4. Structural characterization of N-alkyl thiol monolayers on gold by optical ellipsometry, infrared spectroscopy, and electrochemistry, J. Am. Chem. Soc 109 (1987) 3559–3568.
[70] N.J. Goddard, D. Pollardknight, C.H. Maule, Real-time biomolecular interaction analysis using the resonant mirror sensor, Analyst 119 (1994) 583–588.
[71] H.W. Reinartz, J.G. Quinn, K. Zanker, *et al.*, Bispecific multivalent antibody studied by real-time interaction analysis for the development of an antigen-inhibition enzyme-linked immunosorbent assay, Analyst 121 (1996) 767–771.
[72] K.B. Blodgett, Films built by depositing successive monomolecular layers on a solid surface, J. Am. Chem. Soc. 57 (1935) 1007–1022.
[73] H.T. Tien, A.L. Ottova, The lipid bilayer concept and its experimental realization: from soap bubbles, kitchen sink, to bilayer lipid membranes, J. Membrane Sci. 189 (2001) 83–117.
[74] G. Volkov, D.W. Deamer, D.L. Tanelian, V.S. Markin, Liquid Interfaces in Chemistry and Biology, Wiley, New York, 1998.
[75] J.M. Kauffmann, Development and characterization of electrochemical biosensors based on organic molecular assemblies, Bioelectrochem. Bioenerg. 42 (1997) 1–104.
[76] V. Tvarozek, H.T. Tien, I. Novotny, T. Hianik, J. Dlugopolsky, W. Ziegler, A. Leitmannovaottova, J. Jakabovic, V. Rehacek, M. Uhlar, Thin-Film microsystem applicable in (bio)chemical sensors, Sensor. Actuat. B – Chem. 19 (1994) 597–602.
[77] H.T. Tien, R.H. Barish, L.-Q. Gu, A.L. Ottova, Supported bilayer lipid membranes as ion and molecular probes, Anal. Sci. 14 (1998) 3–14.
[78] F.W. Scheller, F. Schubert, J.e. Fedrowitz, Frontiers in Biosensorics, Vols. I and II, Birkhauser, Berlin, 1996.
[79] B.A. Cornell, V.L.B. Braach-Maksvytis, L.G. King, P.D.J. Osman, B. Raguse, L. Wieczorek, R.J. Pace, A biosensor that uses ion-channel switches, Nature 387 (1997) 580–583.
[80] J.P. Folkers, P.E. Laibinis, G.M. Whitesides, J. Deutch, Phase-behavior of 2-component self-assembled monolayers of alkanethiolates on gold, J. Phys. Chem. 98 (1994) 563–571.

[81] S. Heysel, H. Vogel, M. Sanger, H. Sigrist, Covalent attachment of functionalized lipid bilayers to planar wave-guides for measuring protein-binding to biomimetic membranes, Protein Sci. 4 (1995) 2532–2544.
[82] H. Lang, C. Duschl, H. Vogel, A new class of thiolipids for the attachment of lipid bilayers on gold surfaces, Langmuir 10 (1994) 197–210.
[83] H.M. McConnell, T.H. Watts, R.M. Weis, A.A. Brian, Supported planar membranes in studies of cell–cell recognition in the immune-system, Biochim. Biophys. Acta 864 (1986) 95–106.
[84] A.L. Plant, M. Gueguetchkeri, W. Yap, Supported phospholipid/alkanethiol biomimetic membranes – insulating properties, Biophys. J. 67 (1994) 1126–1133.
[85] J. Rickert, T. Weiss, W. Kraas, G. Jung, W. Gopel, A new affinity biosensor: self-assembled thiols as selective monolayer coatings of quartz crystal microbalances, Biosens. Bioelectron. 11 (1996) 591–598.
[86] C. Steinem, A. Janshoff, W.P. Ulrich, M. Sieber, H.J. Galla, Impedance analysis of supported lipid bilayer membranes: a scrutiny of different preparation techniques, Biochim. Biophys. Acta – Biomembr. 1279 (1996) 169–180.
[87] K. Fukuda, Y. Sasaki, K. Ariga, J. Kikuchi, Dynamic behavior of a transmembrane molecular switch as an artificial cell-surface receptor, J. Mol. Catal. B – Enzym. 11 (2001) 971–976.
[88] J. Kikuchi, K. Ariga, K. Ikeda, Signal transduction mediated by artificial cell-surface receptors: activation of lactate dehydrogenase triggered by molecular recognition and phase reorganization of bile acid derivatives embedded in a synthetic bilayer membrane, Chem. Commun. (1999) 547–548.
[89] J. Kikuchi, K. Ariga, T. Miyazaki, K. Ikeda, An artificial signal transduction system. Control of lactate dehydrogenase activity performed by an artificial cell-surface receptor, Chem. Lett. (1999) 253–254.
[90] J. Kikuchi, Y. Murakami, Steroid cyclophanes as artificial cell-surface receptors. Molecular recognition and its consequence in signal transduction behavior, J. Inclus. Phenom. Mol. Recognition Chem. 32 (1998) 209–221.
[91] Y. Murakami, J. Kikuchi, O. Hayashida, Molecular recognition by large hydrophobic cavities embedded in synthetic bilayer-membranes, Supramol. Chem. II – Host Design Mol. Recogn. 175 (1995) 133–156.
[92] L. Wang, X.P. Hou, A. Ottova, H.T. Tien, Receptor–ligand interactions in a reconstituted bilayer lipid membrane, Electrochem. Commun. 2 (2000) 287–289.
[93] A. Brett, A.M. Oliverira Brett, Electroanalytical chemistry, Electrochim. Acta 43 (1998) 3587–3610.
[94] Y.L. Zhang, Z.X. Guo, H.X. Shen, Modification of bilayer lipid membrane and its application to analytical chemistry, Chin. J. Anal. Chem. 27 (1999) 1096–1102.
[95] J.L. Anderson, L.A.J. Coury, J. Leddy, Dynamic electrochemistry: methodology and application, Anal. Chem. 72 (2000) 4497–4520.
[96] R. Guidelli, G. Aloisi, L. Becucci, A. Dolfi, M.R. Moncelli, F.T. Buoninsegni, New directions and challenges in electrochemistry – bioelectrochemistry at metal/water interfaces, J. Electroanal. Chem. 504 (2001) 1–28.
[97] C. Karolis, H.G.L. Coster, T.C. Chilcott, K.D. Barrow, Differential effects of cholesterol and oxidised-cholesterol in egg lecithin bilayers, Biochim. Biophys. Acta – Biomembr. 1368 (1998) 247–255.
[98] T.Y. Tsong, Electroporation of cell-membranes, Biophys. J. 60 (1991) 297–306.
[99] T.Y. Tsong, On electroporation of cell-membranes and some related phenomena, Bioelectrochem. Bioener. 24 (1990) 271–295.
[100] T.I. Rokitskaya, M. Block, Y.N. Antonenko, E.A. Kotova, P. Pohl, Photosensitizer binding to lipid bilayers as a precondition for the photoinactivation of membrane channels, Biophys. J. 78 (2000) 2572–2580.
[101] F.T. Hong, Interfacial photochemistry of retinal proteins, Prog. Surf. Sci. 62 (1999) 1–237.

[102] M.A. Delarosa, J.A. Navarro, M. Roncel, Solar-energy conversion from water photolysis by biological and chemical-systems, Appl. Biochem. Biotechnol. 30 (1991) 61–81.
[103] G. Dryhurst, K. Niki, Redox Chemistry and Interfacial Behavior of Biological Molecules, Plenum, New York, 1988, pp. 529–556.
[104] A. Domenech, H. Garcia, M.T. Domenech-Carbo, M.S. Galletero, 2,4,6-Triphenylpyrylium ion encapsulated into zeolite y as a selective electrode for the electrochemical determination of dopamine in the presence of ascorbic acid, Anal. Chem. 74 (2002) 562–569.
[105] J.W. Mo, B. Dgorevc, Simultaneous measurement at dopamine and ascorbate at their physiological levels using voltammetric microprobe based on overoxidized poly(1,2-phenylenediamine)-coated carbon fiber, Anal. Chem. 73 (2001) 1196–1202.
[106] M.D. Rubianes, G.A. Rivas, Highly selective dopamine quantification using a glassy carbon electrode modified with a melanin-type polymer, Anal. Chim. Acta 440 (2001) 99–108.
[107] B.R. Cooper, J.A. Jankowski, D.J. Leszczyszyn, R.M. Wightman, J.W. Jorgenson, Quantitative-determination of catecholamines in individual bovine adrenomedullary cells by reversed-phase microcolumn liquid-chromatography with electrochemical detection, Anal. Chem. 64 (1992) 691–694.
[108] H. Cui, L.S. Wu, J. Chen, X.Q. Lin, Multi-mode in situ spectroelectrochemical studies of redox pathways of adrenaline, J. Electroanal. Chem. 504 (2001) 195–200.
[109] S.H. Kim, J.W. Lee, I.H. Yeo, Spectroelectrochemical and electrochemical behavior of epinephrine at a gold electrode, Electrochim. Acta 45 (2000) 2889–2895.
[110] F. Li, H. Cui, X.Q. Lin, Determination of adrenaline by using inhibited Ru(bpy)(3)(2+) electrochemiluminescence, Anal. Chim. Acta 471 (2002) 187–194.
[111] K.O. Lupetti, I.C. Vieira, H.J. Vieira, O. Fatibello, Electroregenerable anion-exchange resin with triiodide carbon paste electrode for the voltammetric determination of adrenaline, Analyst 127 (2002) 525–529.
[112] K. Pihel, T.J. Schroeder, R.M. Wightman, Rapid and selective cyclic voltammetric measurements of epinephrine and norepinephrine as a method to measure secretion from single bovine adrenal-medullary cells, Anal. Chem. 66 (1994) 4532–4537.
[113] J. Sumpter, S. Jobling, Environ. Health Prespect. 103 (1995) 173–178.
[114] D. Crews, J.M. Bergeron, J.A. McLachlan, The role of estrogen in turtle sex determination and the effects of PCBs, Environ. Health Prespect. 103 (1995) 73–77.
[115] C. Desbrow, E.J. Routledge, G.C. Brighty, J.P. Sumpter, M. Waldock, Identification of estrogenic chemicals in STW effluent. 1. Chemical fractionation and *in-vitro* biological screening., Environ. Sci. Technol. 32 (1998) 1549–1558.
[116] V. Granek, J. Rishpon, Detecting endocrine-disrupting compounds by fast impedance measurements, Environ. Sci. Technol. 36 (2002) 1574–1578.
[117] J. Rishpon, S. Gottesfeld, Resolution of fast and slow charging processes in ruthenium oxide films: an AC impedance and optical investigation, J. Electrochem. Soc. 131 (1984) 1960–1968.
[118] J.R. Macdonald, Impedance Spectroscopy: Emphasizing Solid Materials and Systems, Wiley, New York, 1987.
[119] E. Boubour, B.L. Lennox, Insulting properties of self-assembled monolayers monitored by impedance spectroscopy, Langmuir 16 (2000) 4222–4228.
[120] E. Boubour, B.L. Lennox, Potential-induced defects in n-alkenthiol self-assembled monolayers monitored by impedance spectroscopy, J. Phys. Chem. B 104 (2000) 9004–9010.

This page intentionally left blank

CHAPTER 2

Functional Tethered Bimolecular Lipid Membranes (tBLMs)

Ingo Köper,[1,*] Stefan M. Schiller, Frank Giess, Renate Naumann, and Wolfgang Knoll

[1]*Max Planck Institute for Polymer Research, Ackermannweg 10, 55128 Mainz, Germany*

Contents

Abstract

Biological membranes are highly complex architectures. Their central structure consists of a lipid bilayer, which fulfills many tasks and, in particular, serves as a barrier between the inside and outside of the cell. Membrane-related processes have attracted an enormous interest, but systematic studies of such complex systems are difficult and limited to only a few examples. Here, we present two different model systems that enable the study of membrane proteins in a quasi-natural environment. First, the tethered bilayer lipid membrane, where a lipid is anchored to a surface *via* a hydrophilic spacer and the so-formed bilayer serves as a matrix for protein incorporation. In the inverse architecture, a protein is tethered to a surface and then embedded into a lipid bilayer. In both cases, functional studies of the proteins are possible.

1. INTRODUCTION

Biological membranes are highly complex architectures. Their central structure consists of a lipid bilayer, which fulfills many tasks and, in particular, serves as a barrier between the inside and outside of the cell. The bilayer comprises a double layer of lipids that are held together by a variety of interactions, e.g., hydrophobic and van der Waals forces. Transport processes across membranes are controlled by proteins, e.g., ion channels, shuttle proteins or gated pores. A large number of diseases is related to mal-functions of these membrane proteins. Therefore, membrane-related processes have attracted an enormous interest,

*Corresponding author. Tel: +49-613-379164; Fax: +49-6131-379503;
E-mail: Ingo.koeper@mpip-mainz.mpg.de

ADVANCES IN PLANAR LIPID BILAYERS AND LIPOSOMES, VOLUME 3
ISSN 1554-4516 DOI: 10.1016/S1554-4516(05)03002-4

but systematic studies of such complex systems are difficult and limited to only a few examples.

Different model systems have been developed in order to mimic the basic functions of a cell membrane and thus to provide a basis for the systematic study of all kinds of different membrane-related processes [1–3]. A suitable model system should fulfill certain key features in order to display properties as close as possible to the natural analogue: the membrane should separate an inner-membrane space from the outer part. This homogeneous barrier also has to prevent translocation processes from one side to the other. Not only does this include the transport of small molecules as well as of ions, but also the membrane has to be insulating. At the same time, the model membrane has to provide some flexibility and lateral fluidity in order to allow the incorporation and proper function of membrane proteins.

Four different model membrane architectures are schematically depicted in Fig. 1. Very simple model systems are vesicles or liposomes. Their internal part is separated by the membrane bilayer from the outside. The membranes have been shown to be fluid, and the functional incorporation of membrane proteins is possible by reconstitution protocols. Protein-loaded vesicles can be obtained from purified membrane proteins. The number of techniques used to analyze the vesicles as a membrane system, however, is limited, as well as their use in biosensing devices.

The BLM (“black”), on the other hand, is a model system well suitable for the investigation of transport processes of ions or small molecules through lipid bilayers [4]. To this end, a rather simple setup has been developed: a lipid bilayer spans an aperture in a septum that separates two aqueous compartments, each connected to an electrode. Using this configuration, the electrical characterization of the membrane is possible and resistances and capacitances similar to values measured in patch clamp experiments have been obtained. The high electrical sealing properties of BLMs make it even possible to measure ion translocations through single ion channels and to record the resulting stochastic current signals. However, these systems, by their very nature, are rather unstable and difficult to use in practical applications, Several attempts have been made to increase their stability including the polymerization of the lipids or the application of stabilizing layers on one or both sides of the membrane [5].

In order to obtain maximum stability and to provide a suitable platform for biosensing applications, the concept of solid-supported membranes has been proposed [2,6]. In this concept, a lipid bilayer is directly placed on top of a solid support. If this support is an electrode, electrical characterization of the membrane is possible. The drawback of this system is the limited space between the membrane and the support, which is often not more than a thin layer of water. This is usually not enough to serve as an ion reservoir needed to allow for ion transport to occur through the embedded membrane proteins. Additionally, proteins with large extramembrane domains cannot be incorporated without risking

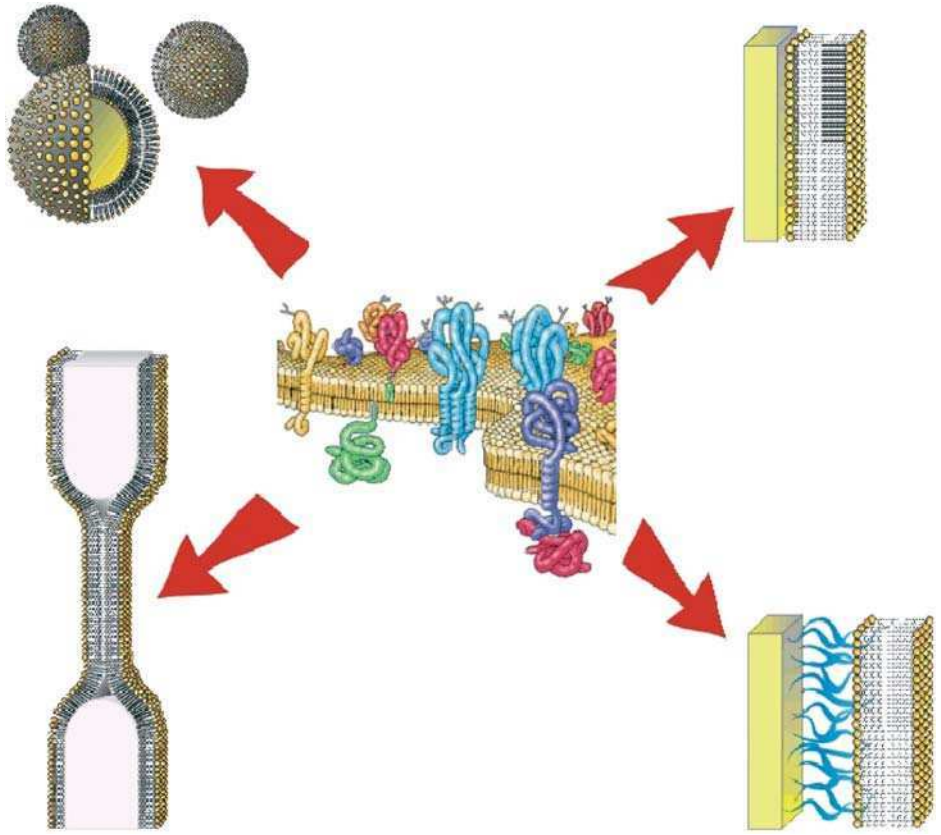

Fig. 1. Schematic assembly of different model membrane systems. Upper left: vesicles, lower left: bimolecular lipid membrane (BLM), upper right: solid-supported membrane, lower right: tethered bilayer lipid membrane (t'BLM), central part: schematic of a biomembrane with incorporated membrane proteins.

denaturation. Another inconvenience of this model system is its reduced stability. A bilayer merely fused to a solid support lacks the robustness needed for practical applications as biosensors.

2. ASSEMBLING THE TETHERED BILAYER

In order to overcome these limitations and drawbacks, we recently introduced a novel model membrane platform, the t'BLM.

As depicted in Fig. 2 a t'BLM consists of a lipid bilayer. Its proximal layer is (partially) covalently attached to a solid support *via* a hydrophilic spacer.

Various architectures and chemical strategies have been tested in an effort to develop the best tethering systems. However, the most successful architecture recently developed is based on a telechelic system, for which the spacer chain

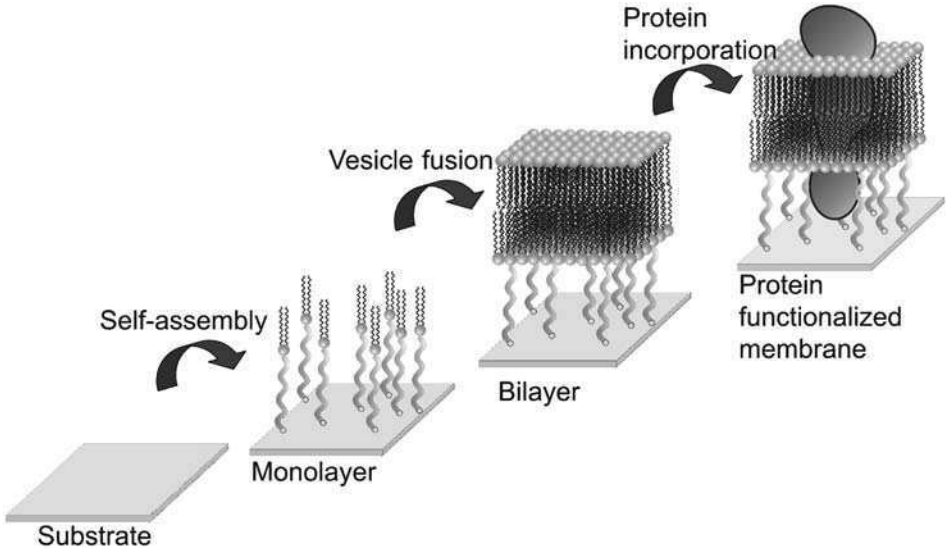

Fig. 2. Schematic assembly of a tBLM in three steps. Firstly, the proximal layer is (partially) bound to a substrate by a self-assembly procedure. The bilayer is completed by vesicle fusion. Solubilized proteins are then functionally incorporated into the bilayer. The last two steps can be combined using proteoliposomes.

molecules are functionalized on one end with a reactive group specifically binding to the substrate, while the other end carries an amphiphile acting as an anchor lipid.

This first layer is built *via* a self assembly process from a dilute solution of the tetherlipid. If the solid support is a gold substrate (used, e.g., for electrochemical measurements and the surface plasmon spectroscopy), the spacer unit can be bound using thiol chemistry. These bonds provide a stable anchoring of the proximal membrane layer to the electrode. The distal layer of the membrane can be completed either by depositing a second (distal) monolayer, which was preorganized at the air/water interface *via* the Langmuir/Blodgett/Kuhn techniques, or by fusion of lipid vesicles to the hydrophobic self-assembled monolayer. Several different systems have been shown to form tBLM architectures, however, with different property profiles. Certain criteria have been established that measure the quality of the bilayer. Homogeneity at the micrometer scale can be investigated using fluorescence microscopy techniques, for which fluorescently labeled lipids are mixed into the distal leaflet of the bilayer. We believe one important factor for the incorporation and proper function of membrane proteins is the fluidity or lateral mobility of membrane constituents (lipids and proteins) within the bilayer. This can be measured by fluorescence recovery after photobleaching (FRAP) techniques. It could be shown that a large tether density in the proximal leaflet can obstruct the free diffusion of integral units [7].

Another main criteria for the quality of a membrane and its suitability for biosensing applications is a high electrical resistance. This factor becomes obvious if one thinks about measuring general electric currents or, more specifically, evaluating the transport of small molecules and ions through the membrane. In order to ensure that these transport processes are dominated by the functional action of the incorporated proteins, one needs to prepare membranes that show as little shunt conductance through uncontrolled defects as possible. The observed currents should be exclusively due to protein action and not to defects in the bilayer.

A method of choice for these investigations is the electrical impedance spectroscopy (EIS). Using the noble metal support as a working electrode, one can perform three electrode measurements in order to obtain parameters such as the resistance and capacitance of the membrane. Values obtained from the various model systems can be compared to those known from patch clamp experiments on real cells or those known from black lipid membrane experiments. Resistances larger than approximately 10 $M\Omega\,cm^2$ and capacitances smaller than 1 $\mu F\,cm^2$ are standard for good membranes.

The first tBLMs with high electrical resistances have been presented by Cornell *et al.* [8]. The authors presented an architecture in which gramicidin was embedded into a tethered bilayer membrane and served as the detection unit of a biosensing prototype [9,10]. Terrettaz *et al.* have presented another electrically insulating system [11–13] with a synthetic ion channel, which was bound to the substrate and served as the active unit.

In 2003, we presented a novel type of tethered thiolipids. The first example of this type is the 2,3-di-*O*-phytanyl-*sn*-glycerol-1-tetraethylene glycol-D,L,α-lipoic acid ester lipid (DPTL) [14]. Its architecture, as shown as the proximal leaflet in Fig. 3, includes phytanyl chains, which are known to guarantee a low phase transition temperature. This ensures a fluid like structure of the membrane at room temperature. Such lipids are known to allow for the formation of dense and stable membranes [15,16]. The link between the lipid tails and the spacer unit contains only ether bonds, which are known to be chemically inert. In nature, these moieties can be found in extremophiles or archaea [17]. The spacer unit consists of a tetraethylene-glycol unit that (i) provides a hydrophilic ion reservoir between the substrate and bilayer, (ii) compensates for surface roughness effects and (iii) separates the bilayer from the substrate. A lipoic acid moiety was used to link the molecule to a gold substrate. The proximal layer can be assembled by adsorption from an ethanolic solution. The best results have been obtained using template stripped gold [18], which helps minimizing surface roughness effects. In short, a thin gold film is firstly evaporated onto a clean silicon substrate used as the template. The gold is then transferred to a glass slide using optical glue that matches the optical properties of the glass. The silicon wafer can then be stripped off, resulting in a gold film displaying the surface roughness of the silicon template, i.e., typically a fraction of a nanometer.

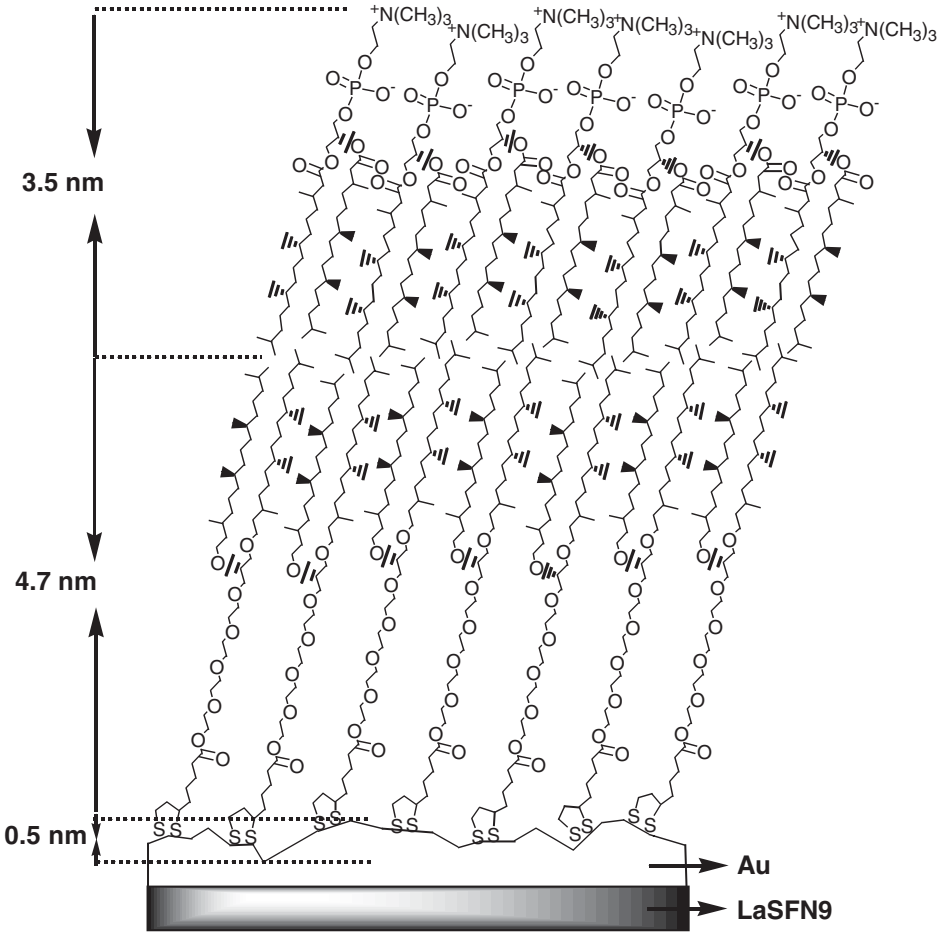

Fig. 3. DPTL-based tBLM on template stripped gold. The dense proximal layer is assembled to an ultrasmooth gold film *via* self-assembly. The distal layer is then deposited by fusion of DPhyPC vesicles. LaSFN9 = high-refractive-index glass. DPTL is now available from DIVERCHIM S.A.

The self-assembled monolayer can then be completed to a full bilayer by fusion of small unilamellar vesicles. The complete architecture is schematically shown in Fig. 3, here, the distal layer is composed of diphytanoylphosphatidylochline (DPhyPC) lipids.

3. STRUCTURAL CHARACTERIZATION

A useful approach for measuring thin film thicknesses at a metal/air or metal/liquid interface is based on the surface plasmon resonance (SPR) technique [19]. At a certain angle of incidence, a laser excites an electromagnetic wave bound to

the interface and which decays exponentially into both media. At this resonance angle, all the energy of the incoming laser beam is coupled into the plasmon wave. This shows up as a narrow drop in the reflected light. The optical parameters (thickness and refractive index) of any adsorbed material at the interface will modify this minimum angle. As an example, Fig. 4 shows the angular shift of the resonance after the formation of a bilayer due to vesicle fusion. Its thickness then can be characterized by knowing the refractive index of the adlayer.

One can also follow the kinetics of such a process when measuring the reflected intensity at a fixed angle of observation. However, it is difficult to discriminate between vesicle fusion and vesicle adsorption, two processes that often interfere with each other and that are yet to be fully understood [20]. The combination of surface plasmon spectroscopy with the quartz crystal microbalance with dissipation (QCM-D) monitoring offers the possibility to address exactly this question. QCM-D works in a way that a quartz crystal is electrically driven at its resonance frequency. If a material adsorbs to the surface, the frequency of this shear mode is shifted. At the same time, one can measure change of the dissipation of the mode, which originates from the viscoelastic properties of the film. In the case of vesicle fusion, the QCM-D signal shows a certain shift in frequency corresponding to the adsorbed mass. If a bilayer membrane (relatively rigid) is formed, there is only little change in the dissipation. However, if whole intact vesicles adsorb to the surface, one also measures a strong increase in mass by a shift in frequency. Moreover, the viscous coupling of the adsorbed vesicles with

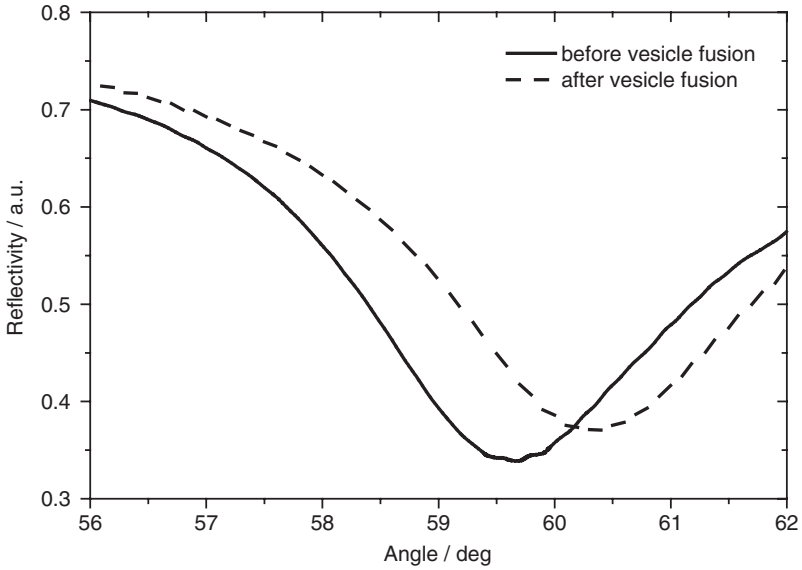

Fig. 4. SPR curves of a DPTL-based tBLM before (solid) and after (dashed) vesicle fusion. The angular shift in the reflectivity minimum corresponds to the addition of the distal layer.

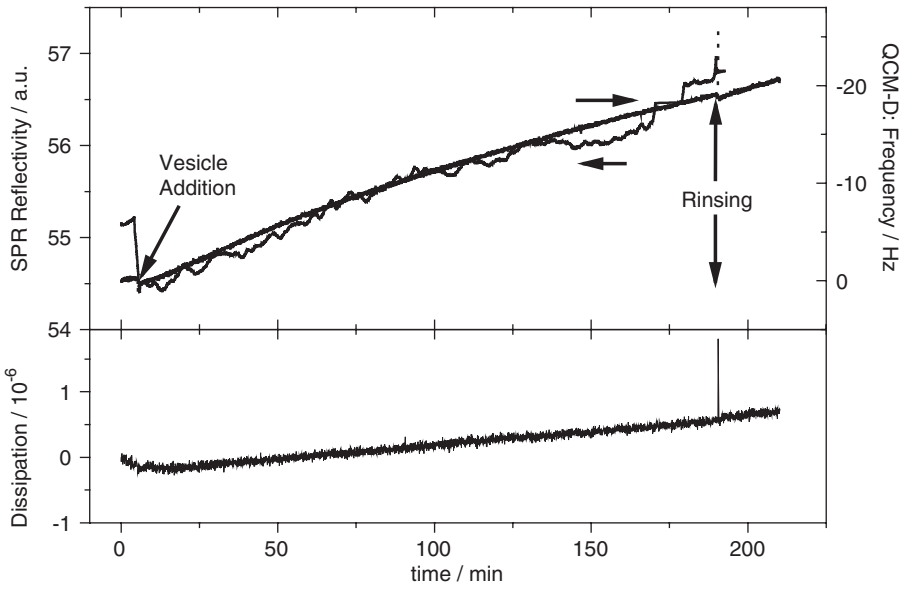

Fig. 5. SPR/QCM-D experiment. The fusion of vesicles can be followed by simultaneous recording (i) by SPR an increase in reflectivity at a fixed angle of observation and (ii) by a shift in frequency in a QCM experiment. The dissipation remains almost constant, signaling the formation of a complete bilayer.

their water load results also in a significant increase of the dissipation. QCM-D measurements are, hence, very well suited to differentiate between mere vesicles adsorption and the formation of a bilayer after vesicle fusion [21].

Contrary to that, SPR is sensitive only to the amount of adsorbed (optical) mass within the evanescent field of the surface plasmon mode, i.e., within about 100–200 nm.

In Fig. 5, a combined SPR/QCM-D experiment is shown. Here, a DPTL monolayer was assembled onto a QCM-D sensor quartz disc which had a sinusoidal surface corrugation that could be used as a grating coupler in SPR. This way, we could follow the increase in thickness by simultaneously recording the SPR signal and the parallel shift in QCM-D frequency. A very similar time-dependence was observed. At the same time, the dissipation remained low indicating the formation of a defined bilayer membrane by vesicle fusion.

4. FUNCTIONAL CHARACTERIZATION

The main criteria for the quality of a model membrane system are the electrical properties, especially if one is interested in studying the functional incorporation of ion transporting peptides and proteins. Electrical impedance measurements

give access to these characteristic parameters. In a typical three-electrode experiment a sinusoidal voltage of small amplitude is applied at various frequencies covering more than eight orders of magnitude and the resulting current is measured. The obtained data is typically displayed in a Bode plot (cf. Fig. 7), where the logarithm of the absolute value of the impedance and the corresponding phase angle shift are plotted as a function of frequency. In such a representation, the phase shift and the slope of the impedance can reveal useful information about the electric properties of the system. In a typical t'BLM system the solution resistance dominates at high frequencies. The mid-frequency region is governed by an increasing impedance with a slope of minus one, thus the capacitance dominates. The drop in phase angle and a plateau in impedance at low frequencies show again an increasing resistive moment. Such plots can be described in good agreement using model circuits that consist of a series of resistor and capacitance elements. One can thus obtain parameters for the bilayer resistance and capacitance which can be compared to values known from experiments with black lipid membranes. With the DPTL system we could measure values up to several $M\Omega\,cm^2$ at less than $1\,\mu F\,cm^{-2}$. Moreover, the system turned out to be extremely robust and it could be prepared very reproducible. These tethered membranes are an ideal platform for the study of ion transport processes mediated by embedded membrane peptides and proteins, e.g., valinomycin [22], gramicidin, mellitin, cytochrome c oxidase [18,22], M2 [23], maxi-K channels [24] or other peptides [25].

From a chemical point of view, the DPTL molecule consists of the three distinct parts as mentioned above: the lipid tails, the spacer unit and the anchor group. In order to modify or improve the system further, one can address each of these parts.

So far, as is the DPTL system, most lipids described in the literature are based on thiol chemistry and gold or noble metal substrates. In contrast, many applications and possible microelectronic readout devices are based on silicon-containing materials.

To meet the corresponding chemical requirements, we could exchange the lipoic acid moiety of the DPTL molecule by different silane groups, especially by monochloro-dimethylsilane (DPTDC) and by trichlorsilane (DPTTC). The chemical formulae are shown in Fig. 6.

The molecules can be self-assembled from a toluene solution. Typically, after 24 h a first hydrophobic layer is formed. However, ellipsometric measurements as

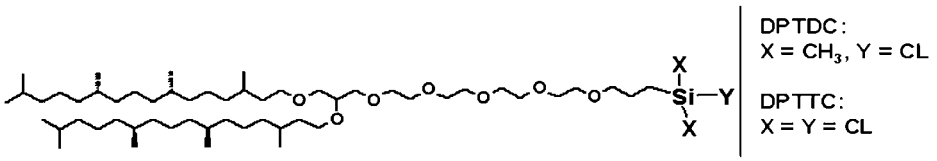

Fig. 6. Chemical structure of the silane-based lipids.

well as the hysteresis in the advancing and receding water contact angles indicate that this proximal layer does not form a dense film, rather is relatively dilute.

Nevertheless electrical characterization is possible. The first layer is assembled on a highly doped silicon wafer with a backside aluminum contact. Figure 7 shows the impedance data of a DPTDC monolayer before and after vesicle fusion. For the monolayer, the capacitance of the thin natural silicon oxide layer at the surface dominates the signal, while the formation of the bilayer leads to a shift of the curve to lower capacitances and a shoulder at low frequencies in the impedance data, the curves can be fitted using an equivalent circuit with an RC (resistor and capacitance in parallel) element describing the SiOx layer in series with a second RC element describing the bilayer properties. Resistances of the bilayer of about 1.5 $M\Omega\,cm^2$ and a capacitance of about 0.9 $\mu F\,cm^2$ could be found [26].

The functionality of these tBLMs could be shown by the incorporation of two different ionophores, i.e., the ion shuttle valinomycin and the pore-forming peptide gramicidin. Valinomycin is a small peptide that transports potassium ions from one side of the bilayer to the other. The functional incorporation of the peptide into the pre-formed bilayer can be seen by a drop in the bilayer resistance. In Fig. 7, this can be seen as a shift of the transition shoulder toward higher frequencies [26].

Valinomycin is highly selective to potassium. The probability for sodium transport is, e.g., reduced by a factor of 10^4. This effect can be used to prove the

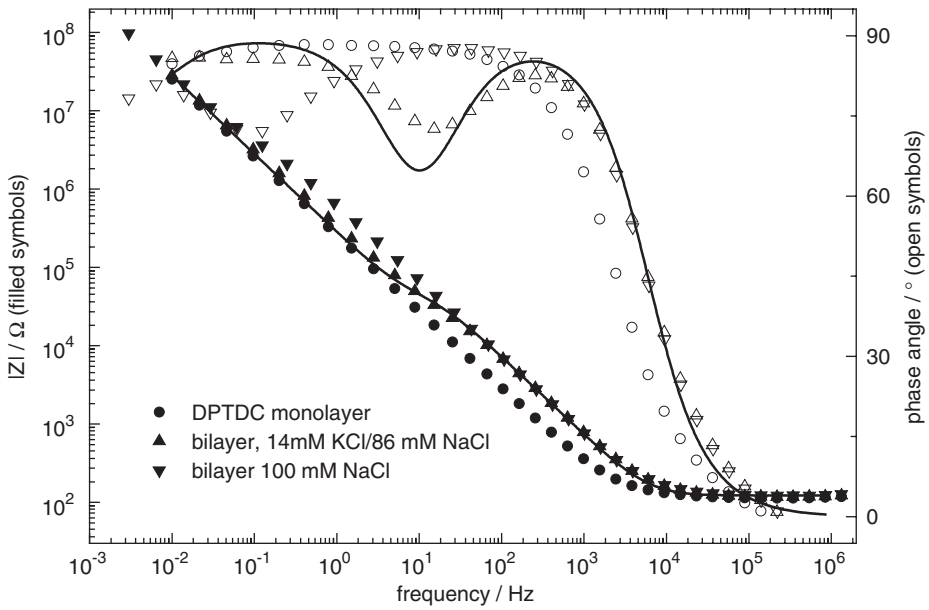

Fig. 7. Bode plot for a DPTDC monolayer, a bilayer after vesicle fusion (in 100 mM NaCl) and after the incorporation of valinomycin (in 14 mM KCl/86 mM NaCl). The curves correspond to a fit using a series of RC elements.

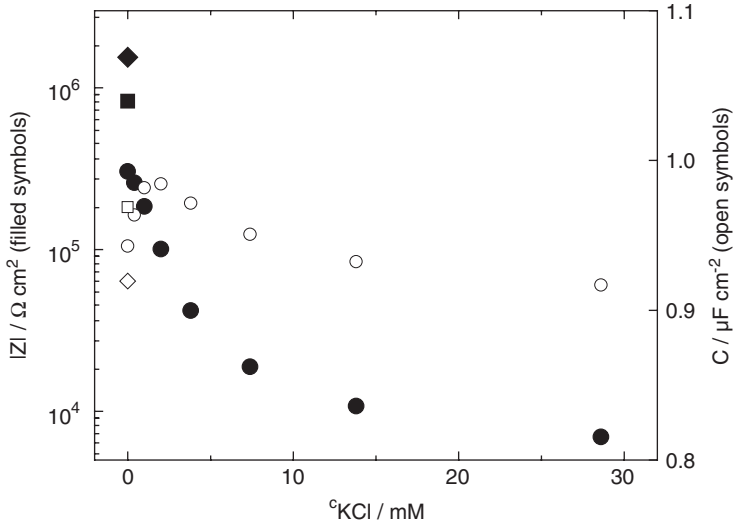

Fig. 8. Impedance and capacitance values of a valinomycin-containing bilayer tethered *via* DPTDC, as a function of the K^+ concentration. ■ Initial value, ◆ after additional rinsing with NaCl at the end of the concentration gradient.

functional incorporation of the peptide. In a potassium-free medium, a bilayer should show a high electrical resistance, which drops after addition of potassium.

Figure 8 shows exactly this behavior for a bilayer on DPTDC containing a small amount of valinomycin. The successive increase of the potassium concentration in a buffer of 100 mM ionic strength results in a decrease of the membrane resistance, which can be obtained by fitting the corresponding impedance data, while the capacitance remains almost constant. The latter confirms the membranes integrity. The square marks the initial value at 100 mM NaCl and the diamond the result obtained at the end of the experiment after having rinsed again with 100 mM NaCl. The difference may be due to initial small traces of potassium in the valinomycin.

5. PROTEIN-TETHERED BILAYER LIPID MEMBRANES

Even though the assembly of the tBLM leads to the structural integrity needed for a bilayer that constitutes a high barrier for the passive permeation of ions, a clear drawback of this architecture is the lack of control during the incorporation of functional units, i.e., peptides, ionophores or proteins: the addition of either solubilized channel proteins or the fusion of proteo-liposomes results in the spontaneous incorporation of proteins into the tethered membrane, but does not allow for the desired control of their density or orientation.

One way to overcome this limitation is to tether the final membrane *via* the incorporated protein. In this approach, the proteins are genetically modified by a

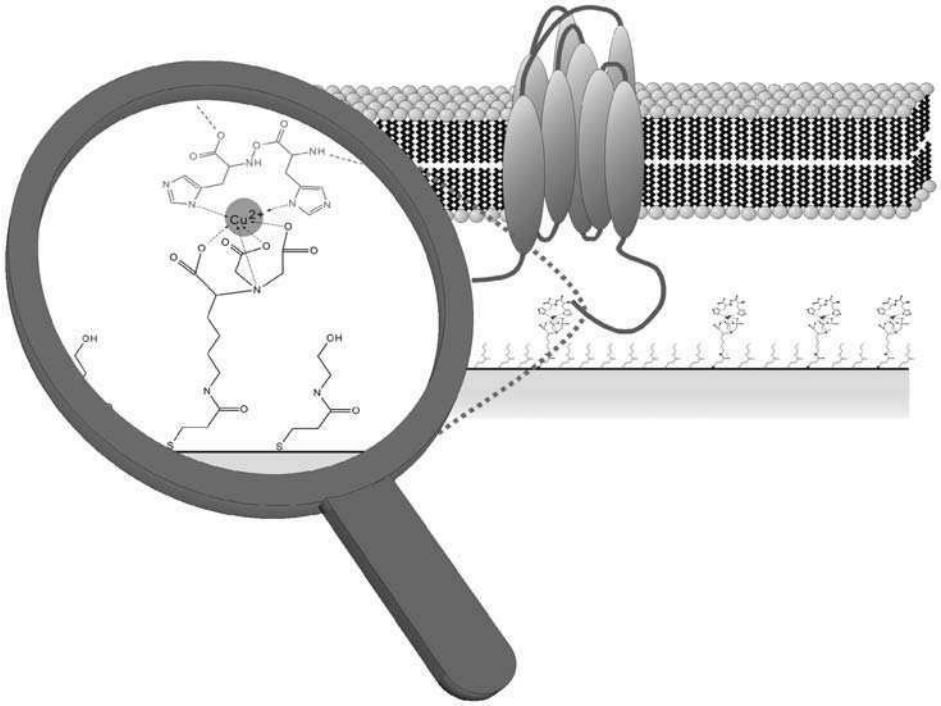

Fig. 9. Schematic tethering of a protein: the protein is bound to a substrate *via* a stretch of histidines. The bilayer is completed by fusion of lipids.

stretch of histidines at either their N- or their C-terminus which allows for their coupling to a NTA/Ni^{2+} modified substrate (sensor) surface. This way, the density of the proteins and, in particular, their orientation can be fully controlled. Fusion of lipid bilayers ''around'' these anchored proteins then completes the desired membrane architecture. This is schematically shown in Fig. 9.

The chemical strategy that we recently introduced is given in Fig. 10. A succinimide derivative is first assembled on an Au substrate (A) followed by the covalent coupling of an amino-terminated NTA derivative (B). After incubation with Cu^{2+} or Ni^{2+} ions the proteins can be assembled *via* their histidine sequence (His-tag). The example shown in Fig. 10(C) corresponds to the redox-active protein Cytochrome c Oxidase, modified at its N-terminus. Thus, the Cytochrome c binding pocket remains exposed to the distal aqueous phase [27–29].

All assembly steps could be followed by surface-enhanced infrared absorption (SEIRA) spectroscopy thus giving full control over the degree of completion of the individual modification steps. For the coupling of the protein this is given in Fig. 11(A) that shows the time-evolution of IR bands in the range of the amide I and amide II vibrations. If plotted as a function of time (Fig. 11(B)) one can see that the process can be stopped at anytime thus determining the degree of

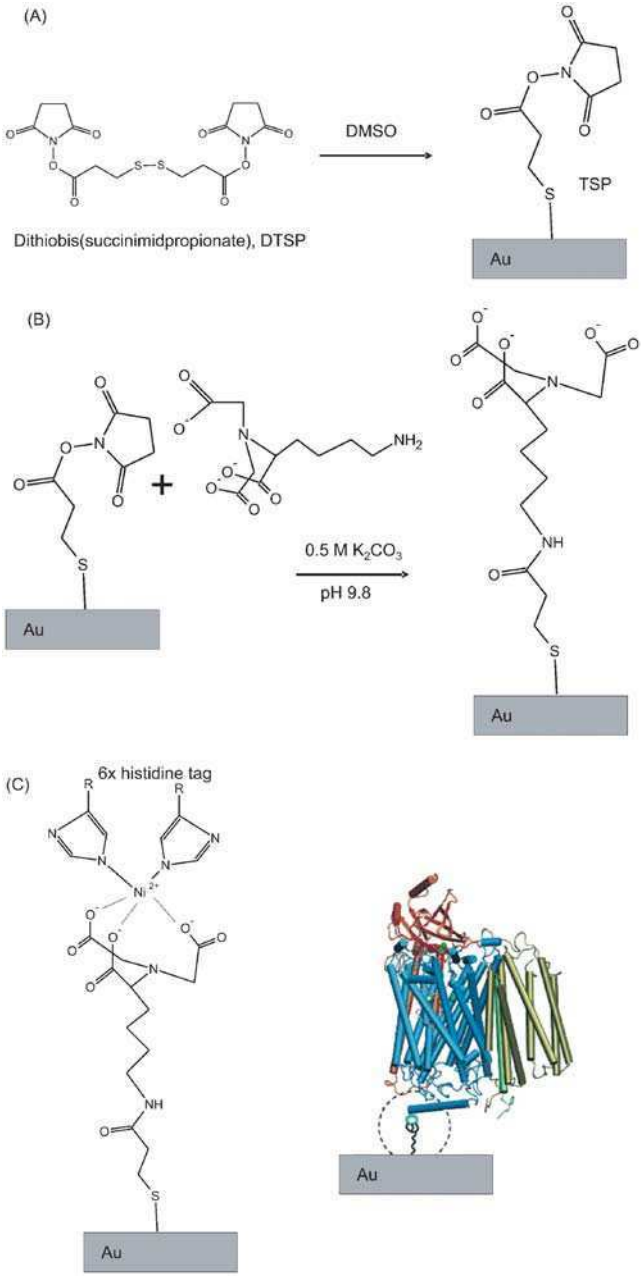

Fig. 10. Chemical strategy how to ''tether'' a protein.

coverage of the surface by protein and, hence, controlling the protein number density of the final tethered membrane.

The critical step is the surface reconstitution, i.e., the assembly of a lipid bilayer architecture ''around'' the tethered proteins. To this end a surface dialysis cell

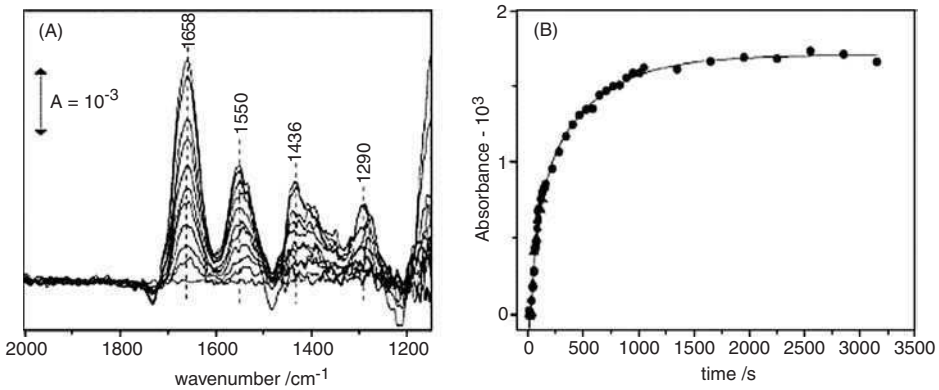

Fig. 11. SEIRA results. (A) Time-evolution of the IR bands. (B) Adsorption kinetics of the binding of the protein. The peak height of the amide II band at 1550 cm^{-1} is plotted against the adsorption time.

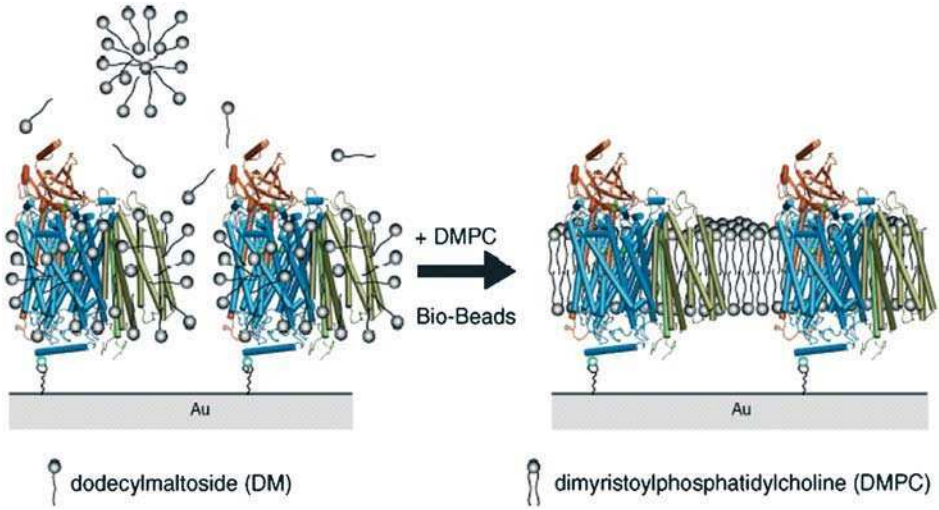

Fig. 12. Surface dialysis: the surface-adsorbed cytochrome c oxidase is exposed to bio-beads and lipid vesicles. The retreat of the detergent leads to a formation of a lipid bilayer around the protein.

was designed that allows for the *in situ* replacement of the solubilizing detergents used to stabilize the protein during the surface-grafting step by the lipids that eventually constitute the final bilayer matrix. This step is schematically depicted in Fig. 12. Again, SPR, QCM and SEIRA spectroscopy could be employed to monitor the successful surface dialysis.

The critical test, however, was again the capacity and resistivity of the obtained membrane. These parameters obtained by EIS are summarized in Table 1. The reconstitutioh step works surprisingly well and results in a membrane that is

Table 1. Resistance and capacitance values from EIS data for the different preparation steps of the cytochrome c oxidase tethered architecture

	Resistance/kΩ cm^2	Capacitance/μF cm^{-2}
DTSP-ANTA-Cu2+-CcO complex	35±10	10±2
Reconstituted	800±300	6±1
After activation	100±20	6±1
After washing	750±300	6±1
After activation in the presence of KCN	750±300	7±1

sufficiently electrically isolating unless the integral proteins, the cytochrome c oxidase, are activated by the addition of cytochrome c. This activation step, however, is fully reversible: rinsing the protein-tethered BLM with cytochrome-c free buffer restores the isolating membrane. (Alternatively, the addition of cyanide ions, well known for their interference with the coupled electron/proton translocation of the cytochrome c oxidase, restores the high resistivity of the membrane in the absence of any other specific ion translocation mechanism.)

6. CONCLUSIONS

After many years of rather moderately successful attempts, the tBLM has finally matured into a novel model membrane platform that deserves to be called a ''membrane'': it fulfills not only the structural requirements of being a bimolecular leaflet that can act as a matrix for the incorporation of peptides, ionophores or proteins as ion-translocating functional units, foremost it constitutes a barrier for the passive translocation of ions. Its structural integrity as well as its local fluidity provide a bilayer with a sufficiently low defect density and, thus, passive leakage currents that match or are even lower than those of our best model membranes so far, the BLMs.

While having focused first on the assembly of tBLMs on Au electrodes that also could be used for the surface-plasmon optical characterization of the individual preparation steps, we also recently introduced silane-based attachment groups thus opening the possibility of building tBLM layers on glass or SiO_2 substrates, hence, spanning the range of experimental formats essentially to any substrate material of interest.

The versatility of the tBLM platform has further been confirmed by the incorporation and functional characterization of a wide variety of ionophores and channel proteins: valinomycin, gramicidin, mellitin, M2, H^+ATPase, cytochrome c oxidase, nAChR, Maxi-K channels and others have been shown to ''work'' in tBLMs.

A particularly promising but also challenging extension of these studies with many functional units embedded into the tBLMs are efforts to incorporate only

individual single channels and monitor the stochastic current through the membrane reflecting the switching between an isolating off-state and a conducting on-state of the pore. The high resistivity of the bare lipid bilayer matrix with the corresponding low current levels in the sub-pA-range are a prerequisite for the successful recording of single channel conductance increments which typically amount to some 10–100 pS thus generating current fluctuations in steps of 1–10 pA. By using a patch-clamp amplifier we recently could demonstrate for the first time channel fluctuations of the M2 peptide incorporated into a tBLM assembled from DPTL [23]. We consider this result to be the final element in a breakthrough for the tethered bilayers that paves their way as a new model membrane platform.

ACKNOWLEDGMENTS

We thank all the colleagues that contributed to the development of tBLMs, in particular, V. Atanasov, P. Atanasova, P. Anderson, C. Breffa, R. Duran, M. Friedrich, E. Gardel, N. Knorr, J. Long, J. Robertson, E.-K. Sinner, I. Vockenroth and D. Walz.

Partial financial support came from the Defense Advanced Research Projects Agency (DARPA) through the MOLDICE program. I.K. acknowledges support from the Laboratoire Européen Associé (LEA) on ''Polymers in Confined Geometries''.

REFERENCES

[1] A. Ottova, V. Tvarozek, J. Racek, J. Sabo, W. Ziegler, T. Hianik, H. Tien, Self-assembled BLMs: biomembrane models and biosensor applications, Supramol. Sci. 4 (1997) 101–112.
[2] E. Sackmann, Supported membranes: scientific and practical applications, Science 271 (1996) 43–48.
[3] W. Knoll, C.W. Frank, C. Heibel, R. Naumann, A. Offenhäusser, J. Rühe, E.K. Schmidt, W.W. Shen, A. Sinner, Functional tethered lipid bilayers, Rev. Mol. Biotechnol. 74 (2000) 137–158.
[4] M. Winterhalter, Black lipid membranes, Curr. Opin. Coll. Interf. Sci. 5 (2000) 250–255.
[5] B. Schuster, D. Pum, O. Braha, H. Bayley, U.B. Sleytr, Self-assembled a-hemolysin pores in an S-layer-supported lipid bilayer, Biochim. Biophys. Acta 1370 (1998) 208–288.
[6] M. Stelzle, G. Weissmüller, E. Sackmann, On the application of supported bilayers as receptive layers for biosensors with electrical detection, J. Phys. Chem. 97 (1993) 2974–2981.
[7] M.A. Deverall, E. Gindl, E.-K. Sinner, H. Besir, J. Rühe, M.J. Saxton, C.A. Naumann, Membrane lateral mobility obstructed by polymer-tethered lipis studied at the single molecule level, Biophys. J. 88 (2005) 1875–1886.
[8] B.A. Cornell, V.L.B. Braach-Maksvytis, L.G. King, P.D.J. Osman, B. Raguse, L. Wieczorek, R.J. Pace, A biosensor that uses ion-channel switches, Nature 387 (1997) 580–583.

[9] B. Raguse, V. Braach-Maksvytis, B.A. Cornell, L.G. King, P.D.J. Osman, R.J. Pace, L. Wieczorek, Tethered lipid bilayer membranes: formation and ionic reservoir characterization, Langmuir 14 (1998) 648–659.
[10] G. Krishna, J. Schulte, B.A. Cornell, R.J. Pace, P.D. Osman, Tethered bilayer membranes containing ionic reservoirs: selectivity and conductance, Langmuir 19 (2003) 2294–2305.
[11] S. Terrettaz, W.-P. Ulrich, R. Guerrini, A. Verdini, H. Vogel, Immunosensing by a synthetic ligand-gated ion channel, Angew. Chem. Int. Ed. 40 (9) (2001) 1740–1743.
[12] S. Terrettaz, M. Mayer, H. Vogel, Highly electrically insulating tethered lipid bilayers for probing the function of ion channel proteins, Langmuir 19 (2003) 5567–5569.
[13] S. Terretaz, H. Vogel, Investigating the function of ion channels in tethered lipid membranes by impedance spectroscopy, MRS Bull. 30 (2005) 207–210.
[14] S.M. Schiller, R. Naumann, K. Lovejoy, H. Kunz, W. Knoll, Archaea analogue thiolipids for tethered bilayer lipid membranes on ultrasmooth gold surfaces, Angew. Chem. 42 (2) (2003) 208–211.
[15] V. Braach-Maksvytis, B. Raguse, Highly impermeable ''soft'' self-assembled monolayers, J. Am. Chem. Soc. 122 (2000) 9544–9545.
[16] B. Raguse, P.N. Culshaw, J.K. Prashar, K. Raval, The synthesis of archaebacterial lipid analogues, Tetrahedron Lett. 41 (2000) 2971–2974.
[17] C.R. Woese, G.E. Fox, Phylogenetic structure of the prokaryotic domain: The primary kingdoms, Proc. Nat. Acad. Sci. 74 (11) (1977) 5088–5090.
[18] R. Naumann, S.M. Schiller, F. Giess, B. Grohe, K.B. Hartman, I. Kärcher, I. Köper, J. Lübben, K. Vasilev, W. Knoll, Tethered lipid bilayers on ultraflat gold surfaces, Langmuir 19 (2003) 5435–5443.
[19] W. Knoll, H. Park, E.-K. Sinner, D. Yao, F. Yu, Supramolecular interfacial architectures for optical biosensing with surface plasmons, Surf. Sci. 570 (2004) 30–42.
[20] B. Kasemo, Biological surface science, Surf. Sci. 500 (2002) 656–677.
[21] J. Ekeroth, P. Konradsson, F. Höök, Bivalent-ion-meditated vesicle adsorption and controlled supported phospholipid bilayer formation on molecular phosphate and sulfate layers on gold, Langmuir 18 (2002) 7923–7929.
[22] R. Naumann, D. Walz, S.M. Schiller, W. Knoll, Kinetics of valinomycin-mediated K+ ion transport through tethered bilayer lipid membranes, J. Electroanal. Chem. 550–551 (2003) 241–252.
[23] H.M. Keizer, B.R. Dorvel, D. Fine, J. Long, A. Dodobalapur, I. Köper, W. Knoll, R.S. Duran, In preparation, 2005.
[24] J. Li, R.S. Duran, I. Köper, W. Knoll, P.A. Anderson, In preparation, 2005.
[25] P. Vitovic, S. Kresak, R. Naumann, S.M. Schiller, R.N.A.H. Lewis, R.N. McElhaney, T. Hianik, The study of the interaction of a model alpha-helical peptide with lipid bilayers and monolayers, Bioelectrochemistry 63 (2004) 169–176.
[26] V. Atanasov, N. Knorr, R.S. Duran, S. Ingebrandt, A. Offenhäuser, W. Knoll, I. Köper, Membrane on a chip. A functional tethered lipid bilayer membrane on silicon oxide surfaces, Biophys. J. 89 (2005) 1780–1788.
[27] K. Ataka, F. Giess, W. Knoll, R. Naumann, S. Haber-Pohlmeier, B. Richter, J. Heberle, Oriented attachment and membrane reconstitution of His-tagged cytochrome c oxidase to a gold electrode: *in situ* monitoring by surface enhanced infrared adsorption spectroscopy, J. Am. Chem. Soc. 126 (2004) 16199–16206.
[28] M.G. Friedrich, F. Giess, R. Naumann, W. Knoll, K. Ataka, J. Heberle, J. Hrabakova, D.H. Murgida, P. Hildebrandt, Active site structure and redox processes of cytochrome c oxidase immobilised in a novel biomimetic lipid membrane on an electrode, Chem. Commun. (2004) 2376–2377.
[29] F. Giess, M.G. Friedrich, J. Heberle, R. Naumann, W. Knoll, The protein-tethered lipid bilayer a novel mimic of the biological membrane, Biophys. J. 87 (2004) 3213–3220.

This page intentionally left blank

CHAPTER 3

Birefringence Studies on Effects of Additives on Bilayer Lipid Membranes

Kiyoshi Mishima*,[1]

Department of Physics, College of Art & Science, Showa University 4562 Kamiyoshida, Fujiyoshida-shi, Yamanashi 4030005, Japan

Contents

Abstract

A new, optical technique to determine molecular order of lipid bilayers is described. This technique is based on birefringence (double refraction) of lipid bilayers and applicable without any kind of labeling. The order including the lipid molecular orientation order and the acyl chain order is determined from the interference light by vesicles due to the birefringence. Because of high sensitivity of the birefringence to the molecular order, it is possible to detect a slight change in the order. Effects of hydrophilic, hydrophobic and amphiphilic additives on bilayer lipid membranes measured by this technique are also described. The experiments show that the birefringence technique is powerful to investigate molecular order of lipid membranes with additives.

*Corresponding author. Tel./Fax: +81-043-271-2642; E-mail: mishima@yellow.plala.or.jp
[1] Yorozu Kohboh, Dome, 2-2804-1 Makuhari Hanamigawa-ku, Chiba-shi, Chiba 262-0032, Japan.

ADVANCES IN PLANAR LIPID BILAYERS AND LIPOSOMES, VOLUME 3
ISSN 1554-4516 DOI: 10.1016/S1554-4516(05)03003-6

1. INTRODUCTION

Much of the knowledge about structural and dynamic properties of bilayer phospholipids was gained by many techniques as X-ray diffraction, DSC, NMR, electron microscopy and so on [1]. Recently, interaction between biological molecules and lipids has been widely noticed because the interaction is a fundamental process in living biological membranes [2,3], and so the interaction has been studied employing a variety of additives. These additives are hydrophilic ones which predominantly affect the headgroup region; hydrophobic ones, which interact with the acyl chains; and amphiphilic ones which affect the entire lipid. Also, a variety of techniques have been newly developed to investigate the structure and dynamics of lipid-additive systems. In this review, a new, optical technique to determine molecular order of lipid bilayers is described. This technique is based on birefringence (double refraction) of lipid bilayers. The order including the lipid molecular orientation order and the acyl chain order is obtained from the interference light by vesicles due to the birefringence [4,5]. Because of the high sensitivity of the birefringence to the molecular order, it is possible to detect a slight change in the order. In this chapter, I will first describe this birefringence method and secondly our recent experiments with various a dditives using this technique. The additives employed in these experiments are as follows:

(a) Hydrophilic: polysaccharide, polysaccharide/cholesterol conjugate and polyethylene glycol (PEG)
(b) Hydrophobic: cholesterol and organohalogen compounds
(c) Amphiphilic: lysolipids, peptide and a local anesthetic.

2. BIREFRINGENCE TECHNIQUE FOR STUDYING MOLECULAR ORDER OF LIPID BILAYERS

Phospholipid bilayers show optical birefringence (double refraction) owing to the liquid-crystal structure of lipid bilayers. Birefringence phenomena of lipid assemblies were observed from long ago [6,7]. However, until recently, the birefringence has been underutilized for studying bilayer structure. The birefringence of pure lipids was measured using lipid lamellar textures [8] and vesicles [9]. The birefringence depends on the order of molecular orientation as well as the acyl chain order of lipids. In particular, in the case of multilamellar bilayers, the birefringence strongly depends on the order of the longitudinal orientation of lipids in the multilamellae.

Interference light due to the birefringence can be easily observed by a polarization microscopy with crossed polarizers. Figure 1 shows micrographs of lipid vesicles observed with parallel polarization and crossed polarization. When a

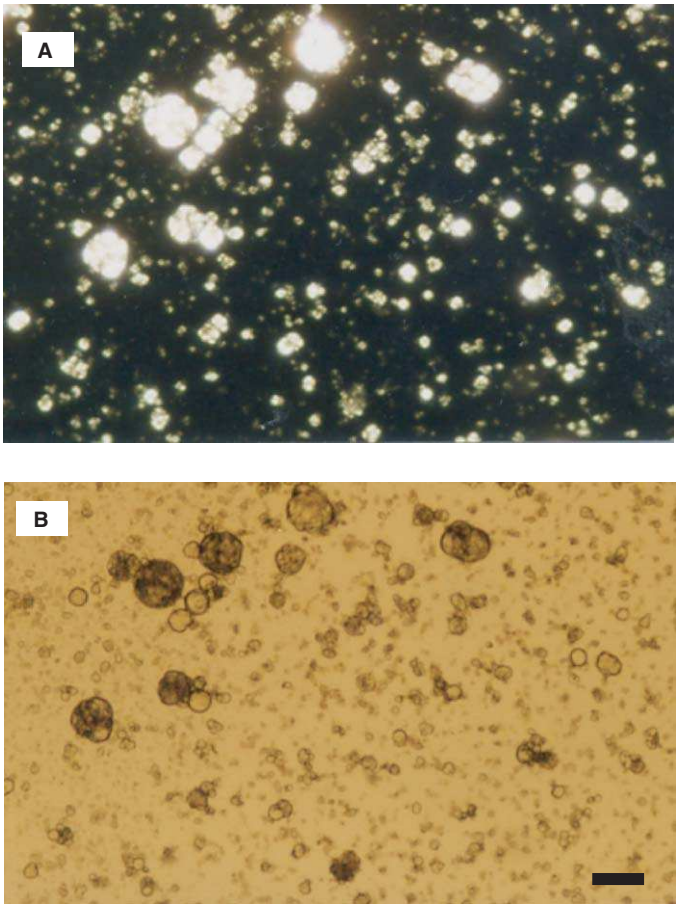

Fig. 1. Optical micrographs of (A) interference light by phosphatidylcholine vesicles observed with crossed polarization and (B) the same place observed with parallel polarization. Bar represents 100 μm.

vesicle is illuminated through a polarizer, the incoming polarized light separates into two beams with different directions of the electric vibration, and the beams emerge from the vesicle with a different phase. As a result of the phase difference, interference occurs between the two beams after passing through another polarizer. The interference light intensity relates both to the birefringence and the vesicle size. We recently proposed a new technique that utilized the birefringence. In this technique, the interference light intensity is determined from the polarized light transmitted through the vesicle suspension, and the molecular order of lipids is obtained from the interference light intensity. This birefringence technique is simple to measure and is applicable to lipid membranes without any kinds of labeling.

2.1. Theory

2.1.1. Interference light by a hollow sphere

I will describe the theory of the birefringence method as presented in Refs. [4,5]. A crystal plane plate placed between a polarizer and an analyzer is firstly considered. Intensity of interference light by the plate is given as [10]

$$i = a\{\cos^2\chi - \sin 2\phi \, \sin 2(\phi - \chi)\sin^2(\delta/2)\} \tag{1}$$

where a is the intensity of the incident light on the plate per unit area, χ the angle between the directions of electric vibrations passed by the polarizer and the analyzer, ϕ the angle between the direction of electric vibration passed by the polarizer and one of the two mutually orthogonal directions of vibrations in the crystal and δ the phase difference between the two emerging beams with different vibration directions, the so-called ordinary and extraordinary beams. In the case that polarizer and analyzer are perpendicular (crossed polarization), the interference light intensity is written as

$$i = a \sin^2 2\phi \, \sin^2(\delta/2) \tag{2}$$

The phase difference is related with the light path and the refractive indices for the two emerging beams. When the refractive, n' and n'' approximate each other, the phase difference is given as

$$\delta = (2\pi/\lambda)(n'' - n')\rho \tag{3}$$

where λ is the wavelength of the incident light and ρ the mean geometrical path of two emerging beams. Difference in the refractive indices is written by the birefringence of the uniaxial crystal Δn as

$$n'' - n' = \Delta n \sin^2\theta \tag{4}$$

with

$$\Delta n = n_\mathrm{e} - n_\mathrm{o} \tag{5}$$

where n_o and n_e are the ordinary and extraordinary refractive indices, respectively, and θ is the angle between the optical axis of the crystal plate and the mean path of the two beams.

Next, a hollow sphere is considered as a model of lipid vesicles. The hollow sphere is composed of an uniaxial crystal with the birefringence of Δn, and the optical axis of the crystal is radially oriented in the shell. It is assumed that the birefringence is far small compared with the refractive indices of the crystal n_o and n_e ($\Delta n \ll n_\mathrm{o}, \ n_\mathrm{e}$), and so $n' \fallingdotseq n''$. The direction of beams propagated in the shell changes with varying the direction of the optical axes. However this change is negligible, if $n' \fallingdotseq n''$ is hold. On the assumption, the mean geometrical path of two beams with different electric vibration is easily written as

$$\rho = 2R_\mathrm{o} \cos\beta \tag{6}$$

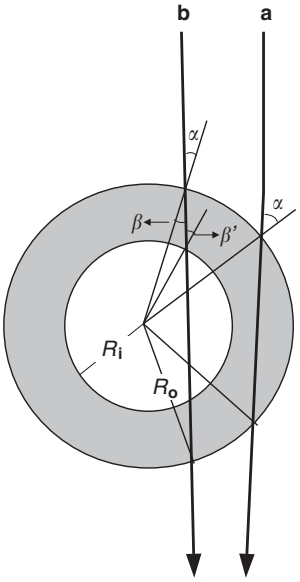

Fig. 2. Geometrical paths of light propagated through the shell (a) and the shell and the inside medium. (b) Each path contains both ordinary and extraordinary beams. From Mishima *et al.* [9].

in the case of the beams propagated through only the shell (a in Fig. 2), and

$$\rho = 2(R_o \cos\beta - R_i \cos\beta') \tag{7}$$

in the case of the beams propagated from the shell to the inside medium (b in Fig. 2), where R_o and R_i are the outer and the inner radii of the shell, respectively, and β the refractive angle between the optical axis and the light path. β' is the incident angle at the interface for the case of the propagation (b). In the limiting case of $\beta' = \pi/2$, equation (7) reduces to equation (6).

On averaging over the light path for the factor $\sin^2\theta$ in equation (4), the difference in the refractive indices $n''-n'$ for the case of (b) is given as

$$\begin{aligned} n'' - n' &= \Delta n < \sin^2\theta >_{AV} \\ &= \frac{\Delta n}{2}\left(1 - \frac{\sin 2\beta - \sin 2\beta'}{2(\beta - \beta')}\right) \end{aligned} \tag{8}$$

The difference $n'' - n'$ for the case of (a) is obtained by replacing β' with $\pi/2$ in equation (8). It is noted that the birefringence Δn is approximately equivalent to that of a plate composed of same uniaxial crystal, when the shell has a large curvature. If the optical axis of the crystal is not radially oriented, it is not easy to express the difference $n'' - n'$. However, when the direction of the optical axis is radial on average, equation (8) is valid. In this case, Δn is the mean birefringence.

Then the phase difference δ for the hollow sphere is given as

$$\delta = \frac{2\pi}{\lambda}\Delta n\left(R_{\mathrm{o}}\cos\beta - R_{\mathrm{i}}\cos\beta'\right)\left(1 - \frac{\sin 2\beta - \sin 2\beta'}{2\left(\beta - \beta'\right)}\right) \tag{9}$$

where in the case of propagation (a), $\beta' = \pi/2$.

Intensity of the interference light by the sphere is given by integration with the incoming angle α over the illuminated area of the sphere. In the case of crossed polarizers, the interference light intensity is expressed:

$$i = \int a \sin^2 2\phi \sin^2(\delta/2)\, \mathrm{d}S \tag{10}$$

where $a\,\mathrm{d}S$ is the intensity of the incident light flux with the cross-sectional area of $\mathrm{d}S$. When the incident light flux illuminates an area of the shell surface $\mathrm{d}S'$ with the incoming angle α, the area $\mathrm{d}S$ is written as

$$\mathrm{d}S = \mathrm{d}S'\cos\alpha = R_{\mathrm{o}}^2\,\mathrm{d}\phi\,\sin(2\alpha)\,\mathrm{d}\alpha/2 \tag{11}$$

Thus, the interference light intensity is

$$i = \int_0^{2\pi}(a/2)R_{\mathrm{o}}^2\sin 2\phi\,\mathrm{d}\phi\int_0^{\pi/2}\sin^2(\delta/2)\sin 2\alpha\,\mathrm{d}\alpha \tag{12}$$

Since the total intensity of the illuminated light i_{o} is $i_{\mathrm{o}} = \pi a R_{\mathrm{o}}^2$, the first integral is equal to $i_{\mathrm{o}}/2$. The second integral is divided into two terms for the cases of propagations (a) and (b) of Fig. 2. Therefore, the interference light intensity per unit incident light with crossed polarization is expressed as

$$A = \frac{i}{i_{\mathrm{o}}} = \frac{1}{2}\left(\int_0^{\alpha_{\mathrm{o}}}\sin^2\left(\frac{\delta}{2}\right)\sin 2\alpha\,\mathrm{d}\alpha + \int_{\alpha_{\mathrm{o}}}^{\pi/2}\sin^2\left(\frac{\delta}{2}\right)\sin 2\alpha\,\mathrm{d}\alpha\right) \tag{13}$$

where α_{o} is the incoming angle of the beam propagated on the interface between the shell and the inside medium of the hollow sphere. The angle is represented by $\alpha_{\mathrm{o}} = \arcsin(mR_{\mathrm{i}}/R_{\mathrm{o}})$ in which m is the relative refractive index of the shell to the medium. In the second term of equation (13), the phase difference is taken as equation (9) with $\beta' = \pi/2$. The interference light intensity A was numerically calculated by the Simpson method. Also, the interference intensity by a single vesicle was experimentally measured using a polarized microscopy with crossed polarizers with varying the wave length of the incident light. Comparing these intensities, the birefringence was estimated to be 0.020 for the gel phase and 0.028 for the ripple phase of dipalmitoylphosphatidylcholine (DPPC) bilayers [9]. These values are in good agreement with the results obtained by the use of lipid lamellar textures [8].

2.1.2. Polarized light transmitted through lipid dispersion

Let us consider lipid dispersion containing various vesicles in size. The total intensity of interference light is a sum of the individual interference light by the vesicles. Since the interference light depends on both inner and outer radii, the mean intensity of the interference light $<A>$ is written as

$$\langle A\rangle = \sum_j \sum_k A(R_{oj}, R_{ik}) f(R_{oj}, R_{ik}) \tag{14}$$

where $A(R_{oj},R_{ik})$ is the interference light by a vesicle with an inner radius of R_{ik} and an outer radius of R_{oj}, and $f(R_{oj},R_{ik})$ the number fraction of the vesicle. The total interference light per unit area is given by $<A>N\ell$ for the dispersion with the number density of N and the light path length of ℓ. Also, the total scattered light is $<S>N\ell$, where $<S>$ is the mean intensity of scattered light as defined by a similar way as equation (14).

We consider the polarized light transmitted through the dispersion with a small path length of d ℓ. Deviation of the light intensity with crossed polarization I_1 to the polarized incoming light is written as

$$\frac{dI_1}{d\ell} = <A>NI_2 - <A>NI_1 - <S>NI_1 \tag{15}$$

where I_2 is the light intensity with parallel polarization. The first term is an increase in the interference light crossly polarized to the incoming light, the second term is a reduction by the interference light polarized in parallel, and the last term is a reduction by scattering light. Since the light intensity of parallel polarization is far larger than that of crossed polarization, i.e., $I_2 \gg I_1$, the second term is neglected in comparison with the first term:

$$\frac{dI_1}{d\ell} = <A>NI_2 - <S>NI_1 \tag{16}$$

Deviation of the light intensity with parallel polarization is similarly written as equation (15), but the effect of the scattered light is dominant rather than that of the interference light. So, the deviation is written as

$$\frac{dI_2}{d\ell} = -<S>NI_2 \tag{17}$$

The light intensity transmitted through the light path of l is given by

$$I_2 = I_o \exp(-\tau l) \tag{18}$$

where I_o is the incident light intensity and $\tau = <S>N$ is the turbidity.

The transmitted-light intensity with crossed polarization is obtained by combining equations (16) and (18) as

$$I_1 = I_o(\phi + <A>Nl)\exp(-\tau l) \tag{19}$$

where ϕ is a ratio I_1/I_o in the absence of vesicles, namely, a background of the optical system. Ratio of the transmitted light intensities I_1/I_2 is related only to the

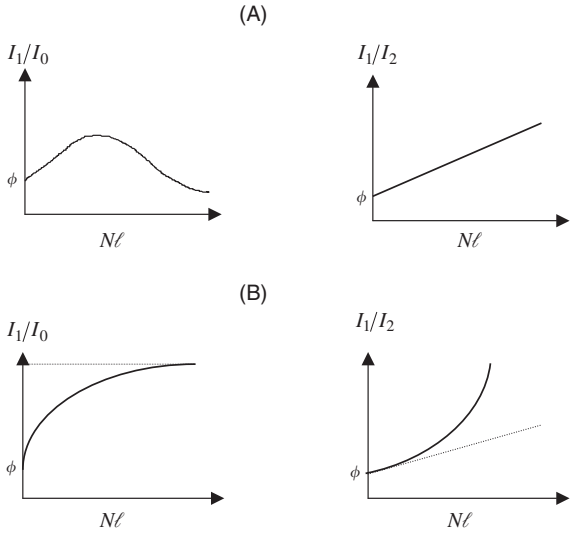

Fig. 3. Schematic representation of transmitted-light intensity with crossed polarization I_1 (left) and ratio of the light intensities with crossed polarization I_1 and with parallel polarization I_2 (right) as a function of number density of vesicles N and light path length ℓ. (A) intensity of the interference light is comparable with that of the scattered light and (B) interference light intensity is far larger than the scattered light intensity. ϕ is a background of the optical system and I_o is the incident light intensity.

interference light as

$$\frac{I_1}{I_2} = \phi + <A> NI \tag{20}$$

The transmitted-light intensity with crossed polarization and the intensity ratio are schematically represented in Fig. 3(A). The mean interference light intensity $<A>$ can be determined from the slope of a linear dependence on the number density of vesicles and the light path length.

However, when the interference light intensity is far larger than the scattered light intensity, i.e. $<A>I_2 \gg <S>I_1$, the intensity ratio becomes a nonlinear dependence. In this case, equation (16) is reduced to

$$\frac{dI_1}{d\ell} = <A> NI_2 \tag{21}$$

Combining equations (18) and (21), the transmitted-light intensity with crossed polarization is given by

$$I_1 = I_o\left(\phi + \frac{<A>}{<S>}(1 - \exp(-\tau\ell))\right) \tag{22}$$

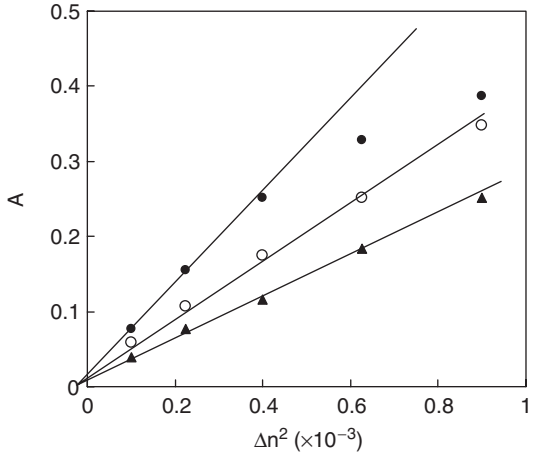

Fig. 4. Relation between the interference light intensity by single vesicle A and the square of the birefringence Δn with different wave length λ of 400 (●), 500 (○) and 600 nm (▲). The intensity values were calculated according to equation (13) for $R_o = 5\,\mu m$, $R_i = 2\,\mu m$ and the relative refractive index of the vesicle to the medium, $m = 1.4$. A linear dependence obtains for the large wavelength, but the intensity for the small wavelength deviates from the straight line at large birefringence.

Ratio of the transmitted-light intensities I_1/I_2 is

$$\frac{I_1}{I_2} = \left(\phi + \frac{<A>}{<S>}\right)\exp(-\tau\ell) - \frac{<A>}{<S>} \tag{23}$$

The intensity ratio deviates positively from a linear dependence, as shown in Fig. 3(B).

Experimentally, it is easy to determine the interference light intensity from the ratio of transmitted-light intensities with a linear dependence. To obtain a linear dependence of the intensity ratio I_1/I_2 on $N\ell$, vesicles with appropriate size and incident light with a larger wave length should be employed. It is necessary to test whether the linear relation holds or not. In addition, use of incident light with a larger wavelength is helpful to analyze data of the interference light. As seen in equation (9), the phase difference δ is in proportion with the birefringence Δn, and becomes small with increasing the wavelength. For the small phase difference, the interference light intensity is approximately proportional to the square of δ (equation (13)). This leads to a linear dependence between the interference light intensity and the square of the birefringence Δn. In fact, this square relation is obtained for the small birefringence at a range of large wavelength, as shown in Fig. 4.

2.1.3. Molecular orientation order in lipid bilayers

As mentioned above, the birefringence of lipid bilayers does not relate to only the acyl chain order but also the molecular orientation order in the bilayers. Let us

consider the relation between the birefringence and the molecular order. According to the theory of an uniaxial liquid crystal, the ordinary and extraordinary refractive indices, n_o and n_e are related with the principal polarizabilities α_o and α_e as [11]

$$\frac{n_e^2 - 1}{n_e^2 + 2} = \frac{4\pi}{3} \frac{N\alpha_e}{1 + A_1\alpha_e} \tag{24}$$

$$\frac{n_o^2 - 1}{n_o^2 + 2} = \frac{4\pi}{3} \frac{N\alpha_o}{1 + A_2\alpha_o} \tag{25}$$

where N is the number density of molecules, and A_1 and A_2 are constants by which the Clausius–Mosotti relation is adapted to the uniaxial crystal. Since the birefringence of lipid bilayers is small, i.e., $n_e \approx n_o$, these adapted factors can be neglected and $(n_e + 1)/(n_e^2 + 2) \approx (n_o + 1)/(n_o^2 + 2)$. Thus, the birefringence, Δn is obtained from the following equation:

$$\Delta n = \left(\tilde{n} - 1 - \frac{\Delta n}{3}\right)\left(\frac{\alpha_e - \alpha_o}{\alpha_o}\right) \tag{26}$$

with the mean refractive index, $\tilde{n}$

$$\tilde{n} = \frac{n_e + 2n_o}{3} \tag{27}$$

Using equation (26), the birefringence was calculated to be 0.079 on the assumption that lipid molecules with fully extended chains are uniformly arrayed [9]. In this assumption, the polarizabilities of the bilayer, α_e and α_o are equal to polarizabilities of the lipid molecule, $\alpha_\parallel$ and $\alpha_\perp$, i.e., $\alpha_e = \alpha_\parallel$ and $\alpha_o = \alpha_\perp$, where the indices $\parallel$ and $\perp$ denote the principal direction of the molecule and a direction perpendicular to it, respectively. The calculated value is far larger than both values measured for the gel phase (0.02) and for the ripple phase (0.028) of DPPC multilamellar bilayers [9]. These smaller values arise from disorders of chains and molecular orientation in the bilayer. In particular, the birefringence of the multilamellar bilayers is strongly affected by a disorder in the longitudinal orientation. The degree of order of the uniaxial liquid crystal is defined by the ratio of the polarizabilities of the crystal to the molecular polarizabilities as [11]

$$S = \frac{\alpha_e - \alpha_o}{\alpha_\parallel - \alpha_\perp} \tag{28}$$

In the case of lipid bilayers, the term $\Delta n/3$ in equation (26) is approximately neglected in comparison with $\tilde{n} - 1$ since the $\Delta n/3$ value is about 2.5% of the $\tilde{n} - 1$ value. In this case, the degree of order S is written as

$$S = \left(\frac{\Delta n}{\tilde{n} - 1}\right)\left(\frac{\alpha_\perp}{\alpha_\parallel - \alpha_\perp}\right) \tag{29}$$

where it is assumed that $\alpha_o \approx \alpha_\perp$. This equation indicates that the order S is in proportion with the birefringence. Considering the square relation of the

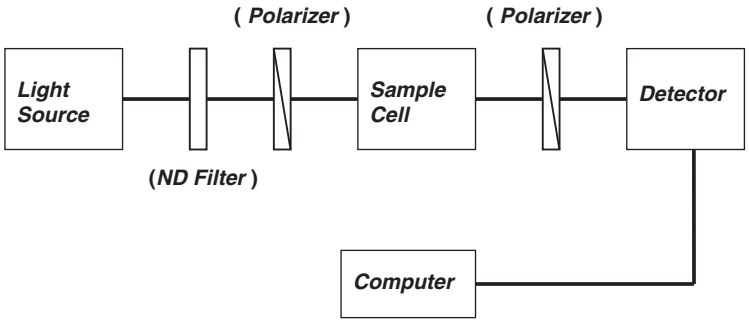

Fig. 5. Experimental arrangement for polarized transmitted-light measurements. ND filter is used to reduce the transmitted-light intensity with parallel polarization.

birefringence Δn with the interference light intensity ($A \propto \Delta n_2$), the order S is proportional to the square root of the interference light intensity, i.e., $S \propto \sqrt{A}$.

2.2. Experimental

Intensity of interference light is obtained from measurements of transmitted-light intensities with parallel and crossed polarization. The measurements were performed using a spectrophotometer (Japan Spectroscopic Co., CT10) or a Laser-diode optical system equipped with two polarizers. The arrangement of measurements is shown in Fig. 5. The polarizers used were Glan–Thompson prisms with extinction ratio of 5×10^{-5} or polarization filters with the ratio of 10^{-4}. The light source was a halogen lamp of 150 W or He–Ne Laser with 632.8 nm. In the case of the halogen lamp, the wavelength was selected to be 500 nm. When the transmitted light with parallel polarization was measured, the incident light was reduced by the use of an *ND* filter placed in the path of the incident beam. The sample cell made of quartz was used in order to reduce the effect on the optical background at the crossed polarization measurement.

There are two ways of measurements of the transmitted light with crossed, I_1 and parallel polarization, I_2, since the ratio I_1/I_2 depends on $N\ell$. One is to measure with varying the light-path length, ℓ using a sample cell of a syringe type. The other is to measure with varying the number density of vesicles, N by diluting the lipid dispersion using a square cell. It is convenient to express the number density N in terms of more directly measurable parameter. Using the lipid concentration c, the number density is given by $N = c/M$, where M is the mean anhydrous mass of a single vesicle. The mean anhydrous mass is a constant value when no vesicle disruption occurs at the dilution. Figure 6 shows typical examples of the intensity ratio I_1/I_2 measured by these two ways. Both results show the linear dependence on the lipid concentration and the cell length at low values. The interference light intensity was determined from the slopes of the lines. To obtain

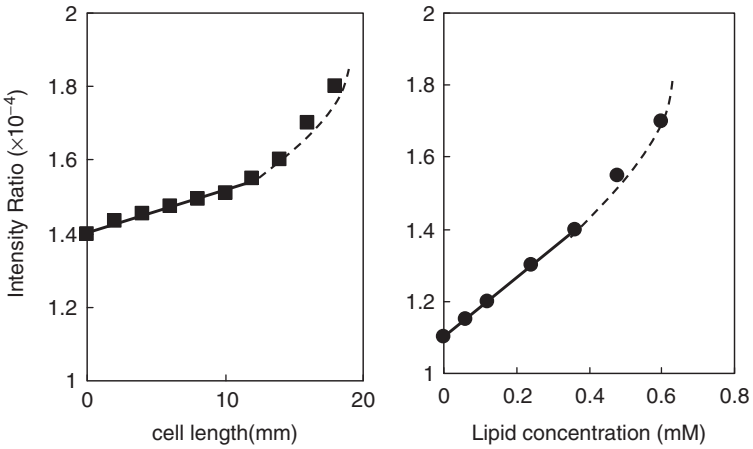

Fig. 6. Examples of intensity ratio of crossed and parallel transmitted light I_1 /I_2 measured with varying (A) the cell length and (B) lipid concentration. Slopes of the solid lines give the interference light intensity. (A) DPPC, concentration, 0.17 μM. (B) DMPC, cell length, 10 mm.

a linear dependence of the intensity ratio I_1/I_2 on $N\ell$, multilamellar vesicles with appropriate size were prepared. Small unilamellar vesicles (SUV) are not suitable for measuring the interference light due to the weak intensity. Sometimes, SUV was removed by filter to avoid vesicle aggregation by addition of additives. The suitable size is roughly more than $\lambda/\tilde{n}$, where λ is the wavelength of the incident light and $\tilde{n}$ the mean refractive index of lipids. Since the interference light strongly depends on the vesicle size, the vesicle aggregation and disruption were usually monitored by the turbidity obtained from the transmitted light with parallel polarization. Occasionally, the size distribution of vesicles in the dispersion was measured by dynamic light scattering.

3. BIREFRINGENCE STUDIES ON THE EFFECT OF ADDITIVES ON MOLECULAR ORDER

Interaction between lipids and biological substances relates to many kinds of factors, such as the shape and size of these molecules, location of the substances in the bilayer, structure and dynamics of the bilayer, and so on. A variety of additives have been employed in the study of the lipid–substance interaction. The additives are classified into three types: (i) Hydrophilic additives which locate the headgroup region or the surface of the bilayer, and predominantly affect the headgroup region; (ii) Hydrophobic ones which locate the chain region and interact with the chains and (iii) Amphiphilic ones which locate across both the headgroup and the acyl chain regions, and affect the entire lipid. Location of these additives is schematically represented in Fig. 7. In this section, I will

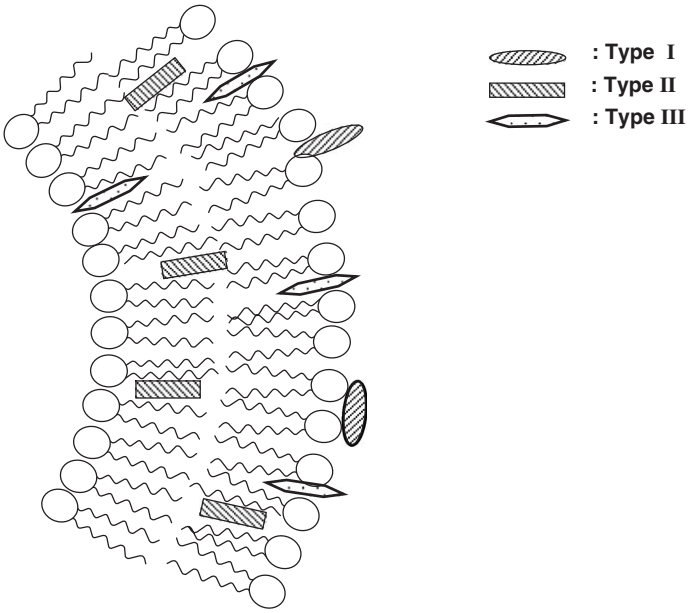

Fig. 7. Schematic representation of additives with three types in lipid bilayers: Type (I) hydrophilic, (II) hydrophobic and (III) amphiphilic additives.

describe the effect of these additives on the molecular order of bilayers measured by the birefringence technique.

3.1. Hydrophilic additives

3.1.1. Polysaccharide and polysaccharide/cholesterol conjugate

Saccharides are bound to the surface of lipid bilayers (Type I) as a result of the hydrophilic property, and interact with the headgroups and the interfacial water. Sucrose and disaccharides are known to strongly affect phases and phase transitions of lipids as phosphatidylethanolamine (PE) [12]. Disaccharides stabilize the gel phase and destabilize the liquid crystalline phase. They induce the formation of the hexagonal phase $H_{II}$and cubic phases [13,14]. These behaviors are owing to their tendency to decrease the surface area of lipids as a result of preferential exclusion from interfacial water. Disaccharide trehalose is known to stabilize the bilayer structure by direct interaction with lipids through hydrogen bonds [15]. Biological cells are coated with polysaccharide moieties from glycoproteins and glycolipids. The complex carbohydrates are known to play a significant role in cellular protection and intercellular recognition processes. For example, lipopolysaccharide in Gram-negative bacteria provides strong protection against membrane lysis induced by antimicrobial peptides as mellitin [16,17]. There have been many attempts to mimic recognition processes in artificial lipid

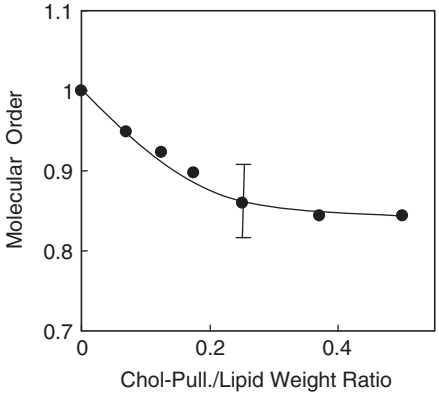

Fig. 8. Effect of surface pullulan modification with a hydrophobic anchor of cholesterol on the molecular orientation order of egg-PC bilayers measured by the birefringence technique. Values of the molecular order are relatively represented to the order without the pullulan derivative. From Mishima *et al.* [5].

membranes. In particular, to obtain target ability for specific cells or tissues in drug delivery systems, modification of liposomes was attempted using complex carbohydrates bearing hydrophobic anchor groups [18,19].

The birefringence studies using polysaccharide pullulan (mean molecular weight of 50,000) to modify egg-yolk phosphatidylcholine (egg-PC) liposomes have shown that the turbidity significantly increases by addition of pullulan at high concentrations above about 10 in the weight ratio to lipid, indicating an aggregation of the liposomes [5]. The interference light also increased, which completely correlated with the change in the turbidity. The increase in the interference light is not attributed to the birefringence of bilayers but the aggregation of liposomes. It was concluded that, although pullulan molecules are bound to the surface of the bilayers, they are of no effect on the molecular order.

However, pullulan-bearing cholesterol as an anchor showed a different effect on bilayers compared with pure pullulan. The interference light remarkably decreased with increasing the concentration of the pullulan derivative from 0 to about 0.25 in the weight ratio, whereas the turbidity is maintained at a constant value. Figure 8 shows the molecular orientation order in the bilayers S, calculated by the square root relationship with the interference light intensity, $S \propto \sqrt{A}$. The molecular order decreases by 15% in maximum. This result is contrary to a dramatic increase by pure cholesterol for DPPC bilayers [4,20,21]. It should be noted that the cholesterol-bearing pullulan concentration (0.5 weight ratio (0.8 mol%) in maximum) is far less than a concentration at which the cholesterol effect occurs (above about 5 mol%). The decrease by the pullulan derivatives seems to be due to disordering of the molecular packing induced by thermal motion of the pullulan moieties through the cholesterol moieties, since the

pullulan moieties wander in an aqueous phase on the liposome surface. No change in the molecular order is seen above about 0.3 in the weight ratio, indicating that all surfaces of the liposomes are fully coated by the pullulan derivatives. The fluorescence microscopic observation has also shown that all the pullulan derivatives are bound to unilamellar vesicles at a concentration of 0.4 weight ratio [18].

3.1.2. Polyethylene glycol (PEG)

Since PEG is a hydrophilic polymer with a large hydrated volume, it is excluded from a water layer near the surface of bilayer membranes and thus raises the water chemical potential at the surface. As a result, PEG causes dehydration of the membrane surface, forcing close contact between membranes, and also an imbalance of osmolarity between the membrane surface and the bulk aqueous phase. Addition of PEG above a certain threshold concentration induces liposome aggregation in order to reduce the volume of the water layer near the liposome surface [22]. Owing to the aggregating ability, PEG has been used as fusogen in the production of somatic cell hybrids and in the fusion injection of macromolecules into cultured cells [23].

The birefringence technique was applied to study the PEG effects on the molecular order of egg-PC bilayers, paying attention to the behavior of the liposomes at a low PEG concentration range without liposome aggregation [24]. Measurements of polarized transmitted light were performed with diluting the liposome suspension with PEG 8000 solution preserving the PEG concentration. The results have shown that the turbidity is approximately constant at PEG concentrations below 2 wt.%, indicating no aggregation occurs, however, the interference light increases abruptly at 1 wt.% of PEG by about 50%. By using the square root relation, the molecular order is estimated to increase by 25% compared with that in the absence of PEG. Generally, an increase in the molecular order leads to a decrease in the membrane fluidity. The birefringence result corresponds to the PEG-induced decrease in membrane fluidity observed by other methods [25]. PEG causes an imbalance of osmolarity between a membrane surface and the bulk aqueous phase because of exclusion from a water layer near the surface. The imbalance of osmolarity exerts an osmotic stress on liposomes [26]. The osmotic stress causes an elastic strain in the membrane to produce elastic pressure, and also a significant change in molecular packing in the membrane owing to a decrease in the surface area per lipid molecule. The increase in the molecular order is resulted from an increase in the molecular packing induced by the osmotic stress. The birefringence result suggests that liposome aggregation does not drive only from the dehydration in the water layer but also the tight packing of lipids, since the tight packing causes for liposome to be mechanically unstable.

3.2. Hydrophobic additives

3.2.1. Cholesterol

Cholesterol is one of the major lipid components of cellular membranes and plays an important role in cell function. Many workers have investigated the effects of cholesterol on physical and chemical properties of the membranes. Despite a great deal of investigation, cholesterol research is still one of the key investigation areas [27]. The membrane properties are strongly affected by the cholesterol content [28]. At high concentration, free cholesterol self-associates and forms microdomains, called rafts, in the plasma membrane [29–31]. Rafts appear to organize some signaling activity, concentrating the interacting proteins of various signal transduction cascades [32]. Understanding the structure and dynamics of rafts could be a key to many crucial membrane-associated processes in cells [33]. Lipid bilayer membranes containing high concentration of cholesterol are more resistant to pore formation, and the pore sizes are smaller than those composed of phospholipid only. This behavior is connected with the phenomenon of raft formation [34].

Cholesterol also regulates lipid bilayer dynamics and structure at low concentration. The interaction of cholesterol with phospholipids has been studied using various techniques. NMR and DSC experiments have showed that a subgel phase, called β phase appears in binary mixtures of DPPC at cholesterol concentrations above 20–25 mol%, and the gel and β phases coexists at cholesterol concentrations from 7.5 to 20 mol% [20]. The β phase is characterized by highly ordered, rigid acyl chains with rapid axially symmetric reorientation. A phase-separated mixture containing pure DPPC and DPPC-cholesterol domains was also found at cholesterol concentrations between 0 and 20 mol%. In addition, small amounts of cholesterol (5 mol%) induces a conversion from the tilted gel phases of pure DPPC (the L β' and P β' phases) to a new, untilted gel phase (the L β phase) [21]. X-ray diffraction experiment on dimyristoylphosphatidylcholine (DMPC)/cholesterol mixtures indicated a dramatic increase in the bilayer repeat spacing of the gel phase above 5 mol% of cholesterol [35]. This result provides evidence of a reduction in the tilt angle of acyl chains by incorporation of cholesterol.

Birefringence experiment also indicated an appearance of the untilted gel phase in DPPC/cholesterol mixtures above 5 mol% of cholesterol [4]. The experiment was performed by diluting the vesicle suspension. The multilamellar vesicles were prepared with varying the cholesterol concentration, and the size distribution of each sample was measured by a dynamic light scattering apparatus of Malvern submicron particle analyzer (4700-V4). Determination of the mean interference light $<A>$ is not easy because the number density of vesicles N differs with samples owing to the different distributions in size, even if the lipid concentrations are the same. The procedure of data analysis will be described briefly. Since cross-sectional areas of cholesterol and two fully extended acyl chains of DPPC are similar, the apparent volumes occupied in the bilayers are

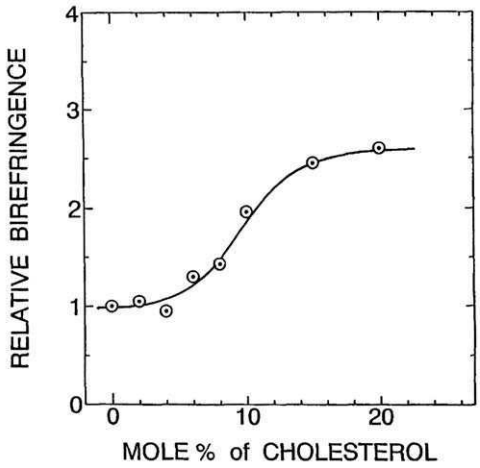

Fig. 9. Relative birefringence in the multilamellar gel phase as a function of cholesterol concentration of DPPC/cholesterol mixtures. The birefringence was determined from the interference light intensity obtained by fitting the slope of I_1/I_2 to the $<A>/<V>$ values calculated using the size distribution data by dynamic light scattering. The ratio of the vesicle wall thickness to the outer radius is assumed to be 0.43. From Mishima *et al.* [4].

assumed to be approximately equal to each other. Using the molecular volume v, number density of the dispersion with molar concentration of M is expressed as $N = vN_{avo}M/<V>$, with the Avogadro's number N_{avo} and the average lipid volume of one vesicle $<V>$. Thus, the intensity ratio of transmitted light I_1 /I_2 of equation (20) is rewritten as

$$\frac{I_1}{I_2} = \phi + vN_{avo}M\,\ell\frac{<A>}{<V>} \tag{30}$$

The slope of the plots of I_1/I_2 *versus* M gives $vN_{avo}M\ell\frac{<A>}{<V>}$. Note that the lipid volume of a vesicle $<V>$ and also the interference light $<A>$ depend on both the diameter and the wall thickness. The interference light $<A>$ for each sample was determined by fitting the slope to the $<A>/<V>$ values calculated using the data of the size distribution. The calculation was carried out for various values of the ratio $(R_o–R_i)/R_o$, but the calculated results showed similar profiles of the interference light as a function of cholesterol concentration indicating no significant dependence on the ratio. Figure 9 shows the birefringence obtained from the interference light. The birefringence increases gradually as cholesterol concentration is raised from 6 to 15 mol%. The increase is attributed to an increase in longitudinal order of the molecular orientation in the multilamellae. The longitudinal order is related to the tilted packing of lipid molecules in bilayers. In the gel phase of pure DPPC, the acyl chains are tilted with a same angle with respect to the bilayer plane, however, the tilt direction is probably different from the bilayers.

Due to the irregularity in the tilt direction, the longitudinal order of the multilamellae is significantly reduced. Thus, the birefringence of multilamellar bilayers appears to be smaller than that of the unilamellar bilayer because the optical anisotropy cancels each other. In fact, as mentioned above, the measured birefringence of the multilamellar bilayers of pure DPPC is about a quarter of that of the single bilayer estimated from the molecular polarizabilities of DPPC [9]. Therefore, the increase in the birefringence is owing to an appearance of the untilted gel phase by cholesterol.

The birefringence increase occurs above 6 mol% of cholesterol which agrees with the concentration of the phase boundary observed by NMR and DSC [20,21]. However, the gradual increase in the birefringence indicates that there is no clear-cut phase separation of the tilted gel phase and the untilted gel phase. It seems that the tilt of chains remains unchanged in the pure DPPC domain because chain tilting is favorable to a tight chain packing in the gel phase. The observed result indicates that the tilted phase of pure DPPC and the untilted phase of DPPC/cholesterol coexist at cholesterol concentrations above 6 mol%, and that the untilted phase domain spreads as cholesterol concentration is increased. The binary mixture of 20 mol% cholesterol is all in the untilted phase since the increase in the birefringence is suppressed around the cholesterol concentration.

3.2.2. Organohalogen compounds

Organohalogen compounds are well known for the in toxic effects on biological organs and cells [36–40]. The compounds usually do damage to plasma membrane functions. The damage is not induced only by a direct attack on proteins but also by changes in physical properties of lipid bilayers. Particularly, lipid order and dynamics in bilayer membranes are important to understand the membrane damage since protein function is partially modulated by these properties. Organohalogen compounds as chloroform and carbon tetrachloride are incorporated into the acyl chain region owing to their hydrophobic property. The birefringence experiment using these compounds was performed by varying the light path length in the syringe-type sample cell [41]. The results show a significant decrease in the interference light by addition of these compounds to DMPC bilayers in the fluid phase, but no rupture of the vesicles is seen at concentrations within the limit of solubility of these compounds in water, i.e., 0.2 v/v% for chloroform and 0.05 v/v% for carbon tetrachloride. The decrease in the interference light results from disordering of the chains by incorporation of these compounds. Figure 10 shows the molecular order S obtained by the square-root relationship. The molecular order decreases by about 17% at 0.2 v/v% of chloroform (mole ratio to lipid, 142:1), and by 23% at 0.05 v/v% of carbon tetrachloride (mole ratio, 29:1) indicating a strong effect of carbon tetrachloride on lipid bilayers

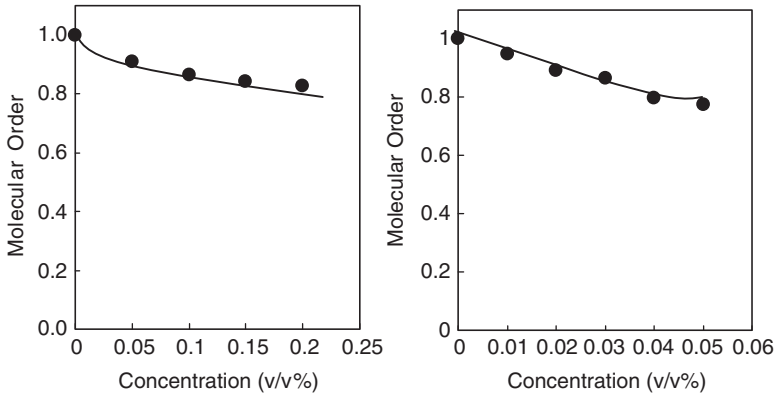

Fig. 10. Effects of chloroform (left) and carbon tetrachloride (right) on molecular order of DMPC bilayers in the fluid phase (24–25 °C) at low concentrations of chloroform and carbon tetrachloride without vesicle rupture. From Mishima *et al.* [41].

compared with that of chloroform. The reduction in the molecular order was correlated with an increase in the membrane fluidity observed by excimer fluorescence of pyrene incorporated to the membrane.

Egg-PC bilayer is primarily lower in the chain packing than DMPC bilayer because of having unsaturated double bonds and different chains in length. Generally, in comparison with synthetic lipids composed of saturated chains, natural lipid bilayers are acceptable for hydrophobic substances without significant disturbance, and readjust themselves to a more favorable hydrophobic match with the substances. In other words, hydrophobic substances can easily enter hydrophobic region of natural lipid bilayers since they have vacancy. However, birefringence study showed that behavior of disordering of egg-PC by these organohalogen compounds was approximately comparable with that of DMPC [41]. This result indicates that these compounds strongly interact with the lipid chains, whether or not the bilayer has the vacancy. It is known that organohalogen compounds transiently form pores in membranes [42]. The significant decrease in the membrane order seems to be partially attributed to a transient pore formation. The results by birefringence suggest that damages of biological membranes by organohalogen compounds are not only induced by a direct attack on proteins but also by a significant membrane perturbation involving pore formation.

3.3. Amphiphilic molecules

3.3.1. Lysolipids

Lysophospholipids are found only in small amounts in biological cell membranes. Early reports are focused on abnormal accumulations of lysophospholipid, which

induces fusion and lysis of cells [43,44]. However, it has been revealed that a variety of lysophospholipids play a role in a wide range of cellular processes involving membrane–protein or membrane–membrane interactions [45]. For example, lysophosphatidylcholine (LPC) is directly involved in signal transduction pathway and gating kinetics of membrane channels by altering mechanical properties of lipid bilayers [46–48]. Also, LPC is involved in lipidic pore formation in bilayer membranes formation [49]. Lysophosphatidic acid (LPA) plays a central role in a broad range of physiological processes, including neuronal function, cancer and mechanotransduction [50,51].

Effects of lysolipids of oleo-LPA and palmitoyl-LPC on molecular order of DMPC and egg-PC bilayers were examined by the birefringence technique [52]. It was found that LPA induces a considerable disorder in molecular orientation for synthetic lipid of DMPC in the fluid phase, whereas a slight order for natural lipid of egg-PC, e.g., the molecular order decreases by 10% at 15 μM of LPA (0.1 mole ratio) for DMPC and increases by 3.4% at 10 μM (0.09 mole ratio) for egg-PC in comparison without LPA (Fig. 11). Similarly, membrane fluidity measured by pyrene fluorescence increased for DMPC but decreased for egg-PC by addition of LPA. These behaviors are resulted from a difference in the chain packing of lipids. The bilayer of egg-PC is looser in the packing than that of DMPC at the fluid phase due to the unsaturated double bonds and different chain length of egg-PC. In fact, the interference light by egg-PC liposomes is far small in comparison with the DMPC vesicles in the absence of lysolipids. It seems that LPA is incorporated into egg-PC bilayers without significant disturbance and readjusts

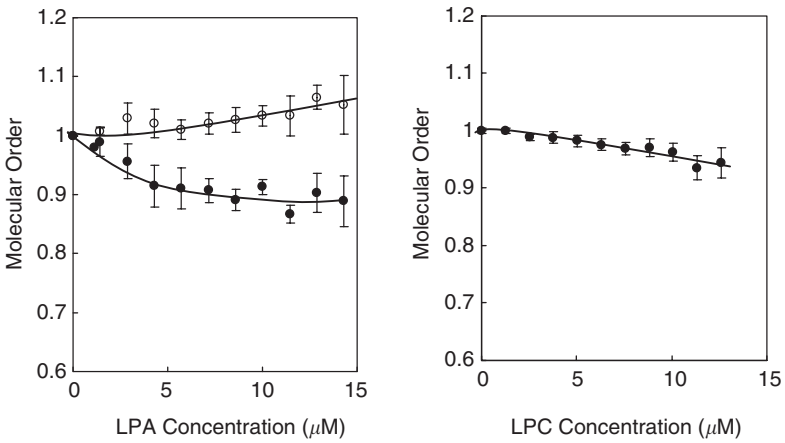

Fig. 11. Effects of lysophophatidic acid (left) and lysophophatidylcholine (right) on molecular order in DMPC (●) and egg-PC (○) bilayers. Values of the molecular order were calculated by the square root relationship from the interference light intensities of Figs. 2, 4 and 5 of Mishima *et al.* [52] and relatively represented to those without lysolipids. Mean ± S.E. of four to seven independent experiments are depicted.

itself to a more favorable hydrophobic match with the lipids. On the contrary, DMPC bilayers are significantly disturbed by incorporation of LPA owing to a higher molecular order. The result of the favorable hydrophobic match with natural lipid bilayers suggests that LPA can play a role in physiological processes in biological cells. In comparison with LPA, LPC induces a slight decrease in the molecular order of DMPC. The decrease at 0.07 mole ratio of LPC is only half compared with that at 0.1 mole ratio of LPA. This discrepancy is possibly resulted from a difference in the binding affinity with the headgroup, and a difference in the partitioning into the bilayers.

3.3.2. Amphiphilic peptide

Peptide–lipid interactions intensively influence membrane function. Research of these interactions is one of the key investigation areas in membrane biology. There has been a great deal of work of these interactions using many kinds of peptides. For example, antibiotic peptides, as melittin, magainin and alamethicin, aggregate in the outer leaflet membrane and form a transmembrane pore, resulting in an increase in permeability [53,54]. The action mechanism is studied in connection with peptide conformation, membrane elasticity and lipid constituent of membranes by many authors [55–59]. Secretory proteins and integral membrane proteins are effectively transported to cell membranes. Many of these proteins have the so-called signal sequences at the N terminal [60,61]. The signal sequences are of an amphiphilic peptide. The signal peptide mediates initiation of the membrane insertion of the following polypeptide segments, and is cleaved by the signal peptidase in the membrane. We have a lot of knowledge about the sequence structure and the steric conformation of these signal peptides [62,63], but information about the effects on lipid membrane structure and dynamics is not yet completed.

Effect of a synthetic model peptide on the molecular order of lipid bilayers was studied using the birefringence technique [64]. The synthetic peptide is modeled on signal sequences of a protein of *E. coli*. It is constituted by 20 amino acid residues and has a hydrophobic region of 7 alanines, 7 leucines and tryptophan at the end. The hydrophobic region forms an α-helix structure, and the hydrophobic length closely matches hydrocarbon thickness of the model membranes used. The experiment was performed for multilamellar vesicles of synthetic (DMPC, DPPC) and natural (egg-PC) lipids with varying the sample cell length. The results are shown in Fig. 12. The molecular order decreases by 5% for DMPC in the fluid phase and by 10% for DPPC in the gel phase with increasing the peptide concentration to 17 μM. The difference in the decrease is mainly owing to a difference in the phase. Since the order of the gel phase is larger than that of the fluid phase, the peptide induces a relatively larger disturbance on the gel phase bilayers. The molecular order is constant above 17 μM of the peptide

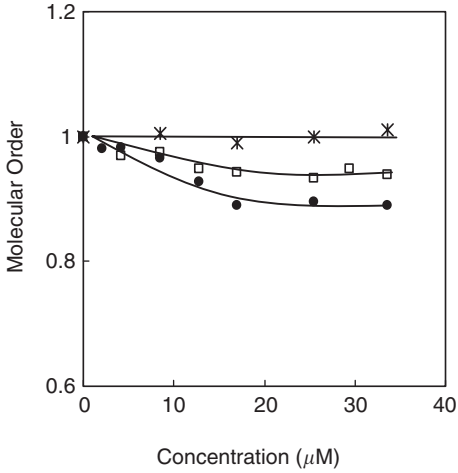

Fig. 12. Effects of an amphiphilic peptide on molecular order in egg-PC (✳), DMPC (□) and DPPC (●) bilayers. Values of the molecular order were calculated by the square root relationship from the interference light intensities of Fig. 3 of Mishima *et al.* [64] and relatively represented to those without peptide. The experiments were done at 24–25 °C, where DPPC was in the gel phase and other lipids in the fluid phase.

for both synthetic lipids, indicating that the membranes are saturated with the peptide at the concentration (∼0.1 mole ratio to lipid). NMR study using a similar peptide showed little effect on chain order of DMPC [65,66], but the peptide concentration (below 0.03 mole ratio) is far lower than that used here. The birefringence results also show that the peptide induces no change in the molecular order for egg-PC, indicating that the peptide enters the bilayers without significant disturbance due to the low chain order, and readjusts itself to a more favorable hydrophobic match with the bilayers. The behavior of egg-PC is suggestive for signal sequences of biosynthetic proteins to play a role of the transport in biomembranes. The signal sequence is probable to mediate the initiation of protein insertion without a significant disturbance in the membrane.

3.3.3. Local anesthetic

Local anesthetics exert their influence in nerve cell membranes by blocking the sodium channels [67]. The action mechanism has been studied by many workers, however, the controversy whether this blocking is the result of a direct anesthetic–protein interaction or a perturbation of the lipid membrane by the anesthetic remains unresolved. The presence of anesthetics within the membrane induces changes in the membrane structure and dynamics that would strongly affect the activity of a membrane protein [68,69]. Local anesthetic molecules have diverse size, shape and chemical structures. Because of this variety, it seems unlikely

that a specific binding site with the protein exists. A correlation between the potency of anesthetics and their lipophilicity, together the variety in their chemical structures, strongly suggest that anesthetic–lipid interaction may play a significant role in the anesthetic action. A wide variety of techniques have been used to examine the interaction of local anesthetics with model and biological lipid membranes, as X-ray [70–72], spin label ESR [73–75], NMR [76–79], infrared spectroscopy [80,81] and fluorescence [82–84]. Most local anesthetics are amphiphilic molecules with an ionizable amino group and a lipophilic aromatic ring. Under physiological conditions, the amino-ester and amino-amide anesthetics are present in both the charged and uncharged forms. Many experiments show that both charged and uncharged anesthetics bind to the membranes, and that the former is located in the headgroup region, while the latter more deeply in the acyl-chain region but near the membrane/water interface. There is some disagreement in the literature concerning the effect of the uncharged form on the chain region. Several reports indicate that uncharged anesthetics decrease chain order [78,85,86] and molecular organization of bilayers [87,88], whereas some others indicate that they increase order of erythrocyte membranes [89] and the organization of micelles [90]. The study of molecular dynamics simulation shows that the uncharged anesthetic increases chain order/packing, like as the effect of cholesterol on lipid bilayers, whereas charged anesthetic decreases chain order/packing, which resulted from formation of micelle-like aggregates of charged anesthetics at the bilayer surface [91]. The formation of micelle-like aggregates is thought to be resulted from cooperative binding of anesthetics to the bilayer surface by replacing lipid-bound water [81] and self-condensation of anesthetics [92].

The birefringence experiment employing local anesthetic tetracaine hydrochloride (Sigma Chemicals) was performed by the addition of the anesthetic to the suspension of DMPC multilamellar vesicle. As shown in Fig. 13, the interference light abruptly decreased with increasing tetracaine concentration. The turbidity also decreased slightly indicating an occurrence of vesicle rupture. It is noted that the decrease in the interference light is remarkable even at low tetracaine concentrations without significant change in the turbidity. This indicates a remarkable reduction in the molecular order. The interference light decrease at higher tetracaine concentrations reflects the molecular order reduction, together with a reduction in vesicle size. The molecular order reduction by the anesthetic is larger than that by the synthetic model peptide (Fig. 12). The effect of the anesthetic on the molecular order is rather comparable with that of the organohalogen compounds, chloroform and carbon tetrachloride (Fig. 10). Generally, membrane disordering by additives incorporated into the hydrophobic core is caused by steric effects originating in the mismatch between the additive and lipid shapes. It seems unlikely that the remarkable disordering observed is induced only by uncharged tetracaine molecules in the hydrophobic core. There is every probability that perturbation by charged forms at the membrane surface, as formation of micelle-like aggregates, affects the molecular order. Interaction between local

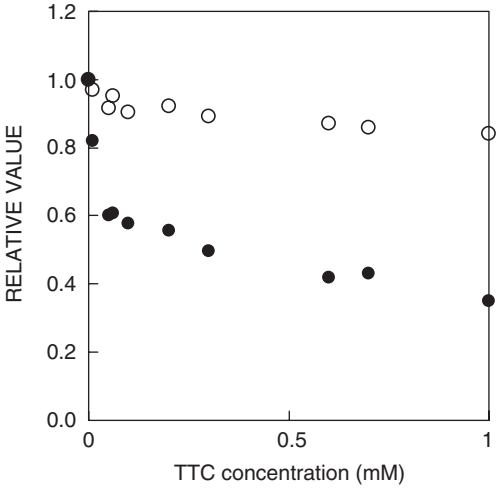

Fig. 13. Interference light intensity (●) measured by birefringence technique and turbidity (○) of DMPC multilamellar vesicles as a function of concentration of local anesthetic tetracaine. The values are relatively represented to those in the absence of tetracaine; Temperature: 21 °C, pH: 7.2.

anesthetics and lipids is not yet fully understood up to the present. Further research focused on the effects of local anesthetics on the membrane/water interface is important to understand mechanisms of local anesthesia.

4. CONCLUDING REMARKS

Interaction between biological molecules and lipids is one of the fundamental processes in living biological membranes. With this view, experiments employing a variety of additives have been extensively performed by many workers. In this chapter, I described the birefringence method and the examples restricted to our recent experiments using this technique. The birefringence technique is simple and powerful to investigate the effects of additives on lipid molecular order in the bilayers without any kind of labeling. The technique shall be extended to a time-resolved technique where changes in the molecular order can be observed in real time.

ACKNOWLEDGMENTS

Many people helped contribute to this work. The author would like to express his appreciation to K. Satoh, K. Suzuki, T. Ogihara, H. Watanabe, S. Kaneko, M. Nakajima, Y. Umehara and N. Inoue. The author is also grateful to Y. Anzai for support in preparing the figures.

REFERENCES

[1] D.M. Small (Ed.), The physical chemistry of lipids, in: D.J. Hanahan, (Series Ed.), Handbook of Lipid Research, Vol. 4, Plenum Press, New York, 1986
[2] J.Katsaras, T.Gutberlet (Eds.), Lipid BilayersStructure and Interactions, Springer, Heidelberg, 1999.
[3] H.T.Tien, A.Ottova (Eds.), Planar Lipid Bilayers (BLMs) and their Applications, Elsevier Science, Amsterdam, New York, 2003.
[4] K. Mishima, K. Satoh, K. Suzuki, Optical birefringence of multilamellar gel phase of cholesterole/phosphatidylcholine mixtures, Colloids, Surf. B: Biointerfaces 7 (1996) 83–89.
[5] K. Mishima, K. Satoh, K. Suzuki, Molecular order of lipid membranes modified with polysaccharide pullulan and a pullulan-derivative bearing a hydrophobic anchor, Colloids Surf. B: Biointerfaces 9 (1997) 9–15.
[6] H. Kelker, History of liquid crystals, Mol. Cryst. Liquid Cryst. 21 (1973) 1–48.
[7] T. Gordon, M.D. Stewart, Liquid crystals in biological systems, Mol. Cryst. 1 (1966) 563–580.
[8] L. Powers, P.S. Pershan, Monodomain samples of dipalmitoyl-phosphatidylcholine with varying concentrations of water and other ingredients, Biophys. J. 20 (1977) 137–152.
[9] K. Mishima, K. Satoh, T. Ogihara, Optical birefringence of phosphatidylcholine liposomes in gel phases, Biochim. Biophys. Acta 898 (1987) 231–238.
[10] M. Born, E. Wolf, Principles of Optics, 2nd edition, Pergamon Press, Oxford, 1964, pp. 694–701
[11] H. Kelker, R. Hatz, Handbook of Liquid Crystal, Verlag Chemie, Florida, 1980, pp. 254–262
[12] R. Koynova, M. Caffrey, Phases and phase transitions of the hydrated phosphatidylethanolamines, Chem. Phys. Lipids 69 (1994) 1–34.
[13] B. Tenchov, M. Rappolt, R. Koynova, G. Rapp, New phases induced by sucrose in saturated phosphatidylethanolamines: an expanded lamellar gel phase and a cubic phase, Biochim. Biophys. Acta, 1285 (1996) 109–122.
[14] B. Tenchov, R. Koynova, G. Rapp, Accelerated formation of cubic phases in phosphatidylethanolamine dispersions, Biophys. J. 75 (1998) 853–866.
[15] C.S. Pereira, R.D. Lins, I. Chandrasekhar, L.C. Freitas, P.H. Hünenberger, Interaction of the disaccharide trehalose with a phospholipid bilayer: a molecular dynamics study, Biophys. J. 86 (2004) 2273–2285.
[16] D. Allende, T.J. McIntosh, Lipopolysaccharides in bacterial membranes act like cholesterol in eukaryotic plasma membranes in providing protection against melittin-induced bilayer lysis, Biochemistry 42 (2003) 1101–1108.
[17] J. Tong, T.J. McIntosh, Structure of supported bilayers composed of lipopolysaccharides and bacterial phospholipids: raft formation and implications for bacterial resistance, Biophys. J. 86 (2004) 3759–3771.
[18] J. Sunamoto, T. Sato, M. Hirota, K. Fukushima, K. Hiratani, K. Hara, A newly developed immunoliposome – an egg phosphatidylcholine liposome coated with pullulan bearing both a cholesterol moiety and an IgMs fragment, Biochim. Biophys. Acta 898 (1987) 323–330.
[19] J.J. Ramsden, P. Schneider, Membrane insertion and antibody recognition of a glycosylphosphatidylinositol-anchored protein: an optical study, Biochemistry 32 (1993) 523–529.
[20] M.R. Vist, J.H. Davis, Phase equilibria of cholesterol/dipalmitoylphosphatidylcholine mixtures: ^{2}H nuclear magnetic resonance and differential scanning calorimetry, Biochemistry 29 (1990) 451–464.
[21] T.P.W. McMullen, R.N. McElhaney, New aspects of the interaction of cholesterol with dipalmitoylphosphatidylcholine bilayers as revealed by high-sensitivity differential scanning calorimetry, Biochim. Biophys. Acta 1234 (1995) 90–98.

[22] B.R. Lentz, Polymer-induced membrane fusion: potential mechanism and relation to cell fusion events, Chem. Phys. Lipids 73 (1994) 91–106.
[23] K. Kostarelos, D. Emfietzoglou, T.F. Tadros, Light-sensitive fusion between polymer-coated liposomes following physical anchoring of polymerisable polymers onto lipid bilayers by self-assembly, Faraday Discuss 128 (2005) 379–388.
[24] K. Mishima, K. Satoh, K. Suzuki, Increase in molecular order of phospholipid membranes due to osmotic stress by polyethyleneglycol, Colloids Surf. B: Biointerfaces 10 (1997) 113–117.
[25] M. Yamazaki, S. Ohnishi, T. Ito, Osmoelastic coupling in biological structures: decrease in membrane fluidity and osmophobic association of phospholipid vesicles in response to osmotic stress, Biochemistry 28 (1989) 3710–3715.
[26] V.S. Malinin, P. Frederik, B.R. Lentz, Osmotic and curvature stress affect PEG-induced fusion of lipid vesicles but not mixing of their lipids, Biophys. J. 82 (2002) 2090–2100.
[27] D.E. Vance, H. Van den Bosch, Cholesterol in the year 2000, Biochim. Biophys. Acta 1529 (2000) 1–8.
[28] S. Raffy, J. Teissie, Control of lipid membrane stability by cholesterol content, Biophys. J. 76 (1999) 2072–2080.
[29] J.R. Silvius, Role of cholesterol in lipid raft formation: lessons from lipid model systems, Biochim. Biophys. Acta 1610 (2003) 174–183.
[30] L. Addadi, M. Geva, H.S. Kruth, Structural information about organized cholesterol domains from specific antibody recognition, Biochim. Biophys. Acta 1610 (2003) 208–216.
[31] E.K. Fridriksson, P.A. Shipkova, E.D. Sheets, D. Holowka, B. Baird, F.W. McLafferty, Quantitative analysis of phospholipids in functionally important membrane domains from RBL-2H3 mast cells using tandem high-resolution mass spectrometry, Biochemistry 38 (1999) 8056–8063.
[32] D.A. Brown, E. London, Functions of lipid rafts in biological membranes, Annu. Rev. Cell Dev. Biol. 14 (1998) 111–136.
[33] K. Bacia, D. Scherfeld, N. Kahya, P. Schwille, Fluorescence correlation spectroscopy relates rafts in model and native membranes, Biophys. J. 87 (2004) 1034–1043.
[34] S. Koronkiewicz, S. Kalinowski, Influence of cholesterol on electroporation of bilayer lipid membranes: chronopotentiometric studies, Biochim. Biophys. Acta 1661 (2004) 196–203.
[35] S.W. Hui, N.-B. He, Molecular organization in cholesterol-lecithin bilayers by X-ray and electron diffraction measurements, Biochemistry 22 (1983) 1159–1164.
[36] J.L. Larson, D.C. Wolf, S. Mery, K.T. Morgan, B.E. Butterworth, Toxicity and cell proliferation in the liver, kidneys and nasal passages of female F-344 rats, induced by chloroform administered by gavage, Food Chem. Toxicol. 33 (1995) 443–456.
[37] D.C. Dorman, K.L. Miller, A. D'Antonio, R.A. James, K.T. Morgan, Chloroform-induced olfactory mucosal degeneration and osseous ethmoid hyperplasia are not associated with olfactory deficits in Fischer 344 rats, Toxicology 122 (1997) 39–50.
[38] C. Guastadisegni, L. Guidoni, M. Balduzzi, V. Viti, E. DiConsiglio, L. Vittozzi, Characterization of a phospholipid adduct formed in Sprague Dawley rats by chloroform metabolism: NMR studies, J. Biochem. Mol. Toxicol. 12 (1998) 93–102.
[39] E. Di Consiglio, G. De Angelis, E. Testai, L. Vittozzi, Correlation of a specific mitochondrial phospholipid-phosgene adduct with chloroform acute toxicity, Toxicology 159 (2001) 43–53.
[40] S.J. Hemmings, V.B. Pulga, S.T. Tran, R.R. Uwiera, Differential inhibitory effects of carbon tetrachloride on the hepatic plasma membrane, mitochondrial and endoplasmic reticular calcium transport systems: implications to hepatotoxicity, Cell Biochem. Funct. 20 (2002) 47–59.
[41] K. Mishima, H. Watanabe, S. Kaneko, T. Ogihara, Membrane disordering induced by chloroform and carbon tetrachloride, Colloids Surf. B: Biointerfaces 28 (2003) 307–312.

[42] M. Engelke, R. Jessel, A. Wiechmann, H.A. Diehl, Effect of inhalation anaesthetics on the phase behavior, permeability and order of phosphatidylcholine bilayers, Biophys. Chem. 67 (1997) 127–138.
[43] F.C. Reman, R.A. Demel, J. De Gier, L.L. Van Deenen, H. Eibl, O. Westphal, Studies on the lysis of red cells and bimolecular lipid leaflets by synthetic lysolecithins, lecithins and structural analogs, Chem. Phys. Lipids 3 (1969) 221–233.
[44] A.R. Poole, J.I. Howell, J.A. Lucy, Lysolecithin and cell fusion, Nature 227 (1970) 810–813.
[45] N. Fuller, R.P. Rand, The influence of lysolipids on the spontaneous curvature and bending elasticity of phospholipid membranes, Biophys. J. 81 (2001) 243–254.
[46] Y. Asaoka, K. Yoshida, Y. Sasaki, Y. Nishizuka, Potential role of phospholipase A2 in HL-60 cell differentiation to macrophages induced by protein kinase C activation, Proc. Natl. Acad. Sci. USA 90 (1993) 4917–4921.
[47] Y. Asaoka, K. Yoshida, Y. Sasaki, Y. Nishizuka, M. Murakami, I. Kudo, K. Inoue, Possible role of mammalian secretory group II phospholipase A2 in T-lymphocyte activation: implication in propagation of inflammatory reaction, Proc. Natl. Acad. Sci. USA 90 (1993) 716–719.
[48] J.A. Lundbaek, O.S. Anderson, Lysophospholipids modulate channel function by altering the mechanical properties of lipid bilayers, J. Gen. Physiol. 104 (1994) 645–673.
[49] G. Basañez, J.C. Sharpe, J. Galanis, T.B. Brandt, J.M. Hardwick, J. Zimmerberg, Bax-type apoptotic proteins porate pure lipid bilayers through a mechanism sensitive to intrinsic monolayer curvature, J. Biol. Chem. 277 (2002) 49360–49365.
[50] C. Luquain, V.A. Sciorra, A.J. Morris, Lysophosphatidic acid signaling: how a small lipid does big things, Trends Biochem. Sci. 28 (2003) 377–383.
[51] H. Ohata, K. Tanaka, N. Maeyama, T. Ikeuchi, A. Kamada, M. Yamamoto, K. Momose, Physiological and pharmacological role of lysophosphatidic acid as modulator in mechanotransduction, Jpn J. Pharmacol. 87 (2001) 171–176.
[52] K. Mishima, M. Nakajima, T. Ogihara, Effects of lysophospholipids on membrane order of phosphatidylcholine, Colloids Surf. B: Biointerf. 33 (2004) 185–189.
[53] D. Andreu, L. Rivas, Animal antimicrobial peptides: an overview, Biopolymers 47 (1998) 415–433.
[54] H.W. Huang, Action of antimicrobial peptides: two-state model, Biochemistry 39 (2000) 8347–8352.
[55] L. Yang, T.A. Harroun, T.M. Weiss, L. Ding, H.W. Huang, Barrel-stave model or toroidal model? A case study on melittin pores, Biophys. J. 81 (2001) 1475–1485.
[56] K. Matsuzaki, Why and how are peptide-lipid interactions utilized for self-defense? Magainins and tachyplesins as archetypes, Biochim. Biophys. Acta 1462 (1999) 1–10.
[57] M. Zasloff, Antimicrobial peptides of multicellular organisms, Nature 415 (2002) 389–395.
[58] O.S. Belokoneva, H. Satake, E.L. Mal'tseva, N.P. Pal'mina, E. Villegas, T. Nakajima, G. Corzo, Pore formation of phospholipid membranes by the action of two hemolytic arachnid peptides of different size, Biochim. Biophys. Acta 1664 (2004) 182–188.
[59] E.E. Ambroggio, F. Separovic, J. Bowie, G.D. Fidelio, Surface behavior and peptide-lipid interactions of the antibiotic peptides, Maculatin and Citropin, Biochim. Biophys. Acta 1664 (2004) 31–37.
[60] G. Blobel, Intracellular protein topogenesis, Proc. Natl. Acad. Sci. USA 77 (1980) 1496–1500.
[61] S.L. Sanders, R. Schekman, Polypeptide translocation across the endoplasmic reticulum membrane, J. Biol. Chem. 267 (1992) 13791–13794.
[62] G. von Heijne, The signal peptide, J. Membr. Biol. 115 (1990) 195–201.
[63] M. Sakaguchi, R. Tomiyoshi, T. Kuroiwa, K. Mihara, T. Omura, Functions of signal and signal-anchor sequences are determined by the balance between the hydrophobic segment and the N-terminal charge, Proc. Natl. Acad. Sci. USA 89 (1992) 16–19.

[64] K. Mishima, H. Watanabe, S. Kaneko, T. Ogihara, Effects of an amphiphilic peptide on membrane order of phosphatidylcholine, Colloids, Surf. B: Biointerfaces 25 (2002) 219–224.
[65] M.R. Morrow, J.C. Huschilt, J.H. Davis, Simultaneous modeling of phase and calorimetric behavior in an amphiphilic peptide/phospholipid model membrane, Biochemistry 24 (1985) 5396–5406.
[66] K. Belohorcova, J. Qian, J.H. Davis, Molecular dynamics and (2)H-NMR study of the influence of an amphiphilic peptide on membrane order and dynamics, Biophys. J. 79 (2000) 3201–3216.
[67] B. Hille, Ionic channels in nerve membranes, Prog. Biophys. Mol. Biol. 21 (1970) 1–32.
[68] R.S. Cantor, Breaking the Meyer–Overton rule: predicted effects of varying stiffness and interfacial activity on the intrinsic potency of anesthetics, Biophys. J. 80 (2001) 2284–2297.
[69] N. Hauet, F. Artzner, F. Boucher, C. Grabielle-Madelmont, I. Cloutier, G. Keller, P. Lesieur, D. Durand, M. Patermostre, Interaction between artificial membranes and enflurane, a general volatile anesthetic: DPPC-enflurane interaction, Biophys. J. 84 (2003) 3123–3137.
[70] H.G.L. Coster, V.J. James, C. Berthet, A. Miller, Location and effect of procaine on lecithin/cholesterol membranes using X-ray diffraction methods, Biochim. Biophys. Acta 641 (1981) 281–285.
[71] V. Luzzati, L. Mateu, G. Marquez, M. Borgo, Structural and electrophysiological effects of local anesthetics and of low temperature on myelinated nerves: implication of the lipid chains in nerve excitability, J. Mol. Biol. 286 (1999) 1389–1402.
[72] V. Luzzati, E. Benoit, G. Charpentier, P. Vachette, X-ray scattering study of pike olfactory nerve: elastic, thermodynamic and physiological properties of the axonal membrane, J. Mol. Biol. 343 (2004) 199–212.
[73] S. Schreier, W.A. Frezzatti Jr., P.S. Araujo, H. Chaimovich, I.M. Cuccovia, Effect of lipid membranes on the apparent pK of the local anesthetic tetracaine. Spin label and titration studies, Biochim. Biophys. Acta. 769 (1984) 231–237.
[74] M.L. Bianconi, A.T. do Amaral, S. Schreier, Use of membrane spin label spectra to monitor rates of reaction of partitioning compounds: hydrolysis of a local anesthetic analog, Biochem. Biophys. Res. Commun. 152 (1988) 344–350.
[75] J. Gallova, F. Andriamainty, D. Uhrikova, P. Balgavy, Interaction of local anesthetic heptacaine homologs with phosphatidylcholine bilayers: spin label ESR study, Biochim. Biophys. Acta. 1325 (1997) 189–196.
[76] H. Hauser, S.A. Penkett, D. Chapman, Nuclear magnetic resonance spectroscopic studies of procaine hydrochloride and tetracaine hydrochloride at lipid-water interfaces, Biochim. Biophys. Acta 183 (1969) 466–475.
[77] J. Cerbon, NMR evidence for the hydrophobic interaction of local anaesthetics. Possible relation to their potency, Biochim. Biophys. Acta 290 (1972) 51–57.
[78] A. Seelig, P.R. Allegrini, J. Seelig, Partitioning of local anesthetics into membranes: surface charge effects monitored by the phospholipid head-group, Biochim. Biophys. Acta 939 (1988) 267–276.
[79] L.F. Fraceto, L.de.M. Pinto, L. Frnzoni, A.A. Braga, A. Spisni, S. Schreier, E. de Paula, Spectroscopic evidence for a preferential location of lidocaine inside phospholipid bilayers, Biophys. Chem. 99 (2002) 229–243.
[80] M. Auger, H.C. Jarrell, I.C. Smith, D.J. Siminovitch, H.H. Mantsch, P.T. Wong, Effects of the local anesthetic tetracaine on the structural and dynamic properties of lipids in model membranes: a high-pressure Fourier transform infrared study, Biochemistry 27 (1988) 6086–6093.
[81] I. Ueda, J.S. Chiou, P.R. Krishna, H. Kamaya, Local anesthetics destabilize lipid membranes by breaking hydration shell: infrared and calorimetry studies, Biochim. Biophys. Acta 1190 (1994) 421–429.

[82] S. Desai, T. Hadlock, C. Messani, R. Chafetz, G. Strichartz, Ionization and adsorption of a series of local anesthetics in detergent micelles: studies of drug fluorescence, J. Pharmacol. Exp. Ther. 271 (1994) 220–228.
[83] J. Garcia-Soto, M.S. Fernandez, The effect of neutral and charged micelles on the acid–base dissociation of the local anesthetic tetracaine, Biochim. Biophys. Acta. 731 (1983) 275–281.
[84] M. Mondal, A. Chakrabarti, Effect of the glycosphingolipid, GM1 on localization of dibucaine in phospholipid vesicles: a fluorescence study, Chem. Phys. Lipids 130 (2004) 175–187.
[85] M. Auger, H.C. Jarrell, I.C. Smith, Interactions of the local anesthetic tetracaine with membranes containing phosphatidylcholine and cholesterol: a 2H NMR study, Biochemistry 27 (1988) 4660–4667.
[86] D.A. Driscoll, S. Samarasinghe, S. Adamy, J. Jonas, A. Jonas, Pressure effects on dipalmitoylphosphatidylcholine bilayers measured by 2H nuclear magnetic resonance, Biochemistry 30 (1991) 3322–3327.
[87] E. de Paula, S. Schreier, Use of a novel method for determination of partition coefficients to compare the effect of local anesthetics on membrane structure, Biochim. Biophys. Acta 1240 (1995) 25–33.
[88] L.M. Pinot, D.K. Yokaichiya, L.F. Fraceto, E. de Paula, Interaction of benzocaine with model membranes, Biophys. Chem. 87 (2000) 213–223.
[89] T. Frangopol, D. Mihailescu, Interactions of some local anesthetics and alcohols with membranes, Colloids Surf. B: Biointerfaces 22 (2001) 3–22.
[90] C.V. Teixeira, R. Itri, F. Casallanovo, S. Schreier, Local anesthetic-induced microscopic and mesoscopic effects in micelles. A fluorescence, spin label and SAXS study. Single angle X-ray scattering, Biochim. Biophys. Acta 1510 (2001) 93–105.
[91] M. Pasenkiewicz-Gierula, T. Rog, J. Grochowski, P. Serda, R. Czarnecki, T. Librowski, S. Lochynski, Effects of a carane derivative local anesthetic on a phospholipid bilayer studied by molecular dynamics simulation, Biophys. J. 85 (2003) 1248–1258.
[92] H. Matsuki, M. Yamanaka, S. Kaneshina, H. Kamaya, I. Ueda, Surface tension study on the molecular-aggregate formation of local anesthetic dibucaine hydrochloride, Colloids Surf. B: Biointerfaces 11 (1998) 87–94.

This page intentionally left blank

CHAPTER 4

Visualization and Characterization of Domains in Supported Model Membranes

Hilde A. Rinia,[1,*] George W.H. Wurpel,[2] and Michiel Müller[1]

[1]*Biophysics and Microscopy Group, Swammerdam Institute for Life Sciences, University of Amsterdam, P.O. Box 94062, 1090 GB Amsterdam, The Netherlands*
[2]*Biosurface and Microscopy Group, FOM Institute of Atomic and Molecular Physics, P.O. Box 41883, 1009 DB Amsterdam, The Netherlands*

Contents

Abstract

Lateral segregation of lipid and protein components within biomembranes can lead to the formation of biologically functional domains. This chapter reviews microdomain formation in supported model membranes, induced by lipid–lipid interactions. The discussed techniques used for bilayer imaging are atomic force microscopy and fluorescence microscopy. Furthermore, we describe the promising capabilities and thus far obtained results of multiplex coherent anti-stokes Raman scattering microscopy with respect to functional imaging of microdomains in lipid model systems.

*Corresponding author. Tel: +31-20-5256204; Fax: +31-20-5256327;
E-mail: rinia@science.uva.nl

ADVANCES IN PLANAR LIPID BILAYERS AND LIPOSOMES, VOLUME 3
ISSN 1554-4516 DOI: 10.1016/S1554-4516(05)03004-8

1. INTRODUCTION

The way in which biological membranes have been visualized has changed considerably over the past decades. In the fluid-mosaic model described by Singer and Nicolson [1] in 1972, the lipids were thought to form a matrix surrounding the integral membrane proteins, and providing them with the appropriate environment to be functional. This model however still left some open questions, like the natural occurrence of a very large variety of lipids, while a few lipid species, with different headgroups and tails, would be sufficient to provide the proper lipid-matrix for any membrane protein. Moreover, it was unclear why certain lipid components, e.g. sphingolipids and cholesterol, have a special affinity for each other or how membranes deal with constituents with different hydrophobic thickness. In 1984, Mouritsen and Bloom [2] published their mattress model, a thermodynamic model which describes peptide–lipid interactions in the light of hydrophobic mismatch. Membrane constituents with a certain hydrophobic thickness would segregate from constituents with a different hydrophobic thickness. Mismatch is believed to be important for protein insertion, activity, stability, and protein sorting and aggregation [3,4]. That in live cells hydrophobic mismatch indeed plays a role in protein sorting, is illustrated by the fact that when the length of a membrane spanning domain of a Golgi protein is increased, it is targeted to the thicker plasma membrane [5]. The plasma membrane is known to be thicker than organelle membranes, due to the fact that it contains (more) cholesterol, which has a thickening effect on fluid-phase bilayers [6]. Furthermore, it contains saturated sphingolipid species, which have longer hydrophobic acyl chains than unsaturated lipids. The facts that the plasma membrane and the trans Golgi network (TGN) are enriched in cholesterol and sphingolipids combined with the fact that these two lipids have a high affinity for each other [7,8] have led to the postulation of the raft-model [9]. The basis of this idea is the existence of the so-called liquid-ordered phase [10], induced by the presence of cholesterol. This would cause liquid–liquid phase-separation in the plasma membrane, leading to the formation of liquid-ordered domains (rafts), enriched in cholesterol and sphingolipids, surrounded by fluid-phase lipids. These rafts are thought to correspond to detergent-resistant membranes, which is the fraction of membranes resistant to detergent extraction at 4 °C [11]. Analysis of such fractions showed that these are indeed enriched in sphingolipids and specific proteins, usually glycosylphosphatidylinositol (GPI)-anchored proteins [12]. The size of rafts is still heavily debated and the values in the literature vary from a few annular lipid molecules [13] to 700 nm, depending on the used technique [13–15]. Generally, rafts are proposed to play a role in several vital biological processes like lipid and protein sorting, vesicular transport, and signal transduction [9,16–18]. Although nowadays most authors assume that rafts indeed exist, the evidence for the presence of rafts in biological membranes is still circumstantial [19]. Nonetheless, for model membranes there is ample proof that domain

formation takes place [20] and model-rafts have been visualized directly in several lipid systems [21–24].

Another open question concerning the lateral organization in membranes involves diffusion coefficients, which for live cells are found to be significantly different compared to values found for model membranes [25,26]. The diffusion coefficients of proteins in fluid-phase bilayers are in the order of several $\mu m/s^2$, while in live cells values are around 10–100 times lower [25,27,28]. Important information concerning this anomalism was found with single molecule tracking or single particle tracking (SPT), which enables one to determine the diffusion of one (or a few) molecule(s) [27]. Experiments with SPT, with a high spatial and temporal resolution, show that membrane proteins and lipids undergo ''hop-diffusion'', meaning they diffuse in a small zone, after which they ''hop'' to the adjacent zone and so on [25,29]. On a large scale, as observed by fluorescence recovery after photobleaching (FRAP), this averages out to lower diffusion coefficients, but within one zone the value of the diffusion coefficient approaches the diffusion coefficient in model membranes [30]. Apparently, cell membranes are divided in confined zones, but it is possible for membrane constituents to cross the barrier between zones, and therefore these zones are also referred to as transient confinement zones [31]. Kusumi *c.s.* coined the picket fence model, which describes how the membrane skeleton network (fences) directly obstructs the diffusion of proteins with large intracellular domains and indirectly, *via* skeleton-linked proteins (pickets), also confines diffusion of lipids [25,28].

In order to systematically investigate lateral segregation in cell membranes, model systems have proven to be quite useful. Supported bilayers consisting of one lipid species can be regarded as simple model membranes. Upon adding more membrane constituents, a more biologically relevant model system is obtained. Although protein–lipid interactions play an important role in the lateral organization of membranes, and although domain formation induced by small peptides has been visualized [32–37], in this chapter we focus on lipid–lipid interactions only, systematically studied using supported lipid bilayers. Such model membranes can be imaged with several different microscopic techniques. This chapter discusses the visualization of domains in supported model membranes, imaged with atomic force microscopy (AFM), fluorescence microscopy (FM) and gives an outlook on imaging of supported bilayers with coherent anti-stokes Raman spectroscopy (CARS) microscopy.

AFM provides one with the height profile of a sample, with a lateral resolution of less than a nanometer and a *z*-resolution of about 1–2 Å [38]. Since domain formation in general and raft formation in particular are accompanied by height differences, AFM is an excellent tool to visualize domains in supported membranes. Due to the high resolution, even domains with the size of only a few nanometers can be visualized [39–42].

In FM studies, bilayers are used with a small amount of lipids with an attached fluorescent group. The contrast in the obtained image is based on the preference

of this fluorescent lipid for different lipid phases. The advantage of this technique is that one can image both supported and freestanding bilayers. The resolution of FM is usually a few hundred nanometers, depending on the wavelength of the emitted light of the used fluorophore. In spite of this limited resolution, FM has proven to be a very elucidative technique in the studies of domains in model systems [43–45].

The field of CARS microscopy is relatively new. As with FM, both freestanding and supported systems can be studied, and the resolution is several hundreds of nanometers. Since it is an analog of Raman scattering, the contrast is based on differences in vibrational spectra, which means that the differences in lipid phases within one sample can be directly visualized [46]. This technique does not require any probes, does not suffer from photobleaching or phototoxicity, and the net energy deposition of the CARS process is zero, making it a potentially non-invasive technique. Since CARS microscopy is based on a non-linear third-order process, it yields much higher signals compared to Raman microscopy. Recently, it was shown that the physical phase of single bilayers can be clearly detected [47] and visualized [48].

We chose to discuss these three imaging techniques because they have been successfully applied to supported lipid model membranes. These techniques each provide unique, and together provide complementary information on lateral organization in model membranes, since their contrast is based on different sample properties: height, fluorophore partitioning, and vibrational transitions.

2. ATOMIC FORCE MICROSCOPY

With AFM, the sample surface is scanned by a sharp tip (radius 1–10 nm, depending on the conditions, see [38,49]), which is integrated at the end of a flexible cantilever. On this cantilever a laser beam is directed, which is deflected in a detector, consisting of a split diode. As the tip encounters height differences on the surface and/or experiences different interactions with the surface, it moves up and down, which in turn causes the cantilever to deflect up and down. This deflection is monitored, *via* the laser beam, by the detector (Fig. 1). In this way, a profile of the scanned surface is obtained with a height resolution of 1–2 Å, and a lateral resolution of less than 1 nm [38].

In air, most surfaces are covered with a nanoscopic layer of water, and the tip is pulled toward the surface by the surface tension of this water layer. Due to these hydration forces, the tip is exerting a relatively large force (10 nN) on the scanned sample, when operating in air. This large force can easily damage biological samples, fragile as they are. This problem can be circumvented by scanning in water, where no hydration forces are present, and forces exerted by the tip are much smaller: several hundreds of picoNewtons [50]. Scanning in water holds an extra benefit of AFM for biologists, since the natural environment

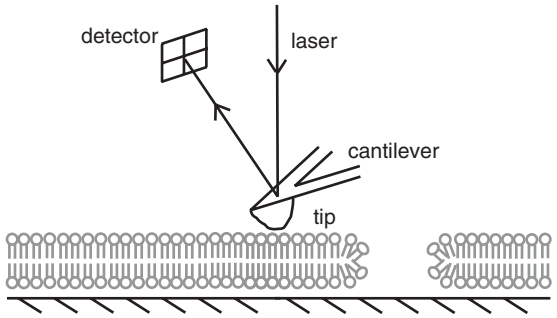

Fig. 1. Principle of AFM. The sample surface, here a supported bilayer, is scanned with a sharp tip mounted on a flexible cantilever (not on scale). Deflection of the tip, caused by differences in height or surface properties of the sample, is followed *via* a laser-beam by the detector.

of biomolecules is usually an aqueous solution. Another advantage is that buffers with variable pH or salt concentration, or with biological relevant components like ATP can be used. Also, the liquid above the sample can be replaced, so that specific molecules can be added or removed.

The thickness and length of a cantilever determine the spring constant of that cantilever, and thus the force exerted on the sample during scanning. Chips are commercially available, with integrated cantilevers, each with their own spring constant. Since biological samples are fragile, usually the cantilever with the lowest spring constant ($\sim$0.06 N/m) is chosen. Chip, cantilever, and tip are made of Si_3N_4, which is hydrophilic and negatively charged. With AFM, strictly spoken, one measures the forces between the tip and the underlying molecules of the scanned sample. When the tip closely approaches the sample, electron orbitals of tip atoms and sample atoms repel each other, and it is at this point where tip and sample are said to be in contact. When scanning an uncharged sample, only contact forces and van der Waals forces play a role. However, many biological molecules, like DNA and anionic lipids, are negatively charged. In this case, the longer ranged electrostatic interactions would cause to repel the, also negatively charged, tip and give rise to artifacts in the measured heights [50,51]. This can be overcome, and even be used to obtain a higher resolution, by adjusting the ionic strength of the buffer solution above the scanned sample [52].

An AFM can operate in different modes. The mode mostly used is contact mode (CM), in which the tip is in constant contact with the sample during scanning. The advantage of this mode is that in principle, when used on sturdy, ordered samples, high resolution can be achieved. The disadvantage is that it can damage the sample, since the tip is ‘‘dragging’’ along the surface, and possibly removes molecules from the sample. This ability to remove molecules has also been used to modify lipid layers on purpose [53,54]. In these cases, the applied force was increased, to let the tip scratch a line or a square in the lipid bilayers.

To avoid damaging the sample, tapping mode (TM) was developed [55]. In TM, the cantilever is oscillating in the *z*-direction, all the time touching the surface briefly during scanning. In this way, no lateral force is exerted, so that scanned samples are less easily damaged. Other commonly used modes are the friction mode and force volume mapping, also referred to as jumping mode. In friction mode the torque of the cantilever during scanning is detected, which reflects the friction encountered by the tip, i.e. differences in lateral surface forces. This mode yields information on the physical surface properties [56,57]. In force volume mapping, at each point the tip–sample interactions are measured by taking a force curve. Images reflect the magnitude of adhesion forces between the tip and sample. Usually, the tip is modified or coated with, for example, specific antibodies. Objects with similar features can be distinguished based on their (bio) chemical properties [58].

The resolution of AFM images highly depends on the sample. For instance, adsorbed proteins, scanned in CM appear hazy, mostly due to damage caused by the tip, as explained above (TM in this case yields better images). However, proteins present in a two-dimensional (2-D) crystal scanned in CM can yield images with subnanometer resolution [59–62]. Membranes when present around whole cells give low resolution images [63–65], due to the presence of the underlying cytoskeleton, cytoplasm, and organelles. The latter three are a soft foundation under the scanned membrane. As a contrast, in some model membranes deposited directly on a solid support, the lipid head groups could be directly resolved [66,67]. As in the case of 2-D crystals of proteins, the lipids in these bilayers were ordered in a lattice. The regularity of samples increases the obtained resolution and facilitates any off-line processing.

2.1. Bilayer preparation and properties

In order to image biological samples with AFM, they have to be deposited onto a solid support [68]. For optical microscopy, glass cover slides or quartz slides are often used as solid support, but for AFM such a substrate should be flat on the molecular level, otherwise height differences arising from the sample cannot be distinguished from height differences arising from the substrate. Substrates that meet this condition are highly orientated pyrolytic graphite (HOPG), which is hydrophobic, and mica and hydrophilized silicon wafer (silica), which are both hydrophilic and negatively charged. Supported lipid bilayers are usually deposited on mica, using the Langmuir–Blodgett (LB) [69] method, by vesicle fusion [70] or a combination of these methods [71].

With the LB technique, first, a monolayer is deposited on a hydrophilic substrate by pulling the substrate through a monolayer on the air–water interface on a Langmuir trough. After this, a second monolayer is deposited by lowering the monolayer-coated substrate again through the monolayer on the air–water

interface, but now going from the air into the subphase (Fig. 2). Thus, bilayers on a hydrophilic surface are always exposed to (and imaged in) water. Following the Langmuir–Schäfer (LS) technique, the second leaflet is deposited by lowering the monolayer-coated substrate horizontally through the monolayer on the air–water interface instead of vertically. Stable bilayers are formed when the first monolayer consists of a solid-phase lipid, deposited at high surface pressures (around 40 N/m) [72].

Figure 3 illustrates the process of vesicle fusion where a small amount of vesicle suspension is applied to the substrate. The suspension should contain

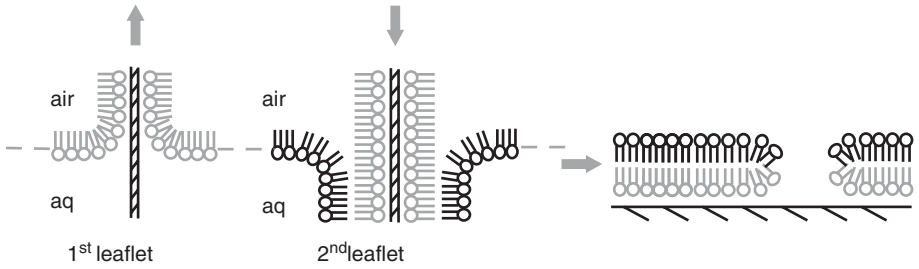

Fig. 2. Bilayer deposition with the LB method [69]. The first leaflet (proximal monolayer) is transferred by pulling a clean hydrophilic substrate through the air–water interface of an aqueous subphase in a Langmuir trough onto which a lipid monolayer (Langmuir layer) is spread. The second leaflet (distal monolayer) is deposited by pushing the substrate coated with the first leaflet, vertically through the air–water interface, going from air in the aqueous subphase. The substrate can also be pushed through the interface horizontally, referred to as the LS method. An asymmetric bilayer can be prepared by using a different lipid-composition for the second leaflet than for the first leaflet.

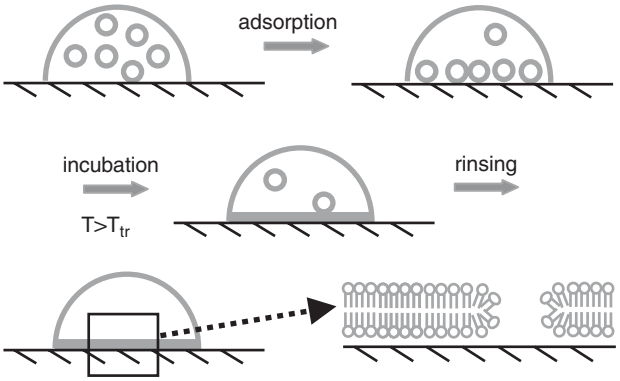

Fig. 3. Bilayer deposition with vesicle fusion. A suspension of ~1 mM unilamellar vesicles (Ø 25–100 nm) is deposited on a clean hydrophilic substrate. After incubation at a temperature higher than the T_m of the highest melting lipid present in the system, the vesicles adsorb to the substrate, open to form a lipid-patch and fuse with other patches until a symmetric, planar-supported bilayer is formed.

small unilamellar vesicles (SUVs) with a diameter of 20–50 nm, although 200 nm vesicles have also been used successfully [73]. These vesicles adsorb to the substrate surface and in an active process, they open and fuse to form a uniform bilayer on the substrate [73–75]. This process is facilitated when the temperature is above the phase-transition temperature of the lipids present in the vesicles. After rinsing excess vesicles, a clean smooth bilayer remains.

2.1.1. Defects and bilayer thickness

Usually in bilayers, defects in the form of holes piercing the entire bilayer are present [71] (Figs. 4 and 5). This means that supported bilayers rarely cover the substrate entirely and thus they are ''leaky''. The width of these defects depends on the sample preparation, but a few hundred nanometers or smaller is not uncommon so they are usually not noticed in studies using FM or other optical imaging techniques. The depth of the defects can be used to confirm that indeed one or more bilayers are present, since in some cases the presence of multiple bilayers is required [76]. Measured values of bilayer thicknesses, as determined with AFM, vary between 4 and 6 nm.The exact depth of the defects gives information on the bilayer thickness and thus on the physical state of the bilayer: bilayers in the fluid phase are generally thinner than bilayers in the solid or in the liquid-ordered phase. This also implies that fluid–solid phase-separation can be visualized by AFM, as is illustrated in Fig. 4C. A prerequisite to use defects to measure bilayer thicknesses is that the defect is wide enough for the tip to unambiguously reach the bottom of the defect (Fig. 4C and D). Another possibility is to use the AFM tip to ''scratch'' a defect in the bilayer by scanning a small area with a high loading force, high speed, and/or prolonged time (few minutes up to an hour). The values found for bilayer thicknesses using AFM are typically 1–2 nm larger than the values found by other techniques like X-ray scattering or NMR (see also Table 1). The consensus is that this is due to a water layer that is present between the support and the bilayer [71].

Although both LB and vesicle fusion yield bilayers with defects, the origin of this defect formation is entirely different for the two preparation methods. In the case of LB, the first monolayer, composed of a solid-phase lipid at high surface pressure, generally contains merely a few small pinholes (Fig. 4A) [54]. During deposition of the second monolayer, lipids of the first leaflet are able to leave the substrate to mix with the monolayer on the trough [77], which gives rise to defects in the eventually formed bilayer. The amount and size of the defects, i.e. the amount of uncovered substrate obviously depends on the number of lipids that move from the first leaflet to the Langmuir layer. This number was found to inversely depend on the speed of deposition of the second monolayer [77] and on the surface pressure [54,72,77] and fluidity [54] of the second monolayer. Qualitatively, it was observed that the lipids that are not orderly packed in the first monolayer, e.g. the lipids at the rim of defects or in grain boundaries, have the

highest probability of leaving the first monolayer [54] and determine the shape of the defects. For example, a monolayer of 1,2-Dipalmitoyl-*sn*-Glycero-3-Phosphocholine (DPPC), at high surface pressure, consists of patches of rigidly packed, tilted lipids. Disordered lipids reside in the grain boundaries between the patches. In monolayers, these boundaries are not detectable with AFM (Fig. 4A). However, after deposition of a second monolayer in the fluid phase, these grain boundaries are visible as defects in the bilayer (see Fig. 4B). Bilayers with a first leaflet of 1,2-Dipalmitoyl-*sn*-Glycero-3-Phosphoethanolamine (DPPE) give rise to round defects [54,72] (Fig. 4E) because the Phosphatidylethanolamine (PE) head groups form a network of hydrogen bonds causing a large line tension energy. Thus, in LB bilayers, the first monolayer seems to determine the shape of the defects, whereas the second monolayer influences the size of the defects.

In bilayers formed by vesicle fusion, composed of lipids in the fluid phase, there are usually only a few small defects present, often induced by contaminations on the substrate. This complete coverage is due to the fluid character of the bilayer, since any hole in the bilayer would immediately be filled with lipid. During the process of making bilayers, composed of lipids in the solid phase, typically these bilayers are heated to well above the phase-transition temperature of the used lipids (Fig. 3). Above their phase-transition temperatures, bilayers are in the fluid phase and presumably cover the whole substrate. When these bilayers are subsequently cooled down, the surface area per lipid decreases and thus there are not enough lipids to cover the substrate. The bilayer ruptures [78], resulting in the presence of defects. However, when there is a supply of lipid during the cooling process, i.e. when the shrinking bilayer is covered with vesicle suspension, the amount of defects is greatly reduced [53].

2.1.2. Bilayer asymmetry and leaflet coupling

With vesicle fusion, symmetric bilayers are formed, which means that both leaflets have the same lipid composition. With the LB method it is possible to make asymmetric bilayers by simply depositing a second leaflet with a different lipid composition than the first leaflet. Since flip-flop in membranes requires proteins and spontaneous flip-flop in lipid bilayers is low [79], it is assumed that this asymmetry is maintained in time. However, due to the molecular organization of the lipids facing the defects, which is presumably as depicted in Figs. 1–3 [54,72,73,80], lipid exchange between both leaflets is possible. It was found that in bilayers with a second leaflet of anionic lipids, around the defects, some of these negatively charged lipids moved to the first leaflet. Since the support of these bilayers was also negatively charged, this lead to electrostatic repulsion between bilayer and substrate, such that the bilayer was locally pushed up (Fig. 4E and F), a phenomena referred to as bilayer blistering [54]. In the presence of divalent cations, the negative charges were screened and the bilayer lay flat on the surface again, a process that was found to be reversible. This

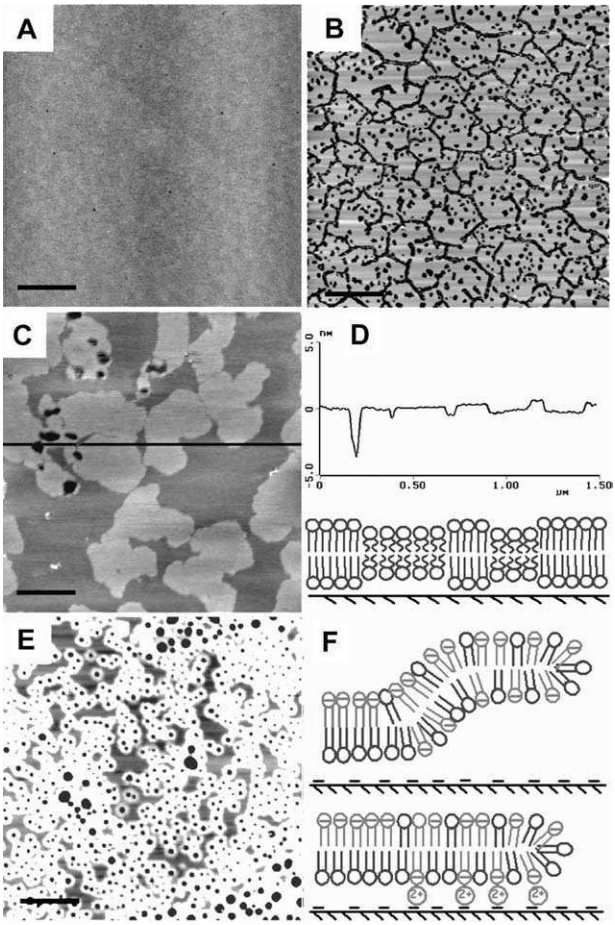

Fig. 4. AFM imaging of several different lipid layers. In all AFM-images conventionally, the *z*-scale is represented by a gray-scale in which black reflects the lowest, and white the highest area. (A) DPPC monolayer, deposited on silicon wafer with LB at a surface pressure of 35 mN/m (condensed phase). A smooth flat layer is seen, with a few pinholes visible as small black dots, reflecting the level of the substrate. (B) Asymmetric bilayer on silicon wafer, with a first leaflet of DPPC, deposited at 35 mN/m (condensed phase) and a second leaflet of DMPG, deposited at 22 mN/m (fluid phase). The (black) hexagonal pattern of defects (6 nm deep) reflects the pattern of the grain boundaries in the first leaflet. (C) Phase-separated bilayer of DPPC and POPC (1:1) deposited with vesicle fusion on mica. Three height levels can be discerned: light gray areas represent solid-phase DPPC domains, surrounded by a lower dark phase of fluid POPC lipids. The black spots reflect defects in the bilayer, marking the level of the underlying mica. (D) Cross-section of the line drawn in (C), showing that although in this case the defects were not wide enough to determine the thickness of the bilayer, the height difference between solid and fluid phase could be determined to be 1 nm.The lower panel shows a molecular model of a phase-separated supported bilayer. (E) LB bilayer on silicon wafer, with a first leaflet of DPPE,

observation is in agreement with the finding that divalent cations favor the vesicle fusion process of vesicles containing anionic lipids [71,81] when using a negatively charged substrate like mica or silica. Depending on the lipid composition of both first and second leaflet, bilayer asymmetry was lost within a few days or even within a few hours [54]. The loss of asymmetry of LB-deposited bilayers is supported by FM studies [24].

Another distinction that can be made between bilayers made by vesicle fusion and bilayers made by LB, is that in the latter the leaflets are not coupled (also referred to as ''not in registration''). This is nicely illustrated in a study of Hollars and Dunn [82], which reports images of bilayers composed of two DPPC monolayers, both phase-separated in liquid expanded (LE) and liquid condensed (LC) domains. AFM images clearly show three height levels, consistent with stacks of LE on LE, LC on LC, and LC on LE (or LE on LC). From different FM studies it was also concluded that LB deposited bilayers are not in registration [24,83].

In phase-separated bilayers made by vesicle fusion, usually two height levels are discerned (Fig. 4C) indicating that the phases of the upper leaflet match with the phases of the lower leaflet and that the leaflets are coupled. Although for certain systems occasionally an intermediate level is observed [21], in general it is assumed that in bilayers prepared with the vesicle fusion method, both leaflets are coupled [40].

2.2. Imaging domains in one-component systems with AFM

In the last decade, much effort has been made to image supported model membranes [41,42]. Single component phospholipid bilayers consisting of Phosphatidylcholine (PC) [53,84–87], PE [66,67], and of polymerizable PC [88] were among the first systems to be imaged by AFM. As mentioned above, these bilayers look flat with some defects, and when the lipids are ordered in a crystalline lattice, molecular resolution can be obtained. Upon treatment of such bilayers, the morphology could be changed dramatically. Fang and Yang [89] found that prolonged heating of DPPC bilayers resulted in lipid loss, visible as an

deposited at 35 mN/m (condensed) and a second leaflet of DPPG, deposited at 26 mN/m (condensed phase). The level of the bilayer (gray) appears 6 nm above the level of the substrate (black). The shape of the defects in this bilayer is round, stemming from the PE lipids in the first leaflet. Around the defects a light ''halo'' is observed, appearing ~2 nm above the level of the bilayer. These elevations are caused by negatively charged DPPG lipids, which diffused from the second leaflet, *via* the edge of the defects, to the first leaflet. Here, they are repelled by the negatively charged silica, which pushes the edges of the bilayer up. In the presence of divalent cations (Ca^{2+}, Mg^{2+}, Ba^{2+}, and Sr^{2+} tested) the entire bilayer lies flat on the substrate [54]. (F) Molecular model for this phenomenon. Scale bars A, B, and E: 2 μm; C: 300 nm.
Panel A, B, E, and F reproduced with permission from Rinia *et al.* [54].

increase in amount and size of defects, and the appearance of lower areas in the bilayer (2 nm lower than the intact bilayer). Such lower areas are generally believed to consist of interdigitated lipids [84,89,90]. Also, interdigitated domains in DPPC bilayers induced by alcohols have been imaged [84].

When single-component bilayers undergo a phase transition, solid–fluid phase-separation occurs and domains are formed. The introduction of the sample heating stage [91] allowed visualization of this process in supported lipid bilayers with AFM in a controlled manner. 1,2-Dimyristoyl-*sn*-glycero-3-Phosphocholine (DMPC) is a convenient lipid for such studies [92] since it has a phase-transition temperature around room temperature (24 °C [79]). This phase transition of a supported DMPC bilayer on mica has been studied recently using AFM [78,93]. In the first study it was found that, upon undergoing a gel- to fluid-phase transition, a single supported DMPC bilayer starts melting at the edge of the defects [93]. Since the lipid packing is more disordered here than in the rigidly packed bulk phase, these lipids are more prone to become fluid. Xie *et al.* [78] observed initially the formation of small nucleation sites in the gel phase from which the fluid phase started to grow, but subsequently melting also started at the defect periphery. They subscribed the nucleating sites also to the presence of small microscopic defects in the gel phase itself. It was found that the phase transition was independent of AFM–tip contact or heating rate, but solely determined by the temperature [93]. Although in one case a slightly lower phase-transition temperature was determined, which was attributed to super cooling [78], in the other study a transition temperature of 28.5 °C was found [93]. This is higher than the 24 °C generally found on DMPC vesicles and the discrepancy is likely to be induced by the substrate, which can influence the phase behavior of lipids [94].

In the above-described studies, where a DMPC bilayer was heated from below its pretransition temperature to well above its main phase-transition temperature, a ripple phase was not seen [78,93]. This has been observed more often when heating single supported bilayers composed of lecithins and other ripple phase forming lipids [89] (unpublished observations) (note that constituents of buffers like Trishydroxymethylaminomethane (Tris) and phosphate buffered saline (PBS), are able to induce ripple phases in single supported bilayers [85,87]. However, ripple phases are often observed in second bilayers, present on top of a bilayer on a solid support [36,76,95,96]. It was postulated that a second bilayer is less influenced by the support and therefore has a more freestanding character than a single supported bilayer [76], which is confirmed by neutron-diffraction studies [97]. This freestanding character allows the bilayer to adopt a rippled structure and to be studied as such with AFM. The growth and disappearance of liquid domains in rippled bilayers of DPPC, going from the ripple to the fluid phase, was investigated thoroughly by Kaasgaard *et al.* [96]. It was found that the domain shape was dominated by the anisotropy in the lipid packing of the ripple phase, leading to straight-edged domains. The phase transition visualized in these systems occurred at 23.4 °C [98]. This temperature is close to the reported

value of 24 °C as found by differential scanning calorimetry (DSC), which implies that a bilayer-supported bilayer indeed has a more freestanding character.

2.3. Imaging domains in binary systems with AFM

One of the first images of fluid–solid phase-separation was taken on DPPC/POPC (1,2-Dioleoyl-*sn*-glycero-3-phosphocholine) bilayers, which showed higher domains, consisting of DPPC in the solid phase surrounded by lower areas, consisting of POPC in the fluid phase [86]. Figure 4C shows an AFM image of such a bilayer, which we prepared using the vesicle fusion method. Defects were seen only in the solid-phase domains and since, besides the level of the mica, only two levels could be discerned, presumably this bilayer is coupled. The difference between these height levels is 1.1 nm, which is in agreement with the difference in bilayer thickness of DPPC (4.8 nm, see Table 1) and POPC (3.7 nm, see Table 1) at room temperature. Later on, more studies on fluid–solid phase-separation at room temperature followed, including DPPC/DOPC (1,2-Dioleoyl-*sn*-Glycero-3-Phosphocholine) [99], DMPC/DSPC [100,101],

Table 1. Acyl chain composition, phase-transition temperatures, and bilayers thicknesses for several phospholipids and sphingolipids

Lipid	Acyl chain composition	T_m (°C)[a] (main)	T_m (°C)[a] (pre)	Bilayer thickness (nm)	Bilayer thickness (nm) (with chol)
DLPC	C12:0/C12:0	−1.9		3.0 (25 °C)[b]	
DMPC	C14:0/C14:0	23.6	13.7	4.2 (20 °C)[b]	
				3.6 (37 °C)[b]	
DPPC	C16:0/C16:0	41.3	34.4	4.7 (20 °C)[b]	
				3.7 (50 °C)[c]	
DSPC	C18:0/C18:0	54.5	49.1	4.7 (25 °C)[b]	
				4.1 (60 °C)[c]	
DAPC	C20:0/C20:0	65.3	63.2		
DOPC	C18:1/C18:1	−18.3		3.7 (30 °C)[b]	
POPC	C16:0/C18:1	−2.5		3.7 (25 °C)[d]	4.1 (25 °C)[d]
Egg-SpM	C16:0/C13:0 (84%)	38[e]			
Brain-SpM	C18:0/C13:0 (46%)	29; 34[f]			
C16:0-SpM	C16:0/C13:0 (100%)	41[g]		5.0 (29 °C)[g]	4.5 (29 °C)[g]
				4.4 (55 °C)[g]	4.5 (55 °C)[g]
C18:0-SpM	C18:0/C13:0 (100%)	45.1[h]		5.2 (29 °C)[h]	4.7 (29 °C)[h]
				4.3 (58 °C)[h]	4.6 (55 °C)[h]

[a] From Ref. [149] unless stated otherwise.
[b] From Ref. [79].
[c] From Ref. [150].
[d] Calculated thickness following Ref. [4]: for the headgroup regions 1.1 nm was added to the hydrophobic thickness as determined by Nezil and Bloom [6].
[e] From Ref. [21].
[f] Brain-SpM is a mixture and was found to have two phase transitions [108].
[g] From Ref. [114].
[h] From Ref. [113].

DLPC/DPPC [102], 1,2-Dilauroyl-*sn*-Glycero-3-Phosphocholine/1,2-Distearoyl-*sn*-Glycero-3-Phosphocholine (DLPC/DSPC) [26], and lately several sphingomyelins (SpM) mixtures with different fluid-phase lipids have been published, the latter in the light of raft formation (see below). These images usually show solid-phase domains, appearing about 1 nm above the level of the surrounding fluid-phase lipids, consistent with the difference in bilayer thickness of a solid- and fluid-phase bilayer.

Apart from fluid–solid phase-separation, also solid–solid phase-separation has been visualized. This can occur in systems of lipids which differ in acyl chain length by four or more carbon atoms. It was found that in the case of gel–gel phase-separation in systems composed of DMPC/DSPC [100,101] or DAPC/DPPC [103], visualization of the phase-separation becomes more difficult, due to the small difference in height (2–5 Å). However, amplification of the height difference is possible by the use of biotinylated lipids, which preferentially, depending on the acyl chain length, participate in one phase. They can subsequently be visualized easily after addition of streptavidin [103], which binds to biotin and, in this study, appears 6–7 nm above the bilayer.

2.3.1. Percolation

In all equimolar phase-separated bilayers made by vesicle fusion imaged so far, the lipids in the solid phase form domains and are surrounded by the fluid phase, i.e. the fluid phase is the percolating phase [21,99,102,104–106]. In systems in which gel–gel phase-separation occurred, the lowest melting lipids formed the percolating phase [103]. A change in percolation point in the fluid–solid coexistence region was visualized directly by heating up a two-component system DMPC/DSPC in the gel phase [93,100]. It was found that first fluid domains appeared (presumably DMPC) surrounded by solid-phase lipid (presumably DSPC). Further heating resulted in the presence of solid domains surrounded by fluid-phase lipid [100]. Eventually all lipids became fluid and thus mixed.

Most fluid–solid phase-separated bilayers studied with AFM are imaged at room temperature and consist of lipids with a T_m well above room temperature and lipids with a T_m well below room temperature. In general during the preparation protocol of the supported bilayer, at some stage the lipids are cooled down from above the T_m of the highest melting lipid. This means that the high T_m lipids have solidified, excluding the fluid-phase lipids, which accordingly form the percolating phase. Upon increasing the concentration of solid-phase lipids, more lipids will be solidified at room temperature and eventually the solid phase forms the percolating phase [26]. This is illustrated by the fact that in a POPC/brain-SpM (1:1) mixture, brain-SpM forms domains [107], while in a POPC/brain-SpM (1:3) mixture, brain-SpM forms the percolating phase [108].

At which lipid ratio the percolating phase changes, is determined by the amount of area occupied by the phases and by the shape of the domains. In the case of

gel-phase irregularly shaped domains, the percolation point should be at an area-fraction of ~0.7 (assuming such domains behave as overlapping disk-shaped structures [109]). This is confirmed by an elegant combined AFM/FM study connecting FRAP measurements (see below) with bilayer morphology. They found that for a DLPC/DSPC system the percolation point lies at 70% area-coverage of the gel-phase lipids [26]. For fluid–liquid ordered phase-separation, which leads to it was determined, using FM images, that the percolation point lies at 50% area [24], which is supported by AFM results [21].

2.4. Imaging domains in ternary systems with AFM

In 1997, Simons and Ikonen [9] published their proposal that plasma membranes of mammalian cells contain small domains, enriched in sphingolipids and cholesterol, which are involved in signal transduction. These domains were baptized "rafts" since they are, with associated signaling proteins, floating around in a sea of fluid-phase lipids. After that many researchers from different fields occupied themselves with finding proof for the existence of rafts in live cells or with investigating the behavior of model systems, containing sphingolipids and cholesterol. Dietrich *et al*. were the first to image rafts in model systems, using fluorescence microscopy [23] and after that came the first AFM images of model-rafts [21]. In the past four years, many papers concerning raft-formation obtained by AFM on several lipid systems have been published. In this paragraph, we give an overview of results concerning ternary mixtures of solid-phase lipids, fluid-phase lipids, and cholesterol in which rafts are expected to form. It is shown that with AFM not only can model-rafts be visualized, it also allows investigation of different raft-related phenomena such as detergent resistance [21], association with GPI-anchored proteins [105,106] and the effect of cholesterol extraction using methyl-β-cyclodextrin (MβCD) [107,110].

2.4.1. Visualizing model-rafts

Several AFM studies show the effect of increasing cholesterol concentration on an equimolar mixture of fluid-phase- and solid-phase lipid. As a fluid-phase lipid, usually DOPC [21,105,106,110] or POPC [107,108] are used, but also results on mixtures with DLPC are available [102]. As a solid-phase lipid, SpM are often used since they are sphingolipids and exhibit a specific affinity for cholesterol [8,20]. The most commonly used SpM in AFM studies is a natural mixture extracted from brain tissue (brain-SpM), which consists for nearly 50% of an SpM-species with C13:0/C18:0 acyl chains. Occasionally, a mixture extracted from egg yolk (egg-SpM) is used, which consists for over 80% of an SpM-species with C13:0/C16:0 acyl chains. Upon addition of increasing amounts of cholesterol to bilayers consisting of SpM and a fluid-phase lipid, the cholesterol will first

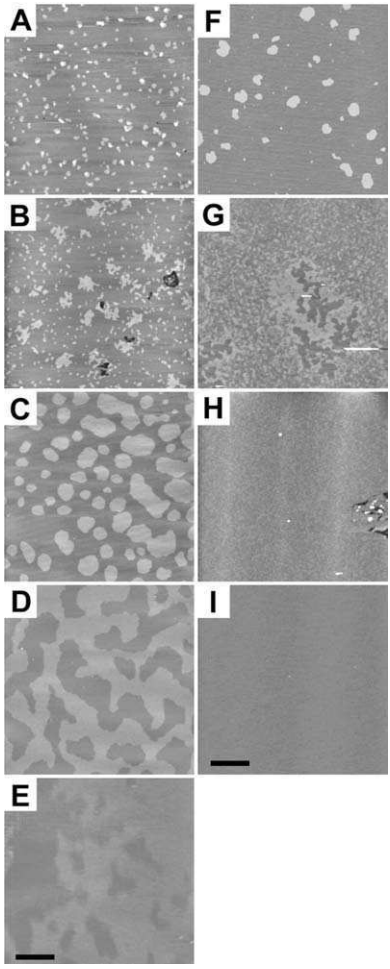

Fig. 5. Model-rafts in bilayers made with vesicle fusion on mica. Bilayers consist of DOPC and ESpM (A–E), or POPC and E-SpM (F–I) with varying amounts of cholesterol. (A) DOPC:SpM (1:1) phase-separate in a fluid phase (dark) surrounding small gel phase domains (light). Domains appear 1 nm above the level of the fluid phase and occupy 20% of the total area. (B) Upon addition of 10 mol% cholesterol, the amount of area occupied by domains increases to 30%, and the height difference is 0.8 nm.(C) Upon increasing the amount of cholesterol to 25 mol%, the domains appear rounder, occupy 40% of the total area and are 0.8 nm above the level of the fluid phase. (D) At 30 mol% cholesterol, the higher phase is now the percolating phase, occupying 60% of the total amount of area, while the height difference is 0.6 nm.(E) At 50 mol% cholesterol, the height difference between both phases is merely 0.4 nm and the amount of occupied area is difficult to determine trustworthy. (F) When changing the unsaturated lipid from DOPC to POPC, the morphology changes markedly. Without cholesterol, solid–fluid phase-separation can be seen, with the level of the solid domains 0.8 nm above the level of the fluid bilayer and the domains occupy 5% of the total area. (G) At 10 mol% cholesterol, the phases are intertwined, it is not clear which

associate with SpM and induce the liquid-ordered phase, and only at higher concentrations, cholesterol will also locate between the fluid-phase lipids [111]. This means that, upon cholesterol addition, first, the solid-phase domains in these bilayers increase in size and/or amount. Furthermore, these domains should decrease in thickness, because although cholesterol has a thickening effect on fluid-phase bilayers of POPC [6], in solid-phase bilayers consisting of SpM, it decreases the bilayer thickness [112–114]. Since we noted some misunderstanding in the literature about the latter effect and because AFM primarily determines height and height differences, we listed some bilayer thicknesses of several lipids in Table 1.

Figure 5 (left panel) illustrates the above-described effect of increasing cholesterol concentration on an egg-SpM/DOPC bilayer. The amount of area occupied by the ordered phase increases from 20 to 30, 40, and 60% with increase of cholesterol concentration from 0 to 10, 25, and 30 mol%, respectively [21]. The height difference between SpM and DOPC in the absence of cholesterol is 1 nm, but at 10 and 25 mol% cholesterol, the difference is 0.8 nm and at 30 mol% it is merely 0.6 nm. At 50 mol% cholesterol, the difference in height decreases to 0.4 nm, most likely because at this concentration, the entire bilayer, i.e. also DOPC, contains cholesterol, which presumably is thickening the DOPC-phase. Note that at 30 mol%, the fluid phase is not continuous anymore and that the system has passed the percolation point. This change in percolating phase is accompanied by an amount of area, occupied by the liquid-ordered phase exceeding 50%. This is in agreement with the analysis that the phase which occupies an amount of area larger than 50% of the total area, forms the percolating phase [24].

Systems with brain-SpM yield similar results in that, upon increase of the cholesterol concentration, the amount of ordered phase increases while the height difference between ordered and disordered phase decreases [105,106]. Also, the size and shape of the cholesterol-containing domains are similar [105,106].

Bilayers of POPC and SPM with increasing amounts of cholesterol show different morphologies [108]. An example is given in Fig. 5 (right panel), which shows clear phase-separation in the absence of cholesterol. Upon addition of cholesterol, the domain shape becomes irregular and both phases become intertwined (Fig. 5G and H). The height difference between the SpM-rich phase and the POPC-rich phase is 0.8 nm at 0% cholesterol, while at 10–25 mol% cholesterol we found it difficult to determine the height difference trustworthy (Fig. 5F and G),

phase is percolating and the amount of occupied area nor the height difference between the two phases could be determined trustworthy. (H) At 20 mol% cholesterol, the bilayer has a grainy appearance and clear phase-separation as with DOPC (C) instead of POPC, is not observed. (I) At 30 mol% cholesterol, the bilayer appears flat and smooth. Scale bars 1 μm. Panels A and E adopted with permission from Rinia *et al.* [21].

but values of 0.3 nm have been reported elsewhere [108]. At 30 mol% cholesterol, no domains can be distinguished anymore (Fig. 5I and [108]). The reason why in raft-forming mixtures POPC leads to such different morphologies compared to DOPC is not clear, but it is interesting to note these differences since usually research is focused on sphingolipid–cholesterol interactions, while the properties of the fluid-phase lipids appear to have a marked influence on the size and shape of the formed domains.

In case of a phase-separated bilayer of DOPC and DPPC, the height difference between solid-phase and fluid-phase lipids (1.1 nm) seems to increase upon addition of cholesterol (unpublished observations). This may be because DPPC looses its tilt in the presence of cholesterol and thus appears higher.

2.4.2. Raft-related phenomena

When live cells are treated with Triton X-100 in the cold (4 °C), there are certain parts of the plasma membrane that are not dissolved [11]. These parts are referred to as detergent-resistant membranes (DRMs) and they were found to be enriched in sphingolipids and GPI-anchored proteins [12]. There is some controversy around DRMs since their composition depends on the used detergent and it is argued that they are generated by the extraction itself [115]. The method, however, is still widely used by different research groups. DRMs are thought to correspond to rafts implying that rafts ought to be detergent resistant. To check whether this was the case for model-rafts, a supported bilayer with a raft-forming composition (egg-SpM:DOPC (1:1) with 25 mol% cholesterol) was cooled down to 4 °C and carefully rinsed with cold Triton X-100. This bilayer was imaged before and after extraction [21] and it showed that indeed the fluid part of the bilayer had been removed while the model-rafts were still present, as can be seen in Fig. 6. The domains were collected and analyzed by thin layer chromatography (TLC) and were found to be enriched in SpM and cholesterol. The domains had slightly increased in size (Fig. 6B), probably due to the cooling, but furthermore they had remained unchanged after the Triton extraction [21]. This does not exclude the possibility that in real cells, phase-separation is induced by the extraction, but it surely means that in supported model systems, rafts or DRMs are not generated by the extraction, but already exist before the treatment and that they remain unaltered by the detergent.

As mentioned above, DRMs are found to be enriched in not only sphingolipids and cholesterol but also in GPI-anchored proteins. Such proteins are linked to one or more acyl chains, mainly unsaturated ones. Consequently, these proteins can associate *via* their acyl chains with lipid bilayers and preferentially with lipids in ordered phases such as the liquid-ordered phase. The preference of such a GPI-anchored protein, alkaline phosphatase (AP) for ordered domains has been visualized using AFM [105,106,116]. It was found that in phase-separated bilayers

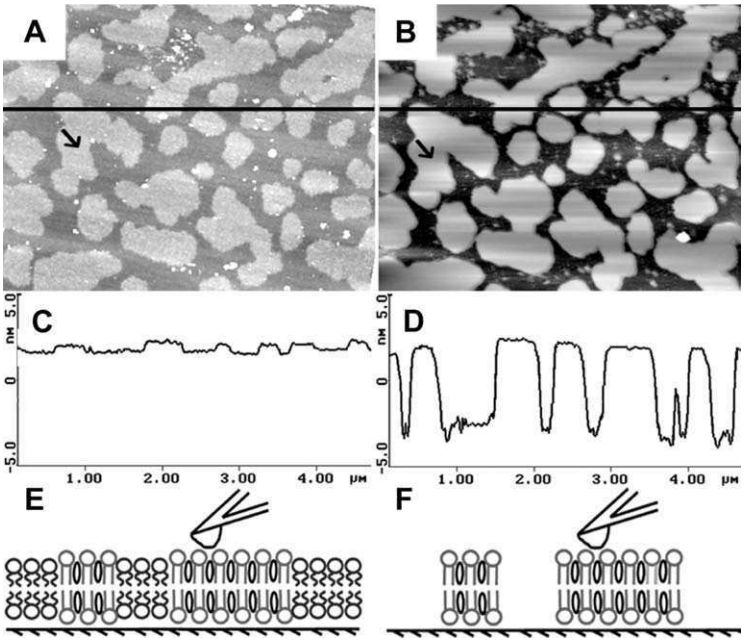

Fig. 6. Detergent resistance of supported model-rafts. (A) Bilayer of DOPC:SpM (1:1) with 25 mol% cholesterol, deposited with vesicle fusion on mica. (B) Same bilayer after rinsing with 0.1% Triton X-100 at 4 °C. The fluid phase is extracted and the domains remained. Using TLC, it was found that the fluid phase was enriched in DOPC and the domains in SpM and cholesterol. (C) Cross-section of the line drawn in A showing that the height difference between domains and fluid phase is ~0.8 nm. (D) Cross-section of the line drawn in B showing that the lower area around the domains is ~5.8 nm lower, thus it corresponds to the mica substrate and that indeed all the fluid-phase lipid has disappeared. (E) Molecular model of the bilayer shown in (A). (F) Molecular model of the bilayer shown in (B). Scale bars 1 μm. Adopted with permission from Rinia *et al.* [21].

of DOPC and brain-SpM (1:1) in the absence of cholesterol, AP spontaneously inserted in the bilayer, but mainly at the edges [105] and rarely in the bulk [105,106] of the SpM domains (Fig. 7B). In the presence of cholesterol, AP again spontaneously inserted in the bilayer, but now it was found to be homogeneously distributed all over the raft-phase (Fig. 7D [105]). These results confirm the assumption that GPI-anchored proteins associate with ordered-phase bilayers, preferentially with liquid-ordered phase bilayers.

MβCD can be used to both extract cholesterol from- and to deliver cholesterol to cell membranes or model membranes [117,118]. This biochemical tool was used to directly follow the changes in morphology of supported bilayers upon addition of- or depletion from cholesterol [107,110]. In Fig. 8, this process is shown in the case of a brain-SpM/DOPC bilayer to which cholesterol-loaded MβCD is added. In time it can be seen that the brain-SpM domains grow due to

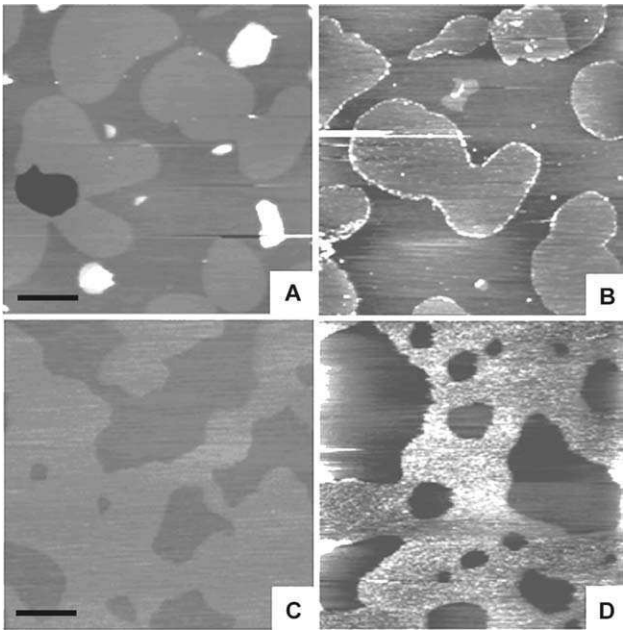

Fig. 7. Preference of AP, a GPI-anchored protein, for the liquid-ordered phase. (A) A phase-separated bilayer of DOPC and brain-SpM (1:1). (B) Upon addition of AP in the aqueous phase above the bilayer, insertion is observed mainly at the edges of the gel-phase domains. (C) Phase-separated bilayer of DOPC and brain-SpM (1:1) with 15 mol% cholesterol in which the liquid-ordered phase is percolating. (D) Same bilayer in the presence of AP showing that the liquid-ordered phase is packed with inserted protein. In both bilayers, insertion in the fluid phase is rarely observed. Scale bars 2 μm. Adopted with permission from Milhiet *et al.* [105].

cholesterol incorporation, they coalesce and become the percolating phase until all domains disappear and the bilayer becomes featureless, presumably because it is saturated with cholesterol. This process is reversible [107,110], in that upon extracting cholesterol from a saturated bilayer, domains appear, which become smaller in size. However, when the extraction is completed, the phase-separated situation in the binary bilayers is not restored: the bilayer become featureless again [107,110]. It is not exactly clear why this is the case. Possibly, SpM is also extracted from the bilayer. Giocondi *et al.* [107] found that in the presence of MβCD, SpM was indeed extracted from a brain-SpM/DOPC bilayer, leaving holes in the bilayer. Lawrence and co-workers [110] however found in similar experiments that in the presence of MβCD, brain-SpM/DOPC bilayers stayed intact and SpM-domains remained unaltered. Futhermore, no formation of defects were observed upon cholesterol extraction. Thus, a more likely possibility is that, after cholesterol extraction, the SpM-molecules are still distributed in the fluid phase and the system needs time to phase-separate [107,110].

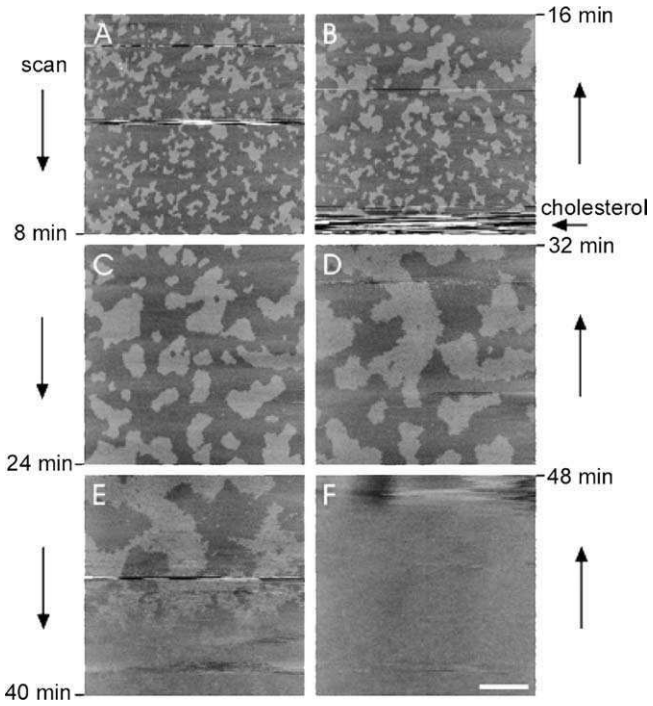

Fig. 8. Addition of cholesterol to a supported bilayer using MβCD. (A) Bilayer of DOPC and brain-SpM (1:1) showing solid–fluid phase-separation. This bilayer was deposited on mica with vesicle fusion. Upon addition of cholesterol-loaded MβCD in the aqueous subphase above the bilayer (bottom of image (B)), cholesterol is inserted in the bilayer. The domains grow and coalesce in time (B–E) until the bilayer appears flat and no phase-separation is observed (E–F). The scan-direction is denoted next to each frame together with the elapsed time. Scale bar 1 μm. Adopted with permission from Lawrence *et al.* [110].

The experiments concerning raft-related events illustrate that although supported bilayers are adsorbed to- and influenced by a substrate, they still undergo the above-mentioned processes as if they were cell membranes. This renders them trustworthy as clean model systems useful to quantitatively investigate biological phenomena related to live cell membranes.

3. FLUORESCENCE MICROSCOPY

With FM, a sample is exposed to the light of a selected wavelength (excitation light), which is absorbed by fluorochromes present in the sample and the subsequent emitted light is collected. The emitted light is separated from the excitation light using a dichroic mirror. The principle of FM is schematically drawn in Fig. 9, where in (A) the path of the excitation light is depicted and in (B) the path of

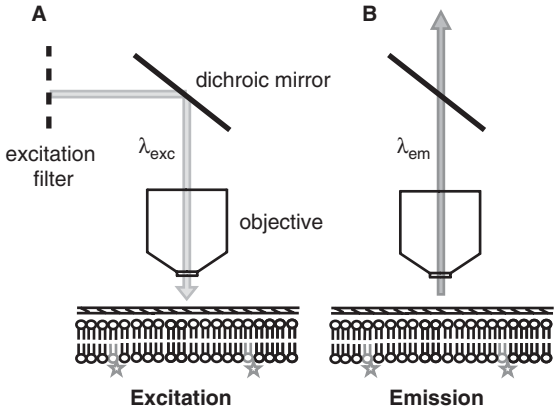

Fig. 9. Principle of FM. The sample, here a supported bilayer with fluorophores in the distal leaflet, is illuminated by the excitation-light coming in *via* a dichroic mirror through the objective. Light that is subsequently emitted by the excited fluorophores goes through the objective, passes the dichroic mirror and can be recorded by a CCD camera.

the emitted light. The lateral resolution R is determined by the wavelength of the emitted light and the numerical aperture (NA) of the used objective, *via* equation (1):

$$R = \frac{0.6 \cdot \lambda}{NA} \tag{1}$$

The wavelength of the emitted light of generally used fluorochromes such as Texas Red, NBD, Fluoresceine, and Rhodamine lies between 500 and 600 nm, so for a high NA objective, the lateral resolution of FM is roughly 200–250 nm. For research concerning lateral segregation in membranes this means that domains larger than 250 nm can in principle be resolved. More advanced optical techniques, like scanning near-field optical microscopy (SNOM) can detect domains on smaller scales, typically 50–100 nm [82].

The fluorochromes in the sample can be intrinsically present in the sample, in which case the fluorescence process is referred to as auto-fluorescence, or added to the sample, in which case the process is referred to as secondary fluorescence. FM on model membranes always deals with secondary fluorescence and the added fluorophores or fluorescent probes are usually lipids onto which a fluorochrome is attached [22–24,44,83,119]. Apart from fluorescent–lipid analogs, also hydrophobic organic dyes can be used or fluorescent ligands, binding to a specific lipid. A well-known example of the latter is the combination of fluorescently labeled cholera toxin B, which strongly binds to GM1, a glycosphingolipid and thus a raft-marker [120–122].

The properties of the probe, like the position where the fluorescent group is attached, or the acyl chains and headgroup of the lipid, determine whether the

probe preferentially mixes with solid-, fluid-, or liquid–ordered phase lipids. This is important since the contrast in FM is based on the partitioning of the fluorophore(s). In general, due to the bulky fluorescent group, fluorophores prefer to be situated in the fluid phase. However, there are exceptions to this rule, for example, DPEE with a nitrobenzoxadiazolyl (NBD) group attached to the PE headgroup (NBD-DPPE), which preferentially partitions in ordered phases [23,24]. Thus, it is not always straightforward to predict in which phase a fluorescent probe will partition or how it will distribute over different phases (see also below).

3.1. Diffusion in bilayers

Apart from imaging, FM can also be used to quantify the diffusion of fluorophores in a sample by intentionally bleaching a part of the sample with very high light intensity. Subsequently, fluorescent probes from outside the bleached area will diffuse into the bleached spot, thus the fluorescence in this spot is partially restored. This is called fluorescence photobleaching recovery (FPR) or FRAP [123,124]. By following the fluorescence recovery in time, one can determine the lateral mobility in a membrane. Diffusion coefficients of fluorescently labeled lipids in fluid-phase bilayers, deposited on glass or quartz, as determined with FRAP, varies between 1 and 5 $\mu m^2/s$ [24,125,126]. This is comparable to values found on similar systems with other techniques [23,126]. Diffusion coefficients measured on supported systems are usually lower than the values determined on freestanding or multilayered systems ($\sim$6 $\mu m^2/s$ for fluid-phase bilayers and 0.4–2.5 $\mu m^2/s$ for liquid–ordered phase bilayers [125,127]). Apparently, the substrate has a restricting influence on the bilayer. Initially it was found that the diffusion in both leaflets is essentially the same [125], but it has also been reported that diffusion in the proximal leaflet (facing the substrate) is twice as low as in the distal leaflet (facing the aqueous phase) [128]. With FRAP experiments on both supported model systems and live cell membranes, usually less than 100% fluorescence is recovered, suggesting the presence of an immobile fraction [27,28,125]. Such a fraction can stem from obstacles present in the bilayer, photobleaching of the returning fluorophores or from immobilization due to the cytoskeleton or due to inhomogeneities in the substrate surface [24,26].

3.2. Imaging domains in supported bilayers with FM

There is a substantial amount of published papers dealing with phase-separation in lipid layers, studied with FM. A large part comprises supported monolayers [129–134] complemented by studies concerning giant unilamellar vesicles (GUVs) [22,43–45,135]. In this chapter, we confine ourselves to supported and unsupported planar bilayers, but the results reviewed in this section will be

analyzed and discussed using the information from the literature on other lipid systems.

McKiernan *et al.* [136] investigated the morphology of mica-supported single component bilayers made by vesicle fusion, of cationic phospholipids, with either two saturated C_{14} acyl chains [1,2-Dimyristoyl-3-trimethylammonium Propane (DMTAP)] or C_{16} acyl chains [1,2-Dipalmitoyl-3-trimethylammonium-Propane (DPTAP)]. These lipids were found to form distinguished domains exhibiting fractal- and feathery patterns, after they had been cooled from above, to below their phase-transition temperature. The authors investigated the influence of various parameters on the domain size and shape, like the effect of the support or the cooling rate, and their findings should be generally applicable to domain formation in supported lipid bilayers. The fluorescent probe that was used in this study, NBD-PC, which contains the fluorochrome in one of the acyl chains, was excluded from the domains. By using FRAP it was found that the mobility of the lipids in the probe-containing phase was very low. AFM imaging showed that this phase had a thickness of 4 nm and that the probe-excluding domains were 1.4 nm thicker. It was concluded that both phases were ordered and the difference in thickness stemmed from differences in tilt [136]. Bilayers of DPTAP on glass gave the same results as for such bilayers on mica, except that the domains were somewhat larger, which was attributed to a slightly higher surface charge of glass compared to mica, at the used pH. The amount of probe had an evident effect on the shape of the domains, showing more fractalic growth at higher probe concentrations. Decreasing the cooling rate from 2 to 0.2 °C/min resulted in an increase of the size of the domains. These results indicate that domain sizes and shapes in supported lipid bilayers are markedly influenced by the probe, the substrate –properties, and the cooling rate used in the preparation method.

A few years after the raft hypothesis had been formulated, the first studies concerning the visualization of ‘‘model-rafts’’ in bilayers using fluorescence appeared [23,137]. Dietrich *et al.* [23] published a thorough study on GUVs and fluorescently labeled monolayers deposited on either silanized glass or on a monolayer of egg-PC. Concerning the supported lipid layers they found that indeed a mixture of a fluid-phase lipid (POPC) and cholesterol yielded featureless images, while in a mixed layer of POPC, brain-SpM and cholesterol (2:1:1) domains were formed. These domains excluded the used probe (0.5% Fl-DPPE) while the raft-marker GM1 preferentially partitioned in them, as was visualized by the use of fluorescently labeled cholera toxin. Furthermore, they were found to be detergent resistant and thus it was assumed that such domains are in the liquid-ordered phase. Also in monolayers of a natural lipid mixture, a lipid extract from brush border membranes, domains were present. Single particle tracking indicates that the diffusion constant of lipids in the continuous, fluid phase was 2–3 times higher than in the liquid-ordered domains. This is in agreement with values measured in unsupported systems [127].

Samsonov *et al.* [137] investigated black lipid membranes of raft-forming compositions using FM. They used a 2:1 mixture of DOPC and DOPE to form the fluid phase and a 1:1 mixture of cholesterol and egg-SpM to form the liquid-ordered phase, with a rather high concentration of fluorescent probe: 5 mol% Rho-DOPE. Above 30 mol% Chol + SpM, round domains were observed, which excluded the probe. GM1 with a fluorochrome, BODIPY, attached to its headgroup was found to preferentially participate in these domains, indicating that these domains were ordered. The use of this GM1 is particularly elegant since it omits the need for (fluorescently labeled) cholera toxin B, which, due to its multiple binding sites, by itself is able to cluster GM1 lipids and to induce phase-separation [138]. Upon oxidizing the cholesterol in a domain, by locally applying cholesterol oxidase, the domain disappeared. Additionally, it was shown that domains were more susceptible to a force along the bilayer, which was applied by stirring the adjacent solutions. Hence it was concluded that the domains protrude from the bilayer, i.e. are thicker than the surrounding phase, which is in agreement with AFM measurements. Also, the bilayers were coupled, as was deduced from the absence of intermediate fluorescence intensities in the images.

When dealing with liquid–liquid phase-separations, as in raft studies, the exact partitioning of the used probe becomes prominent, since this generates the contract in fluorescence images. The used fluorescent probe has a distinct effect on the morphology of phase-separated layers [24], which is illustrated in a study of Crane and Tamm (see Fig. 10). These systems consist of bilayers of a mixture of a fluid PC and brain-SpM (1:1) with various amounts of cholesterol. They were deposited with the LS method and the second monolayer contained 0.5–1 mol% probe. Most probes prefer the disordered phase (Rho-DOPE, NBD-DOPE, $DiIC_{12}$, $DiIC_{18}$, TR-DPPE, and FL-DPPE [23,24,83,137], but NBD-DPPE participated in the ordered phase [23,24]. The most striking effect of the probe is in the presence of 50 mol% cholesterol, where with Rh-DOPE, NBD-DOPE, and $DiIC_{12}$ domains are visible, while NBD-DPPE and $DiIC_{18}$ are evenly distributed over both phases since bilayers with these probes look uniform. Another notable feature is that in some cases, not only the domains in the second (stained) leaflet were visible, but also domains in the first monolayer could be seen, even though this layer was unstained when deposited. This phenomenon has also been observed in a recent study on LB deposited bilayers concerning model-rafts [83] and is attributed to probe-molecules, which moved to the first leaflet [24,83]. As stated above, in LB and LS deposited bilayers, lipid exchange between the first and second monolayer can occur during deposition of the second leaflet and afterward *via* the connections between both leaflets due to the presence of defects [54,77]. The defects, which make the exchange possible, are too small to be resolved with FM and therefore remain unnoticed. In AFM studies, they are found to be always present and thus, logically, they also exist in similarly deposited bilayers, but imaged with FM. We want to emphasize that we believe that the exchange is not caused by spontaneous flip-flop, since this is a slow process (hours to days [79]).

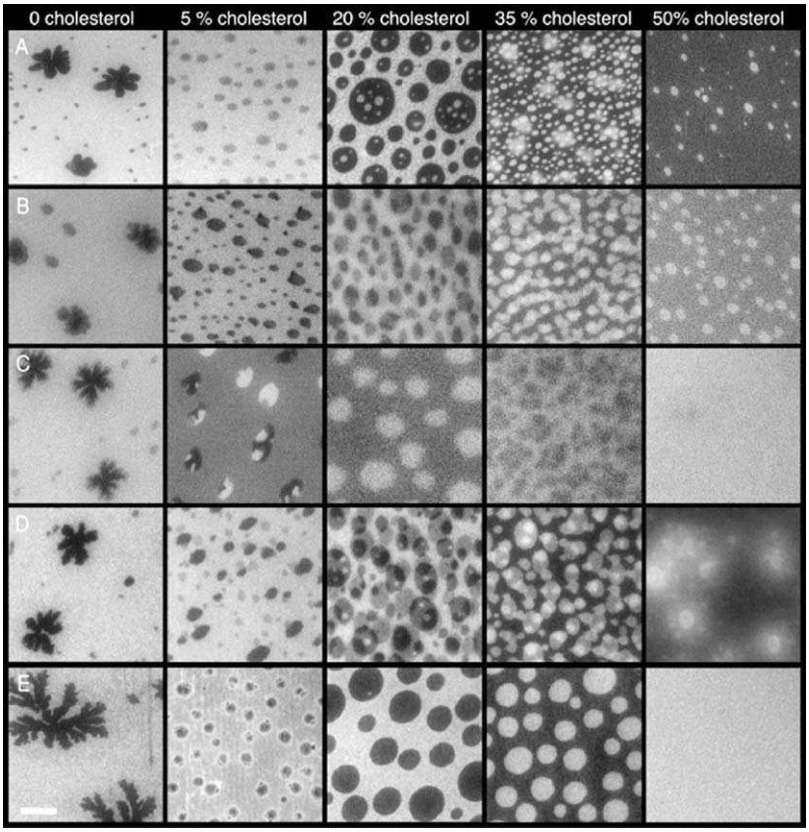

Fig. 10. Influence of fluorescent probes on the morphology of supported bilayers. Bilayers consist of brain-PC and brain-SpM (1:1) with increasing amounts of cholesterol and were deposited with the LS technique on quartz. The second leaflet was stained with (A) 0.5 mol% Rho-DOPE, (B) 1 mol% NBD-DOPE, (C) 1 mol% NBD-DPPE, (D) 0.5 mol% $DiIC_{12}$, and (E) 0.5 mol% $DiIC_{18}$. Although only the second leaflet was stained, in several cases (middle panels in (B) and (D)) probe also appears in the first monolayer and reveals the domains in that leaflet. This illustrates that diffusion between both leaflets is possible and that an asymmetric lipid composition in supported bilayers cannot be maintained for prolonged times. Also, the domains in both leaflets are not aligned and thus the monolayers are not coupled. Scale bar 10 μm. Adopted with permission from Crane and Tamm [24].

Generally, in bilayers deposited by vesicle fusion (see above) or in freestanding bilayers [22,137], the leaflets are coupled. In these systems, the domains start to form when the lipids are organized as a bilayer. In the case of LB bilayer, domains are formed in the monolayer on the trough, before they are deposited to form a bilayer. Such a system would be far away from thermodynamic equilibrium and there is no reason to assume that two of such separate leaflets would be coupled. In the next section, the dynamics of supported bilayers is considered.

3.2.1. Dynamics in supported bilayers: influence of support

The size of the domains in and within all studies discussed so far varied between 10 nm and 10 μm. What exactly determines the size of domains in these systems is still not entirely clear, but they are distinctly influenced by the preparation method. It is clear that bilayers deposited with LB or LS contain large domains (μm-range), whereas vesicle fusion yields bilayers with domains as small as 10–100 nm. Furthermore, with vesicle fusion, the domains-size is influenced by the cooling rate during the preparation: quenching yields smaller domains, while cooling slowly yields larger domains [26,136]. Although supported bilayers are quite stable in time [26,125], after prolonged time domains indeed change in size [99] and slowly coalesce (Fig. 11). We assume that freshly prepared supported bilayers have not reached their equilibrium yet. For bilayers made with LB or LS this means that the bilayers are asymmetric and not coupled. For bilayers made with vesicle fusion this means that possibly the domains have not reached their full-size yet.

In freestanding lipid layers like GUVs or Langmuir layers, with similar lipid compositions, domains are large and in the case of GUVs, it is observed that equilibrium is reached very rapidly (seconds to minutes) [22]. Supported systems equilibrate very slowly (hours or days, Fig. 11). However, lipid diffusion in supported bilayers is reduced with merely a factor 3 or so, and FRAP experiments showed that fluorescence was recovered also in isolated domains in the middle of the bleached spot [23,83]. This indicates that the lipids themselves are mobile and that lipid exchange between different phases is rather rapid. The domains on the contrary appear to be immobile entities. It was suggested that domains in supported bilayers are immobilized by inhomogeneities in the underlying glass, such as strong contact sites or spikes, acting as pinning centers [23,83,139].

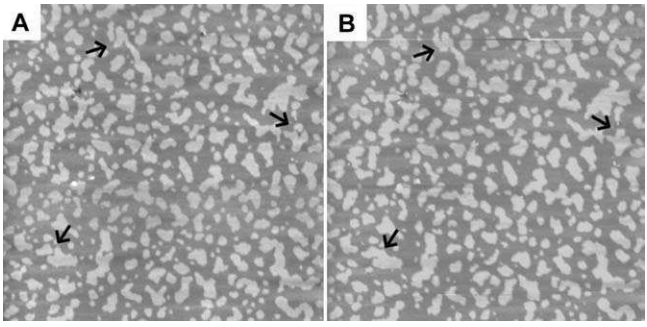

Fig. 11. Immobility of domains in a fluid–liquid ordered phase-separated bilayer. (A) AFM image of a bilayer consisting of egg-SpM and DOPC (1:1) with 25% cholesterol, deposited on mica with vesicle fusion. (B) Same bilayer 2.5 h later. Only a few domains have merged, indicated with arrows in the image, but overall the morphology has remained the same. Image size 7.5 μm.

Relaxation of supported systems may be speeded up by heating the bilayer. This was done by Stottrup *et al.* [83], with a phase-separated LB/LS-deposited bilayer, composed of DOPC, brain-SpM, and cholesterol (1:1:1). They found that upon heating, the domains disappeared and one uniform phase was formed. After cooling, however no domain formation was observed, but it was found that ''speckles'' appeared [83] which could correspond to small domains.

Although the morphology of bilayers, deposited with vesicle fusion, indicates that they are coupled, a recent study reveals that both leaflets have their own phase-transition temperature. In a phase-separated bilayer of DPPC and a fluid-phase lipid, DPPC in the distal leaflet was in the fluid phase at about 40 °C, while the DPPC in the proximal leaflet was still solid and did not melt until around 50 °C [140]. This indicates that the substrate and the first leaflet are very strongly coupled. Although it was found that in the presence of salt this coupling is much weaker, it is still important to realize that the substrate can have a marked influence on the phase behavior and thus on the morphology of supported bilayers.

4. COHERENT ANTI-STOKES RAMAN SCATTERING (CARS) MICROSCOPY

Vibrational spectroscopic techniques have the potential to directly address molecular properties of supported bilayers. Vibrational spectroscopy probes the intra- and intermolecular vibrational structure of molecules and molecular assemblies. It can provide detailed information on both the chemistry and physics of the sample, with a remarkable specificity even at room temperature and in samples as complex as whole cells [141]. Traditionally, spontaneous Raman scattering and infrared (IR) absorption have been used to determine vibrational spectra. IR absorption however does not lend itself for high resolution microscopy because of the long wavelengths involved. Also, water absorption in this wavelength region can be a serious problem. On the other hand, the generally very weak signal from spontaneous Raman scattering, due to its extremely small scattering cross-section, is readily overwhelmed by natural luminescence or requires acquisition times, which often are prohibitive for high resolution microscopic imaging.

CARS is the non-linear optical analogue of spontaneous Raman scattering. While amplifying the Raman signal by many orders of magnitude and enhancing the detectability of the signal against background luminescence, it retains the unique spectral specificity of Raman scattering. The Raman spectrum can provide a molecular ''fingerprint'' even at room temperature and in complex environments such as living cells. In addition, it is sensitive to intermolecular interactions. Recent developments in laser technology have permitted introduction of this well-known non-linear spectroscopic technique into the field of high resolution microscopy [142,143]. In addition to the significant Raman signal enhancement, there are a number of features that make CARS especially suitable

to incorporate vibrational spectroscopy into high resolution microscopy. Near-IR wavelengths can be used that ensure submicron optical resolution and minimal sample heating and damage. The non-linear dependence of the CARS signal to input laser intensity provides inherent optical sectioning capability (similar to that of two-photon absorption fluorescence microscopy). Finally, the signal propagates coherently and is of shorter wavelength than all the input fields making it readily detectable.

CARS is a third-order non-linear optical process where three laser fields, denoted by *pump*, *Stokes*, and *probe* with frequencies ω_{pu}, ω_s and ω_{pr}, respectively, are mixed in the sample to generate an *anti-Stokes* signal at frequency $\omega_{as} = \omega_{pu} - \omega_s + \omega_{pr}$. The induced third-order polarization, for a unique and linear polarization direction, can generally be written as

$$P^{(3)}(\omega_{as}) \propto N \cdot E_{pu}(\omega_{pu}) E_s^*(\omega_s) E_{pr}(\omega_{pr}) \chi^{(3)}_{1111}(-\omega_{as}; \omega_{pr}, -\omega_s, \omega_{pu}) \tag{2}$$

where $\chi^{(3)}_{1111}(-\omega_{as}; \omega_{pr}, -\omega_s, \omega_{pu})$ is the third-order susceptibility, N the molarity (number of moles per unit volume), and $E_i(\omega_i)$ denotes the respective electric field. In the most common arrangement all laser field are narrow band ($\sim 5\,\mathrm{cm}^{-1}$) and the generated CARS signal consequently represents a single point in the vibrational spectrum. Additional frequency tuning of one of the lasers is required to acquire the full CARS spectrum. Alternatively, the *Stokes* laser can be made broad band ($> 100\,\mathrm{cm}^{-1}$), in which case the so-called multiplex CARS spectrum is generated concurrently over a significant part of the vibrational spectrum [46].

Far away from one-photon resonances, the non-linear susceptibility can in general be written as a sum of two terms:

$$\chi^{(3)}_{1111}(\omega) = \chi_{NR} + \chi_R(\omega) \tag{3}$$

where the non-resonant term (χ_{NR}) is independent of frequency and real, while the resonant term ($\chi_R(\omega_{as}) = \sum_j R_j/(\omega_{as} - \omega_{pu} - \Omega_j - i\Gamma_j)$) is a complex sum over all involved vibrational resonances with eigenfrequency Ω_j, oscillator strength R_j, and linewidth Γ_j. In practice, *pump* and *probe* are usually derived from the same laser and most CARS microscopy configurations employ point-by-point signal acquisition using either specimen or laser beam scanning. It follows from equations (2) and (3) that the CARS signal intensity is propotional to

$$I_{CARS} \propto I_{pu} I_s I_{pr} \cdot |\chi_{NR} + \chi_R|^2 \tag{4}$$

Thus the signal is a sum of a purely non-resonant contribution, a purely resonant contribution and a cross-product between the two. The latter is responsible for the characteristic dispersive lineshape of CARS spectra. Various approaches have been developed to eliminate the non-resonant contribution from the signal (see e.g. [144]). Alternatively, the non-resonant background is used in multiplex CARS experiments to increase the sensitivity in a heterodyne fashion [145].

4.1. Measurement of acyl chain ordering in supported bilayers

CARS microscopy is a rapidly growing new microscopic technique, which can be used in biology and biophysics as well as the material sciences. In the following, the potential of technique in providing detailed molecular information in supported lipid bilayers is illustrated. For other applications, the reader is referred to a recent review of the field [144].

Both the CH-stretch and CC-stretch vibrational spectral regions are rich in information on lipid acyl chain order (in particular, the amount *trans-gauche* kinks and long-range intermolecular coupling) [146]. For instance, lipid phase-transition temperatures can be readily determined by recording Raman spectral parameters as a function of temperature. Whereas it is extremely difficult to obtain spontaneous Raman signals from a single lipid bilayer, vibrational spectra with unprecedented signal-to-noise have been recorded using multiplex CARS microscopy [47].

An example of this is shown in Fig. 12A, which shows CARS spectra of a single lipid bilayer in the liquid crystalline (lower trace) and gel phase (upper trace), respectively. From these spectra the lipid chain order, defined as the ratio of the signal intensity from the anti-symmetric and symmetric methylene stretching modes, respectively, can be determined to increase from 0.74 ± 0.08 in the fluid phase to 0.99 ± 0.09 in the gel phase. For multilamellar systems, a lower lipid chain order parameter was found: 0.69 ± 0.03 and 0.79 ± 0.04 for fluid and gel phase, respectively. This means that the supported bilayers are more ordered, presumably due to coupling with the substrate. The above demonstrates the

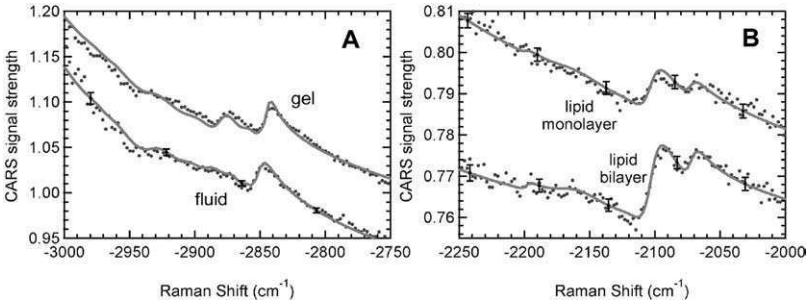

Fig. 12. (A) Multiplex CARS signal from a fluid phase bilayer (DOPC; lower curve) and a gel phase bilayer (DPPC; upper curve). Even though only one lipid bilayer is present, the difference in phase can be clearly deduced from the spectra. (B) Multiplex CARS signal from a lipid bilayer of deuterated DPPC (lower curve) and of a bilayer of which only the first monolayer consisted of deuterated DPPC and the second of DPPC, not contributing to the shown signal (upper curve). The signal of the bilayer (1.6) is exactly twice as high as the signal from the monolayer (0.8), indicating that at these low lipid concentrations, the strength of the multiplex CARS signal depends linearly on the lipid concentration. Adopted with permission from Wurpel *et al.* [47]

unique ability of non-linear vibrational spectroscopy to determine the phase of the lipid bilayer from inherent molecular parameters.

Another important feature of multiplex CARS microscopy is that since all spectral channels are recorded simultaneously, the resonant contribution can be determined quantitatively against the non-resonant background. This is demonstrated in Fig. 12B, where the signal from a lipid bilayer shows a signal strength, which is exactly twice that of a lipid monolayer. More recently, polarization techniques have been used to determine absolute lipid density and lipid chain orientational disorder in multilamellar vesicles and influence of cholesterol partitioning [147].

The continuing development of ultrashort laser pulse technology allows the application of a whole range of non-linear optical spectroscopic techniques to microscopy of biological or biomimetic systems. The strength of these techniques is the fact that they can provide direct detailed chemical and physical information of the sample by using the inherent molecular properties. Thus, they can provide complementary information to that which can be derived from more traditional techniques such as AFM and FM. Of particular interest to lipid bilayers is the recent application of sum-frequency generation (SFG) to biomimetic systems [148]. This second-order non-linear optical technique is particularly sensitive to surface and interfaces and thus highly suited to investigate the special properties of asymmetric bilayers, which are the rule in natural membranes. In addition, it has similar vibrational specificity as CARS microscopy. As illustrated by the examples above, the field of non-linear optical microscopy has only just started to flourish and is expected to come to full fruition over the years to come.

5. CONCLUSION

Supported lipid bilayers are suitable systems to visualize domain formation in model membranes. Because they are planar, a large area of bilayer is in focus at once so there is no need for 3-D imaging like with GUVs. They can be routinely deposited on mica or glass, which are commonly used substrates for AFM and optical microscopy, respectively. One leaflet is exposed to bulk-water, so exogenous components (e.g. proteins, detergents, or agents) can easily be added and interaction with the bilayer can be visualized directly. The phase transition in supported bilayers is retained and the lateral diffusion in supported bilayers is merely a few times lower than in freestanding bilayers. The diffusion coefficients in different phases in supported systems relate in the same way as diffusion coefficients in unsupported systems.

Despite these arguments in favor of supported systems, there are also several drawbacks to the use of supported bilayers. Supported bilayers do not form sealed systems: they contain defects and therefore are leaky. Moreover, the presence of defects allows lipid exchange between proximal and distal leaflet of

the bilayer and thus in time, bilayers loose their possible asymmetric composition. As is the case with freestanding bilayers, bilayers deposited with vesicle fusion are coupled. However with LB or LS, two independent monolayers are deposited on each other and these layers are not coupled.

The influence of the support appears to be quite substantial. The acyl chains in supported bilayers are more ordered than the acyl chains of multilamellar systems and although phase transitions are retained in supported bilayers, the transition is considerably broadened. In certain cases each monolayer undergoes its transition separately, with up to 10 °C difference in phase-transition temperature [140]. Additionally, differences in diffusion coefficients have been found for both leaflets [128]. In spite of the fact that the lateral mobility in supported bilayers is only a few times lower than in freestanding systems, domains behave as immobile entities on the support. The size of the domains depends on the deposition technique. In LB or LS deposited bilayers, the domains are initially formed in a freestanding monolayer and these domains are larger than found in bilayers made with vesicle fusion, although in the latter systems, domain size can be tuned by the cooling rate in the vesicle fusion protocol [26]. In freestanding systems, domains coalesce rapidly in time (seconds–minutes) and can quickly become up to micrometers in size. In supported systems, domains coalesce slowly in time (hours–days), and therefore essentially remain in the same size. The immobility of domains has been ascribed to inhomogeneities on the substrate surface, like spikes acting as pinning centers. However, since domains are equally immobile on an atomically flat surface as mica, other factors have to be involved. Possibly local differences in surface charge densities play a role, but what exactly causes the paralysis of domains on the substrate remains to be elucidated.

It is important that researchers realize the described drawbacks of supported bilayers when working with them. The use of supported membranes remains advantageous and especially when one takes their shortcomings in account, supported bilayers are excellent model systems to work with and to use as model membranes.

REFERENCES

[1] S.J. Singer, G.L. Nicolson, The fluid mosaic model of the structure of cell membranes, Science 175 (1972) 720–731.
[2] O. Mouritsen, M. Bloom, Mattress model of lipid–protein interactions in membranes, Biophys. J. 46 (1984) 141–153.
[3] J.A. Killian, Hydrophobic mismatch between proteins and lipids in membranes, BBA-rev. biomembranes 1376 (1998) 401–416.
[4] F. Dumas, M.C. Lebrun, J.F. Tocanne, Is the protein/lipid hydrophobic matching principle relevant to membrane organization and functions? FEBS Lett. 458 (1999) 271–277.
[5] S. Munro, An investigation of the role of transmembrane domains in golgi protein retention, EMBO J. 14 (1995) 4695–4704.

[6] F. Nezil, M. Bloom, Combined influence of cholesterol and synthetic amphiphillic peptides upon bilayer thickness in model membranes, Biophys. J. 61 (1992) 1176–1183.
[7] J.P. Slotte, Sphingomyelin–cholesterol interactions in biological and model membranes, Chem. Phys. Lipids 102 (1999) 13–27.
[8] M.B. Sankaram, T.E. Thompson, Interaction of cholesterol with various glycerophospholipids and sphingomyelin, Biochemistry 29 (1990) 10670–10675.
[9] K. Simons, E. Ikonen, Functional rafts in cell membranes, Nature 387 (1997) 569–572.
[10] J.H. Ipsen, G. Karlstrom, O.G. Mouritsen, H. Wennerstrom, M.J. Zuckermann, Phase equilibria in the phosphatidylcholine-cholesterol system, Biochim. Biophys. Acta 905 (1987) 162–172.
[11] F.D. Yu J, T.L. Steck, Selective solubilization of proteins and phospholipids from red blood cell membranes by nonionic detergents, J. Supramol. Struct. 1 (1973) 233–248.
[12] D.A. Brown, J.K. Rose, Sorting of GPI-anchored proteins to glycolipid-enriched membrane subdomains during transport to the apical cell-surface, Cell 68 (1992) 533–544.
[13] R.G.W. Anderson, K. Jacobson, Cell biology – a role for lipid shells in targeting proteins to caveolae, rafts, and other lipid domains, Science 296 (2002) 1821–1825.
[14] K. Simons, W.L.C. Vaz, Model systems, lipid rafts, and cell membranes, Annu. Rev. Biophys. Biom. 33 (2004) 269–295.
[15] M. Edidin, Shrinking patches and slippery rafts: scales of domains in the plasma membrane, Trends Cell Biol. 11 (2001) 492–496.
[16] K. Simons, G. Vanmeer, Lipid sorting in epithelial-cells, Biochemistry 27 (1988) 6197–6202.
[17] D.A. Brown, E. London, Functions of lipid rafts in biological membranes, Annu. Rev. Cell Dev. Biol. 14 (1998) 111–136.
[18] D.A. Brown, E. London, Structure and function of sphingolipid- and cholesterol-rich membrane rafts, J. Biol. Chem. 275 (2000) 17221–17224.
[19] S. Munro, Lipid rafts: elusive or illusive? Cell 115 (2003) 377–388
[20] J.R. Silvius, Role of cholesterol in lipid raft formation: lessons from lipid model systems, BBA-Biomembranes 1610 (2003) 174–183.
[21] H.A. Rinia, M.M.E. Snel, J. van der Eerden, B. de Kruijff, Visualizing detergent resistant domains in model membranes with atomic force microscopy, FEBS Lett. 501 (2001) 92–96.
[22] S.L. Veatch, S.L. Keller, Separation of liquid phases in giant vesicles of ternary mixtures of phospholipids and cholesterol, Biophys. J. 85 (2003) 3074–3083.
[23] C. Dietrich, L.A. Bagatolli, Z.N. Volovyk, N.L. Thompson, M. Levi, K. Jacobson, E. Gratton, Lipid rafts reconstituted in model membranes, Biophys. J. 80 (2001) 1417–1428.
[24] J.M. Crane, L.K. Tamm, Role of cholesterol in the formation and nature of lipid rafts in planar and spherical model membranes, Biophys. J. 86 (2004) 2965–2979.
[25] K. Ritchie, R. Iino, T. Fujiwara, K. Murase, A. Kusumi, The fence and picket structure of the plasma membrane of live cells as revealed by single molecule techniques (review), Mol. Membr. Biol. 20 (2003) 13–18.
[26] T.V. Ratto, M.L. Longo, Obstructed diffusion in phase-separated supported lipid bilayers: a combined atomic force microscopy and fluorescence recovery after photobleaching approach, Biophys. J. 83 (2002) 3380–3392.
[27] M.J. Saxton, K. Jacobson, Single-particle tracking: applications to membrane dynamics, Annu. Rev. Biophys. Biom. 26 (1997) 373–399.
[28] A. Kusumi, C. Nakada, K. Ritchie, K. Murase, K. Suzuki, H. Murakoshi, R.S. Kasai, J. Kondo, T. Fujiwara, Paradigm shift of the plasma membrane concept from the two-dimensional continuum fluid to the partitioned fluid: high-speed single-molecule tracking of membrane molecules, Annu. Rev. Biophys. Biom. 34 (2005) 351–378.

[29] T. Fujiwara, K. Ritchie, H. Murakoshi, K. Jacobson, A. Kusumi, Phospholipids undergo hop diffusion in compartmentalized cell membrane, J. Cell Biol. 157 (2002) 1071–1082.
[30] A. Kusumi, I. Koyama-Honda, K. Suzuki, Molecular dynamics and interactions for creation of stimulation-induced stabilized rafts from small unstable steady-state rafts, Traffic 5 (2004) 213–230.
[31] C. Dietrich, B. Yang, T. Fujiwara, A. Kusumi, K. Jacobson, Relationship of lipid rafts to transient confinement zones detected by single particle tracking, Biophys. J. 82 (2002) 274–284.
[32] J.B. de la Serna, J. Perez-Gil, A.C. Simonsen, L.A. Bagatolli, Cholesterol rules – direct observation of the coexistence of two fluid phases in native pulmonary surfactant membranes at physiological temperatures, J. Biol. Chem. 279 (2004) 40715–40722.
[33] M. Amrein, A. von Nahmen, M. Sieber, A scanning force- and fluorescence light microscope study of the structure and function of a model pulmonary surfactant, Eur. Biophys. J. 26 (1997) 349–357.
[34] D. Knebel, M. Sieber, R. Reichelt, H.J. Galla, M. Amrein, Fluorescence light microscopy of pulmonary surfactant at the air–water interface of an air bubble of adjustable size, Biophys. J. 83 (2002) 547–555.
[35] H.A. Rinia, R.A. Kik, R.A. Demel, M.M.E. Snel, J.A. Killian, J. van der Eerden, B. de Kruijff, Visualization of highly ordered striated domains induced by transmembrane peptides in supported phosphatidylcholine bilayers, Biochemistry 39 (2000) 5852–5858.
[36] J.X. Mou, D.M. Czajkowsky, Z.F. Shao, Gramicidin A aggregation in supported gel state phosphatidylcholine bilayers, Biochemistry 35 (1996) 3222–3226.
[37] H.A. Rinia, J.W.P. Boots, D.T.S. Rijkers, R.A. Kik, M.M.E. Snel, R.A. Demel, J.A. Killian, J. van der Eerden, B. de Kruijff, Domain formation in phosphatidylcholine bilayers containing transmembrane peptides: specific effects of flanking residues, Biochemistry 41 (2002) 2814–2824.
[38] A. Engel, D.J. Muller, Observing single biomolecules at work with the atomic force microscope, Nat. Struct. Biol. 7 (2000) 715–718.
[39] H.A. Rinia, B. de Kruijff, Imaging domains in model membranes with atomic force microscopy, FEBS Lett. 504 (2001) 194–199.
[40] P.E. Milhiet, M.-C. Giocondi, C. Le Grimellec, AFM imaging of lipid domains in model membranes, The Scientific World J. 3 (2003) 59–74.
[41] Y.F. Dufrene, G.U. Lee, Advances in the characterization of supported lipid films with the atomic force microscope, BBA-Biomembranes 1509 (2000) 14–41.
[42] A. Janshoff, C. Steinem, Scanning force microscopy of artificial membranes, Chembiochem 2 (2001) 799–808.
[43] S.L. Veatch, S.L. Keller, Organization in lipid membranes containing cholesterol, Phys. Rev. Lett. 89 (2002) 268101-1–268101-4.
[44] T. Baumgart, S.T. Hess, W.W. Webb, Imaging coexisting fluid domains in biomembrane models coupling curvature and line tension, Nature 425 (2003) 821–824.
[45] J. Korlach, P. Schwille, W.W. Webb, G.W. Feigenson, Characterization of lipid bilayer phases by confocal microscopy and fluorescence correlation spectroscopy, Proc. Natl. Acad. Sci. USA 96 (1999) 8461–8466.
[46] M. Müller, J.M. Schins, Imaging the thermodynamic state of lipid membranes with multiplex CARS microscopy, J. Phys. Chem. B 106 (2002) 3715–3723.
[47] G.W.H. Wurpel, J.M. Schins, M. Müller, Direct measurement of chain order in single phospholipid mono- and bilayers with multiplex CARS, J. Phys. Chem. B 108 (2004) 3400–3403.
[48] E.O. Potma, X.S. Xie, Direct visualization of lipid phase segregation in single lipid bilayers with coherent anti-stokes Raman scattering microscopy, Chemphyschem 6 (2005) 77–79.

[49] S. Sheng, D.M. Czajkowsky, Z. Shao, AFM tips: how sharp are they? J. Microsc.-Oxford 196 (1999) 1–5.
[50] H.J. Butt, Electrostatic interaction in atomic force microscopy, Biophys. J. 60 (1991) 777–785.
[51] D.J. Müller, A. Engel, The height of biomolecules measured with the atomic force microscope depends on electrostatic interactions, Biophys. J. 73 (1997) 1633–1644.
[52] D.J. Müller, D. Fotiadis, S. Scheuring, S.A. Muller, A. Engel, Electrostatically balanced subnanometer imaging of biological specimens by atomic force microscope, Biophys. J. 76 (1999) 1101–1111.
[53] M. Beckmann, P. Nollert, H.A. Kolb, Manipulation and molecular resolution of a phosphatidylcholine-supported planar bilayer by atomic force microscopy, J. Membr. Biol. 161 (1998) 227–233.
[54] H.A. Rinia, R.A. Demel, J. van der Eerden, B. de Kruijff, Blistering of Langmuir–Blodgett bilayers containing anionic phospholipids as observed by atomic force microscopy, Biophys. J. 77 (1999) 1683–1693.
[55] H.G. Hansma, R.L. Sinsheimer, J. Groppe, T.C. Bruice, V. Elings, G. Gurley, M. Bezanilla, I.A. Mastrangelo, P.V.C. Hough, P.K. Hansma, Recent advances in atomic-force microscopy of DNA, Scanning 15 (1993) 296–299.
[56] Y.F. Dufrene, W.R. Barger, J.B.D. Green, G.U. Lee, Nanometer-scale surface properties of mixed phospholipid monolayers and bilayers, Langmuir 13 (1997) 4779–4784.
[57] J. Schneider, Y.F. Dufrene, W.R. Barger, G.U. Lee, Atomic force microscope image contrast mechanisms on supported lipid bilayers, Biophys. J. 79 (2000) 1107–1118.
[58] M. Grandbois, W. Dettmann, M. Benoit, H.E. Gaub, Affinity imaging of red blood cells using an atomic force microscope, J. Histochem. Cytochem. 48 (2000) 719–724.
[59] H. Seelert, A. Poetsch, N.A. Dencher, A. Engel, H. Stahlberg, D.J. Muller, Structural biology – proton-powered turbine of a plant motor, Nature 405 (2000) 418–419.
[60] D.M. Czajkowsky, H. Iwamoto, T.L. Cover, Z.F. Shao, The vacuolating toxin from Helicobacter pylori forms hexameric pores in lipid bilayers at low pH, Proc. Natl. Acad. Sci. USA 96 (1999) 2001–2006.
[61] S. Scheuring, P. Ringler, M. Borgnia, H. Stahlberg, D.J. Müller, P. Agre, A. Engel, High resolution AFM topographs of the Escherichia coli water channel aquaporin, Z EMBO J. 18 (1999) 4981–4987.
[62] D.J. Müller, J.B. Heymann, F. Oesterhelt, C. Moller, H. Gaub, G. Buldt, A. Engel, Atomic force microscopy of native purple membrane, BBA-Bioenergetics 1460 (2000) 27–38.
[63] F.O. Ahimou, A. Touhami, Y.F. Dufrene, Real-time imaging of the surface topography of living yeast cells by atomic force microscopy, Yeast 20 (2003) 25–30.
[64] E. Lesniewska, P.E. Milhiet, M.C. Giocondi, C. Le Grimellec, Atomic force microscope imaging of cells and membranes, in: J.K.H. Horber, B.P. Jena, P. Matsudaira, L. Wilson (Eds.), Atomic Force Microscopy in Cell Biology, Academic Press, New York, 2002, pp. 51–65.
[65] A.H. Swihart, J.M. Mikrut, J.B. Ketterson, R.C. MacDonald, Atomic force microscopy of the erythrocyte membrane skeleton, J. Microsc. 204 (2001) 212–225.
[66] J. Zasadzinski, C. Helm, M. Longo, A. Weisenhorn, S. Gould, P. Hansma, Atomic force microscopy of hydrated phosphatidylethanolamine bilayers, Biophys. J. 59 (1991) 755–760.
[67] S.W. Hui, R. Viswanathan, J.A. Zasadzinski, J.N. Israelachvili, The structure and stability of phospholipid-bilayers by atomic-force microscopy, Biophys. J. 68 (1995) 171–178.
[68] D.J. Müller, A. Engel, M. Amrein, Preparation techniques for the observation of native biological systems with the atomic force microscope, Biosens. Bioelectron. 12 (1997) 867–877.

[69] K.B. Blodgett, Films built by depositing successive monomolecular layers on a solid surface, J. Am. Chem. Soc. 57 (1935) 1007–1022.
[70] A.A. Brian, H.M. McConnell, Allogeneic stimulation of cytotoxic T cells by supported planar membranes, Proc. Natl. Acad. Sci. USA 81 (1984) 6159–6163.
[71] Z.F. Shao, J. Mou, D.M. Czajkowsky, J. Yang, J.Y. Yuan, Biological atomic force microscopy: what is achieved and what is needed, Adv. Phys. 45 (1996) 1–86.
[72] M. Benz, T. Gutsmann, N. Chen, R. Tadmor, J. Israelachvili, Correlation of AFM and SFA measurements concerning the stability of supported lipid bilayers, Biophys. J. 86 (2004) 870–879.
[73] I. Reviakine, A. Brisson, Formation of supported phospholipid bilayers from unilamellar vesicles investigated by atomic force microscopy, Langmuir 16 (2000) 1806–1815.
[74] R. Richter, A. Mukhopadhyay, A. Brisson, Pathways of lipid vesicle deposition on solid surfaces: a combined QCM-D and AFM study, Biophys. J. 85 (2003) 3035–3047.
[75] R.P. Richter, A.R. Brisson, Following the formation of supported lipid bilayers on mica: a study combining AFM, QCM-D, and ellipsometry, Biophys. J. 88 (2005) 3422–3433.
[76] C. Leidy, T. Kaasgaard, J.H. Crowe, O.G. Mouritsen, K. Jorgensen, Ripples and the formation of anisotropic lipid domains: imaging two-component double bilayers by atomic force microscopy, Biophys. J. 83 (2002) 2625–2633.
[77] P. Bassereau, F. Pincet, Quantitative analysis of holes in supported bilayers providing the adsorption energy of surfactants on solid substrates, Langmuir 13 (1997) 7003–7007.
[78] A.F. Xie, R. Yamada, A.A. Gewirth, S. Granick, Materials science of the gel to fluid phase transition in a supported phospholipid bilayer, Phys. Rev. Lett. 89 (2002) 246103-1–246103-4.
[79] D. Marsh, Handbook of Lipid Bilayers, CRC Press, Boca Raton, 1990.
[80] M. Grandbois, H. Clausen-Schaumann, H. Gaub, Atomic force microscope imaging of phospholipid bilayer degradation by phospholipase A(2), Biophys. J. 74 (1998) 2398–2404.
[81] I. Reviakine, W. Bergsma-Schutter, A. Brisson, Growth of protein 2-d crystals on supported planar lipid bilayers imaged in situ by AFM, J. Struct. Biol. 121 (1998) 356–362.
[82] C.W. Hollars, R.C. Dunn, Submicron structure in L-alpha -dipalmitoylphosphatidylcholine monolayers and bilayers probed with confocal, atomic force, and near-field microscopy, Biophys. J. 75 (1998) 342–353.
[83] B.L. Stottrup, S.L. Veatch, S.L. Keller, Nonequilibrium behavior in supported lipid membranes containing cholesterol, Biophys. J. 86 (2004) 2942–2950.
[84] J.X. Mou, J. Yang, C. Huang, Z.F. Shao, Alcohol induces interdigitated domains in unilamellar phosphatidylcholine bilayers, Biochemistry 33 (1994) 9981–9985.
[85] J.X. Mou, J. Yang, Z.F. Shao, Tris(hydroxymethyl)aminomethane (C4h11no3) induced a ripple phase in supported unilamellar phospholipid-bilayers, Biochemistry 33 (1994) 4439–4443.
[86] J.X. Mou, J. Yang, Z.F. Shao, Atomic-force microscopy of cholera-toxin B-oligomers bound to bilayers of biologically relevant lipids, J. Mol. Biol. 248 (1995) 507–512.
[87] D.M. Czajkowsky, C. Huang, Z.F. Shao, Ripple phase in asymmetric unilamellar bilayers with saturated and unsaturated phospholipids, Biochemistry 34 (1995) 12501–12505.
[88] J. Yang, L.K. Tamm, T.W. Tillack, Z. Shao, New approach for atomic force microscopy of membrane-proteins – the imaging of cholera-toxin, J. Mol. Biol. 229 (1993) 286–290.
[89] Y. Fang, J. Yang, The growth of bilayer defects and the induction of interdigitated domains in the lipid-loss process of supported phospholipid bilayers, BBA-Biomembranes 1324 (1997) 309–319.

[90] A. Janshoff, D.T. Bong, C. Steinem, J.E. Johnson, M.R. Ghadiri, An animal virus-derived peptide switches membrane morphology: possible relevance to nodaviral transfection processes, Biochemistry 38 (1999) 5328–5336.
[91] I. Musevic, G. Slak, R. Blinc, Temperature controlled microstage for an atomic force microscope, Rev. Sci. Instrum. 67 (1996) 2554–2556.
[92] F. Tokumasu, A.J. Jin, G.W. Feigenson, J.A. Dvorak, Atomic force microscopy of nanometric liposome adsorption and nanoscopic membrane domain formation, Ultramicroscopy 97 (2003) 217–227.
[93] F. Tokumasu, A.J. Jin, J.A. Dvorak, Lipid membrane phase behaviour elucidated in real time by controlled environment atomic force microscopy, J. Electron Microsc. 51 (2002) 1–9.
[94] J. Yang, J. Appleyard, The main phase transition of mica-supported phosphatidylcholine membranes, J. Phys. Chem. B 104 (2000) 8097–8100.
[95] Y. Fang, J. Yang, Role of the bilayer–bilayer interaction on the ripple structure of supported bilayers in solution, J. Phys. Chem. 100 (1996) 15614–15619.
[96] T. Kaasgaard, C. Leidy, J.H. Crowe, O.G. Mouritsen, K. Jorgensen, Temperature-controlled structure and kinetics of ripple phases in one- and two-component supported lipid bilayers, Biophys. J. 85 (2003) 350–360.
[97] G. Fragneto, T. Charitat, F. Graner, K. Mecke, L. Perino-Gallice, E. Bellet-Amalric, A fluid floating bilayer, Europhys. Lett. 53 (2001) 100–106.
[98] O. Enders, A. Ngezahayo, M. Wiechmann, F. Leisten, H.-A. Kolb, Structural calorimetry of main transition of supported DMPC bilayers by temperature-controlled AFM, Biophys. J. 87 (2004) 2522–2531.
[99] M.-C. Giocondi, V. Vie, E. Lesniewska, P.E. Milhiet, M. Zinke-Allmang, C. Le Grimellec, Phase topology and growth of single domains in lipid bilayers, Langmuir 17 (2001) 1653–1659.
[100] M.-C. Giocondi, L. Pacheco, P.E. Milhiet, C. Le Grimellec, Temperature dependence of the topology of supported dimirystoyl-distearoyl phosphatidylcholine bilayers, Ultramicroscopy 86 (2001) 151–157.
[101] M.-C. Giocondi, C. Le Grimellec, Temperature dependence of the surface topography in dimyristoylphosphatidylcholine/distearoylphosphatidylcholine multibilayers, Biophys. J. 86 (2004) 2218–2230.
[102] F. Tokumasu, A.J. Jin, G.W. Feigenson, J.A. Dvorak, Nanoscopic lipid domain dynamics revealed by atomic force microscopy, Biophys. J. 84 (2003) 2609–2618.
[103] T. Kaasgaard, O.G. Mouritsen, K. Jorgensen, Lipid domain formation and ligand-receptor distribution in lipid bilayer membranes investigated by atomic force microscopy, FEBS Lett. 515 (2002) 29–34.
[104] P.E. Milhiet, V. Vie, M.C. Giocondi, C. Le Grimellec, AFM characterization of model rafts in supported bilayers, Single Mol. 2 (2001) 109–112.
[105] P.E. Milhiet, M.C. Giocondi, O. Baghdadi, F. Ronzon, B. Roux, C. Le Grimellec, Spontaneous insertion and partitioning of alkaline phosphatase into model lipid rafts, EMBO Rep. 3 (2002) 485–490.
[106] D.E. Saslowsky, J. Lawrence, X.Y. Ren, D.A. Brown, R.M. Henderson, J.M. Edwardson, Placental alkaline phosphatase is efficiently targeted to rafts in supported lipid bilayers, J. Biol. Chem. 277 (2002) 26966–26970.
[107] M.-C. Giocondi, P.E. Milhiet, P. Dosset, C.L. Grimellec, Use of cyclodextrin for AFM monitoring of model raft formation, Biophys. J. 86 (2004) 861–869.
[108] P.E. Milhiet, M.C. Giocondi, C. Le Grimellec, Cholesterol is not crucial for the existence of microdomains in kidney brush-border membrane models, J. Biol. Chem. 277 (2002) 875–878.
[109] S.B. Lee, S. Torquato, Monte-Carlo study of correlated continuum percolation – universality and percolation thresholds, Phys. Rev. A 41 (1990) 5338–5344.
[110] J.C. Lawrence, D.E. Saslowsky, J.M. Edwardson, R.M. Henderson, Real-time analysis of the effects of cholesterol on lipid raft behavior using atomic force microscopy, Biophys. J. 84 (2003) 1827–1832.

[111] R.A. Demel, J.W. Jansen, P.W. van Dijck, L.L. van Deenen, The preferential interaction of cholesterol with different classes of phospholipids, Biochim. Biophys. Acta 465 (1977) 1–10.
[112] P.R. Maulik, P.K. Sripada, G.G. Shipley, Structure and thermotropic properties of hydrated *N*-stearoyl sphingomyelin bilayer-membranes, Biochim. Biophys. Acta 1062 (1991) 211–219.
[113] P.R. Maulik, G.G. Shipley, Interactions of *N*-stearoyl sphingomyelin with cholesterol and dipalmitoyl phosphatidylcholine in bilayer membranes, Biophys. J. 70 (1996) 2256–2265.
[114] P.R. Maulik, G.G. Shipley, *N*-palmitoyl sphingomyelin bilayers: structure and interactions with cholesterol and dipalmitoylphosphatidylcholine, Biochemistry 35 (1996) 8025–8034.
[115] H. Heerklotz, Triton promotes domain formation in lipid raft mixtures, Biophys. J. 83 (2002) 2693–2701.
[116] P.E. Milhiet, M.C. Giocondi, O. Baghdadi, F. Ronzon, C. Le Grimellec, B. Roux, AFM detection of GPI protein insertion into DOPC/DPPC model membranes, Single Mol. 3 (2002) 135–140.
[117] A.E. Christian, M.P. Haynes, M.C. Phillips, G.H. Rothblat, Use of cyclodextrins for manipulating cellular cholesterol content, J. Lipid Res. 38 (1997) 2264–2272.
[118] H. Ohvo, J.P. Slotte, Cyclodextrin-mediated removal of sterols from monolayers: effects of sterol structure and phospholipids on desorption rate, Biochemistry 35 (1996) 8018–8024.
[119] D. Scherfeld, N. Kahya, P. Schwille, Lipid dynamics and domain formation in model membranes composed of ternary mixtures of unsaturated and saturated phosphatidylcholines and cholesterol, Biophys. J. 85 (2003) 3758–3768.
[120] T. Harder, P. Scheiffele, P. Verkade, K. Simons, Lipid domain structure of the plasma membrane revealed by patching of membrane components, J. Cell Biol. 141 (1998) 929–942.
[121] K. Bacia, D. Scherfeld, N. Kahya, P. Schwille, Fluorescence correlation spectroscopy relates rafts in model and native membranes, Biophys. J. 87 (2004) 1034–1043.
[122] A.K. Kenworthy, N. Petranova, M. Edidin, High-resolution FRET microscopy of cholera toxin B-subunit and GPI-anchored proteins in cell plasma membranes, Mol. Biol. Cell 11 (2000) 1645–1655.
[123] R. Peters, J. Peters, K. Tews, W. Bahr, A microfluorimetric study of translational diffusion in erythrocyte membranes, Biochim. Biophys. Acta 367 (1974) 282–294.
[124] D. Axelrod, D. Koppel, J. Schlessinger, E. Elson, W. Webb, Mobility measurement by analysis of fluorescence photobleaching recovery kinetics, Biophys. J. 16 (1976) 1055–1069.
[125] L.K. Tamm, Lateral diffusion and fluorescence microscope studies on a monoclonal-antibody specifically bound to supported phospholipid-bilayers, Biochemistry 27 (1988) 1450–1457.
[126] G.J. Schutz, H. Schindler, T. Schmidt, Single-molecule microscopy on model membranes reveals anomalous diffusion, Biophys. J. 73 (1997) 1073–1080.
[127] N. Kahya, D. Scherfeld, K. Bacia, B. Poolman, P. Schwille, Probing lipid mobility of raft-exhibiting model membranes by fluorescence correlation spectroscopy, J. Biol. Chem. 278 (2003) 28109–28115.
[128] M. Hetzer, S. Heinz, S. Grage, T.M. Bayerl, Asymmetric molecular friction in supported phospholipid bilayers revealed by NMR measurements of lipid diffusion, Langmuir 14 (1998) 982–984.
[129] H.M. McConnell, A. Radhakrishnan, Condensed complexes of cholesterol and phospholipids, BBA-Biomembranes 1610 (2003) 159–173.
[130] A. Radhakrishnan, H.M. McConnell, Condensed complexes of cholesterol and phospholipids, Biophys. J. 77 (1999) 1507–1517.

[131] S.L. Keller, W.H. Pitcher, W.H. Huestis, H.M. McConnell, Red blood cell lipids form immiscible liquids, Phys. Rev. Lett. 81 (1998) 5019–5022.
[132] E. Kalb, S. Frey, L.K. Tamm, Formation of supported planar bilayers by fusion of vesicles to supported phospholipid monolayers, Biochim. Biophys. Acta 1103 (1992) 307–316.
[133] R.M. Weis, Fluorescence microscopy of phospholipid monolayer phase-transitions, Chem. Phys. Lipids 57 (1991) 227–239.
[134] C.M. Knobler, Seeing phenomena in flatland – studies of monolayers by fluorescence microscopy, Science 249 (1990) 870–874.
[135] K. Bacia, P. Schwille, T. Kurzchalia, Sterol structure determines the separation of phases and the curvature of the liquid-ordered phase in model membranes, Proc. Natl. Acad. Sci. USA 102 (2005) 3272–3277.
[136] A.E. McKiernan, T.V. Ratto, M.L. Longo, Domain growth, shapes, and topology in cationic lipid bilayers on mica by fluorescence and atomic force microscopy, Biophys. J. 79 (2000) 2605–2615.
[137] A.V. Samsonov, I. Mihalyov, F.S. Cohen, Characterization of cholesterol-sphingomyelin domains and their dynamics in bilayer membranes, Biophys. J. 81 (2001) 1486–1500.
[138] A.T. Hammond, F.A. Heberle, T. Baumgart, D. Holowka, B. Baird, G.W. Feigenson, Crosslinking a lipid raft component triggers liquid ordered-liquid disordered phase separation in model plasma membranes, Proc. Natl. Acad. Sci. USA 102 (2005) 6320–6325.
[139] J. Radler, H. Strey, E. Sackmann, Phenomenology and kinetics of lipid bilayer spreading on hydrophilic surfaces, Langmuir 11 (1995) 4539–4548.
[140] D. Keller, N.B. Larsen, I.M. Moller, O.G. Mouritsen, Decoupled phase transitions and grain-boundary melting in supported phospholipid bilayers, Phys. Rev. Lett. 94 (2005) 025701-1–025701-4.
[141] G.J. Puppels, J. Greve, Whole cell studies and tissue characterization by Raman spectroscopy, in: R.J.H. Clark, R.E. Hester (Eds.), Biochemical Applications of Spectroscopy, Wiley, New York, 1996, pp. 1–47.
[142] M. Müller, J. Squier, C.A. De Lange, G.J. Brakenhoff, CARS microscopy with folded BoxCARS phasematching, J. Microsc. 197 (2000) 150–158.
[143] A. Zumbusch, G.R. Holtom, X.S. Xie, Three-dimensional vibrational imaging by coherent anti-stokes Raman scattering, Phys. Rev. Lett. 82 (1999) 4142–4145.
[144] J.X. Cheng, X.S. Xie, Coherent anti-stokes Raman scattering microscopy: instrumentation, theory, and applications, J. Phys. Chem. B 108 (2004) 827–840.
[145] M. Müller, J.M. Schins, G.W.H. Wurpel, Shot-noise limited detection sensitivity in multiplex CARS microscopy, SPIE 5323 (2004) 195–204.
[146] I.W. Levin, Vibrational spectroscopy of membrane assemblies, in: R.J.H. Clark, R.E. Hester (Eds.), Advances in Infrared and Raman Spectroscopy, Wiley Heyden, New York, 1984, pp. 1–48.
[147] G.W.H. Wurpel, H.A. Rinia, M. Muller, Imaging orientational order and lipid density in multilamellar vesicles with multiplex CARS microscopy, J. Microsc. 218 (2005) 37–45.
[148] S. Roke, J. Schins, M. Muller, M. Bonn, Vibrational spectroscopic investigation of the phase diagram of a biomimetic lipid monolayer, Phys. Rev. Lett. 90 (2003) 128101-1–128101-4.
[149] R. Koynova, M. Caffrey, Phases and phase transitions of the phosphatidylcholines, BBA-rev. biomembranes 1376 (1998) 91–145.
[150] B.A. Lewis, D.M. Engelman, Lipid bilayer thickness varies linearly with acyl chain length in fluid phosphatidylcholine vesicles, J. Mol. Biol. 166 (1983) 211–217.

This page intentionally left blank

CHAPTER 5

Physicochemical Insights into Equilibria in Bilayer Lipid Membranes

Aneta Dorota Petelska,[1] Monika Naumowicz,[1] and Zbigniew Artur Figaszewski[1,2,*]

[1]*Institute of Chemistry, University of Bialystok, Al. J. Pilsudskiego 11/4, 15-443 Bialystok, Poland*

[2]*Laboratory of Electrochemical Power Sources, Faculty of Chemistry, University of Warsaw, Pasteur St. 1, 02-093 Warsaw, Poland*

Contents

*Corresponding author. Tel: +48856647487; Fax: +48856647489; E-mail: elchem@uwb.edu.pl

ADVANCES IN PLANAR LIPID BILAYERS AND LIPOSOMES, VOLUME 3
ISSN 1554-4516 DOI: 10.1016/S1554-4516(05)03005-X

Abstract

This chapter concerns the equilibria of some biomolecules in bilayer lipid membranes. The presented research of biolipid interaction was concentrated on quantitative description of experiments that take part within the bilayer as well as on its surface. Assumed models of interaction between amphiphilic molecules, between transport proteins and monovalent cations and the equilibria that take place there as well as acid–base equilibria were described by mathematical equations for the systems studied. These theoretical models were verified experimentally using interfacial tension and electrochemical impedance spectroscopy techniques.

For systems of two kinds of lipids, the possibility of a 1:1 complex formation was assumed what would explain the deviation from the additivity rule. Calculated values of parameters (equilibrium constants, molecular areas of complexes, interfacial tensions, capacitances and resistances of molecules and complexes) were used for calculation model curves. The comparison of model curves and experimental points verified assumed models.

The complex formation between the gramicidin molecule and K^+ ion was investigated by the interfacial tension method. Electrochemical impedance spectroscopy was used for the study of gramicidin D dimerization and transport of monovalent cations across lipid bilayers by the dimers. Both experimental methods mentioned were used for the research ability of valinomycin to form a 1:1 potassium-ion complex on the lipid bilayer/electrolyte solution interface. Very simple methods were proposed to determine the parameters used to describe the gramicidin dimer and ionophore-K^+ complexes. It could be demonstrated that determined parameters values were of a similar order of magnitude to those obtained by other measuring techniques.

The effect of pH of electrolyte solution on the bilayer lipid membrane built from different lipids was also determined. The obtained curves demonstrate the maximal interfacial tension values at the isoelectric point. A course of these curves was well characterized by the simplified description based on the Gibbs isotherm, but only in proximity of the isoelectric point. While, using the exact definition of surface excess within the Gibbs equation (taking into account volumes of adsorbed ions at the membrane surface) permits us to explain the run of experimental curves in the whole pH range. Also in this chapter the models derived to describe adsorption of the H^+ and OH^- ions at lipid surfaces formed from phospholipids were proposed, which would reproduce changes in interfacial tension more correctly, particularly in the ranges distant from the isolelectric point. In models, contribution of the individual forms of lipid molecule to interfacial tension of the bilayer was assumed to be additive.

This chapter concentrated especially on phospholipids because they are major fractions of lipids found in biological membranes: phosphatidylcholine (PC), phosphatidylethanolamine (PE) and phosphatidylserine (PS) were chosen. PC was the basic component of the formed bilayers because it has been widely examined and described in the literature, but also because it creates permanent monolayers and bilayers, of which one can easily build in the other components. Cholesterol, gramicidin and valinomycin were also studied since they play an important biochemical role in cell membranes. Cholesterol is an important factor in controlling physical properties of biological membranes and their functions. Gramicidin is a model of more complicated biological ionic channels. For this reason, many studies have been done using this simple channel-forming polypeptide. It has been reported that valinomycin acts as a selective carrier of K^+ ions in a variety of cell membranes as well as on liposomes and lipid bilayers.

The interactions between membrane lipids are nowadays intensively developed. This results from the suitability of this research for understandings of phenomena proceeding in

cellular membranes. However, there is still the lack of the quantitative description of the systems. It is required for a better understanding of the processes that take place in biological membranes with the aim of forming the artificial membrane that would very closely resemble the properties of the natural membrane. Therefore, the knowledge of molecular structure and organization of phospholipids is necessary. Data presented in this work, received from mathematical derivation and confirmed experimentally are of great importance for interpretation of phenomena occurring in lipid monolayers and bilayers. These results can help in a better understanding of biological membranes and in their biophysical studies. Simple and very interesting methods proposed in this chapter can be used with success for the determination of the equilibrium constant value of any 1:1 lipid–other lipid complex and any 1:1 ionophore–monovalent ion complex and for acid–base equilibria between any phospholipids and ions from electrolyte solution (H^+ and OH^-).

ABBREVIATIONS

Names of compounds

Ch	cholesterol
G	gramicidin
GG	dimer of gramicidin–gramicidin
GK^+	gramicidin-K^+ ion complex
PC, L	phosphatidylcholine (lecithin)
PC–Ch	lecithin–cholestrol complex
PC–PE	lecithin–cephalin complex
PE, E	phosphatidylethanolamine (cephalin)
PE–Ch	cephalin–cholesterol complex
PS	phosphatidylserine
V	valinomycin
VK^+	valinomycin-K^+ ion complex

Variables

A	surface area of the lipid membrane
$a_{H^+}, a_{OH^-}, a_{K^+}$	activity of H^+, OH^- and K^+ ions
B	partition coefficient
C_i	electric capacitance of component "i"
c_i^s	surface concentration of component "i"
c_i^b	volume concentration of component "i"
D	diffusion coefficient of ion in the aqueous phase
E_s	surface energy
F	Faraday constant
K_i	equilibrium constant of adequate process
k_a	association rate constant
k_d	dissociation rate constant
m_i	mass of component "i"

M_i	molar mass of component "i"
N_A	Avogadro's constant
n_G	the analytical lecithin and gramicidin concentrations ratio in the membrane
R	gas constant
R_i	electric resistance of component "i"
T	environment temperature
V	volume of component "i"
Z'	real part of electric impedance
$Z''(-jX)$	imaginary part of electric impedance
z_i	valency of ion "i"
x_i	molar fraction of component "i"
γ_i	interfacial tension value of component "i"
γ_i^0	specific interfacial tension value of component "i"
γ_{max}	maximal interfacial tension value
Γ_i	surface excess of component "i"
δ	lipid bilayer thickness
θ	coverage ($0 < \theta > 1$)
$\bar{\mu}_i$	electrochemical potential of component "i"
μ_i	mobility of component "i"
σ	Warburg coefficient
v	stoichiometric coefficient
ω	angular frequency

1. COMPLEXES FORMATION EQUILIBRIA

1.1. Membranes composed of two kinds of lipids

Biological membrane contains a heterogeneous mixture of lipids differing from each other with respect to their head-group structure, hydrocarbon chain length, degree of unsaturation of the acyl chain, and mode of attachment of the hydrocarbon chain. Due to this complexity, it is difficult to ascertain the physical properties and functional roles of individual lipids and their mode of interaction with other lipids in natural membranes. Therefore model systems consisting of phospholipids and sterols have been a valuable tool in obtaining basic information on membrane lipid interactions.

Most of the lipid bilayer studies concentrate on the surface potential or surface pressure measurements, spectroscopy and microscopic visualization of lateral domains [1]. In spite of a wide variety of experimental methods for the study of lipid bilayers, some long-lasting problems remain. One of them is the complex formation between phospholipid and cholesterol and between two kinds of phospholipids in a bilayer or in a monolayer at the air/water interface [2,3].

1.1.1. Theoretical considerations

Nevertheless, whether it is a three-dimensional bilayer or a two-dimensional monolayer, each two-compound system can be described by a set of equations presented below [4–6]:

$$\begin{gathered}\gamma_1 c_1^{\mathrm{s}} A_1 + \gamma_2 c_2^{\mathrm{s}} A_2 = \gamma \\ \frac{c_1^{\mathrm{s}}}{c_1^{\mathrm{s}} + c_2^{\mathrm{s}}} = x_1 \\ x_1 + x_2 = 1\end{gathered} \tag{1}$$

where γ ($\mathrm{N\,m^{-1}}$) is the interfacial tension of the membrane; γ_1, γ_2 ($\mathrm{N\,m^{-1}}$) the interfacial tension of the membrane built of compound 1 and 2, respectively; A_1^{-1}, A_2^{-1} ($\mathrm{mol\,m^{-2}}$) the maximal surface concentration of compound 1 and 2, respectively, per unit area of the membrane; c_1^{s}, c_2^{s} ($\mathrm{mol\,m^{-2}}$) the surface concentration of compound 1 and 2, respectively, per unit area of the membrane and x_1, x_2 the molar fraction of compound 1 and 2, respectively, in the solution forming the membrane.

Elimination of c_1^{s} and c_2^{s} yields the linear equation:

$$(\gamma - \gamma_1)x_1 = \frac{A_2}{A_1}(\gamma_2 - \gamma)x_2 \tag{2}$$

To the fact that the first stability constant in complexes, as the essential one, is usually the biggest and should be taken into consideration [7], existence of 1:1 complexes in lipid–lipid or lipid–cholesterol systems was assumed. This assumption was verified experimentally using interfacial tension method (the interface tension values reported below refer to the one side of bilayer membrane surface area unit).

Then, the set of equations (1) is modified because the interfacial tension is the sum of the contributions of all compounds:

$$\begin{gathered}\gamma_1 c_1^{\mathrm{s}} A_1 + \gamma_2 c_2^{\mathrm{s}} A_2 + \gamma_3 c_3^{\mathrm{s}} A_3 = \gamma \\ K = \frac{c_3^{\mathrm{s}}}{c_1^{\mathrm{s}} \cdot c_2^{\mathrm{s}}} \\ \frac{c_1^{\mathrm{s}} + c_3^{\mathrm{s}}}{c_1^{\mathrm{s}} + c_2^{\mathrm{s}} + 2c_3^{\mathrm{s}}} = x_1 \\ x_1 + x_2 = 1\end{gathered} \tag{3}$$

where γ_3 ($\mathrm{N\,m^{-1}}$) is the interfacial tension of the complex; A_3^{-1} ($\mathrm{mol\,m^{-2}}$) the maximal surface concentration of the complex per unit area of the membrane; c_3^{s} ($\mathrm{mol\,m^{-2}}$) the surface concentration of the complex per unit area of the membrane and K the stability constant of the complex.

Elimination of c_1^s, c_2^s and c_3^s yields the basic equation:

$$\begin{aligned}&\left[(\gamma-\gamma_1)B_2x_1+(\gamma-\gamma_2)B_1x_2\right]\left[(\gamma_3-\gamma_1)B_2x_1+(\gamma_3-\gamma_2)B_1x_2+(\gamma_1-\gamma_2)(x_1-x_2)\right]\\&=KA_3^{-1}B_1B_2\left[(\gamma-\gamma_1)(x_2-x_1)+(\gamma_3-\gamma)B_1x_2\right]\left[(\gamma-\gamma_2)(x_1-x_2)+(\gamma_3-\gamma)B_2x_1\right]\end{aligned} \tag{4}$$

where $B_1=\frac{A_3}{A_1}$ and $B_2=\frac{A_3}{A_2}$.

Equation (4) is the equation of a second degree with respect to γ, to the complex composition as well as with respect to the constants: γ_1, γ_2, γ_3, B_1, B_2. Opening of the parentheses results in a great complexity of the equation, and is troublesome when directly applied to the determination of constants. The constants mentioned above can be determined in individual cases using simplified forms of this equation.

Equation (4) may be simplified taking into account the high stability constant of the complex. With this assumption, it presents a straight line for small x_2 values ($x_2<x_1$):

$$(\gamma_1-\gamma)\frac{x_1-x_2}{x_2}=-B_1\gamma_3+B_1\gamma \tag{5}$$

while for the high x_2 values ($x_2>x_1$) it can represent another straight line:

$$(\gamma_2-\gamma)\frac{x_2-x_1}{x_1}=-B_2\gamma_3+B_2\gamma \tag{6}$$

Equation (4) can be simplified in some other way. In the case where $x_1=x_2$, it assumes the form:

$$\begin{aligned}&K\left(A_1^{-1}\right)^2\left(A_2^{-1}\right)^2\left(A_3^{-1}\right)^{-1}(\gamma-\gamma_3)^2=\left[\gamma_2A_1^{-1}+\gamma_1A_2^{-1}-\gamma\left(A_1^{-1}+A_2^{-1}\right)\right]\\&\left(\gamma_2A_1^{-1}+\gamma_1A_2^{-1}\right)-\left[\gamma_2A_1^{-1}+\gamma_1A_2^{-1}-\gamma\left(A_1^{-1}+A_2^{-1}\right)\right]\left(A_1^{-1}+A_2^{-1}\right)\gamma_3\end{aligned} \tag{7}$$

The parameters describing the complex determined from equations (4) and (7) could be applied to the calculation of theoretical points using equation presented below (the agreement between theoretical and experimental values means that the system is well described by the equations above):

$$\begin{aligned}&KA_1^{-1}A_2^{-1}(\varepsilon_1+\varepsilon_2)(\varepsilon_3-\varepsilon_1)\gamma^2+\Big[KA_1^{-1}A_2^{-1}(\gamma_1\varepsilon_1-\gamma_3\varepsilon_3)(\varepsilon_1+\varepsilon_2)\\&-KA_1^{-1}A_2^{-1}(\gamma_2\varepsilon_1+\gamma_3\varepsilon_2)(\varepsilon_3-\varepsilon_1)+\varepsilon_4A_3^{-1}(\varepsilon_3+\varepsilon_2)\Big]\gamma\\&+KA_1^{-1}A_2^{-1}\varepsilon_3\gamma_3(\gamma_3\varepsilon_2+\gamma_1\varepsilon_2)-KA_1^{-1}A_2^{-1}\varepsilon_1\gamma_1(\varepsilon_1\gamma_2+\varepsilon_2\gamma_3)\\&-\varepsilon_4A_3^{-1}(\gamma_2\varepsilon_3+\gamma_1\varepsilon_2)=0\end{aligned} \tag{8}$$

where:

$$\varepsilon_1 = A_3^{-1}(x_2 - x_1)$$
$$\varepsilon_2 = A_2^{-1}x_1$$
$$\varepsilon_3 = A_1^{-1}x_2$$
$$\varepsilon_4 = \left[A_3^{-1}(\gamma_1 - \gamma_2)(x_2 - x_1) + (\gamma_1 - \gamma_3)x_1A_2^{-1} + (\gamma_2 - \gamma_3)x_2A_1^{-1}\right]$$

The equations above (1–8) can be derived in an analogous manner, taking into account the capacity C_m or conductance R_m^{-1} (instead interfacial tension γ) [8].

1.1.2. Phosphatidylcholine– cholesterol complex

Researchers from many years have been trying to define physical properties of mixtures of cholesterol and phospholipids in monolayer and bilayer membranes. These quasi two-dimensional systems are of intrinsic interest to physical chemists. They also help understand certain properties of the membranes of animal cells [9,10]. The interactions between PC (lecithin, L) and cholesterol (Ch) are manifested in significant deviations from the additivity rule. Non-ideal behaviour of the PC–Ch system was explained by the condensing effect of cholesterol (increases surface density of the membrane in presence of sterol) or by the ordering effect (presence of sterol causes order of the hydrocarbon chains). Condensing and ordering effects of cholesterol have been observed both in model and in biological membranes [11–13]. There have also been a number of proposals for existence of the complexes at different stoichiometries. But there is no agreement concerning what stoichiometries of the formed complexes have. The 1:1, 1:2, 2:1, 1:3 and 3:1 complexes are mostly claimed to be in monolayers or bilayers [14,15]. On the other hand, subsequent investigators have suggested that specific associates [16], phase separation [17], domains [18] or lattice-based structures [19] could be formed in the PC–Ch membranes.

In this paragraph, a 1:1 PC–Ch complex has been proposed to exist in bilayer composed of egg lecithin and cholesterol. It was verified experimentally using the interfacial tension γ and electrochemical impedance spectroscopy techniques (the interface tension and impedance values reported below refer to the one side of the bilayer membrane (monolayer) surface area unit).

The dependences of interfacial tension, capacitance C_m and resistance R_m (reciprocal of conductance R_m^{-1}) of PC–Ch membrane as a function of molar fraction of cholesterol x_2 were studied in all the concentration range and are presented in Fig. 1. The resulting dependences deviate from linearity indicating that some bonds are formed in the membrane. The interfacial tension, capacitance and conductance values of pure lecithin membrane are $0.81 \times 10^{-3}\,\mathrm{N\,m^{-1}}$, $0.31\,\mu\mathrm{F\,cm^{-2}}$ and $8.70 \times 10^{-6}\,\Omega^{-1}\,\mathrm{cm^{-2}}$, respectively. The interfacial tension, capacitance and conductance values of the pure cholesterol

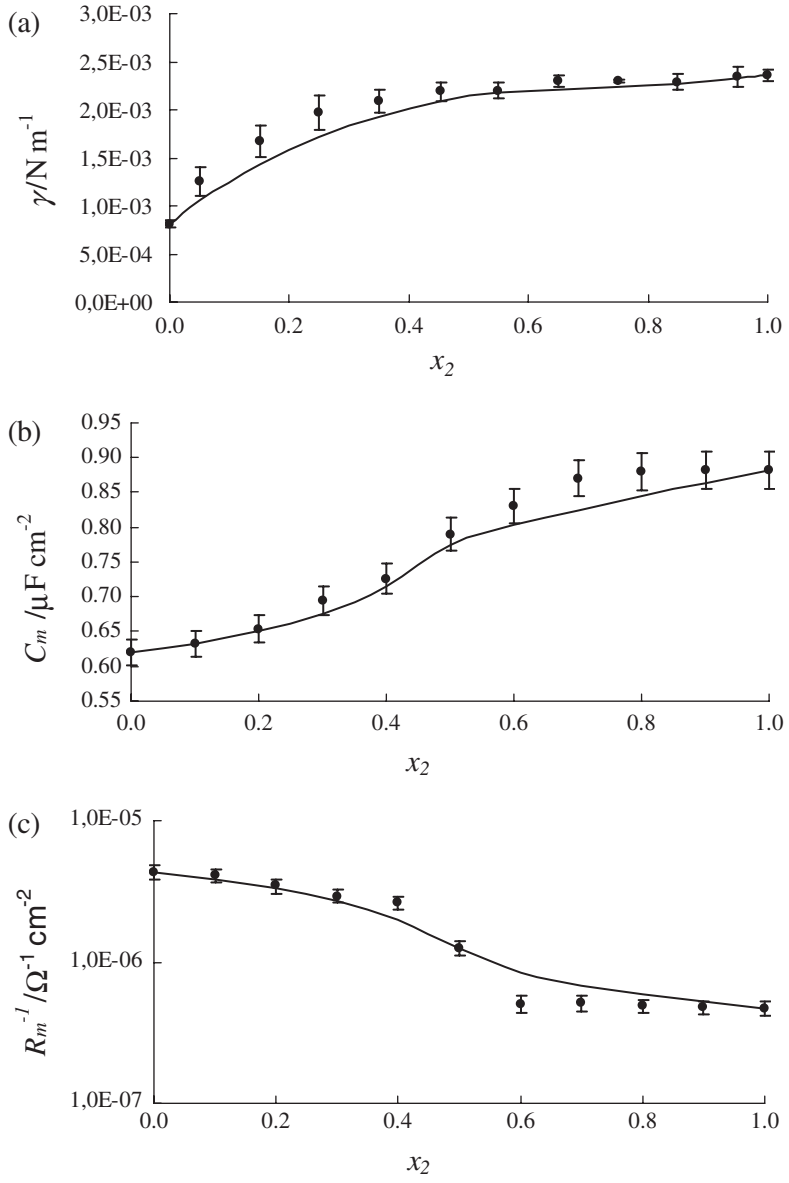

Fig. 1. The interfacial tension γ (a), capacitance C_m (b) and conductance R_m^{-1} (c) of the PC–Ch membrane as a molar fraction of cholesterol x_2 (the experimental values are marked by points and the theoretical ones by curves).

membrane are $2.36 \times 10^{-3}\,\mathrm{N\,m^{-1}}$, $0.44\,\mu\mathrm{F\,cm^{-2}}$ and $9.43 \times 10^{-7}\,\Omega^{-1}\,\mathrm{cm^{-2}}$, respectively [6,8]. Figure 1 also represents the theoretical values, marked by the curves, obtained from equation (8). The values of γ_3, C_3, R_3^{-1}, A_3^{-1} and K whose determination will be described in further parts of the paragraph were

required for the calculation of these theoretical values. Equation (8) can yield two solutions, as it is a square equation. The values yielding a better agreement of the experimental points with equations describing the complex formation between membrane lipid components were chosen. It can be seen from this figure that the agreement between experimental and theoretical points is quite good, which verifies the assumption of the formation of a 1:1 PC–Ch complex in the lipid membrane. The small variances between points indicate that complexes at different stoichiometries or associates are possible in the lecithin–cholesterol bilayer, but one can neglect their influence on the studied system.

The plots of the functions (5) and (6) are presented in Fig. 2 (examples for interfacial tension measurements). The B_1 and B_2 values determined from the line slopes are 1.08 and 7.90, respectively. The intersections of the straight lines with ordinate yield the $-B_1\gamma_3$ and $-B_2\gamma_3$ values, which can be used to determine the interfacial tension of the PC–Ch complex. The mean value γ_3 obtained from both points equals $2.17 \times 10^{-3}\,\mathrm{N\,m^{-1}}$. The C_3 and R_3^{-1} mean values obtained in the same way are equal to $0.39\,\mu\mathrm{F\,cm^{-2}}$ and $4.30 \times 10^{-6}\,\Omega^{-1}\,\mathrm{cm^{-2}}$, respectively.

The interfacial tension and impedance values determined as a function of composition made it possible to calculate the maximal surface concentrations of the membranes composed of pure components. At least one of them is necessary for determination of the A_3^{-1} value. The surface area occupied by a lecithin molecule equal to $85\,\mathrm{Å}^2$ was determined in the work [20]. The surface area occupied by a cholesterol molecule amounts to $38\,\mathrm{Å}^2$ [21].

Knowing the A_1^{-1} and A_2^{-1} as well as B_1 and B_2 the maximal surface concentration of the membrane composed of the lecithin–cholesterol complex could be determined. The resulting A_3^{-1} values were equal to $1.19 \times 10^{-6}\,\mathrm{mol\,m^{-2}}$ (from

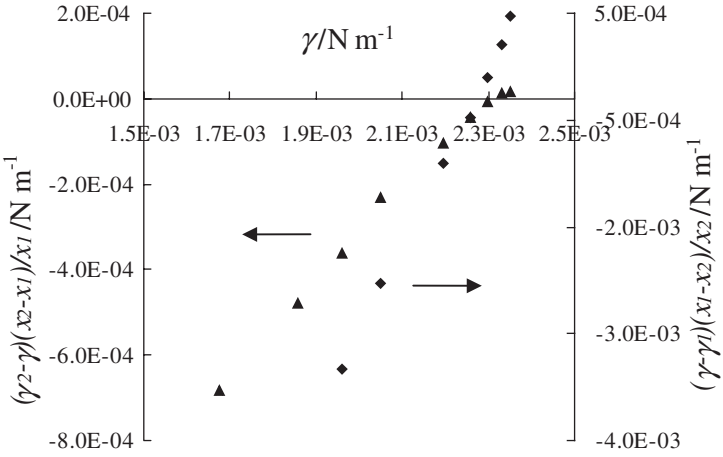

Fig. 2. A plots illustrating equations (5) and (6), from which parameters B_1, B_2, γ_3 for PC–Ch complex can be determined.

interfacial tension measurements) and 1.47×10^{-6} mol m^{-2} (from impedance spectroscopy measurements).

The only value to be determined was the stability constant of the lecithin–cholesterol complex. It could be determined from equation (7) when $x_1 = x_2 = 0.5$; this parameter is 8.59×10^{10} m^2 mol^{-1} (from interfacial tension) and 1.81×10^9 m^2 mol^{-1} (from electrochemical impedance). These values are relatively high, giving additional evidence for the prevalence of the 1:1 complex in mixed phospholipid–cholesterol bilayers. These values also confirm that the assumptions used to simplify equation (4) were correct.

1.1.3. Phosphatidylcholine– phosphatidylethanolamine and phosphatidylethanolamine– cholesterol complexes

Phosphatidylcholine–phosphatidylethanolamine (PC–PE) and phosphatidylethanolamine–cholesterol (PE–Ch) complexes have not been described quantitatively (using mathematical equations) in the literature so far. One can assume that a chemical complex with the stoichiometry of 1:1 is formed as a result of existence of the equilibrium in the two-compound system [7].

Interfacial tension values of the membranes formed using pure components were measured directly. The interfacial tension value of pure PE membrane was 1.67×10^{-3} N m^{-1} [22]; the interfacial tension values of pure PC membrane and pure cholesterol membrane were given in the previous paragraph.

The dependences of the interfacial tension of the lipid membrane as a function of composition for PC–PE and PE–Ch systems were studied in all the concentration range and are presented in Fig. 3. The experimental values are marked in Fig. 3 by points and the theoretical ones obtained from equation (8) by lines. It can be seen from this figure that the theoretical and the experimental interfacial tension values of PC–PE and PE–Ch membranes agree in the whole ranges, which verifies the assumption of the formation of a 1:1 PC–PE and a 1:1 PE–Ch complexes in the lipid membranes [6].

From equations (5) and (6) the interfacial tension γ_3 for PC–PE and PE–Ch complexes were calculated. These values are equal to 1.58×10^{-3} and 2.30×10^{-3} N m^{-1}, respectively. Equations (5) and (6) could also be applied to calculate the maximal surface concentrations of the PC–PE and PE–Ch complexes per unit area of the membranes (the surface area occupied by PE molecule was found to be equal to 74.6 Å^2 [22]). Then the A_3^{-1} values permitted on determining the area occupied by PC–PE and PE–Ch complexes; these were 154 and 127 Å^2 values, respectively.

The only parameters remained to be determined are the stability constants of the PC–PE and PE–Ch complexes. The 2.85×10^8 and 4.16×10^{10} m^2 mol^{-1} values were found using equation (7).

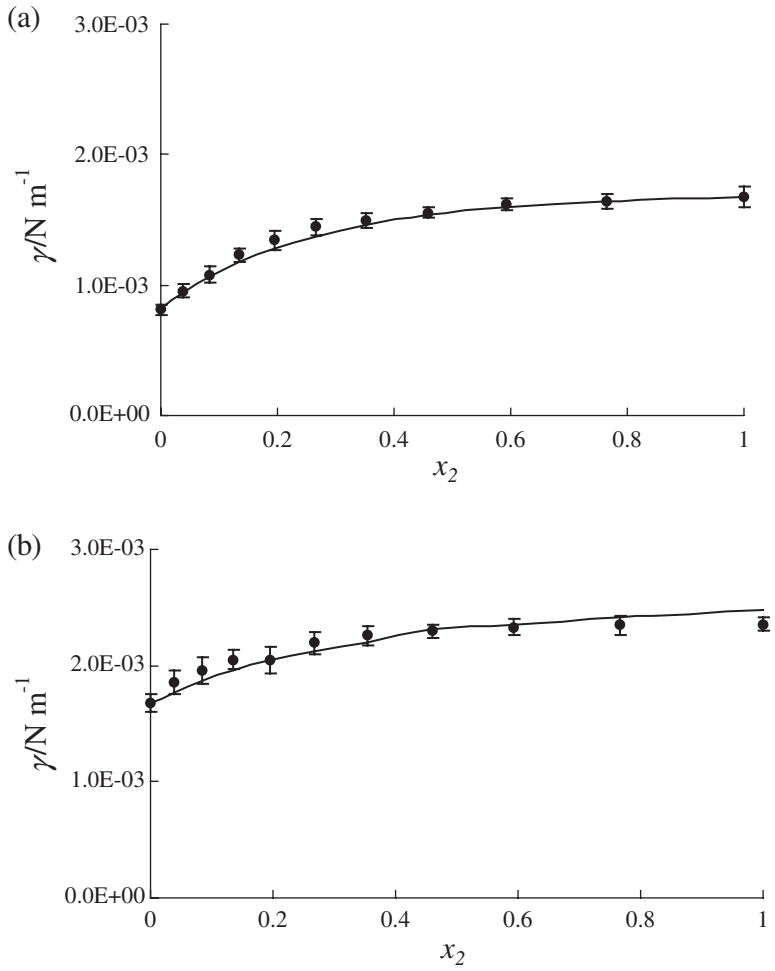

Fig. 3. The dependences of the interfacial tensions γ of (a) PC–PE membrane as a molar fraction of PE x_2 and (b) PE–Ch membranes as a molar fraction of cholesterol x_2 (the experimental values are marked by points and the theoretical ones by curves).

1.1.4. Conclusions

The obtained stability constant of the PC–Ch complex is $8.59 \times 10^{10}\,m^2\,mol^{-1}$ (from interfacial tension measurements) and $1.81 \times 10^{9}\,m^2\,mol^{-1}$ (from impedance spectroscopy measurements), whereas the stability constants of the other complexes are: $2.85 \times 10^{8}\,m^2\,mol^{-1}$ in the case of the PC–PE complex and $4.16 \times 10^{10}\,m^2\,mol^{-1}$ in the case of the PE–Ch complex. High values of these three stability constants confirm the legitimacy of the foundation to simplifying equation (4). It can be observed that the stability constants of the

cholesterol-containing complexes are higher. It means that the PE–Ch and PC–Ch complexes are more stable than the PC–PE complex.

The calculated area occupied by one PC–Ch complex is 127 $Å^2$ (the mean value taken from interfacial tension and impedance measurements) whereas the areas occupied by other complexes are: 154 $Å^2$ for PC–PE and 127 $Å^2$ for PE–Ch. It can be observed that areas of complexes are lower in the cases where cholesterol is involved. Cholesterol condenses some membrane components (the so-called condensation effect) making the membrane structures more rigid. Sterol also improves the packing of membrane lipids as they occupy more places in the hydrophobic layer of the membrane and few places in the polar groups range unlike the phospholipid molecules.

Good agreement of the experimental and theoretical points verifies the assumption of formation of a 1:1 complex in the lipid membrane. Small variances between points indicate that complexes at different stoichiometries or associates are possible in the PC–Ch membrane. Lack of variances in the PC–PE and PE–Ch membranes justifies the statement that other complexes or associates do not appear in these systems.

1.2. Phosphatidylcholine membranes containing transport proteins

In biological membranes, among many different transport phenomena, ion transport is one of the major processes that are vital for all kinds of cell function. This ion transport is all protein-mediated, and a wide variety of mechanisms have been elucidated by which solute flux across membranes is achieved. The extensive studies over the past few decades of the mechanisms of ion transport across artificial membranes have revealed a great deal both about ionophores themselves and about the properties lipid membranes must have for the ionophores to function efficiently. In the case of a carrier molecule, for example, it is of little value for it to have high ion selectivity if it does not combine with the membrane or, if it does combine, if it does not move or bind ions in the membrane. In the case of pore-forming molecules, binding to different membranes may be very similar, but the efficiency of the transport process may depend critically on the state of ionization of the lipid or on the membrane thickness [23,24].

The functional roles played by channels and carriers are quite diverse. The complex formation equilibria between ionophores and monovalent cations in the examples of systems: gramicidin-K^+ ion and valinomycin-K^+ ion and the dimerization equlibrium of gramicidin D are considered in points 1.2.1 and 1.2.2. The presented experimental interfacial tension and impedance values refer to the bilayer surface area unit. Measurements were carried out with unmodified membranes and with the membranes modified by four or five different ionophores concentrations and at five different KCl concentrations. Except for the *Z* values, all recorded impedance spectra are characterized by common general features

and the same dynamic behaviour. For this reason, the data for one KCl concentration and for one gramicidin D or valinomycin concentration are shown.

1.2.1. Gramicidin D as a model of biomembrane ionic channels

Gramicidin D is a natural mixture of 85% of gramicidin A, 10% of gramicidin C and 5% of gramicidin B. Linear gramicidin A, B and C are able to induce ion transfer across both natural and artificial lipid membranes. These pentadecapeptides are built of L- and D-amino acids arranged alternately in a chain, their terminal amino group is formylated and ethanolamine is substituted to their terminal carboxy group. Gramicidin A, B and C differ with only one amino acid: the tryptophan residue appearing at position 11 in gramicidin A is replaced by the L-phenylalanine residue in gramicidin B and by the L-tyrosine residue in gramicidin C [25–27].

Due to unusual D-amino acids present in this structure, gramicidin cannot be used as a model for structures, which may occur in membrane proteins. However, this peptide does illustrate one way to form a selective intermolecular channel through the bilayer. Also, gramicidin, because of its availability, has frequently been used as a ‘‘model membrane protein’’ in studying the perturbing influence of membrane proteins on lipids [23].

1.2.1.1. Gramicidin-K^+ complex analysis by interfacial tension method

The effect of the presence of gramicidin in the phospholipid bilayer on interfacial tension can be described as similar to that of cholesterol (the interfacial tension of such membrane should be a sum of the lecithin and gramicidin interfacial tensions values) presented in point 1.1.2, because gramicidin is the compound, which can be integrally built-in into the membrane [4]. It can be written taking advantage of the additivity of the individual gramicidin–lipid membrane component contributions:

$$\gamma = \gamma_L c_L^s A_L + \gamma_G c_G^s A_G + \gamma_{GK^+} c_{GK^+}^s A_{GK^+} \tag{9}$$

where γ_L, γ_G, γ_{GK^+} ($N\,m^{-1}$) are the interfacial tensions of the membrane formed from lecithin, gramicidin and the GK^+ complex, respectively; c_L^s, c_G^s, $c_{GK^+}^s$ ($mol\,m^{-2}$) are the surface concentrations of lecithin, gramicidin and the GK^+ complex, respectively; A_L, A_G, A_{GK^+} ($m^2\,mol^{-1}$) are the surface areas occupied by lecithin, gramicidin and the GK^+ complex, respectively.

Reaction of formation of the gramicidin-K^+ complex can be presented as [28]

$$G + K^+ \rightleftharpoons GK^+ \tag{10}$$

and then the stability constant describing this complex has the form:

$$K = \frac{c_{GK^+}^s}{c_G^s \cdot a_{K^+}} \tag{11}$$

here a_{K^+} ($mol\,m^{-3}$) is K^+ ions activity in the solution.

The analytical lecithin and gramicidin concentrations ratio in the membrane are denoted by n_G. It was assuming that the gramicidin and lecithin ratio in the membrane is the same as in the forming solution. Thus, n_G is described by the equation:

$$\frac{c_L^s}{c_G^s + c_{GK^+}^s} = \frac{m_L M_G}{m_G M_L} = n_G \tag{12}$$

where m_L, m_G (g) are the masses of lecithin and gramicidin in the forming solution, respectively; M_L, M_G (g mol^{-1}) the molar masses of lecithin and gramicidin, respectively.

Elimination of c_L^s, c_G^s, $c_{GK^+}^s$ yielded the equation:

$$\gamma = -\frac{(A_L n_G^{-1} + A_{GK^+})K}{A_L n_G^{-1} + A_G} a_{K^+}\gamma + \frac{(\gamma_L A_L n_G^{-1} + \gamma_{GK^+} A_{GK^+})K}{A_L n_G^{-1} + A_G} a_{K^+} + \frac{\gamma_L A_L n_G^{-1} + \gamma_G A_G}{A_L n_G^{-1} + A_G} \tag{13}$$

Equation (13) expresses the dependence of interfacial tension of the lipid membrane modified with gramicidin D on the K^+ ion concentration; this dependence is presented in Fig. 4 for various gramicidin D concentrations in the membrane.

Equation (13) can be written in the form $y = m_1 x_1 + m_2 x_2 + b$. The m_1, m_2 and b coefficients were determined using linear regression. Eight constants are present in the equation whereas only three of them are available. Therefore, combinations of individual constants only can be calculated instead of the constants themselves.

The m_1, m_2 and b coefficients were applied to present the agreement of the equation (13) data (solid lines) with the experimental data (points) in Fig. 4 using

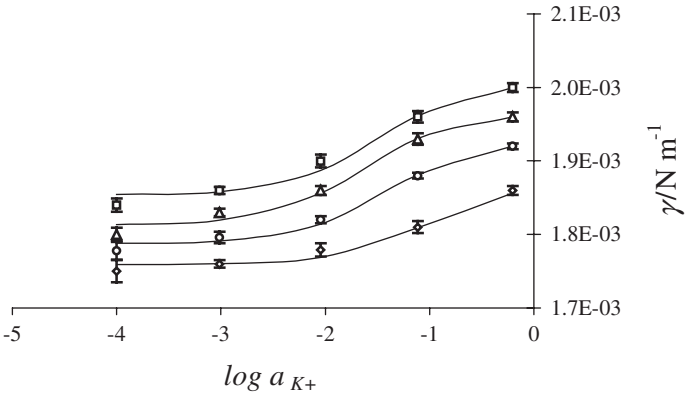

Fig. 4. The dependence of the interfacial tension γ of a lipid membrane formed from PC modified with gramicidin D on the logarithm of electrolyte solution concentration log a_{K^+} for different gramicidin D: PC ratio where (□) 1:40; (Δ) 1:30; (○) 1:20 and (◇) 1:10; the experimental values are marked by points and the theoretical ones by curves.

equation (14) presented below:

$$\gamma = \frac{m_2 a_{K^+} + b}{1 - m_1 a_{K^+}} \tag{14}$$

The coefficients values, presented in the Table 1, were used to calculate the following constants: the surface areas occupied by gramicidin membrane and GK^+ complex, interfacial tensions of the gramicidin membrane and GK^+ complex and the stability constant of the gramicidin-K^+ complex.

The parameters m_1, m_2 and b were described by equations (15–17):

$$m_1 = -\frac{\left(A_L n_G^{-1} + A_{GK^+}\right)K}{A_L n_G^{-1} + A_G} \tag{15}$$

$$m_2 = \frac{\left(\gamma_L A_L n_G^{-1} + \gamma_{GK^+} A_{GK^+}\right)K}{A_L n_G^{-1} + A_G} \tag{16}$$

and

$$b = \frac{\gamma_L A_L n_G^{-1} + \gamma_G A_G}{A_L n_G^{-1} + A_G} \tag{17}$$

All magnitudes: γ_G, γ_{GK^+}, A_G, A_{GK^+} and K can be determined from the equations (15–17) when the lecithin membrane interfacial tension γ_L ($1.623 \times 10^{-3}\,N\,m^{-1}$) and the area occupied by lecithin membrane A_L values ($85\,Å^2$) are known [4,20].

The linear equation was derived by elimination of the constants K and A_G from equations (15) and (16) in order to calculate the constants A_{GK^+} and γ_{GK^+}. This calculation was illustrated in the paper [28]. Values obtained for the interfacial tension of the gramicidin-K^+ ions complex γ_{GK^+} and the area occupied by gramicidin-K^+ ions complex A_{GK^+} are equal to $1.89 \times 10^{-3}\,N\,m^{-1}$ and $156\,Å^2$, respectively.

The values A_G and γ_G were then calculated from equation (17) by a similar method. This calculation was illustrated graphically in the paper [28]. The determined values of the area occupied by gramicidin molecule in membrane and

Table 1. The parameters m_1, m_2 and b determined from equation (13) used to calculate the interfacial tension value of membrane built from gramicidin, γ_G; gramicidin-K^+ ion complex, γ_{GK^+}; area occupied by gramicidin molecule, A_G; area occupied by gramicidin-K^+ ion complex, A_{GK^+} and stability constant of gramicidin-K^+ ion complex K

Gramicidin D:PC ratio	n_G^{-1} ($\times 10^{-2}$)	m_1	m_2 ($\times 10^{-5}$)	b
1:10	6.19	−0.03027	6.076	0.001854
1:20	3.10	−0.04382	8.612	0.001813
1:30	2.06	−0.02539	4.89	0.001788
1:40	1.55	−0.01058	1.98	0.001759

interfacial tension of the gramicidin membrane are equal to $188\,\text{Å}^2$ and $1.76 \times 10^{-3}\,\text{N m}^{-1}$, respectively. No unequivocal determination of the area occupied by gramicidin molecule has been presented in the literature. The proposed values range from 120 to $150\,\text{Å}^2\,\text{molecule}^{-1}$, and even to $250\,\text{Å}^2\,\text{molecule}^{-1}$ [29–31].

The last value, i.e. the stability constant of complex K, was determined from the two separate equations (15) and (16) by substitution of the determined earlier values of parameters γ_G, γ_{GK^+}, A_G, A_{GK^+} relative to values the m_1 or m_2. The obtained K values are identical and are equal to $0.033\,\text{m}^3\,\text{mol}^{-1}$.

It would be interesting to calculate the surface energy of the membrane formed from gramicidin or the gramicidin-ion K^+ complex. This is the energy needed to change the surface for 1 mol. For these calculations, it is necessary to find the surface concentration of the membrane built from the pure gramicidin and gramicidin-K^+ complex. These constants were calculated from the equation:

$$c^s = \frac{1}{A \cdot N_A} \tag{18}$$

where N_A (mol^{-1}) is the Avogadro's constant.

The obtained c^s_G and $c^s_{GK^+}$ values are equal to 8.82×10^{-7} and $1.06 \times 10^{-6}\,\text{mol m}^{-2}$, respectively. Knowing the surface concentrations of the membrane made from the pure gramicidin and pure gramicidin-K^+ complex and its interfacial tensions, the surface energy E_s of these compounds can be calculated using equation (19):

$$E_s = \frac{\gamma}{c^s} \tag{19}$$

where γ (N m^{-1}) is the interfacial tension of the membrane formed from gramicidin or the gramicidin-K^+ complex and c^s (mol m^{-2}) the surface concentration of the gramicidin or the gramicidin-K^+ complex.

The obtained value of the surface energy for gramicidin membrane is equal to $1995.7\,\text{J mol}^{-1}$ and for gramicidin-ion K^+ complex membrane is equal to $1782.5\,\text{J mol}^{-1}$. The result of subtraction of these energies ($-213.2\,\text{J mol}^{-1}$) is the energy required for entrance of the K^+ ions into the pore of the gramicidin channel.

It is very difficult to interpret these values, because the energy required for entrance of the K^+ ions into the pore of the gramicidin channel has a small value. It is very hard to compare this value with different values of the energy of the bonds.

The gramicidin channel has about a 0.4 nm diameter and is full with water. It permits water and the partly hydrated K^+ ions to pass through a membrane. The determined nominal value of the energy needed for K^+ ions to enter the pore of the gramicidin channel is connected with the pushing out the water from the gramicidin channel and inserting the ion K^+ inside the channel.

1.2.1.2. Gramicidin dimer analysis by impedance spectroscopy method

The gramicidin D monomers introduced into the bilayer can form formyl-NH to formyl-NH (N-to-N) dimeric species. The dimers stretch across the bilayer and they can constitute ionic channels, which are able to transport monovalent cations. In the N-to-N dimer model the monomers are connected by 12 intermolecular hydrogen bonds and the dimer is stabilized by 6 intermolecular hydrogen bonds linking the formyl groups and the N-terminal amino acids mutually [32,33]. It is suggested that opening and closing of the channels is connected with the association of the intermolecular hydrogen bonds. The dimer-building monomers separate if their bonds are broken hereby destroying the transmembrane channel. At low concentration, gramicidin in the lipid bilayer can exist both as monomers and as dimers [34]; at relatively high concentrations it appears as dimers only [33]. The dimerization of gramicidin has been suggested to be responsible for the ion-conducting transmembrane channels in bilayers [35].

Gramicidin channels are formed by transmembrane dimerization of the monomers originating from different monolayers composing the bilayer. The dimerization equilibrium constant of gramicidin K_{GG} can be written in the form [31]:

$$K_{GG} = \frac{c^{s}_{GG}}{\left(c^{s}_{G}\right)^{2}} \tag{20}$$

where c^{s}_{G} ($\mathrm{mol\,cm^{-2}}$) is the surface concentration of the gramicidin monomers and c^{s}_{GG} ($\mathrm{mol\,cm^{-2}}$) the surface concentration of the gramicidin dimers.

The sum of the monomer (on both bilayer sides) and of dimer surface concentrations is equal to the total gramicidin concentration in the bilayer c_T:

$$c_T = c^{s}_{G} + c^{s}_{GG} \tag{21a}$$

The total gramicidin D concentration can also be determined from the equation (the results are presented in Table 2 with other parameters determined as described further on):

$$c_T = \frac{s^{s}_{PC} M_{PC}}{n M_G} \tag{21b}$$

in which s_{PC} ($\mathrm{mol\,cm^{-2}}$) is the PC surface concentration in the membrane built of lipid only and n the gramicidin to PC weight ratio in the forming solution.

Substitution of the gramicidin monomers surface concentration obtained from the total gramicidin concentration (equation (21a)) in equation (20) followed by simple transformations yield another relation to determine the equilibrium constant of the gramicidin dimerization:

$$K_{GG}^{-1/2} = c_T\left(c^{s}_{GG}\right)^{-1/2} - \left(c^{s}_{GG}\right)^{1/2} \tag{22}$$

Impedance of lipid bilayers modified with gramicidin D was measured in a system arranged in series. It is diagrammatically presented on Scheme 1 in Fig. 5:

Table 2. Total gramicidin concentration in the bilayer c_T, coverage Θ and surface concentration of gramicidin dimers c_{GG} as function of gramicidin D:PC weight ratio

Gramicidin D:PC ratio	$10^6\ c_T$ (mol cm^{-2})	$10^5\ \Theta$	$10^7\ c_{GG}$ (mol cm^{-2})
1:1.0 × 10^4	1.23	6.97 ± 0.01	9.33 ± 0.02
1:2.5 × 10^4	0.49	2.37 ± 0.01	3.15 ± 0.02
1:5.0 × 10^4	0.24	1.01 ± 0.01	1.36 ± 0.02
1:7.5 × 10^4	0.16	0.55 ± 0.01	0.73 ± 0.02
1:1.0 × 10^5	0.12	0.40 ± 0.01	0.53 ± 0.02

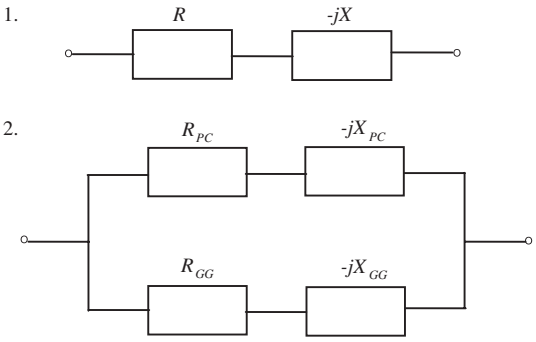

Fig. 5. Equivalent circuits representing electric properties of PC membranes contained gramicidin D. R is real part of impedance (after substracting electrolyte solution resistance) and $-jX\left(X = \frac{1}{\omega C}\right)$ is imaginary part of impedance on the simplified Scheme 1. R_{PC}, $-jX_{PC}$ is impedance of pure PC bilayer, and R_{GG}, $-jX_{GG}$ is impedance related to the presence of gramicidin channels able to transport monovalent ions across the membrane on the Scheme 2.

Effect of gramicidin on the PC bilayer impedance can be determined by assuming that the double layer capacity at the membrane/solution interface is unmodified by gramicidin and by distinguishing the impedance of pure PC bilayer from the impedance related to the presence of gramicidin channels is able to transport monovalent ions across the membrane (Scheme 2 in Fig. 5).

A comparison of real and imaginary parts of impedances presented by both schemes in Fig. 5 yields the relationship, which can be used for the determination of impedance components, related to the presence of gramicidin channels in the membrane [31]:

$$R_{GG} = \frac{R(R_{PC}^2 + X_{PC}^2) - R_{PC}(R^2 + X^2)}{(R_{PC} - R)^2 + (X_{PC} - X)^2} \tag{23a}$$

$$X_{GG} = \frac{X(R_{PC}^2 + X_{PC}^2) - X_{PC}(R^2 + X^2)}{(R_{PC} - R)^2 + (X_{PC} - X)^2} \tag{23b}$$

Very simple impedance diagrams were obtained in the absence of channel-forming gramicidin D (Fig. 6a); they had the form of impedance semicircles in the entire analysed frequency range; it was the evidence of the lipid bilayer being a dielectric layer with leakage. The semicircles were distorted because the lipid bilayer itself was not a simple and uniform dielectric layer. The impedance spectra of the gramicidin-containing bilayers (Fig. 6b) had the form of a capacitance semicircle and, in addition, Warburg impedance appeared at frequencies lower than 2.51 Hz, probably due to potassium-ion transport in the area near the membrane surface. Both imaginary and real parts of PC bilayer impedance proved to be by two orders of magnitude lower when it was modified with gramicidin than those obtained from pure lipid membranes. Impedance of gramicidin dimers (Fig. 6c) was calculated, using equations (23a) and (23b), from the impedance spectra of pure PC membrane (Fig. 6a) and the membrane modified with gramicidin (Fig. 6b).

It can be deduced from Fig. 6c that the impedance due to the presence of gramicidin dimers consists of the Warburg impedance Z_W only; the impedance characteristic for the diffusion at the electrode layer which is presented by the equation [36]:

$$Z_W = \sigma\omega^{1/2} - j\sigma\omega^{1/2} \tag{24}$$

The Warburg coefficients σ modelling ion transport near surface of the lipid bilayer were determined by plotting the straight lines in the $R_{GG} = f(\omega^{-1/2})$ coordinate system; the slope of the line yielded the σ value. The Warburg coefficient values obtained in this way in the logarithmic form are presented in Fig. 7 vs. potassium-ion concentration logarithm (KCl concentrations in mol cm^{-3}).

The Warburg coefficient can also be calculated from the well-known equation [37]:

$$\sigma = RT(2D)^{1/2}F^2z^2cA \tag{25}$$

here R, T, z and F are denoted as usual, D is diffusion coefficient of the ion in the aqueous phase, supporting electrolyte concentration is denoted by c and membrane surface area by A.

The above equation describes the diffusion to a flat uniform surface while the ion transport across the bilayer containing gramicidin D depends on the number of open gramicidin channels. The surface fraction occupied by active gramicidin dimers can be denoted as coverage Θ ($0 < \Theta < 1$). This parameter can be substituted in equation (25) as the membrane surface area.

Coverage values were determined for gramicidin-containing membranes from the intersection points with the ordinate in the plots presented in Fig. 7 using the Warburg coefficient equation in the form (the results are presented in Table 2):

$$\log\ \sigma = \log\left(\frac{RT}{(2D)^{1/2}F^2z^2c\Theta}\right) - \log\ c_{K^+} \tag{26}$$

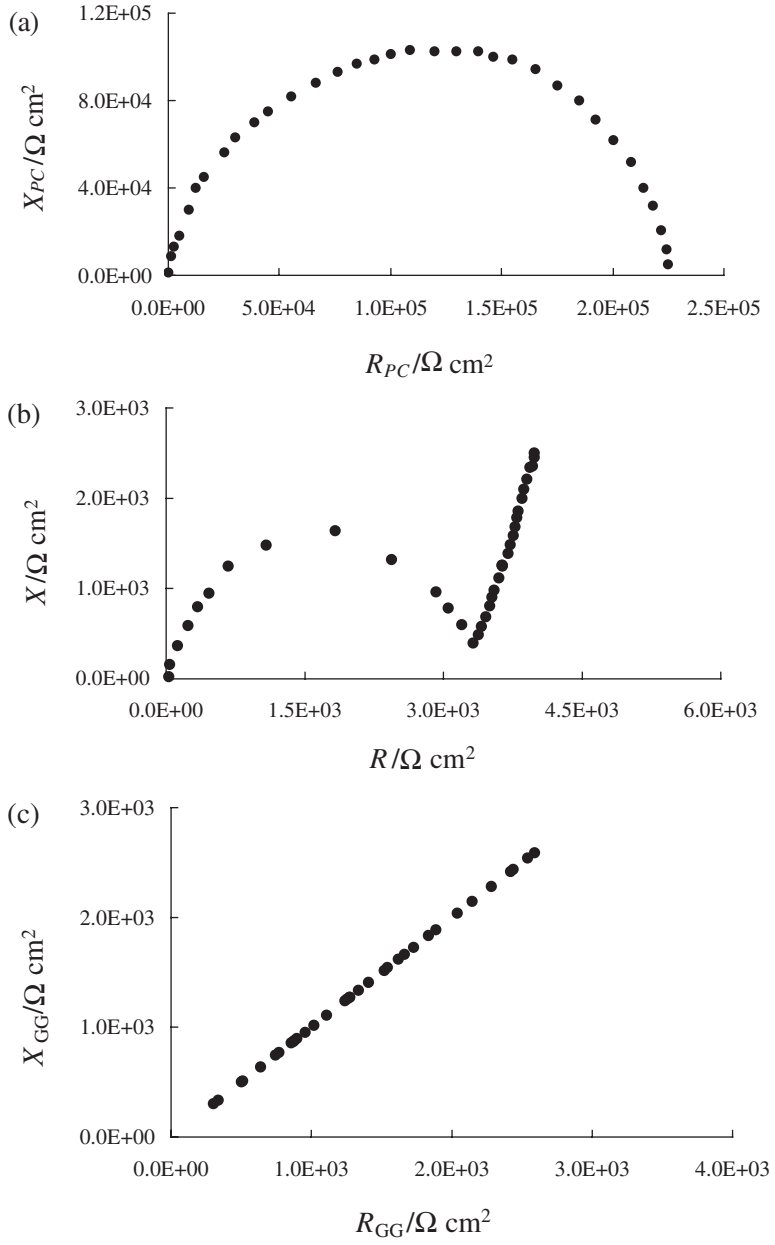

Fig. 6. Dependence of an imaginary part $-Z''$ on the real part Z' recorded for 1.0×10^{-3} KCl mol cm^{-3} (a) of pure PC bilayer, (b) of PC bilayer modified with gramicidin D (total gramicidin concentration $= 4.92 \times 10^{-7}$ mol cm^{-2}) and (c) of gramicidin channels ($f \geq 100$ Hz).

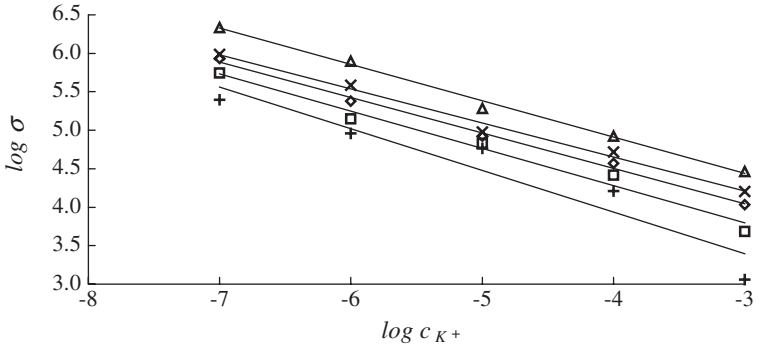

Fig. 7. Dependence of Warburg coefficient logarithm logσ on potassium-ion concentration logarithm logc_K^+. The following total gramicidin D concentrations were used: (+) 1.23×10^{-6} mol cm^{-2}, (□) 4.92×10^{-7} mol cm^{-2}, (◇) 2.41×10^{-7} mol cm^{-2}, (×) 1.64×10^{-7} mol cm^{-2} and (Δ) 1.23×10^{-7} mol cm^{-2}.

Coverage can also be presented in the following way:

$$\Theta = c^{s}_{GG} A_{GG} \tag{27}$$

where A_{GG} (cm^2 mol^{-1}) is the area occupied by 1 mol of channels.

Substituting the expression of surface concentration of the dimer obtained by transformation of equation (27) to equation (22) yields a linear dependence (this dependence is shown in Fig. 8):

$$\Theta^{1/2} = A_{GG} c_T \Theta^{-1/2} - K_{GG}^{-1/2} A_{GG}^{1/2} \tag{28}$$

The slope value of the straight line (equation 28) is equal to the surface area occupied by 1 mol of channels. Substituting this value to equation (27) yields the surface concentration of the gramicidin dimers (Table 2).

The area occupied by a single gramicidin dimer A_G can be readily calculated if the surface area occupied by 1 mol channels is known. The A_G value obtained in this way is 124 Å^2 molecule^{-1}.

Intersection of the straight line with the ordinate (equation (28)) yields the equilibrium constant of the gramicidin dimerization equal to 1.06×10^7 cm^2 mol^{-1}. This K_{GG} value is similar to the values proposed by other authors, ranging from 10^8 to 10^{17} cm^2 mol^{-1} [38,39].

1.2.2. Valinomycin as a model of selective membranes carrier of K^+ ions

Valinomycin is one of a number of cyclic depsipeptides that have been shown to function by increasing membrane cation permeability. These kinds of ionophores have been found to increase the electrical conductivity of the lipid barrier in membranes of bilayers because of their ion-complex ability. As is known from monolayer and bilayer studies, valinomycin binds K^+ ions very strongly in

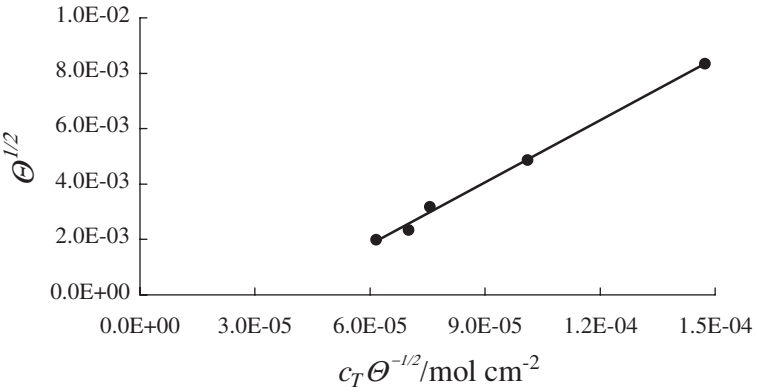

Fig. 8. The plot illustrating equation (28) used to determine area occupied by 1 mol of channels A_{GG} and dimerization equilibrium constant of gramicidin K_{GG}.

comparison, for example, to Na^+ [25]. The complexed ion is situated inside the ring-shaped valinomycin molecule. In addition, the valinomycin molecule binds water molecules of the first hydration layer of the cation and its hydrocarbon groups oriented outside the molecule facilitate complex dissolution in the hydrophobic membrane phase. The valinomycin molecule complex with the cation is electrically charged; it diffuses across the membrane. The reverse process occurs at the opposite membrane surface – the ion passes to the aqueous phase [40].

1.2.2.1. Interfacial tension analysis

Dependence of K^+ ion surface excess should be expressed as a function of the K^+ ion concentration in the solution before the effect of valinomycin on interfacial tension of a lipid bilayer will be described.

The valinomycin-K^+ ion complex is formed in the medium containing the K^+ ion [41]:

$$V_W + K_W^+ \rightleftharpoons VK_W^+ \tag{29}$$

The equilibrium between the valinomycin in electrolyte solution (presented as VK_W^+) and valinomycin in lipid bilayer membrane (presented as VK_b^+) is showed below:

$$VK_W^+ \rightleftharpoons VK_b^+ \tag{30}$$

The relative K^+ ion excess in the bilayer to bulk phase can be expressed by the equation:

$$\Gamma_{K^+} = \frac{\delta A c^b_{VK_b^+} - \delta A a_{K^+}}{A} \tag{31}$$

where $c^{b}_{VK^{+}_{b}}$ (mol m^{-3}) is the volume concentration of the K^+ ion in the bilayer, δ (m) the lipid bilayer thickness and a_{K^+} (mol m^{-3}) the K^+ ion activity in the solution.

The above relationship yields:

$$\Gamma_{K^+} = \delta c^{b}_{VK^{+}_{b}} - \delta a_{K^+} \tag{32}$$

The adsorption of K^+ ions on the lecithin membrane surface was not taken into account when the surface access of K^+ ions, using the Gibbs equation, was described.

Stability constant of the valinomycin-K^+ ion complex K has the form:

$$K = \frac{c^{b}_{VK^{+}_{W}}}{c^{b}_{V_W} a_{K^+}} \tag{33}$$

where $c^{b}_{VK^{+}_{W}}$ (mol m^{-3}) is the volume concentration of the K^+ ion in the solution and $c^{b}_{V_W}$ (mol m^{-3}) the concentration of the valinomycin in the solution.

The partition coefficient takes a form:

$$B = \frac{c^{b}_{VK^{+}_{b}}}{c^{b}_{VK^{+}_{W}}} \tag{34}$$

and then

$$c^{b}_{V_W} V_W + c^{b}_{VK^{+}_{W}} V_W + c^{b}_{V_b} V_b + c^{b}_{VK^{+}_{b}} V_b = m_V \tag{35}$$

where $c^{b}_{V_b}$ (mol m^{-3}) is the concentration of the valinomycin in the membrane, V_W (m^3) the volume of the electrolyte solution, V_b (m^3) the volume of the lipid bilayer and m_V (mol) the total quantity of the valinomycin.

Because the volume of the bilayer lipid membrane is small in comparison with the volume of the aqueous phase, the terms defining the valinomycin quantities in the lipid bilayer can be neglected.

Therefore the equation (35) may be presented as:

$$c^{b}_{V_W} V_W + c^{b}_{VK^{+}_{W}} V_W = m_V \tag{36}$$

Then,

$$\frac{c^{b}_{VK^{+}_{b}} V_W}{BKa_{K^+}} + \frac{c^{b}_{VK^{+}_{b}} V_W}{B} = m_V \tag{37}$$

$c^{b}_{VK^{+}_{b}}$ is determined from equation (37) and it is substituted in equation (32). The result is:

$$\Gamma_{K^+} = \frac{m_V}{V_W(1 + Ka_{K^+})} KB\delta a_{K^+} - a_{K^+}\delta \tag{38}$$

The Gibbs equation is presented in the form:

$$d\gamma = -\Gamma_{K^+} d\mu_{K^+} \tag{39}$$

Substitution of equation (37) in equation (38) yields:

$$d\gamma = -\left(\frac{m_V BKa_{K^+}}{V_W(1+Ka_{K^+})}\delta - a_{K^+}\delta\right)RT\frac{da_{K^+}}{a_{K^+}} \tag{40}$$

a_{K^+} integration of the above equation yields the relationship:

$$\gamma = \delta RTa_{K^+} - \frac{m_V}{V_W}RT\delta B \ \ \ln(1+Ka_{K^+}) + \text{const} \tag{41}$$

For $a_{K^+} = 0$, $\gamma = \gamma_0$ and $\frac{m_V}{V_W} = c_V^b$ the equation results to:

$$\gamma = \gamma_0 + \delta RTa_{K^+} - \delta BRTc_V^b \ \ \ln(1+Ka_{K^+}) \tag{42}$$

where c_V^b (mol m^{-3}) is the volume concentration of the valinomycin.

Dependence of the interfacial tension of valinomycin-modified lipid membrane in the K^+ ion medium on valinomycin concentration in the membrane is given by equation (42) and is presented in Fig. 9.

The bilayer membranes were created from the drop of forming solution, which contained valinomycin. When the lipid membranes were formed, the valinomycin partly passed to the aqueous phase as being soluble in water and in the phospholipid in accordance with the partition coefficient.

It is indicated by equation (42) that the dependence of interfacial tension on the valinomycin concentration in the bilayer should be a straight line of a negative slope. It is also determined from this equation that the slope should increase with increasing K^+ ion concentration in the solution; this can also be seen. The values of interfacial tension of pure lecithin membranes increase together with the

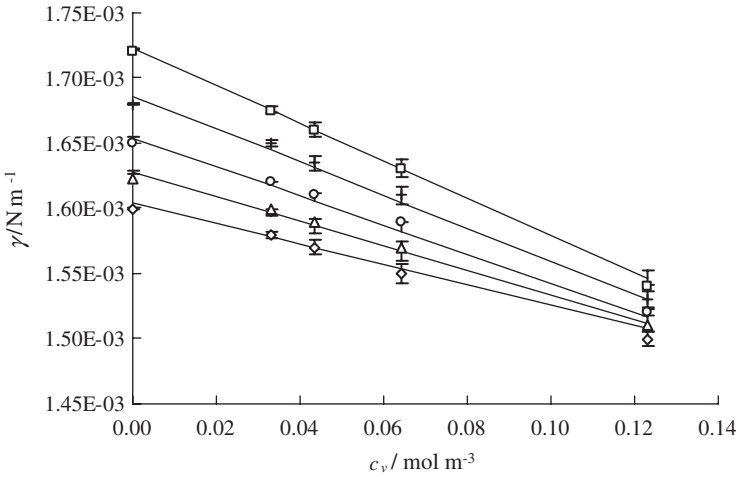

Fig. 9. The dependence of the interfacial tension γ of lecithin membrane in K^+ ion medium on valinomycin concentration c_v for different electrolyte concentration. (◇) 0.0001 M KCl, (Δ) 0.001 M KCl, (○) 0.01 M KCl, (+) 0.1 M KCl, (□) 1 M KCl (the experimental values are marked by points and the theoretical ones by curves).

increasing the K^+ ions concentration. This growth should be proportional to K^+ ions concentration in electrolyte solution in the absence of valinomycin, which results from equation (42). However, as can be seen in Fig. 9 this proportionality is not noticed.

In the paper [42] the figure illustrating the coverage of lecithin membrane by H^+ and OH^- ions as a function of pH electrolyte solution was reported. The surface of lecithin bilayer was built from $-PO^{(-)}$ and $-\overset{(+)}{N}(CH_3)_3$ groups. In neutral pH (about 7, as in the electrolyte solution) the $-\overset{(+)}{N}(CH_3)_3$ groups of the lecithin membrane were covered by OH^- ions and the $-PO^{(-)}$ groups were not covered. It is possible that the K^+ ions (from electrolyte solution – KCl) are adsorbed on free $-PO^{(-)}$ groups, however, in the description of the valinomycin presence on the interfacial tension of lecithin membrane, the adsorption of K^+ ions on lecithin membrane surface was not take into account.

Probably the lack of proportionality of the interfacial tension for K^+ ions concentration is the result of increasing the negative surface access of K^+ ions during the growing of the electrolyte solution concentration in the absence of valinomycin.

The equation (42) is of the $y = ax + b$ type. The a and b constants presented in Table 3 were determined using the linear regression, where

$$a = RT\delta B \quad \ln(1 + Ka_{K^+}) \tag{43}$$

and

$$b = \gamma_0 + RT\delta \tag{44}$$

It is possible to determine the γ_0 value from equation (44) knowing the thickness of the lipid bilayer formed from stock solution containing lecithin in *n*-decane. The calculated value γ_0 is equal to $1.59 \times 10^{-3}\,\mathrm{N\,m^{-1}}$.

The parameters K and B could be determined from equation (43). However this is very difficult because the value of the stability constant of the valinomycin-K^+ ion complex is in the expression $\ln(1 + Ka_{K^+})$. Both these parameters were calculated using the ''self-agreement'' method from equation (45):

$$a = \delta RTB \ln(1 + Ka_{K^+}) \tag{45}$$

Table 3. The parameters a and b determined from equation (42) used to calculate the partition coefficient B and stability constant of valinomycin-K^+ ion complex K

C_{KCl} (mol dm^{-3})	a_{K^+} (mol m^{-3})	a	b
0.0001	0.10	8.320×10^{-4}	1.604×10^{-3}
0.001	0.97	9.354×10^{-4}	1.628×10^{-3}
0.01	9.02	1.064×10^{-3}	1.654×10^{-3}
0.1	77.0	1.241×10^{-3}	1.686×10^{-3}
1.0	624.0	1.470×10^{-3}	1.723×10^{-3}

Using the $\ln(1 + Ka_{K^+})$ value, it is possible to use the calculation by the assumption of a certain value for the stability constant K. Then the B value could be determined by graphic representation of the values of straight-line parameters a (from the Table 3) as a function $\ln(1 + Ka_{K^+})$. Applying the obtained value of parameter B to equation (46) allows one to determine the K value.

$$\ln\ a_{K^+} = -\ln\ K + \ln(e^{a/RTB} - 1) \tag{46}$$

Equation (46) was received by transformation of equation (43) to the following expression:

$$a_{K^+} = \frac{1}{K}(e^{-a/RTB} - 1) \tag{47}$$

and then this expression was logarithmic.

The action, described above, of substituting K and B in equations (45) and (46) were made as long as it is possible to obtain the ascertained values of these parameters (best fits). The calculated value of the stability constant of the valinomycin-K^+ ion complex K equals $3.52 \times 10^5\ m^3\ mol^{-1}$. This value is in good agreement with the literature values of the stability constant (equal to 0.1 or 1.5 to 5×10^3, and even $2 \times 10^6\ dm^3\ mol^{-1}$ [43–46].

The partition coefficient B obtained in this way equals 6.0. This indicates, that the valinomycin concentration in the lecithin membrane is six times higher than the concentration of valinomycin in electrolyte solution.

Knowing the partition coefficient and stability constant values, the theoretical values of the interfacial tension of the lecithin membrane with the presence of valinomycin were calculated using equation (42). The theoretical values obtained are presented in Fig. 9 and are marked by lines; points on the same figure show the experimental values. It can be seen that the agreement between experimental and theoretical points is very good, which verifies the assumption of the formation of a valinomycin-K^+ ion complex in the lipid membrane.

1.2.2.2. Impedance spectroscopy analysis

Membrane component concentrations can be related to its surface area by multiplying volume concentrations by lipid bilayer thickness. The complex formation equilibrium constant can then be written in the form:

$$K = \frac{c^s_{VK^+}}{c^s_V a_{K^+}} \tag{48}$$

where $c^s_{VK^+}$ ($mol\ cm^{-2}$) is the surface concentration of the complex and c^s_V ($mol\ cm^{-2}$) the surface concentration of valinomycin.

Determination of membrane conductivity in terms of the second Ohm law yields:

$$R_m^{-1} = \frac{A}{\delta}\mu_{VK^+}\frac{c^s_{VK^+}}{d}F \tag{49}$$

here μ_{VK^+} ($cm^2\ V^{-1}\ s^{-1}$) is the mobility of the VK^+ complex.

Surface concentration of the complex can be presented as:

$$c^{s}_{VK^+} = \frac{Ka_{K^+}c_T}{1 + Ka_{K^+}} \tag{50}$$

taking advantage of the following set of equation:

$$\begin{aligned} c^{s}_{V} + c^{s}_{VK^+} &= c_T \\ c^{s}_{VK^+} &= Kc^{s}_{V}a_{K^+} \end{aligned} \tag{51}$$

Substituting equation (50) in equation (49) yields the dependence permitting to determine conductivity as function of total valinomycin and/or electrolyte concentration:

$$R_m^{-1} = \frac{A}{\delta^2}\mu_{VK^+}F\frac{Ka_{K^+}c_T}{1 + Ka_{K^+}} \tag{52}$$

In the absence of the ion carrier, the impedance diagrams exhibited very simple profiles, showing a capacitive semicircle in the analysed frequency range, indicating that the lipid bilayer behaves as an isotropic sheet (Fig. 10a). The frequency response was drastically different when valinomycin was present in the membrane (Fig. 10b). Then, the impedance spectra contained a capacity semicircle and, in addition, a low-frequency semicircle related to the potassium-ion transport in the area close to the membrane surface (formation of the second semicircle was observed to start at 0.01 M KCl only).

The electric properties of the pure lipid membrane are described by the electric circuit No. 1, presented in Fig. 11. The possibility of misinterpretation of the recorded data is reduced by simplicity of the circuit. R_0 is the electrolyte solution resistance; it was assumed to be of ohmic nature and not to perturb the membrane properties. R_m represents the resistance of the membrane and C_m is the membrane capacitance. Resistance and capacity of the PC membranes change insignificantly with increasing electrolyte concentration in the studied KCl concentration range: resistance decreases and capacity increases. It can be explained by great membrane elasticity caused by the process of its formation. Increased elasticity results in reduced ordering of phosphatidyl hydrocarbon chains and in decreased membrane resistance. In addition, a greater amount of water can be dispersed in the membrane causing increase in its electric permittivity and, consequently, in capacity.

A simple membrane model taking into account impedance components of the membrane and the impedance representing the situation at the membrane interface is represented by Scheme 2 of Fig. 11. The membrane impedance is composed of electric capacity of the membrane C_m and of electric resistance of the VK^+ complex transport inside the membrane R_m. Capacity and resistance of the membrane/electrolyte solution phase transition are denoted by C_{pt} and R_{pt}, respectively (pt stands for phase transfer). Such symbols of electric equivalent circuit characterizing ion transport have been commonly used in the literature [32,47].

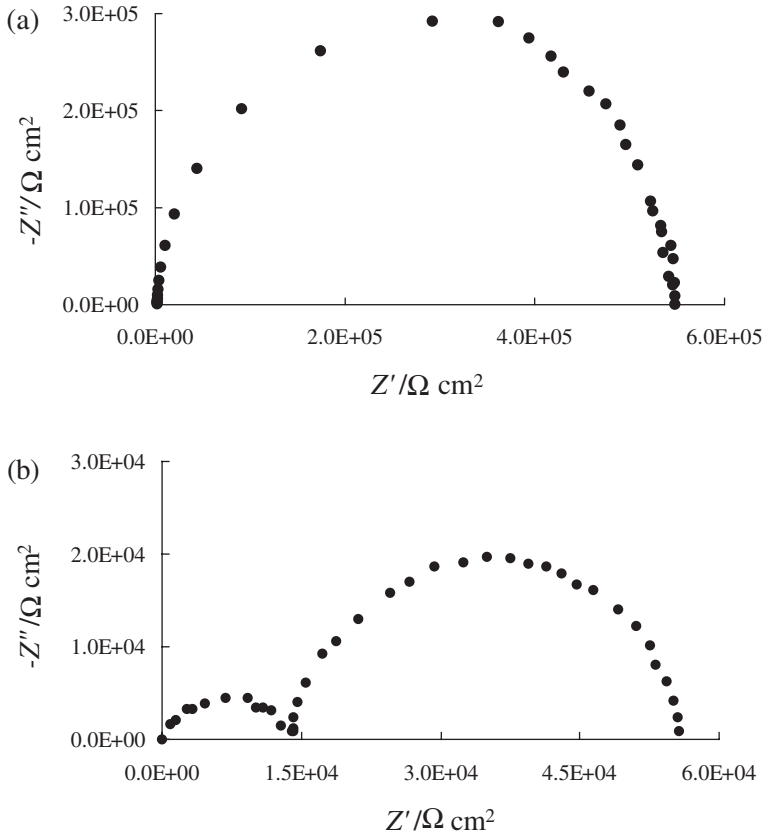

Fig. 10. Dependence of an imaginary part -Z″ on the real part Z′ recorded for 0.001 M KCl: (a) a bilayer formed by PC only, (b) a PC bilayer modified with valinomycin (total valinomycin concentration is equal to 5.2×10^{-12} mol cm^{-2}).

Experimental values of the R_m, C_m, R_{pt} and C_{pt} parameters are presented in Figs. 12–15 as functions of potassium-ion concentration in the solution and of total valinomycin concentration in the membrane. For the sake of clarity, experimental errors have been omitted in Figs. 12 and 14 (deviations amounted up to 15% of mean resistance values and the divergences of results increased with increasing amount of the ionophore, which made the membrane instable). The C_{pt} and R_{pt} values of the membranes were not determined for the 0.1 and 1 M KCl solutions because the formation of the second semicircle was observed to start at 0.01 M KCl only.

It can be concluded that an increase in potassium-ion concentration at constant valinomycin concentration provokes a marked decrease in R_m (Fig. 12) and R_{pt} (Fig. 14) as well as a marked increase in C_{pt} (Fig. 15). Dependence of C_m on KCl concentration was not taken into account in Fig. 14 because no clear variation was observed in the C_m values with electrolyte concentration (more or less

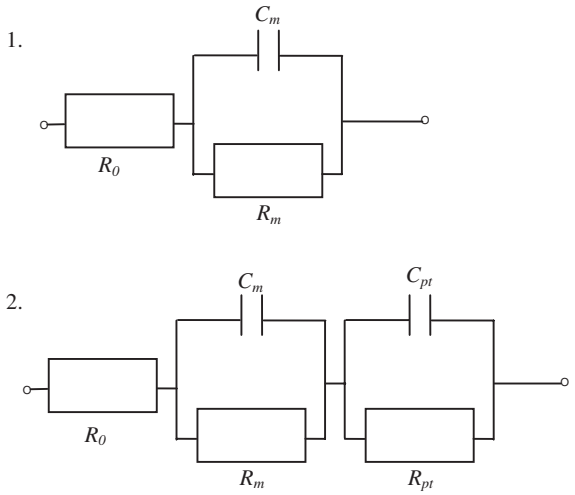

Fig. 11. Equivalent circuits representing the electrical properties of pure PC membrane (1) and PC membrane containing valinomycin (2). R_0, electrolyte resistance; C_m and R_m, capacitance and resistance of the membrane, respectively; C_{pt} and R_{pt}, capacitance and resistance of the membrane/electrolyte solution phase transition, respectively.

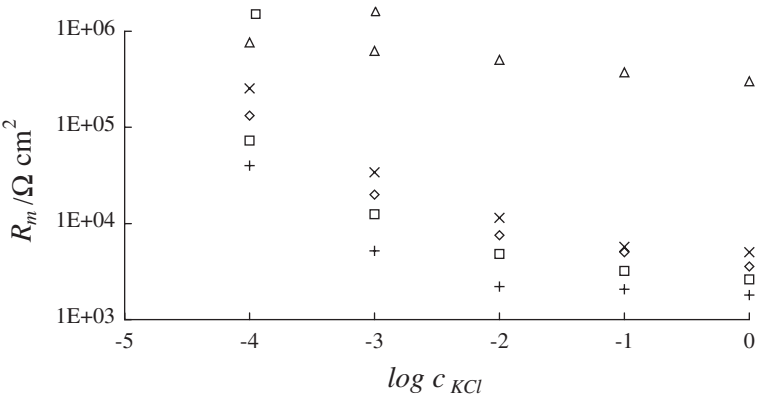

Fig. 12. The dependence of the resistance of the membrane R_m on potassium-ion concentration logarithm log c_{KCl} at various total valinomycin concentrations. The following total valinomycin concentrations were used: (+) 2.08×10^{-11} mol cm^{-2}, (□) 1.04×10^{-11} mol cm^{-2}, (◇) 6.94×10^{-12} mol cm^{-2}, (×) 5.20×10^{-12} mol cm^{-2} and (Δ) 0 mol cm^{-2}.

constant membrane capacity value was also observed by other authors who studied the effect of valinomycin on potassium-ion transport across lipid bilayers [48]. Both resistance values were also observed to decrease with increasing carrier concentration at constant K^+ ion concentration (increasing membrane

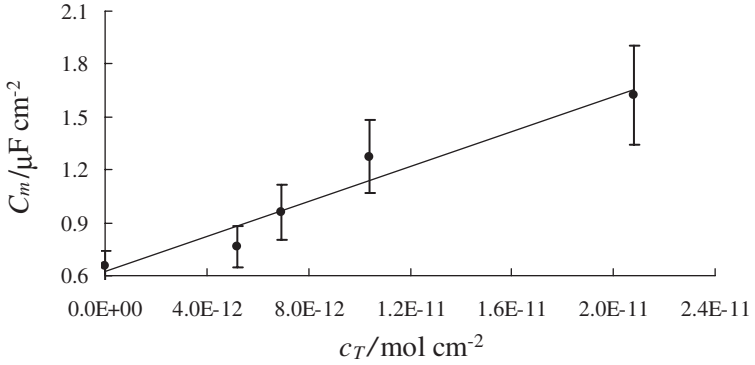

Fig. 13. The dependence of the capacitance of the membrane C_m on total valinomycin concentration c_T at various electrolyte concentrations.

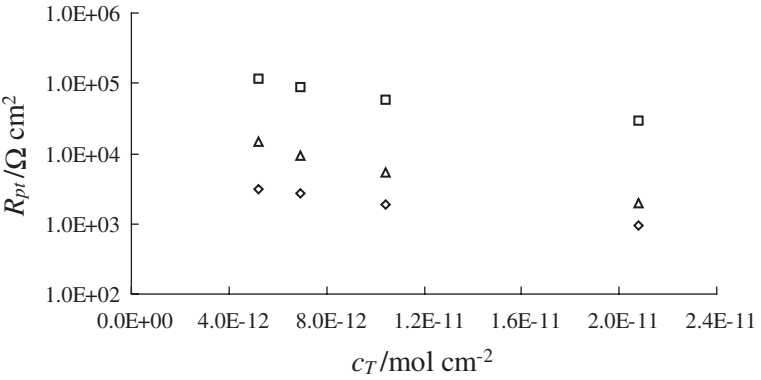

Fig. 14. The dependence of the resistance of phase transfer R_{pt} on total valinomycin concentration c_T at various electrolyte concentrations. (◇) 0.01 M KCl, (Δ) 0.001 M KCl and (□) 0.0001 M KCl.

conductivity), whereas capacity of transfer and membrane capacitance values were observed to increase. Increase in the membrane capacity can be explained by increasing valinomycin amount in the membrane, which results in increasing electric permittivity of the lipid bilayer.

Slope of the straight line described by equation (52) was determined by linear regression method. Agreement of equation (52) with the experimental data is shown in Fig. 16 where the equation (52) results are presented by solid lines and the experimental results by points. Proportionality of membrane conductance to total valinomycin concentration is the evidence that the single valinomycin molecule is the smallest transporting unit. Linearity of this dependence in a broad concentration range is also the evidence that the molecule participates as a carrier not as a channel [41]. Conductance is proportional to the potassium-ion concentration logarithm if the K^+ concentration is lower than 0.1 M (Fig. 14). This

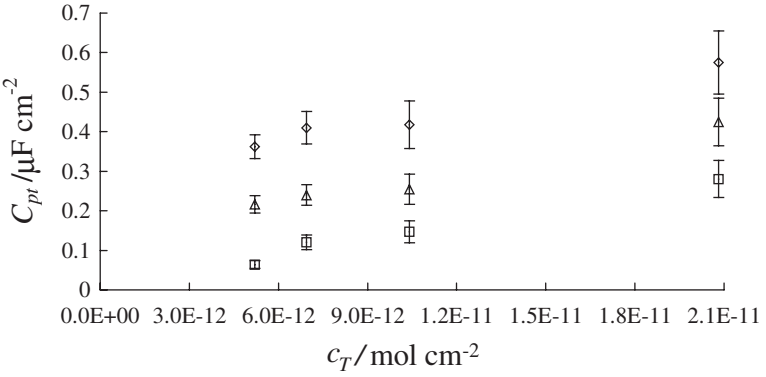

Fig. 15. The dependence of the capacitance of phase transfer C_{pt} on total valinomycin concentration c_T at various electrolyte concentrations. (◇) 0.01 M KCl, (Δ) 0.001 M KCl and (□) 0.0001 M KCl.

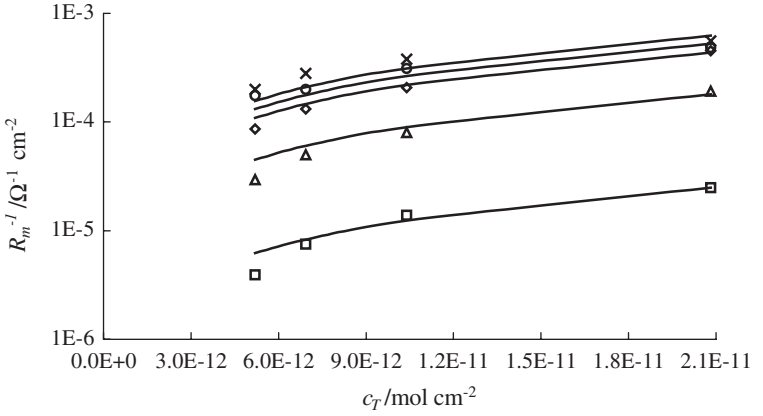

Fig. 16. The variation of the membrane conductance R_m^{-1} as a function of total valinomycin concentration c_T at various electrolyte concentrations. (×) 1 M KCl, (o) 0.1 M KCl, (◇) 0.01 M KCl, (Δ) 0.001 M KCl and (□) 0.0001 M KCl (the experimental values are marked by points and the theoretical ones by curves).

fact, together with the Fig. 16 data, suggests that the 1:1 valinomycin-K^+ complex are the carrier of charge in the membrane. Deviations from linearity observed at greater potassium-ion concentrations suggest that the conductance increase is slower than the increase in potassium-ion concentration. Such saturation is characteristic for a carrier system at high concentration of transported individuals where a great part of the carrier appears in the form of complex. It is in agreement with the earlier results obtained for classical bilayer lipid membrane (BLM) systems [41].

The equilibrium constant of complex formation can be calculated from equation (52). The slope of the straight line (now denoted by p) can be presented in the following way:

$$p = \frac{A}{\delta^2}\mu_{VK^+}F\frac{Ka_{K^+}}{1 + Ka_{K^+}} \tag{53}$$

The above equation can be presented as linear dependence:

$$\frac{p}{a_{K^+}} = \frac{A}{\delta^2}\mu_{VK^+}FK - Kp \tag{54}$$

This dependence is presented in Fig. 17.

The equilibrium constant of the VK^+ complex formation calculated from the slope of the straight line (equation (54)) amounts to about 0.44×10^3 dm^3 mol^{-1}.

Knowledge of the stability constant of the VK^+ complex permitted one to determine theoretical membrane conductance values as a function of potassium-ion concentration at a given valinomycin concentration and to compare them with the experimental data (Fig. 18). As it can be seen in Fig. 18, the theoretical and experimental results agree. Very good agreement of theoretical lines and of experimental points can be observed in the high valinomycin concentration range in the bilayer. Small divergences were observed at small ionophore concentrations in the bilayer. A low VK^+ concentration in the bilayer can cause experimental errors resulting in differences of experimental and theoretical conductance values.

The reaction of the VK^+ complex formation at the membrane surface is characterized by the association rate constant (k_a). The stage of complex dissociation and potassium-ion liberation to the aqueous phase can be described by the dissociation rate constant (k_d). The k_d value can be expressed using the equations determining real and imaginary parts of membrane/electrolyte solution phase transition impedance (at low frequencies where ω is considerably smaller

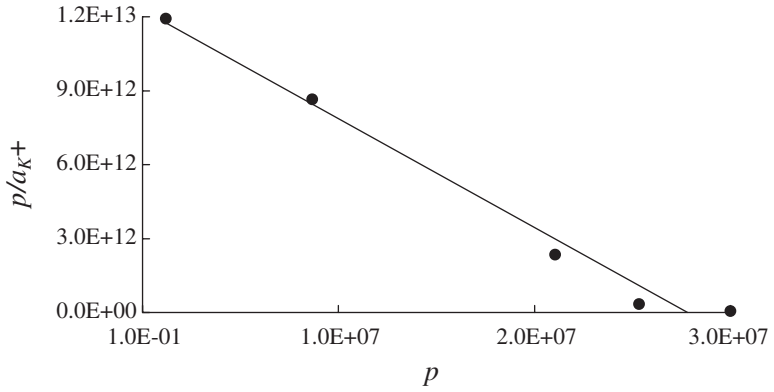

Fig. 17. The plot representing equation (54).

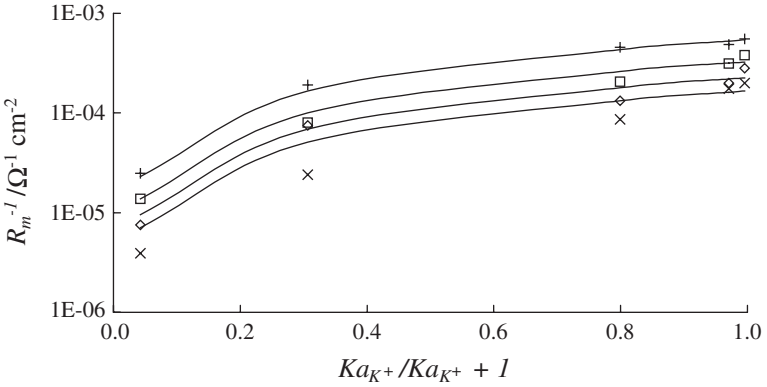

Fig. 18. The variation of membrane conductance R_m^{-1} as a function of potassium-ion concentration at various valinomycin concentrations. The experimental values are marked by points and the theoretical ones by solid lines.

than *k*) [49]:

$$R_{pt} = \frac{v^2 RT}{n^2 F^2} \frac{1}{c^s_{VK^+} k_d} \tag{55}$$

$$\frac{1}{\omega C_{pt}} = \frac{v^2 RT}{n^2 F^2} \frac{1}{c^s_{VK^+} k_d} \frac{\omega}{k_d} \tag{56}$$

here *v* is the stoichiometric coefficient of the complex.

It can be deduced from equations (55) and (56) that resistance of transition is frequency independent for the frequencies tending to zero whereas $1/\omega \cdot C_{pt}$ increases proportionally to ω.

In order to determine the k_d value and to propose a correct equivalent circuit to reproduce electric properties of the PC membrane modified with valinomycin, the experimental data were substituted both in equations (55) and (56). The results were found to agree at low frequencies as it has been shown in Fig. 19 for the imaginary part of the impedance. This fact was decisive in that the phase transition parameters could be related to the semicircle occurring in the impedance spectrum at low frequencies.

The k_d values determined from equations (55) and (56) are equal to 4 ± 2 and $15 \pm 5\,s^{-1}$, respectively. The dissociation rate constant of the complex being known, the association rate constant was calculated from the $k_a = K \times k_d$ relationship. The resulting value was $(1.76 \pm 0.88) \times 10^3$ and $(6.6 \pm 2.2) \times 10^3\,M^{-1}\,s^{-1}$, respectively. Very different association and dissociation rate constant values of the complex could be found in the literature; the same applies to the complex formation equilibrium constant. The presented k_d values range from $21 \pm 5\,s^{-1}$ (from the studies of ionophore behaviour in semi-polar solvents system) to $2 \times 10^4\,s^{-1}$ (the case phosphatidylinositol membranes) to $2 \times 10^5\,s^{-1}$ (the

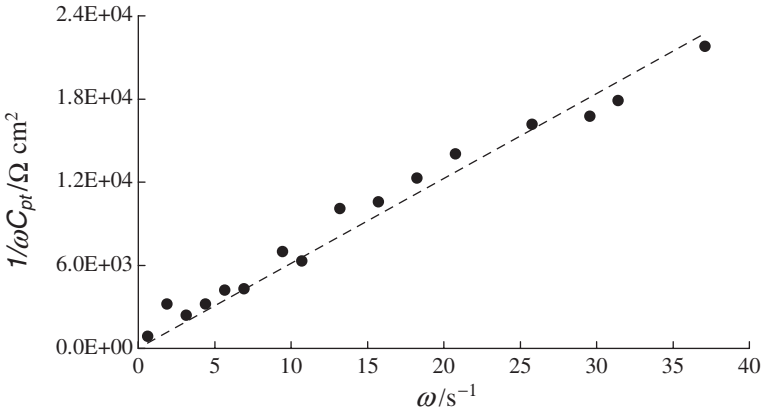

Fig. 19. Frequency ω dependence of the imaginary part of the impedance $1/\omega C_{\mathrm{pt}}$ ($\omega = 2\pi \mathrm{f}$, and $\mathrm{f} < 5.906$ Hz).

case of monooleic membranes). The k_a were found to range from 5×10^4 (the case phosphatidylinositol membranes) to $2 \times 10^5\ \mathrm{M}^{-1}\ \mathrm{s}^{-1}$ (the case of monooleic membranes); even a value larger by four orders of magnitude was given in the case of valinomycin and potassium-ion association in methanol [44,45–48,50]. The rate constant values can depend on membrane structure and fluidity. Evidence can be found in the literature for a great effect of lipids within the membrane (the hydrocarbon chain length, the number of double bonds, the resulting functional group charge) upon the ion transport intermediated by valinomycin [51–53]. The relatively low dissociation constant value obtained by us suggests that the behaviour of valinomycin at the membrane/electrolyte solution interface could be similar to that of the ionophore in semi-polar solvents. Similar conclusions have appeared in the works by other authors [54,55].

1.2.3. Conclusions

Separation was proposed for the ion transport effect by gramicidin channels (or valinomycin molecule) in the equivalent circuit by presenting it as the separate branch. Correctness of such a separation is supported by analysis of the experiments. The branch corresponding to the effect of gramicidin channels in the equivalent circuit contains Warburg impedance only, probably due to transport of the potassium-ion in the area near to the membrane surface. The impedance due to ion transport in valinomycin-containing membrane is composed of three elements: the resistance R_{m}, characterizing the ion flow across the membrane and the parameters characterizing the interfacial barrier: capacity C_{pt} and the resistance R_{pt}.

It is very interesting to observe the obtained values of the surface energy for membrane formed from gramicidin and gramicidin-ion K^+ complex. These values

are equal to 1995.7 and 1782.5 J mol^{-1}, respectively. The result of subtraction of these energies (-213.2 J mol^{-1}) are the energy required for entrance of the K^+ ions to the pore of the gramicidin channel. In the literature there were a lot of mathematical simulation data reporting the energy required for entrance of the K^+ ions into the pore of the gramicidin channel using molecular dynamics simulations (MD simulations). For K^+ the values are $r_{min} = 2.350$ Å and $e = -0.010$ kcal mol^{-1}. The authors [56] compared the potassium parameter to those from various other studies reported in the literature, for example those used by Åqvist [57–59] (for K^+ $r_{min} = 2.66$ Å and $e = -0.000328$ kcal mol^{-1}). Theoretical values determined by many authors of the energy required for entrance of K^+ ions into the pore of the gramicidin channel using a MD simulation method are of a similar value to the energy needed for K^+ ions to enter the pore of the gramicidin channel calculated by interfacial tension methods, which is equal to -213.2 J mol^{-1} (-0.0509 kcal mol^{-1}).

Simple and very interesting methods proposed above can be used with success for determination of characteristic forming complexes equilibria parameters. The parameters values obtained both from interfacial tension and electrochemical impedance are in agreement with the literature data.

2. ACID–BASE EQUILIBRIA BETWEEN THE LIPID MEMBRANE AND ELECTROLYTE SOLUTION

A cell membrane is a very complex system; it contains various elements influencing its interfacial tension. Therefore, it is easier to study the effect of various factors; for example, pH of the electrolyte solution, using artificial membranes. The dependences of interfacial tension of lipid bilayers on pH of electrolyte solution can be described in terms of acid–base equlibria. Theoretical equations based on Gibbs isotherm or models make assumptions that additivity of the different forms of lipids is derived to describe these dependences. The H^+ and OH^- ions are adsorbed by the phospholipid surface. The lipid is present in the membrane only. Therefore, the volume or surface concentration of the lipid is equal to its amount related to the solution volume or to the membrane surface area. The interfacial tension values reported in this paragraph refer to both the sides of bilayer membrane surface area unit.

2.1. Phosphatidylcholine or phosphatidylethanolamine membrane

PC and PE (cephalin) molecules are electrically neutral lipids, because they have two electric charges, one positive and one negative, on their surface. The lecithin or cephalin molecule forms ampholyte ions and can participate in equilibrium with ions H^+ as well as with OH^-. When hydrogen ions are in excess, equilibria (1)

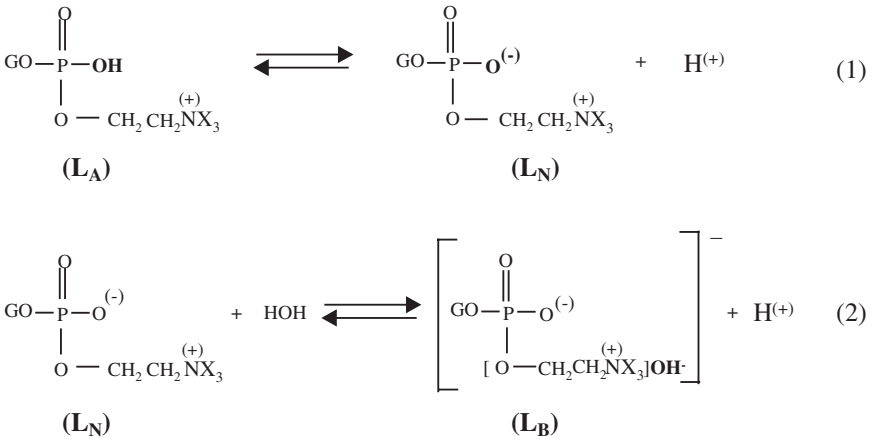

Fig. 20. The acid–base equilibria for PC and PE molecule, where *G* is the doubly acylated glycerol group [60,61]; $X = CH_3$ for PC molecule and $X = H$ for PE molecule.

and (2) presented in Fig. 20 are shifted to the left, which means that PC or PE cations L_A dominate in the solution. However, in basic solutions, the equilibria (1) and (2) are moved to the right, so anions L_B dominate in the solution.

2.1.1. The simplified description based on Gibbs isotherm

The phospholipid molecule is in acid–base equilibria with the H^+ and OH^- ions from electrolyte solution [20]:

$$AH \rightleftharpoons A^- + H^+ \tag{57}$$

$$B^+ + OH^- \rightleftharpoons BOH \tag{58}$$

$$HOH \rightleftharpoons H^+ + OH^- \tag{59}$$

It results from (58) and (59), that

$$B^+ + HOH \rightleftharpoons BOH + H^+ \tag{60}$$

The dissociation constants of the lipid membrane are given by the equations:

$$K_a = \frac{c^s_{A^-} a_{H^+}}{c^s_{AH}} \tag{61}$$

$$K_b = \frac{c^s_{BOH} a_{H^+}}{c^s_{B^+}} \tag{62}$$

where K_a and K_b ($mol^1\,m^{-3}$) are the acid and base equilibrium constants, respectively; $c^s_{A^-}$, $c^s_{B^+}$, c^s_{AH}, c^s_{BOH} ($mol\,m^{-2}$) the surface concentrations of AH, BOH,

A^- and B^+ forms at the lipid surface and a_{H^+}, a_{OH^-} ($\mathrm{mol\,m^{-3}}$) the activity of H^+ and OH^- ions.

The adsorption equilibria are described by the equations:

$$A^- + H^+ \rightleftharpoons AH \tag{63}$$

$$B^+ + OH^- \rightleftharpoons BOH \tag{64}$$

These concentrations and the volume concentrations of hydrogen or hydroxyl ions according to the relationships determine the acid–base constants:

$$K_1 = \frac{c^s_{AH}}{c^s_{A^-} a_{H^+}} \tag{65}$$

$$K_2 = \frac{c^s_{BOH}}{c^s_{B^+} a_{OH^-}} \tag{66}$$

The dissociated and non-dissociated form concentrations of the lipid appear in the same power (one) in the above equations.

In the case where the adsorbed molecules are electrically charged, the molar free energy of charged components depends on the inner potential of the considered phase. Therefore, the chemical potentials in Gibbs equation should be replaced by electrochemical potentials.

Then Gibbs equation assumes the form:

$$\mathrm{d}\gamma = -\sum \Gamma_i \, \mathrm{d}\bar{\mu}_i \tag{67}$$

If the H^+ and OH^- ions are adsorbed, then the above equation takes the form:

$$\mathrm{d}\gamma = -a_{H^+} \, \mathrm{d}\bar{\mu}_{H^+} - a_{OH^-} \, \mathrm{d}\bar{\mu}_{OH^-} \tag{68}$$

The dependence of the interfacial tension on the pH of electrolyte solution was introduced in the papers [20,22], and final equation is presented below:

$$\gamma = \gamma_{max} + 2A^{-1}RT\ln\left(\sqrt{\frac{K_a}{K_b}} + 1\right) - A^{-1}RT\ln\left[\left(\frac{K_a}{a_{H^+}} + 1\right)\left(\frac{a_{H^+}}{K_b} + 1\right)\right] \tag{69}$$

where γ_{max} ($\mathrm{N\,m^{-1}}$) is the maximal interfacial tension value and A^{-1}($\mathrm{mol\,m^{-2}}$) the maximal lipid surface concentration value.

The acid–base equilibrium constants for PC membrane are $K_a = 2.63 \times 10^{-3}\,\mathrm{mol\,m^{-3}}$ and $K_b = 2.04 \times 10^{-6}\,\mathrm{mol\,m^{-3}}$ and for PE membrane are equal to $K_a = 2.63 \times 10^{-2}\,\mathrm{mol\,m^{-3}}$ and $K_b = 9.55 \times 10^{-5}\,\mathrm{mol\,m^{-3}}$.

The dependences on an interfacial tension of a lipid membrane formed from lecithin (a) and cephalin (b) on the pH of the electrolyte solution are presented in Fig. 21. The maximal interfacial tension value of the lecithin membrane was found to be $3.53 \times 10^{-3}\,\mathrm{N\,m^{-1}}$ at pH equal to 4.15 [19]. For cephalin membrane the maximal interfacial tension value is $4.07 \times 10^{-3}\,\mathrm{N\,m^{-1}}$ at pH equal to 4.12 [22].

The experimental values in Fig. 21 are marked by points and the theoretical ones obtained from equation (69) by lines. It can be seen from this figure that the

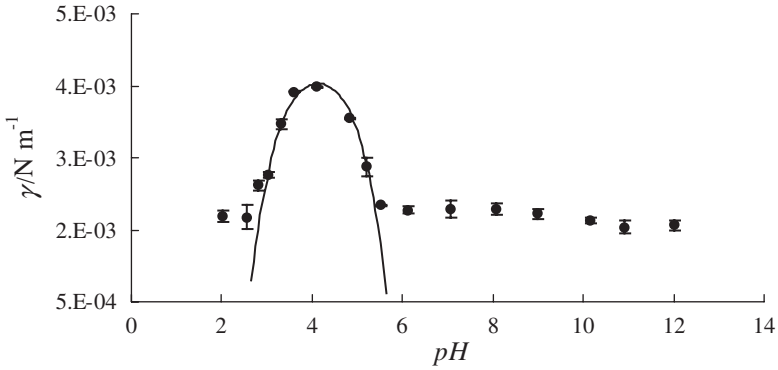

Fig. 21. The dependence of interfacial tension γ of a lipid membrane formed from lecithin of the pH of the electrolyte solution (the experimental values are marked by points and the theoretical ones by curve).

theoretical and the experimental interfacial tension values of the lecithin membrane agree in the pH ranges 2.5–5.8 and they diverge in the 2.0–2.5 and 5.8–12.0 pH ranges. The equation (69) allows one to determine the maximal interfacial tension value at pH $= 4.15$ and the maximal lecithin surface concentration.

The dependence resulting from equation (69) is presented in Fig. 22 in the coordinate system in which it should be a straight line. This equation was plotted in the pH range 2.5–5.8 for PC membrane and in pH range 2.8–5.6 for PE membrane, because the theoretical interfacial tension values of PC and PE membranes agree then with the experimental ones.

The PC and PE surface concentrations amounting to 1.96×10^{-6} and $2.23 \times 10^{-6}\,\mathrm{mol\,m^{-2}}$ were calculated from the slope of the lines. The line determines the γ_{max} values equal to $3.53 \times 10^{-3}\,\mathrm{N\,m^{-1}}$ for PC membrane and $4.07 \times 10^{-3}\,\mathrm{N\,m^{-1}}$ for PE membrane on the abscissa. The maximal interfacial tension value for lecithin membrane is in a good agreement with the value given in paper [20,62].

The surface area occupied by a lecithin and cephalin molecule could be determined from the surface concentrations; 85 and 74.6 $\mathrm{Å}^2$ [20,22]. The literature values ranged from 54 to 96 $\mathrm{Å}^2$ for lecithin molecule [63,64] and for cephalin molecule about 4 $\mathrm{Å}^2$ less than for analogous PC [65].

2.1.2. The full description based on Gibbs isotherm

It was assumed in the papers [20,22] and in the previous paragraph, that surface excess of the H^+ and OH^- ions is equal to their surface concentration. This assumption is common in describing adsorption phenomena [66,67] but it is correct in the case only where the adsorption is strong and the concentration of the

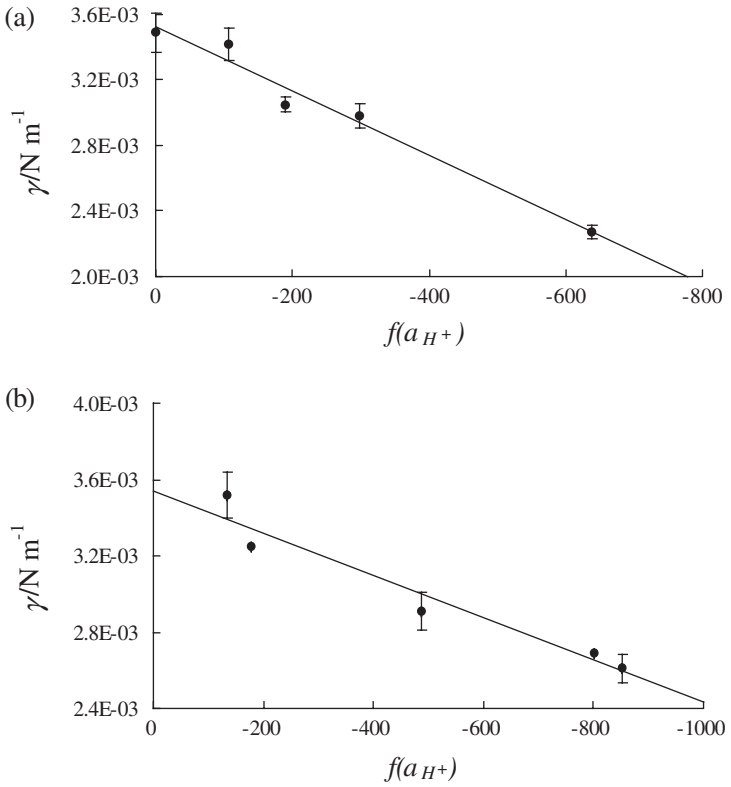

Fig. 22. A plot illustrating equation (69) in the pH range 2.5–5.8 for PC membrane (a) and in the pH range 2.8–5.6 for PE membrane (b).

adsorbed ion in the solution is low. In the present case, the surface excess definition resulting from deduction of the Gibbs equation [68] should be strictly respected.

The equations describing surface excess of the H^+ and OH^- ions in terms of the definition resulting from the Gibbs equation can be presented in the form [22,69]:

$$\Gamma_{OH^-} = c^s_{BOH} - V_{H^+} c^s_{AH} a_{OH^-} - V_{OH^-} c^s_{BOH} a_{OH^-} \tag{70}$$

$$\Gamma_{H^+} = c^s_{AH} - V_{H^+} c^s_{AH} a_{H^+} - V_{OH^-} c^s_{BOH} a_{H^+} \tag{71}$$

where V_{H^+} and V_{OH^-} (m^3) are the H^+ and OH^- ions volumes in the adsorption layer.

The dependence of interfacial tension on the pH of electrolyte solution taking into account the definition of surface excess was introduced in paper [22,69] and

is shown below:

$$\gamma = \gamma_{max} - A^{-1}RT\left(1 + \frac{V_{H^+}}{K_A} - V_{H^+}K_WK_A\right)\ln\frac{1 + K_Aa_{H^+}}{1 + K_Aa_{H^+}^{max}} - A^{-1}RT\left(1 + \frac{V_{OH^-}}{K_B} - V_{OH^-}K_WK_B\right)\ln\frac{1 + K_Ba_{OH^-}}{1 + K_Ba_{OH^-}^{max}} - A^{-1}RTV_{H^+}K_WK_A\ln\frac{a_{H^+}}{a_{H^+}^{max}} - A^{-1}RTV_{OH^-}K_B\ln\frac{a_{OH^-}}{a_{OH^-}^{max}} + A^{-1}RTV_{H^+}\left(a_{H^+} - a_{H^+}^{max}\right) + A^{-1}RTV_{OH^-}\left(a_{OH^-} - a_{OH^-}^{max}\right) \quad (72)$$

here $a_{H^+}^{max}$ and $a_{OH^-}^{max}$ (mol m^{-3}) are the activities of H^+ and OH^- ions at the isoelectric point (at this point the interfacial tension value is maximal), respectively.

The points in Fig. 23 represent the experimental data concerning the interfacial tensions of the membrane formed from PC (a) and PE (b) depending on pH of the electrolyte solution.

Equation (72) is of the $y = m_1x_1 + m_2x_2 + m_3x_3 + m_4x_4 + m_5x_5 + m_6x_6 + b$ type. The interfacial tension values were calculated by the substituting calculated coefficients m_1, m_2, m_3, m_4, m_5, m_6, and b in equation (72); the results are presented in Fig. 23 as a solid line. As it is seen, the experimental data agree with the calculation results. Equation (72), educed theoretically, describes the experimental results in the whole pH range.

The m_1, m_2, m_3, m_4, m_5, m_6, and b coefficients contain the equilibrium constants and volumes of the adsorbed H^+ and OH^- ions. Thus, having the equation coefficients calculated and using the equilibrium constants from papers [20,42] the volumes of adsorbed the H^+ and OH^- ions in the PC membrane were calculated; they are equal to 2026 and 3190 Å^3, respectively [69]. The mean intermolecular distance of the PC molecules on the bilayer surface can be determined if the area per molecule is known. Assuming this area to be 85 Å^2 [20], the mean H^+ ion adsorption centres distance amounts to 9.9 Å. The solvated H^+ ion in the bulk solution is spherical but, if adsorbed at an active centre, it loses a part of its solvation layer as it is shown in the figure in the paper [69]. Therefore, the volume of the adsorbed solvated ion can be expected to be smaller than that of the ion in the bulk. The radius of adsorbed the H^+ ion was determined from the experimental volume assuming its hemispherical shape; the result was 9.89 Å. This value is in agreement with the estimated distance between PC molecules in the membrane was presented above [70].

The volume and radius of the solvated OH^- ion on the lipid membrane surface can be determined in a similar way from equation (72). However, the OH^- ion is adsorbed by an active centre at the end of the hydrophilic PC chain. The chain can be bent and the active centre can appear at various distances from the interface. The chain length amounts to 5.0–7.5 Å [71]. Therefore, the adsorbed OH^- ions can be imagined to be present in two layers: a layer of ions bonded to

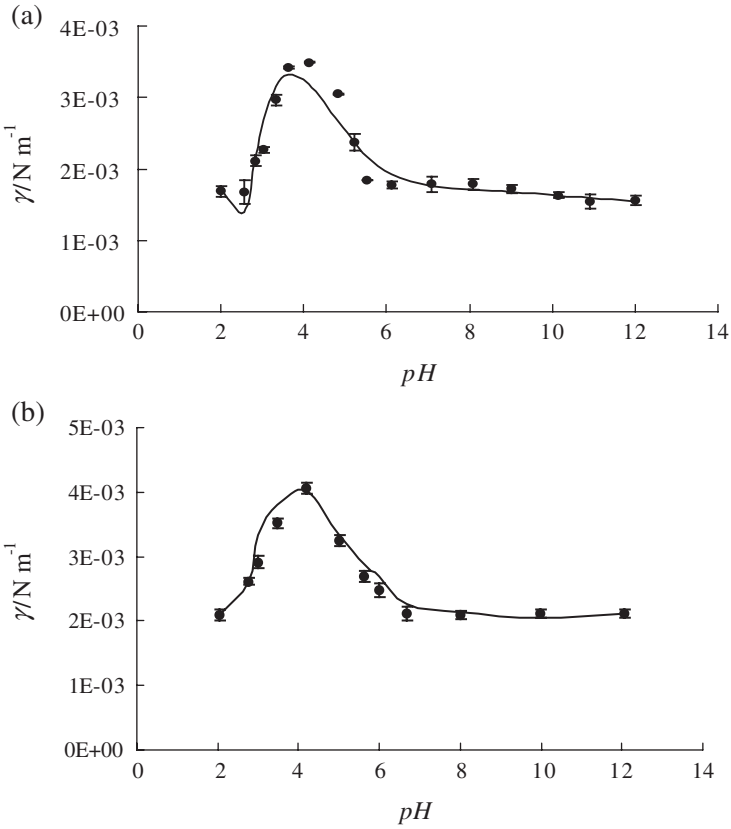

Fig. 23. The dependence of the interfacial tension γ of lipid membrane formed from PC (a) and PE (b) as a function of the pH of the electrolyte solution (full descriptions based on the Gibbs equation); the experimental values are marked by points and the theoretical ones by line.

active centres at the ends of straight chains and a layer of molecules situated at the interface at the ends of bent chains, as it is presented in the paper [69]. Assuming that half of the hydrophilic PC chains are straight and half are bent at the surface, the surface concentration of straight-chain lecithin is half of the total PC surface concentration and the distances between straight-chain PC molecules are about 14 Å [72]. Similar estimates can be made for the chains bent at the membrane surface. In this case, too, the radius of partly desolvated OH^- ion can be evaluated from its volume determined by equation (72) assuming its hemispherical shape; it amounts to about 20 Å. This value is in only approximate agreement with the distance of adsorption centres, which is equal to 14 Å (as already presented above). These values are rough estimates only because of doubtlessly strong deformation of the OH^- ion solvation shell due to dense packing of the layers. The above discussed radii of hydrated H^+ and OH^- ions are longer than the literature values [72,73], which were determined from hydration

energies and corresponding to the ions with one hydration shell. Actually, the number of hydration shells can be greater because of hydrogen bonding between water molecules. Thus, the radius of an ion adsorbed at the membrane can be longer than that determined by formation energy of a single solvation layer.

2.1.3. Model based on the additivity of different forms of lipid in membrane

The phospholipid layer observed from the aqueous solution side has uniformly distributed $-PO^{(-)}$ and $-\overset{(+)}{N}X_3$ groups because it is built of the molecules each having one $-PO^{(-)}$ group and one $-\overset{(+)}{N}X_3$ group, where $X = CH_3$ for PC molecule; $X = H$ for PE molecule.

Therefore, two descriptions of the lecithin or cephalin surface can be adopted. In Description I, the membrane surface is continuous with uniformly distributed functional groups being the active centres of adsorption of the H^+ and OH^- ions. In Description II the lipid surface is composed of non-bonded lipid molecules and of the molecules with bounded H^+ and OH^- ions.

The model described above is presented in Fig. 24.

2.1.3.1. Description I

Uniformly distributed active centres at which the H^+ and OH^- ions can be adsorbed are present at the aqueous solution side. They are schematically described with the following equations:

$$-\underset{(A^-)}{PO^{(-)}} + H^{(+)} \rightleftharpoons -\underset{(AH)}{PO^{(-)}} - H^{(+)} \tag{73}$$

$$-\underset{(B^+)}{\overset{(+)}{N}X_3} + OH^{(-)} \rightleftharpoons -\underset{(BOH)}{\overset{(+)}{N}X_3} - OH^{(-)} \tag{74}$$

where $X = CH_3$ for PC molecule and $X = H$ for PE molecule.

Thus, four groups: A^-, AH, B^+ and BOH are present at the layer surface. Assuming the contributions of individual forms to the interfacial tension to be additive, the following equation can be written as:

$$\gamma = \gamma_{A^-} + \gamma_{AH} + \gamma_{B^+} + \gamma_{BOH} \tag{75}$$

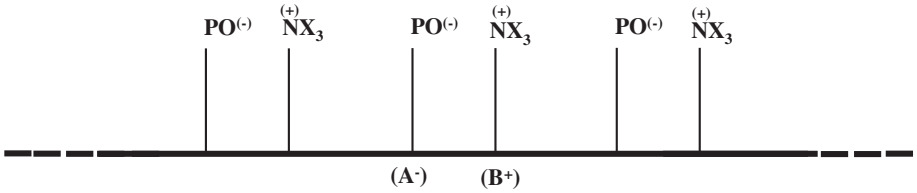

Fig. 24. The model of the bilayer lipid surface, which presents the equilibria between H^+ and OH^- ions from solution and the functional groups distributed on its surface, where $X = CH_3$ for PC molecule and $X = H$ for PE molecule.

Therefore

$$\gamma = \gamma^0_{A^-}\left(\frac{1}{1+K_A a_{H^+}}\right) + \gamma^0_{AH}\left(\frac{K_A a_{H^+}}{1+K_A a_{H^+}}\right) + \gamma^0_{B^+}\left(\frac{1}{1+K_B a_{OH^-}}\right) + \gamma^0_{BOH}\left(\frac{K_B a_{OH^-}}{1+K_B a_{OH^-}}\right) \quad (76)$$

where K_A and K_B ($m^3\,mol^{-1}$) are the acids and base association constants, $\gamma^0_{A^-}$, γ^0_{AH}, $\gamma^0_{B^+}$ and γ^0_{BOH} ($N\,m^{-1}$) the specific interfacial tensions of the membrane component, respectively.

Equation (76) presents the dependences of interfacial tension of the membrane formed from lecithin or cephalin on the pH of electrolyte solution based on Description I [22,42].

Interfacial tension of the membrane formed from PC and PE are plotted in Fig. 25 vs. pH of the electrolyte solution. Points present the experimental values; the total values calculated from equation (76) are presented by a continuous line. The interfacial tension values of lecithin or cephalin membrane components are marked with broken lines. Figure 25 refers to the Description I, where the distribution of the $-PO^{(-)}$ and $-\overset{(+)}{N}X_3$ groups on the aqueous solution side of the lipid layer has been assumed to be uniform.

As is seen in equation (76), the total interfacial tension value of the lecithin or cephalin membrane is a sum of the interfacial tension values of its components, i.e. sum of its A^-, AH, B^+ and BOH. Specific interfacial tension values of individual components of the lecithin and cephalin membranes were determined. The $\gamma^0_{A^-}$, γ^0_{AH}, $\gamma^0_{B^+}$ and γ^0_{BOH} values were determined by linear regression and are presented in the paper [42]. When the interfacial tension of the bilayer lipid membrane formed from only individual forms has negative values, it is possible to suppose, that the bilayer membrane formed from this forms does not exist.

Coverage of the lipid membrane surface by the H^+ and OH^- ions vs. pH of electrolyte solution is presented in paper [42]. The PC membrane surface is not covered by the H^+ and OH^- ions in proximity of its isoelectric point, i.e. at pH equal to about 4.

2.1.3.2. Description II

As a result of adsorption of the H^+ and OH^- ions on the surface of lecithin or cephalin, the lipid membrane can exist in four different forms presented in Fig. 26; XH^+ with H^+ adsorbed, XOH^- with OH^- adsorbed, XHOH with both H^+ and OH^- ions adsorbed on the surface and a free lipid molecule X with no ions adsorbed.

The sum of interfacial tension contributions of the forms composing the lecithin or cephalin surface in the Description II is as follows:

$$\gamma = \gamma_{XHOH} + \gamma_{XH^+} + \gamma_{XOH^-} + \gamma_X \quad (77)$$

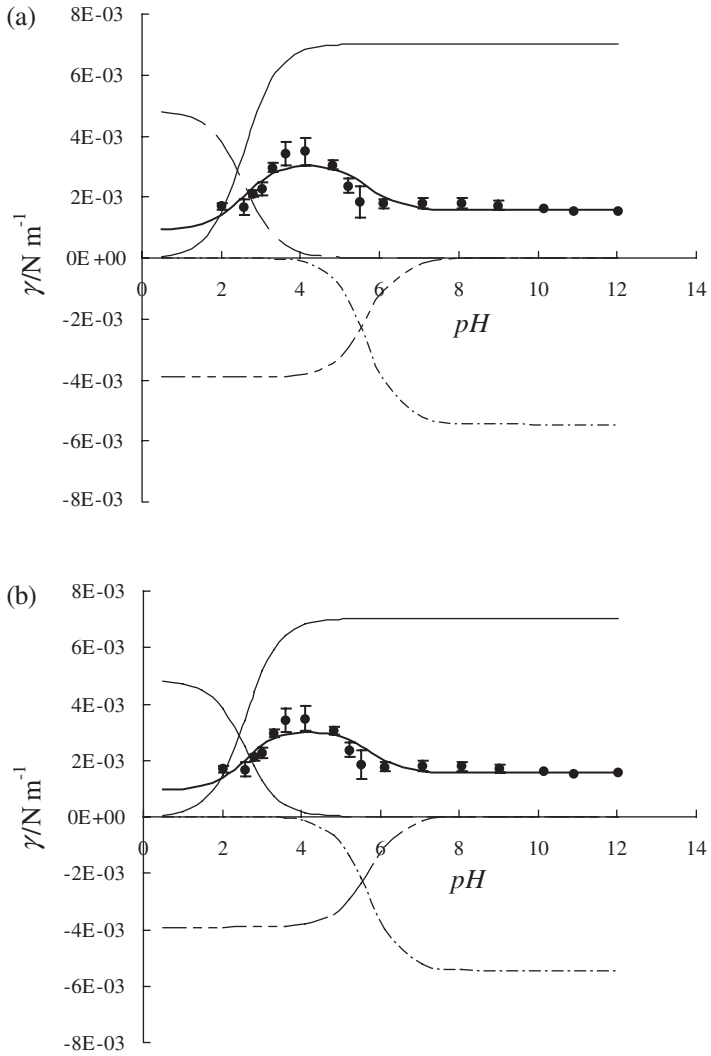

Fig. 25. The participation of the A and B groups, calculated from the Description I, in dissociated and associated forms in the interfacial tension γ of the bilayer formed from PC (a) and PE (b), as a function of pH of electrolyte solution; the experimental values are marked by points and the theoretical ones by solid curve.

The expressions describing the contributions of the individual forms of the lecithin and cephalin molecule to the interfacial tensions are in papers [20,22], these results in describing of the dependence on interfacial tension of the membrane formed from lecithin or cephalin of the pH of electrolyte solution based on Description II.

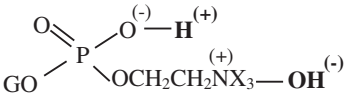

(XHOH)

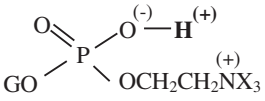

(XH^+)

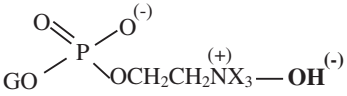

(XOH^-)

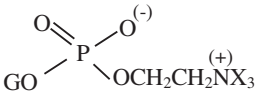

(X)

Fig. 26. Four different forms of the PC or PE molecule at the membrane surface.

Therefore:

$$\gamma = \gamma^0_{XHOH}\left(\frac{K_A a_{H^+}}{1+K_A a_{H^+}}\right)\left(\frac{K_B a_{OH^-}}{1+K_B a_{OH^-}}\right) + \gamma^0_{XH^+}\left(\frac{K_A a_{H^+}}{1+K_A a_{H^+}}\right)\left(\frac{1}{1+K_B a_{OH^-}}\right) + \gamma^0_{XOH^-}\left(\frac{1}{1+K_A a_{H^+}}\right)\left(\frac{K_B a_{OH^-}}{1+K_B a_{OH^-}}\right) + \gamma^0_X\left(\frac{1}{1+K_A a_{H^+}}\right)\left(\frac{1}{1+K_B a_{OH^-}}\right) \quad (78)$$

where γ^0_{XHOH}, $\gamma^0_{XH^+}$, $\gamma^0_{XOH^-}$ and γ^0_X ($N\,m^{-1}$) are the specific interfacial tensions of the membrane component, respectively; X = L for lecithin membrane and X = E for cephalin membrane.

Interfacial tension of the membrane formed from PC is also plotted in Fig. 27 vs. pH of electrolyte solution. Points present the experimental values, the total values calculated from equation (78), which has been derived according to Description II, are presented by a continuous line and the interfacial tension values of the PC membrane components are marked with broken lines.

It is seen in equation (78) that the total interfacial tension values of the lecithin membrane is the sum of its individual components, i.e. XHOH, XH^+, XOH^- and X, where X = L for lecithin membrane and X = E for cephalin membrane.

Specific interfacial tension values of individual lecithin membrane components $\gamma^0_{LHOH}, \gamma^0_{LH^+}, \gamma^0_{LOH^-}$ and γ^0_L were determined using linear regression and these values are presented in paper [42].

Coverage of the lipid membrane surface by the H^+ and OH^- ions vs. pH of electrolyte solution is presented in paper [42]. As in Description II, the L form predominates in the lecithin membrane surface in proximity of its isoelectric point; the surface is not covered by the H^+ and OH^- ions there. In both descriptions, coverage of the lipid membrane surface by the H^+ and OH^- ions remains unchanged in the ranges below 1.5 and above 7.0.

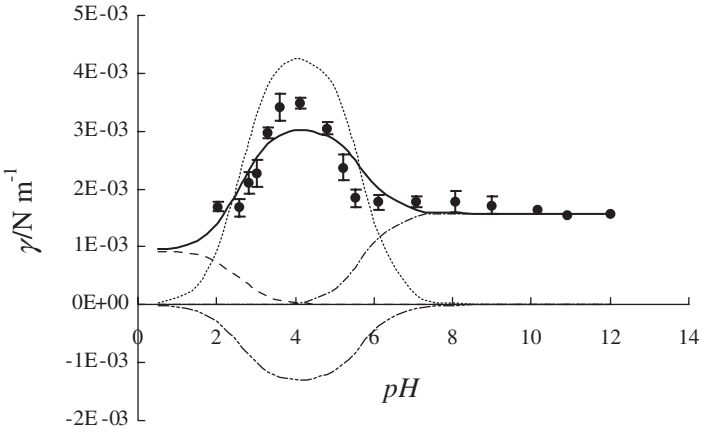

Fig. 27. The participation of the individual form of lecithin molecules, calculated from the Description II, in the interfacial tension γ of the bilayer formed from PC, as a function of pH of electrolyte solution; the experimental values are marked by points and the theoretical ones by solid curve.

Interfacial tension of the membrane formed from PE is also plotted in Fig. 28 vs. pH of electrolyte solution. Points present the experimental values. The total values calculated from equation (78), which have been derived according to Description II, are presented by a continuous line. The interfacial tension values of PE membrane components are marked with broken lines.

Considerations of equilibria by considering the H^+ and OH^- ions in terms of the Model II presented in Fig. 29 and calculations of contributions of those forms with respect to interfacial tension of the lipid bilayer resulted in disagreement with the experimental.

The above presented description in which the contributions of various forms of the lecithin or cephalin molecule to interfacial tension of the bilayer were assumed to be additive resulted in markedly better description of the dependence on pH than the description based on the Gibbs's isotherm [20,22], particularly at far distances from the isoelectric point.

2.2. Phosphatidylserine membrane

It has been proved in earlier studies [20,22,42] that interfacial tension of lipid membranes formed from lecithin or cephalin are affected by pH. Maximal interfacial tension of such membranes was attained at a pH equal to 4.15 and 4.20, respectively. The lecithin and cephalin molecules have two electric charges, one positive and one negative, on its surface. It is interesting to examine the effect of pH on interfacial tension of a membrane formed from a polar lipid of different molecular structure. PS has been chosen; its molecule has two negative groups

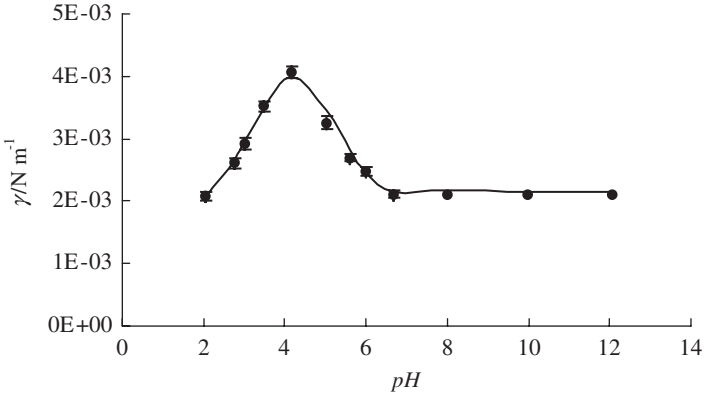

Fig. 28. The dependence of the interfacial tension γ of a lipid membrane formed from PE on the pH of the electrolyte solution calculated from the Description II (the experimental values are marked by points and the theoretical ones by solid curve).

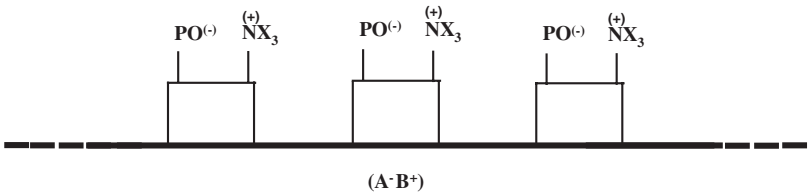

Fig. 29. The model of the bilayer lipid surface, which presents the equilibria between H^+ and OH^- ions from solution and the functional groups distributed on its surface, where $X = CH_3$ for PC molecule and $X = H$ for PE molecule.

and one positive, its net charge being negative. The PS molecule is in equilibria with the H^+ and OH^- ions; the equilibria (1)–(3) can be shown in the Fig. 30.

2.2.1. The simplified description based on Gibbs isotherm

The H^+ and OH^- ions are also adsorbed at the PS surface [42]:

$$A_1^- + H^+ \rightleftharpoons A_1H \tag{79}$$

$$A_2^- + H^+ \rightleftharpoons A_2H \tag{80}$$

$$B^+ + OH^- \rightleftharpoons BOH \tag{81}$$

Thus, adsorption equilibria can be written in the form:

$$K_{A_1} = \frac{c^s_{A_1H}}{c^s_{A_1^-} a_{H^+}} \tag{82}$$

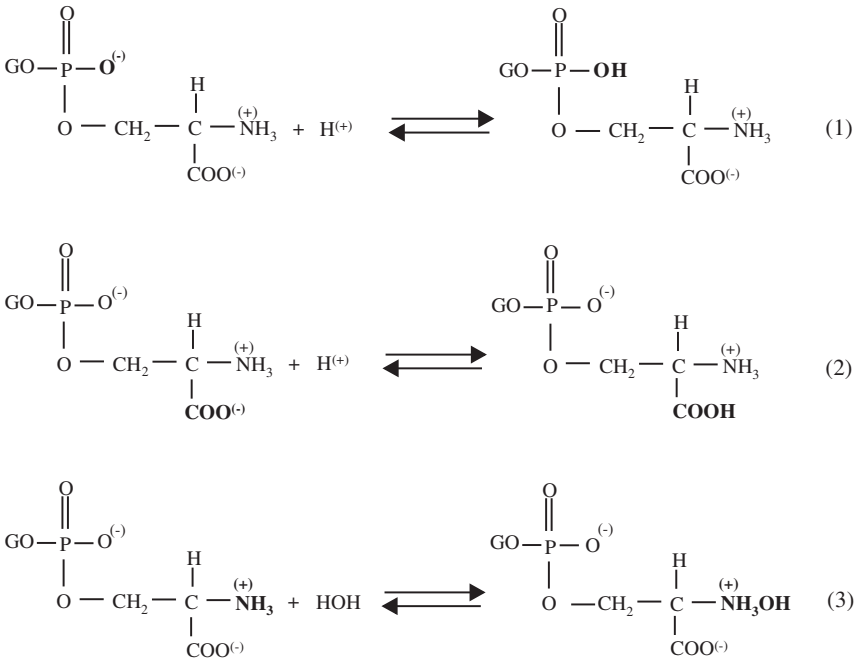

Fig. 30. The acid–base equilibria for PS molecule.

$$K_{A_2} = \frac{c^s_{A_2H}}{c^s_{A_2^-} a_{H^+}} \tag{83}$$

$$K_B = \frac{c^s_{BOH}}{c^s_{B^+} a_{OH^-}} \tag{84}$$

where K_{A_1}, K_{A_2} and K_B ($m^3\,mol^{-1}$) are the acids and base association constants, respectively; $c^s_{A_1^-}$, $c^s_{A_2^-}$, $c^s_{B^+}$, $c^s_{A_1H}$, $c^s_{A_2H}$ and c^s_{BOH} ($mol\,m^{-2}$) are the surface concentrations of $A_1^-, A_2^-, B^+, A_1H, A_2H$ and BOH forms at the lipid surface.

If the H^+ and OH^- ions are adsorbed at the PS membrane surface then the Gibbs equation assumes the form:

$$d\gamma = -c^s_{A_1H}\, d\bar{\mu}_{H^+} - c^s_{A_2H}\, d\bar{\mu}_{H^+} - c^s_{BOH}\, d\bar{\mu}_{OH^-} \tag{85}$$

The case of PS can be treated like that of lecithin or cephalin and the final equation was introduced below:

$$\gamma = \gamma_{max} - A^{-1}RT\ln\left(\frac{1 + K_{A_1} a_{H^+}}{1 + K_{A_1} a_{H^{+max}}}\right) - A^{-1}RT\ln\left(\frac{1 + K_{A_2} a_{H^+}}{1 + K_{A_2} a_{H^{+max}}}\right) - A^{-1}RT\ln\left(\frac{1 + K_B a_{OH^-}}{1 + K_B a_{OH^{-max}}}\right) \tag{86}$$

The association constant values obtained in this way were $K_1 = 2.29 \times 10^3\,m^3\,mol^{-1}$ and $K_2 = 3.55 \times 10^9\,m^3\,mol^{-1}$, respectively. As two association

constants only could be determined in this way and three were needed, the association constant corresponding to the $-PO^{(-)}$ group, $K_{A_1} = 3.80 \times 10^2\,m^3\,mol^{-1}$ was taken from the work [20]. Thus, the K_1 constant determined by titration was the geometric mean of the K_{A_1} and K_{A_2} constants. On this ground, the $K_{A_2} = 1.38 \times 10^4\,m^3\,mol^{-1}$ could be determined. The K_B constant was determined titrimetrically and it was found to be $3.55 \times 10^9\,m^3\,mol^{-1}$.

Effect of the pH on interfacial tension of the lipid bilayer formed from PS has been studied in the whole pH range. The dependence of interfacial tension of the membrane formed of PS on the pH of the electrolyte solution is presented in Fig. 31. The maximal interfacial tension value is $2.94 \times 10^{-3}\,N\,m^{-1}$ at pH equal to 3.80 [42].

The experimental values are marked in Fig. 31 by points and the theoretical ones obtained from equation (86) by lines. It can be seen from this figure that the theoretical and the experimental interfacial tension values of the PS membrane do not agree in the whole pH range.

2.2.2. *The full description based on Gibbs isotherm*

The exact definition of surface excess from the Gibbs equation lead to a description of the pH effect of electrolyte solution on interfacial tension of the membrane formed from lecithin or cephalin. Both compounds are similar and the experimental points are in agreement with theoretical ones obtained from equation (72) in whole pH range was very good. Therefore, it was necessary to check whether that description would also be right for more complicated compounds, for example, PS.

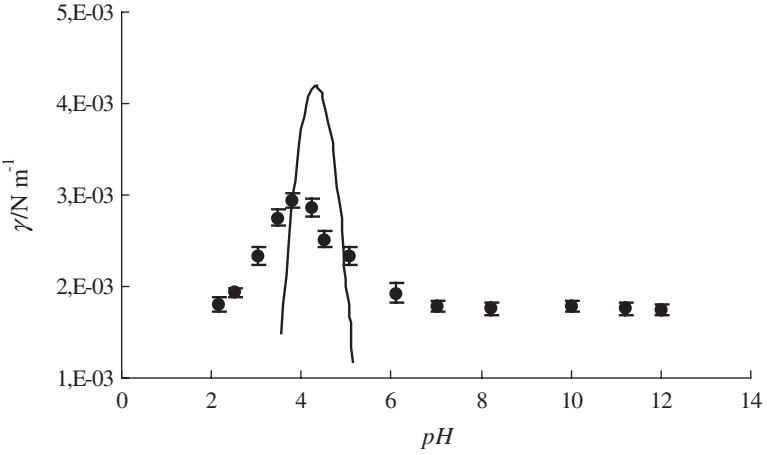

Fig. 31. The dependence of interfacial tension γ of a lipid membrane formed from PS of the pH of the electrolyte solution (the experimental values presented as points and the theoretical ones as line).

Dependences of surface excesses of the H^+ and OH^- ions in the PS membrane surface are as follows [74]:

$$\Gamma_{OH^-} = c^s_{BOH} - V_{H^+}\left(c^s_{A_1H} + c^s_{A_2H}\right)a_{OH^-} - V_{OH^-}c^s_{BOH}a_{OH^-} \tag{87}$$

$$\Gamma_{H^+} = c^s_{A_1H} + c^s_{A_2H} - V_{H^+}\left(c^s_{A_1H} + c^s_{A_2H}\right)a_{H^+} - V_{OH^-}c^s_{BOH}a_{H^+} \tag{88}$$

and therefore have:

$$\begin{aligned}\gamma = \gamma_{max} &- A^{-1}RT\left(1 + \frac{V_{H^+}}{K_{A_1}} - V_{H^+}K_WK_{A_1}\right)\ln\frac{1 + K_{A_1}a_{H^+}}{1 + K_{A_1}a^{max}_{H^+}} \\ &- A^{-1}RT\left(1 + \frac{V_{H^+}}{K_{A_2}} - V_{H^+}K_WK_{A_2}\right)\ln\frac{1 + K_{A_2}a_{H^+}}{1 + K_{A_2}a^{max}_{H^+}} \\ &- A^{-1}RT\left(1 + \frac{V_{OH^-}}{K_B} - V_{OH^-}K_WK_B\right)\ln\frac{1 + K_Ba_{OH^-}}{1 + K_Ba^{max}_{OH^-}} \\ &- A^{-1}RTV_{H^+}K_WK_{A_1}\ln\frac{a_{H^+}}{a^{max}_{H^+}} - A^{-1}RTV_{H^+}K_WK_{A_2}\ln\frac{a_{H^+}}{a^{max}_{H^+}} \\ &- A^{-1}RTV_{OH^-}K_wK_B\ln\frac{a_{OH^-}}{a^{max}_{OH^-}} \\ &+ 2A^{-1}RTV_{H^+}\left(a_{H^+} - a^{max}_{H^+}\right) + A^{-1}RTV_{OH^-}\left(a_{OH^-} - a^{max}_{OH^-}\right)\end{aligned} \tag{89}$$

The points in Fig. 32 present the experimental data concerning the interfacial tension of the membrane formed from PS depending on pH of the electrolyte solution.

Equation (89) is of type:

$$y = m_1x_1 + m_2x_2 + m_3x_3 + m_4x_4 + m_5x_5 + m_6x_6 + m_7x_7 + m_8x_8 + b$$

The interfacial tension values of the membrane formed from PS were calculated by substituting the calculated coefficients m_1, m_2, m_3, m_4, m_5, m_6, m_7, m_8, and b in equation (89), the result is presented in Fig. 32 as a solid line. It can be observed that the theoretical results agree well with the experimental data. The deduced theoretical equation (89) describes the experimental results in the whole pH range.

The m_1, m_2, m_3, m_4, m_5, m_6, m_7, m_8, and b coefficients contain the equilibrium constants and volumes of the adsorbed H^+ and OH^- ions. Thus, the equation coefficients calculated using the equilibria constants from paper [42] and were calculated for the volumes of adsorbed H^+ and OH^- ions as in previous paragraph. Volumes occupied by the H^+ and OH^- ions can be deducted from equation (89); they equal to 18,844 and 28,889 $Å^3$, respectively.

Assuming the most dense packing of the PS molecules in two-dimensional space, the surface occupied by a molecule corresponds to two equilateral triangles of a side equal to the intermolecular distance. If the area occupied by a PS molecule is known then mean intermolecular distance of phosphatidyserine on the bilayer surface can be estimated. Assuming the area occupied by a PS

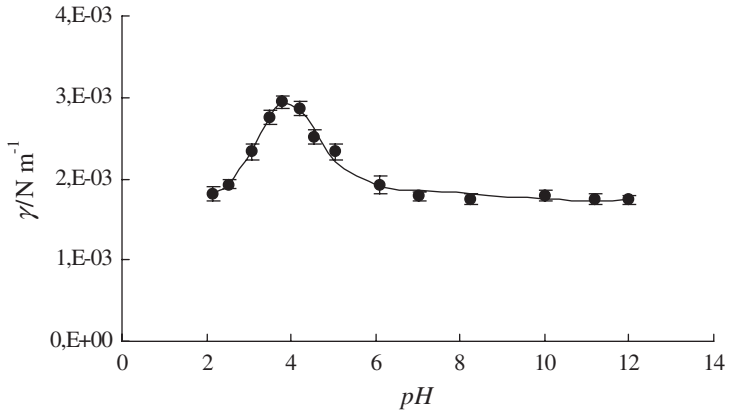

Fig. 32. The dependence of interfacial tension γ of the lipid membrane formed from PS of pH of electrolyte solution (full description based on the Gibbs equation); the experimental values are marked by points and the theoretical ones by solid curve.

molecule to be 68.5 Å^2 [42], the mean distance from an H^+ ion to an OH^- ion adsorption centre is about 11 Å.

For this reason, the volume of the adsorbed solvated H^+ ion can be assumed to be smaller than that of the solvated ions in the bulk. The radius of the adsorbed H^+ ion was calculated from its volume assuming its hemispherical shape; the result was about 10 Å. It is in agreement with the estimated distances of PS molecules in the membrane calculated above (11 Å).

The volume and radius of the solvated OH^- ion at the lipid membrane surface can be determined in a similar way from equation (89). However, the OH^- ion is adsorbed at an active centre that is present at the end of the hydrophilic PS chain. The chain can appear in various conformations with the result that the active centres were in various distances from the interface. The chain length is 5.0–7.5 Å [70]. Thus, the adsorbed OH^- ions are present in two layers: a layer of adsorption centres at the end of straight chains and the other layer with the centres at the ends that the absorb OH^- ion to stay at the interface; the situation is presented in paper [74]. It was assumed that parts of the PS molecule with hydrophilic chains and with the absorbed OH^- ions are straight and a part is bent towards the surface. For this reason, the straight-chain PS molecule surface concentration is half that of total PS concentration and distances between straight hydrophilic chains are approximately 16 Å. Similar estimates can be carried out for the chains bent towards the membrane surface.

The radius of the partly desolvated OH^- ion could be determined in this case, too, from its volume calculated using equation (89) assuming its hemispherical shape; it amounts to about 24 Å. It only approximately agrees with the 16 Å distance presented above between the adsorption centres.

The above numbers are rough estimates because of doubtlessly strong deformation of the OH^- ion solvation layer caused by dense packing of two layers.

The radii discussed above of hydrated H^+ and OH^- ions are greater than those given in the literature [71–73] that have been determined from hydration energy and correspond to ions having one hydration layer. Actually, the ions can be covered by more hydration layers due to hydrogen bonds acting between water molecules. Thus, the radius of an ion adsorbed by the layer can be greater than the value determined by formation energy of a single hydration layer.

2.2.3. *Models based on the additivity of different form of lipid in membrane*

The $-PO^{(-)}$, $-\overset{(+)}{N}H_3$ and the $-COO^{(-)}$ groups are presented at the phospholipid layer surface at the aqueous solution side; the surface is built of molecules each of them containing one $-PO^{(-)}$, one $-\overset{(+)}{N}H_3$ and one $-COO^{(-)}$ groups. Various models of membrane surface structure can be adopted to be analysed and describe the equilibria between the bilayer and the solution ions.

2.2.3.1. Model I

In this model, the surface is continuous with uniformly distributed functional groups constituting the active centres of H^+ and OH^- ions adsorption. The scheme of the membrane surface in this model is presented in the paper [42]. The system is schematically presented by equations (90–92):

$$\underset{(A_1^-)}{-PO^{(-)}} + H^{(+)} \rightleftharpoons \underset{(A_1H)}{-PO^{(-)}-H^{(+)}} \tag{90}$$

$$\underset{(B^+)}{-\overset{(+)}{N}H_3} + OH^- \rightleftharpoons \underset{(BOH)}{-\overset{(+)}{N}H_3-OH^{(-)}} \tag{91}$$

$$\underset{(A_2^-)}{-COO^{(-)}} + H^{(+)} \rightleftharpoons \underset{(A_2H)}{-COO^{(-)}-H^{(+)}} \tag{92}$$

Thus, six kinds of groups are present on the layer surface: $A_1^-, A_1H, B^+, BOH, A_2^-$ and A_2H. The adsorption equilibria are described by the equations as in the previous paragraph and are presented in the paper [42]. The following equation can be written assuming that contributions of the individual forms are additive:

$$\gamma = \gamma_{A_1^-} + \gamma_{A_1H} + \gamma_{B^+} + \gamma_{BOH} + \gamma_{A_2^-} + \gamma_{A_2H} \tag{93}$$

and therefore:

$$\begin{aligned}\gamma = {} & \gamma^0_{A_1^-}\left(1 - \frac{K_{A_1}a_{H^+}}{1+K_{A_1}a_{H^+}}\right) + \gamma^0_{A_1H}\left(\frac{K_{A_1}a_{H^+}}{1+K_{A_1}a_{H^+}}\right) + \gamma^0_{B^+}\left(1 - \frac{K_B a_{OH^-}}{1+K_B a_{OH^-}}\right) \\ & + \gamma^0_{BOH}\left(\frac{K_B a_{OH^-}}{1+K_B a_{OH^-}}\right) + \gamma^0_{A_2^-}\left(1 - \frac{K_{A_2}a_{H^+}}{1+K_{A_2}a_{H^+}}\right) + \gamma^0_{A_2H}\left(\frac{K_{A_2}a_{H^+}}{1+K_{A_2}a_{H^+}}\right)\end{aligned} \tag{94}$$

Equation (94) presents the dependence of the interfacial tension of the lipid membrane formed from PS on pH of electrolyte solution based on the Model I.

The interfacial tension of the membrane formed from PS is plotted in Fig. 33 vs. pH of the electrolyte solution (the experimental values are marked by points and the theoretical ones obtained from equation (94) by lines; broken lines present the interfacial tensions of the individual membrane components, i.e. $A_1^-, A_1H, B^+, BOH, A_2^-$ and A_2H). Fig. 33 refers to the structural Model I described earlier of the lipid membrane surface in which the functional groups have been assumed to be uniformly distributed on its surface on the aqueous solution side. As it is seen in equation (94), the total interfacial tension value of the PS membrane is the sum of interfacial tension values of it components presented above.

Introducing the K_{A_1}, K_{A_2} and K_B values obtained previous [42] to equation (94) yielded specific interfacial tension values of the individual forms of the PS membrane. The $\gamma_{A_1^-}, \gamma_{A_1H}, \gamma_{B^+}, \gamma_{BOH}, \gamma_{A_2H}$ and $\gamma_{A_2^-}$ values were obtained using the linear regression method and presented in the paper [42].

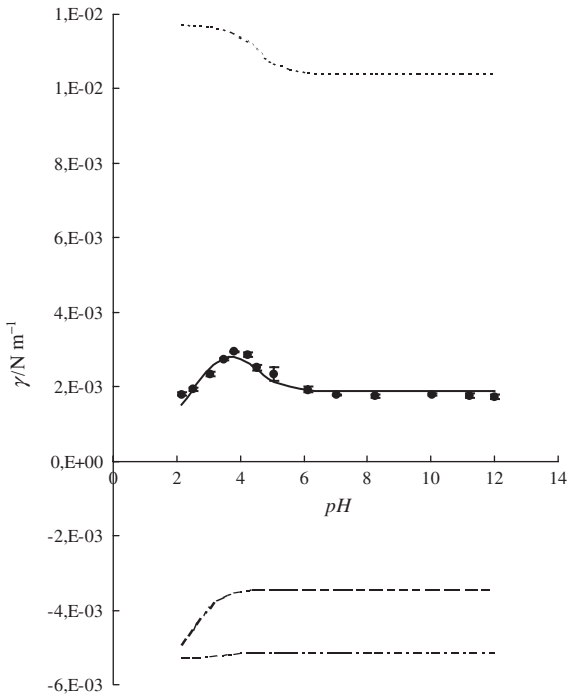

Fig. 33. The participation of the A_1, B and A_2 groups, calculated from the Model I, in dissociated and associated forms in the interfacial tension γ of the bilayer formed from PS, as a function of pH of electrolyte solution (the experimental values are marked by points and the theoretical ones by line).

2.2.3.2. Model II

In this model, the acid equilibrium between the $-PO^{(-)}$ group and the H^+ ion and the species containing the $-\overset{(+)}{N}H_3$ and the $-COO^{(-)}$ group with the H^+ and OH^- ion of solution are distinguished. This model is presented in the paper [42].

The adsorption equilibria are described by the equations:

$$A_1^- + H^+ \rightleftharpoons A_1H \tag{95}$$

$$B^+A_2^- + OH^- \rightleftharpoons BOHA_2^- \tag{96}$$

$$B^+A_2^- + H^+ \rightleftharpoons B^+A_2H \tag{97}$$

$$BOHA_2^- + H^+ \rightleftharpoons BOHA_2H \tag{98}$$

Thus, six groups: $A_1^-, A_1H, B^+A_2^-, BOHA_2^-, B^+A_2H$ and $BOHA_2H$ can be distinguished at the layer surface. Assuming that contributions of the individual forms for the interfacial tension are additive, the following equation can be written [42]:

$$\gamma = \gamma_{A_1^-} + \gamma_{A_1H} + \gamma_{B^+A_2^-} + \gamma_{BOHA_2^-} + \gamma_{B^+A_2H} + \gamma_{BOHA_2H} \tag{99}$$

and therefore [42]:

$$\gamma = -m_1 a_{H^+}^2 \gamma - m_2 a_{H^+}\gamma - m_3 a_{OH^-}\gamma + m_4 a_{H^+}^2 + m_5 a_{H^+} + m_6 a_{OH^-} + b \tag{100}$$

where

$$m_1 = \frac{K_1K_3}{M}$$

$$m_2 = \frac{K_1 + K_3 + K_1K_2K_4K_w}{M}$$

$$m_3 = \frac{K_2}{M}$$

$$m_4 = \frac{K_1K_3\left(\gamma^0_{A_1H} + \gamma^0_{B^+A_2H}\right)}{M}$$

$$m_5 = \frac{K_3\gamma^0_{A_1H} + K_1K_2K_4K_w\gamma^0_{A_1H} + K_1\gamma^0_{B^+A_2^-} + K_1K_2K_4K_w\gamma^0_{BOHA_2H}}{M}$$

$$m_6 = \frac{K_2\gamma^0_{A_1^-}}{M}$$

$$b = \frac{\gamma^0_{A_1^-} + \gamma^0_{A_1H} + \gamma^0_{B^+A_2^-} + \gamma^0_{BOHA_2^-} + \gamma^0_{B^+A_2H} + \gamma^0_{BOHA_2H}}{M} + \frac{K_2K_4K_w\gamma^0_{A_1^-} + K_1K_2K_w(\gamma^0_{A_1H} + \gamma^0_{BOHA_2^-})}{M}$$

$$M = 1 + (K_1 + K_4)K_2K_w$$

here $\gamma^0_{A_1^-}, \gamma^0_{A_1H}, \gamma^0_{B^+A_2^-}, \gamma^0_{BOHA_2^-}, \gamma^0_{B^+A_2H}$ and $\gamma^0_{BOHA_2H}$ ($N\,m^{-1}$) are the specific interfacial tensions of the membrane components, respectively.

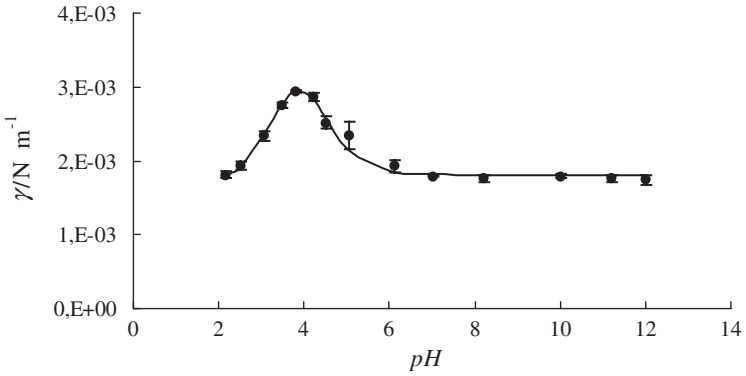

Fig. 34. The participation of the A_1 and BA_2 groups, calculated from the Model II, in dissociated and associated forms in the interfacial tension γ of the bilayer formed from PS, as a function of pH of electrolyte solution; the experimental values are marked by points and the theoretical ones by line.

Equation (100) presents the dependence of the interfacial tension of the lipid membrane on pH of electrolyte solution based on the Model II.

In Fig. 34, the experimental interfacial tension values are represented as points and those calculated for Model II from equation (100) as solid lines. Figure 34 refers to the Model II in which the PS surface is built from forms of PS molecules. However, determination of the interfacial tension of the individual components was difficult because the association constant values K_1, K_2, K_3 and K_4 were unknown. For this reason, the individual equation coefficients, m_1, m_2, m_3, m_4, m_5, m_6, m_7, m_8, and b were obtained using the linear regression method. As it is seen in Fig. 34, Model II yields a much better agreement of the calculated and experimental data in all the pH range. It indicates that it is closer to the reality.

Another structural model of PS bilayer surface was considered; it is presented in the paper [42]. This model was considered to explain acid–base equilibria between the functional groups of the PS molecule and the H^+ and OH^- ions in solution. However, the presentation and the discussion of the equilibria in the forms envisaged by this model and calculations of their contribution on the interfacial tension of the lipid bilayer results in disagreement with the experiment.

2.3. Conclusions

The results of pH on interfacial tension of the bilayer lipid membrane formed from PC, PS and from PE have permitted us to determine the effect of the hydrophilic head of lipids on interfacial tension values of bilayer lipid membranes. Hydrophilic heads have been demonstrated to affect the interfacial tension values and, consequently, cell membrane properties. Unlike other phospholipids, e.g. lecithin

or PS, small hydrophilic head characterizes PE molecule. Regularity has been found: the larger hydrophilic head of a lipid brings about lower interfacial tension.

Calculated interfacial tension values are $\gamma = (4.06 \pm 0.12) \times 10^{-3}\,\mathrm{N\,m^{-1}}$ for PE, $\gamma = (3.53 \pm 0.12) \times 10^{-3}\,\mathrm{N\,m^{-1}}$ for PC (large hydrophilic head), and $\gamma = (2.93 \pm 0.10) \times 10^{-3}\,\mathrm{N\,m^{-1}}$ for PS.

In addition, a relationship has been found for the size of the hydrophilic head of lipid with the isoelectric point pH value. With a larger hydrophilic head, the isoelectric point appears at lower pH. The isoelectric point of PE was found to be at pH 4.20, while those of lecithin and phospatidylserine appear at pH 4.15 and 3.80, respectively.

Interestingly, the interfacial tension value of the isoelectric point increases with decreasing hydrophilic head diameter of lipid. Surface area of the isoelectric points for PC, PS and PE related to 1 mol of the substance are similar and amount to 1800, 1824 and 1854 $\mathrm{J\,mol^{-1}}$, respectively.

3. MATERIALS AND EXPERIMENTAL DETAILS

3.1. Reagents

The following chemicals were used for preparation of the forming solution:

1. Lecithin (3-sn-phosphatydylcholine 99%) from Fluka. It had been obtained from egg yolk. The composition of fatty acids in the lecithin was 16:0∼33%, 18:0∼4%, 18:1∼30%, 18:2∼14% and 20:4∼4%. Lecithin was dissolved in chloroform to prevent oxidizing and the solvent was evaporated in an argon medium
2. 99% cholesterol of molecular formula $C_{27}H_{45}OH$ made by Sigma
3. PE (99%) from Fluka
4. 3-sn-Phosphatidyl-L-serine from bovine brain (99%) from Fluka
5. Gramicidin D produced by Sigma.
6. Valinomycin (90%) by Sigma.

The stock solutions used to form the artificial membrane contained 20 $\mathrm{mg\,cm^{-3}}$ of lipids in appropriate solvents: decane or decane-butanol (3:1 by volume) for interfacial tension measurements and hexadecane-butanol (10:1 by volume) for impedance measurements.

The forming solutions modified with gramicidin were prepared by adding the peptide in trifluoroethanol to lecithin and the solvent was again removed by argon. Dried residues were dissolved in decane or a hexadecane-butanol mixture (10:1 by volume). The stock solutions contained 10 $\mathrm{mg\,cm^{-3}}$ of gramicidin D and PC (weight ratios: $1{:}1.0 \times 10^4$, $1{:}2.5 \times 10^4$, $1{:}5.0 \times 10^4$, $1{:}7.5 \times 10^4$ and $1{:}1.0 \times 10^5$) for impedance measurements and 20 $\mathrm{mg\,cm^{-3}}$ of gramicidin D and PC (1:10, 1:20, 1:30 and 1:40 weight ratio) for interfacial tension experiments.

Valinomycin was added as a solution in chloroform (20 mg cm^{-3}) and the solvent was again removed by argon. For impedance measurements dried residues were dissolved in a hexadecane-butanol mixture (10:1 by volume). The forming solutions contained PC or a PC–valinomycin mixture (total valinomycin concentrations: 2.08×10^{-11}, 1.04×10^{-11}, 6.94×10^{-12} and 5.20×10^{-12} mol cm^{-2}). For the interfacial tension measurements the membrane components were dissolved in *n*-decane and the forming solutions contained pure lecithin and lecithin–valinomycin mixtures of 1:10, 1:20, 1:30 and 1:40 weight ratio.

All experiments connected with investigation of the complex forming equilibria were carried out in the whole composition range of the membrane concentrations.

Potassium chloride solutions were used as electrolyte in those experiments, in which forming complexes was assumed. The electrolyte solutions were prepared from mili-Q water and KCl form POCh. 1, 0.1, 0.01, 0.001 and 0.0001 M electrolyte solutions were used for experiments. Potassium chloride was calcinated to remove organic impurities.

The buffers of 2–12 pH ranges prepared according to Britton and Robinson were used in the interfacial tension measurements of the bilayer lipid membrane as a function of the pH of the electrolyte solution [20,22]. They were prepared by adding 0.2 M sodium hydroxide to 100 cm^3 of solution having the composition: 0.04 M acetic acid (80%, POCh), 0.04 M phosphoric acid (POCh) and 0.04 M boric acid (POCh). A suitable pH of the buffer was imposed depending on the amount of added sodium hydroxide (at 291 K).

The solvents were of chromatographic standard grade: *n*-decane was from Merck, hexadecane was from Fluka and chloroform, butanol and trifluoromethanol were from Aldrich. Water purified by Milli-QII (18.2 M, Millipore, USA) was used to make all solutions in all cleaning procedures.

All experiments were carried out at room temperature (295–297 K).

3.2. Interfacial tension measurements

The interfacial tension of a lipid bilayer was determined by measuring the radius of the curvature of a convex surface formed by pressure difference applied on both sides. The applied technique is based on the Young's and Laplace's equation [75].

The apparatus and the measurement method were described in the papers [4,6,20,22,42,69,74]. The measuring vessel consisted of two glass chambers separated by a mount in which a circular Teflon element was set with a 1.5 mm outer diameter containing an orifice along its axis. An electrolyte solution was present on both sides of the orifice.

The membranes were formed by the Mueller–Rudin method [76] on the flat end of the Teflon element. Both chambers of the measuring vessel were filled with the electrolyte solution. The forming solution was brought with a micropipette to the

flat wall of the Teflon element. Then, a pressure was applied to the left chamber using a manometer.

The convexity of the lipid membrane cap was measured with 0.05 mm precision instrument reading. This value together with the Teflon element diameter corresponding to the lipid cap diameter yielded the radius of curvature.

3.3. Impedance analysis

Electrochemical impedance measurements were carried out using an alternative current (AC) impedance system (EG&G, Princeton Applied Research, Model 388) including a personal computer, a two-phase lock-in amplifier (Model 5208) and a potentiostat/galvanostat (Model 273). The electrochemical cell was connected with a potentiostat via a differential amplifier with high-impedance inputs. The electrochemical cell in the four-electrode configuration contained two identical reversible silver–silver chloride electrodes and two identical current platinum electrodes, and was described exactly in [5,7,31]. The A 4-mV amplitude sine-wave signal perturbation was applied in the 0.1–10,000 Hz frequency range. Data analysis was performed by means of software using a non-linear least-square fit (Equivcrt.Pas) elaborated by Boukamp [77].

Bilayer membranes were obtained as bubbles at the teflon cap constituting a measuring vessel component. The use of hexadecane as the solvent allows obtaining membranes of thickness and capacity values similar to those of membranes formed of monolayers (*n*-butanol contained in the forming solution dissolved in aqueous solution). The thinning of the BLMs was observed visually. Capacity of membranes increased with time after bilayers formation until a steady-state value was reached some 10–20 min later. The measurements were started 20–30 min after the membranes turned completely black. The bilayers area was determined with a microscope with micrometer scale built-in in the lens and was between $4 \times 10^{-2} - 8 \times 10^{-2}$ cm^2 (the values were given for the bilayers area with a subtracted margin).

3.4. Preparation of liposomes and isoelectric point determination

The bilayer lipid membranes were also used in the form of liposomes. These can be formed owing to the fact that most phospholipids undergo spontaneous aggregation in water or in aqueous electrolyte solutions if shaken or subjected to ultrasounds. Bubbles of spherical or cylindrical shape, sized from less than a little to a fraction of millimetre, are then formed [78,79]. They were formed as follows [80]: 10 mg of lipids were dissolved in 1–2 cm^3 of chloroform and the solvent was evaporated in the atmosphere of argon until 25–50 μm^3 of lipid film remained in the beaker. 15 cm^3 of 0.9% NaCl were added and the beaker was placed in a

water bath (at about 280 K). The head of an UD-20 ultrasound generator was immersed in the solution and the solution was subjected to ultrasounds five times for 1.5 minutes each time. The liposomes of 10–20 nm were obtained [81].

The isoelectric point of a lipid membrane can be determined if the acid–base equilibrium constants are known. However, it was difficult to determine those magnitudes because the phospholipid was insoluble in water. For this reason, the needed values were determined using liposomes. It was accepted in the calculations that only the lecithin molecules present in the outer layer of liposome took part in acid–base equilibria. Thus, the phospholipid concentrations used in the equations were half of that introduced into the solution.

The dissociation constants of the membrane formed from phospholipid were determined by titration of the previously obtained liposomes with hydrochloric acid and with sodium hydroxide. A 736GP Titrino apparatus from Metrohm (Switzerland) was used in the titration.

Having determined the dissociation constants of the membrane, isoelectric point could be calculated from equations presented in the paper [42].

ACKNOWLEDGMENT

The points about valinomycin and gramicidin interfacial tension measurements were supported by a grant from the Polish Committee of Scientific Research No 3 T09A 006 15.

REFERENCES

[1] F.T. Presti, R.J. Pace, S.I. Chan, Cholesterol-phospholipid interaction in membranes. 2. Stoichiometry and molecular packing of cholesterol-rich domains, Biochemistry 21 (1982) 3831–3835.
[2] A. Darke, E.G. Finer, A.G. Flook, M.C. Phillips, Nuclear magnetic resonance study of lecithin-cholesterol interactions, J. Mol. Biol. 63 (1972) 265–279.
[3] S.L. Regen, Lipid–lipid recognition in fluid bilayers: solving the cholesterol mystery, Curr. Opin. Chem. Biol. 6 (2002) 729–735.
[4] A.D. Petelska, Z.A. Figaszewski, Interfacial tension of the two-component bilayer lipid membrane modelling of the cell membrane, Biolectrochem. Bioenerg. 46 (1998) 199–204.
[5] M. Naumowicz, A.D. Petelska, Z.A. Figaszewski, Capacitance and resistance of the bilayer lipid membrane formed of phosphatidylcholine and cholesterol, Cell. Mol. Biol. Lett. 8 (2003) 5–18.
[6] A.D. Petelska, M. Naumowicz, Z.A. Figaszewski, The interfacial tension of the lipid membrane formed from lipid–cholesterol and lipid–lipid systems, Cell Biochem. Biophys. 44 (2006) 205–211.
[7] J. Inczendy, Analytical Applications of Complex Equlibria, Chapter 1, Akademia Kiado, Budapest, 1976.
[8] M. Naumowicz, A.D. Petelska, Z.A. Figaszewski, Impedance analysis of phosphatidylcholine–cholesterol system in bilayer lipid membranes, Electrochim. Acta 50 (2005) 2155–2161.

[9] P.L. Yeagle, Cholesterol and the cell membrane, Biochim. Biophys. Acta 822 (1985) 267–287.
[10] T.X. Xiang, J. Chen, B.D. Anderson, A quantitative model for the dependence of solute permeability on peptide and cholesterol content in biomembranes, J. Membrane Biol. 177 (2000) 137–148.
[11] T. Hianik, M. Haburcak, K. Lohner, E. Prenner, F. Paltauf, A. Hermetter, Compressibility and density of lipid bilayers composed of polyunsaturated phospholipids and cholesterol, Colloids Surf. A Physicochem. Eng. Aspects 139 (1998) 189–197.
[12] M.R. Prestom, T.N. Tulenko, R.F. Jacob, Direct evidence for cholesterol crystalline domains in biological membranes: role in human pathobiology, Biochim. Biophys. Acta 1610 (2003) 198–207.
[13] T. Rog, M. Pasenkiewicz-Gierula, Non-polar interactions between cholesterol and phospholipids: a molecular dynamics simulation study, Biophys. Chem. 107 (2004) 151–164.
[14] A. Darke, E.G. Finer, A.G. Flook, M.C. Phillips, Complex and cluster formation in mixed lecithin cholesterol bilayers. Cooperativity of motion in lipid system, FEBS Lett. 18 (1971) 326–330.
[15] D.A. Cadenhead, Monolayers of synthetic phospholipid, in: J.F. Danielli, A.C. Riddiford, M. Rosenberg (Eds.), Recent Progress in Surface Science, Vol. 3, Academic Press, New York, London, 1970.
[16] H. Ohvo-Rekila, B. Ramstedt, P. Leppimaki, J.P. Slotte, Cholesterol interactions with phospholipids in membranes, Prog. Lipid Res. 41 (2002) 66–97.
[17] D. Shigematsu, M. Matsutani, T. Furuya, T. Kiyota, S. Lee, G. Sugihara, Roles of peptide–peptide charge interaction and lipid phase separation in helix–helix association in lipid bilayer, Biochim. Biophys. Acta 1564 (2002) 271–280.
[18] N. Kahya, D. Scherfeld, K. Bacia, P. Schwille, Lipid domain formation and dynamics in giant unilamellar vesicles explored by fluorescence correlation spectroscopy, J. Struct. Biol. 147 (2004) 77–89.
[19] P. Somerharju, J.A. Virtanen, K.H. Cheng, Lateral organisation of membrane lipids: the superlattice view, Biochim. Biophys. Acta 1440 (1999) 32–48.
[20] A.D. Petelska, Z.A. Figaszewski, Effect of pH on the interfacial tension of bilayer lipid membrane, Biophys. J. 78 (2000) 812–817.
[21] M.K. Jain, F. Ramirez, T.M. McCaffrey, P.V. Ioannou, J.F. Marecek, J. Leunissen-Bijvelt, Phospholipidcholesterol bilayers a model for phospholipid–cholesterol interaction, Biochim. Biophys. Acta 600 (1980) 678–688.
[22] A.D. Petelska, Z.A. Figaszewski, The effect of pH on the interfacial tension of bilayer lipid membrane formed from phosphatidylethanolamine, Biochim. Biophys. Acta 1567 (2002) 79–86.
[23] R.B. Gennis, Biomembranes: Molecular Structure and Function, Chapter 2, Springer, New York, 1989.
[24] K.S. Birdi, Lipid and Biopolymer Monolayers at Liquid Interfaces, Plenum Press, New York, 1989.
[25] O.S. Andersen, Gramicidin channels, Annu. Rev. Physiol. 46 (1984) 531–548.
[26] A.E. Vallejo, C.A. Gervasi, Impedance analysis of ion transport through gramicidin channels in supported lipid bilayers, Bioelectrochemistry 57 (2002) 1–7.
[27] B.M. Burkhart, N. Li, D.A. Langs, W.A. Pangborn, W.L. Duax, The conducting form of gramicidin A is a right-handed double-stranded double helix, Proc. Natl. Acad. Sci. USA 95 (1995) 12950–12955.
[28] A.D. Petelska, M. Naumowicz, Z.A. Figaszewski, The effect of interaction between K^+ ions and gramicidin D on the lecithin membrane interfacial tension, Bioelectrochemistry 65 (2005) 143–148.
[29] D.A. Haydon, S.B. Hladky, Ion transport across thin lipid membranes: a critical discussion of mechanisms in selected systems, Q. Rev. Biophys. 5 (1972) 187–282.
[30] N. Davion-Van Mau, P. Daumas, D. Lellevre, Y. Trudelle, F. Heitz, Linear gramicidins at the air–water interface, Biophys. J. 51 (1987) 843–845.

[31] M. Naumowicz, Z. Figaszewski, Impedance analysis of phosphatidylcholine membrane modified with gramicidin D, Bioelectrochemistry 61 (2003) 21–27.
[32] S. Alonso-Romanowski, L.M. Gassa, J.R. Vilche, An investigation by EIS of gramicidin channels in bilayer lipid membrane, Electrochim. Acta 40 (1995) 1561–1567.
[33] W. Jing, Z. Wu, E. Wang, Electrochemical study of gramicidin D forming ion-permeable channels in the bilayer lipid membranes, Electrochim. Acta 44 (1998) 99–102.
[34] W.R. Veatch, L. Stryer, The dimeric nature of the gramicidin A transmembrane channel: conductance and fluorescence energy transfer studies of hybrid channel, J. Mol. Biol. 113 (1977) 89–102.
[35] D.W. Urry, The gramicidin A transmembrane channel: a proposed $\pi_{(L,D)}$ helix, Proc. Natl. Acad. Sci. USA 68 (1971) 672–676.
[36] M. Sluyters-Renbach, Impedances of electrochemical systems: terminology, nomenclature and representation. Part I. Cells with metal electrodes and liquid solutions, Pure Appl. Chem. 66 (1994) 1831–1891.
[37] M. Sluyters-Renbach, J.H. Sluyters, in: J. Bard, (Ed.), Electroanalytical Chemistry, Vol. 4, Marcel Dekker, Inc., New York, 1970.
[38] E. Bamberg, P. Lauger, Channel formation kinetics of gramicidin A in lipid bilayer membranes, J. Membrane Biol. 11 (1973) 177–194.
[39] W.R. Veatch, R. Mathies, M. Eisenberg, L. Stryer, Simultaneous fluorescence and conductance studies of planar bilayer membranes containing a highly active and fluorescent analog of gramicidin A, J. Mol. Biol. 99 (1975) 75–92.
[40] S. Shobana, S. Vishveshwara, Structure of valinomycin by molecular dynamics studies, Indian J. Biochem. Biophys. 28 (1991) 363–368.
[41] P. Lauger, Carrier-mediated ion transport, Science 178 (1972) 24–30.
[42] A.D. Petelska, Z.A. Figaszewski, Effect of pH on the interfacial tension of the lipid bilayer membrane formed from phosphatidylcholine or phosphatidylserine, Biochim. Biophys. Acta 1561 (2002) 135–146.
[43] H.D. Haynes, The kinetic of potassium ion complexation by ionophores, FEBS Lett. 20 (1972) 221–224.
[44] P. Lauger, Kinetic properties of ion carries and channels, J. Membrane Biol. 57 (1980) 163–178.
[45] G. Stark, B. Ketterer, R. Benz, P. Lauger, The rate constants of valinomycin-mediated ion transport through thin lipid membranes, Biophys. J. 11 (1971) 981–994.
[46] Y.A. Ovchinnikov, V.T. Ivanov, A.V. Evstratov, V.F. Bystrov, N.D. Abdullev, E.M. Popov, G.M. Lipkind, S.F. Arhipova, E.S. Efremov, M.M. Shemyakin, The physicochemical basis of the functioning of biological membranes: dynamic conformational properties of enniatin B and its K^+ complex in solution, Biochim. Biophys. Res. Commun. 37 (1969) 668–676.
[47] C. Steinem, A. Janshoff, W.P. Ulrich, M. Sieber, H.J. Galla, Impedance analysis of supported lipid bilayer membranes: a scrunity of different preparation techniques, Biochim. Biophys. Acta 1279 (1996) 169–180.
[48] R. Naumann, D. Waltz, S.M. Schiller, W. Knoll, Kinetics of valinomycin-mediated K^+ ion transport through tethered bilayer lipid membranes, J. Electroanal. Chem. 550–551 (2003) 241–252.
[49] K.J. Vetter, Elektrochemische kinetik, Springer, Berlin, 1961.
[50] E. Grell, T. Funck, F. Eggers, Proceedings of the symposium on molecular mechanisms of antibiotic action on protein in biosynthesis and membranes, Elsevier, Amsterdam, 1972.
[51] R. Benz, G. Stark, K. Janko, P. Lauger, Valinomycin-mediated ion transport through neutral lipid membranes: influence of hydrocarbon chain length and temperature, J. Membrane Biol. 14 (1973) 339–364.
[52] R. Benz, O. Frohlich, P. Lauger, Influence of membrane structure on the kinetics of carrier-mediated ion transport through lipid bilayers, Biochim. Biophys. Acta 464 (1977) 465–481.

[53] R. Benz, D. Cros, Influence of sterols on ion transport through lipid bilayer membranes, Biochim. Biophys. Acta 506 (1978) 265–280.
[54] B.C. Pressman, D.H. Haynes, Symposium on the molecular basis of membrane function, Prentice-Hall, New York, 1970.
[55] D.H. Haynes, A. Kowalsky, B.C. Pressman, Application of neutral magnetic resonance to the conformational changes in valinomycin during complexation, J. Biol. Chem. 244 (1969) 502–505.
[56] P.C. Biggin, G.R. Smith, I. Shrivastava, S. Choe, M.S.P. Sansom, Potassium and sodium ions channel studied by molecular dynamics simulations, Biochim. Biophys. Acta 1510 (2001) 1–9.
[57] J. Åqvist, V. Luzhakov, Ion permeation of the potassium channel, Nature 404 (2000) 881–884.
[58] J. Åqvist, Ion-water interaction potentials derived from free energy perturbation simulations, J. Phys. Chem. 94 (1990) 8021–8024.
[59] V. Luzhakov, J. Åqvist, K(+)/Na(+) selectivity of the KcsA potassium channel from microscopic free energy perturbation calculations, Biochim. Biophys. Acta 1548 (2001) 194–202.
[60] R.T. Morison, R.N. Boyd, Organic Chemistry, 3rd edition, Allyn and Bacon, Inc., Boston, 1985, pp. 281–286.
[61] C.A. Stace, A Guide to Subcellular Botany, Green & Co. Ltd., London, 1965, pp. 50–51.
[62] H.G.L. Coster, R. Simons, Energy of formation of bimolecular lipid membranes, Biochim. Biophys. Acta 163 (1968) 234–239.
[63] M.K. Jain, The Biomolecular Lipid Membrane, Litton Educational Publishing, Inc., New York, 1972, pp. 90–92.
[64] P. Joos, R.A. Demel, The interaction energies of cholesterol and lecithin in spread mixed monolayers at the air–water interface, Biochim. Biophys. Acta 183 (1969) 447–457.
[65] D.J. Vaughan, K.M. Keough, Changes in transitions of phosphatidylethanolamine and phosphatidylcholine–water dispersions induced by small modifications in the headgroup and backbone regions, FEBS Lett. 47 (1974) 158–161.
[66] J. Gawłowski, P. Zelenay, M. Szklarczyk, Interdependence and accuracy of parameters determined from adsorption isotherms, Polish J. Chem. 69 (1995) 1046–1053.
[67] B.R. Scharifker, P. Zelenay, The comparison of thermodynamic quantities in adsorption from solution described by different isotherms, Quim. Acta Cient. Venez. 39 (1988) 315–318.
[68] J.J. Bikerman, Surface Chemistry. Theory and Applications, Academic Press, New York, 1958.
[69] A.D. Petelska, Z.A. Figaszewski, Acid–base equilibria at interface separating electrolyte solution and lipid bilayer formed from phosphatidylcholine, Biophys. Chem. 104 (2003) 13–19.
[70] D.R. Laver, J.R. Smith, H.G.L. Coster, The thickness of the hydrophobic and polar regions of glycerol monooleate bilayers determined from the frequency-dependence of bilayer capacitance, Biochim. Biophys. Acta 772 (1984) 1–9.
[71] Y. Marcus, Ion solvatation, Wiley, London, 1985.
[72] Y. Marcus, Ion properties, Marcel Dekker, Inc., New York, 1997.
[73] J. Padova, Ion-solvent interaction. II. Partial molar volume and electrostriction: a thermodynamic approach, J. Chem. Phys. 39 (1963) 1552–1557.
[74] A.D. Petelska, Z.A. Figaszewski, Acid–base equilibria at interface separating electrolyte solution and lipid bilayer formed from phosphatidylserine, Biophys. Chem. 104 (2003) 5–11.
[75] A.W. Adamson, Physical Chemistry of Surfaces, Interscience Publishers, Inc., New York, 1960, pp. 4–9.
[76] P. Mueller, D.O. Rudin, H.T. Tien, W.C. Wescoot, Methods for the formation of single bimolecular lipid membranes in aqueous solution, J. Phys. Chem. 67 (1963) 534–535.

[77] B.A. Boukamp, Equivalent Circuit (equivcrt.pas), University of Twente, Enschede, 1988.
[78] S.M. Jahnson, A.D. Bagham, H.W. Hill, E.D. Korn, Single bilayers liposomes, Biochim. Biophys. Acta 233 (1971) 820–826.
[79] E. Ziętkiewicz, R. Słomski, Liposomes as carriers in the transfer of substances of biological importance into cell, Post. Biochem. 30 (1984) 149–172.
[80] D.D. Lasic, Liposomes: From Physics to Application, Elsevier Science B.V., Amsterdam, 1995, pp. 63–100.
[81] C. Huang, Studies on phosphatidylcholine vesicles. Formation and physical characteristics, Biochemistry 8 (1963) 344–352.

This page intentionally left blank

CHAPTER 6

Effects of Sugars on the Stability and Structure of Lipid Membranes During Drying

Dirk K. Hincha,[1,*] Antoaneta V. Popova,[1,2] and Constança Cacela[1]

[1]*Max-Planck-Institut für Molekulare Pflanzenphysiologie, D-14424 Potsdam, Germany*
[2]*Institute of Biophysics, Bulgarian Academy of Sciences, 1113 Sofia, Bulgaria*

Contents

Abstract

Most plants, microbes, and animals that can survive complete dehydration (anhydrobiotes) accumulate high concentrations of sugars in their cells during desiccation. Since cellular membranes are a primary target of desiccation damage in cells, liposomes have been widely used as comparatively simple model systems to study the effects of sugars on the properties of membranes during drying. In addition, there is a pronounced technical interest in the stabilization of liposomes with encapsulated medical drugs in the dry state for pharmaceutical purposes. Most sugars induce a depression of the membrane phase transition temperature of the dry lipid and form a glass (vitrify) during drying. In this paper, we critically review the current state of knowledge about the physical mechanisms that may lead to membrane stabilization in dry systems, with a special emphasis on possible interactions between membrane lipids and sugars in the dry state. For this purpose we compare the effects of soluble disaccharides, oligosaccharides, and polysaccharides, and also the effects of lipid-bound sugars on the stability and physical behavior of liposomes.

1. THE ROLE OF SUGARS IN THE DESICCATION TOLERANCE OF CELLS AND ORGANISMS

For most living organisms, water is an essential prerequisit of survival and even a moderate loss of cellular water can lead to physiological damage and ultimately death. Several species of microbes, plants, and animals, however, have evolved

*Corresponding author. Tel: +49 331 567 8253; Fax: +49 331 567 8250;
E-mail: hincha@mpimp-golm.mpg.de

ADVANCES IN PLANAR LIPID BILAYERS AND LIPOSOMES, VOLUME 3
ISSN 1554-4516 DOI: 10.1016/S1554-4516(05)03006-1

the ability to survive almost complete dehydration, often for prolonged periods of time. This life without water, or anhydrobiosis, is dependent on a coordinated and controlled set of biochemical adaptations, that are still far from being fully understood. Several mechanisms participate in the protection of living cells during the removal of water (see [1] for a review). These include, but are not limited to, the maintenance of macromolecules in their biologically functional structures. This pertaines to nucleic acids, soluble proteins and protein complexes, and membranes. In yeast, tardigrades, and nematodes, in many algae, and desiccation tolerant higher plants (resurrection plants), but also in the pollen and seeds of many plant species that are not desiccation tolerant in their vegetative state, the accumulation of the disaccharides sucrose or trehalose is thought to play a major role in cellular desiccation tolerance (see [2–4] for reviews).

In addition to the accumulation of disaccharides, many other biochemical adaptations take place in anhydrobiotic cells during the drying process. Many organisms accumulate not only disaccharides, but also other compatible solutes, such as some amino acids (e.g. proline), quaternary ammonium compounds (e.g. betaine), oligosaccharides, sugar alcohols, and several others (see [5,6] for reviews). However, not all compatible solutes are effective in stabilizing cellular structures during complete dehydration [7,8]. In addition to the accumulation of compatible solutes during slow drying, the pattern of gene expression changes dramatically in desiccation tolerant cells [9]. In addition to many genes that may be related to biochemical and physiological adaptation to low water content, many of the expressed genes encode specific dehydration-related proteins, such as late embryogenesis abundant (LEA) proteins. Their functional role in dehydration tolerance, however, remains to be shown [10].

An important further point is the defense of dry cells against oxidative damage. Since enzymatic antioxidant systems are probably not functional under conditions of extreme dehydration, chemical antioxidants, such as flavonoids, will have to take their place [11,12]. These molecules, however, are amphiphilic in nature and will partition into the lipid phase of membranes during dehydration [13,14]. This can, in addition to the antioxidant effects, also have pronounced direct effects on membrane stability. Whether the effects will be stabilizing or destabilizing, depends not only on the chemical nature of the amphiphilic molecules, but also on membrane lipid composition and the additional presence of protective solutes such as sugars [15–19].

The importance of non-disaccharide-based protective systems in anhydrobiosis [20] is highlighted by the recent investigations into the desiccation tolerance of rotifers, which are highly desiccation tolerant without accumulating any sugars during drying [21,22]. It is therefore clear that the accumulation of sugars is not the only possible strategy for a cell to become desiccation tolerant. It is, nevertheless, the most prevalent adaptation to the loss of water found in nature. In addition, the biophysical mechanisms underlying the protection of cellular structures have been most thoroughly investigated with sugars.

In addition to the biological interest, there is considerable technical interest in the stabilization of cellular membranes by sugars [4]. In recent years, efforts have been directed at the preservation of biological cells in the dry state. This involves e.g. blood components such as platelets [23,24], but also other mammalian cells [25–27]. In these cases, trehalose has been accumulated in the cells, either by endocytosis, or by genetically engineering the cells to take up or synthesize trehalose.

Since cellular membranes are primary targets of desiccation damage, considerable effort has been directed toward understanding the mechanisms of protection of membranes by sugars during drying (see [1,28] for reviews). Many of these investigations have used liposomes as comparatively simple model systems to elucidate the physical details of membrane protection. In addition, there is considerable interest in the stability of liposomes as vehicles for the delivery of medical drugs. The present article will therefore review our current understanding of how sugars stabilize liposomes, and presumably biological membranes, in the dry state.

2. THE STABILIZATION OF MEMBRANES BY VITRIFICATION OF SUGARS DURING DRYING

Cytoplasmic vitrification is considered to be an important mechanism in cellular desiccation tolerance in many species of plants, animals, and microbes [29–31]. Many sugars form glasses (vitrify) during drying at ambient temperatures (see [32,33] for reviews). Physically, a glass is a metastable solid. It is spatially homogeneous, but it has no defined long-range structure, such as a crystal lattice [33]. Due to the high viscosity, all processes that require diffusion are slowed down to a degree that makes them stop on the scale of human observation [29]. Therefore, most deteriorative biological, chemical, and physical reactions should be prevented in the vitreous state. Obviously, the effectiveness of stabilization of biological structures by glasses depends on the physical stability of the glass.

The melting temperature of a sugar glass (glass transition temperature; T_g) is a convenient and often used measure of glass stability, but it may not be the only important parameter when the stabilizing effects of a carbohydrate glass are considered [8,34]. The collapse temperature, or critical temperature, (T_c) can be significantly above T_g and may be more closely related to the stability of biological structures in the dry state than T_g. T_c, however, is more difficult to measure and therefore the calorimetrically determined glass transition temperature T_g is more commonly used to compare the vitrification properties of biological glass formers such as sugars.

In general, T_g increases with molecular weight of the solute [35]. This is also true for oligosaccharides such as raffinose family oligosaccharides (RFO) [36],

fructo-oligosaccharides [37,38], and malto-oligosaccharides [39]. It has also been shown recently that the addition of small anions such as phosphate [40] or citrate [41], or the addition of proteins [42,43] can significantly increase the T_g of vitrified sucrose or glucose. Water, on the other hand, is an effective plasticizer of sugar glasses, although the degree of plasticization varies between different di-, oligo-, or polysaccharides [38,39,44]. In general, a sugar with a higher T_g will vitrify at a higher water content at a given temperature during drying. Therefore, a higher T_g will be beneficial during drying, because it allows vitrification at an earlier stage of the drying process, leaving less time for deteriorative processes.

In liposomes, damage during drying and rehydration is commonly determined as the leakage of a soluble marker such as carboxyfluorescein (CF) from the interior of the lipid vesicles. One of the mechanisms that can lead to leakage is the fusion of liposomes under conditions of severe water loss. In most cases, the fusion of liposomes will be accompanied by the formation of transient pores in the membranes, which allow soluble molecules to diffuse out of the vesicles [45,46]. Vitrification during drying will fix the position of the liposomes in the glassy matrix, so that the close approach of vesicles necessary for fusion is prohibited. Raising the temperature of a vitrified sample above the T_g of the system leads to increased fusion and leakage from liposomes [47]. On the other hand, using sugars with increasing T_g, such as longer-chain RFO, results in reduced liposome fusion in the dry state, especially at elevated temperatures [48].

Disaccharides such as sucrose and trehalose are highly effective in preventing both fusion of and leakage from liposomes in the dry state. The close linear correlations between leakage and fusion for both sugars (Fig. 1) stress the importance of fusion events for the overall severity of damage indicated by the amount of CF leakage. It should be noted, however, that fusion decreases much more strongly with increasing sugar concentration than leakage (Fig. 1), a fact that has also been observed in previous studies [48–50]. This indicates that in addition to fusion, another mechanism or mechanisms contribute to overall damage, that require higher concentrations of sugar for protection. One factor that has been recognized and analyzed in detail is the dehydration-induced increase in the gel to liquid-crystalline phase transition temperature (T_m) of membrane lipids. When T_m increases above the ambient temperature, the lipids will undergo two phase transitions, one from liquid-crystalline to gel phase during drying and the other from gel to liquid-crystalline phase during rehydration (see [3,20] for reviews). The effects of H-bonding interactions between different parts of the membrane lipid molecules and various carbohydrates on lipid phase transitions in the dry state will be extensively discussed in the remaining parts of this review. It should, however, be mentioned at this point that an alternative explanation for the effects of sugars on lipid phase transitions has also been proposed [51,52] that involves direct effects of vitrification of the sugar matrix on lipid phase behavior. We will discuss this hypothesis in more detail in Section 6.

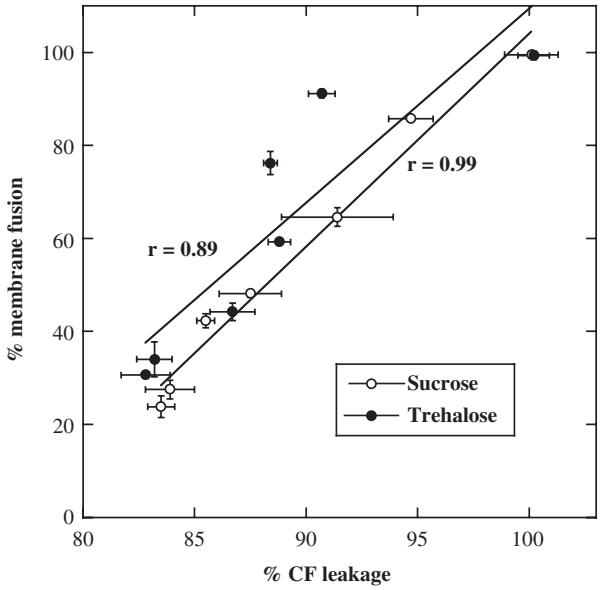

Fig. 1. Correlation between CF leakage and membrane fusion after air-drying and rehydration of EPC liposomes in the presence of different concentrations of sucrose or trehalose. The lines were fitted to the data (mean $\pm$ SD) by linear regression analysis and the correlation coefficients are indicated. Data redrawn from Hincha and Hagemann [8].

3. INTERACTIONS OF SUGARS AND WATER WITH PHOSPHOLIPIDS: SIMILARITIES AND DIFFERENCES

Water plays an essential role in the formation of bilayers from lipids, as the hydrophobic fatty acyl chains are not soluble in water and are therefore driven into aggregation by entropic forces, leaving the hydrophilic headgroups on the outside to interact with the aqueous medium. Different parts of the lipid headgroups interact with water through H-bonding and ensure spacing of the lipid molecules in the liquid-crystalline state (see [53] for a comprehensive review), which is the functional state for biological membranes. When membranes are dehydrated, the water molecules that help to maintain this spacing between the lipid headgroups are removed, allowing a closer approach of the lipid molecules. This leads to an increase in van der Waals interactions between the fatty acyl chains and to an increase in the membrane T_m by as much as 70 °C [1]. This elevation of T_m in dry membranes is especially important if the membrane lipids have a sub-ambient T_m under hydrated conditions, as is the case for most biological membranes. In these circumstances, T_m increases during dehydration, which causes a phase change from the liquid-crystalline to the gel phase at constant temperature (lyotropic phase transition). When water is added again

during rehydration, T_m shifts back to the hydrated value, and the membrane undergoes another lyotropic phase transition, resulting in transient leakage of soluble cell contents through the membrane [54,55]. This leakage is thought to be due to inhomogeneities in the membrane during the phase transition [56], because of the coexistance of gel and fluid phase lipids that results in packing defects and increased permeability [57].

In contrast, when membranes are dried in the presence of sufficiently high amounts of trehalose or sucrose, leakage of soluble content from liposomes can be largely prevented [47,48,59]. The water replacement hypothesis suggests that the sugar molecules prevent the close approach of lipids through H-bonding interactions between the sugar OH-groups and the lipid headgroups. This would prevent the dehydration-induced increase in T_m [3] and consequently phase transitions and solute leakage. Fourier-transform infrared spectroscopy (FTIR) and nuclear magnetic resonance spectroscopy (NMR) have provided evidence for such interactions between disaccharides and phospholipid headgroups (see e.g. [8,60]). However, while such spectroscopic data are qualitatively consistent with the water replacement hypothesis, there are some quantitative discrepancies that have not been adequately addressed so far.

H-bonding interactions between either water or disaccharides and lipids have been mostly studied at the level of the P=O moiety of phosphatidylcholines. Figure 2 shows typical FTIR spectra in the P=O asymmetric stretching region of egg phosphatidylcholine (EPC). It is apparent that both the presence of sucrose or trehalose, or the addition of water lead to a large downfield shift of the P=O peak. This shift has been shown to be due to H-bonding of OH-groups to the P=O groups, both in the case of water [61,62] and sugars [1]. But while sucrose and trehalose are able to depress T_m below the value in the fully hydrated state [47,51,52,63], these sugars induce a shift in the P=O peak that is considerably smaller than that obtained by hydration (Fig. 2; [64]). This indicates that there is no simple linear correlation between the extent of H-bonding to the P=O groups in the lipid and the lipid T_m. In fact, when small amounts of water are present together with the sugar, there are no additive effects on T_m, but instead the water replaces the sugar, leading to an increase in T_m compared to the dry state in the presence of sugar [65]. Recent molecular dynamics (MD) simulations indicate that sucrose and trehalose H-bond to the lipid P=O even in the presence of excess water. Under these circumstances, however, the replacement of water by sugar OH-groups has no apparent effects on the dynamic properties of the fatty acyl chains of the simulated PC molecules [66–68].

In addition to the P=O moiety, the C=O groups in diacyl lipids are potential partners for H-bonding interactions with water [69] or sugars. Figure 3 shows FTIR spectra in the region of the C=O stretching vibration. It can be seen that the C=O peak is shifted downfield and broadened on the downfield side in the presence of water, compared to the dry membranes (compare also [19,61,62,64,70]). There is, however, no apparent shift in the C=O stretching band in the dry

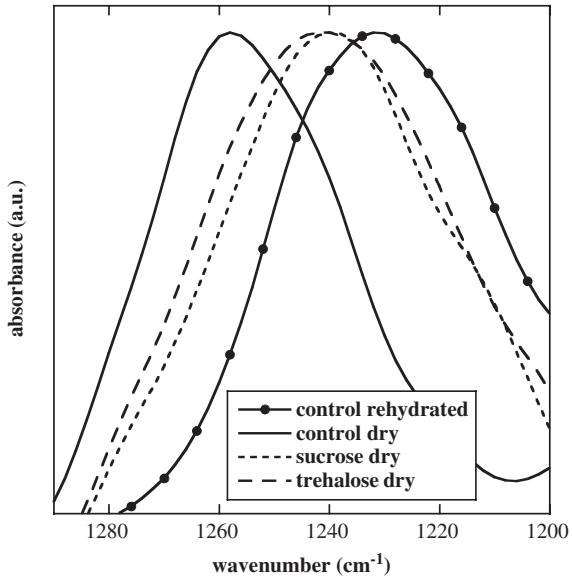

Fig. 2. Interactions of sucrose and trehalose with EPC membranes. Normalized FTIR spectra in the asymmetric P=O stretching region are shown for liposomes in the dry or rehydrated state. Samples were dried at 0% relative humidity for 24 h at 28 °C. For rehydration, dry samples were incubated in closed containers over distilled water (100% relative humidity) for 24 h at 28 °C. Samples measured in the dry state contained either only liposomes (control dry), or liposomes in the presence of sucrose (sucrose dry) or trehalose (trehalose dry) at a 2:1 mass ratio (sugar:lipid). The rehydrated sample (control rehydrated) contained only liposomes. Data for dry samples were taken from Hincha and Hagemann [8]. The absorbance maxima are located at 1232 cm^{-1} (control hydrated), 1259 cm^{-1} (control dry), 1240 cm^{-1} (sucrose dry), 1241 cm^{-1} (trehalose dry).

membranes, when samples in the absence and presence of disaccharides are compared (Fig. 3; [8]).

It has been shown in previous studies that the C=O stretching vibration is composed of more than one peak and that H-bonded and nonbonded C=O groups may contribute to these bands [69]. H-bonded C=O groups are indicated by lowfield peaks, while nonbonded groups are indicated by upfield peaks. The shift and the broadening on the lowfield side of the C=O peak in the hydrated state (Fig. 3) indicate that the proportion of H-bonded C=O groups has increased relative to the proportion of nonbonded groups, compared to the dry state. Deconvolution of these peaks also gives evidence for this shift to lower frequency vibrations [19,70]. More detailed studies involving careful deconvolution of the C=O peak into its components will have to be performed to see whether any H-bonding of the sugars to C=O groups takes place or not. Evidence for H-bonding of disaccharides to the lipid C=O has been obtained for hydrated systems both experimentally by FTIR [71], and from MD simulations [68]. It is

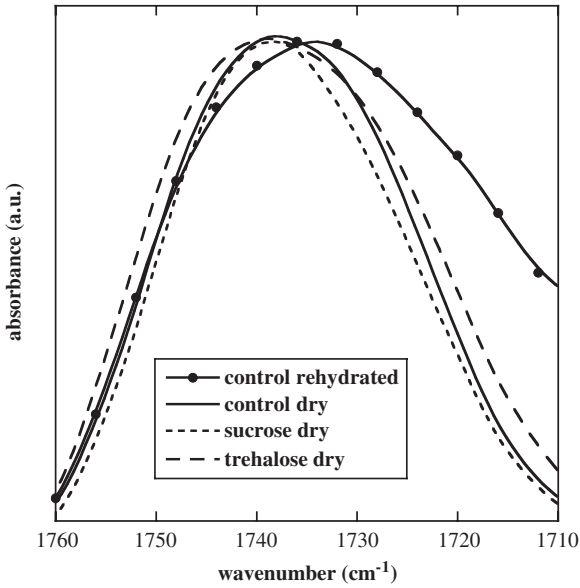

Fig. 3. Interaction of sucrose and trehalose with EPC membranes. Normalized FTIR spectra in the C=O stretching region are shown for liposomes in the dry or rehydrated state (compare Fig. 2). Samples measured in the dry state contained either only liposomes (control dry), or liposomes in the presence of sucrose (sucrose dry) or trehalose (trehalose dry) at a 2:1 mass ratio (sugar:lipid). The rehydrated sample (control rehydrated) contained only liposomes. Data for dry samples were taken from Hincha and Hagemann [8].

clear from the data shown in Fig. 3, however, that the level of H-bonding to the C=O groups achieved by sugars must be significantly lower than the level achieved by water molecules. As in the case of the P=O group there is no simple, quantitative replacement of H-bonded water by sugar OH-groups.

Similar interactions have also been described for choline in lipid headgroups, and water or sugars [62,70,72,73]. In this case, however, it was originally suggested that no H-bonding would be possible between the choline group and OH-groups and instead, polar interactions were postulated, without any clear physical description [72]. Further careful analysis suggests that the interactions of water and the choline group are indeed H-bonding interactions, where the methyl and methylene groups of the choline act as donors in CH···OH interactions [64,73]. Since the shifts in the choline asymmetric stretching vibration determined by FTIR are the same when water is added to dry EPC membranes, or when a glycolipid is present in addition to EPC in the dry membranes ([70]; see also Section 4) we suggest that the interactions of water and of sugars with the choline group are qualitatively and quantitatively the same. Therefore, in this case, the sugar molecules completely replace the water molecules in the appropriate H-bonds. This is difficult to investigate with soluble sugars, because the choline

asymmetric stretching vibration at about 970 cm^{-1} [70] strongly overlaps with vibrations from the sugars. We are currently investigating the possibility of using other choline vibrations in the FTIR spectrum for this purpose [61].

In conclusion, the water replacement hypothesis provides a qualitative explanation of the effects of disaccharides on the phase behavior of dry membranes. Quantitatively, H-bonding patterns, and effects of sugars and water on T_m are not well correlated and studies at different low-sugar concentrations will be necessary to obtain detailed quantitative information on the influence of water replacement by sugar OH-groups on lipid phase transitions.

4. EFFECTS OF COVALENTLY BOUND SUGARS ON THE STABILITY AND PHYSICAL PROPERTIES OF LIPOSOMES DURING DRYING

As discussed above, sugars are able to stabilize liposomes during drying, but relatively high sugar/lipid weight ratios are needed to achieve a high degree of protection [47,58,59]. It is possible that the concentration of sugar molecules that are located close to the membrane surface and therefore easily interact with the lipid headgroups, could be limiting for the protective activity of soluble sugars. A high local concentration of sugars specifically at the membrane surface can be achieved by incorporating either synthetic or natural glycolipids into phospholipid membranes. The approach of incorporation of synthetic glycolipids into phospholipid liposomes has been used by several researchers and a stabilizing effect has been observed during freezing [74,75] or freeze-drying [76]. In all these cases, di- or trisaccharides were used as sugar headgroups, but a polysaccharide (hyaluronan) linked to the membrane surface through a phosphatidylethanolamine anchor has also been successfully used to stabilize liposomes with encapsulated drugs during freeze-drying [77]. Such a stabilizing effect has not been observed for the natural plant glycolipids digalactosyldiacylglycerol (DGDG) or monogalactosyldiacylglycerol (MGDG) either during freezing [78,79], or during air-drying [79]. Also, in some cases an increased efficiency has been observed in the protection of glycolipid-containing liposomes by soluble sugars during freeze-drying [76], while decreased efficiency has been observed with different lipids during freezing [75,80]. This suggests that the functional properties of glycolipids for the stabilization of liposomes during freezing and drying are quite complex and will need further detailed studies to determine, whether this approach can make a significant contribution to the preservation technology of liposomes.

While the functional role of both synthetic and natural glycolipids in membrane stabilization is still unclear, the physical interactions of membrane-bound sugars with phospholipids in the dry state are much better characterized. We have focused our research on the effects of plant chloroplast galactolipids on the physical behavior of liposomes [19,70]. The galactolipids MGDG and DGDG

comprise about 70–80% of the total chloroplast lipids in plants [81]. In addition, DGDG can make up almost 50% of the lipid in the plasma membrane in severely phosphate-starved plants [82]. DGDG is a bilayer-forming lipid with a T_m below –30 °C in both the dry [70] and fully hydrated [70,83] states. It is highly unsaturated, with mainly 18:3 fatty acids [84,85], which may contribute to the low T_m. MGDG, on the other hand, is a nonbilayer-forming lipid that forms hexagonal or cubic phases under all investigated conditions of temperature and hydration (see [86] for a review). In combination with bilayer-forming lipids such as EPC, however, it can form bilayers with a low permeability for soluble markers [79], but with a greatly reduced physical stability during hyperosmotic stress, freezing, or drying [78,79]. It has generally been observed for natural and synthetic lipids that monoglycolipids tend to adopt nonbilayer phases, depending on the degree of unsaturation of the fatty acids [87–89], while diglycolipids form stable bilayers [90–93].

Similar to the situation for soluble sugars (see Section 3), interactions of sugar moieties of glycolipids with the P=O group of phospholipids have been most thoroughly studied. Figures 4 and 5 show that the galactose groups from both MGDG and DGDG interact with the P=O in dry mixed EPC/galactolipid liposomes. Similar to the situation for soluble sugars, these membrane-bound sugars are not able to shift the P=O peak to the same extent as hydration does (compare panels A and B in Figs. 4 and 5). The shift is more pronounced, however, in the digalactolipid than in the monogalactolipid, indicating that in DGDG more OH-groups are available for H-bonding with the phospholipid than in MGDG. This may be due to the higher number of OH-groups available for H-bonding in DGDG, but also to the more flexible structure of the disaccharide, as compared to the monosaccharide. It has been shown that even in fully hydrated membranes, the DGDG headgroup is oriented almost parallel to the membrane surface, thus increasing the possibility of interlipid interactions [94]. In the presence of excess water, there is no difference in the position of the P=O vibration with or without MGDG or DGDG. Similar H-bonding interactions between phospholipids and glycolipids have also been reported for synthetic glycolipids [95,96]. In the case of both synthetic glycolipids and DGDG, this H-bonding was accompanied by a decrease in the T_m of the dry membranes [70,95–97]. The effects of MGDG on membrane phase behavior, especially in the dry state, are more complex, since it is a nonbilayer-forming lipid [86].

The C=O band in FTIR spectra in dry EPC was not influenced by the presence of 50% DGDG or MGDG in the membranes, indicating that the lipid-bound galactoses are not able to penetrate deeply enough into the membrane to interact with the C=O groups, but are rather completely bonded to the P=O groups ([70] and unpublished data). With a maltose-containing synthetic lipid, on the other hand, interactions with the C=O group of phosphatidylcholine were clearly detected by Raman spectroscopy [95]. This indicates that penetration depth of a lipid sugar headgroup into the membrane depends on structural features that may

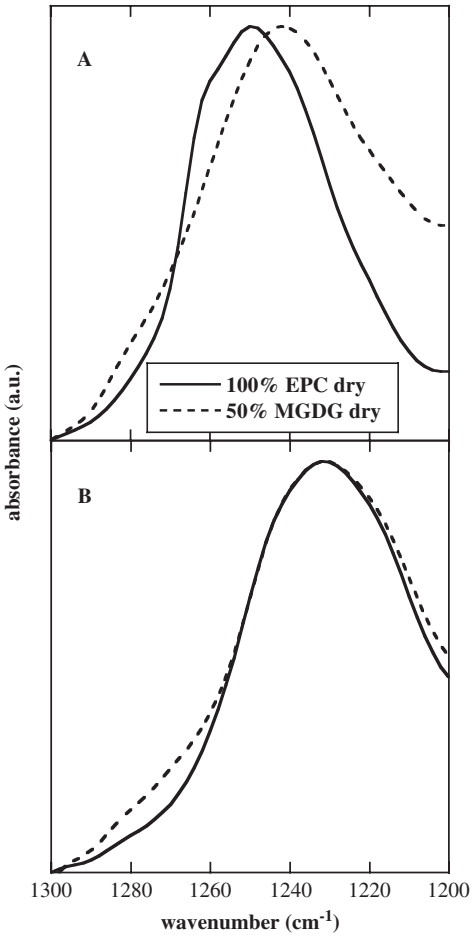

Fig. 4. Interactions of membrane-bound galactose with EPC. Normalized FTIR spectra in the asymmetric P=O stretching region are shown for liposomes in the dry (A) or rehydrated (B) state. The membranes were composed of either pure EPC (solid lines), or 50% EPC and 50% MGDG (dashed lines). The absorbance maxima are located at 1250 cm^{-1} (EPC dry), 1232 cm^{-1} (EPC hydrated), 1242 cm^{-1} (EPC/MGDG dry), 1232 cm^{-1} (EPC/MGDG hydrated).

be related to the sugar, but also to the hydrophobic lipid part that anchors the sugar in the membrane. Further studies will be necessary to separate the effects of sugar and lipid structure on H-bonding interactions and membrane phase behavior.

In the case of EPC/DGDG and EPC/MGDG mixed membranes, there was a clear indication in the FTIR spectra of an interaction of the sugar with the choline part of the headgroup ([70] and unpublished data), indicating H-bonding interactions between the sugar OH-groups and the choline CH-groups (compare Section 3).

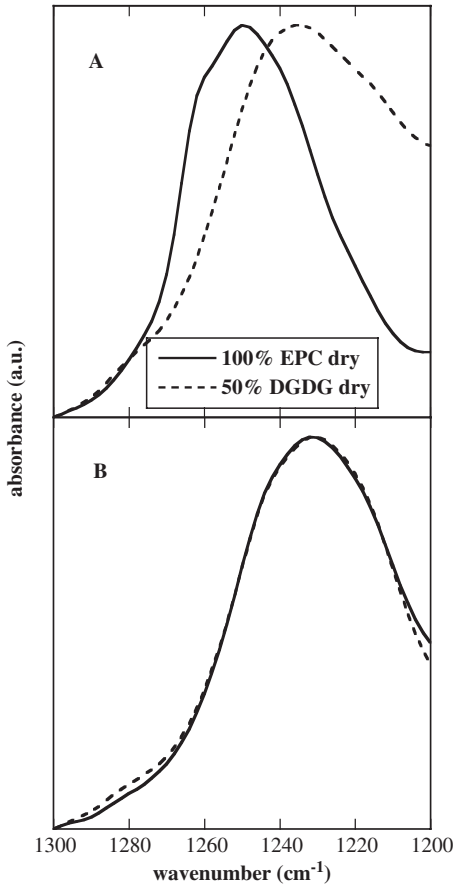

Fig. 5. Interactions of membrane-bound galactose with EPC. Normalized FTIR spectra in the asymmetric P=O stretching region are shown for liposomes in the dry (A) or rehydrated (B) state (compare Fig. 4). The membranes were composed of either pure EPC (solid lines), or 50% EPC and 50% DGDG (dashed lines). Data redrawn from Popova and Hincha [70]. The absorbance maxima are located at 1250 cm^{-1} (EPC dry), 1232 cm^{-1} (EPC hydrated), 1236 cm^{-1} (EPC/DGDG dry), 1232 cm^{-1} (EPC/DGDG hydrated).

5. STABILIZATION OF LIPOSOMES BY POLYSACCHARIDES DURING DRYING

Polysaccharides could be expected to be good protectants for liposomes during drying, because in the dry state, all polysaccharides that have been investigated in this regard showed high T_g values (fructans 154 °C [37]; hydroxyethyl starch (HES) >100 °C [44,54]; dextran >100 °C [51]). Therefore, they are expected to be efficient protectants against liposome fusion in the dry state (compare Section 2). Such protection has actually been shown during air-drying for HES [54,63], dextran, and fructan [98], and an extracellular polysaccharide (EPS) from the

cyanobacterium *Nostoc commune* [99]. Interestingly, HES did not provide any protection from fusion to liposomes during freeze-drying [100]. This could be due to a separation of the samples into HES- and liposome-rich domains, which would prohibit the vitrified HES from protecting the liposomes against close approach and the resulting fusion. However, this needs to be experimentally verified.

The polysaccharides did not, or only to a very small degree, protect liposomes against leakage (see Fig. 6; [98] for dextran, [54,63,100] for HES, and [99] for EPS), indicating that vitrification is not sufficient to protect liposomes during drying. The reason for this high degree of leakage could be found in the inability of HES [54,60,63,100], dextran [101,102], and bacterial EPS [99] to depress T_m in dry membranes. This has been related to the inability of such polysaccharides to H-bond to the lipid P=O groups [54,58,60,63,100]. Interestingly, mixtures of HES and glucose, and of EPS and sucrose/trehalose have been shown to be very efficient in preventing both leakage and fusion in dry liposome systems [54,63,99]. The explanation in these cases is that the polysaccharides as good glass formers protect the liposomes from fusion, while the mono- or disaccharides efficiently H-bond to the lipid P=O groups and thereby depress T_m and the resulting leakage. It should be mentioned at this point that both sucrose and trehalose are also good glass formers, which can prevent both leakage and

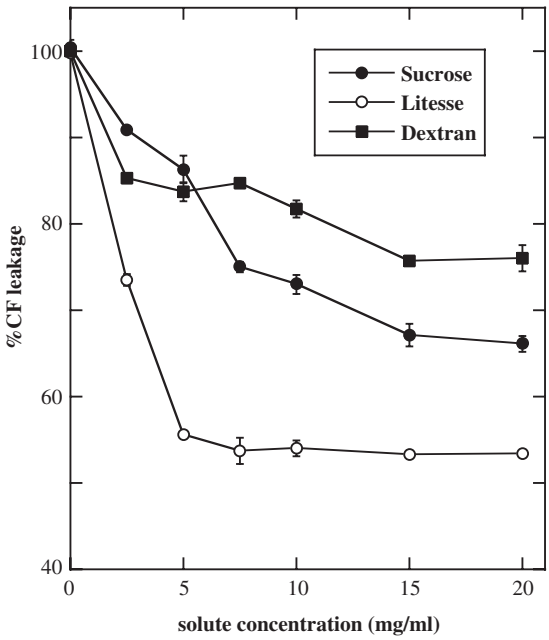

Fig. 6. CF leakage from EPC liposomes air-dried and rehydrated in the presence of different concentrations of sucrose, dextran, and Litesse. Litesse is a polydextrose that consists of randomly bonded glucose units with sorbitol as the chain-terminating units (Litesse® Ultra™, Danisco, Copenhagen, Denmark).

fusion in the absence of polysaccharides (see Sections 2 and 3). However, in the presence of EPS the disaccharides are more efficient in preventing leakage during drying, i.e. less sucrose and trehalose is needed to achieve a given degree of protection [99]. Glucose, on the other hand, is a poor glass former and therefore this monosaccharide alone is not able to prevent liposome fusion and the associated leakage [54,63].

The ineffectiveness of EPS, HES, and dextran to interact with lipid headgroups in membranes could be due to steric hindrance, because of the large size of these polysaccharides. If this were the only explanation, all polysaccharides above a certain size limit should show the same effect. This, however, is clearly not the case. Figure 6, for example, shows the effect of a commercial polysaccharide preparation (Litesse®) on CF leakage from liposomes during air-drying. It is obvious that this polysaccharide, which is a polydextrose that consists of randomly bonded glucose units with sorbitol as the chain-terminating unit, protects the liposomes with a higher efficiency than sucrose. Clearly, the mere size of a molecule resulting in steric hindrance of interactions is at best one of the factors that determines the effectiveness of a polysaccharide as a protectant during drying. An analysis of the mechanism by which Litesse® protects membranes in the dry state is still outstanding and therefore it is not known yet whether it depresses T_m and H-bonds to the lipid P=O groups.

The class of polysaccharides that has been most thoroughly investigated with regard to their protective effects on liposomes during drying are fructans. These polyfructoses are biosynthetically derived from sucrose. They can be found in many species of bacteria, fungi, and plants and are classified on the basis of their glycosidic linkages. The linear inulins contain only $\beta(2\rightarrow1)$ linkages, while the levans contain mainly $\beta(2\rightarrow6)$ linkages. Fructans are accumulated in many plant species under stress conditions such as cold and drought, and may play an important role in plant freezing and desiccation tolerance (see [103,104] for reviews on fructan structure, biosynthesis, and function).

Both a plant inulin (from chicory roots) and a bacterial levan (from *Bacillus subtilis*) have been shown to protect liposomes from leakage during freeze-drying or air-drying [98,100]. The physical mechanisms of protection, however, may be different for the two structural classes of fructans.

The chicory inulin is a mixture of polysaccharides with a degree of polymerization (DP) between 10 and 30, corresponding to molecular masses between approximately 1600 and 5000 [100]. During freeze-drying, the presence of the chicory inulin in phosphatidylcholine liposome preparations reduces the degree of leakage from the liposomes after rehydration [100]. This protective effect is related to a depression of T_m in the dry membranes by about 20 °C compared to liposomes dried without the fructan, as judged from the temperature-dependent changes in the CH_2 symmetric stretching vibration in infrared spectra of the lipid fatty acyl chains (Fig. 7). By FTIR it could also be shown that the inulin establishes H-bonds with the lipid P=O, despite its large size [100]. This indicates that

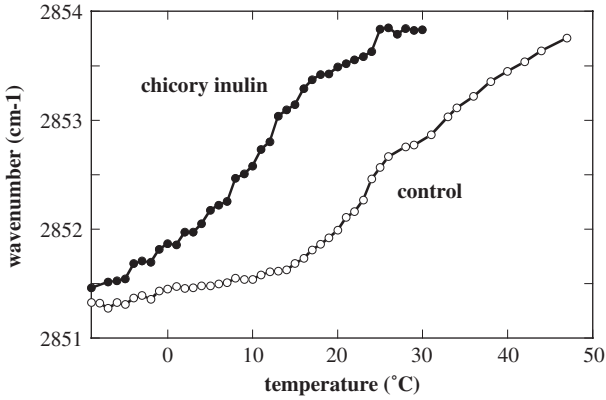

Fig. 7. Lipid melting curves of freeze-dried EPC liposomes as determined by FTIR spectroscopy. The wavenumber of the symmetric CH_2 stretching vibration is plotted as a function of sample temperature. The lipid gel to liquid-crystalline phase transition temperature (T_m) is taken as the midpoint of the melting curves. The samples contained either only EPC (control; $T_m = 29\,^{\circ}C$), or EPC and chicory inulin at a 1:1 mass ratio (chicory inulin; $T_m = 8\,^{\circ}C$). Data redrawn from Hincha *et al*. [100].

steric factors can be overcome even by large molecules to enable the insertion of at least part of the polysaccharide into the lipid headgroup region. It was shown in the same study that HES was not able to interact with the P=O groups in the dry membrane or depress T_m, under identical experimental conditions. This indicates that the fructan has specific structural properties that this glucan does not possess. During slow air-drying, the chicory inulin provides no protection to liposomes [50]. This is presumably due to the fact that the chicory inulin has a low solubility and therefore precipitates during the slow drying process. It would then not be available for interactions with the membrane lipids anymore. For freeze-drying, on the other hand, the samples are rapidly frozen in liquid nitrogen, thus immobilizing the inulin and keeping it available for H-bonding, when water is removed during the drying process. Inulins with a lower DP (≤ 10), which are more soluble, do not precipitate during air-drying and provide protection to liposomes [50,98]. The effects of such oligosaccharides on membrane stability are discussed in detail in Section 6.

The levan isolated from *Bacillus subtilis* has a DP of about 125, corresponding to a molecular mass of approximately 25,000 [105]. Although this fructan has a much higher DP than the chicory inulin, it also has a much higher solubility. This is reflected in the fact that it will not precipitate from solution during air-drying and that it protects liposomes from leakage and fusion during drying and rehydration [98]. It has been shown by X-ray diffraction measurements that the levan is located between the liposomes in the dry state, thus enabling both encasement in a glassy matrix and direct interactions with the membrane lipids [98]. In contrast

to HES and dextran, the presence of the levan resulted in a clear depression of T_m and increased mobility of the fatty acyl chains in the dry membranes, as determined by FTIR and NMR spectroscopy [102]. However, no evidence for an interaction of the levan with the lipid P=O groups was found by FTIR, although NMR measurements indicated a strong immobilization of the headgroup both at the P=O and the choline level in the presence of levan [102]. It was hypothesized that due to the immobilization of the headgroups in the sugar glass, the spacing of the headgroups would be kept during drying and therefore phase transitions would be inhibited. It was suggested from MD simulations [106] and investigations of the physical properties of the levans [105] that hydrophobic interactions may contribute significantly to the interaction of the levan with the lipids, rather than H-bonding interactions. This would constitute a completely different mode of action of the levan, compared to that proposed for all other sugars that had previously been investigated.

While hydrophobic interactions may play a role in the interactions of the levan with membrane lipids, and may also play a role in such interactions in other sugars (see Section 7 for a more detailed discussion), we believe that H-bonding interactions also take place between the levan and the lipid P=O groups and that these interactions may be important for the function of this polysaccharide as a membrane protectant in the dry state. Figure 8 shows a comparison of the effects of HES, levan and sucrose on the asymmetric P=O stretching vibration in dry dimyristoylphosphatidylcholine (DMPC) liposomes. Two important observations can be made in this figure. On the one hand, levan clearly shifts the P=O peak by $5\,cm^{-1}$ downfield, compared to the control sample without any sugar. This is much less than the shift induced by sucrose, but it clearly indicates H-bonding between levan and the lipid P=O group. Also, the peak is much broader than the peak of the pure lipid and, similar to the situation with sucrose, the peak is broadened on the lowfield side, indicating a more heterogeneous H-bonding pattern in the presence of both sucrose and levan, compared to the control situation. These data suggest that levan and sucrose both interact with the lipid P=O groups through H-bonding, but to quantitatively different degrees.

This point is stressed by a comparison of the effects of levan with those of HES. HES is a polysaccharide that shows no interactions with the P=O groups. In fact, we found that the P=O peak vibration increased by $5\,cm^{-1}$ in the presence of HES, compared to the control samples containing only lipid. This indicates that the presence of HES reduces the interactions of the P=O groups with other groups in the lipid molecules. This can be rationalized as follows. It has been shown by NMR that the presence of HES in dry lipid samples leads to a slight immobilization of the lipid headgroups [60]. This could be due to an interaction of the HES with the lipid choline groups. Alternatively, the presence of HES could influence the conformation of the headgroups in other, more unspecific ways, not involving direct interactions. It has been shown that in the absence of any solutes, the PC headgroup is oriented almost parallel to the membrane

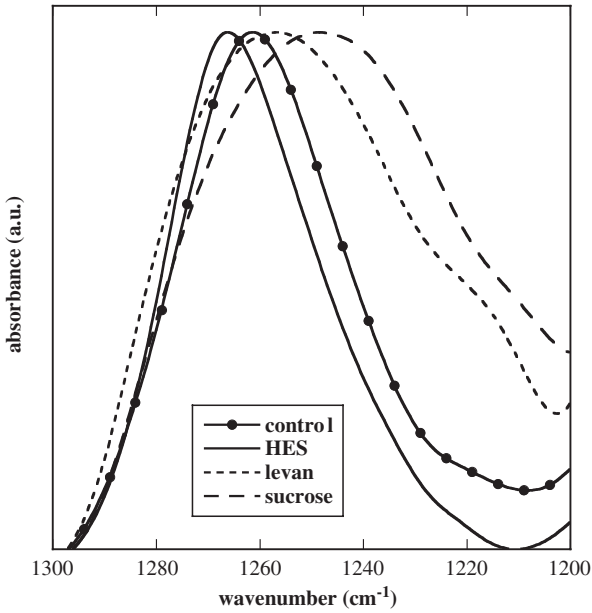

Fig. 8. Interactions of sucrose, HES, and levan with dry DMPC liposomes. Normalized FTIR spectra in the asymmetric P=O stretching region are shown for liposomes in the absence of sugars (control), or in the presence of a 2:1 (sugar:lipid) mass ratio of the three carbohydrates. Samples were dried for 24 h at 0% relative humidity at 28 °C. The dry samples were heated under vacuum for 2 h to 100 °C, i.e. above the T_m of dry DMPC (70 °C; [70]), to facilitate interactions of the sugars with the membranes. Spectra were recorded after cooling of the samples, at 50 °C. The absorbance maxima are located at 1261 cm^{-1} (control), 1266 cm^{-1} (HES), 1256 cm^{-1} (levan), and 1247 cm^{-1} (sucrose). The levan was a kind gift of Dr. I.J. Vereyken and was purified from *Bacillus subtilis* as described [105]. The HES was a kind gift of Dr. A.E. Oliver and was dialyzed extensively against distilled water to remove impurities before use.

surface [107–110]. This leads to H-bonding interactions between the choline and the P=O groups of neighboring lipid molecules in the membrane [61,111]. Similar H-bonding interactions have also been described for choline in lipid headgroups, and water or sugars [62,70,72,73], as discussed in detail in Section 3. When the HES interacts with the lipid headgroups, the H-bonding interactions between the P=O groups and the choline groups are interrupted, leading to an increase in the P=O vibrational frequency, as observed in Fig. 8. *Ab-initio* calculations [61] indicate that the frequency of the "totally free" P=O group would be located at about 1268 cm^{-1}, in good agreement with our FTIR data of the dry EPC/HES samples.

If we now compare the effects of HES and levan, which have both been shown to immobilize the lipid headgroups in the dry state, presumably through an interaction with the choline group, it becomes clear that the levan has substantial

H-bonding interactions with the P=O group, shifting the peak frequency downfield by 10 cm^{-1}, compared to samples in the presence of HES. On the basis of these data, it can be proposed that the effect of the levan on T_m is due, at least in part, to H-bonding, and that the ability of the fructan to H-bond to the P=O group is the decisive difference to HES, which has no influence on T_m.

6. DIFFERENTIAL STABILIZATION OF LIPOSOMES DURING DRYING BY DIFFERENT FAMILIES OF OLIGOSACCHARIDES

In many plant species, oligosaccharides such as RFO, or fructans are considered as protectants for cellular structures during freezing, drought stress, or seed desiccation [103,112]. In some cases, studies with transgenic plants accumulating such sugars have provided experimental evidence for their efficacy as stress protectants [113–115], while others found no effects [116].

To gain further insight into the physical mechanisms and structural determinants of membrane protection by oligosaccharides, we investigated the effects of different structural families of oligosaccharides on liposomes during drying. One prominent aspect of these studies is the comparison of oligosaccharides of different DP within the same structural family. Figure 9 shows as an example the effect of inulins of different chain length on CF leakage from EPC liposomes after air-drying and rehydration. It can be clearly seen that the ability of the inulins to protect the liposomes increases with increasing DP and that the higher DP fructans are better protectants than the DP 2 inulin, i.e. sucrose. In this figure, the differences between the different DPs are enhanced by plotting molar concentrations of the sugars, instead of mass ratios between sugar and lipid. However, the same trend is apparent when such leakage data are plotted on a mass basis [50].

This is a surprising result, because it had been suggested in other studies that oligosaccharides show reduced protection for liposomes during drying, compared to sucrose, and that strongly reduced protective effects can be expected above DP 3 [63,117]. Further studies showed that this was specifically true for glucans, while fructans and RFO showed the opposite behavior (Fig. 10; [48,50]). Also, a cyclic inulin of DP 6 (cycloinulohexaose) showed good protection of liposomes during freeze-drying [118], indicating that it may be structural features of the fructose (fructan), or galactose (RFO) units, as opposed to glucose (glucan) moieties, that determine the efficacy of oligosaccharides as membrane stabilizers during drying. We will discuss these structural points further in Section 7.

Here, we will discuss some functional aspects of the observed differences between the different families of oligosaccharides. Following the structure of the earlier sections, we can divide this into effects on fusion and effects on T_m. In general, one would expect better protection against fusion from longer oligosaccharides, because of the expected increase in T_g (compare Section 2). This expectation is borne out by the RFO [34,48], and the glucans (T_g values from

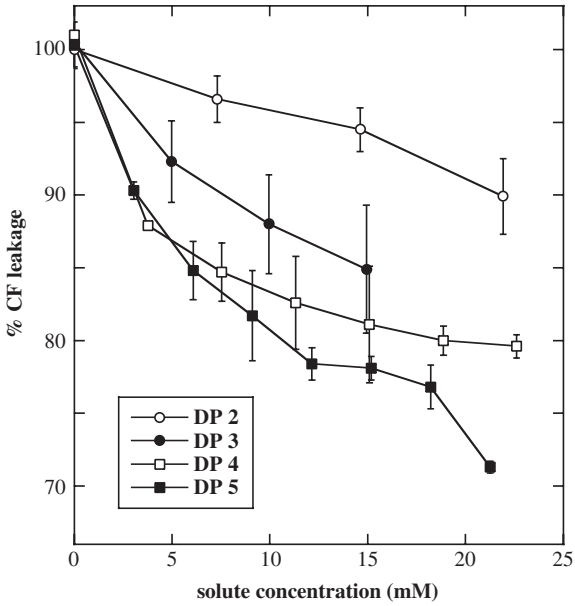

Fig. 9. CF leakage from EPC liposomes air-dried and rehydrated in the presence of different concentrations of fructo-oligosaccharides. The oligosaccharides vary in the number of fructose units. A DP of 2 corresponds to sucrose and the higher DPs correspond to sugars with additional fructose units attached by β(2→1) linkages to the terminal fructose, leaving a glucose at one end of the molecules. It should be noted that concentration in this figure is given on a molar rather than on a mass basis.

Oliver, A.E. and Hincha, D.K., unpublished, and fusion data in [50]), which show increases in both T_g and protection against fusion, with increasing DP. Protection against fusion, however, decreases with DP in the presence of inulins [50], although T_g increases with DP, albeit to a smaller degree than for the glucans (Oliver, A.E. and Hincha, D.K., unpublished). This emphasizes our point made earlier, that T_g may not be the most appropriate measure for the effects of carbohydrate glasses on membrane stability in the dry state. More subtle structural properties of these glasses will have to be considered, to understand the differential protection against fusion provided by these different oligosaccharides.

The effects of the sugars on T_m follow a different pattern than the effects on fusion. All oligosaccharides depress T_m, but while the inulins lead to a slight decrease with DP [50], the RFO lead to a slight increase [48], and the glucans to a strong increase [50]. The shift in the spectral position of the P=O vibration in FTIR spectra, indicating H-bonding between sugar and lipid headgroup (compare Section 3) shows a slight reduction for RFO and inulins, but a strong reduction for glucans, in general agreement with the T_m data [48,50]. Vibrations stemming from other parts of the lipid headgroup (C=O, choline) have so far not been investigated for effects of these oligosaccharides.

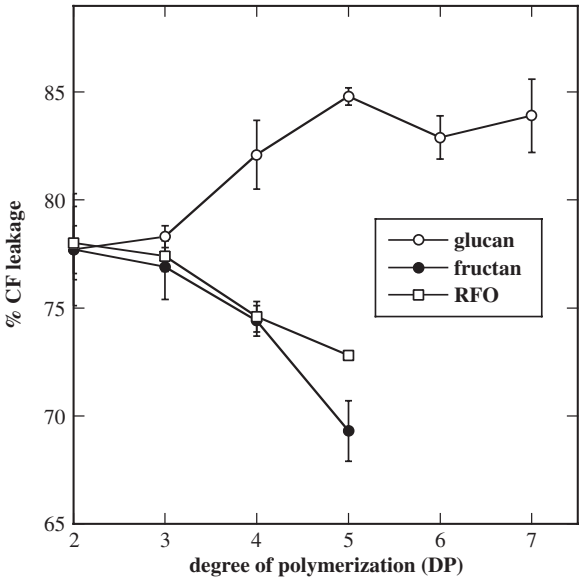

Fig. 10. CF leakage from EPC liposomes air-dried and rehydrated in the presence of 10 mg/ml of glucans (malto-oligosaccharides), fructans (inulins), or RFO (raffinose family oligosaccharides). The sugars were present both inside of the liposomes and outside. CF leakage is plotted as a function of the degree of polymerization (DP) of the different oligosaccharides. Within one family the members of different DP vary in the number of glucose (glucans), fructose (fructans), or galactose (RFO) units. Data were partly adapted from Hincha *et al*. [48,50].

There has been some discussion in the literature [51,52,54,58,63,101], whether the depression of T_m observed in dry membranes in the presence of sugars is primarily due to H-bonding of the sugars to the lipid headgroups (water replacement hypothesis), or whether nonspecific osmotic and volumetric effects are sufficient to explain the depression in T_m. The results discussed above from our experiments with different oligosaccharides seem to favor the first hypothesis. High DP glucans, for instance, are very good protectants against fusion, indicating that they form a stable glass around the unilamellar liposomes used in these studies. This, however, does not lead to a strong depression in T_m, in agreement with the small effect on the P=O peak position in FTIR spectra. On the other hand, inulins show less protection against fusion with increasing DP, indicating less stable glasses around the liposomes, but increased effects on T_m. We therefore feel that these results are more consistent with the water replacement hypothesis than with the volumetric arguments of the vitrification hypothesis, although a fully quantitative description of the relationship between T_m and H-bonding still needs to be developed in the future (compare Section 3).

7. STRUCTURAL CONSIDERATIONS FOR THE STABILIZATION OF LIPOSOMES DURING DRYING BY OLIGO- AND POLYSACCHARIDES

An interesting and surprising aspect of our recent work on the effects of oligosaccharides on liposome stability in the dry state is the strong influence of the chemical nature of the monosaccharide moieties on protection and interaction potential, as opposed to pure size (DP) effects (see Section 6 for details). These data suggest that specific structural features of the different oligosaccharide families determine their effects. This may also be true for the structurally even more complex polysaccharides (Section 5). Recent work on oligosaccharides suggests that such molecules may possess relatively defined and stable structures in aqueous solution [119]. There are various levels at which the structure of oligosaccharides could differ and thereby influence the interactions with membrane surfaces. These could include different degrees of structural flexibility around the glycosidic bonds, chair-boat conformational transitions, and differences in exposed hydrophobic surface area that might facilitate interactions with membrane lipids. We should of course emphasize at this point that any data that have been obtained from oligosaccharides in dilute solution can only give us hints at what differences may be present during the drying process when a large part of the water has been removed. It seems quite likely that under such conditions additional stresses act on the oligosaccharide molecules and may force conformational transitions that are not readily observed in the fully hydrated state. Evidence for this hypothesis comes from MD simulations that show large differences in oligosaccharide structure between gas phase and solution, and indicate a major influence of H-bonding interactions between water and sugars on oligosaccharide structure [120–122].

The oligosaccharides we have investigated so far have as their basic building blocks either fructose, which may be linked by $\beta\,2\rightarrow1$ (inulin) or by $\beta\,2\rightarrow6$ (levan) glycosidic linkages, glucose with an $\alpha\,1\rightarrow4$ linkage (malto-oligosaccharides), or galactose with an $\alpha\,1\rightarrow6$ linkage (RFO). Therefore, both the structures of the monosaccharide units and their different linkages may have an influence on the structure and membrane interaction potential of the different oligosaccharide families.

For fructans, specific secondary structures have been proposed. For inulin, both a helical structure [123,124] or a random coil structure [106] were postulated, while for levan also a helical structure has been proposed [106]. In general, however, it is assumed that oligosaccharides have no defined secondary structure and rather have random and rapidly changing conformations in aqueous solution.

While the type of glycosidic linkage will certainly have an effect on the mechanical properties of sugars, there are no simple rules to link the two properties.

1→6 linked oligosaccharides are considered to be structurally, highly flexible [125]. However, different β 1→4 linked polysaccharides vary in their mechanical properties and bond flexibility between highly rigid (e.g. chitin, cellulose) and highly flexible (e.g. xylan, hyaluronan) [121], indicating that depending on other structural features, the same glycosidic bond can result in opposite mechanical properties for different saccharides. An additional degree of flexibility is inherent in most sugars from the ability for transitions between boat and chair conformations. These conformational transitions have been investigated using atomic force microscopy (see [126] for a review) and it has been shown that different oligosaccharides require different amounts of energy for such transitions [127–130]. It is unclear, whether such transitions also occur during drying, but the forces that act on the solute molecules during drying may be big enough to force such conformational transitions, at least in some oligo- and polysaccharides.

It has been suggested that sugars, although they are usually highly soluble in water, nevertheless have hydrophobic properties. These are brought about by the fact that many sugars form planar, rigid rings with a CH-rich hydrophobic plane on one side and an OH-rich hydrophilic plane on the other side [131]. This hydrophobicity has been quantified as the ration of hydrophobic to hydrophilic surface area, or hydrophobic index (HI) [132]. It has been shown that there is a close correlation between the HI of a sugar and its effect on lipid T_m in systems of low water content [133]. This would indicate that hydrophobic interactions play an important role in determining the effectiveness of at least simple sugars on membrane behavior at low hydration. Unfortunately, these studies have so far not been extended to more complex oligo- and polysaccharides. It can, however, be assumed that for such larger molecules, more complex behavior would be observed, that would be the result of several different properties and structural constraints. This will have to be elucidated, if we are to understand the differences in the protective properties of different saccharides for membranes during drying.

REFERENCES

[1] J.H. Crowe, F.A. Hoekstra, L.M. Crowe, Anhydrobiosis, Annu. Rev. Physiol. 54 (1992) 579–599.
[2] F.A. Hoekstra, E.A. Golovina, J. Buitink, Mechanisms of plant desiccation tolerance, Trends Plant Sci. 6 (2001) 431–438.
[3] A.E. Oliver, L.M. Crowe, J.H. Crowe, Methods for dehydration tolerance: depression of the phase transition temperature in dry membranes and carbohydrate vitrification, Seed Sci. Res. 8 (1998) 211–221.
[4] J.H. Crowe, L.M. Crowe, A.E. Oliver, N. Tsvetkova, W. Wolkers, F. Tablin, The trehalose myth revisited: introduction to a symposium on stabilization of cells in the dry state, Cryobiology 43 (2001) 89–105.
[5] G.N. Somero, Adapting to water stress: convergence on common solutions, in: G.N. Somero, C.B. Osmond, C.L. Bolis (Eds.), Water and Life, Springer, Berlin, 1992, pp. 3–18.

[6] P.H. Yancey, M.E. Clark, S.C. Hand, R.D. Bowlus, G.N. Somero, Living with water stress: evolution of osmolyte systems, Science 217 (1982) 1214–1222.
[7] J.H. Crowe, J.F. Carpenter, L.M. Crowe, T.J. Anchordoguy, Are freezing and dehydration similar stress vectors? A comparison of modes of interaction of stabilizing solutes with biomolecules, Cryobiology 27 (1990) 219–231.
[8] D.K. Hincha, M. Hagemann, Stabilization of model membranes during drying by compatible solutes involved in the stress tolerance of plants and microorganisms, Biochem. J. 383 (2004) 277–283.
[9] J. Ingram, D. Bartels, The molecular basis of dehydration tolerance in plants, Annu. Rev. Plant Physiol. Plant Mol. Biol. 47 (1996) 377–403.
[10] M. Wise, A. Tunnacliffe, POPP the question: what *do* LEA proteins do? Trends Plant Sci. 9 (2004) 13–17.
[11] R.A. Larson, The antioxidants of higher plants, Phytochemistry 27 (1988) 969–978.
[12] C.A. Rice-Evans, N.J. Miller, G. Paganga, Antioxidant properties of phenolic compounds, Trends Plant Sci. 2 (1997) 152–159.
[13] J. Buitink, O. Leprince, F.A. Hoekstra, Dehydration-induced redistribution of amphiphilic molecules between cytoplasm and lipids is associated with desiccation tolerance in seeds, Plant Physiol. 124 (2000) 1413–1425.
[14] F.A. Hoekstra, E.A. Golovina, The role of amphiphiles, Comp. Biochem. Physiol. 131A (2002) 527–533.
[15] D.K. Hincha, A.E. Oliver, J.H. Crowe, Lipid composition determines the effects of arbutin on the stability of membranes, Biophys. J. 77 (1999) 2024–2034.
[16] A.E. Oliver, D.K. Hincha, L.M. Crowe, J.H. Crowe, Interactions of arbutin with dry and hydrated bilayers, Biochim. Biophys. Acta 1370 (1998) 87–97.
[17] A.E. Oliver, D.K. Hincha, N.M. Tsvetkova, L. Vigh, J.H. Crowe, The effect of arbutin on membrane integrity during drying is mediated by stabilization of the lamellar phase in the presence of nonbilayer-forming lipids, Chem. Phys. Lipids 111 (2001) 37–57.
[18] A.V. Popova, A.G. Heyer, D.K. Hincha, Differential destabilization of membranes by tryptophan and phenylalanine during freezing: the roles of lipid composition and membrane fusion, Biochim. Biophys. Acta 1561 (2002) 109–118.
[19] A.V. Popova, D.K. Hincha, Specific interactions of tryptophan with phosphatidylcholine and digalactosyldiacylglycerol in pure and mixed bilayers in the dry and hydrated state, Chem. Phys. Lipids 132 (2004) 171–184.
[20] A.E. Oliver, O. Leprince, W.F. Wolkers, D.K. Hincha, A.G. Heyer, J.H. Crowe, Non-disaccharide-based mechanisms of protection during drying, Cryobiology 43 (2001) 151–167.
[21] J. Lapinski, A. Tunnacliffe, Anhydrobiosis without trehalose in bdelloid rotifers, FEBS Lett. 553 (2003) 387–390.
[22] A. Tunnacliffe, J. Lapinski, Resurrecting van Leeuwenhoek's rotifers: a reappraisal of the role of disaccharides in anhydrobiosis, Phil. Trans. R. Soc. Lond. B 358 (2003) 1755–1771.
[23] J.H. Crowe, F. Tablin, W.F. Wolkers, K. Gousset, N. Tsvetkova, J. Ricker, Stabilization of membranes in human platelets freeze-dried with trehalose, Chem. Phys. Lipids 122 (2003) 41–52.
[24] W.F. Wolkers, N.J. Walker, F. Tablin, J.H. Crowe, Human platelets loaded with trehalose survive freeze-drying, Cryobiology 42 (2001) 79–87.
[25] T. Chen, J.P. Acker, A. Eroglu, S. Cheley, H. Bayley, A. Fowler, M. Toner, Beneficial effect of intracellular trehalose on the membrane integrity of dried mammalian cells, Cryobiology 43 (2001) 168–181.
[26] N. Guo, I. Puhlev, D.R. Brown, J. Mansbridge, F. Levine, Trehalose expression confers desiccation tolerance on human cells, Nat. Biotechnol. 18 (2000) 168–171.
[27] A. Tunnacliffe, A.G. de Castro, M. Manzanera, Anhydrobiotic engineering of bacterial and mammalian cells: is intracellular trehalose sufficient? Cryobiology 43 (2001) 124–132.

[28] F.A. Hoekstra, W.F. Wolkers, J. Buitink, E.A. Golovina, J.H. Crowe, L.M. Crowe, Membrane stabilization in the dry state, Comp. Biochem. Physiol. 117A (1997) 335–341.
[29] W.Q. Sun, A.C. Leopold, Cytoplasmic vitrification of anhydrobiotic organisms, Comp. Biochem. Physiol. 117A (1997) 327–333.
[30] R.J. Williams, A.C. Leopold, The glassy state in corn embryos, Plant Physiol. 89 (1989) 977–981.
[31] C. Walters, Temperature dependency of molecular mobility in preserved seeds, Biophys. J. 86 (2004) 1253–1258.
[32] J. Buitink, O. Leprince, Glass formation in plant anhydrobiotes: survival in the dry state, Cryobiology 48 (2004) 215–228.
[33] J.H. Crowe, J.F. Carpenter, L.M. Crowe, The role of vitrification in anhydrobiosis, Annu. Rev. Physiol. 60 (1998) 73–103.
[34] J. Buitink, I.J. van den Dries, F.A. Hoekstra, M. Alberda, M.A. Hemminga, High critical temperature above Tg may contribute to the stability of biological systems, Biophys. J. 79 (2000) 1119–1128.
[35] H. Levine, L. Slade, Principles of ''cryostabilization'' technology from structure/property relationships of carbohydrate/water systems – a review, CryoLetters 9 (1988) 21–63.
[36] J. Buitink, M.A. Hemminga, F.A. Hoekstra, Is there a role for oligosaccharides in seed longevity? An assessment of intracellular glass stability, Plant Physiol. 122 (2000) 1217–1224.
[37] W.L.J. Hinrichs, M.G. Prinsen, H.W. Frijlink, Inulin glasses for the stabilization of therapeutic proteins, Int. J. Pharm. 215 (2001) 163–174.
[38] L.A. Schaller-Povolny, D.E. Smith, T.P. Labuza, Effect of water content and molecular weight on the moisture isotherms and glass transition properties of inulin, Int. J. Food Prop. 3 (2000) 173–192.
[39] P.D. Orford, R. Parker, S.G. Ring, A.C. Smith, Effect of water as a diluent on the glass transition behaviour of malto-oligosaccharides, amylose and amylopectin, Int. J. Biol. Macromol. 11 (1989) 91–96.
[40] W.F. Wolkers, H. Oldenhof, F. Tablin, J.H. Crowe, Preservation of dried liposomes in the presence of sugar and phosphate, Biochim. Biophys. Acta 1661 (2004) 125–134.
[41] E.P.W. Kets, P.J. Ijpelaar, F.A. Hoekstra, H. Vromans, Citrate increases glass transition temperature of vitrified sucrose preparations, Cryobiology 48 (2004) 46–54.
[42] W.F. Wolkers, S. McCready, W.F. Brandt, G.G. Lindsey, F.A. Hoekstra, Isolation and characterization of a D-7 LEA protein from pollen that stabilizes glasses in vitro, Biochim. Biophys. Acta 1544 (2001) 196–206.
[43] W.F. Wolkers, M.G. van Kilsdonk, F.A. Hoekstra, Dehydration-induced conformational changes of poly L-lysine as influenced by drying rate and carbohydrates, Biochim. Biophys. Acta 1425 (1998) 127–136.
[44] W.Q. Sun, C.T. Wagner, J. Connor, The glass transition behaviors of hydroxyethyl starch solutions, Cell Preserv. Technol. 2 (2004) 55–65.
[45] V.A. Frolov, A.Y. Dunina-Barkovskaya, A.V. Samsonov, J. Zimmerberg, Membrane permeability changes at early stages of *Influenza* hemagglutinin-mediated fusion, Biophys. J. 85 (2003) 1725–1733.
[46] M. Müller, K. Katsov, M. Schick, A new mechanism of model membrane fusion determined from Monte Carlo simulation, Biophys. J. 85 (2003) 1611–1623.
[47] W.Q. Sun, A.C. Leopold, L.M. Crowe, J.H. Crowe, Stability of dry liposomes in sugar glasses, Biophys. J. 70 (1996) 1769–1776.
[48] D.K. Hincha, E. Zuther, A.G. Heyer, The preservation of liposomes by raffinose family oligosaccharides during drying is mediated by effects on fusion and lipid phase transitions, Biochim. Biophys. Acta 1612 (2003) 172–177.

[49] L.M. Crowe, J.H. Crowe, A. Rudolph, C. Womersley, L. Appel, Preservation of freeze-dried liposomes by trehalose, Arch. Biochem. Biophys. 242 (1985) 240–247.
[50] D.K. Hincha, E. Zuther, E.M. Hellwege, A.G. Heyer, Specific effects of fructo- and gluco-oligosaccharides in the preservation of liposomes during drying, Glycobiology 12 (2002) 103–110.
[51] K.L. Koster, Y.P. Lei, M. Anderson, S. Martin, G. Bryant, Effects of vitrified and nonvitrified sugars on phosphatidylcholine fluid-to-gel phase transitions, Biophys. J. 78 (2000) 1932–1946.
[52] K.L. Koster, M.S. Webb, G. Bryant, D.V. Lynch, Interactions between soluble sugars and POPC (1-palmitoyl-2-oleoylphosphatidylcholine) during dehydration: vitrification of sugars alters the phase behavior of the phospholipid, Biochim. Biophys. Acta 1193 (1994) 143–150.
[53] J. Milhaud, New insights into water-phospholipid model membrane interactions, Biochim. Biophys. Acta 1663 (2004) 19–51.
[54] J.H. Crowe, A.E. Oliver, F.A. Hoekstra, L.M. Crowe, Stabilization of dry membranes by mixtures of hydroxyethyl starch and glucose: the role of vitrification, Cryobiology 35 (1997) 20–30.
[55] S.B. Leslie, S.A. Teter, L.M. Crowe, J.H. Crowe, Trehalose lowers membrane phase transitions in dry yeast cells, Biochim. Biophys. Acta 1192 (1994) 7–13.
[56] L.M. Hays, J.H. Crowe, W. Wolkers, S. Rudenko, Factors affecting leakage of trapped solutes from phospholipid vesicles during thermotropic phase transitions, Cryobiology 42 (2001) 88–102.
[57] P.J. Quinn, A lipid-phase seperation model of low-temperature damage to biological membranes, Cryobiology 22 (1985) 128–146.
[58] J.H. Crowe, S.B. Leslie, L.M. Crowe, Is vitrification sufficient to preserve liposomes during freeze-drying? Cryobiology 31 (1994) 355–366.
[59] T.D. Madden, M.B. Bally, M.J. Hope, P.R. Cullis, H.P. Schieren, A.S. Janoff, Protection of large unilamellar vesicles by trehalose during dehydration: retention of vesicle content, Biochim. Biophys. Acta 817 (1985) 67–74.
[60] N.M. Tsvetkova, B.L. Phillips, L.M. Crowe, J.H. Crowe, S.H. Risbud, Effect of sugars on headgroup mobility in freeze-dried dipalmitoylphosphatidylcholine bilayers: solid-state 31P NMR and FTIR studies, Biophys. J. 75 (1998) 2947–2955.
[61] J. Grdadolnik, J. Kidric, D. Hadzi, Hydration of phosphatidylcholine reverse micelles and multilayers – an infrared spectroscopic study, Chem. Phys. Lipids 59 (1991) 57–68.
[62] P.T.T. Wong, H.H. Mantsch, High-pressure infrared spectroscopic evidence of water binding sites in 1,2-diacyl phospholipids, Chem. Phys. Lipids 46 (1988) 213–224.
[63] J.H. Crowe, F.A. Hoekstra, K.H.N. Nguyen, L.M. Crowe, Is vitrification involved in depression of the phase transition temperature in dry phospholipids? Biochim. Biophys. Acta 1280 (1996) 187–196.
[64] J. Grdadolnik, D. Hadzi, FT infrared and Raman investigation of saccharide–phosphatidylcholine interactions using novel structure probes, Spectrochim. Acta A 54 (1998) 1989–2000.
[65] H. Nagase, H. Ueda, M. Nakagaki, Effect of water on lamellar structure of DPPC/sugar systems, Biochim. Biophys. Acta 1328 (1997) 197–206.
[66] C.S. Pereira, R.D. Lins, I. Chandrasekhar, L.C.G. Freitas, P.H. Hünenberger, Interaction of the disaccharide trehalose with a phospholipid bilayer: a molecular dynamics study, Biophys. J. 86 (2004) 2273–2285.
[67] A. Sum, R. Faller, J. de Pablo, Molecular simulation study of phospholipid bilayers and insights of the interactions with disaccharides, Biophys. J. (2003) 2830–2844.
[68] M.A. Villarreal, S.B. Diaz, E.A. Disalvo, G.G. Montich, Molecular dynamics simulation study of the interaction of trehalose with lipid membranes, Langmuir 20 (2004) 7844–7851.

[69] A. Blume, W. Hübner, G. Messner, Fourier transform infrared spectroscopy of $^{13}C{=}O$-labeled phospholipids. Hydrogen bonding to carbonyl groups, Biochemistry 27 (1988) 8239–8249.
[70] A.V. Popova, D.K. Hincha, Intermolecular interactions in dry and rehydrated pure and mixed bilayers of phosphatidylcholine and digalactosyldiacylglycerol: a Fourier-transform infrared spectroscopy study, Biophys. J. 85 (2003) 1682–1690.
[71] M.C. Luzardo, F. Amalfa, A.M. Nunez, S. Diaz, A.C. Biondi de Lopez, E.A. Disalvo, Effect of trehalose and sucrose on the hydration and dipole potential of lipid bilayers, Biophys. J. 78 (2000) 2452–2458.
[72] H. Akutsu, Direct determination by Raman scattering of the conformation of the choline group in phospholipid bilayers, Biochemistry 20 (1981) 7359–7366.
[73] W. Pohle, D.R. Gauger, M. Bohl, E. Mrazkova, P. Hobza, Lipid hydration: headgroup CH moieties are involved in water binding, Biopolymers 74 (2004) 27–31.
[74] R.P. Goodrich, J.D. Baldeschwieler, The cryoprotective action of synthetic glycolipids, Cryobiology 28 (1991) 327–334.
[75] Y.S. Park, L. Huang, Cryoprotective activity of synthetic glycophospholipids and their interactions with trehalose, Biochim. Biophys. Acta 1124 (1992) 241–248.
[76] G. Bendas, F. Wilhelm, W. Richter, P. Nuhn, Synthetic glycolipids as membrane-bound cryoprotectants in the freeze-drying process of liposomes, Eur. J. Pharm. Sci. 4 (1996) 211–222.
[77] D. Peer, A. Florentin, R. Margalit, Hyaluronan is a key component in cryoprotection and formulation of targeted unilamellar liposomes, Biochim. Biophys. Acta 1612 (2003) 76–82.
[78] D.K. Hincha, Effects of calcium-induced aggregation on the physical stability of liposomes containing plant glycolipids, Biochim. Biophys. Acta 1611 (2003) 180–186.
[79] D.K. Hincha, A.E. Oliver, J.H. Crowe, The effects of chloroplast lipids on the stability of liposomes during freezing and drying, Biochim. Biophys. Acta 1368 (1998) 150–160.
[80] D.K. Hincha, J.H. Crowe, Trehalose increases freeze-thaw damage in liposomes containing chloroplast glycolipids, Cryobiology 36 (1998) 245–249.
[81] M.S. Webb, B.R. Green, Biochemical and biophysical properties of thylakoid acyl lipids, Biochim. Biophys. Acta 1060 (1991) 133–158.
[82] M.X. Andersson, M.H. Stridh, K.E. Larsson, C. Liljenberg, A.S. Sandelius, Phosphate-deficient oat replaces a major portion of the plasma membrane phospholipids with the galactolipid digalactosyldiacylglycerol, FEBS Lett. 537 (2003) 128–132.
[83] G.G. Shipley, J.P. Green, B.W. Nichols, The phase behaviour of monogalactosyl, digalactosyl, and sulphoquinovosyl diglycerides, Biochim. Biophys. Acta 311 (1973) 531–544.
[84] D. Klaus, H. Härtel, L.M. Fitzpatrick, J.E. Froehlich, J. Hubert, C. Benning, P. Dörmann, Digalactosyldiacylglycerol synthesis in chloroplasts of the Arabidopsis *dgd1* mutant, Plant Physiol. 128 (2002) 885–895.
[85] P.J. Quinn, W.P. Williams, The structural role of lipids in photosynthetic membranes, Biochim. Biophys. Acta 737 (1983) 223–266.
[86] A.G. Lee, Membrane lipids: it's only a phase, Current Biol. 10 (2000) R377–R380.
[87] D.A. Mannock, R.N.A.H. Lewis, R.N. McElhaney, Physical properties of glycosyl diacylglycerols. 1. Calorimetric studies of a homologous series of 1,2-di-*O*-acyl-3-*O*-(α-D-glucopyranosyl)-*sn*-glycerols, Biochemistry 29 (1990) 7790–7799.
[88] A. Sen, S.-W. Hui, D.A. Mannock, R.N.A.H. Lewis, R.N. McElhaney, Physical properties of glycosyl diacylglycerols. 2. X-ray diffraction studies of a homologous series of 1,2-di-*O*-acyl-3-*O*-(α-D-glucopyranosyl)-*sn*-glycerols, Biochemistry 29 (1990) 7799–7804.
[89] D.A. Mannock, R.N. McElhaney, Thermotropic and lyotropic phase properties of glycolipid diastereomers: role of headgroup and interfacial interactions in determining phase behavior, Curr. Opin. Colloid Interface Sci. 8 (2004) 426–447.

[90] P.J. Foht, Q.M. Tran, R.N.A. Lewis, R.N. McElhaney, Quantitation of the phase preferences of the major lipids of the *Acholeplasma laidlawii* B membrane, Biochemistry 34 (1995) 13811–13817.
[91] H.-J. Hinz, H. Kuttenreich, R. Meyer, M. Renner, R. Fründ, R. Koynova, A.I. Boyanov, B.G. Tenchov, Stereochemistry and size of sugar head groups determine structure and phase behavior of glycolipid membranes: densitometric, calorimetric, and X-ray studies, Biochemistry 30 (1991) 5125–5138.
[92] H.M. von Minden, G. Milkereit, V. Vill, Effects of carbohydrate headgroups on the stability of induced cubic phases in binary mixtures of glycolipids, Chem. Phys. Lipids 120 (2002) 45–56.
[93] A. Wieslander, J. Ulmius, G. Lindblom, K. Fontell, Water binding and phase structures for different *Acholeplasma laidlawii* membrane lipids studied by deuteron nuclear magnetic resonance and X-ray diffraction, Biochim. Biophys. Acta 512 (1978) 241–253.
[94] R.V. McDaniel, Neutron diffraction studies of digalactosyldiacylglycerol, Biochim. Biophys. Acta 940 (1988) 158–164.
[95] R.P. Goodrich, J.H. Crowe, L.M. Crowe, J.D. Baldeschwieler, Alterations in membrane surfaces induced by attachment of carbohydrates, Biochemistry 30 (1991) 5313–5318.
[96] M.A. Testoff, A.S. Rudolph, Modification of dry 1,2-dipalmitoylphosphatidylcholine phase behavior with synthetic membrane-bound stabilizing carbohydrates, Bioconj. Chem. 3 (1992) 203–211.
[97] R.P. Goodrich, T.M. Handel, J.D. Baldeschwieler, Modification of lipid phase behavior with membrane-bound cryoprotectants, Biochim. Biophys. Acta 938 (1988) 143–154.
[98] I.J. Vereyken, V. Chupin, A. Islamov, A. Kuklin, D.K. Hincha, B. de Kruijff, The effect of fructan on the phospholipid organization in the dry state, Biophys. J. 85 (2003) 3058–3065.
[99] D.R. Hill, T.W. Keenan, R.F. Helm, M. Potts, L.M. Crowe, J.H. Crowe, Extracellular polysaccharide of *Nostoc commune* (Cyanobacteria) inhibits fusion of membrane vesicles during desiccation, J. Appl. Phycol. 9 (1997) 237–248.
[100] D.K. Hincha, E.M. Hellwege, A.G. Heyer, J.H. Crowe, Plant fructans stabilize phosphatidylcholine liposomes during freeze-drying, Eur. J. Biochem. 267 (2000) 535–540.
[101] K.L. Koster, K.J. Maddocks, G. Bryant, Exclusion of maltodextrins from phosphatidylcholine multilayers during dehydration: effects on membrane phase behavior, Eur. Biophys. J. 32 (2003) 96–105.
[102] I.J. Vereyken, V. Chupin, F.A. Hoekstra, S.C.M. Smeekens, B. de Kruijff, The effect of fructan on membrane lipid organization and dynamics in the dry state, Biophys. J. 84 (2003) 3759–3766.
[103] T. Ritsema, S. Smeekens, Fructans: beneficial for plants and humans, Curr. Opin. Plant Biol. 6 (2003) 223–230.
[104] I. Vijn, S. Smeekens, Fructan: more than a reserve carbohydrate? Plant Physiol. 120 (1999) 351–359.
[105] I.J. Vereyken, V. Chupin, R.A. Demel, S.C.M. Smeekens, B. de Kruijff, Fructans insert between the headgroups of phospholipids, Biochim. Biophys. Acta 1510 (2001) 307–320.
[106] I.J. Vereyken, J.A. van Kuik, T.H. Evers, P.J. Rijken, B. de Kruijff, Structural requirements of the fructan–lipid interaction, Biophys. J. 84 (2003) 3147–3154.
[107] G. Büldt, H.U. Gally, J. Seelig, Neutron diffraction studies on phosphatidylcholine model membranes. I. Head group conformation, J. Mol. Biol. 134 (1979) 673–691.
[108] P.L. Yeagle, W.C. Hutton, C.-H. Huang, R.B. Martin, Structure in the polar head region of phospholipid bilayers: a ^{31}P (^{1}H) nuclear Overhauser effect study, Biochemistry 15 (1976) 2121–2124.

[109] P.L. Yeagle, W.C. Hutton, C.-H. Huang, R.B. Martin, Phospholipid head-group conformations: intermolecular interactions and cholesterol effects, Biochemistry 16 (1977) 4344–4349.
[110] R.J. Mashl, H.L. Scott, S. Subramaniam, E. Jacobsson, Molecular simulation of dioleoylphosphatidylcholine lipid bilayers at differing levels of hydration, Biophys. J. 81 (2001) 3005–3015.
[111] M. Pasenkiewicz-Gierula, Y. Takaoka, H. Miyagawa, K. Kitamura, A. Kusumi, Charge pairing of headgroups in phosphatidylcholine membranes: a molecular dynamics simulation study, Biophys. J. 76 (1999) 1228–1240.
[112] R.L. Obendorf, Oligosaccharides and galactosyl cyclitols in seed desiccation tolerance, Seed. Sci. Res. 7 (1997) 63–74.
[113] T. Konstantinova, D. Parvanova, A. Atanassov, D. Djilianov, Freezing tolerant tobacco transformed to accumulate osmoprotectant, Plant Sci. 163 (2002) 157–164.
[114] E.A.H. Pilon-Smits, M.J.M. Ebskamp, M.J. Paul, M.J.W. Jeuken, P.J. Weisbeek, S.C.M. Smeekens, Improved performance of transgenic fructan-accumulating tobacco under drought stress, Plant Physiol. 107 (1995) 125–130.
[115] T. Taji, C. Ohsumi, S. Iuchi, M. Seki, M. Kasuga, M. Kobayashi, K. Yamaguchi-Shinozaki, K. Shinozaki, Important roles of drought- and cold-inducible genes for galactinol synthase in stress tolerance in *Arabidopsis thaliana*, Plant J. 29 (2002) 417–426.
[116] E. Zuther, K. Büchel, M. Hundertmark, M. Stitt, D.K. Hincha, A.G. Heyer, The role of raffinose in the cold acclimation response of *Arabidopsis thaliana*, FEBS Lett. 576 (2004) 169–173.
[117] T. Suzuki, H. Komatsu, K. Miyajima, Effects of glucose and its oligomers on the stability of freeze-dried liposomes, Biochim. Biophys. Acta 1278 (1996) 176–182.
[118] K. Ozaki, M. Hayashi, Cryoprotective effects of cycloinulohexaose on freezing and freeze-drying of liposomes, Chem. Pharm. Bull. 44 (1996) 2116–2120.
[119] A. Almond, B.O. Petersen, J.O. Duus, Oligosaccharides implicated in recognition are predicted to have relatively ordered structures, Biochemistry 43 (2004) 5853–5863.
[120] J.W. Brady, R.K. Schmidt, The role of hydrogen bonding in carbohydrates: molecular dynamics simulations of maltose in aqueous solution, J. Phys. Chem. 97 (1993) 958–966.
[121] A. Almond, J.K. Sheehan, Predicting the molecular shape of polysaccharides from dynamic interactions with water, Glycobiology 13 (2003) 255–264.
[122] K.N. Kirschner, R.J. Woods, Solvent interactions determine carbohydrate conformation, Proc. Natl. Acad. Sci. USA 98 (2001) 10541–10545.
[123] R.H. Marchessault, T. Bleha, Y. Deslandes, J.-F. Revol, Conformation and crystalline structure of $(2>1)-\beta$-D-fructofuranan (inulin), Can. J. Chem. 58 (1980) 2415–2422.
[124] C.F. Phelps, The physical properties of inulin solutions, Biochem. J. 95 (1965) 41–47.
[125] G. Lee, W. Nowak, J. Jaroniec, Q. Zhang, P.E. Marszalek, Molecular dynamics simulations of forced conformational transitions in 1,6-linked polysaccharides, Biophys. J. 87 (2004) 1456–1465.
[126] D.A. Brant, Novel approaches to the analysis of polysaccharide structures, Curr. Opin. Struct. Biol. 9 (1999) 556–562.
[127] P.E. Marszalek, H. Li, A.F. Oberhauser, J.M. Fernandez, Chair-boat transitions in single polysaccharide molecules observed with force-ramp AFM, Proc. Natl. Acad. Sci. USA 99 (2002) 4278–4283.
[128] P.E. Marszalek, A.F. Oberhauser, Y.-P. Pang, J.M. Fernandez, Polysaccharide elasticity governed by chair-boat transitions of the glucopyranose ring, Nature 396 (1998) 661–664.
[129] P.E. Marszalek, Y.-P. Pang, H. Li, J.E. Yazal, A.F. Oberhauser, Atomic levers control pyranose ring conformations, Proc. Natl. Acad. Sci. USA 96 (1999) 7894–7898.

[130] M. Rief, F. Oesterhelt, B. Heymann, H.E. Gaub, Single molecule force spectroscopy on polysaccharides by atomic force microscopy, Science 275 (1997) 1295–1297.
[131] Y. Yano, K. Tanaka, Y. Doi, M. Janado, The polystyrene affinity of methylglucosides, deoxysugars and glucooligosaccharides, J. Solution Chem. 17 (1988) 347–358.
[132] K. Miyajima, K. Machida, T. Taga, H. Komatsu, M. Nakagaki, Correlation between the hydrophobic nature of monosaccharides and cholates, and their hydrophobic indices, J. Chem. Soc. Faraday Trans. 84 (1988) 2537–2544.
[133] H. Nagase, H. Ueda, M. Nakagaki, Relationship between hydrophobic index of saccharide and gel-liquid crystal transition temperature of the L-α-dipalmitoyl phosphatidylcholine (DPPC)/saccharide/water system, Chem. Pharm. Bull. 47 (1999) 607–610.

This page intentionally left blank

CHAPTER 7

Atomic Force Microscopy of Lipid Bilayers

Hans-Jürgen Butt* and Ann-Katrin Awizio

Max-Planck-Institute for Polymer Research, Ackermannweg 10, 55128 Mainz, Germany

Contents

Abstract

With the invention of the atomic force microscope (AFM) it became possible to image lipid bilayers at a high resolution in natural environment. Therefore, they have to be adsorbed to a solid support. The structure of solid-supported lipid bilayers can be studied – in some cases at molecular resolution. Phenomena such as two-dimensional phase separation and the formation of lipid rafts were imaged in real time. By taking force-*versus*-distance curves it is possible to measure local mechanical properties and to determine the interaction between lipid bilayers and thus study vesicle fusion and related phenomena.

*Corresponding author. Tel: 0049-6131-379 111; Fax: 0049-6131-379 310;
E-mail: butt@mpip-mainz.mpg.de

ADVANCES IN PLANAR LIPID BILAYERS AND LIPOSOMES, VOLUME 3
ISSN 1554-4516 DOI: 10.1016/S1554-4516(05)03007-3

ABBREVIATIONS OF LIPIDS

DAPC 1,2-Diarachidoyl-*sn*-glycero-3-phosphocholine
DGDG Digalactosyldiglyceride
DLPC 1-Palmitoyl-2-linoleoyl-sn-glycero 3-phosphocholine
DLPE 1,2-Dilauroyl-*sn*-glycero-3-phosphoethanolamine
DMPC 1,2-Dimyristoyl-*sn*-glycero-3-phosphocholine
DMPE 1,2-Dimyristoyl-*sn*-glycero-3-phosphoethanolamine
DMTAP 1,2-Dimyristoyl-3-trimethylammonium-propane
DODAB Dimethyl-dioctadecylammonium bromide
DOPC 1,2-Dioleoyl-*sn*-glycero-3-phosphocholine
DOPE 1,2-Dioleoyl-*sn*-glycero-3-phosphodylethanolamine
DOPS 1,2-Dioleoyl-*sn*-glycero-3-phospho-L-serine
DOTAP 1,2-Dioleoyl-3-trimethylammonium-propane chloride
DPPC 1,2-Dipalmitoyl-*sn*-glycero-3-phosphocholine
DPPE 1,2-Dipalmitoyl-*sn*-glycero-3-phosphoethanolamine
DPTAP 1,2-Dipalmitoyl-3-trimethylammonium-propane
DSPC 1,2-Distearoyl-*sn*-glycero-3-phosphocholine
DSPE 1,2-Distearoyl-*sn*-glycero-3-phosphoethanolamine
MGDG Monogalactosyldiacylglycerol
PLPC 1-Palmitoyl-2-linoleoyl-*sn*-glycero-3-phosphocholine
POPC 1-Palmitoyl-2-oleoyl-*sn*-glycero-3-phosphocholine
POPE 1-Palmitoyl-2-oleoyl-*sn*-glycero-3-phosphoethanolamine
POPG 1-Palmitoyl-2-oleoyl-*sn*-glycero-3-(phospho-rac-(1-glycerol))
POPS 1-Palmitoyl-2-oleoyl-*sn*-glycero-3-phospho-L-serine
SOPG 1Stearoyl-2-oleoyl-*sn*-glycero-3-(phospho-rac-(1-glycerol))
SpM Sphingomyelin

1. INTRODUCTION

With the invention of the atomic force microscope (AFM) in 1986 by Binnig *et al*. [1], it became possible to analyze the structure of lipid bilayers and biological membranes with a high resolution in aqueous electrolyte [2]. When the AFM was first applied to image lipid bilayers the aim was to solve the molecular packing structure. Therefore, lipids below their phase transition temperature were prepared by Langmuir–Blodgett (LB) transfer and imaged in aqueous medium. Weisenhorn *et al*. [3] analyzed bilayers composed of a first monolayer made of cadmium arachidate plus a second layer of cadmium arachidate or dioctadecyldimethylammonium bromide (DODAB). Zasadzinski *et al*. [4] deposited bilayers of dimyristoylphosphatidylcholine (DMPE). In both cases, the molecular packing was revealed. These are the first molecularly resolved images of lipid bilayers in their natural environment. Imaging in native medium was a significant step forward and complemented ‘‘classical’’ techniques such as electron microscopy, light microscopy, and X-ray scattering.

In general, the AFM is a tool to image the topography of surfaces. For imaging, the sample is scanned underneath a tip, sometimes called ''probe'', which is mounted to a cantilever spring. The sample is scanned by a piezoelectric scanner. While scanning, the force between the tip and the sample is measured by monitoring the deflection of the cantilever. To get a topographic image of the sample, the deflection of the cantilever *versus* its position on the sample is plotted. Alternatively, it is possible to plot the height position of the scanner. In this case, the height is controlled by a feedback loop, which maintains a constant force between tip and sample. Image contrast arises because the force between the tip and sample is a function of both tip–sample separation, and the material properties of the tip and sample. To date, the AFM was used in most applications to image surface topography in the contact mode. In this mode image contrast is obtained from the very short-range repulsion, which occurs when the electron orbitals of tip and sample overlap (Born repulsion). However, further interactions between tip and sample can be used to investigate material properties on a nanometer scale.

Soon after the invention of the AFM, it was realized that valuable information about surfaces can be obtained by taking force-*versus*-distance measurements [5,6]. These measurements are usually known as ''force measurements''. Force measurements with the AFM were first driven by the need to reduce the total force between tip and sample in order to be able to image fragile, biological structures [7,8]. Therefore, it was obligatory to understand the different components of the force. Nowadays, most force measurements are done by surface scientists, electrochemists, or colloidal chemists who are interested in surface forces *per se*. Short [9] or comprehensive [10] reviews about surface force measurements with the AFM have been published.

In this contribution we first describe how an AFM works, which are the main components, the technical limitations, and we mention important aspects of the resolution. Then, results obtained with the AFM on solid–supported membranes are highlighted. We focus on lipid bilayers rather than dealing with biological membranes containing proteins. Excellent reviews on the imaging of membrane proteins and structure have appeared [11–13]. Only few, however, focus on lipid bilayers and highlight the physicochemical aspects [14,15] rather than protein structure. Sample preparation, a prerequisite for any good AFM experiment, is described next. To learn more about the properties of lipid bilayers, force experiments have become more and more popular during the last years. They are described in the last section.

2. THE ATOMIC FORCE MICROSCOPE

2.1. Components and principle

The basic components of an AFM are the tip attached to a cantilever, a piezoelectric scanner to position and move either the sample or the tip, a system to

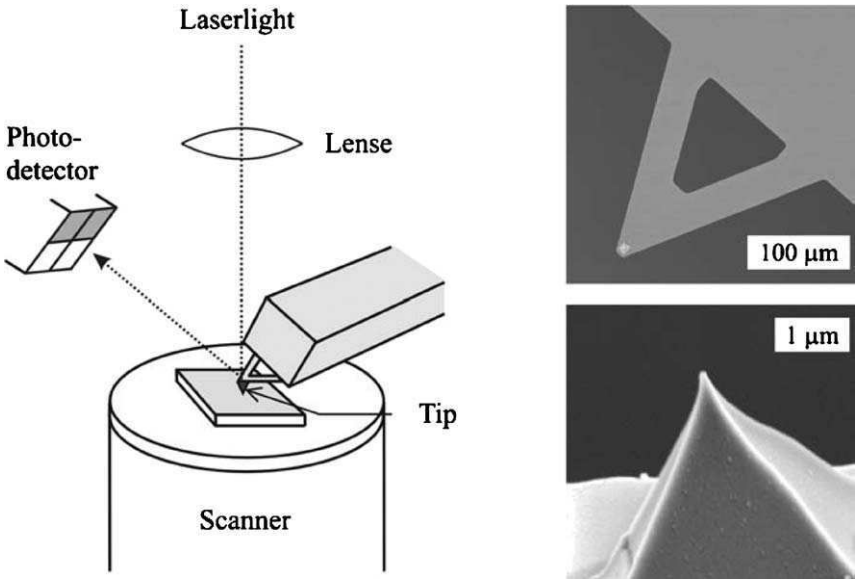

Fig. 1. Schematic of an atomic force microscope. On the right, scanning electron micrographs show a cantilever (top) and a tip (bottom) in more detail. The tip, which in operation points downwards to the sample, is pointing toward the observer (top) and upwards (bottom). The picture was taken from Ref. [16].

detect cantilever deflection, and the electronics with a computer to provide a feedback loop, for data storage, and for the analysis of results (Fig. 1). We start our discussion with the tip. The end of the tip is usually in mechanical contact with the sample. The quality of the tip and the mechanical properties of the cantilever determine the behavior of an AFM. Tip and cantilever are usually made using microfabrication techniques from materials such as silicon or silicon nitride. Tip properties are described below when discussing resolution.

Essential for the information provided by AFM experiments are the mechanical properties of the cantilever. Cantilevers should have a high resonance frequency. A high resonance frequency reduces noise and it allows for fast scanning. For a rectangular cantilever the resonance frequency is given by $\nu = 0.162 \cdot d/L^2 \cdot \sqrt{E/\rho}$, where d is the thickness of the cantilever, L is its length, E is Young's modulus of the material, and ρ is the density. High resonance frequencies are obtained by making cantilevers short. Short cantilever also provides a high sensitivity at a given deflection. At the same time cantilevers should be soft and have a low spring constant to allow imaging at low force. The spring constant of a rectangular cantilever is given by $K = Ewd^3/(4L^3)$, where w is the width of the cantilever. To obtain a low spring constant, the cantilever should be long. Both requirements – high-resonance frequency and low spring constant – are achieved by making cantilevers as small as possible.

When imaging in liquids – and lipid bilayers can only be imaged in liquids – the resonance frequency is typically a factor 5–10 lower than in air or vacuum [17]. This is due to the hydrodynamic drag experienced by a moving cantilever [18]. It is a severe drawback because it limits the scanning velocity and also makes imaging in tapping mode difficult.

Typical commercial cantilevers are 100–200 μm long, 0.5–2 μm thick and 10–30 μm wide. Usually, they are produced with a rectangular cross-section or V-shaped to minimize torsion. Resonance frequencies are typically 5–300 kHz in air. Recently, several research groups made significant progress in designing and using smaller cantilevers. This not only involves a refined fabrication process for the cantilevers but also requires a perfect alignment and focusing of the optical system and a fast electronic and data recording system [19].

A less critical component is the piezoelectric scanner. Piezoelectric scanners and control electronics of sufficient quality are commercially available. Different configurations are possible. Usually, the sample is scanned in *xy*-direction and also the height of the sample is adjusted by the *xyz*-scanner. In some instruments, tip and cantilever are scanned and the sample is fixed. This is, for instance, the case when the sample is mounted on an inverted light microscope. Also combinations are possible in which the sample is scanned but the height of the cantilever is controlled.

In order to measure the up and down movements of the tip, a laser beam is focused on to the back of the cantilever. From there, the laser beam is reflected toward a position sensitive photodetector. If the cantilever moves, the position of the reflected beam changes. With the help of the photodetector this change is converted into an electrical signal. An electronic feedback control keeps the cantilever deflection constant by adjusting the *z*-position of the sample. This height information of the sample is finally plotted *versus* the *xy*-position and a topographic picture of the sample surface is obtained. Since the deflection of the cantilever and thus the force applied by the tip to the sample remains constant, this mode is referred to as ‘‘constant force mode’’. Alternatively, the feedback loop is kept slow so that it only regulates the average height of the sample. Then small features deflect the cantilever. The deflection is plotted *versus* the lateral position on the sample. In this case, the force changes but the height remains relatively constant. For this reason this mode is called ‘‘constant height mode’’.

2.2. Resolution

If we think of tip and sample as non-deformable continuous solids with no interaction except the hard-core repulsion, it is obvious that the tip geometry determines the resolution. The main basic parameter to describe tip geometry is the radius of curvature of the tip. Different methods have been devised to measure this tip radius. One possibility is to image the end of the tip with a scanning

electron microscope. Practically, the resolution is limited by charging effects to typically 5–10 nm.With a transmission electron microscope the shadow of a tip can be imaged, and the tip radius at least in one direction can be obtained [20,21]. This method requires the design of suitable cantilever holders. An alternative method is to use the tip and image a very sharp structure, where the edges are even sharper than the tip itself. From these images the tip radius is obtained, or at least an upper limit of the tip radius. Gratings with sharp protrusions are commercially available for this purpose.

In reality, the tip is not a perfect continuous solid and there are several aspects to be considered. First, tip and in particular the sample can and will deform. This might sound surprising because the force between tip and sample is low; typical forces range between 0.1 and 1 nN. It is even lower than the force required to break a single covalent bond of typically 1–10 nN. The pressure underneath the tip, however, can reach several thousand atmospheres because the contact area is so small. This can lead to deformation or even destruction of organic and biological structures.

A second aspect is the roughness of the tip on the atomic scale and the range of the effective interaction forces. When it comes to resolution on the nanometer or subnanometer scale, the tip radius is certainly not sufficient to describe its behavior anymore. Single atoms or groups of atoms might protrude from the mean structure and make a significant contribution to an image. In other words: Depending on the length scale of the relevant interaction and the structure investigated, different radii of curvature are effective. From the image of the membrane protein bacteriorhodopsin, Müller *et al*. [22] for example deduced an effective tip radius of few nanometers, which is significantly lower than a tip radius determined by electron microscopy.

A third aspect, often neglected, is surface layers of adsorbed material. No surface except a freshly cleaved surface in UHV is clean and even then only for several minutes. There is always adsorbed material such as water or hydrocarbons. The adsorption depends sensitively on the medium. In air, for example, water tends to adsorb to hydrophilic surfaces. In water, on the other hand, hydrocarbons are driven toward interfaces. Adsorption is also influenced by the chemical nature of the tip and sample surface and it is by this effect that identical topographic structures of different chemical composition can lead to different images. Depending on the force and the strength of adsorption, one might image the real solid surface, or the adsorbates, most likely something in between. Thus, to understand an AFM image not only the topography of sample and tip is important but also the deformability and possible adsorbed materials have to be considered.

The resolution obtained is often judged by features resolved in an image. Here we have to distinguish two cases. When crystalline samples are imaged, often periodicities with a period much smaller than the radius of curvature of the tip are resolved. Solid crystal surfaces can often be imaged with ‘‘atomic resolution’’,

which in fact means that periodicities of atomic spacing are reproduced. It is much more difficult to resolve defects and non-periodic features. Therefore, it is necessary to specify whether single features or periodicities are meant when reporting a resolution.

2.3. Imaging modes

In most applications of biological substances in aqueous medium the AFM is used to image surface topography in the contact mode. In contact mode, the tip of the AFM is continuously in actual contact with the sample surface. Image contrast is obtained from the very short-range repulsion, which occurs when the electron orbitals of tip and sample overlap (Born repulsion). To be able to adjust the force applied by the tip to the sample cantilevers with relatively low spring constants of typically 0.01–0.2 N/m are used.

One risk in atomic force microscopy is the destruction of fragile objects. A way to avoid deformation of fragile objects is to use the so-called tapping mode. In tapping mode, the cantilever is vibrated at its resonance frequency. In most applications this vibration is initiated by a piezo, which is included in the cantilever holder. This is called ''acoustic tapping''. Alternatively, the cantilever is coated with a magnetic material and an oscillating magnetic field causes the vibration [23]. Unfortunately, cantilevers with magnetic coating are difficult to manufacture and are therefore expensive. At the end of the cantilever, where the tip is, the vibration amplitude is typically 1–10 nm.When we approach the surface with such a vibrating cantilever, at some point the amplitude will decrease, simply because the tip starts to hit the surface. Instead of scanning the surface at constant deflection or constant height, we scan at constant reduction of the vibration amplitude. As a result, most of the time the tip is not in actual contact with the surface (Fig. 2). It just taps the surface for a short time at intervals given by the resonance frequency. Cantilevers for tapping mode have high spring constants of the order of 10–50 N/m to reach a high resonance frequency.

The tapping mode is often less destructive than the contact mode because the contact time is very short and shear is prevented. In addition, we can get information about the local mechanical properties such as the elasticity [24,25].

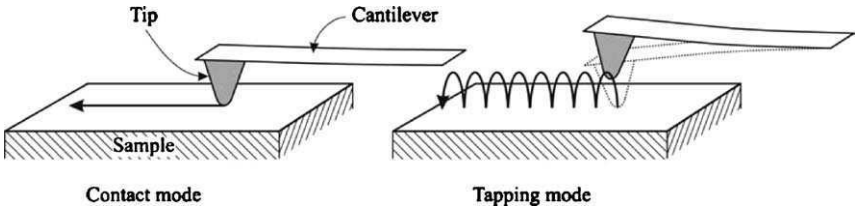

Fig. 2. Actual movement of the AFM tip with respect to the sample in the standard contact mode and in the tapping mode. The picture was reproduced from Ref. [16].

Disadvantages of the tapping mode are the slightly lower resolution and the fact, that the resonance peak is broad in liquid media.

3. FORMATION OF SOLID-SUPPORTED LIPID BILAYERS

To prepare lipid bilayers for AFM studies two methods usually are applied: The LB technique and spontaneous vesicle fusion [26]. In very few cases the Langmuir–Schäfer method [27] was used. It is not further described here.

3.1. Langmuir–Blodgett transfer

Lipid monolayers can be transferred layer-by-layer onto solid substrates by the LB technique (Fig. 3) [28,29]. This is done with a film balance, also called a Langmuir trough. The modern version of a film balance consists of a temperature-controlled trough, which contains the aqueous medium, called "subphase". Lipids are not (or only weakly) soluble in water and go to the surface, where they form a monolayer. Through a movable barrier the film balance allows to adjust the density of molecules on the aqueous surface by compression or expansion of the film.

If the barrier could move freely, it would drift in the direction of the liquid with higher surface tension. In this way the system is able to reduce its entire free energy. We could imagine that this movement is caused by a so-called film pressure. The film pressure π is defined as the difference between the surface tension of the bare aqueous medium γ_0 and the surface tension of the subphase

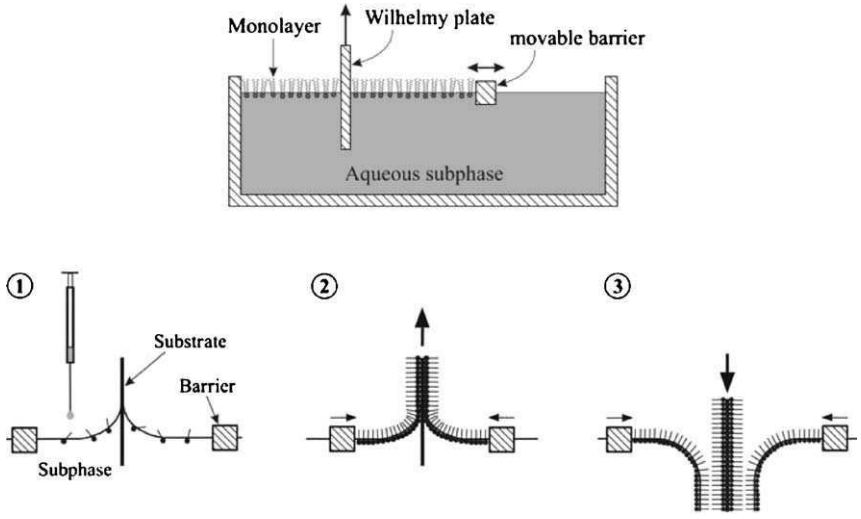

Fig. 3. Langmuir–Blodgett transfer of lipid monolayers from water onto a solid substrate. The picture was reproduced from Ref. [16].

in the presence of lipids γ: $\pi = \gamma_0 - \gamma$ The film pressure is determined by the Wilhelmy plate method, which usually contains a piece of absorbent paper hanging into the aqueous subphase. The force acting on this piece of paper having a width l is $2l\gamma$. By measuring this force the surface tension and thus the film pressure can be determined. If we compress a surfactant film on water we observe that the surface tension decreases and the surface pressure increases.

To deposit a lipid bilayer onto a hydrophilic substrate such as a silicon wafer or mica one proceeds as follows (Fig. 3):

- First, the lipid is dissolved in a solvent, which evaporates easily and is not miscible with water (usually chloroform). After the hydrophilic solid substrate has been moved into the aqueous subphase, drops of the lipid-containing solvent are set carefully onto the water surface between the movable barriers by a syringe (''spreading''). After solvent evaporation the monolayer is compressed to the desired pressure, typically some 20–40 mN/m.
- The hydrophilic substrate is moved continuously out of the water subphase at constant film pressure. During the upstroke the monolayer is transferred onto the wafer with the headgroups oriented toward the solid substrate and the alkyl chains exposed to the air. This renders the hydrophilic solid surface hydrophobic. Thereby, the surface energy of the solid surface decreases from typically 0.05 to 0.02–0.03 J/m^2.
- Then the substrate is moved into the subphase again. Another monolayer is deposited onto the first monolayer. The alkyl chains are oriented toward the solid substrate in a ''tail-to-tail'' configuration. As a result, a lipid bilayer is formed. This has to be kept in water all the time. Otherwise, it is immediately destroyed since the hydrophobic effect, which holds the bilayer together, does not exist in air.

In this way, lipid bilayers can be formed from a large variety of lipids. The density of molecules in a monolayer can be adjusted by choosing the appropriate film pressure. A possible drawback is that in some cases it is difficult to produce homogeneous films covering a large area. This, however, is not a severe limitation in AFM studies because inhomogeneities are usually spaced more than several micrometers and are easily detected.

3.2. Vesicle fusion

Vesicle fusion provides a technique, which is easy to handle and which leads to spontaneous formation of a bilayer in the liquid cell of the AFM. Brian and McConnell [30,31] were the first to use vesicle fusion to form a lipid bilayer on a solid surface. They observed that vesicles of phosphatidylcholine spontaneously adsorb, spread, and form a bilayer on glass. Meanwhile, vesicle fusion has been observed on several solid surfaces such as silicon oxide [32–37], silicon nitride

[37,38], glass [39], alumina [40], titanium oxide [37,41], mica [42,43], platinum [37], gold [37], and some thiol-coated gold surfaces [43,44,45]. Only lipids in their fluid state can be used for spontaneous vesicle fusion. For lipids, which are in their gel phase at room temperature, vesicle fusion is enhanced by heating to temperatures above the phase transition temperature. Depending on the substrate, the lipid, the pH, and salts present in the solution the lipids are able to diffuse laterally and a molecular layer of water is entrapped or the lipid molecules are laterally immobile [46].

Formation of a continuous lipid bilayer on a solid support involves several steps [47]. Initially, the vesicles diffuse to the solid substrate and adsorb. The adsorption kinetics has been modelled by Zhdanov *et al*. [48]. Depending on the substrate, the chemical nature of the lipids, the pH, and salt concentrations vesicles remain intact and do not spread or form a planar bilayer [49]. In particular, divalent cations influence vesicle adsorption [47,50]. A certain critical coverage of adsorbed vesicles is required before spreading sets in [37]. Then the vesicles rupture or may fuse with each other before they can rupture [51,52]. In either case, lipid bilayer discs are formed. The top bilayer of the ruptured vesicles rolls or slides over the bottom bilayer [53] and the solid-supported bilayer grows [54,55]. Eventually the discs coalesce to form a continuous layer.

4. IMAGING LIPID BILAYERS

4.1. Formation of solid-supported bilayers by vesicle fusion and changes in bilayer shape

AFM studies have significantly contributed to our understanding of the process of vesicle fusion on solid surfaces [43,56] because it is the only tool to study the process in situ with a high resolution. In one of the early studies Egawa and Furusawa [57] observed the first stages of vesicle fusion on mica: The vesicles adsorb, flatten, and rupture. They observed a difference between phosphatidylcholine (PC) and phosphatidylethanolamine (PE). With PE vesicles the second bilayer remained intact and two bilayers are typically formed while for PC the second bilayer slided over the first to adsorb to empty places on the mica surface resulting in one homogenous bilayer. The rate of bilayer formation increased with the salt and the vesicle concentration. The authors relate this to the different hydration degree of the headgroups. The same process was observed by Leonenko *et al*. [43] for dioleoylphosphatidylcholine (DOPC) on mica. The presence of the polypeptide gramicidin in the vesicle did not change the process.

Jass *et al*. [53] observed vesicle fusion even in more detail using tapping mode and proteoliposomes made of a mixture of dipalmitoylphosphatidylcholine (DPPC), dipalmitoylphosphatidylethanolamine (DPPE), dipalmitoylphosphatidylglycerol (DPPG), cholesterol and an acetylcholine receptor (Fig. 4): After

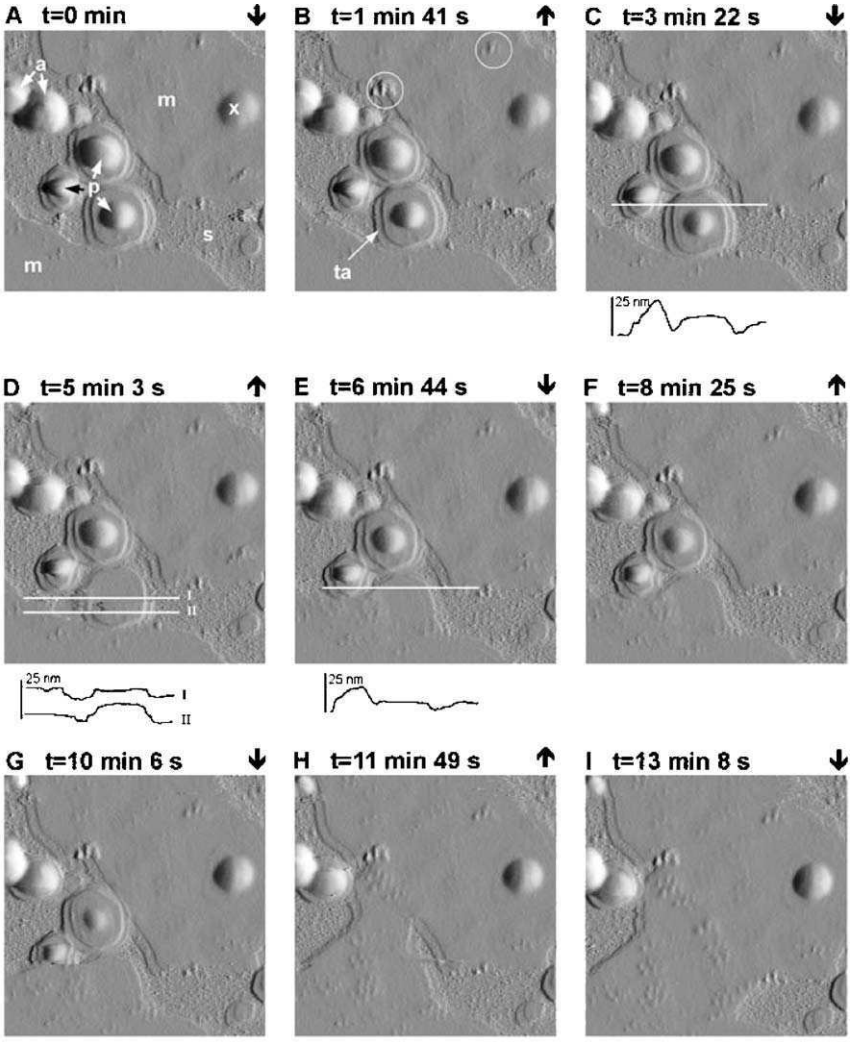

Fig. 4. Sequence of AFM images showing proteoliposome flattening, rupture, and spreading on a hydrophilic silica surface. Images were taken in Tris-HCl/ NaCl buffer in tapping mode. Images were kindly provided by G. Puu [53].

adsorption, the vesicles flatten from the outer edges toward the center until the two bilayers are stacked on top of each other. Then the top bilayer rolls or slides over the bottom bilayer, the adjacent edges join so that a larger membrane patch is formed. Calcium increases the rate of the process so that above a calcium concentration of 4 mM the intermediate stages could not be imaged anymore.

The fusion process of two spherical patches on mica was observed by Muresan and Lee [58] who imaged egg-PC membrane patches after vesicle fusion in tapping mode in the presence of 10–30 mM $MgCl_2$. After the patches get

into contact they merge and after typically 10 min, one rounded, circular patch is formed. As the driving force they identified the line tension. The line tension is the energy per unit length for the formation of an edge of a bilayer patch. Assuming reasonable values for the diffusion of lipid molecules they calculated a line tension of 10^{-18} N. This is much higher than theoretically estimated values of the order of 10^{-10} N, so that additional factors not yet identified have to be considered.

Recent studies in the subject involve the use of complementary techniques like the quartz crystal microbalance (QCM) [59]. With the QCM the adsorbed amount can be measured with a time resolution in the range of 1 s. Therefore, it provides additional information complementing the detailed structural information obtained with the AFM [56,60].

4.2. Phase separations in lipid mixtures

Lipid phase separation phenomena are likely to play an important role in the lateral organization of biological membranes and as such in the function of membrane proteins. Phase changes and phase separation have extensively been studied in monolayers at the air–water interface using optical techniques such as fluorescence and Brewster angle microscopy. These studies are limited to structures, which are larger than the wavelength of light. Using the AFM, they could be extended to smaller sizes, although only on monolayers, which have to be transferred to a solid support [61,62]. Using the AFM, however, phase separation could also be studied on whole bilayers and at a small scale.

Hui *et al*. [63] and Dufrêne *et al*. [64] analyzed phase separation of bilayers with the AFM. Their films were prepared by LB transfer of a first monolayer of distearoylphosphatidylethanolamine (DSPE) onto mica followed by a second monolayer of a mixture of DSPE and dioleoylphosphatidylethanolamine (DOPE). Although DSPE (18:0) and DOPE (18:1) have the same chain length the unsaturated carbon bond is enough to induce the formation of different domains. Domains are recognizable not only on topographic images but also by friction analysis and the measurement of the adhesion force. DSPE domains of typically few microns diameter are higher and show a lower friction and adhesion than the surrounding DOPE matrix.

Tokumasu *et al*. [65] took advantage of the high resolution of AFMs. They studied mixed bilayers on mica from dilauroylphosphatidylcholine (DLPC), DPPC, and cholesterol. They observed DPPC-rich domains of 26–46 nm extension, which increased in the presence of cholesterol to 33–48 nm.In a further study, they added fluorescent lipid analogs and correlated topographic AFM images with optical images obtained with a near-field scanning optical microscope (NSOM) [66]. In both studies, the lipid bilayers were formed by spontaneous vesicle fusion. Tokumasu *et al*. were, however, not the first ones to correlate

topographic structure with the distribution of fluorescently labelled markers. In a thorough study, Burns [67] combined AFM and confocal fluorescence microscopy to study DPPC/DOPC lipid bilayers. DPPC tends to form gel domains while DOPC-rich phases are disordered.

At molecular resolution Valdre *et al*. observed a phase separation in mixtures of PLPC and cardiolipin (tetra-acyl-diphosphatidyl-glycerol) [68]. These lipids are theoretically predicted to phase separate because of a difference in chain length (hydrophobic mismatch). The authors were able to observe the packing structure of the lipids with molecular resolution. Based on these images they could discriminate different phases and, in combination with NMR experiments, confirm the theoretical prediction.

To make phase separations better detectable Kaasgaard *et al*. [69] labelled dipalmitoylphosphatidylethanolamine (DPPE) with biotin. They added 0.7 mol% of labelled lipid to a mixture of DPPC and diarachidoylphosphatidylcholine (DAPC) and transferred bilayers to mica by LB transfer. DPPC and DAPC phases separate with the labelled DPPE partitioning into the DPPC phase. After addition of the protein avidin, which binds specifically to biotin, the DPPC phase could be clearly identified by an increase in height of 6 nm.

4.3. Temperature-induced phase changes

Phase changes can be induced by cooling a lipid bilayer below its melting temperature. At the melting temperature even in a one-component lipid bilayer two phases exist. The AFM is in this case a useful tool to show intermediate stages during phase transitions while the temperature is changing. McKierna *et al*. [70] studied for example, the process of nucleation and growth of domains when the temperature of a dipalmitoyltrimethylammoniumpropane (DPTAP) or a dimyristoyltrimethylammonium-propane (DMTAP) bilayer formed by vesicle fusion on mica was cooled below its melting temperature. Fractal structures were formed in DPTAB, whereas in DMTAP domains were elongated and triangular. The cooling rate and salt concentration affected the shape and size of domains. By adding a fluorescent label, AFM images could be correlated with images obtained by fluorescence microscopy.

Usually the fluid and gel phases differ in their two-dimensional packing density. Without providing some reservoir in the form of vesicles in the liquid cell when cooling a bilayer below the phase transition temperature, the density of the molecules increases and defects occur. The resulting evolution of defects and holes was observed by Xie *et al*. [71] for dimyristoylphosphatidylcholine (DMPC) on mica. Tokumasu *et al*. [72] not only observed phase changes depending on temperature but also studied the effect of the incubation time. Depending on how long mica was exposed to a suspension of DMPC, bilayers or multilayers are formed.

Phase changes in mixtures are usually accompanied with a change in the composition of the two phases. These phase changes can take hours to be completed. One example is mixtures of DMPC and distearoylphosphatidylcholine (DSPC), which have been extensively studied and the phase diagram is well known. Giocondi *et al*. [73] analyzed equimolar mixtures of the two lipids and could clearly observe the fluid-to-gel transition. The fluid DMPC enriched phase and the DSPC enriched gel phase could be distinguished because the gel phase protrudes ≈ 1 nm from the fluid phase. Such a visible domain growth allowed them also to determine growth rates of domain sizes and compare them to theoretical predictions. In a mixture of DOPC/DPPC (3 mol:1 mol), they could quantitatively follow the growth of gel domains when cooling below the fluid-to-gel transition temperature [74]. The area of an average gel domain A increased with time t proportion to $A \propto t^{2/3}$ after quenching the temperature well below the phase transition temperature. It is not proportional to the circumference because the two monolayers are coupled and are forced to grow simultaneously.

4.4. Ripple phase

Phosphatidylcholines can form ripple phases, denoted $P_{\beta'}$, as an intermediate phase between the gel phase and the fluid phase [75]. This ability is attributed to the molecular characteristics of the headgroup region. The ripple phase appears below the main phase transition temperature and above the so-called pretransition temperature. Outside of the ripple phase the bilayer is planar, whereas within the ripple phase the membrane adopts a characteristic structure of parallel lines with a defined periodic spacing of 10–30 nm.To gain insight in the melting of lipid mixtures the temperature-dependent formation of the ripple phase was investigated by Kaasgaard, Leidy *et al*. [76,77] for DPPC and DMPC/DSPC bilayers on mica (Fig. 5).

The bilayers of Kaasgaard, Leidy *et al*. were formed by vesicle fusion and they were symmetric. Czajkowsky *et al*. [78] studied asymmetric bilayers formed by LB transfer. They found that bilayers with DPPC or DSPC in one and POPG, SOPG, or POPE in the second leaflet form the ripple phase at room temperature. Thus, the conditions for ripple phase formation are different than the conditions for symmetric bilayers, indicating a coupling between the two leaflets.

Molecular interactions between lipid molecules account for their ability to exist in various phases, that are distinguishable by packing order and fluidity. These interactions and thus the phases can be influenced by other molecules. Mou *et al*. [42] find that a common buffer, *tris*(hydroxylmethyl)aminomethane ($C_4H_{11}NO_3$), can reversibly induce the formation of a ripple phase in 1,2-dipentadecanoyl-*sn*-glycero-3-phosphatidylcholine bilayers. Czajkowsky *et al*. [78] also found that the presence of phosphate and sodium in the buffer is required to induce a ripple phase in their asymmetric bilayers.

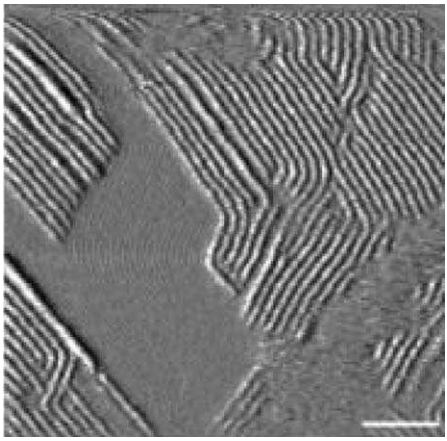

Fig. 5. AFM image showing a ripple phase in a 1:1 DMPC/DSPC bilayer at 24.5 °C. The scale bar is 200 nm long. The image was kindly provided by K. Jorgensen [76].

4.5. Lipid rafts

In biological membranes, the lipids are not perfectly and homogeneously mixed but they are organized. This lateral organization probably results from a preferential packing of sphingolipids and cholesterol into moving platforms, called rafts, onto which specific proteins attach within the bilayer. Over the last years, the research done on lipid rafts and their formation in lipid bilayers increased rapidly due to their importance for cellular processes inside and outside of the cell [79]. Lipid rafts are domains in membranes that are predominantly enriched in sphingolipids and in cholesterol, since the latter prefers sphingolipids over phospholipids. One of the characteristic properties of lipid rafts is that they are insoluble to non-ionic surfactants, such as Triton X-100.

Rinia *et al*. [80] imaged solid-supported bilayers from a mixture of sphingomyelin (SpM)/DOPC/cholesterol. They could clearly observe domain formation of solid SpM cholesterol rich domains and fluid domains of DOPC. The fluid domains are extractable with Triton X-100 and the solid domains remain as detergent-resistant patches. When replacing SpM by DPPC the domains become very small [81]. While with SpM solid domains extend over typically few 100 nm, in the presence of DPPC domain sizes are in the order of few 10 nm. Rinia *et al*. could interpret their results by assuming that cholesterol interacts preferentially with SpM rather than DPPC.

Since lipid rafts are thought to be part of signalling pathways across membranes the enrichment of certain additional molecules in these domains is also subjected to investigation. Yuan *et al*. [82] showed that ganglioside GM1, a glycolipid marker for rafts, accumulates in the ordered SpM/cholesterol rich phase. Several membrane-associated proteins are inserted in the bilayer by a

GPI-anchor as is demonstrated by Milhiet *et al*. [83], who coupled alkaline-phosphatase to a GPI-anchor and visualized its enrichment at the rim of gel phase, SpM rich domains, in a DOPC/SpM bilayer. The same phenomenon was observed in the more ordered SpM/cholesterol domains in a SpM/DOPC/cholesterol bilayer. Bilayers made only by SpM/DOPC or SpM/POPC also form SpM rich domains. After addition of cyclodextrin loaded with cholesterol the domains disappeared, because the SpM is extracted by the cholesterol [84]. A second experiment with the same system using only cyclodextrin led to holes in the bilayer, which proves that not only cholesterol extracts SpM but cyclodextrin alone has an effect.

4.6. Phase changes due to alcohols and peptides

Some chemicals and drugs are thought to exert their physiological or pharmacological effect by dissolving in the membrane and changing its structure. One example is the buffer *tris*(hydroxylmethyl)aminomethane, which reversibly induces the formation of a ripple phase in phospholipid bilayers [42]. Another example is the effect of certain alcohols. AFM images of DPPC and DSPC bilayers showed that ethanol and 2-propanol induce interdigitation of the lipid molecules leading to thinner domains [85]. This interdigitation can also be induced by a 10% 2-propanol and repeated heating to 60°C in DPPC bilayers [86].

More specific is the action of certain peptides. Janshoff *et al*. [87] studied the effect of an amphipathic α-helix of the N-terminal domain of the capsid protein cleavage product of the flock house virus. This peptide induces the formation of the interdigitated gel phase ($L_{\beta}I$) in DPPC bilayers. Rinia *et al*. [88,89] worked with DPPC bilayers as well and added WALP peptides and their analogs. These are peptides with an $(\text{alanine-leucine})_{7,8}$ stretch in the middle and two short flanking regions. The resulting domain formation was visible as ordered supramolecular structures and models for this interaction are presented (Fig. 6). A review of their work as well as that of others is seen in Ref. [89].

4.7. Manipulation of solid-supported bilayers

For some application it might be desirable to change or even reversibly switch the properties of lipid bilayers. Two examples illustrate that the AFM can be useful to characterize such manipulations. Last *et al*. [90] prepared DSPC membranes on mica by vesicle fusion. To the DSPC bilayers they add a synthetic lipid (PSIDA), which can bind copper ions (Cu^{2+}). They observe that PSIDA aggregates reversibly when no Cu^{2+} is present. By adding or withdrawing Cu^{2+} they could reversibly induce phase separation.

In order to form stable bilayers Morigaki *et al*. used a photopolymerizable diacetylene phospholipid (1,2-*bis*(10,12-tricosadiynoyl)-*sn*-glycero-3-phosphocholine) [91]. These lipids were transferred by LB and Schäfer transfer onto mica.

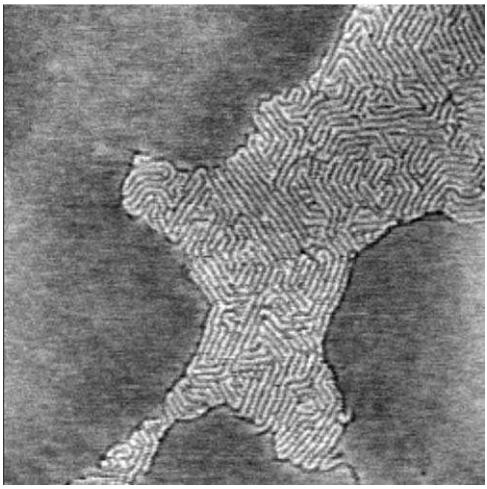

Fig. 6. DPPC bilayers with 2 mol% of a peptide WALP23, which contains tryptophanes as flanking residues. The width is 500 nm.The image was kindly provided by B. de Kruijff [89].

Then they were polymerized by UV light. Bilayers treated in this way were less sensitive to rinsing with sodium dodecyl sulfate. By using a mask for the illumination process the authors could form micropatterns of lipid bilayers on the surface.

Until now we only reported AFM studies, where the AFM was used to analyze lipid bilayers. It can also be used for manipulation and for doing lithography. Creating patterns of microstructured arrays of functional material is of interest in many areas of current surface science and microsensing techniques. Mueller *et al*. [92] created polylysine or protein islands in the lipid bilayer. Therefore, first a solid-supported lipid bilayer was formed by spontaneous vesicle fusion. The vesicle suspension was replaced by a solution containing polylysine (or the protein). Polylysine tends to bind to the solid support. It is, however, prevented from adsorption by the lipid bilayer. By scanning a certain area several times at high force in the presence of the polymer in solution, islands of polylysine were created within the lipid bilayers (Fig. 7). The experiments suggest that at least part of the polylysine is anchored to the solid support below the lipid bilayer.

At this point it is appropriate not only to discuss deliberate manipulation of lipid bilayers but also changes of the bilayers during the imaging process. The question ‘‘how does the AFM tip change the structure of a bilayer while imaging?’’ is certainly important for image interpretation. A distinction between bilayers in the fluid and the gel phase is necessary. This is for two reasons:

– In the fluid phase the lipid bilayer is a laterally homogeneous structure. The reason is that the time Δt required to image one pixel is between 0.1 and 10 ms. If we assume a lateral translational diffusion coefficient of $D = 10^{-11}$ m^2/s for

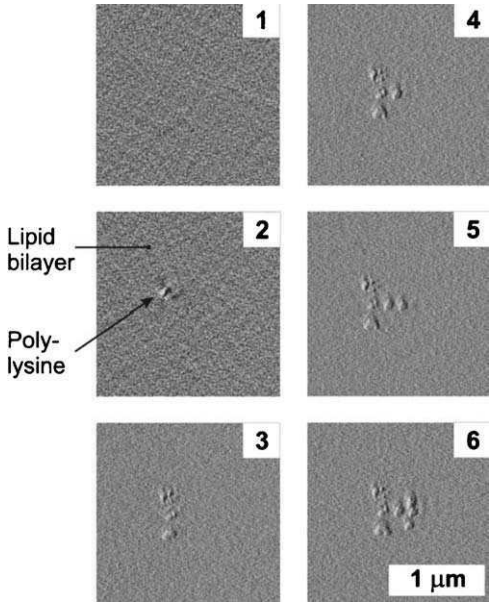

Fig. 7. Sequence of deliberately created structures by penetration of the lipid bilayer in force mode. The bilayer is a mixture of DOPS and DOPC formed by spontaneous vesicle fusion on mica. Image 1 shows a bare bilayer without features. By taking force curves at designated points in the presence of polylysine, patches of ~150 nm in diameter and 0.8 nm height could be formed. Deflection images 2–6 show 1, 3, 4, 5, and 7 deliberately created patches, respectively. The figure was taken from Ref. [92].

lipid molecules, in 0.1 ms the mean diffusion distance is $\sqrt{2D\Delta t} = 45$ nm. While the tip is imaging a single pixel the molecules underneath diffuse in and out at a high rate. Therefore, there is no hope to image individual lipid molecules in their fluid phase.

– The fluid phase is self-healing in the sense that even when the tip penetrates the lipid bilayer, after tip withdrawal the lipid bilayers spontaneously heals again.

In the gel phase it is in principle possible to image the packing structure of the lipid molecules [3,4] as long as they form two-dimensional crystals. However, one has to be careful: Beckmann *et al*. point out, that the tip of the AFM might change the molecular arrangement of the lipids in the gel phase and create structures, which have not been there before [93]. Repeated scanning in contact mode led not only to an ordered pattern (Schallamach waves) of a 1,2-dipentadecanoyl-*sn*-glycero-3-phosphocholine bilayer but also reduced the height of previously observed defects.

The stability of lipid bilayers is an important issue in AFM studies. Hui *et al*. [63] and later Benz *et al*. [94] studied the stability of DSPC, DPPE, and dilinoleoylphosphatidylcholine (DLPE) bilayers formed by LB transfer to mica. The

first ones are solid and for DPPE rows with spacing of 0.49 nm were observed. DSPC and DPPE were stable when being scanned with the AFM. The stability of the negatively charged DLPE, however, decreased with decreasing pH. Rädler *et al*. [95] highlight that the stability also depends on the scanning speed. At low tip velocity the tip can penetrate the lipid bilayer even at low force while at high speed a much higher force is needed for the tip to penetrate the bilayer.

5. FORCE MEASUREMENTS

5.1. Motivation, principle, and technique of force measurements

In the previous chapter we described microscopic applications of the AFM. Images at high resolution and in aqueous environment help to get information about phase separation, the influence of certain substances, and structural changes in lipid bilayers. In this chapter we focus on another application of the AFM: force measurements. In a force measurement the bilayer is not scanned laterally but it is moved up and down with respect to the tip, while measuring the cantilever deflection. The result of such a measurement is a graph, which shows the cantilever deflection Δz_c *versus* the height position of the piezo. From this, a force-*versus*-distance curve, briefly called ''force curve'', is calculated by multiplying the cantilever deflection with its spring constant K to obtain the force, $F = K \cdot \Delta z_c$, and subtracting the cantilever deflection from the height position to obtain the distance.

When measuring force curves on lipid bilayer often a jump of the tip is observed once a certain threshold force has been exceeded (Fig. 8). Such jumps occur not only on solid-supported lipid bilayers [96–103] but also in other systems such as surfactant layers on various substrates [104–107]. This jump is interpreted as a penetration of the AFM tip through the film.

Force curves are highly relevant for several reasons. First, they provide information, which helps interpreting images. Therefore, we first need to understand and interpret force curves correctly. Second, they contain information on bilayer properties such as electric charge or stability. For example, for a relatively unstable bilayer we expect a low breakthrough force while for a stable bilayer we expect a high breakthrough force. Third, once the technique is developed enough we might be able to use force experiments to get information about bilayer–bilayer or bilayer–protein interaction or even about the influence of proteins on the interaction between two bilayers [108].

5.2. Understanding tip–sample interactions

In a series of papers Schneider, Dufrêne, Lee *et al*. [96–98] studied the influence of the tip chemistry on the tip–lipid bilayer interaction. To make a tip with a defined

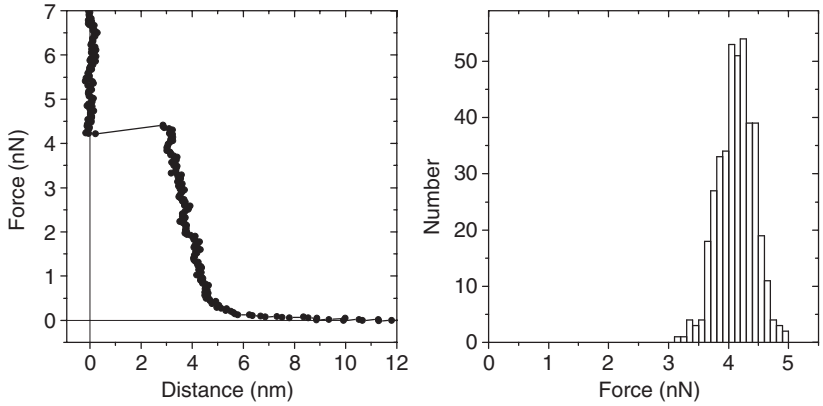

Fig. 8. Left: A typical approach part of a force curve measured on a lipid bilayer of DOTAP on mica with a standard silicon nitride tip in aqueous buffer (150 mM NaCl, 5 mM KH_2PO_4, pH 7.4). The lipid bilayer was formed by spontaneous vesicle fusion. Right: Distribution of breakthrough forces observed in one experiment. For details see Ref. [111].

surface chemistry, they evaporated 2–4 nm of chromium plus 15–60 nm of gold onto commercial silicon nitride tips. Chromium serves as ''glue'', because gold evaporated directly on silicates tends to come off when it gets into contact with water. Afterwards, the tips were immersed in a 0.01 mM ethanolic solution of mercapto hexadecanol or mercapto hexadecane for several hours. The thiols spontaneously form a dense, ordered monolayer on gold. With mercapto hexadecane a more hydrophilic surface is formed while with mercapto hexadecane a hydrophobic surface is produced. With these tips they studied different lipid bilayers formed by LB transfer on mica. The first leaflet was DSPE, which provides a relatively rigid substrate for the second leaflet of DSPE, monogalactosyldiglyceride (MGDG), digalactosyldiglyceride (DGDG), or DOPE. With hydrophilic tips they observe breakthrough forces, which depend on the lipid. It is zero for DOPE in the second layer and increases from DSPE to MGDG and to DGDG. With hydrophobic tips the breakthrough force is always zero. Also pull-off forces are much higher with hydrophobic tips. This is the first clear proof that the tip chemistry drastically changes force curves.

5.3. Quantitative description of force curves

Dûfrene *et al*. [98] also started analyzing force curves quantitatively. Before the jump-in the bilayer is compressed. They fit this part using Hertz model of elastic compression [109]. Hertz calculated the force F *versus* indentation δ for two spheres. If we assume that the tip is described by a sphere of radius R (which corresponds to the tip radius of curvature) and that it is infinitely stiff compared to

the relatively soft lipid bilayer, the following relation is obtained:

$$F = \frac{4E}{3\pi} \cdot \sqrt{R\delta^3} \tag{1}$$

Here, E is Youngs modulus of the lipid. In Hertz model surface forces and adhesion are neglected. Only the elastic compression is taken into account. Dufrêne *et al*. get Youngs moduli of $E = 17$ and 21×10^7 Pa for DSPE and DGDG, respectively.

Hertz treated the solid surface as one continuous body. In reality, the lipid bilayer is only a thin layer on top of a relatively incompressible surface. For this reason the elastic foundation model [110] is more likely to be appropriate. In the elastic foundation model force and indentation are related by

$$F = \frac{\pi E R \delta^2}{h}, \tag{2}$$

where h is the thickness of the uncompressed lipid bilayer. Though both equations are different, Youngs moduli obtained from fitting experimental force curves are not much different.

Intuitively it is obvious that the breakthrough (jump-in) force is a measure for the stability of the lipid bilayer. Stable solid-supported bilayers should break at a higher force than unstable layers. One of the authors developed a theory to describe this layer rupture and to relate microscopic parameters to measurable quantities [100]. It was assumed that the tip has to overcome an activation energy before the bilayer ruptures. A universal relation between the force dependence of the activation energy and the approaching velocity of the tip is derived. One prediction of the theory is that the breakthrough force should increase with increasing approaching speed. This was indeed observed [101,111]. Two complementary models for calculating the activation energy are presented: A continuum nucleation model and a discrete molecular model. Both models predict a narrow distribution of breakthrough forces in agreement with experimental results.

One promising step forward with respect to a quantitative evaluation of force curves is the cluster analysis introduced by Janshoff *et al*. [103]. In a cluster analysis not only the distribution of one parameter is plotted but it is correlated with another parameter. For example, rather than just plotting how often a certain breakthrough force is observed the breakthrough force and the breakthrough distance are plotted on the two axes and each result is represented by one point in this plot (Fig. 9). From the density of points the distribution and at the same time a possible correlation between the two parameters is deducible.

5.4. Surface charges

In aqueous medium most surfaces are charged. Also the tip of an AFM usually bears a surface charge, which depends on pH. At neutral pH it is negatively

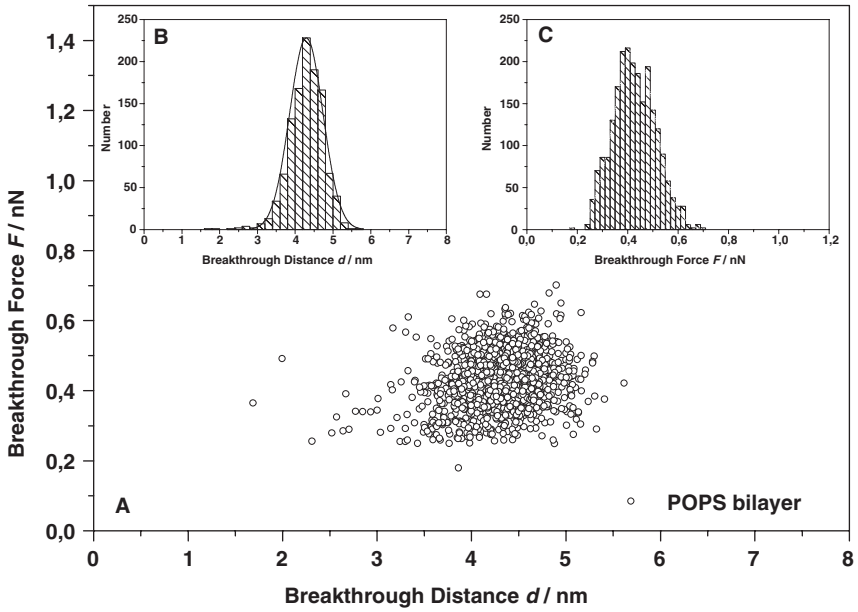

Fig. 9. Distribution of breakthrough forces and jump-in distances shown in a two-dimensional plot. The figure shows results of an AFM experiment with a POPS bilayer. The figure was kindly provided by A. Janshoff [103].

charged. These surface charges cause the diffuse electric double layer to form. When the double layers of tip and sample overlap, they experience an electrostatic double-layer force. It can be approximated by [112]

$$F = \frac{4\pi\sigma_t\sigma_s R\lambda_D}{\varepsilon\varepsilon_0} \cdot e^{-D/\lambda_D} \tag{3}$$

Here, σ_t and σ_s are the charge densities of tip and sample surface, ε and ε_0 are the dielectric permittivity of water and the permittivity of free space, D is the distance, and λ_D is the Debye length. For monovalent salt it is $\lambda_D = 0.3/\sqrt{c}$ nm, where the salt concentration has to be given in mol/L. Equation (3) is valid for $D \gg \lambda_D$.

The double-layer force is proportional to the surface charge density of the sample. Thus, it can be used to detect and measure local surface charge densities. Local surface charges were first measured on purple membranes [113]. Purple membranes are membrane fragments isolated from the plasma membrane of *Halobacterium halobium*, which contain the membrane protein bacteriorhodopsin, a light-driven proton pump. The effect of the electrostatic force on imaging was further analyzed by Müller and Engel [114]. A systematic study on pure lipid bilayers and images of the electric charge distribution are presented by Rotsch and Radmacher [115]. They studied patches of DODAB on mica. DODAB is positively charged, mica is negative. Since the AFM tip is also

negatively charged and thus repelled by mica, they observed a reversal of the image contrast at very low loading force. Mica appeared higher than the DODAB patches because the tip was repelled by the electrostatic double-layer force and scanned some distance over the actual contact zone.

5.5. Lipid–lipid interaction

The force measurements discussed until now were done in order to better understand images of solid-supported bilayers and to get more information about the stability and formation of solid-supported membranes. In addition, the AFM can be used to study bilayer–bilayer interaction. The interactions between lipid bilayers have been studied for the last 30 years, with different methods and under various conditions [116–122]. The motivation comes from two directions, one biological and one physico-chemical. From the biological point of view, knowledge about the interaction between membranes is essential to understand processes such as exo- and endocytosis, intracellular trafficking, cell division, adhesion, fusion, metastasis. From the physico-chemical point of view, lipid bilayers are one possible stable phase, namely a lamellar phase, adopted by amphiphilic molecules in aqueous medium. Questions related to the properties of membranes, the internal organization of a bilayer, the understanding of vesicle fusion by rupturing the bilayers and, the forces governing this interaction may be investigated. By clarifying this latter aspect, a quantitative answer to some of the biological questions may be obtained.

Several forces governing bilayer–bilayer interactions have been identified [121]. The van der Waals force is long-range, attractive, and relatively weak. It is opposed by a short-range repulsive force. This repulsive force decays exponentially with a typical decay length of 0.2–0.5 nm.It is not yet clear which effect dominates this short range repulsion: the hydration pressure, arising from ordering of water molecules by the hydrophilic head groups of the lipids, or an entropic ''protrusion'' effect of molecular groups that are thermally excited to protrude from the fluid-like lipid bilayers. Charged lipids repel each other by electrostatic double-layer forces. For bilayers, which are not supported on a solid surface, an undulation or fluctuation pressure, due to thermally driven undulations of the entire bilayer surface which couple hydrodynamically to other bilayers keep the surface apart.

Several methods have been developed to determine the forces between two lipid bilayers. In the osmotic stress method [123–125], a suspension of multiwalled vesicles or oriented multilayers in the lamellar phase is equilibrated in an aqueous solution containing solute such as dextran or polyvinylpyridine. These solutes cannot enter the lipid phase and they compete for water with lipid multilayers, thereby applying an osmotic pressure. The spacing between the multilayers is measured by X-ray diffraction. In this way one obtains pressure-*versus*-spacing curves. One advantage of the osmotic stress method is that undulation forces can be measured because the lipid bilayers are freely suspended.

An alternative device is the surface forces apparatus (SFA). In the SFA the force between two lipid bilayers supported on two crossed mica cylinders is measured directly [94,126]. In a third method the interaction between two large vesicles formed at the end of micropipettes and imaged by a light microscope is determined [127]. The method is highly sensitive and small pressures can be applied and detected. It also allows determining the mechanical properties of membranes. Since the maximal pressure is given by the Laplace pressure and the size of the vesicles should be large enough for optical detection the method is restricted to low repulsive forces.

How can the AFM be used to measure forces between two bilayers? The answer is relatively simple: We only need to form a lipid bilayer on the tip. Unfortunately this is difficult to achieve. Though, many researchers believe that often a second bilayer has formed on the tip, it seems to be not reproducible and the force to break through the bilayer on the tip seems to be insignificantly small (e.g. Ref. [102]). Why are bilayers at the tip surface so unstable? One possible reason why bilayers adsorb spontaneously to a planar surface, but not to the tip, is the high curvature. The energy per unit area required to bend a bilayer with zero spontaneous curvature to a spherical cap is $2\kappa/R^2$. Here, κ is the bending rigidity, also called bending elastic modulus. For phosphatidylcholine bilayers in the liquid phase κ is typically 10^{-19} J [128–132]. For the spontaneous adsorption of a bilayer, the adsorption energy must be higher than the bending energy. With typical adsorption energies per unit area of $W_A = 0.2 - 2 \times 10^{-4}$ J/m^2 [128,133] the minimal radius of curvature is estimated to be $R = \sqrt{2\kappa/W_A} = 100 - 32\,\text{nm}$, respectively. Only for a strong adhesion between the bilayer and the solid surface we expect that the tip surface be covered. The stronger the adsorption, the smaller the tip can be. In any case: very sharp tips are not going to be covered by bilayers.

To overcome this problem and to spontaneously adsorb lipid bilayers also on the AFM tip, Pera *et al*. [134] first coated tips with gold and a monolayer of mercapto undecanol. Calculations indicate that long-chain hydroxyl terminated

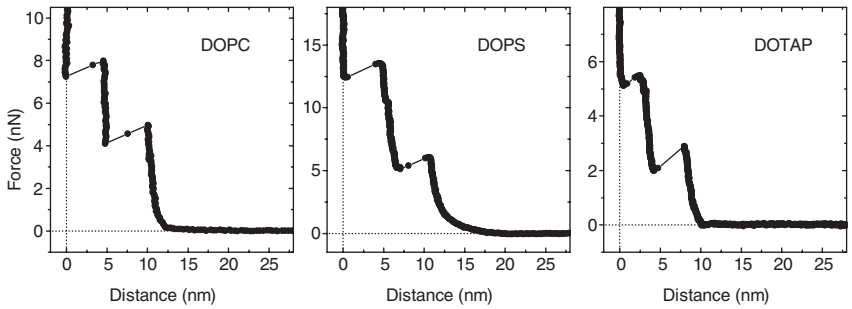

Fig. 10. Typical force-*versus*-distance curve measured on a planar mica surface in buffer after exposure to DOPC, DOPS, and DOTAP vesicles. The AFM tips were first coated with chromium and gold and then with a monolayer of mercapto undecanol ($HS(CH_2)_{11}OH$). For details see Ref. [134].

alkyl thiols tend to enhance spontaneous vesicle fusion because of an increased van der Waals attraction as compared to short-chain thiols. When coating AFM tips in this way indeed two jumps of typically 4 nm were observed (Fig. 10). In this way, the interaction between DOPC, dioleoylphosphatidylserine (DOPS), and DOTAP bilayers could be measured.

6. CONCLUSION

Solid-supported bilayers can routinely be imaged with the AFM in aqueous environment, in different phases, and at different temperature. Force measurements provide information about the mechanical stability and the electric charge. One of the challenges is to get even more detailed information on the lateral organisation of the lipids, even when they are not separated into large clearly distinct domains. Therefore, an even better understanding of the tip–sample is required.

REFERENCES

[1] G. Binnig, C.F. Quate, C. Gerber, Atomic force microscope, Phys. Rev. Lett. 56 (1986) 930–933.
[2] B. Drake, C.B. Prater, A.L. Weisenhorn, S.A.C. Gould, T.R. Albrecht, C.F. Quate, D.S. Cannell, H.G. Hansma, P.K. Hansma, Imaging crystals, polymers, and processes in water with the atomic force microscopy, Science 243 (1989) 1586–1589.
[3] A.L. Weisenhorn, M. Egger, F. Ohnesorge, S.A.C. Gould, S.P. Heyn, H.G. Hansma, R.L. Sinsheimer, H.E. Gaub, P.K. Hansma, Molecular-resolution images of Langmuir-Blodgett films and DNA by atomic force microscopy, Langmuir 7 (1991) 8–12.
[4] J.A.N. Zasadzinski, C.A. Helm, M.L. Longo, A.L. Weisenhorn, S.A.C. Gould, P.K. Hansma, Atomic force microscopy of hydrated phosphatidylethanolamine bilayers, Biophys. J. 59 (1991) 755–760.
[5] A.L. Weisenhorn, P.K. Hansma, T.R. Albrecht, C.F. Quate, Forces in atomic force microscopy in air and water, Appl. Phys. Lett. 54 (1989) 2651–2653.
[6] E. Meyer, H. Heinzelmann, P. Grütter, T. Jung, H.R. Hidber, H. Rudin, H.J. Güntherodt, Atomic force microscopy for the study of tribology and adhesion, Thin Solid Films 181 (1989) 527–544.
[7] A.L. Weisenhorn, P. Maivald, H.-J. Butt, P.K. Hansma, Measuring adhesion, attraction, and repulsion between surfaces in liquids with an atomic force microscope, Phys. Rev. B 45 (1992) 11226–11232.
[8] J.H. Hoh, J.P. Revel, P.K. Hansma, Tip-sample interactions in atomic force microscopy: I. Modulating adhesion between silicon nitride and glass, Nanotechnology 2 (1991) 119–122.
[9] S. Manne, H.E. Gaub, Force microscopy: Measurement of local interfacial forces and surface stresses, Curr. Opin. Colloid Interface Sci. 2 (1997) 145–152.
[10] H.J. Butt, B. Cappella, M. Kappl, Force-measurements with the atomic force microscope, Surf. Sci. Reports 59 (2000) 1–152.
[11] J. Yang, L.K. Tamm, A.P. Somlyo, Z. Shao, Promises and problems of biological atomic force microscopy, J. Microscopy 171 (1993) 183–198.
[12] D.J. Müller, J.B. Heymann, F. Oesterhelt, C. Möller, H. Gaub, G. Büldt, A. Engel, Atomic force microscopy of native purple membrane, Biochim. Biophys. Acta 1460 (2000) 27–38.

[13] P.J.L. Werten, H.-W. Rémigy, B.L. de Groot, D. Fotiadis, A. Philippsen, H. Stahlberg, H. Grubmüller, A. Engel, Progress in the analysis of membrane protein structure and function, FEBS Lett. 529 (2002) 65–72.
[14] Y.F. Dufrêne, G.U. Lee, Advances in the charaterization of supported lipid films with the atomic force microscope, Biochim. Biophys. Acta 1509 (2000) 14–41.
[15] A. Janshoff, C. Steinem, Scanning force microscopy of artifical membranes, Chem. Phys. Chem. 2 (2001) 798–808.
[16] H.-J. Butt, K. Graf, M. Kappl, Physics and Chemistry of Interfaces, Wiley-VCH, Berlin, 2003.
[17] H.-J. Butt, P. Siedle, K. Seifert, K. Fendler, T. Seeger, E. Bamberg, A.L. Weisenhorn, K. Goldie, A. Engel, Scan speed limit in atomic force microscopy, J. Microscopy 169 (1993) 75–84.
[18] F.J. Elmer, M. Dreier, Eigenfrequencies of a rectangular atomic force microscope cantilever in a medium, J. Appl. Phys. 81 (1997) 7709–7714.
[19] T.E. Schäffer, Force spectroscopy with a large dynamic range using small cantilevers and an array detector, J. Appl. Phys. 91 (2002) 4739–4746.
[20] P. Siedle, H.-J. Butt, E. Bamberg, D.N. Wang, W. Kühlbrandt, J. Zach, M. Haider, Determining the form of atomic force microscope tips, Inst. Phys. Conf. Ser. 130 (1992) 361–364.
[21] G. Hüttl, V. Klemm, R. Popp, F. Simon, E. Müller, Tailored colloidal probes and their easy way TEM investigation, Surf. Interface Anal. 33 (2002) 50–53.
[22] D.J. Müller, C.A. Schoenenberger, G. Büldt, A. Engel, Immuno-atomic force microscopy of purple membrane, Biophys. J. 70 (1996) 1796–1802.
[23] I. Revenko, R. Proksch, Magnetic and acoustic tapping mode microscopy of liquid phase phopholipid bilayers and DNA molecules, J. Appl. Phys. 87 (2000) 526–533.
[24] S.N. Magonov, V. Elings, M.H. Whangbo, Phase imaging and stiffness in tapping-mode atomic force microscopy, Surf. Sci. Lett. 375 (1997) L385–L391.
[25] R. Garcia, R. Pérez, Dynamic atomic force microscopy methods, Surf. Sci. Rep. 47 (2002) 197–301.
[26] L.K. Tamm, Z. Shao, The application of AFM to biomembranes, in: P.I. Haris, D. Chapman (Eds.), Biomembrane Structures, IOS Press, Amsterdam, 1998, pp. 169–185.
[27] I. Langmuir, V.J. Schaefer, J. Am. Chem. Soc. 60 (1937) 1351–1360.
[28] I. Langmuir, Mechanical properties of monomolecular films, J. Franklin Inst. 218 (1934) 143–171.
[29] K.B. Blodgett, Films built by depositing successive monomolecular layers on a solid surface, J. Am. Chem. Soc. 57 (1935) 1007–1022.
[30] A.A. Brian, H.M. McConnell, Allogeneic stimulation of cytotoxic T cells by supported planar membranes, Proc. Natl. Acad. Sci. USA 81 (1984) 6159–6163.
[31] R.G. Horn, Direct measurement of the force between two lipid bilayers and observation of their fusion, Biochim. Biophys. Acta 778 (1984) 224–228.
[32] T.M. Bayerl, M. Bloom, Physical properties of single phospholipid bilayers adsorbed to micro glass beads, Biophys. J. 58 (1990) 357–362.
[33] S.J. Johnson, T.M. Bayerl, D.C. McDermott, G.W. Adam, A.R. Rennie, R.K. Thomas, E. Sackmann, Structure of an adsorbed dimyristoylphosphatidylcholine bilayer with specular reflection of neutrons, Biophys. J. 59 (1991) 289–294.
[34] C. Naumann, T. Brumm, T.M. Bayerl, Phase transition behavior of single phosphatidylcholine bilayers on a solid spherical support studied by DSC, NMR and FT-IR, Biophys. J. 63 (1992) 1314–1319.
[35] B.W. Koenig, S. Krueger, W.J. Orts, C.F. Majkrzak, N.F. Berk, J.V. Silverton, K. Gawrisch, Neutron reflectivity and atomic force microscopy studies of a lipid bilayer in water adsorbed to the surface of a silicon single crystal, Langmuir 12 (1996) 1343–1350.
[36] R. Rapuano, A.M. Carmona-Ribeiro, Physical adsorption of bilayer membranes on silica, J. Colloid Interface Sci. 193 (1997) 104–111.

[37] E. Reimhult, F. Höök, B. Kasemo, Intact vesicle adsorption and supported biomembrane formation from vesicles in solution: Influence of surface chemistry, vesicle size, temperature, and osmotic pressure, Langmuir 19 (2003) 1681–1691.
[38] G. Puu, I. Gustafson, Planar lipid bilayers on solid supports from liposomes – factors of importance for kinetics and stability, Biochim. Biophys. Acta 1327 (1997) 149–161.
[39] J.T. Groves, S.G. Boxer, Electric field-induced concentration gradients in planar supported bilayers, Biophys. J. 69 (1995) 1972–1975.
[40] D. Ottenbacher, F. Jähnig, W. Göpel, A prototype biosensor based on transport proteins: electrical transducers applied to lactose permease, Sensors and Actuators B 13–14 (1993) 173–175.
[41] T.E. Starr, N.L. Thompson, Formation and characterization of planar phospholipid bilayers supported on TiO2 and SrTiO3 single crystals, Langmuir 16 (2000) 10301–10308.
[42] J. Mou, J. Yang, Z. Shao, Tris(hydroxymethyl)aminomethane ($C_4H_{11}NO_3$) induced a ripple phase in supported unilamellar phospholipid bilayers, Biochemistry 33 (1994) 4439–4443.
[43] Z.V. Leonenko, A. Carini, D.T. Cramb, Supported planar bilayer formation by vesicle fusion: the interaction of phospholipid vesicles with surfaces and the effect of gramicidin on bilayer properties using atomic force microscopy, Biochim. Biophys. Acta 1509 (2000) 131–147.
[44] S. Lingler, I. Rubinstein, W. Knoll, A. Offenhäuser, Fusion of small unilamellar lipid vesicles to alkanthiol and thiolipid self-assembled monolayers on gold, Langmuir 13 (1997) 7085–7091.
[45] A.T.A. Jenkins, T. Neumann, A. Offenhäuser, Surface plasmon microscopy measurements of lipid vesicle adsorption on a micropatterned self-assembled monolayer, Langmuir 17 (2001) 265–267.
[46] L.K. Tamm, E. Kalb, Microspectrofluorometry on supported planar bilayers, in: S.G. Schulman, (Ed.), Molecular Luminescence Spectroscopy, Wiley, New York, 1993, pp. 253–305.
[47] I. Reviakine, A. Brisson, Formation of supported phospholipid bilayers from unilamellar vesicles investigated by atomic force microscopy, Langmuir 16 (2000) 1806–1815.
[48] V.P. Zhdanov, C.A. Keller, K. Glasmäster, B. Kasemo, Simulation of adsorption kinetics of lipid vesicles, J. Chem. Phys. 112 (2000) 900–909.
[49] C.A. Keller, B. Kasemo, Surface specific kinetics of lipid vesicle adsorption measured with a quartz crystal microbalance, Biophys. J. 75 (1998) 1397–1402.
[50] G. Csúcs, J.J. Ramsden, Interaction of phospholipid vesicles with smooth metal-oxide surfaces, Biochim. Biophys. Acta 1369 (1998) 61–70.
[51] R. Lipowsky, U. Seifert, Adhesion of vesicles and membranes, Mol. Cryst. Liq. Cryst. 202 (1991) 17–25.
[52] U. Seifert, Configurations of fluid membranes and vesicles, Adv. Phys. 46 (1997) 13–137.
[53] J. Jass, T. Tjärnhage, G. Puu, From liposomes to supported, planar bilayer structures on hydrophilic and hydrophobic surfaces: An atomic force microscope study, Biophys. J. 79 (2000) 3153–3163.
[54] J. Nissen, S. Gritsch, G. Wiegand, J.O. Rädler, Wetting of phospholipid membranes on hydrophilic surfaces – concepts towards self-healing membranes, Eur. Phys. J. B 10 (1999) 335–344.
[55] I. Vikholm, J. Peltonen, O. Teleman, Atomic force microscope images of lipid layers spread from vesicle suspension, Biochim. Biophys. Acta 1233 (1995) 111–117.
[56] B. Pignataro, C. Steinem, H.J. Galla, H. Fuchs, A. Janshoff, Specific adhesion of vesicles monitored by scanning force microscopy, Biophys. J. 78 (2000) 487–498.
[57] H. Egawa, K. Furusawa, Liposome adhesion on mica surface studied by atomic force microscopy, Langmuir 15 (1999) 1660–1666.

[58] A.S. Muresan, K.Y.C. Lee, Shape evolution of lipid bilayer patches adsorbed on mica: an atomic force microscopy study, J. Phys. Chem. 105 (2001) 852–855.
[59] R. Richter, A. Mukhopadhyay, A. Brisson, Pathways of lipid vesicle deposition on solid surfaces: A combined QCM-D and AFM study, Biophys. J. 85 (2003) 3035–3047.
[60] B. Seantier, C. Breffa, O. Felix, G. Decher, In situ investigations of the formation of mixed supported lipid bilayers close to the phase transition temperature, Nanoletters 4 (2004) 5–10.
[61] M. Deleu, M. Paquot, P. Jacques, P. Thonart, Y. Adriaensen, Y.F. Dufrêne, Nanometer scale organization of mixed surfactin/phosphatidylcholine monolayers, Biophys. J. 77 (1999) 2304–2310.
[62] C.G. Hollars, R.C. Dunn, Submicron structure in l-α−dipalmitoylphosphatidylcholine monolayers and bilayers probed with confocal, atomic force, and near-field microscopy, Biophys. J. 75 (1998) 342–353.
[63] S.W. Hui, R. Viswanathan, J.A. Zasadzinski, J.N. Israelachvili, The structure and stability of phospholipid bilayers by atomic force microscopy, Biophys. J. 68 (1995) 171–178.
[64] Y.F. Dufrêne, W.R. Barger, J.B.D. Green, G.U. Lee, Nanometer-scale surface properties of mixed phospholipid monolayers and bilayers, Langmuir 13 (1997) 4779–4784.
[65] F. Tokumasu, A.J. Jin, G.W. Feigenson, J.A. Dvorak, Nanoscopic lipid domain dynamics revealed by atomic force microscopy, Biophys. J. 84 (2003) 2609–2618.
[66] F. Tokumasu, J. Hwang, J.A. Dvorak, Heterogeneous molecular distribution in supported multicomponent lipid bilayers, Langmuir 20 (2004) 614–618.
[67] A.R. Burns, Domain structure in model membrane bilayers investigated by simultaneous atomic force microscopy and fluorescence imaging, Langmuir 19 (2003) 8358–8363.
[68] G. Valdrè, A. Alessandrini, U. Muscatello, U. Valdrè, V. Vannini, Coexistence of nanoscopic domains in synthetic membranes, Phil. Mag. B 79 (1999) 1549–1559.
[69] T. Kaasgaard, O.G. Mouritsen, K. Jörgensen, Lipid domain formation and ligand-receptor distribution in lipid bilayer membranes investigated by atomic force microscopy, FEBS Lett. 515 (2002) 29–34.
[70] A.E. McKierna, T.V. Ratto, M.L. Longo, Domain growth, shapes, and topology in cationic lipid bilayers on mica by fluorescence and atomic force microscopy, Biophys. J. 79 (2000) 2605–2615.
[71] A.F. Xie, R. Yamada, A.A. Gewirth, S. Granick, Materials science of the gel to fluid phase transition in a supported phospholipid bilayer, Phys. Rev. Lett. 89 (2002) 246103.
[72] F. Tokumasu, A.J. Jin, J.A. Dvorak, Lipid membrane phase behaviour elucidated in real time by controlled environment atomic force microscopy, J. Electron Microscopy 51 (2002) 1–9.
[73] M.C. Giocondi, L. Pacheco, P.E. Milhiet, C.L. Grimellec, Temperature dependence of the topology of supported dimirystoyl-distearoyl phosphatidylcholine bilayers, Ultramicroscopy 86 (2001) 151–157.
[74] M.C. Giocondi, V. Vié, E. Lesniewska, P.E. Milhiet, M. Zinke-Allmang, C. Le Grimellec, Phase topology and growth of single domains in lipid bilayers, Langmuir 17 (2001) 1653–1659.
[75] R. Koynova, M. Caffrey, Phases and phase transitions of phosphatidylcholines, Biochim. Biophys. Acta 1376 (1998) 91–145.
[76] C. Leidy, T. Kaasgaard, J.H. Crowe, O.G. Mouritsen, K. Jorgensen, Ripples and the formation of anisotropic lipid domains: Imaging two-component supported double bilayers by atomic force microscopy, Biophys. J. 83 (2002) 2625–2633.
[77] T. Kaasgaard, C. Leidy, J.H. Crowe, O.G. Mouritsen, K. Jorgensen, Temperature-controlled structure and kinetics of ripple phases in one- and two-component supported lipid bilayers, Biophys. J. 85 (2003) 350–360.

[78] D.M. Czajkowsky, C. Huang, Z. Shao, Ripple phase in asymmetric unilamellar bilayers with saturated and unsaturated phospholipids, Biochemistry 34 (1995) 12501–12505.
[79] K. Simons, E. Ikonen, Functional rafts in cell membranes, Nature 387 (1997) 569–572.
[80] H.A. Rinia, M.M.E. Snel, J.P.L.M. van der Erden, B. de Kruijff, Visualization detergent resistant domains in model membranes with atomic force microscopy, FEBS Lett. 501 (2001) 92–96.
[81] B.Y. van Duyl, D. Ganchev, V. Chupin, B. de Kruijff, J.A. Killian, Sphingomyelin is much more effective than saturated phosphatidylcholine in excluding unsaturated phosphatidylcholine from domains formed with cholesterol, FEBS Lett. 547 (2003) 101–106.
[82] C. Yuan, J. Furlong, P. Burgos, L.J. Johnston, The size of lipid rafts: An atomic force microscopy study of ganglioside GM1 domains in sphingomyelin/DOPC/cholesterol membranes, Biophys. J. 82 (2002) 2526–2535.
[83] P.E. Milhiet, M.C. Giocondi, O. Baghdadi, F. Ronzon, B. Roux, C.L. Grimellec, Spontaneous insertion and partitioning of alkaline phosphatase into model lipid rafts, EMBO Rep. 3 (2002) 485–490.
[84] M.C. Giocondi, Use of cyclodextrin for AFM monitoring of model raft formation, Biophys. J. 86 (2004) 861–869.
[85] J. Mou, J. Yang, C. Huang, Z. Shao, Alcohol induces interdigitated domains in unilamellar phosphatidylcholine bilayers, Biochemistry 33 (1994) 9981–9985.
[86] R.L. McClain, J.J. Breen, The image-based observation of the L_bl-to-L_b' phase transition in solid-supported lipid bilayers, Langmuir 17 (2001) 5121–5124.
[87] A. Janshoff, D.T. Bong, C. Steinem, J.E. Johnson, M.R. Ghadiri, An animal virus-derived peptide switches membrane morphology: Possible relevance to nodaviral transfection process, Biochemistry 38 (1999) 5328–5336.
[88] H.A. Rinia, J.W.P. Boots, D.T.S. Rijkers, R.A. Kik, M.M.E. Snel, R.A. Demel, J.A. Killian, J.P.L.M. van der Erden, B. de Kruijff, Domain formation in phosphatidylcholine containing transmembrane peptides: Specific effects of flanking residues, Biochemistry 41 (2002) 2814–2824.
[89] H.A. Rinia, B. de Kruijff, Imaging domains in model membranes with the atomic force microscope, FEBS Lett. 504 (2001) 194–199.
[90] J.A. Last, T.A. Waggoner, D.Y. Sasaki, Lipid membrane reorganization induced by chemical recognition, Biophys. J. 81 (2001) 2737–2742.
[91] K. Morigaki, H. Schönherr, C.W. Frank, W. Knoll, Photolithographic polymerization of diacetylene-containing phospholipid bilayers studied by multimode atomic force microscopy, Langmuir 19 (2003) 6994–7002.
[92] H. Mueller, H.-J. Butt, E. Bamberg, Atomic force microscopy deposition of poly-L-lysine structures onto lipid bilayers, Langmuir 16 (2000) 9568–9570.
[93] M. Beckmann, P. Nollert, H.-A. Kolb, Manipulation and molecular resolution of a phosphatidylcholine-supported planar bilayer by atomic force microscopy, J. Membrane Biol. 161 (1998) 227–233.
[94] M. Benz, T. Gutsmann, N. Chen, R. Tadmor, J. Israelachvili, Correlation of AFM and SFA measurements concerning the stability of supported lipid bilayers, Biophys. J. 86 (2004) 870–879.
[95] J. Rädler, M. Radmacher, H.E. Gaub, Velocity-dependent forces in atomic force microscopy imaging of lipid films, Langmuir 10 (1994) 3111–3115.
[96] J. Schneider, Y.F. Dufrene, W.R. Barger, G.U. Lee, Atomic force microscope image contrast mechanisms on supported lipid bilayers, Biophys. J. 79 (2000) 1107–1118.
[97] J. Schneider, W. Barger, G.U. Lee, Nanometer scale surface properties of supported lipid bilayers measured with hydrophobic and hydrophilic atomic force microscope probes, Langmuir 19 (2003) 1899–1907.
[98] Y.F. Dufrêne, T. Boland, J.W. Schneider, W.R. Barger, G.U. Lee, Characterization of the physical properties of model biomembranes at the nanometer scale with the atomic force microscope, Faraday Discuss. 111 (1998) 79–94.

[99] R.P. Richter, A. Brisson, Characterization of lipid bilayers and protein assemblies supported on rough surfaces by atomic force microscopy, Langmuir 19 (2003) 1632–1640.
[100] H.-J. Butt, V. Franz, Rupture of molecular thin films observed in atomic force microscopy. I. Theory, Phys. Rev. E 66 (2002) 031601.
[101] S. Loi, G.X. Sun, V. Franz, H.-J. Butt, Rupture of molecular thin films observed in atomic force microscopy. II. Experiment, Phys. Rev. E 66 (2002) 031602.
[102] L.M. Grant, F. Tiberg, Normal and lateral forces between lipid covered solids in solution: Correlation with layer packing and structure, Biophys. J. 82 (2002) 1373–1385.
[103] S. Künnecke, D. Krüger, A. Janshoff, Scrutiny of the failure of lipid membranes as a function of headgroups, chain length, and lamellarity measured by scanning force microscopy, Biophys. J. 86 (2004) 1545–1553.
[104] I. Burgess, C.A. Jeffrey, X. Cai, G. Szymanski, Z. Galus, J. Lipkowski, Direct visualization of the potential-controlled transformation of hemimicellar aggregates of dodecyl sulfate into a condensed monolayer at the Au(1 1 1) electrode surface, Langmuir 15 (1999) 2607–2616.
[105] W.A. Ducker, D.R. Clarke, Controlled modification of silicon nitride interactions in water via zwitterionic surfactant adsorption, Colloids & Surfaces A 94 (1994) 275–292.
[106] S. Manne, J.P. Cleveland, H.E. Gaub, G.D. Stucky, P.K. Hansma, Direct visualization of surfactant hemimicelles by force microscopy of the electric double layer, Langmuir 10 (1994) 4409–4413.
[107] M. Jaschke, H.-J. Butt, H.E. Gaub, S. Manne, Surfactant aggregates at a metal surface, Langmuir 13 (1997) 1381–1384.
[108] L.R. Fisher, A.R. Malloy, Molecular interactions of biomembranes, Annu. Rep. Prog. Chem., Sect. C 95 (1999) 373–400.
[109] H. Hertz, Über die Berührung fester elastischer Körper, J. Reine Angewandte Mathematik 92 (1882) 156–171.
[110] K.L. Johnson, Contact Mechanics, Cambridge University Press, Cambridge, 1985.
[111] V. Franz, S. Loi, H. Müller, E. Bamberg, H.-J. Butt, Tip penetration through lipid bilayers in atomic force microscopy, Colloids & Surfaces B 23 (2002) 191–200.
[112] H.-J. Butt, Measuring electrostatic, van der Waals, and hydration forces in electrolyte solutions with an atomic force microscope, Biophys. J. 60 (1991) 1438–1444.
[113] H.-J. Butt, Measuring local surface charge densities in electrolyte solutions with a scanning force microscope, Biophys. J. 63 (1992) 578–582.
[114] D.J. Müller, A. Engel, The height of biomolecules measured with the atomic force micoscope depends on electrostatic interactions, Biophys. J. 73 (1997) 1633–1644.
[115] C. Rotsch, M. Radmacher, Mapping local electrostatic forces with the atomic force microscope, Langmuir 13 (1997) 2825–2832.
[116] D.M. LeNeveu, R.P. Rand, V.A. Parsegian, D. Gingell, Measurement and modification of forces between lecithin bilayers, Biophys. J. 18 (1977) 209–230.
[117] S. Nir, M. Andersen, Van der Waals interactions between cell surfaces, J. Membrane Biol. 31 (1977) 1–18.
[118] L.J. Lis, M. McAlister, N. Fuller, R.P. Rand, V.A. Parsesgian, Interactions between neutral phospholipid bilayer membranes, Biophys. J. 37 (1982) 657–666.
[119] J. Marra, J. Israelachvili, Direct measurement of forces between phosphatidylcholine and phosphatidylethanolamine bilayers in aqueous electrolyte solutions, Biochemistry 24 (1985) 4608–4618.
[120] P.K.T. Persson, B.A. Bergenstrahl, Repulsive force in lecithin gylcol lamellar phases, Biophys. J. 47 (1985) 743–746.
[121] J.N. Israelachvili, H. Wennerström, Entropic force between amphiphilic surfaces in liquids, J. Phys. Chem. 96 (1992) 520–531.
[122] T.J. McIntosh, S.A. Simon, Short-range pressure between lipid bilayer membranes, Colloids & Surfaces A 116 (1996) 251–268.

[123] D.M. LeNeveu, R.P. Rand, V.A. Parsegian, Measurement of forces between lecithin bilayers, Nature 259 (1976) 601–603.
[124] V.A. Parsegian, N. Fuller, R.P. Rand, Measured work of deformation and repulsion between lecithin bilayers, Proc. Natl. Acad. Sci. USA 76 (1979) 2750–2754.
[125] R.V. McDaniel, T.J. McIntosh, S.A. Simon, Nonelectrolyte substitution for water in phosphatidylcholine bilayers, Biochim. Biophys. Acta 731 (1983) 97–108.
[126] C.A. Helm, J.N. Israelachvili, P.M. McGuiggan, Molecular mechanisms and forces involved in the adhesion and fusion of amphiphilic bilayers, Science 246 (1989) 919–922.
[127] E. Evans, M. Metcalfe, Free energy potential for aggregation of giant, neutral lipid bilayer vesicles by van der Waals attraction, Biophys. J. 46 (1984) 423–426.
[128] E. Evans, D. Needham, Physical properties of surfactant bilayer membranes: Thermal transitions, elasticity, rigidity, cohesion, and colloidal interactions, J. Phys. Chem. 91 (1987) 4219–4231.
[129] R.M. Servuss, W. Harbich, W. Helfrich, Measurement of the curvature-elastic modulus of egg lecithin bilayers, Biochim. Biophys. Acta 436 (1976) 900–903.
[130] E. Sackmann, H.P. Duwe, H. Engelhardt, Membrane bending elasticity and its role for shape fluctuations and shape transformations of cells and vesicles, Faraday Discuss. Chem. Soc. 81 (1986) 281–290.
[131] T.J. McIntosh, S. Advani, R.E. Burton, D.V. Zhelev, D. Needham, S.A. Simon, Experimental tests for protrusion and undulation pressures in phospholipid bilayers, Biochemistry 34 (1995) 8520–8532.
[132] H.I. Petrache, N. Gouliaev, S. Tristram-Nagle, R. Zhang, R.M. Suter, J.F. Nagle, Interbilayer interactions from high-resolution x-ray scattering, Phys. Rev. E 57 (1998) 7014–7024.
[133] J. Rädler, H. Strey, E. Sackmann, Phenomenology and kinetics of lipid bilayer spreading on hydrophilic surfaces, Langmuir 11 (1995) 4539–4548.
[134] I. Pera, R. Stark, M. Kappl, H.-J. Butt, F. Benfenati, Using the atomic force microscope to study the interaction between two solid supported bilayers and the influence of synapsin I, Biophys. J. 87 (2004) 2446–2455.

This page intentionally left blank

CHAPTER 8

Interfaces, Bifaces, and Nanotechnology

Jian-Shan Ye,[1] Hui-Fang Cui,[1] Angelica Ottova,[2,3,*] and H. Ti Tien[2,†]

[1]*Department of Biological Sciences, National University of Singapore, 14 Science Drive 4, Singapore 117543, Singapore*

[2]*Membrane Biophysics Laboratory, Department of Physiology, 2201 Biomedical and Physical Sciences Building, Michigan State University, East Lansing, MI 48824, USA*

[3]*Center for Interface Sciences, Slovak University of Technology, Faculty of Electrical Engineering & Information Technology, Department of Microelectronics, Bratislava, Slovak Republic*

Contents

Abstract

Nanotechnology is the construction and use of functional structures designed from atomic or molecular scale with at least one characteristic dimension measured in nanometers. Nanomaterials, such as carbon nanotubes (CNTs) and nanoparticles, exhibit novel and significantly improved physical, chemical, and biological properties, phenomena, and processes because of their size. Functionalization of nanomaterials is one of the most active fields in nanotechnology. In natural systems, such as cells, nano-scale structures are formed at room temperature using the approach of self-assembly. Alignment of linear molecules in an ordered array on the surface of CNTs or nanoparticles (self-assembled monolayer and/or bilayer) can function as a new generation of nanomaterials for chemical and biological sensors. The developments of self-assembled lipid-CNTs nanocomposites and/or lipid-nanoparticle hybrids have opened research opportunities in studying hitherto unapproachable phenomena at interfaces and bifaces. Particular emphasis is directed to the use of lipid-functionalized CNTs as well as lipid-nanoparticle nanocomposites for sensors and biosensors and for the fabrication of photo switched-functional devices.

*Corresponding author. E-mail: ottova@pilot.msu.edu

† Deceased.

ADVANCES IN PLANAR LIPID BILAYERS AND LIPOSOMES, VOLUME 3
ISSN 1554-4516 DOI: 10.1016/S1554-4516(05)03008-5

1. SELF-ASSEMBLED LIPID MEMBRANES AT INTERFACES AND BIFACES

It is well known that the fundamental structural element of all cell membranes is a 5–7 nm thick liquid-crystalline phospholipid bilayer. Thus, the lipid bilayer principle of biological membranes may be summarily stated that all living organisms are made of cells, and every cell is enclosed by a plasma membrane, the indispensable component of which is a lipid bilayer. Colloid and interfacial chemistry have played a pivotal role as evidenced by the work of Hooke, Newton, Gibbs, Langmuir, and others [1]. Several methods of forming bilayer lipid membranes (BLMs) have been discovered. The development of planar lipid bilayers or conventional black or bilayer lipid membranes (c-BLMs) and later supported BLMs (s-BLMs, sb-BLMs, and t-BLMs, etc.) have made it possible for the first time to investigate, directly, electrical properties and transport phenomena across a 5 nm ultrathin lamina separating two phases [2]. The process of formation of these BLMs is based on the self-assembly. Nature uses the self-assembly as a strategy to create complex, functional structures such as viral protein coatings, and DNA, besides the lipid bilayer of cell membranes. Supported BLMs (s-BLMs), formed on metallic wires, conducting glasses, and gel substrates, as well as on microchips, possess properties resembling those of biomembranes. These self-assembled, s-BLMs, have opened research opportunities in studying hitherto unapproachable phenomena at interfaces and bifaces. Some recent findings demonstrate potentials for investigating processes at solid–liquid interfaces. As a result of these studies, biomembranes have now been recognized as the basic structure of Nature's sensors and molecular devices. For example, the plasma membrane of cells provides sites for a host of ligand–receptor contact interactions such as the antigen–antibody binding. To impart relevant functions in BLMs, a variety of compounds such as ionophores, enzymes, receptors, pigments, and so on have been embedded. Some of these incorporated compounds cause the BLMs to exhibit nonlinear phenomena and photoelectric effects. A modified or reconstituted BLM is viewed as a dynamic system that changes both in time and in response to environmental stimuli. The self-assembled lipid bilayer, the crucial component of most, if not all biomembranes, is in a liquid crystalline and dynamic state. The self-assembly of lipid membranes at the interfaces may provide a simple yet useful method for the functionalization of nanomaterials.

2. LIPID-CARBON NANOTUBE NANOCOMPOSITES

2.1. Introduction of carbon nanotubes

Carbon nanotubes (CNTs) have captured the imagination of researchers worldwide since they were first observed by Iijima in 1991 [3], because their small dimensions, unique structures, strength, and remarkable physical properties

make CNT a very unique material with a wide range of potential applications. In the past decade, the significant advances in CNTs have been made in their unique structures, physical properties, synthesis methods, chemical modification, and potential applications.

CNTs, consisting of only sp^2 hybridized carbon atoms, are cylindrical nanostructures with a diameter ranging from 1 nm to several nanometers and a length of tens of micrometers. They are made of graphene sheets wrapped into a hollow cylinder and capped by fullerene-like structures. There are two typical types of CNTs, singlewalled carbon nanotubes (SWNTs) and multiwalled carbon nanotubes (MWNTs). High resolution transmission electron microscope (HRTEM) results showed that the first observed CNTs by Iijima in 1991 [3], were fullerene-like tubes consisting of coaxial multiple shells. These tubes were MWNTs. The interlay spacing is 0.34 nm, which is slightly greater than that of graphite (0.335 nm) due to a combination of tubule curvature and van der Waals force interactions between successive grapheme layers.

After two years, it was discovered that the use of transition metals as a catalyst leads to the formation of CNTs with a single shell or wall only [4]. These nanotubes were SWNTs. An ideal SWNT can be viewed as an ''extended'' fullerene, and consists of a single-layer graphite wrapping into one seamless hollow cylinder. SWNTs normally have a narrow diameter distribution (with diameter of the order of 1 nm) but tend to assemble in nanotube bundles during the growth process [5].

There are three types of SWNTs: 'arm-chair' (n, n) tubes, 'zig-zag' (n, 0) tubes, and chiral (all the other tubes with independent n and m) tubes. Theoretical calculations indicate that the electronic properties for a single-walled nanotube will vary as a function of its diameter and helicity [6–8]. A SWNT may behave as a semiconductor or metal, and a slight change in the chirality can transform a nanotube from a metal to a semiconductor. In general, about one-third of SWNTs are metallic, characterized with wrapping vectors of $n - m = 3l$ ($l = 0, 1, 2 \ldots$). All the other tubes are semiconductors [9,10]. Carbon–carbon covalent bonds are one of the strongest in nature, a structure based on a perfect arrangement of these bonds oriented along the axis of nanotubes would produce an exceedingly strong material. Early theoretical work and recent experiments on individual nanotubes have confirmed that nanotubes are one of the stiffest structures ever made [11–13].

CNTs possess high electrical conductivity, high chemical stability, and extremely high mechanical strength and modulus. These special properties of both SWNTs and MWNTs, respectively, have attracted much attention in electrocatalysis [14–19] and chemical sensors/biosensors [20–26].

2.2. Supramolecular self-assembly of lipid monolayer at carbon nanotubes

Surfactant adsorption at interfaces has been widely studied because of its importance in detergents, lubrication, and colloid stabilization [27]. CNTs are

insoluble in organic solvents and in water, which at present considerably restricts their area of use. In order to enhance the solubility of CNTs, detergent is mixed and shaken with nanotubes to form stable suspensions [28]. The chemical adsorption of sodium dodecyl sulphate (SDS) molecules on the surface of the nanotubes creates a distribution of negative charges that prevents their aggregation and induces stable suspensions in water. The SDS molecules can be oriented perpendicularly to the surface of the nanotube, forming a monolayer. The molecular organizations of surfactant at the solid–liquid interface can be: (1) the hydrophobic part of the SDS is adsorbed on the graphite by van der Waals interactions, likely following the carbon network, and (2) the hydrophilic part of the surfactant is oriented toward the aqueous phase, forming half-cylinders on the surface of the graphite plane [29]. Because CNTs are rolled-up grapheme sheets, the SDS molecules may form similar half-cylinders on the surface of the tubes, either oriented parallel or perpendicularly to the tube axis.

The self-assembly of lipid at metallic–aqueous interfaces has been well studied. In order to determine whether lipid molecules could adsorb and self-organize on CNTs, creating stable assemblies, Richard et al. [30] designed and synthesized new reagents, which form lipidic ‘‘rings’’ made up of supramolecular half-cylinders. Transmission electron microscopy (TEM) results indicated the formation of supramolecular assemblies of these molecules on the surface of the nanotubes. It was found that the reagents formed micellar structures in aqueous solution and then spontaneously self-organized into half-cylinders on the CNTs. To explore the possibility of functionalizing the surface of CNTs in a noncovalent but permanent way with different reagents, the self-assembly of a series of molecules made of a double lipidic chain was further tested. In contrast to the single-chain lipids, no organization was detected by TEM when an aqueous solution (1 mg/ml) of the second series of molecules was directly sonicated with 1 mg of MWNTs. To investigate whether micelles are necessary to form these supramolecular assemblies, the MWNTs were sonicated in the presence of mixed micelles. TEM observations showed perfectly organized striations on the CNTs. The size of the striations, determined by TEM, varied from 55 to 75 Å, in perfect agreement with the length of the different lipidic chains. These results are also coherent with a half-cylinder arrangement of the double-chain lipids on the surface of the nanotubes. Hence, the formation of micelles appears to be a key step for the formation of supramolecular assemblies on the CNT surface. This process constitutes a simple and versatile protocol for the noncovalent functionalization of nanotubes.

One of the most exciting applications of CNTs is in the exploration of proteins and cells in aqueous solution. Few of these applications have yet been realized, however, because of the incompatibility of the CNT surface, which is hydrophobic and prone to nonspecific bioadsorption, with biological components such as cells and proteins. In addition, the aqueous environment required for biological materials is not suitable for unfunctionalized CNTs [31]. In nature, cells are faced

with a similar challenge of resisting nonspecific biomolecule interactions while engaging in specific molecular recognition. These functions can be simultaneously fulfilled by mucin glycoproteins, defined by their dense clusters of O-linked glycans. Zettl and associates [32] described a biomimetic surface modification of CNTs using glycosylated polymers designed to mimic natural cell-surface mucins. A C_{18} lipid at one end of a mucin mimic polymer is introduced to enable surface modification of CNTs. Lipids are known to self-assemble on the surface of CNTs through hydrophobic interactions in the presence of water [30] and lipid functionalized glycopolymers have been shown to form ordered arrays on graphite surfaces [33]. The lipid-functionalized mucin mimics is self-assembled on CNTs in a similar manner as the organization of native mucins in the cell membrane, with the glycosylated polymers projecting into the aqueous medium. CNTs modified with mucin mimics were soluble in water, resisted nonspecific protein binding, and bound specifically to biomolecules through receptor–ligand interactions. This strategy for biomimetic surface engineering provides a means to bridge CNTs and biological systems.

2.3. Self-assembly of lipid bilayer at multiwalled carbon nanotubes

CNTs are of significant interest due to their unique properties and potential applications [34]. Several successful strategies using covalent or noncovalent chemistry have been applied to functionalize the sidewall of CNTs. Among these, noncovalent methods are attractive as they may preserve the inherent properties of the nanotubes [30,35]. The s-BLM has attracted increasing interest in recent years due to its vast potential applications as electrochemical biosensors, in developing molecular devices, and for investigating the photo-induced electron transfer in the bio-membranes [36,37]. Stable s-BLMs without or with modification have been formed by self-assembling on the hydrophilic surfaces of several kinds of materials, including hydrogel and freshly prepared metallic surfaces [38,39].

Recently, the self-assembly of s-BLM on the surface of MWNTs by using Tien's method [37,39] was described [40]. The cyclic voltammetric (CV) responses of BLMs-coated MWNTs in phosphate buffer solution (PBS) were studied. At bare MWNTs electrode, a large background current i (in the range of 10^{-5} A) was observed. When MWNTs electrode was coated with BLMs, the background current was dramatically reduced to the range of 10^{-9} A, indicating a strong insulation effect of the lipid assembled on the surface of the MWNTs. Since membrane capacitance (C_m) can be obtained from the background current of the CV ($C_m = i/v$), the thickness of lipid membrane T_m on MWNTs can be calculated from the equation: $T_m = \frac{2.2\varepsilon_0 A}{C_m}$ (ε_0, vacuum dielectric permittivity; A, surface area). The T_m calculated was thus calculated to be about 4.38 nm, which is approximately a double of the molecular size of phosphatidylcholine, consistent with a bilayer structure of the lipid membrane [37]. The static water contact angles on

the surface of MWNTs were measured to be 6–7°, indicating a hydrophilic property of the MWNTs surface. The BLM can thus be formed with the hydrophilic moiety of one lipid layer absorbed on the surface of MWNTs, and that of another lipid layer faced to the testing PBS solution. This result is in agreement with that reported by Kanyó *et al.* [41] but different from that found by Richard *et al.* [30]. Kanyó *et al.* [41] reported that the surface of MWNTs without heat treatment was hydrophilic. In contrast, Richard *et al.* [30] reported that a monolayer of synthetic lipid was self-assembled at the surface of CNTs, in which the van der Waals interaction between hydrophobic part of lipid and the carbon network was suggested. The different hydrophilicity reported may come from the different fabrication methods of the CNTs. When MWNTs were synthesized from the chemical source of ethylenediamine, chemical elemental analysis indicated that 1.8–2.8% nitrogen existed in the MWNTs used in the present study [42]. Functional groups containing nitrogen on the MWNTs surface may contribute partly to the hydrophilic property on the MWNTs synthesized and used here. In addition, it is known that the carbon shell (i.e., each carbon shell of the MWNT) is closed by various functional groups, most frequently by COOH, –OH, and CO groups. For MWNTs, the outer shell may often contain discontinuous spots of imperfection. These local vacancies could be also closed by the functional groups just mentioned above [41]. Possibilities existed for these functional groups to confer the hydrophilic surface of the MWNTs.

2.4. Application of lipid-carbon nanotube nanomaterials

Since their inceptions, bilayer lipid membranes (c-BLMs) in 1961, and supported lipid bilayers (s-BLMs) in 1978, respectively, have been widely used as models for biomembranes [43,44] and sensing devices in biotechnology [44]. These experimental lipid bilayers, along with liposomes, have been used in fundamental and applied studies of lipid assembly on interfaces, membrane structure and function, ligand–receptor interactions, electrochemical properties, and the development of lipid bilayer-based biosensors. Planar BLMs can now be created routinely with long-term stability on various substrates (microporous filters, metal, hydrogels, conducting glass, etc.), thereby opening the way for basic research and development work in the domains such as membrane biophysics [2], biotechnology [1], catalysis [45], electrochemistry [46], and microelectronics [47].

Sensors represent a most plausible and exciting application area for nanobiotechnology; and nanosensors based on CNTs are expected to emerge in the marketplace in significant volumes over the next 10 years. Despite the tremendous excitement recently generated by experimental breakthroughs that have led to realistic possibilities of using CNTs in electrochemical sensors, further experimental and theoretical research is still necessary. The forming of stable lipid-CNT assemblies offers a simple and efficient method for the development of

sensors/biosensors. The supramolecular structure of lipid-CNTs may lead to a number of applications in the field of nanobiotechnology: it could be used for the development of molecular sensors (biosensors) for detecting the body's molecules. This structure could also make it possible to create new vectors of hydrophobic components, in particular complex drugs. To actualize and optimize the full commercial potential of CNT-based electrochemical sensors, efforts must continue to be devoted to integrate the nanotube-arrays with power, miniaturized and easy-to-use electrochemical instruments for bimolecular sensing, genetic analysis, and drug discovery or screening.

The photoelectric effects of BLMs and electron mediator modified BLMs have been extensively studied, on account of their potential applications in understanding the mechanism of natural photosynthesis, and in developing artificial photoelectric devices [2,44,48] and mimicking functionalities of natural photosynthetic systems, which are represented by photoactive groups, electron donors, and acceptors [49]. Various attempts have been made to realize an artificial photosynthesis and solar-energy conversion system under laboratory conditions. For example, synthetic dyes have been used to dope BLMs and the corresponding photo responses have been investigated [50].

Fullerenes, in particular C_{60} as a modifier of BLM, have attracted much interest in the study of photoelectric conversion because of the affinity of these molecules for electrons and, also, because of their highly hydrophobic properties for doping BLMs [51–54]. However, past experiments on the photoelectric properties of C_{60}-doped BLMs were mostly conducted on the conventional planar BLMs [51,55], the defect of which is the fragility, thus precluding protracted investigations and practical applications. Gao and associates [56] reported that s-BLMs (with and without the doping of fullerene C_{60}) self-assembled on indium–tin oxide (ITO) glass were fabricated and characterized by cyclic voltammetry and electrochemical impedance spectroscopy using a three-electrode system. The photoelectric conversion experiment indicates that a photoinduced electron could transfer across BLMs self-assembled on ITO conducting glass and the mediators doping BLMs could facilitate this transmembrane photoinduced electron transfer. Since the ITO/s–BLM probes possess biological compatibility, biomaterials could be further embedded and their photoresponse properties could be investigated. It seems evident that this novel self-assembled ITO/s–BLM probe will be a promising tool for the study of the light-induced properties of biomembranes (e.g., photodynamic therapy) and the development of biomimetic photoelectric devices.

More recently, Ye and associates [40] described the self-assembly of BLM and C_{60}-containing BLM at well-aligned MWNTs. The thickness of lipid membrane at MWNTs is estimated to be 4.38 nm, which is approximately double of the molecular size of phosphatidylcholine, indicating that BLM at the surface of nanotubes has a bilayer structure. Lipid membrane self-assembled at the MWNTs acts as an insulating layer while the incorporated C_{60} can mediate the transportation of electrons as well as photocurrent across BLM. The membrane

resistance of C_{60}-BLM/MWNTs is 369.3 Ω, which is much smaller than that of BLM/MWNTs (3.238×10^6 Ω). Furthermore, C_{60}-BLM/MWNTs possess photoelectric properties due to the electron mediation of C_{60} in the lipid membrane. The photoelectric conversion properties of MWNTs, BLM/MWNTs, and C_{60}-BLM/MWNTs were thus studied using amperometric technique. In lipid interface, C_{60} transports about 30–40% of electrons, compared with that of pure MWNTs, from MWNTs to the redox species in solution. The successful self-assembly of BLM and incorporation of C_{60} into the BLM at MWNTs may provide an easy way for construction of new biosensors and bioelectronic materials using BLM/MWNTs and/or C_{60}-BLM/MWNTs nanocomposites.

2.5. Conclusion and perspectives

CNTs are among the novel emerging technologies with potential application to nanosensors, photo-switched devices,and drug and gene delivery. Functionalization of their surface can result in highly soluble materials, which can be further modified with active molecules, making them compatible with biological systems. Therefore, many applications can be envisaged. With the creation of bifaces and interfaces at lipid-CNTs nanocomposites, progress in CNT technology may well lead to better insights into biological and physical chemistry processes. This will make it possible to find compounds more compatible with CNT technology and facilitate more effective use in electrochemical applications.

3. NANOSTRUCTURED LIPID-NANOPARTICLE NANOCOMPOSITES

3.1. Lipid-nanoparticle interfaces and bifaces

The s-BLM has attracted considerable interest in recent years due to its many potential applications as an electrochemical biosensor and in molecular devices [2,57,58]. BLMs have been used in various experimental paradigms as models of actual living cell membranes [59–61]. BLMs provide a natural environment for embedding a host of compounds such as proteins, receptor, membrane/tissue fragments, and even whole cells under nondenaturing conditions and in a well-defined orientation. Thus, the embedding of nanoparticles at the interfaces of BLMs will create new nanomaterials for wide application.

It is noted that BLMs containing semiconductor nanoparticles has been successfully prepared [62]. For example, CdS crystallites can be formed in situ in the pores of a polycarbonate membrane at the interfaces of aqueous solutions. When the CdS-membrane was irradiated, open-circuit photopotentials up to 500 mV were obtained. A number of substances, such as Cu, CuS, CdS, FeS, and AgBr having typical metallic or semiconducting features, have been deposited onto the

surface of BLMs [62,63]. Nanoparticle-doped BLMs show very good stability in comparison with unmodified BLMs, which usually lacked satisfactory durability. Metallic or semiconducting layers deposited onto the BLM surface can serve as electrodes directly contacting the membrane, which eliminate electrolytic contact with the lipid bilayers and may be useful in the development of biomolecular electronic devices.

Similar studies in semiconductor-containing BLMs have been reported [63]. To prepare semiconductor-containing BLMs, H_2S and appropriate metal ion precursors were added onto bathing solutions on opposite sides of the BLM. Subsequent to the injection of H_2S, the first observable change was the appearance of fairly uniform white dots on the blank film. These dots rapidly moved around and grew in size, forming islands that then merged with each other and with a second generation of dots, which ultimately led to a continuous film that continued to grow in thickness. The semiconductor penetration depth onto the BLM can be assessed by an equivalent RC circuit. Metallic or semiconducting layers formed onto the BLMs may have potential utilization in membrane mimetic chemistry. The deposition of nanoparticles onto the surface of BLMs or inside the BLMs can drastically alter the mechanical, electrical, and optical properties of the BLM. Nanoparticles doped through the s-BLMs may perform as an array of nanoelectrodes, while s-BLMs retain biocompatible microenvironment.

Supramolecular assemblies of self-organized, functionally cooperating molecules are essential for biological systems, and have broad potential to downscale and control (bio)chemical and (bio)technological process on the nanometer scale [64]. This process has been successfully used to produce supramolecular assemblies of semiconducting nanocrystals (NCs) with various biomolecular recognition sites for *in vitro* and *in vivo* bioanalytical applications [65,66]. Recently, Vogel *et al.* [67] developed a general and versatile procedure to make NCs water-soluble and simultaneously decorate them with a diverse range of multiple functionalities. Their approach is based on the self-assembly of single lipid monolayers on hydrophobic NCs. Based on this approach, the physical (electrical charges, structures, entropic shielding) and chemical (reactive group, biological recognition elements) surface properties of the NCs can be tuned by varying the polar head groups of the lipid. This effect can be simply controlled by the composition of the lipids used for self-assembly. More interestingly, the multifunctionalized lipid-coated NCs can bind different proteins per particle specifically and subsequently position themselves on micropatterned surfaces to form nanometer-sized supramolecular structures of higher complexity. Compared to the existing polymer-coated NCs, which are commercially available, the lipid-NCs offer complementary novel applications. Specific interaction between such NCs and different proteins through multiple high-affinity binding sites enabled site-selective controlled formation of supramolecular assemblies. The multifunctional NCs serve as local light sources, which can be positioned with nanometer precision within supramolecular assemblies and can emit light over distances from 1 to

more than 10 nm, again controlled with nanometer precision. Such concepts might be of importance for the development of biotechnology and bioanalytics on a nanometer and attoliter scale.

3.2. Nanoparticles at lipid membranes

The s-BLMs have been widely used in miniaturized biosensors. The PC simulator 'BLM' has been developed based on electrical elements (resistance, capacitance, diode) for simulations of electrical, electromechanical (electrostriction), and electrochemical (redox reactions) properties of s-BLMs [1]. At the nanolevel, Ye and associates [68] described the preparation of s-BLM doped with metal nanoparticles for the design of biosensors. Platinum (Pt) nanoparticles were deposited through s-BLM to build a hybrid device of nanoscale electrode array by potential cycling in 1 mM K_2PtCl_6 solution containing 0.1 M KCl. The properties of Pt nanoparticle-doped s-BLM composite were then characterized by cyclic voltammetry, electrochemical impedance (EIS) and AFM. The results showed that Pt nanoparticles grew in voids of the s-BLMs, through which the underlying glassy carbon (GC) electrode was connected, with maximum length extended out of the lipid membrane around 40 nm. Doping of Pt nanoparticles through s-BLM increased the membrane capacitance and decreased the membrane resistance of s-BLM. AFM images showed that the topography of lipid-coated GC is relatively smooth with a height variation of about 20 nm. Incorporation of Pt nanoparticles is manifested by the formation of numerous domains with a height variation of around 40 nm. These images provide a direct verification of Pt nanoparticles deposited through the lipid membranes. It reveals that a portion of the Pt nanoparticles embedded in the lipid membrane extend from the membrane by as much as 20 nm.

3.3. Lipid-coated nanoparticles

Many methods have been achieved for the synthesis of lipid-coated nanoparticles. Bhattacharya and Srivastava [69] recently reported the synthesis of novel gold nanoparticles bearing cationic single-chain, double-chain, and cholesterol based amphiphilic units. These nanoparticles represent size-stable entities in which various cationic lipids have been immobilized through their thiol group onto the gold nanoparticle core. The resulting colloids have been characterized by UV-vis, H-1 NMR, FT–IR spectroscopy, and TEM. The average size of the resultant nanoparticles could be controlled by the relative bulkiness of the capping agent. Thus, the average diameters of the nanoparticles formed from the cationic single-chain, double-chain, and cholesterol-based thiolate-coated materials were 5.9, 2.9, and 2.04 nm, respectively. Furthermore, the interaction of these cationic gold

nanoparticles with vesicular membranes generated from dipalmitoylphosphatidylcholine (DPPC) lipid suspensions was examined. Gole *et al.* [70] described the formation of gold nanoparticle-lipid composite films by glucose-induced reduction of chloroaurate ions entrapped in thermally evaporated fatty amine films. Simple immersion of films of the salt of octadecylamine and chloroaurate ions (formed by immersion of thermally evaporated fatty amine films in chloroauric acid solution) in glucose solution leads to the facile in situ reduction of the metal ions to form gold nanoparticles in the fatty amine matrix. The formation of gold nanoparticles is readily detected by the appearance of a violet color in the film and thus forms the basis of a possible new, gold nanoparticle-based colorimetric sensor for glucose. More recently, Terheiden *et al.* [71] reported that metallic nanoparticles are deposited on multilayers of an unsaturated phospholipid to form a planar nano-composite material. At temperatures near or above the main transition of the lipid, the organic layers exhibit a high degree of mobility and allow for a significant rearrangement of the metallic particles. Originally after deposition, the inter-particle distances correspond to the average bilayer thickness of the given phospholipid. After annealing of the composite structure in the presence of moisture, the spacing between the particles is significantly reduced, associated with an interdigitation of aliphatic chains in the hydrophobic region.

The comparison of the synthesis of metal nanoparticles at the surfaces of polymerized and unpolymerized phospholipid vesicles has been undertaken [72]. It was found that the divalent palladium ion bound to the negatively charged phospholipids in the vesicle membrane initiated electroless metallization of gold or cobalt on the vesicle surface leading to the formation of metallic nanoparticles. By using the internal volume of polymerized vesicles as the reaction vials, two types of unagglomerated nanoparticles, Au (4–10 nm) and Co/Co(OH)(x) (30–100 nm), have been synthesized. Metallization of unpolymerized vesicles resulted in the formation of size controlled, unagglomerated Au nanoparticles (20–28 nm). TEM results suggest that composites of lipid and metal were formed. For both the polymerized and unpolymerized vesicles, HRTEM studies have demonstrated that particle nucleation and growth occurred at the vesicle membrane surfaces and that particle growth could be initiated by either single or multiple nucleation sites.

Besides gold nanoparticles, the formation of supported lipid bilayers on silica nanoparticles (nanoSLBs) has also been achieved [73]. The successive steps of the adsorption of lipid vesicles on nanoparticles and the formation of nanoSLBs are revealed in detail by cryotransmission electron microscopy (cryo-EM). The formation of nanoSLBs was achieved for liposomes with positive, neutral, and low net negative charge, while liposomes with a high net negative charge adsorbed to silica nanoparticles but did not rupture. The nanoSLBs were found to follow faithfully the surface contours of the particles, information yet unavailable for SLB formation on planar solid substrates.

3.4. Application of lipid-nanocomposites

The extreme fragility of the conventional BLM (c-BLM) seriously limits its utility as a practical tool because it cannot be easily produced and will not endure rugged laboratory handling. This problem of fragility was finally overcome by forming BLMs on solid supports [2,57,58], which substantially improve the stability. Because the s-BLMs have been proven to be very useful and easy to work in the field of membrane research and have solved the shortcomings of the c-BLM, stable s-BLMs on solid substrates are of practical and scientific interest, especially the s-BLMs based on GC in electrochemical investigation. Upon further modification of the BLM by embedding appropriate receptors, their counterparts in the bathing solution may be selectively detected, thereby affirming the principle of ligand–receptor interactions [61,62,74–80]. In such a biomimetic approach, a lipid bilayer is used to construct electrochemical biosensor [75]. The functions of biomembranes are mediated by specific modifiers, which can improve the specificity and the selectivity of the biosensors.

A recent study showed that Pt nanoparticles electrochemically deposited through the lipid films can improve the functions of s-BLMs [68]. Pt nanoparticles array in s-BLM electrocatalyzed the reduction of oxygen (O_2) in PBS. Practical application of Pt nanoparticle-doped s-BLM for the construction of glucose biosensor was also demonstrated by Ye *et al.* [68] in terms of its dose-response curve, stability, and reproducibility. The response time (reaching 90% of the maximum response) of this kind of biosensor was 17 s, which indicated a fast diffusional process and a high activity of the GOx in this nanoparticle lipid composite. The immobilization of Pt nanoparticles indicates that the Pt nanoparticles grow in nanoscale voids in the s-BLMs through which the underlying GC electrode is connected to the circuit. This implicates that the Pt nanoparticles serve as nanoscale conductors that are electrically connected to the GC substrate and that it penetrates through the s-BLMs to distances of tens of nanometers beyond the membrane surface. The advantage and novelty of this device is an electrode system at the nanoscale that can probe through the membrane to investigate the molecular interaction and recognition at the external surface of s-BLMs. Thus, lipid membrane doped with Pt nanoparticles is a novel electrode system at nanoscale that can penetrate through the insulating membrane to probe molecular recognition and catalytic events at the lipid membrane–solution interface. The incorporation of Pt particles through the s-BLMs resulted in a unique nanoelectrode array, which not only enhanced the capacitance and decreased the resistance of s-BLMs, but also increased the sensitivity for s-BLMs in electrocatalyzing the reduction of O_2 as well as rendering s-BLMs as glucose sensor when GOx was incorporated into s-BLMs. In this connection, Wang's [75] group reported the electrochemistry of protein by using monolayer-protected nanoparticles . They synthesized a kind of gold nanoparticle protected by a synthetic lipid (didodecyidimethylammonium bromide, DDAB) with a diameter of around

6.42 nm. With the help of these gold nanoparticles, hemoglobin can exhibit a direct electron transfer (DET) reaction. The formal potential locates at −169 mV vs. Ag/AgCl. Spectral data indicated the hemoglobin on the electrode was not denatured. The lipid-protected gold nanoparticles were very stable (for at least 8 months).

There have been numerous reports within the last decade on self-assembled molecules and supported membranes and their closely related systems such as Langmuir–Blodgett films [2,38,59,76,81–83]. The sustained and continued interest is due to the fact that BLMs provide a natural environment for embedding of proteins, pigments, and other membrane constituents with little denaturation. The key successful construction of BLM-based sensors is the ability to embed functional molecules into the lipid bilayer environment, which is hydrophobic, liquid-like, and self-organizing. The essential idea is to use the s-BLM as a backdrop for the incorporation of materials of interest as well as to use it for signal transduction. To improve the properties of BLM for practical application, many compounds, such as semiconducting nanoparticles, polymeric materials, and fullerenes, have been successfully incorporated into BLM [84]. The recent achievement of the lipid-nanoparticle nanocomposites showed that: (1) nanoparticles can be successfully deposited through BLM as a novel nanoelectrode array system; and (2) s-BLM with doping of nanoparticles retains a biocompatible microenvironment for enzymes to maintain its active conformation for catalytic reaction. Many metallic nanoparticles, such as Cu, Pd, Rh, and Au, may be deposited through s-BLM. In addition, supported lipid biomembrane at the interface of electrode-aqueous interfaces, can also be employed for embedding a variety of compounds such as peptides, enzymes, antibodies, receptors, ionphores, and redox species [2,59]. The bifaces and interfaces of the lipid-nanoparticles will open the possibility for the detection of biological molecules such as antigens, hormones, ions, and electron donors or acceptors. The nanostructured metallic lipid bilayer composite may provide a rationale for the construction of ligand-specific biosensors.

3.5. Conclusion and perspectives

Nanoparticles have unique physicochemical and optoelectronic properties, which is promising to the application in the fast-developing area of nanotechnology [85,86]. Many chemical protocols have been developed and improved upon to synthesize nanoparticles [87]. Molecular self-assembly is ubiquitous in nature and has recently emerged as a new approach in nanotechnology for the synthesis of functional nanoparticles. Molecular self-assembly systems lie at the interface between molecular biology, chemistry, polymer science, materials science, and engineering. Molecular self-assembly of lipid-nanoparticle nanocomposites represent a significant advance in the nanomaterials for a wide range of applications.

REFERENCES

[1] H.T. Tien, A.L. Ottova, Planar Lipid Bilayers (BLMs) and their Applications, Elsevier, Amsterdam, 2003.
[2] H.T. Tien, A.L. Ottova, Membrane Biophysics: As Viewed from Experimental Bilayer Lipid Membranes (Planar Lipid Bilayers and Spherical Liposomes), Elsevier, Amsterdam, 2000.
[3] S. Iijima, Helical microtubules of graphitic carbon, Nature 354 (1991) 56–58.
[4] S. Iijima, T. Ichihashi, Single-shell carbon nanotubes of 1-nm diameter, Nature 363 (1993) 603–605.
[5] A. Thess, R. Lee, P. Nikdaev, H. Dai, P. Petit, J. Robert, C. Xu, Y.H. Lee, S.G. Kim, A.G. Rinzler, D.T. Colbert, G.E. Scuseria, D. Tomanek, J.E. Fischer, R.E. Smalley, Crystalline ropes of metallic carbon nanotubes, Science 273 (1996) 483–487.
[6] R. Saito, M. Fujita, G. Dresselhaus, M.S. Dresselhaus, Electronic structure of graphene tubules based on C_{60}, Phys. Rev. B 46 (1992) 1804–1811.
[7] R. Saito, M. Fujita, G. Dresselhaus, M.S. Dresselhaus, Electronic structure of chiral graphite tubules, Appl. Phys. Lett. 60 (1992) 2204–2206.
[8] J.H. Weaver, D.M. Poirier, Solid state properties of fullerenes and fullerene-based materials, Solid State Phys. – Adv. Res. Appl. 48 (1994) 1–108.
[9] J.W. Mintmire, B.I. Dunlap, C.T. White, Are fullerene tubules metallic, Phys. Rev. Lett. 68 (1992) 631–634.
[10] N. Hamada, S. Sawade, A. Oshiyama, New one-dimensional conductors: graphitic microtubules, Phys. Rev. Lett. 68 (1992) 1579–1581.
[11] B.I. Yakobson, C.J. Brabec, J. Bernholc, Nanomechanics of carbon tubes: instabilities beyond linear response, Phys. Rev. Lett. 76 (1996) 2511–2514.
[12] M.M.J. Treacy, T.W. Ebbesen, J.M. Gibson, Exceptionally high Young's modulus observed for individual carbon nanotubes, Nature 381 (1996) 678–680.
[13] E.W. Wong, P.E. Sheehan, C.M. Lieber, Nanobeam mechanics: elasticity, strength, and toughness of nanorods and nanotubes, Science 277 (1997) 1971–1975.
[14] P.J. Britto, K.S.V. Santhanam, P.M. Ajayan, Carbon nanotube electrode for oxidation of dopamine, Bioelectrochem. Bioenerg. 41 (1996) 121–125.
[15] E. Pennisi, Simple recipe yields Fullerene tubules, Sci. News 142 (1992) 36.
[16] Z.H. Wang, J. Liu, Q.L. Liang, Y.M. Wang, G. Luo, Carbon nanotube-modified electrodes for the simultaneous determination of dopamine and ascorbic acid, Analyst 127 (2002) 653–658.
[17] J.J. Davis, R.J. Coles, H.A.O. Hill, Protein electrochemistry at carbon nanotube electrodes, J. Electroanal. Chem. 440 (1997) 279–282.
[18] H.X. Luo, Z.J. Shi, N.Q. Li, Z.N. Gu, Q.K. Zhuang, Investigation of the electrochemical and electrocatalytic behavior of single-wall carbon nanotube film on a glassy carbon electrode, Anal. Chem. 73 (2001) 915–920.
[19] P.J. Britto, K.S.V. Santhanam, A. Rubio, J.A. Alonso, P.M. Ajayan, Improved charge transfer at carbon nanotube electrodes, Adv. Mater. 11 (1999) 154–157.
[20] J. Kong, N.R. Franklin, C. Zhou, M.G. Chapline, S. Peng, K. Cho, H. Dai, Nanotube molecular wires as chemical sensors, Science 287 (2000) 622–625.
[21] P.G. Collins, K. Bradley, M. Ishigami, A. Zettl, Extreme oxygen sensitivity of electronic properties of carbon nanotubes, Science 287 (2000) 1801–1804.
[22] M. Musameh, J. Wang, A. Merkoci, Y. Lin, Low-potential stable NADH detection at carbon-nanotube-modified glassy carbon electrodes, Electrochem. Commun. 4 (2002) 743–746.
[23] J. Wang, M. Musameh, Y.H. Lin, Solubilization of carbon nanotubes by Nafion toward the preparation of amperometric biosensors, J. Am. Chem. Soc. 125 (2003) 2408–2409.
[24] J. Wang, M. Musameh, Carbon nanotube/teflon composite electrochemical sensors and biosensors, Anal. Chem. 75 (2003) 2075–2079.

[25] X. Yu, D. Chattopadhyay, I. Galeska, F. Papadimitrakopoulos, J.F. Rusling, Peroxidase activity of enzymes bound to the ends of single-wall carbon nanotube forest electrodes, Electrochem. Commun. 5 (2003) 408–411.
[26] J.J. Gooding, R. Wibowo, J.Q. Liu, W.R. Yang, D. Losic, S. Orbons, F.J. Mearns, J.G. Shapter, D.B. Hibbert, Protein electrochemistry using aligned carbon nanotube arrays, J. Am. Chem. Soc. 125 (2003) 9006–9007.
[27] A.C. Zettlemoyer, Hydrophobic surfaces, J. Colloid Interface Sci. 28 (1968) 343–368.
[28] J.M. Bonard, T. Stora, J.P. Salvetat, F. Maier, T. Stockli, C. Duschl, L. Forro, W.A. deHeer, A. Chatelain, Purification and size-selection of carbon nanotubes, Adv. Mater. 9 (1997) 827–832.
[29] S. Manne, J.P. Cleveland, H.E. Gaub, G.D. Stucky, P.K. Hansma, Direct visualization of surfactant hemimicelles by force microscopy of the electrical double layer, Langmuir 10 (1994) 4409–4413.
[30] C. Richard, F. Balavoibe, P. Schultz, T.W. Ebbesen, C. Mioskowski, Supramolecular self-assembly of lipid derivatives on carbon nanotubes, Science 300 (2003) 775–778.
[31] Y. Lin, S. Taylor, H.P. Li, K.A.S. Fernando, L.W. Qu, W. Wang, L.R. Gu, B. Zhou, Y.P. Sun, Advances toward bioapplications of carbon nanotubes, J. Mater. Chem. 14 (2004) 527–541.
[32] X. Chen, G.S. Lee, A. Zettl, C.R. Bertozzi, Biomimetic engineering of carbon nanotubes by using cell surface mucin mimics, Angew. Chem. Int. Ed. 43 (2004) 6111–6116.
[33] N.B. Holland, Y.X. Qiu, M. Ruegsegger, R.E. Marchant, Biomimetic engineering of non-adhesive glycocalyx-like surfaces using oligosaccharide surfactant polymers, Nature 392 (1998) 799–801.
[34] P.M. Ajayan, Nanotubes from carbon, Chem. Rev. 99 (1999) 1787–1799.
[35] X.B. Wang, Y.Q. Liu, W.F. Qiu, D. Zhu, Immobilization of tetra-tert-butylphthalocyanines on carbon nanotubes: a first step towards the development of new nanomaterials, J. Mater. Chem. 12 (2002) 1636–1639.
[36] C.M. Drain, Self-organization of self-assembled photonic materials into functional devices: photo-switched conductors, Proc. Natl. Acad. Sci. USA 99 (2002) 5178–5182.
[37] H.T. Tien, L.G. Wang, X. Wang, A.L. Ottova, Electronic processes in supported bilayer lipid membranes (s-BLMs) containing a geodesic form of carbon (fullerene C-60), Bioelectrochem. Bioenerg. 42 (1997) 161–167.
[38] Y.L. Zhang, H.X. Shen, C.X. Zhang, A.L. Ottova, H.T. Tien, The study on the interaction of DNA with hemin and the detection of DNA using the salt bridge supported bilayer lipid membrane system, Electrochim. Acta 46 (2001) 1251–1257.
[39] H.T. Tien, Z. Salamon, A.L. Ottova, Lipid bilayer-based sensors and biomolecular electronics, Crit. Rev. Biomed. Eng. 18 (1991) 323–340.
[40] J.S. Ye, H.F. Cui, W.D. Zhang, A.L. Ottova, H.T. Tien, F.S. Sheu, Self-assembly of bilayer lipid membrane at multiwalled carbon nanotubes towards the development of photo-switched functional device, Electrochem. Commun. 7 (2005) 81–86.
[41] T. Kanyó, Z. Kónya, Á. Kukovecz, F. Berger, I. Dékány, I. Kiricsi, Quantitative characterization of hydrophilic-hydrophobic properties of MWNTs surfaces, Langmuir 20 (2004) 1656–1661.
[42] W.D. Zhang, Y. Wen, S.M. Lin, W.C. Tjiu, G.Q. Xu, L.M. Gan, Synthesis of vertically aligned carbon nanotubes on metal deposited quartz plates, Carbon 40 (2002) 1981–1989.
[43] H.T. Tien, A.L. Ottova, The lipid bilayer concept and its experimental realization: from soap bubbles, the kitchen sink, to bilayer lipid membranes, J. Membr. Sci. 189 (2001) 83–117.
[44] A.L. Ottova, H.T. Tien, Bilayer lipid membranes: an experimental system for biomolecular electronic devices development, Prog. Surf. Sci. 41 (1992) 337–445.
[45] A.L. Ottova, H.T. Tien, Supported planar BLMs (lipid bilayers): formation methods of study and applications, in: A.G. Volkov (Ed.), Interfacial Catalysis, Marcel Dekker Inc., New York, 2003, Chapter 15, pp. 421–469.

[46] H.T. Tien, A.L. Ottova, Membrane electrochemistry, in: G.S. Wilson, (Ed.), Encyclopedia of Electrochemistry, Vol. 9, Wiley-VCH, New York, 2002.
[47] L. Barsanti, P. Gualtieri, I. Willner (Eds.), Molecular Electronics: Bio-sensor and Biocomputer, NATO Advanced Study Institute, 2003, pp. 197–225.
[48] W.S. Xia, C.H. Huang, L.B. Gan, H. Li, X.S. Zhao, Electronic response of a bilayer lipid membrane doped with an azo pyridinium containing a rare-earth-metal complex, J. Chem. Soc., Faraday Trans. 92 (1996) 769–772.
[49] K. Uosaki, T. Kondo, X.Q. Zhang, M. Yanagida, Very efficient visible-light-induced uphill electron transfer at a self-assembled monolayer with a porphyrin–ferrocene–thiol linked molecule, J. Am. Chem. Soc. 119 (1997) 8367–8368.
[50] H. Fujiwara, Y. Yonezawa, Photoelectric response of a black lipid membrane containing an amphiphilic azobenzene derivative, Nature 351 (1991) 724–726.
[51] E. Tronel-Peyroz, G. Miquel-Mercier, P. Vanel, P. Seta, Influence of adsorption on photoinduced electron transfer in supported liquid membranes: the case of C_{60}, Chem. Phys. Lett. 285 (1998) 294–298.
[52] H.T. Tien, L.G. Wang, X. Wang, Electronic processes in supported bilayer-lipid membranes (s-BLMs) containing a geodesic form of carbon (Fullerene-C_{60}), Bioelectrochem. Bioenerg. 42 (1997) 1–104.
[53] J.L. Garaud, J.M. Janot, G.J. Miquel, Photoinduced electron transfer properties of porous polymer membranes doped with the fullerene C_{60}, J. Membr. Sci. 91 (1994) 259–264.
[54] B. Eom, A.F. Hebard, L.E. Trimble, G.K. Celler, Fabrication and properties of free-standing C_{60} membranes, Science 259 (1993) 1887–1890.
[55] J.L. Garaud, J.M. Janot, G.J. Miquel, Photoinduced electron transfer properties of porous polymer membranes doped with the fullerene C_{60}, J. Membr. Sci. 91 (1994) 259–264.
[56] H. Gao, G.A. Luo, J. Feng, A.L. Ottova, H.T. Tien, Fabrication and photoelectric properties of self-assembled bilayer lipid membranes on conducting glass, J. Photochem. Photobiol. B: Biol. 59 (2000) 87–91.
[57] O. Purrucker, H. Hillebrandt, K. Adlkofer, M. Tanaka, Deposition of highly resistive lipid bilayer on silicon–silicon dioxide electrode and incorporation of gramicidin studied by ac impedance spectroscopy, Electrochim. Acta 47 (2001) 791–798.
[58] G. Wiegand, N. Arribas-Layton, H. Hillebrandt, E. Sackmann, P. Wagner, Electrical properties of supported lipid bilayer membranes, J. Phys. Chem. B 106 (2002) 4245–4254.
[59] R. Guidelli, G. Aloisi, L. Becucci, A. Dolfi, M.R. Moncelli, F.T. Buoninsegni, New directions and challenges in electrochemistry–bioelectrochemistry at metal/water interfaces, J. Electroanal. Chem. 504 (2001) 1–28.
[60] M. Eray, N.S. Dogan, A micromachined polymide aperture for stable bilayer-lipid membrane (BLMs), IEEE Trans. Electron. Dev. 40 (1993) 2137–2138.
[61] A. Ottova, V. Tvarozek, J. Racek, J. Sabo, W. Ziegler, T. Hianik, H.T. Tien, Self-assembled BLMs: biomembrane models and biosensor applications, Supramol. Sci. 4 (1997) 101–112.
[62] H.T. Tien, Z. Salamon, J. Kutnik, P. Krysinski, J. Kotowski, D. Ledermann, T. Janas, Bilayer lipid-membrane (BLM) – an experimental system for biomolecular electronic device development, J. Mol. Electron. 4 (1988) S1–S30.
[63] X.K. Zhao, S. Baral, J.H. Fendler, Electrochemical characterization of bilayer lipid-membrane semiconductor junctions, J. Phys. Chem. 94 (1990) 2043–2052.
[64] H. Kuhn, H.D. Försterling, Principles of Physical Chemistry: Understanding Molecules, Molecular Assemblies, Supramolecular Machines, Wiley, New York, 2000.
[65] A.R. Clapp, I.L. Medintz, J.M. Mauro, B.R. Fisher, M.G. Bawendi, H. Mattoussi, Fluorescence resonance energy transfer between quantum dot donors and dye-labeled protein acceptors, J. Am. Chem. Soc. 126 (2004) 301–310.
[66] B. Dubertret, P. Skourides, D.J. Norris, V. Noireaux, A.H. Brivanlou, A. Libchaber, *In vivo* imaging of quantum dots encapsulated in phospholipid micelles, Science 298 (2002) 1759–1762.

[67] I. Geissbuehler, R. Hovius, K.L. Martinez, M. Adrian, K.R. Thampi, H. Vogel, Lipid-coated nanocrystals as multifunctionalized luminescent scaffolds for supramolecular biological assemblies, Angew. Chem. Int. Ed. 44 (2005) 1388–1391.
[68] J.S. Ye, A. Ottova, H.T. Tien, F.S. Sheu, Nanostructured platinum–lipid bilayer composite as biosensor, Bioelectrochemistry 59 (2003) 65–72.
[69] S. Bhattacharya, A. Srivastava, Synthesis and characterization of novel cationic lipid and cholesterol-coated gold nanoparticles and their interactions with dipalmitoylphosphatidylcholine membranes, Langmuir 19 (2003) 4439–4447.
[70] A. Gole, A. Kumar, S. Phadtare, A.B. Mandale, M. Sastry, Glucose induced in situ reduction of chloroaurate ions entrapped in a fatty amine film: formation of gold nanoparticle-lipid composites, Phys. Chem. Comm. 19 (2001) Art. No. 19
[71] A. Terheiden, B. Rellinghaus, M. Acet, C. Mayer, Structural transitions of lipid monolayers on metallic nanoparticles, Phase Transitions 78 (2005) 25–34.
[72] M.A. Markowitz, G.M. Chow, A. Singh, Nanotechnology ACS Symposium Series 622 (1996) 162–175.
[73] S. Mornet, O. Lambert, E. Duguet, A. Brisson, The formation of supported lipid bilayers on silica nanoparticles revealed by cryoelectron microscopy, Nano Lett 5 (2005) 281–285.
[74] H. Gao, J. Feng, G.A. Luo, A.L. Ottova, H.T. Tien, Some electrochemical features of supported bilayer lipid membranes, Electroanalysis 13 (2001) 49–53.
[75] Z. Wu, B. Wang, Z. Cheng, X. Yang, S. Dong, E. Wang, A facile approach to immobilize protein for biosensor: self-assembled supported bilayer lipid membranes on glassy carbon electrode, Biosens. Bioelectron. 16 (2001) 47–52.
[76] D. Ivnitski, E. Wilkins, H.T. Tien, A. Ottova, Electrochemical biosensor based on supported planar lipid bilayers for fast detection of pathogenic bacteria, Electrochem. Commun. 2 (2000) 457–460.
[77] Y.L. Zhang, H.X. Shen, C.X. Zhang, A. Ottova, H.T. Tien, The study on the interaction of DNA with hemin and the detection of DNA using the salt bridge supported bilayer lipid membrane system, Electrochim. Acta 46 (2001) 1251–1257.
[78] P. Diao, D. Jiang, X. Cui, D. Gu, R. Tong, B. Zhong, Cyclic voltammetry and ac impedance studies of Ca^{2+}-induced ion channels on Pt-BLM, Bioelectrochem. Bioenerg. 45 (1998) 173–179.
[79] K. Asaka, A. Ottova, H.T. Tien, Mediated electron transfer across supported bilayer lipid membrane (s-BLM), Thin Solid Films 354 (1999) 201–207.
[80] J. Sabo, A.L. Ottova, G. Laputkova, M. Legin, L. Vojcikova, H.T. Tien, A combined AC–DC method for investigating supported bilayer lipid membranes, Thin Solid Films 306 (1997) 112–118.
[81] W. Schulmann, S.P. Heyn, H.E. Gaub, Immobilization of enzymes on Langmuir–Blodgett films via a membrane-bound receptor: possible application for amperometric biosensors, Adv. Mater. 3 (1991) 388–391.
[82] K.T. Kinnear, H.G. Monbouquett, Direct electron transfer to *Escherichia-coli* fumarate reductase in self-assembled alkanethiol monolayers on gold electrodes, Langmuir 9 (1993) 2255–2257.
[83] T. Miyashita, Y. Ito, Spreading behavior of polymerizable monolayers of acrylamides with double alkyl chains and polymerization of the LB films, Thin Solid Films 260 (1995) 217–221.
[84] H.T. Tien, A.L. Ottova, Supported planar lipid bilayers (s-BLMs) as electrochemical biosensors, Electrochim. Acta 43 (1998) 3587–3610.
[85] E. Katz, I. Willner, Nanoparticle arrays on surfaces for electronic, optical, and sensor applications, ChemPhysChem 1 (2000) 18–52.
[86] E. Katz, I. Willner, Integrated nanoparticle-biomolecule hybrid systems: synthesis, properties, and applications, Angew. Chem. Int. Ed. 43 (2004) 6042–6108.
[87] D.A. Handley, in: M.A. Hayat (Ed.), Colloidal Gold: Principles, Methods, and Applications, Vol. 1, Academic Press, San Diego, 1989, Chapter 2.

This page intentionally left blank

CHAPTER 9

Interaction of Polyene Macrolide Antibiotics with Lipid Model Membranes

Maciej Baginski,[1,*] Barbara Cybulska,[1,3] and Wieslaw I. Gruszecki[2]

[1]*Department of Pharmaceutical Technology and Biochemistry, Faculty of Chemistry, Gdansk University of Technology, Narutowicza St 11/12, 80-952 Gdansk, Poland*
[2]*Department of Biophysics, Institute of Physics, Maria-Curie-Sklodowska University, 20-031 Lublin, Poland*
[3]*The Elblag University of Humanities and Economy, 82-300 Elblag, Poland*

Contents

Abstract

Polyene macrolide antibiotics (PMAs) comprise over 200 natural compounds produced usually by *Streptomyces* spp. Molecules of these antibiotics contain: (i) large lactone ring with several conjugated double bonds, and (ii) generally one aminosugar moiety and carboxyl group which are attached to this ring. Subgroup of polyene macrolides, the so-called aromatic heptaenes, additionally contains side chain with aromatic ring, which is attached to a lactone moiety. Most of the polyene macrolides exhibit antifungal activity. Some of them are also active against parasites. Only few of polyene macrolides are sufficiently non-toxic to be used as antifungal drugs. Among them the most important one is Amphotericin B (AmB), which is used to treat systemic fungal infections (as Fungizone®

*Corresponding author. Tel: +48-58-3471596; Fax: +48-58-3471144;
E-mail: maciekb@hypnos.chem.pg.gda.pl

ADVANCES IN PLANAR LIPID BILAYERS AND LIPOSOMES, VOLUME 3
ISSN 1554-4516 DOI: 10.1016/S1554-4516(05)03009-7

or as liposomal formulations). Nystatin – another known member of the PMA group – also possesses chemotherapeutic application but only for topical infections. Aromatic polyene macrolides compared to AmB or nystatin were less studied but still they may be regarded as the source of new potent antifungal drugs. Due to space limit the content of this chapter will focus mainly on AmB with some references to nystatin and aromatic PMAs.

Generally accepted mode of action of PMA is interaction of their molecules with cellular membranes. PMAs cause an impairment of membrane function of sensitive cells, usually leakage of cellular constituents and eventually cell death. Detergent type of action or channel formation in cellular membrane is responsible for the disturbance of membrane barrier function. Studies on molecular action of PMAs (especially for AmB) carried out within last 45 years resulted in huge collection of data. Nevertheless, the mechanism responsible for AmB chemotherapeutic selectivity (pathogen cells *versus* host cells) is still not well understood. Chemotherapeutic application of AmB is based on higher sensitivity of ergosterol-containing fungal cells to the antibiotic compared to cholesterol-containing mammalian cells. Therefore, it is postulated that sterol molecules are necessary for AmB channel formation and participate in the channel structure. Due to the complex mode of action of PMAs on membranes of living organisms many simpler models were worked out, namely, lipid monolayers, bilayers, and liposomes and recently *in silico* models. In our review, we focused mainly on studies performed on mentioned models in our laboratories but we also made a critical evaluation of data published in the literature upto 2003. Particularly, the following studies are reviewed and critically discussed in the chapter.

Interaction with planar lipid layers. The molecular dimension of AmB corresponds to a single monolayer of the lipid bilayer membranes and therefore monomolecular layers formed with lipids and modified with AmB seem to be a model system suitable of studying interaction of this antibiotic with lipids. Two-component monomolecular layers formed with AmB and lipids were in several cases deposited to a solid support by means of the Langmuir–Blodgett technique and analyzed with the application of numerous spectroscopic techniques (such as electronic absorption and fluorescence spectroscopy or FTIR) and scanning force microscopy (SFM). The two aspects of these interactions have been studied in a monolayer model system, in particular, a molecular organization of AmB in the lipid environment, including formation of porous structures, and an effect of the drug on structural properties of a lipid phase. These studies are reviewed and critically discussed in the chapter.

Interactions with liposomes. Liposomes, artificial lipid vesicles, attracted widespread interest by the importance of the lipid bilayers as the structural elements of natural membranes. Vesicular model membranes appeared particularly well adapted to study mode of PMA action. Different types of liposomes (MLVs, LUVs, and SUVs) composed of various lipids have been used. Studies on PMA membrane interaction comprise the drug conformational changes, the perturbation in membrane structure, and changes of membrane properties as permeability barrier. We reviewed herein: (i) methods to study PMA membrane interactions, (ii) antibiotic affinity to membrane components (phospholipids and different sterols), and (iii) alteration of the overall membrane organization and membrane permeability characteristics.

Interaction with in silico model membrane. The development of computational chemistry and molecular modeling methods within the last two decades has enabled to use these techniques in studies of interactions between AmB and model phospholipid membranes. These studies include interactions of AmB with the surface of phospholipid bilayer as well as studies of ionic channels formed by molecules of AmB in the lipid bilayer. In particular, molecular dynamic (MD) studies were performed to analyze interaction of single AmB molecule with the surface of lipid membrane and membrane components. MD studies

were also carried out to analyze molecular properties of ionic channels built from AmB molecules and sterols (cholesterol or ergosterol). The simulations applying Monte Carlo methods (MC) and Poisson–Boltzmann electrostatic model were used to study ion passage through AmB membrane channels as well as to study distribution of molecular electrostatic potential for AmB and their supramolecular complexes in the lipid bilayer. Molecular modeling studies of AmB membrane channels presented above was reviewed in the chapter and confronted with available experimental data.

1. INTRODUCTION

Polyene macrolide antibiotics (PMAs) are natural compounds and most of them are produced by soil bacteria *Actinomycetes*, mainly belonging to the genus *Streptomyces*. The first polyene macrolide, i.e. fungicidin, was discovered by Hazen and Brown [1] in 1950 and it was later named nystatin. Since then more than 200 compounds belonging to this group have been found. PMAs produced by *Streptomyces* are present in bacterial mycelium and the antibiotics isolation is carried out by different extraction methods. Due to the fact that closely related polyene macrolide are present in the same cellular extract, isolation of the single compound is difficult (see recent review [2]). Problems with isolations, purification, and additionally complex structure of all polyene macrolides caused that not many more than 40 structures of PMAs have been elucidated [3]. The polyene macrolides, in general, exhibit antifungal and antiprotozoal activity but little or no antibacterial activity. Due to this fact several of PMAs are used as antifungal drugs, e.g. AmB, nystatin, pimaricin, and candicidin (Fig. 1). Polyene macrolides, however, are highly toxic to the host and cause many serious side effects. This disadvantage as well as poor water solubility limits their application. Nevertheless, other much desired chemotherapeutic features such as broad fungal spectrum, fungicidal action, or low occurrence of resistant strains among pathogens make polyene macrolides still valuable group of antifungal drugs. Several reviews, concerning chemical, physical, and chemotherapeutic properties of PMAs were published within the last two decades [3–10]. The most known PMA is AmB, which is still used as a life saving drug (golden standard or rather drug of choice) to treat systemic fungal infections. It is worth to mention here that AmB is probably the oldest antibiotic still used in clinical practice. It was discovered in early 1950s [11,12] and introduced as a drug in 1959. Several very interesting reviews concerning just properties of AmB and its mode of action were published within recent years [10,13–17].

Cellular mechanism of action of PMAs is very complex and still not known in details. Generally, it is accepted that PMAs interact with plasma membranes of sensitive organisms (containing sterols [18]) causing an impairment of barrier function, leakage of cellular constituents, and ultimately cell death ([19–22] and reviewed in Refs. [4,6,7,13,15,16,23]). However, data collected from many laboratories suggest that lethality of sensitive cells is not a simple consequence of

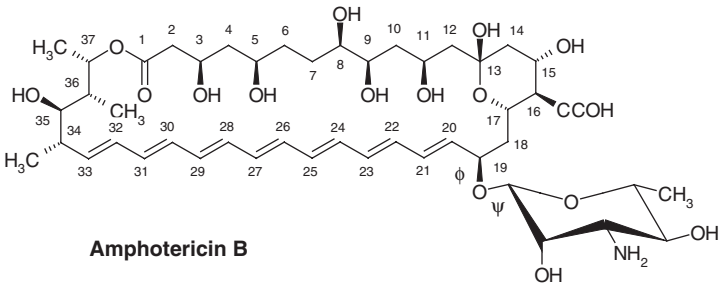

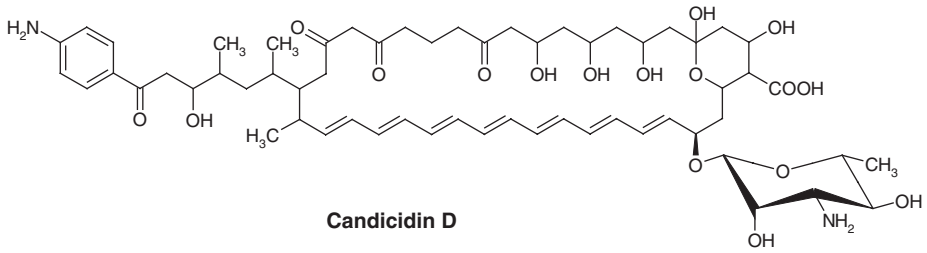

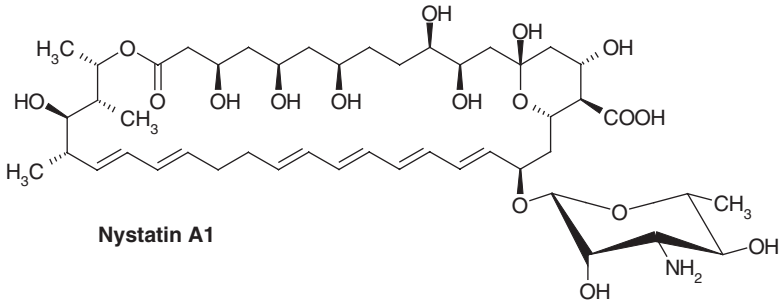

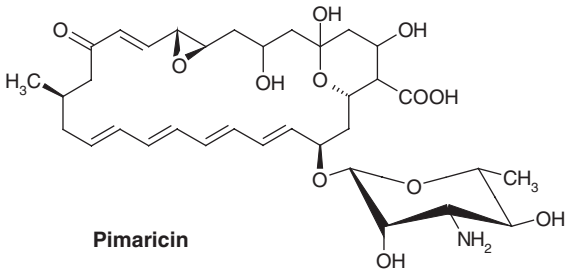

Fig. 1. The structures of selected PMAs. Numbering of atoms was introduced for lactone ring of AmB.

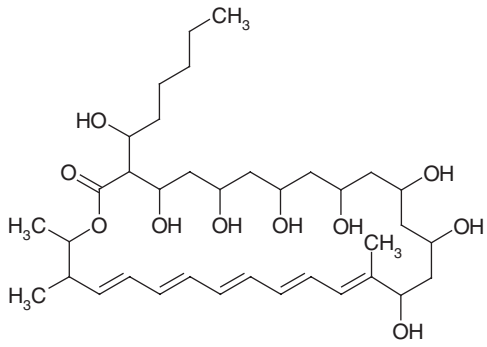

Filipin

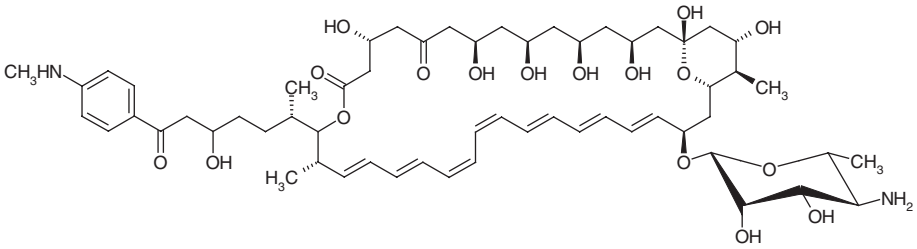

Perimicin A

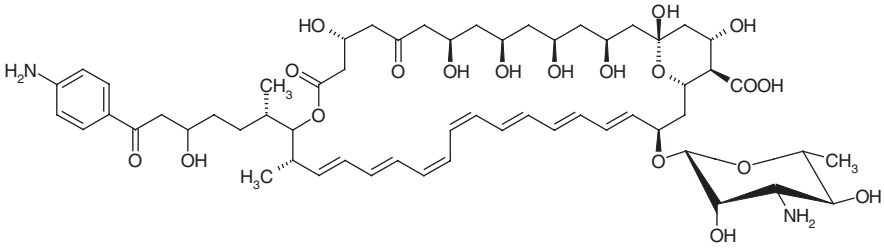

Vacidin A

Fig. 1. (continued).

changes in permeability of cell membranes for all polyene macrolides [13,24–29]. Concerning mechanism of action of two important PMAs, AmB and nystatin, it is known that they form membrane channels which cause leakage of monovalent ions (K^+, Na^+, H^+, Cl^-) and small organic molecules [19–21,30,31]. Chemotherapeutic application of AmB is based on higher sensitivity of ergosterol-containing fungal cells to the antibiotic compared to cholesterol-containing mammalian cells [32–34]. There are only minor differences in the chemical structure between cholesterol and ergosterol molecules (Fig. 2) and reasons why the ergosterol-containing membranes are more sensitive than the cholesterol-containing membranes are still

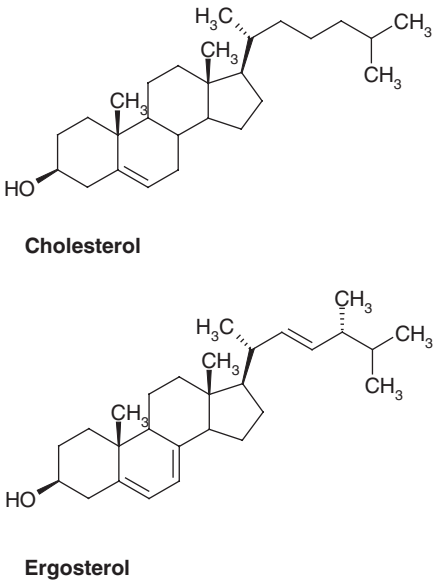

Fig. 2. The structures of cholesterol and ergosterol molecules.

poorly understood. The question still remains whether these differential effects originate solely from a preferential binding of AmB to ergosterol, or whether they originate from a different modulation of the membrane properties by ergosterol and by cholesterol, which then results in differences in susceptibility to AmB. Taking into account current data three phenomena can be considered as responsible for selective toxicity of AmB: (i) ergosterol and cholesterol membranes in a different way accommodate the antibiotic molecules, and extant of association of the antibiotic in the extracellular medium (presumably also the structure of associates) is important for the penetration of the antibiotic into the membrane [35,36] or (ii) for unknown reasons, the ability to form channel by antibiotic molecules present in the membrane is greater in ergosterol- as compared to cholesterol-containing membranes or (iii) structure and stability of channels in ergosterol and cholesterol membranes are different and therefore, only the channels formed in ergosterol-containing membranes are active [37]. One may also think that all three or two of the above mentioned factors work together in a cooperative way and are responsible for the selective toxicity of AmB and its derivatives.

Due to increasing number of immunocompromised patients and uncontrolled use of wide spectrum antibacterial antibiotics, fungal infections have become more frequent. The increase of fungal infections is also caused by uncontrolled use of wide spectrum antibacterial antibiotic. Therefore, searching for new antifungal drugs [38–41] or development of polyene macrolides (old standards) toward less-toxic derivatives [42,43] or formulations [44,45] becomes more and more important. However, rational elaboration of new less-toxic AmB derivatives

will be possible when mechanism of PMA action is known in details. Application of modern approaches in the development of novel polyene macrolides is also very welcome. These new efforts apply recent genetic studies of microorganisms producing polyene macrolides [46] and, *via* genetic engineering, open way to biosynthesis of novel polyene macrolides. Such new PMAs may contain modified groups, which are currently not accessible for chemical synthesis [9].

Due to the importance of polyene macrolides antibiotics for fungal chemotherapy as well as their unique mode of action, this critical review is aimed at presenting recent studies on PMA mechanism of action. This mechanism is based on PMA interaction with biological and model membranes, formation of different supramolecular structures inside the membranes, and changing properties and permeability of these membranes. In particular, we will focus on mechanisms, which concern interaction of PMAs with lipid membranes and their components. Cellular membranes are complex heterogenic structures and studies of interaction between PMAs and natural membranes are difficult and results are not easy to interpret at the molecular level. Therefore, molecular aspects of PMA–membrane interactions have been studied on different simpler membrane systems, which are good models of cellular membranes. These systems include lipid monomolecular layers, lipid bilayers, lipid vesicles, and ''*in silico*'' computer membrane models. Reviewed studies on PMA–membrane interactions (comprising results from our and other laboratories) were aimed at understanding which molecular factors determine selective toxicity of polyene macrolides toward fungal cells compared to mammalian cells.

1.1. Structure and physicochemical properties of PMAs

Structure of PMAs is very complex because PMA molecules contain a macrolide ring, polyene double bonds system, many functional groups, and asymmetric centers [3]. Due to such complex structure and problems with purification, only limited number of PMA 3D structures (including configuration and conformation) were resolved by X-ray [47,48] or NMR methods (e.g. recent works [49–54]). Structure of PMAs determines their chemotherapeutic action and particularly their mode of interaction with membranes. Therefore, detailed presentation of PMA structure is described below and will further help to understand and to discuss the mode of action of PMAs. Molecules of PMAs contain: (i) 20–40 carbon atom lactone ring (the so-called macrolide ring) with several (three to eight) conjugated double bonds and (ii) generally one aminosugar moiety and carboxyl group which are attached to this ring (Fig. 1). Subgroup of polyene macrolides, the so-called aromatic heptaenes, additionally contains side chain with aromatic ring, which is attached to a lactone moiety.

The PMAs are divided, with regard to the size of the macrolide ring (which determines their mode of action), into two groups: containing small (e.g. filipin or

pimaricin) or large macrolide ring (e.g. AmB or nystatin). PMAs containing small macrolide ring usually exhibit detergent type of activity in lipid membranes (e.g. filipin). On the other hand, PMAs containing large macrolide ring are prone to form ionic channels in membranes. With regard to the number of conjugated double bonds in a polyenic chromophore PMAs are classified into trienes, tetraenes, pentaenes, hexaenes, heptaenes, and octaenes [3]. Number of conjugated carbon–carbon double bonds determines spectral properties of PMAs and rigidity of the macrolide ring.

In addition to chromophore, the macrolide ring of PMAs contains other functional groups such as hydroxyls, carbonyls, or epoxides. These groups are located opposite to chromophore region in the macrolide ring (Fig. 1). This part of the PMA ring, containing polyol chain, is rather polar and is presumably responsible for PMA–water or PMA–PMA interactions (e.g. self-association or interaction of PMA molecules in the channel structure). Most PMAs also contain fragment comprising several carbon atoms that forms hemiketal moiety (Fig. 1) [55]. This region is located close to carboxyl group and presumably influences both rigidity of the macrolide ring and polarity of this region.

The aminosugar moiety (usually mycosamine and sometimes perosamine) together with carboxyl group defines a polar fragment (‘‘polar head’’) of the molecule. The aminosugar is linked *via* a glycosidic bond to the first carbon atom after the chromophore region (Fig. 1). One may expect some free rotation of the aminosugar moiety around glycosidic bond and indeed it is expected that mutual position of macrolide ring and aminosugar part is important for biological action of PMAs (some conformational studies were performed only for AmB) [37,56–62].

Several structural requirements for biological activity of PMAs were assigned [63]. To be active, PMAs need to contain macrolide ring with double bond system. Heptaenes are the most active against fungi and aromatic polyene macrolides are more active against fungi than non-aromatic PMAs [64]. The polar head plays important role in antifungal activity of PMAs. Protonable amino group should be present in this polar head to preserve the activity [64–67]. On contrary, the carboxyl group is not important for activity but substitution of this group improves selective toxicity of PMAs [67,68].

Those PMA molecules which possess at the same time both free carboxyl and amino group exhibit amphoteric properties under physiological conditions [69]. Due to chemical properties of carboxyl and amino groups, both of them are the most typical locations for chemical modifications (different *N*-substitutions of amino group and amides or esters of carboxyl group). Numerous of such modifications, leading to different derivatives, were mainly obtained for AmB [42,43,70–76] but also for some other PMAs [67,77–79]. Some other regions of AmB, namely position C-13, C-14, and C-16 (Fig. 1) were also modified [80–82]. Numerous modifications of the above-mentioned groups led to changes in physicochemical and biological properties of PMAs. These studies created the base both for better understanding the mode of PMA biological action and for rational

designing of new less-toxic derivatives of parent compounds (hopefully new drugs). For instance, different modifications of AmB and biological studies of these new AmB derivatives revealed that bulky substituents at amino group and lack of the free carboxyl group may improve selective toxicity of this antibiotic [42,43,68]. These data apparently also show that known PMAs still can be regarded as an unexplored source of new potent antifungal agents exhibiting highly desired chemotherapeutic features.

Polyene macrolides also exhibit amphiphilic properties that stem from structural elements of macrolide ring. Traditionally, one may distinguish (i) polar part containing polar head and polyol chain and (ii) hydrophobic part containing chromophore region. This simple view, however, is more complex. For instance, the amphiphilic property of AmB was shown at molecular level by distribution of molecular electrostatic properties for this molecule [83].

Due to amphiphilic and amphoteric properties, PMAs are very poorly soluble in water but also in pure non-polar solvents. Solubility and the state of PMAs in aqueous media are well characterized only for AmB and some its derivatives [36]. AmB in polar organic solvents (e.g. methanol, ethanol, DMF, and DMSO) exists as a monomolecular dispersion and its optical absorption spectra are not concentration dependent. On the other hand, in aqueous media the optical absorption spectrum of AmB is concentration dependent [84,85]. AmB is fully soluble in water only below concentration 10^{-7} M (monomeric forms). When the concentration increases above 10^{-7} M, AmB undergoes complicated processes of self-association and formation of dimers, soluble oligomers, and at concentrations higher than 10^{-5} M, insoluble aggregates are observed. The associated forms of AmB are characterized by totally new UV–Vis spectra. Several models of aggregation of AmB in aqueous media were proposed: small close packing units [86], big aggregates having helical structure with a repeat unit containing two AmB molecules [87–89], tube-like hydrophobic pores formed by several AmB molecules [90,91], and dimers of different structure [91–93]. Extent of aggregation of AmB depends on various parameters [66,85,86,90–104], which were studied extensively in order to improve solubility of this drug. It has been found that presence of fixed charge in the molecule of the antibiotic improve solubility [85]. It has also been established that the state of aggregation of AmB determines ergosterol/cholesterol selectivity in antibiotic sterol suspensions as well as in of model and cell membranes [35,98,100,105–108].

Due to amphiphilic properties PMA molecules not only form different aggregates in aqueous solution but also tend to form specific monolayers in contact with polar surfaces. For instance AmB forms monolayers at the air/water interface [109–112]. This ability of PMA molecules was used to study interaction between AmB molecules and sterols or lipids in monolayers (Langmuir monolayer techniques and Brewster angle microscopy) [107,113–121].

PMAs due to conjugated double bond system exhibit characteristic spectroscopic properties. UV–Vis and circular dichroism (CD) spectroscopy appeared

to be a powerful monitoring technique to follow the organization of PMAs in various experimental systems due to the dependency of the shape and position of absorption maxima on the dipole–dipole interaction between chromophores of neighbor molecules in the formation of aggregates. The UV–Vis spectra of PMAs show characteristic shapes with several absorption bands in the region (350–450 nm) [3]. Molar extinction coefficient, spectrum shape, and position of bands are dependent on the number of conjugated double bonds system in the polyenic chromophore and their geometry (all-*trans* AmB, *cis*–*trans* aromatic heptaenes) as well as properties of the environment. Absorption spectrum of the monomeric form of heptaenes presents a vibronic structure and four bands are generally observed. Spectra are independent on concentration and absorbency increase with concentration in accord with Lambert–Beer's law. In water, PMAs are poorly soluble and in monomeric form they exist only in very low concentrations (AmB $< 10^{-7}$ M). At higher concentrations, they undergo self-association, reflected in drastic changes of their spectroscopic properties. In aqueous media, spectra are concentration dependent and are well characterized only for AmB and some its derivatives. Spectrum of the monomeric form of AmB in water is similar to that in organic solvents, but the new UV–Vis spectrum exhibit a hypsochromic as well as a batochromic spectral shift with two new bands [85,90] and molar extinction coefficient (ε) is lower (in methanol and water ε are 160,000 and about 100,000, respectively).

Circular dichroic spectra of polyene macrolides are also concentration dependent [85,86,94,95]. CD spectra of the monomeric form of AmB show weak positive bands located at the same wave length as in UV–Vis spectra. This CD spectrum undergoes dramatic changes for aggregated forms of AmB and other PMAs [6,85]. Self-associated species of PMAs are characterized by very intense dichroic doublet around 340 nm ($\Delta\varepsilon$ amplitude 1000 $cm^{-1}\,mol^{-1}$ in water) and a signal above 435 nm. Intensity of the doublet reflects extent of association and is used in the quantitative determinations of the proportion of monomeric and self-associated forms of the antibiotic [85,86,92,101,106].

Fluorescence spectroscopy was less extensively applied than UV–Vis or CD methods in studies of PMA molecular properties mainly due to low quantum yield of fluorescence for polyenes [91,122,123]. The polyenes with shorter polyenic chromophores (filipin, pimaricin, etruscomycin, and nystatin) are fluorescent. Lifetime and quantum yield measurements suggested that in solution, the fluorescent properties of nystatin are identical to those of parinaric acid containing tetraenic fluorophore and similar to those of diphenylhexatriene [124]. Therefore, fluorescence properties of nystatin have been used to investigate behavior of this antibiotic in solutions and membrane preparations and comprised intermolecular interactions, incorporations into bilayers, and effect on bilayer structure. It was generally regarded that the heptaene antibiotics, aromatic, and non-aromatic do not exhibit fluorescence. Until recently, the fluorescence of AmB has been thought to be due to pentaene impurities [125]. However, AmB fluorescence was

established and both emission and excitation spectra appeared to be especially useful in analyzing monomer/dimer transitions of AmB molecules in solution and in lipid membranes [91,126]. The analysis of fluorescence spectra of AmB in 2-propanol–water solvent mixture revealed existence of the two separate excitation bands and the corresponding emission bands shifted approximately by 50 nm [91]. The short wavelength fluorescence excitation spectrum has been assigned to dimeric forms of AmB, on the basis of the exciton splitting theory and van't Hoff dependency [91]. The fact that these two bands can be analyzed in parallel in the same system, provided a tool for studying dimer formation by AmB in the lipid membrane environment as a function of the drug concentration and temperature [91,127].

1.2. Chemotherapeutic value

From the very beginning it was found that PMAs exhibit antifungal activity [1,128]. Fungal cells are highly sensitive to all PMAs, mammalian cells are somewhat less sensitive, while bacteria and blue-green algae are insensitive [18]. Some past and recent studies report also other types of biological action of PMAs, namely: antiparasitic activity [129–133], antiviral (including anti-HIV) activity [134–137], antiprion activity [138–141], and prevention of fibrillization in amyloid diseases [142]. It was also found that PMAs exhibit immunostimulatory effects [13,143–146].

Antifungal activity of PMAs is of primary importance for their practical application in chemotherapy. Several of PMAs are used as antifungal drugs: AmB, nystatin, pimaricin, candicidin, methyl partricin, and trichomycin [9]. AmB is applied in the treatment of fungal systemic infections and the other above-listed drugs are used only for topical infections. Usefulness of AmB for antifungal chemotherapy of various internal mycoses stems from the unique properties of this drug: (i) a very broad antifungal spectrum, (ii) a very high antifungal activity, (iii) a fungicidal type of action, and (iv) a reluctance to induce resistance (resistant fungal strains to AmB appear infrequently) [4,10,14,15,17]. However, the use of AmB is limited by two factors: high toxicity and poor solubility. AmB can produce a wide variety of acute and chronic side effects (including anaphylaxis, nausea, phlebitis, and chills), the most important of which is nephrotoxicity [147–150]. If this drug were not effective against so many fungal pathogens and exhibit other useful properties, it would have been abandoned many years ago. But AmB remains the most effective drug in treating systemic fungal infections (especially as a life saving drug of the first choice) despite the recent opinions that "treatment standards are beginning to grow old" [151].

To overcome problems with toxicity of AmB several approaches have been applied. The most rational approach would be to recognize differences between mechanisms of antifungal action of PMAs (reviewed in Refs.

[4,6,7,9,13,15,17,23,33]) and mechanism of their toxicity [29,149,152–158]. Knowing bases of selective toxicity would enable to design less-toxic (more selective against fungal *versus* mammalian cells) derivatives of parent compounds. These studies have been performed for a long time and are continued with a hope that finally new AmB derivatives or other PMAs will be introduced as an antifungal drug against systemic infections. Such studies, however, take time and in case of polyene macrolides are extremely difficult.

Other approaches, based rather on experimental trial and fail efforts, were focused on screening type search for new less-toxic AmB derivatives [72]. This approach was successful only to some extent. Amphotericin B methyl ester (AME) [70], a result of such search, appeared to be less toxic and better soluble in water than AmB itself and therefore, it was admitted to clinical trials. The AME apparently appeared to be neurotoxic [159,160] and eventually was not further developed, although some later studies on purified compound did not confirm its high neurotoxicity [161]. In order to lower toxicity of AmB, new delivery systems (i.e. liposomes, lipid formulations [17,45,162–167] and micellar systems [168–170]) were developed. First trials with liposomal AmB delivery systems come from early 1980s [171–173]. Within the last 20 years several liposomal and lipid-complex formulations of AmB were developed and few of them are allowed to use in clinical practice (i.e. Abelcet, AmBisome, and Amphotec) (reviewed in Ref. [167]). Many accumulated data show that these new formulations are not less active than classical AmB formulations (i.e. Fungizone, which is amphotericin B deoxycholate complex) and in some infections are superior to Fungizone due to their lower toxicity. However, the serious limitation of a wide practical application of new AmB lipid formulations is their cost, which is much higher than for conventional Fungizone [174].

1.3. Mechanisms of antifungal and toxic action of PMAs

Mechanism of antifungal activity of PMAs is pleiotropic. It is generally assumed that primary mode of action of PMAs responsible for fungicidal as well as toxic effect is destruction of cell membrane as a permeability barrier [19,21,30,31,175]. However, increase of membrane permeabilization, especially for ions, not always is lethal for the cell [24,25,176]. It has been suggested that other mechanism, such as lipid peroxidation and membrane enzyme inhibition may occur [13,176–178]. Also endocytosis detected for AmB in case of mammalian cells may take part in toxic effects of PMAs.

Channel formation by PMA molecules (especially AmB and other heptaenes) is regarded as the principal factor responsible for membrane permeability, consequently leading to lethal effects. First models of such ionic channels were proposed on the bases of permeability studies on model black lipid membranes (BLM) and cells [30,179]. It was postulated that the channel is formed by two

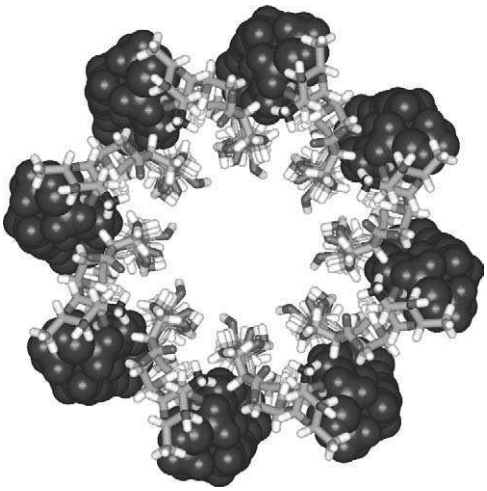

Fig. 3. Computer model of AmB–sterol channel in the lipid membrane based on the idea from work of De Kruijff and Demel [179] and subsequently used in the MD studies of Baginski *et al*. [61]. AmB molecules are presented as sticks and cholesterol molecules as a dark space filling models.

half-pores located one above the other in the bilayer (which was later named double length channel (DLC)). Each half-pore contains eight molecules of antibiotic and eight molecules of sterol arranged alternately (Fig. 3). Molecules of the antibiotic are oriented parallel to each other and perpendicular to the plane of the membrane. The polyhydroxyl parts of AmB molecules form the channel interior (filled with water molecules) and the hydrophobic parts of the antibiotic molecules interact with the lipids. Further this model was elaborated in experimental studies comprising conditions of its formation, permeability characteristics, and role of antibiotic structure [16,29,180–183] as well as in theoretical studies on chemical structure and molecular properties of these channels [37,61,184–191].

Half-pore AmB channel has been named a single length channel (SLC). Two SLCs arranged in a tail-to-tail configuration may form a DLC. It was postulated that SLC AmB channels are formed when AmB is administered to only one side of the lipid bilayer, and DLCs are formed when AmB is added to both sides of the membrane [35,182]. Both channels can permeate ions, and depending on the membrane parameters (i.e. lipid composition and membrane thickness), and on the availability of AmB, both SLC and DLC types of channels can coexist and function. Since under medical usage conditions AmB is administered only from the extracellular side of the cell plasma membrane, it is more likely that only SLCs would be formed in such case. In experiments using artificial BLM, single length AmB channels have been observed to have selective permeability to monovalent cations over anions [30,180,182,192]. Moreover, experiments using single length

AmB channels formed in small and large unilamellar vesicles showed that the ion selectivity depends on the AmB concentration [193]. Even though SLC has cation selectivity, the difference between ion permeabilities is not significant and both negatively or positively charged monovalent ions are transmitted through both types of AmB channels at physiological conditions. The reason for poor ion selectivity is probably the large size of the AmB channel; the pore diameter has been measured to be 7–10 Å, which is larger than the diameter of many protein channels.

Recently, it has been shown that AmB, at high concentration may also form channels in sterol-free membranes [194–197]. However, one may expect that molecular properties (and especially structure) of channels formed in sterol-free and sterol-containing membranes are different. Therefore, it is very unlikely that channels formed without sterol would be of chemotherapeutic relevance.

The mechanism of polyene macrolide channel formation in cell membranes is mostly undiscovered. Two main pathways of channel formation may be postulated: (i) one-step mechanism and (ii) sequential mechanism. In one-step mechanism, a critical number of polyene macrolide molecules (studies concerned AmB) on a membrane surface are necessary to form a pore [198]. AmB molecules tend to form monolayers at the air/water interface and the same behavior of polyene molecules is expected at the water/membrane interface (membrane surfaces). Accumulation of AmB molecules at the membrane surface was recently observed by atomic force microscopy studies [89]. These studies may support one-step mechanism. On the other hand, hypothesis describing sequential mechanism is also attractive. Due to amphiphilic properties, AmB single molecule of this antibiotic is rather not able to enter the membrane [330]. However, different AmB dimers or higher associates (including postulated helical structures [88]) may first interact with membrane surface and then penetrate the membrane. Associated species of AmB, present in water, have to isolate hydrophobic parts of the molecules from an aqueous environment [86–88,90–92]. Entering the membrane requires structural rearrangement of such AmB complexes and exposition of hydrophobic fragments of polyene molecules into the membrane environment. Sequential mechanism suggests that presumably dimers are building blocks of the channels. Such dimers while entering the membrane may interact with phospholipids and sterols. Sterols may play a crucial role in orientation and guiding the polyene macrolide complexes (e.g. dimers) inside the membranes. Additionally, sterols may stabilize the channels when they are formed. In this case, sterols can be necessary both for AmB–sterol interaction as well as for separation of AmB channels from destructive effects of phospholipids [37,61,199].

Why and how structural differences between cholesterol and ergosterol may lead to higher AmB–ergosterol than AmB–cholesterol containing membrane affinity was only hypothesized [65,200]. It was postulated that the molecular structure of ergosterol better complements to AmB [201] and that the presence of

additional carbon–carbon double bonds in the sterol side chain reinforces the electrostatic interaction between ergosterol and AmB molecules [83,202,203]. One may also postulate that small structural differences lead to small differences of interactions between AmB and sterol molecules. However, since many AmB molecules are involved in the formation of a single membrane channel, cumulative effect of such small differences can have a significant influence on the stability of the channel. The importance of structural features of sterols for AmB activity is further supported by experiments showing that AmB resistant fungal strains contain modified sterols, which have structures very similar to that of ergosterol, in their plasma membrane [204]. These small structural differences between sterols are suggested as the source of resistance. Also studies with enantiomeric forms of cholesterol indicated that geometry of AmB–sterol interaction is very important for activity/toxicity of this antibiotic [205,206]. One may also consider that structural differences and various integrities of cholesterol and ergosterol-containing membranes can be responsible for selective toxicity of AmB. In this case, sterol–phospholipid interactions may influence permeability of AmB in a different way in cholesterol- and ergosterol-containing membranes.

1.4. Importance of studies on model membranes

Due to the fact that a cellular target for PMAs is the cell membrane, studies of interaction between PMAs and membranes (natural and model) as well as with their components are of primary importance to understand details of chemotherapeutic action of PMAs and especially selectivity of these antibiotics against fungal *versus* mammalian cells.

Biological membranes contain, as their fundamental structural element, the lipid bilayers, which are the assembly of amphiphatic lipids. Lipid bilayers are relatively impermeable barriers separating the cells from their environment and controlling the entry of materials into a cell and the exit of materials from a cell. Cell membranes are composed of a complex array of glycerophospholipids and sphingolipids that vary in head group and acyl chain composition. The main membrane lipid classes are phospholipids (among which the most common are phosphatidylcholines), sphingolipids, and sterols (cholesterol in mammalian cells, ergosterol in eukaryotic microorganisms, and stigmasterol and sitosterol in plant cells). Each biomembrane contains a complex, but characteristic, mixture of different phospholipid species with variations in aliphatic chains and polar head groups.

According to current domain model of cell membranes, the lipid bilayers are presented as more mosaic than fluid structures. Classical view of cell membranes as fluid–mosaic model of Singer and Nicolson [207] was recently extended by the introduction of lipid rafts. Lipid rafts are conceived as functional lipid microdomains, rich in sphingolipids and cholesterol, responsible for trafficking of lipids,

and lipid-anchored proteins [208,209]. Sterols are essential constituents of most eukaryotic cellular membranes and in many other biological membranes they occur at high concentrations. In living cells, sterols perform two functions: metabolic and structural at the membrane level. The sterols, characteristic for phylogenetic group, are essential growth factors. This metabolic role requires very small amount of specific structure sterol. The other, bulk sterol function in the membrane is to maintain membrane integrity under a variety of physiological conditions by mediating membrane fluidity *via* its effect on the properties of the phospholipid bilayers. This function has less-stringent structural requirements. The main role of sterols in model membranes is to stabilize the arrangement of phospholipids in the bilayer. The effects of sterols on phospholipids are very complex and depend on both: the sterol structure and the fatty acid acyl chain structure of the phospholipid. There have been very few detailed studies as to the effects of sterols other than cholesterol on the structure and physical properties of the phospholipid bilayer [210]. Numerous studies on model membranes showed that cholesterol molecules intercalated into the phospholipid matrix release the rotation and translation of the phospholipid molecule in the gel phase while they restrict this motion in the liquid-crystalline phase. Above 25 mol% in both saturated and unsaturated phospholipid membranes, the intermediate fluid phase, discovered by Chapman some years ago, is formed. The phase combines properties characteristic of gel and liquid-crystalline bilayers [211]. Three main structural features of sterols have been linked to its characteristic effects on lipid bilayer membranes: a planar ring system (Fig. 2), 3β-OH group, and long hydrophobic side chain linked to C 17 [212,213] (Fig. 2). However, all sterols that meet these requirements were less efficient than cholesterol in modulating phospholipids bilayers properties. In lipid membrane, cholesterol can be incorporated up to 50 mol%. Such sterol–phospholipid ratio is found in some mammalian cells, for example erythrocytes. Ergosterol content in fungal cell membrane is around 15 mol% or lower. In experiments using spin-labeled probes it has been shown that 15 mol% was the effective solubility limit for ergosterol in yolk egg phosphatidylcholine (EPC) planar multilayers. In the presence of dicetylphosphate, uniform incorporation of ergosterol can be increased up to 30 mol% [214]. The latest ^{2}H NMR results obtained for dipalmitoylphosphatydylcholine (DPPC) containing 12.5 or 28 mol% cholesterol or ergosterol with respect to the phospholipid content indicate that both sterols cause increase of the acyl chain order of DPPC, this increase being slightly greater with cholesterol [215]. On the other hand, recent steady-state fluorescence anisotropy experiments with a fluorescence probe revealed that DPPC membranes (studies on liposomes) in their liquid-crystalline state are more ordered by ergosterol than cholesterol molecules [210].

Thus cellular membranes are very complex heterogeneous systems modulated by many components. Therefore, studies of molecular interaction of AmB or other polyenes with cell membranes are very difficult and hindered. Results coming

from experiments with cells treated by AmB are usually susceptible to various interpretations. Due to this fact other simpler systems such as membrane models are taken into account. Model membranes such as lipid vesicles, lipid monolayers and bilayers, as well as *in silico* computer models are good representatives of cellular membranes. These systems, usually containing only one or two types of lipids, are much simpler than regular cellular membranes. These models were also extensively used in studies of interaction of polyene macrolides with membranes and are the subject of our review.

2. INVESTIGATION OF AmB IN LIPID MONOLAYERS

2.1. AmB in planar lipid bilayers

Black or bimolecular lipid membranes (BLMs) are a powerful model of studying transport properties of lipid membranes [216]. Originally, the bimolecular lipid membranes were formed on a small aperture ($\sim$1 mm), separating two electrolyte compartments [216]. Such a model has appeared very useful to demonstrate that AmB, incorporated to lipid membranes, facilitates transport of monovalent cations across a membrane [217–220] and therefore provide a background to the hypotheses on AmB membrane channels.

2.2. Why study AmB in monomolecular layers?

When amphiphilic molecules are deposited at the polar–non-polar interface, they adopt such an orientation that polar groups of the molecules are anchored in the polar phase and apolar portions of the molecules are placed in the non-polar phase. Very similar molecular arrangements can be obtained when amphiphilic molecules are deposited at the air–water interface. The portions of the molecules with polar groups will remain in contact with the water phase since the hydrophobic portions of the molecules will be located in air. Lipids are a very good example of such a localization and orientation at the air–water interface. When molecules at the interface are compressed with a hydrophobic barrier a compact monomolecular layer of lipids is formed, which is a very good model of a single leaflet of the lipid bilayer, playing the role of a biomembrane. Monitoring of surface pressure (π), which is a difference between the surface tension of pure water and the surface tension of water with the surfactant deposited, makes it possible to perform detailed analysis of molecular arrangements and interactions at the interface [221–223]. For example, when surface pressure recorded during the monolayer compression *versus* mean molecular area is plotted (A, a current surface occupied by deposited molecules divided by the number of molecules),

one obtains the so-called isotherm of compression or π–*A* curve that can be used to determine the surface occupied by the single molecule at the interface called specific molecular area. In order to do this, we extrapolate the linear part of the isotherm of compression corresponding to higher surface pressure values (in the phase of compression before collapse) to zero surface pressure and the line points the specific molecular area value in the abscissa axis (see Fig. 4). Compressed monolayers can also be deposited to a solid support at certain, selected surface pressure, by means of the Langmuir–Blodgett technique and may be subjected to examination with the application of different spectroscopic techniques such as electronic absorption spectroscopy, fluorescence spectroscopy, and Fourier transform infrared spectroscopy [221–223]. The length of AmB molecule corresponds to the thickness of the single lipid monolayer forming the bilayer membrane. Therefore, it might be expected that the drug, present in the lipid bilayer membranes, will be distributed among both membrane-forming monolayers [179]. According to this, it seems that a monomolecular layer model system provides very good conditions for the study of AmB and AmB interaction with lipids and sterols. This system has been applied to study molecular organization of AmB [111,112,224], interaction of AmB with lipids and sterols [109,112,113,225,226], and sorption and desorption of AmB to/from lipid monolayers also containing sterol molecules [107,186,227]. Selected aspects of these studies will be addressed below.

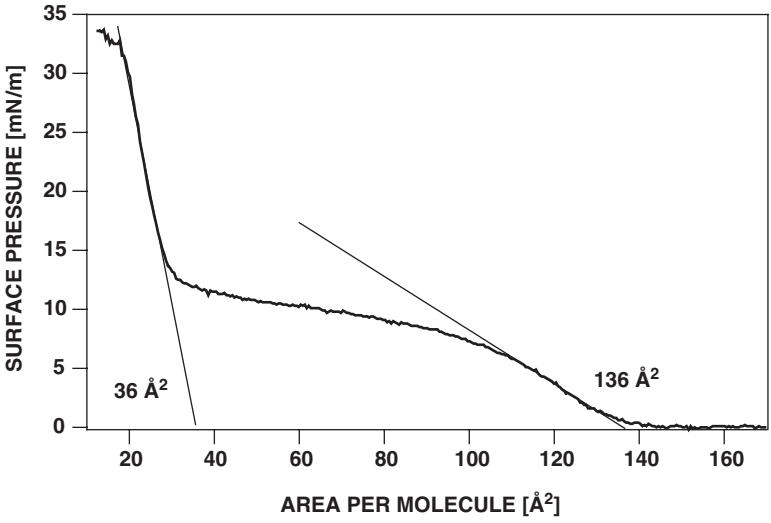

Fig. 4. Isotherm of compression of monomolecular layer of AmB formed at the argon–water interface. The linear fits to the linear portions of the isotherm of compression extrapolated to zero surface pressure point to the specific molecular areas. The speed of compression is $4.8\,cm^2\,min^{-1}$. All experimental details of monolayer deposition and compression are given elsewhere [112].

2.3. Investigation of AmB in monomolecular layers

Figure 4 presents the isotherm of compression of AmB monolayer formed at the argon–water interface. Three distinct phases of compression of AmB in a monolayer can be observed [112]. The surface pressure rises up to 10 mN m^{-1} during the initial phase of compression, preceding the phase of plateau. This phase of compression is characterized by a specific molecular area 136 Å^2. Comparison of the molecular dimensions of AmB and the value of this molecular area indicates that the molecules of the drug are oriented horizontally at the interface under such conditions. Most probably such an orientation is governed by interactions of polar groups located along the AmB molecule (in particular, the hydroxyl groups in the positions 5, 8, 9, and 11) with the subphase. The phase of plateau, in which the surface pressure is almost constant, can be analyzed in terms of a phase transition within the monolayer. Most probably, this transformation consists in reorientation of AmB molecules at the interface [112]. Such an interpretation has a strong support from the Brewster angle microscopy. The thickness of the AmB monolayer during the compression increases by a factor 3, which corresponds to the reorientation of the drug from a horizontal to a vertical position [111]. Indeed, the final phase of compression (preceding the collapse) is characterized by a specific molecular area 36 Å^2, which corresponds exceptionally well to the molecular cross-section of AmB based on the crystallographic data (approximately 6×7 Å [186]). Such a small specific molecular area indicates very compact packing of the drug in a monolayer, despite amphiphilic nature of AmB molecule also along the longer molecular side. Most probably this is possible owing to the formation of molecular assemblies. Indeed, absorption spectrum recorded from the Langmuir–Blodgett film deposited from AmB monolayer indicates strong excitonic interactions between the drug molecules in monomolecular layers (see Fig. 5). The fact that such structures are stable even at surface pressures higher than 30 mN m^{-1} indicates that formation of the same or similar molecular assemblies is possible in the environment of natural lipid membranes [227]. The analysis of the isotherms of very slow compression of two-component system composed of AmB and DPPC (9:1, mol/mol), in terms of the additivity rule, reveals an ordering effect of lipid with respect to the drug in monomolecular membranes, demonstrated as slightly under-additivity [112]. On the other hand, the over-additivity, being an indication of the destructive effect of AmB with respect to the lipid phase, has been observed at relatively low concentrations of the drug, that do not promote formation of aggregated structures of AmB in the lipid phase [113]. The electronic absorption spectra of AmB in monolayers (Fig. 5) and incorporated to lipid bilayers [91,127] are very similar and display similar hypsochromic shifts of the main absorption maxima. The absorption maximum of monomeric AmB that appears at 418 nm and corresponds to the 0–0 vibrational transition in the main absorption band is shifted toward 350 nm upon formation of the aggregated molecular structures. The analysis of such a shift in terms of the

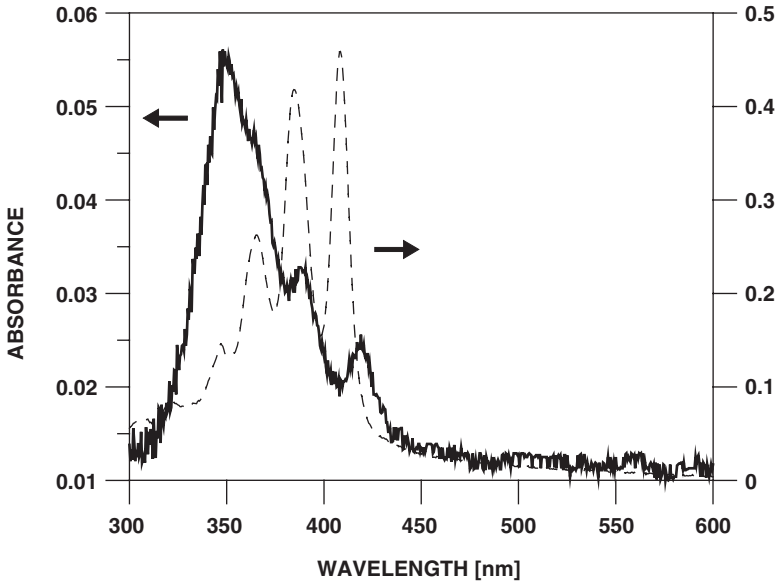

Fig. 5. Electronic absorption spectra of AmB in monomeric form in solution (2-propanol/water, 2:3 by volume, dashed line) and in aggregated form in two-component monomolecular layer composed of AmB and lipid dipalmitoylphosphatidylcholone (9:1, mol/mol, solid line) recorded from the Langmuir–Blodgett film deposited at 30 mN m^{-1}. See Ref. [112] for further experimental details.

exciton splitting theory [228–230] leads to the distance 7.8 Å between the centers of the chromophores (polyene chains) of neighboring AmB molecules [112]. This distance corresponds well to the model of pore-like molecular assemblies of AmB formed with 6–9 molecules [91,112,127]. Deposition of AmB monolayers to mica support by means of the Langmuir–Blodgett technique enabled analysis of the topography of AmB films with SFM [112]. It appeared that AmB in the lipid environment forms cylindrical structures characterized by the internal diameter 6 ± 1 Å and the external diameter 17 ± 3 Å [112]. Figure 6 presents an SFM image of two-component monolayer of AmB and dipalmitoylphospatydylcholine (DPPC) (9:1, mol/mol). The formation of the pore-like structures (also visible in Fig. 6) may be associated with the pharmacological activity of AmB. Formation of such structures may be expected owing to the fact that formation of hydrophilic pores in the hydrophobic core of the membrane would minimize energy of the system. Interestingly, linear dichroism study revealed that binding of AmB to lipid membranes is not limited to molecules oriented vertically, with respect to the plane of the membrane, able to form pore-like structures [127]. It appeared that certain fraction of AmB bound to the lipid membranes (*ca*. 38%) was oriented in the plane of the lipid layer [127]. This fraction of the drug cannot be involved in the formation of membrane channels but may act in reinforcement of the membrane structure *via* creating a network of hydrogen bonds between lipids and AmB. This

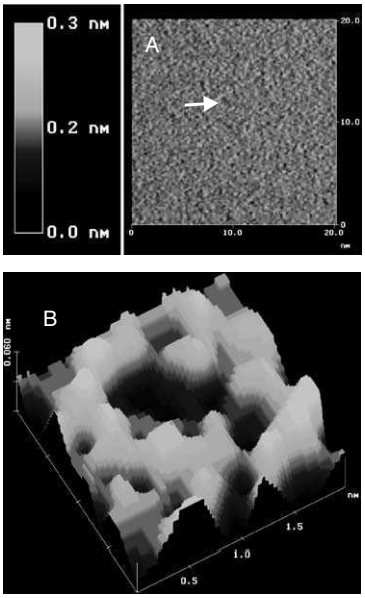

Fig. 6. SFM images recorded in deflection mode of two-component monomolecular layer composed of AmB and dipalmitoyl-phosphatidylcholine (9:1, mol/mol) deposited on mica (A) and 3D view of the selected molecular structure marked in panel A with the white arrow (B). See Ref. [112] for experimental details. The image comes from the unpublished work by P. Kernen, M. Gagos and W.I. Gruszecki.

effect influences, most probably, penetration of lipid monolayers by AmB present in the subphase [109,186,227]. The effect of reinforcement of the membrane structure by AmB also has strong support from the studies of proton transfer across model lipid membranes [331]. It appeared that incorporation of AmB at very low concentration (0.1 mol% with respect to lipid), which does not promote formation of aggregated molecular forms, slows down proton transport across the membranes. On the other hand, the incorporation of AmB at higher concentrations (3 mol%) efficiently facilitates the proton transport, most probably owing to the formation of membrane channels also observed directly in monomolecular layers.

3. INTERACTION OF PMAs WITH LIPOSOMES

3.1. Liposomes as a model of biological membranes – general characteristics

Liposomes, artificial lipid vesicles, are microscopic structures consisting of one or more concentric lipid bilayers surrounding aqueous compartments. Liposomes

have been studied extensively because of their usefulness as models for natural membranes. Phospholipids are a class of lipids most commonly used for liposomes preparations. Upon hydration phospholipids having suitably balanced sizes of their polar head groups and hydrophobic parts adopt the bilayer organization and spontaneously form closed, lamellar membrane-like structures. In the process of formation they trap solutes. Hydrophobic agents can be embedded in the lipid bilayers and hydrophilic agents can be entrapped in the internal aqueous space of the liposomes.

Liposomes were first time described in 1965 [231]. Since their discovery, liposome research and application have been evolved synergistically in different fields, mainly in biophysics, cell biology, and medicine. Within few years liposomes became the favorite systems for studying a variety of membrane physicochemical properties and membrane functions at the molecular level. In fact, liposomal studies played an essential part in developing our current understanding of biological membrane structure and function. During the early 1970s there has been a growing interest in liposomes not only as a model membranes but also as vector systems introducing various foreign molecules into cells or altering the tissue distribution of various substances in the whole organisms. Actually liposomes, besides application as a model of natural membranes in the fundamental studies, they are used as drug carriers, as a tool for the controlled DNA transfer, as well as red blood cells substitutes.

Liposomes are generally classified on the basis of size and number of bilayers. The main shapes encountered are multilamellar vesicles (MLVs), large unilamellar vesicles (LUVs), and small unilamellar vesicles (SUVs). The liposome size can range from very small (0.025 μm) to large (2.5 μm). Many different methods have been developed for preparation of liposomes. Bangham *et al*. [231] first succeeded in making multilayered liposomes that entrapped aqueous compartments and were osmotically active. The standard method for producing MLVs involves vacuum drying lipid dissolved in a solvent such as chloroform, to a thin film onto the bottom of a round-bottom flask. Liposomes are formed by adding the aqueous solution and shaking or vortexing until dry film is removed from the wall of the flask. Unilamellar vesicles of uniform size (30 nm), SUVs, were soon prepared by Huang [232] using extensive sonication. LUVs are generally made at solvent–water interfaces or by detergent removal methods. Of these, the reverse-phase evaporation method is the most commonly used procedure for the preparation of LUVs [233]. In all procedures of vesicles formation, lipids have to be in the fluid state.

The use of liposomes depends on their material properties as well as their chemical composition. The charge, rigidity, size, and surface properties of liposomes can be varied and controlled by incorporating different types of lipids and by varying the preparation methods. Liposomes made of the same components but formed by different procedures differ with respect to their properties. In fact, an almost infinite number of liposome versions exhibiting well-defined behavior in

a given environment can be produced to satisfy particular needs. In practice, the most frequent components of liposomal membrane are natural egg yolk phosphatidylcholine and synthetic ones, DPPC, DMPC, and distearoylphosphatidylcholines (DSPC). Charged liposomes are formed by including 2–10 mol% of stearylamine (positively charged) or phosphatidic acid or dicetylphosphate (negatively charged). Often liposomes are made of phospholipid–-sterol mixtures. The most commonly used cholesterol and a number of related sterols can be incorporated in the bilayer up to 1:1 molar ratio.

Bimolecular layer arrangement is a privilege structure for majority of phospholipids. The main driving forces in the bimolecular layer formation are hydrophobic interactions between aliphatic chains of phospholipids. In aqueous environment, assembling of hydrophobic aliphatic chains of lipids in the apolar interior of the bilayer release water molecules and leads to great increase of entropy in the whole system. Besides, bilayer structure is stabilized by various non-covalent forces comprising of Van der Waals interactions between apolar parts, electrostatic interactions between charged polar heads of lipids, and hydrogen bonds between their polar heads as well as between polar heads of lipids and water molecules present around. Due to the lack of covalent bonds between lipid components bilayers are dynamic structures. Lipids have freedom of rotation and lateral diffusion in the monolayer plane. On the contrary, perpendicular dislocation of the lipid molecules between monolayers (flip-flop) is energetically unfavorable.

Structure and physical state of the artificial membranes are dependent on their composition. Membrane composed of pure phospholipids may exist in a liquid-crystalline state or more ordered gel state and can undergo a thermal phase transition from one state to the other. Each phospholipid has characteristic transition temperature that is determined mainly by length and unsaturation of the phospholipid acyl chains and content of sterols, which also influence the order of phospholipid side chains. It has generally been accepted that natural membranes are in the liquid-crystalline state.

One of the functions of lipid bilayer is to form an appropriate permeability barrier. The rate of movement of water soluble molecules across lipid membranes depends on the degree of packing and the order of hydrocarbon chains of phospholipids. Ordered membranes are less permeable. Liposomes consisting mainly of uninterrupted bilayer exhibit a low permeability for ions but high permeability for water and small non-electrolytes, which is in agreement with the passive diffusion pattern of biological membranes. It is known from many types of studies that cholesterol effectively reduces membrane permeability and alters transport rate of cations, anions, and neutral solutes in liposome systems. The decrease in permeability is generally proportional to the concentration of cholesterol. The intermediate gel phase formed in the presence of cholesterol, at temperatures above and below phase transition, suggests that cholesterol could regulate the permeability of model and biological membranes by affecting the

internal viscosity and molecular motion of the lipids in the membrane. Permeability properties of liposomes have been studied either by monitoring release of previously trapped substances (radioactive or fluorescent markers, ions) or by using osmotic properties of liposomes, MLVs and LUVs (but not SUVs), behavior as ideal osmometers and exhibit linear swelling or shrinking rates when placed in the hypotonic or hypertonic solutions, respectively.

3.2. Liposomes as a model membrane system in the studies of PMA mode of action

It is well established that primary site of action of PMAs is lipid bilayer structure of cell membrane. Studies with liposomes, which are the most adequate model of natural membranes, provided an opportunity for better understanding of the mechanisms of PMAs action. Vesicular models allow evaluation of the PMA influence on overall membrane structure, properties, and permeability characteristic as well as studies of their interactions with particular membrane components. The excellent reviews of [6,16,29,234] give extensive coverage of the literature up to 1998. In this chapter, a short review of the methods used in the studies on liposomes and some new ideas about the mode of PMAs action resulting from studies on lipid vesicles will be discussed.

Liposomes of different size and composition have been extensively used in the studies of various aspects of the PMAs mode of action. First studies were performed on MLVs, later the more frequently used systems were SUVs and LUVs. SUVs have special properties not necessarily found in cellular membranes. Due to high vesicles curvature lipid molecules are more tightly packed in the internal leaflets when compared to the external leaflets of the lipid bilayer. Interfacial packing defects facilitate PMA incorporation into vesicles in the gel state [6,235]. LUVs, especially those made of natural lipids, seem to be a close model of biological membranes. MLVs are the most thermodynamically stable form of vesicles but unilamellar vesicles are advantageous than MLVs because homogeneous populations of uniform size and known amount of lipids enable to work with defined antibiotic/lipid ratio. Optical spectroscopic measurements performed with SUVs or LUVs are not obscured by the intense light scattering caused by MLVs. The parameters taken into account in PMA action on vesicular membrane included fluid or gel state of the membrane, membrane thickness, sterol presence, concentration and structure, vesicle charge and curvature, as well as stability of the antibiotic membrane binding. PMAs can readily be incorporated into a variety of liposomal systems by (i) cosolubilization of the phospholipid or phospholipid/sterol and antibiotic mixture in organic solvents before vesicles formation and (ii) by addition of the antibiotic solution to a dispersion of the preformed vesicles. In the first method antibiotic has access to both sides of bilayer and possibility of incorporation into internal and external monolayers. This type of

vesicles is analogous to ''liposomal AmB formulations'' lately introduced to clinical practice. In the second method usually small amounts of concentrated antibiotic solutions in DMSO or DMF are added to aqueous vesicle suspension. In this case, antibiotic is in contact only with the external side of the bilayer. Whether incorporation of PMAs into membranes occurs *via* fusion of self-associated species or whether it involves insertion of monomers is not yet established even for AmB. Our experimental results, based on permeability properties of studied vesicles, suggested that from the aqueous suspension, monomers of AmB are incorporated only by ergosterol-containing membranes but not by cholesterol-containing membranes [35]. Cholesterol-containing and probably sterol-free membranes incorporate antibiotic self-associated species. Madden *et al*. [236] examined the spontaneous incorporation of self-associated AmB from aqueous solution into phospholipid vesicles as a function of the lipid composition of the vesicles and their physical state. Virtually, no insertion of the antibiotic into EPC vesicles was observed even when cholesterol was also present in the bilayer. In contrast, rapid incorporation occurred into vesicles containing an anionic phospholipid (phosphatidyl-glicerol or phosphatidyl-serine) with the fastest rate observed for lipids containing the saturated dimyristoyl fatty acid species. Insertion of AmB into vesicles composed of DMPC/DMPG (dimyristoyl-posphatydyl-glycerol) mixture (7:3 mole ratio) was rapid either above, below, or within the gel- to liquid-crystalline phase transition temperature (23 °C). Authors suggested that the inability of AmB to incorporate from an aqueous suspension might indicate its inability to penetrate the bilayer in the absence of a solvent vector.

3.3. Interaction of PMAs with liposomes studied by selected methods

Liposomes have been used as models in the structural as well as functional studies of the PMAs mode of action. Structural studies comprised two aspects: (i) effect of the PMAs on overall membrane structure and (ii) the PMAs action at the molecular level concerning conformational changes of the antibiotic in the lipid membrane environment, effects of PMAs on lipid membrane components as well as on the overall membrane properties.

Influence of PMAs on the overall membrane structure has been studies by various electron microscopy (EM) methods. Initial studies using freeze-etching EM tried to associate antibiotic structure with an extent of membrane damage mainly in cells [6]. Later, freeze fracture and negative staining EM were applied in the structural studies of liposomal and other lipid AmB formulations [237,238]. Analysis of sonicated and unsonicated mixtures of DMPC/DMPG (7:3) containing various proportion of AmB showed that at low antibiotic concentration (>5 mol%), vesicular structures are formed. At AmB/lipid mole ratios of 1:3 to 1:1, unusual ribbon-like structures appeared. Negative stain EM of these ribbon-like structures

indicated that the ribbon-like appearance arises as a consequence of the cross-fracturing of what are aggregated, collapsed single lamellar, presumably interdigitated membranes. It was proposed that a ribbon-like structure results from phase separation of AMB–phospholipid complexes within the phospholipid matrix. Scanning electron microscopy (SEM) and transmission electron microscopy (TEM) examination showed that the LUVs prepared by reverse phase evaporation method, composed of phospholipids/cholesterol/AmB mixed in various molar ratios are spherical, unilamellar, or oligolamellar structures [239].

Fluorescence microscopy was used in the investigation of the spatial distribution of the AmB and nystatin in MLV suspension – composed of dilauroylphosphatidylcholine (DLPC) labeled with rhodamine B. These studies revealed that MLVs form clusters inside which the antibiotic is strongly concentrated and lipid superstructures appear to be characterized by special properties [240]. Microscopic observations were similar with AmB and nystatin and did not dependent on the mode of antibiotic incorporation into vesicles (from aqueous medium or during vesicle preparation).

Examinations of the conformational changes of the PMAs in the lipid vesicle membranes were based on the optical properties of the polyenic chromophore. The most commonly used and convenient method has been electronic absorption (UV–Vis), CD, and fluorescence. The UV–Vis and CD spectra of monomeric as well as associated forms of AmB are modified in the presence of lipidic vesicles. The changes in spectra, reflecting antibiotic vesicle interactions are dependent on the nature of lipids, antibiotic/lipid ratio, presence, structure and concentration of sterols, as well as experimental conditions. However, when antibiotic is incorporated from aqueous medium into preformed vesicle suspension, quantitative determinations of the binding constant are reliable only for antibiotic in the monomeric form. Decrease of the maximal band absorption in the presence of sterol-free and sterol-containing egg yolk, phosphatydylcholine SUV was used for determination of the association constants of AmB, candicidin, mediocidin, and water soluble guanidine derivative of AmB, with sterol-free, ergosterol-, and cholesterol-containing vesicles. The dissociation kinetics of the bound antibiotics were monitored by following the absorbency increase at one of the maxima [241]. The appearance of the antibiotic in the medium indicated reversibility of the binding and exchange of the antibiotic molecules between vesicles [242].

At higher PMA concentrations, free and bound antibiotic spectra overlap and their interpretation is difficult. In the studies in which antibiotic is added to preformed vesicle suspension, a quantitative analysis of the data obtained is hampered by the complex equilibrium that involved antibiotic aggregation in the aqueous solution [66,85], partition into lipid bilayers, and self-association in the bilayer. Interaction of AmB with lipid membrane was identified by the appearance of a new band around 415 nm and decrease in intensity or blue shift of the band around 340 nm characteristic of free self-associated antibiotic [90,234]. In DPPC LUVs containing AmB this new band was located at 415.2, 414.9, and

416.9 nm in sterol-free, cholesterol- and ergosterol-containing vesicles, respectively [243].

Situation is less complicated when antibiotic is incorporated into membrane during vesicle formation. Spectroscopic characteristics of AmB in DPPC SUVs with different relative cholesterol/AmB ratio indicated that in the membrane AmB changes from an aggregated state into a dissociated state through interaction with cholesterol. Similar determinations done in the aqueous solutions showed that cholesterol at low concentrations increase the aggregation of AmB but at higher concentrations caused dissociation of the aggregates [114].

CD spectroscopy is especially convenient in the comparative studies of the antibiotic state in various aqueous and non-aqueous environments. CD spectra of the monomeric form of AmB show weak positive bands located at the same wave length as in UV–Vis spectra. Self-associated species are characterized by very intense dichroic doublet around 340 nm ($\Delta\varepsilon$ amplitude 1000 $cm^{-1}\,mol^{-1}$ in water) and a signal above 435 nm. Intensity of the doublet reflects extent of association and is used in the quantitative determinations of the proportion of monomeric and self-associated forms of the antibiotic. Upon interaction with lipid membrane, dichroic doublet usually disappears, whereas other bands may change sign, intensity, and position. Modification of the dichroic spectra is dependent on lipid composition, sterol presence, its structure and concentration, as well as vesicle curvature and experimental conditions. For AmB many spectroscopic species have been recognized. A reduction of the intensity of the dichroic signal due to the antibiotic binding enabled quantitative determination of free and bound drug. CD method for quantitative determination of AmB binding to liposomes has been proposed [244].

Electronic absorption and CD have been the most commonly used methods in the studies of various aspects of PMA – lipid membrane interactions of several antibiotics: AmB and its derivatives, aromatic heptaenes, nystatin, filipin, and etruscomycin. The results are reviewed in Refs. [6,234]. Also in the more recent studies UV–Vis and CD were used together with other methods in the examinations of interactions of AmB [89], nystatin [240,245], and filipin [234] with lipid vesicles as well as in the studies of the properties of various new AmB formulations [246].

Quantitative analysis of the spectroscopic data has been done by Fujii *et al*. [183] for AmB stably associated with SUVs – composed of DSPC, distearoylphosphatydylglycerol (DSPG), and cholesterol. When AmB is present only in the membrane, the spectral changes reflect the specific interactions of individual AmB molecules with each other and with the surrounding lipids. Changes in the aggregation state of AmB indicated by UV–Vis and CD spectra pointed to the association/dissociation process occurring within the lipid bilayer. A large absorbency peak with maximum at 325 nm dominating in the spectrum at antibiotic lipid ratio $> 10^{-2}$ has been attributed to an aggregated state of AmB. There were also three minor peaks with absorbency maxima at 365, 388, and 415 nm. As the

antibiotic/lipid ratio decreased, the 325 nm peak intensity decreased and three minor peak intensities, characteristic of monomeric AmB increased. Singular value decomposition analysis of the CD spectra of AmB at different AmB/lipid ratios suggested that AmB exist primary in only two states in the bilayer: monomeric and aggregated. The transition from monomeric to the aggregated state begins to occur at 1 AmB per 1000 lipids in the membrane and coincides with the appearance of channel activity.

Fluorescent properties of filipin and pimaricin have been used to characterize their interactions with sterols in solution and in some membrane preparation. The changes in the partial quantum efficiency and corrected fluorescence caused by addition of sterols were different for both the antibiotics. In the presence of cholesterol decrease of these parameters were observed for filipin and strong increase for pimaricin. A strong enhancement of etruscomycin fluorescence was observed in the presence of sterol-containing lipid vesicles [247]. In the recent studies, fluorescence resonance energy transfer (FRET) between a fluorescent analog of ergosterol, dehydroergosterol (DHE) and filipin as well as steady-state fluorescence intensity, anisotropy, and absorption were measured in DPPC SUV (gel phase) [248]. Filipin emits fluorescence in both aqueous and lipid environment with similar quantum yields. FRET between DHE and filipin was sensitive to filipin concentration only in bilayer whereas in water it did not occur. The results point to the formation of both DHE–filipin aggregates and filipin–filipin aggregates. These results point out that apparently contradictory biochemical models for action of filipin (some based on the presence of sterols, others not) can be equally valid. In the membrane with low sterol concentration both the models can coexist. It means that biochemical mode of action of filipin probably involves a ''multiple-path strategy'' where several different phenomena may occur simultaneously, depending on the local filipin and sterol concentrations.

Fluorescence properties of nystatin have been used to investigate the behavior of this antibiotic in solutions and membrane preparations and comprised intermolecular interactions, incorporations into bilayers, and effect on bilayer structure. The quantum yields, lifetimes, and anisotropies as functions of temperature and nystatin to phospholipid molar ratios in dispersion of small vesicles composed of DMPC and the antibiotic have been measured [249]. In phospholipid membrane, the fluorescence lifetime of nystatin increased at least 10-fold in their gel phase as compared to non-polar solvents (THF, dioxane). Analysis of the results indicated that nystatin in all concentrations was predominantly in the bilayer in both the gel- and liquid-crystalline states and its properties in both the phases were similar. Nystatin complexes were formed with equal ease in both rigid and fluid membranes. According to the authors, the fluorescence of all parameters measured (lifetimes, quantum yields, and anisotropies) are characteristics of the emission from the monomeric species in phospholipid matrix. The nystatin emission is quenched by the increasing density of nystatin in the membrane; the nystatin aggregates cannot emit fluorescence, while the monomeric

species in the bilayer can. In the other reports [235,250], nystatin interaction with phosphatidylcholine liposomes of different size (LUVs and SUVs) was investigated by steady-state and time-resolved fluorescence measurements. The enhancement in the fluorescence intensity of antibiotic was applied to study the membrane-binding of nystatin. The results provided evidence for the formation of strongly fluorescent antibiotic aggregates in gel-phase membranes and no antibiotic self-association was detected in a liquid-crystalline lipid bilayer within the antibiotic concentration range studied (0–14 μM). The emission decay kinetics of the antibiotic interacting with the gel-phase DPPC vesicles was controlled by the mean number of membrane-bound antibiotic molecules per liposome. The transition from a monomeric to an oligomeric state of the antibiotic, which is associated with a sharp increase (about four-fold) in nystatin, mean-fluorescence lifetime begins to occur at a critical concentration of 10 antibiotic molecules per vesicle. This interpretation is in variance with a previous study [249].

Degree of antibiotic penetration into the membrane was determined in depth-dependent quenching experiments using spin-labeled fatty acid as a probe (5- and 16-doxyl stearic acid). The results obtained suggested that monomeric nystatin is anchored at the phospholipid/water interface and that nystatin oligomerization was accompanied by its insertion into the membrane. The process was quantitatively described by a cooperative partition model [235]. A fluorescent 7-nitrobenz-2-oxa-1,3-diazol-4-yl derivative of AmB, nystatin, and pimaricin have been synthesized and characterized. Nystatin and AmB derivatives have been used in photobleaching measurements of diffusion in L-cell membranes. They were not used on model membranes [251,252].

The membrane fluorescent probes, trimethylammonium-diphenyl hexatriene (TMA-DPH) [253], and cyanine dyes [254] were applied in the studies of AmB and some of its derivatives interaction with lipid membranes by energy-transfer method.

The methods of choice to investigate perturbations in the overall membrane organization upon PMA incorporation are differential scanning calorimetry (DSC) and nuclear magnetic resonance (NMR). Lipid membranes composed of pure phospholipids are characterized by a sharp endothermic peak at the transition temperature (T_m) corresponding to the gel–fluid transition. It reflects temperature-induced change in the conformation of fatty acyl chains, which form a fully extended to less ordered in the highly cooperative process. Incorporation of any component to phospholipid bilayer usually causes broadening and shift of this peak what is interpreted as a diminution of fatty acyl chain cooperativity and destabilization of the organization of the aliphatic chains. Thermotropic properties of AmB, nystatin, and filipin incorporated into liposomes composed of various phospholipids containing saturated (7:3 DMPC/DMPG mixture, DMPC, DLPC, DPPC) or unsaturated oleolyl-stearoyl-phosphatydylcholine (OSPC) acyl chains, and antibiotic free liposomes were examined. In the presence of PMAs, the average transition temperature of phospholipids was shifted upward indicating a solidifying effect on the bilayers [237,245,255,256].

In the first calorimetric determinations on the cholesterol/DPPC/AmB vesicles (SUVs) [114] it was shown that a lipid bilayer is influenced by complex formation between AmB and cholesterol. Calorimetric and spectroscopic data indicated that due to interaction with cholesterol AmB in lipid vesicles changes from an aggregated state into a dissociated one.

Comparative DSC studies were performed on sterol-free, ergosterol-, and cholesterol-containing DPPC LUVs containing various molar ratios of AmB in the membrane [243]. Data obtained have shown that in pure phospholipid/AmB membrane three phases coexist. One corresponds to the phospholipid alone and two others to the drug interacting with aliphatic chains of lipids. The fact that the transition temperatures of these additional components are higher than that of the pure phospholipids suggested that AmB interacts strongly with aliphatic chains of phospholipids. This is consistent with the idea that AmB may form aggregates or pores in pure phospholipid membranes. Thermograms of cholesterol-containing bilayers also reflected coexistence of three phases but important broadening of these components in this case indicated destabilization of the organization of the aliphatic chains by AmB. The situation was strikingly different in ergosterol-containing membranes. A broad transition was independent on AmB concentration and decomposition of the thermograms revealed only two components. Coexistence of two interacting units, e.g. AmB + DPPC and (AmB + ergosterol) + DPPC, within the membrane was proposed. These units involve the phospholipid and hence contribute to its structurization. The important differences between the thermograms obtained with ergosterol-containing bilayers when compared to cholesterol-containing bilayers provided strong evidences for different mechanism of action of AmB in these two membranes.

^{2}H NMR provides more molecular information on the dynamic state of lipid molecules when compared to other NMR techniques, and mainly this method has been applied in the studies of PMAs (AmB, nystatin, and filipin) interaction with lipid membranes composed of pure phospholipids or phospholipid–sterol mixtures. The quadrupolar splitting of the ^{2}H NMR spectra of deuterated phospholipids or sterols was measured and interpreted in terms of order parameter of the fatty acyl chain and stability of the antibiotic lipid complexes formed. ^{2}H NMR was applied in the studies of interaction of filipin [257–259] and nystatin [245] in sterol-free DLPC MLVs, AmB [199,260] with DMPC and cholesterol or epicholesterol/DMPC vesicles and lately with pure and ergosterol- or cholesterol-containing DPPC membranes [215]. In all these determinations, antibiotics were incorporated into lipid dispersions during their preparation. Filipin had some disordering effect on DMPC lipid matrix below the T_m of the gel-to-fluid phase transition and above $T_m + 11\,^{\circ}C$. In the range between these two temperatures, two lipid regions of very different dynamic properties were observed: one region which was attributed to a filipin–lipid complex had the properties of gel-like phase; the other had those of fluid-like phase, but was more ordered than the pure lipid at corresponding temperatures. In the presence of 30 mol% of cholesterol, DMPC

spectra did not exhibit any indication of a gel-like phase and filipin action was probably masked by cholesterol [258]. Experiments with vesicles containing cholesterol and different antibiotic/lipid ratios showed that filipin binds competitively to cholesterol and phospholipid and filipin–phospholipid association can occur when sterol sites are occupied. These interpretations have been suggested by parallel CD and ESR measurements [257].

In the multibilayer DMPC membranes, AmB had an overall ordering effect on lipid fatty acyl chains. At high AmB concentrations (30 mol% with respect to lipids) and at a temperature in which lipids are in fluid state (above 25 °C), DMPC experienced two different environments which are in slow exchange on the ^{2}H NMR time scale. In one of these environments, the lipid was immobilized by AmB in approximately 1:1 molar ratio, whereas the lipid unsequestered by the antibiotic was more ordered than in its pure state. The AmB/lipid system undergoes a phase transition of 5–10 °C below that of the pure DMPC. Even at high temperatures, these aggregates are embedded in a lipid matrix whose properties are similar to those of the pure lipid system [260]. The addition of AmB to cholesterol/DMPC (3:7) was perceived differently by the lipid depending upon the depth in the bilayer. The ^{2}H NMR results using labeled sterols and labeled lipids lead to the conclusion that the AmB–sterol complex exhibited ordering properties only at the level of bilayer center.

Lately [215], the effect of AmB has been investigated on pure DPPC and on cholesterol- and ergosterol-containing DPPC bilayers by ^{2}H NMR powder spectra. The ^{2}H NMR results first confirmed that AmB forms a complex with sterol-free DPPC bilayers. This interaction causes the ordering of the lipids and the increase of gel-to-lamellar fluid DPPC phase transition temperature with increasing concentration of the antibiotic. The effects of AmB on cholesterol- and ergosterol-containing DPPC bilayers are remarkably different. On the one hand, the drug causes an increase of the order of lipid acyl chains in cholesterol-containing membranes, mostly in high cholesterol content membranes. On the other, the addition of AmB disorders the DPPC acyl chains when ergosterol is present. This is thought to be due to the direct complexation of the ergosterol by AmB, causing the sterol ordering effect to be weaker on the lipids.

DSC and NMR results suggest that the general consequence of PMA association with lipid bilayer is the ordering effect on the lipid chains of phospholipids in the liquid-crystalline state.

3.4. PMAs – membrane permeability induction

Since their discovery, lipid vesicles have been commonly used in the studies of PMA influence on the membrane permeability characteristics. Most studies on the membrane permeability induction concerned ionophoric properties of PMAs. Among these properties selectivity of the permeability pathway characteristic, as

a part of antifungal and toxic action of PMAs, was examined. Another permeability property extensively studied on vesicles was dependence of channel formation and function on lipid composition of the membrane (especially concerning presence of sterol and its structure). This approach has enabled to test ''sterol hypothesis'' and to establish some relation between PMAs structure, channel formation, and functionality in vesicular membranes.

Various florescent probes, entrapped inside vesicles appeared to be convenient in the determinations of PMA-induced ion fluxes. Assays exploiting fluorescence of the pH-sensitive fluorescent probe, pyranine, encapsulated in unilamellar vesicles have been used in determination of membrane permeability to monovalent cations. Pyranine displays linear changes in fluorescence intensity with changing pH (between pH 6.4 and pH 7.8); decreasing when protonated and increasing when deprotonated. In solution composed of cation and impermeant anion, electroneutral exchange with protons is necessary to maintain the PMA-induced cation flux. When the H^+ current is facilitated by a protonophore, the drug-induced cation flux becomes the rate-limiting step. The exchange is triggered either by a trans-membrane pH gradient or a salt gradient. Many important properties of PMAs and parameters determining membrane damage have been discovered using this method.

Using kinetic fluorescence methods it has been found that AmB and nystatin have different activities on sterol-free SUVs composed of synthetic dioleoylphosphatydylcholine (DOPC) and natural EPC. Significant K^+ permeability enhancement was observed for AmB (stoichiometry AmB/lipid $>1{:}1000$) in EPC vesicles and much lower in DOPC. On the contrary, in the same experiments nystatin was not active even at 10 times higher concentration. Experiments on vesicles composed of other synthetic lipids indicated that AmB activity on sterol-free SUVs is strongly influenced even by small variations of bilayer thickness [261]. Osmotic stress greatly increases sensitivity of sterol-free LUVs to AmB present in the soluble oligomer state; these vesicles were completely insensitive under isoosmotic conditions. The related antibiotics, AME and nystatin, showed almost no activity. These differences may be attributable to various abilities of self-association and different properties of oligomers determined by antibiotic structure. Membrane defects caused by osmotic pressure were highly selective for monovalent cations (K^+) over anions (Cl^-) and were strongly dependent on bilayer thickness [196]. It was proposed that AmB worked as a ''molecular harpoon,'' an expression coined to describe substances, which can selectively target osmotically stressed, strained, or curved membranes. These results may provide a rationale for reported anti-HIV activity of AmB and activity against sterol-free highly curved SUVs. The stress dependence may be responsible for the renal toxicity of AmB as some parts of the nephron are submitted to strong osmotic stress. It was suggested that changes in the phospholipid bilayer induced by osmotic stress may catalyze the formation and assembly of AmB channel

structure within the vesicle membrane and evidenced that sterols are not necessary to produce highly cation-selective AmB channels [194].

Temperature effects on permeability induction by AmB in ergosterol- or cholesterol-containing EPC LUVs were used in the studies that supported a model of AmB action assuming that antibiotic aggregates are the major channel-inducing species in cholesterol-containing membrane whereas monomers are active only on ergosterol-containing membranes [105].

Determinations of the ionic selectivity of the pathway formed by PMAs were based on changes in the membrane potential followed by fluorescence changes of 3,3′-dipropylthiadicarbocyanine DiSC3(5). Membrane diffusion potentials induced by AmB, AME, *N*-fructosyl AmB, and vacidin A in ergosterol- or cholesterol-containing EPC LUVs were measured in various media, in order to determine the relative selectivity of Na^+, K^+, Cl^-, and other ions in these environments. Cation over anion selectivity varied with the PMA structure. It was very strong with vacidin (below 5×10^{-7} M), smaller with AmB, and none with AME and *N*-fructosyl AmB. The selectivity observed were antibiotic, concentration, and time dependent, which confirms the existence of different types of channels [193]. Subtle changes in the intercationic selectivity of the pathway formed by PMAs were monitored by measuring biionic potentials, using pyranine probe. In case of AmB, it was found that selectivity was concentration dependent. Above 5×10^{-7} M, the sequence determined for sterol-free SUVs and cholesterol-containing SUVs and LUVs was the following: $Na^+ > K^+ > Rb^+ \geq Cs^+ > Li^+$ (sulfate salts) corresponded closely to Eisenman selectivity sequence number VII. At the antibiotic concentration 5×10^{-7} M and below, the selectivity switched from $Na^+ > K^+$ to $K^+ > Na^+$. In contrast, Li^+ was the most permeant ion for AmB channels in the presence of ergosterol. In fact, the intercationic selectivity of the permeability pathways formed by AmB was weak when compared to that of typical protein biological channels.

Measurement of an increase in fluorescence due to the antibiotic-induced efflux of self-quenched encapsulated in side vesicles carboxyfluorescein (CF) or calcein (CC) was applied in the studies of membrane permeabilization by filipin. These dyes were released freely through the membranes in their anionic forms and their efflux was controlled by the release of alkaline counter ion, i.e. Na^+. CF or CC entrapped in EPC SUVs due to the filipin action was released according to an ‘‘all-or-none’’ mechanism, leaving the depleted vesicles intact. Percentage of released probes as a function of the filipin/phospholipid ratios was the same whether or not membranes contained sterol. The permeabilization of vesicles proceeded concomitantly with filipin–phospholipid binding while filipin binding leveled off. These observation and binding measured by spectroscopic methods together with previous structural findings have led to a new interpretation of the filipin mode of action. Inducement of permeability would result from the high intrinsic permeability of the interfacial region at the boundaries of the gel-like

domains corresponding to the filipin–phospholipid aggregates without any membrane-disruptive effect [262].

Calcium permeability induced by AmB in sterol-containing EPC LUVs was studied by following the modification of the absorbency of encapsulated Arsenazo III. The results obtained suggested that the channels responsible for the AmB-induced Ca^{2+} permeability have different structures in cholesterol- and ergosterol-containing membranes [263].

Monitoring of the intravesicular pH by ^{31}P NMR spectroscopy (using phosphate ions as a probe) has proved to be especially useful in the studies of ionophoric properties of PMAs. Under the conditions of obligatory proton/cation exchange, the ionophore-induced permeability can be followed by monitoring in time the position and intensity of intravesicular phosphate signals, which show simultaneously both: the total phosphate concentration and pH distribution in the whole population of vesicles. EPC LUVs are characterized by their relatively high basic permeability to protons. However, proton movement is observed only when electroneutrality is ensured. In the case of vesicles prepared and suspended in a medium containing only Na^+, phosphate, and sulfate, since none of these anions can cross the membrane, any proton movement can occur only by electroneutral H^+/Na^+ exchange. A trans-membrane proton gradient established in the vesicle suspension is a driving force for this exchange providing that proton efflux is not a limiting factor [263].

The activity of an ionophore depends on the intrinsic permeability properties of the pathway this ionophore provides and on its mode of interaction and incorporation in the membrane. The permeabilization of each vesicle by PMAs requires the gathering of a certain number of molecules sufficient to form a channel inside the vesicle membrane (or at the surface – if one concerns one-step mechanism of channel formation). Due to the very high ion mobility in the channel, the ion flux rate did not reflect the channel permeability, but rather the kinetics of channel formation. The cation release depends then on the comparative rates of the following processes: (i) the channel formation by accumulating a proper amount of antibiotic molecules in the membrane (or on the surface) and (ii) exchange of the drug between vesicles. Two extreme cases can be distinguished. If the rate of the channel formation is much higher than the exchange of the antibiotic between vesicles depletion of the pH gradient occurs by an ''all-or-none'' mechanism, and two populations of vesicles coexist. Only part of population of vesicles is permeabilized due to channel formation and has the pH of the external medium. Remaining vesicles have the initial pH. If the exchange is fast the depletion occurs by a ''progressive'' mechanism in which all vesicles are simultaneously permeabilized and lost only a part of their pH gradient [264].

Natural polyene antibiotics and their *N*-acetyl and methyl ester derivatives, which differ mainly in their electric net charge, were compared for their ability to increase the ionic permeability of LUVs. The zwitterionic compounds (AmB, vacidin, and negatively charged *N*,*N*′-diacetyl vacidin) induced permeability

according to an all-or-none process on both cholesterol- and ergosterol-containing membranes. The same mechanism of permeability induction was observed only in ergosterol-containing membranes for positively charged antibiotics (perimicin A, vacidin A methyl ester, AME) [265]. A different type of action is observed for the latter group of ionophores in cholesterol-containing vesicles. In this case, a progressive proton flux occurred in which the whole vesicle population was involved. This quantitative difference in the kinetics of ionic fluxes induced by antibiotics without free carboxyl group in cholesterol-containing membranes when compared to ergosterol-containing membranes was ascribed to differences in polyene–sterol interactions as well as in the lifetime of the ionic path formed. Antibiotics and derivatives that have a free ionizable carboxyl group induced biphasic ''all-or-none permeability'' typical of channel-forming ionophores, whatever the sterol present. In sterol-free membranes, they have no significant activity. Antibiotic and derivatives which lack a free ionizable carboxyl group exhibit this channel-like mode of action only in membranes containing ergosterol or sterols with an alkyl chain like that of ergosterol. In membrane containing cholesterol or sterols whose alkyl chain was alike, a slow and progressive permeability is observed at high concentrations of the antibiotic. These compounds are active in sterol-free vesicles as well. The greatest decrease in activity was observed for *N*-acetyl derivatives. Substitution of the amino groups has no effect on the mode of action. A model of interaction of the antibiotics with sterol was presented accounting for the data obtained on vesicles and the observed selective toxicity of polyene derivatives in biological membranes [65,264,265].

Lately, ^{31}P NMR method was applied in the studies of cholesterol concentration influence on vesicle sensitivity to AmB. It was demonstrated that cholesterol markedly inhibited ion permeability induced by AmB present in the membrane (the antibiotic was incorporated during vesicle formation) [266]. This could be accounted for a membrane-thickening effect of cholesterol since AmB action is known to be markedly affected by the thickness of membrane. Upon addition of AmB to preformed LUV suspension, the ion flux gradually increased with increasing molar ratios of cholesterol up to 20 mol%. These biphasic effects of cholesterol could be explained at least in part, by ordering effect of cholesterol [266].

Electron paramagnetic resonance (EPR) technique has been applied in the studies of AmB-induced permeability of both unilamellar and multilamellar liposomes. The loss of EPR signal of a spin probe TEMPO choline, trapped in the aqueous compartment of MLVs or SUVs upon addition of ascorbate ions to the bulk aqueous phase was monitored. The effect of antibiotic was dependent upon the antibiotic/sterol molar ratio as well as on the state of the membrane [267]. AmB caused large increase in permeability of cholesterol-containing EPC membranes (liquid-crystalline state), whereas the effect was small in the absence of sterol and did not depend on the vesicle surface charge. When phospholipids in the gel phase were used, AmB caused large increase in permeability independently of the presence or absence of sterol. It suggests that mechanism of action

of AmB is different for membrane in the liquid-crystalline and gel states. The antibiotic appears to be unable to cross the membrane, acting only on the outermost bilayer of a multilamellar dispersion [267].

The effect of AmB on the proton/hydroxide and potassium-ion permeability of EPC SUVs has been investigated by using potential dependent paramagnetic probes [268]. The spin-labeled phosphonium measured trans-membrane potential resulting from ion current and *n*-hexylamine nitroxide directly monitored the trans-membrane pH gradient in vesicle systems. Several intriguing features of AmB-induced ionic conductance pathways in lipid vesicles were observed. The striking selectivity for cholesterol over ergosterol was found when H^+/OH^- currents were examined. AmB (1–10 molecules/vesicle) caused dramatic increase in the background H^+/OH^- permeability only in cholesterol-containing vesicles, whereas in sterol-free vesicles only 4–8-fold increase and even lower in ergosterol-containing vesicles was observed. No significant sterol dependence was found for K^+ permeability induction. These findings strongly suggested that the induction of K^+ and H^+/OH^- currents in vesicles by AmB occurred *via* two distinct molecular mechanisms. It was the next evidence undermining the sterol-dependent pore hypothesis. It was suggested that the H^+/OH^- current, which is seen in the presence of cholesterol might partially account for the high toxicity of AmB to humans. Many side effects accompanied AmB therapy are similar to those of protonophoric poisons such as dinitrophenol.

It was known from many experiments that the permeability alteration induced by AmB in many cell and model systems is concentration and time dependent. It suggested the existence of possible functional intermediates in the spontaneous insertion process leading to the formation of AmB permeabilizing units. A sequential mechanism for the formation of aqueous channels by AmB in liposomes has been investigated by osmotic stopped-flow method [29,269]. Determination of AmB-induced permeability to urea and glucose in liposomes indicated that both the phospholipid composition and the type of sterol are involved in determining the rate of aqueous pore formation. The formation of aqueous pores by AmB was always preceded by the formation of transient, non-aqueous pre-pore structure. The non-aqueous pre-pore structure made the liposomes more permeable to urea, whereas aqueous pore formation was indicated by glucose permeability. When liposomes were composed of EPC and cholesterol, the formation of non-aqueous and aqueous channels by AmB occurred after a lag time of several minutes. Such a lag time for AmB action was not observed in cholesterol-containing DMPC liposomes. Both non-aqueous and aqueous channels were always formed at lower concentrations of AmB in liposomes-containing ergosterol when compared to those with cholesterol. In sterol-free liposomes, non-aqueous channels were formed in DMPC but not in EPC liposomes at polyene concentration equal to that found for cholesterol-containing liposomes. No evidence of the formation of aqueous channels by AmB was found in sterol-free DMPC liposomes. These data were consistent with the concept of a sequential mechanism of the

membrane permeabilization by AmB. First AmB forms non-aqueous channels without the participation of sterol molecules, which subsequently interact with the sterols to form aqueous channels having enlarged diameter. The presence of either ergosterol or cholesterol is strictly required for the formation of aqueous channels. It was also demonstrated that two types of channels are equilibrium structures that differ in cation/anion selectivity [29]. By following the membrane potential with the fluorescent probe, it was found that at AmB concentrations lower than 10^{-7} M channels formed are permeable only to monovalent cations (K^+). Beyond this concentration they become permeable to K^+ and Cl^- what was consistent with an increase of radius of the structures formed. In sterol-free liposomes, the AmB channels formed were only permeable to cations.

4. INTERACTION OF PMAs WITH *IN SILICO* MODEL MEMBRANES: THEORETICAL STUDIES

4.1. Development of *in silico* models of cell membranes

As it was stated in the Introduction cell membranes are heterogenic and complex structures, which can be described as fluid mosaic domain systems. Such entities are difficult to study by experimental methods at the molecular level. Even recent improved methods such as atomic force microscopy, single particle tracking methods, or different spectroscopic methods only to some extant enable to monitor dynamic and static properties of cell membranes at atomic resolution. Therefore, simpler models of cell membranes, such as vesicles and layers, containing only defined type of lipids have been used in experimental studies of cell membranes and their components (see previous paragraphs of this chapter). On the other hand, new methodology was needed to study, at the molecular level, both pure lipid membranes and different ligands (e.g. drugs or proteins) interacting with such membranes. The development of computational chemistry and molecular modeling methods within the last two decades have enabled to use these techniques in studies of such systems (see recent reviews [270–274]). To study lipid membranes by computational chemistry methods, construction and development of *in silico* membrane models were necessary. These models evolve in time and are more complex now than a decade ago when only homogenic lipid systems were studied. Due to the fact that lipid bilayers are periodic lateral systems, simulations of such models are primarily limited by the system size, accessible time scale, and accuracy of the methodology.

Concerning methodology, in general, four type of methods are widely used to study lipid membranes namely: molecular dynamics (MD), Monte Carlo methods (MC), Brownian dynamics (BD), and methods calculating electrostatic properties of studied systems usually based on treating medium (in this case water or/and lipids) as continuum (continuum electrostatic methods (CEM)). MD, BD, and MC

methods are an irreplaceable tool to study structural and dynamic properties of lipid membranes at atomistic level. These three methods were applied to study both pure lipid membranes [270–273,275,276] as well as membranes containing ligands (usually drugs, anesthetics or small molecules, and ions e.g. [270,277–282]) or proteins (usually channels, e.g. reviews [276,283–290]). CEM methods, on the other hand, were used to study surface properties of lipid membranes [291–293], interaction of ligands with membranes [294,295], as well as conducting properties of membrane ion channels [293,296–299].

Size of *in silico* models of lipid membranes has been expanding along with the development of the computational technology, especially power of computers and introduction of parallel calculations. First *in silico* models of lipid membranes contained not more than 64 lipids [270]. Currently, simulations typically involve a few hundred of lipids and are confined to a few nanoseconds in case of MD simulations [273,300–302]. Usually, lipids are represented explicit (all atom approach) or as a simpler models (united atoms) [303]. Recently also very simple representation of lipids, the so-called coarse grain models [304–306], were introduced. In this model, lipids are represented as a polar head and apolar tail. Such models can be useful to expend time of simulation. There are also other, even simpler models, where lipid membrane is represented as a slab geometry, e.g. rectangular box, in which explicit represented ionic channels are inserted. Such models may be applied in calculations of electrostatic properties of studied channels. Typical models of lipid membranes used in MD simulations usually contain only one type of lipid [270,271,273,307]. The most commonly used are DPPC and DMPC bilayer systems. More elaborated models of lipid membranes used by MD contain a mixture of lipids [308,309]. One of the most common lipids present in mammalian cell membranes is cholesterol and therefore, several MD simulations were performed with model membranes containing except phospholipids also this type of molecule [310–320]. Since ergosterol is regarded as a molecular target for some polyene macrolides, it is worth to mention that only one MD simulation of lipid membrane was performed with ergosterol [315].

Development of methodology (concerns mainly MD and BD) and *in silico* models is made *via* improvement of force fields, better treatment of long-range electrostatic interactions, application of proper macroscopic boundary conditions, and improvement of numerical algorithms [270,273,302,321,322]. Using different methods one may monitor static and dynamic microscopic and macroscopic properties of studied systems. Usually, the following quantities are calculated: area per one lipid, ordering parameter of lipid acyl chains, area compressibility of lipids, dipole potential across the membrane and dipole moments, thickness of the membrane (atom density distribution), and diffusion coefficients of membrane components. These values together with analysis of dynamic properties and electrostatic interaction can gain insight into molecular behavior of lipid membrane components and ligands (i.e. small molecules, complexes or even proteins, and large supramolecular structures) present inside the membranes or at their surfaces.

4.2. Interaction of PMAs with *in silico* lipid membranes

Molecular modeling of PMA interaction with lipid membranes is still very young. This approach boosted in recent years and stems from previous computational chemistry and molecular modeling studies of molecular properties of polyene macrolides and their membrane targets.

Conformational analysis of isolated AmB [56,57,60] and its methyl ester [58] was performed and revealed that mutual location of lactone ring and aminosugar moiety (defined by ϕ, ψ dihedral angles Fig. 1) takes only two positions called ''open'' and ''closed'' conformation. In ''closed'' conformation, amino group of AmB tends to form intramolecular hydrogen bond, *via* water molecule, with carboxyl group. On the other hand, ''open'' conformation of both fragments enable AmB to form intermolecular hydrogen bonds with other partners. This ''open'' conformation of the polar head of AmB was also found as preferable conformation in some of AmB amide derivatives, which are more selective than AmB against fungal *versus* mammalian cells [62]. Therefore, this property of AmB polar head is postulated to be important for the interaction of AmB in channels or other supramolecular structures [37,62]. MD simulations of AmB monomer and dimer (head-to-tail orientation) also showed that aminosugar moiety may take both ''open'' and ''closed'' conformation [59,102,323].

In addition to structural properties of AmB electrostatic properties of this antibiotic and its derivatives were also studied. Calculation of proton affinity of amino group in AmB and in some its derivatives revealed the correlation between basicity of defined amino groups and biological activity of studied compounds [324]. On the other hand, distribution of molecular electrostatic potential calculated for AmB, cholesterol, and ergosterol indicated that both sterols exhibit different electrostatic pattern [83,203]. Different distributions of molecular electrostatic potential together with different structural properties of both sterols [201] were postulated as a source of different affinity of both sterols toward AmB. More flat overall shape of the ergosterol molecule than the cholesterol molecule and more extensive generation of a negative molecular electrostatic potential by ergosterol may be responsible for stronger interaction between AmB and ergosterol when compared to cholesterol. Interaction between sterols or other lipids and AmB were also studied by computational chemistry methods [323,325,326]. Generally, it was found that cholesterol [325], ergosterol [326], and DPPC [323] can form binary complexes with AmB molecule which are stabilized by Van der Waals forces in apolar parts of molecules and by hydrogen bonds in polar parts of molecules. The hydrogen bonds are formed between hydroxyl group of sterols and aminosugar moiety of AmB. DPPC molecule also can strongly interact with AmB molecule *via* oxygen atoms from phosphate group that can form hydrogen bonds with one of hydroxyl groups of the AmB aminosugar. The latter interaction between phospholipid and aminosugar part of AmB can be responsible for trafficking of AmB within the membrane but also for the destruction of the

AmB channel structure and was also observed in later studies of AmB ionic channels [61].

AmB membrane ionic channels are regarded as a principal element of the antifungal action of this drug and therefore, these channels were one of the main targets of computational chemistry and molecular modeling studies. The initial attempts using simple models (only AmB and sterol molecules were included) were quite modest but, on the other hand, were very promising that the theoretical approach can bring new insight into molecular level of observed phenomena. Conformational analysis of an isolated AmB–cholesterol channels performed by molecular mechanics methods revealed that stoichiometry, topology, and structure of the channel model proposed by De Kruijff [179] is very reasonable and stable concerning intermolecular interactions [186–188,190]. Studies of different models of the channel showed that stoichiometry AmB–sterol (8:8) is optimal [188] but, on the other hand, it was also found that channels with different stoichiometry of components may exhibit similar conducting properties of the pore [186]. In the latter studies, the electrostatic energy profile for a monovalent ion passing through the channel was also calculated. Presented profiles satisfactorily explains the permeability characteristics and selectivity properties of studied channels, i.e. cation selectivity of SLC and anion selectivity of DLC [186]. The initial MD studies of AmB–cholesterol channel also brought information about permeability properties of studied channel [189]. Studies of Khutorsky [189] showed that AmB molecules within the channel can interact *via* different polar groups and form intermolecular hydrogen bond chains. In these studies, the microscopic model of AmB channel was used [189] and interaction of sodium and chloride ions with the groups forming interior of the pore was analyzed. It was also found that both ions when present together in the pore could interact and form a pair, which goes together within the channel. Recent thermodynamic free energy studies of the AmB–cholesterol channel showed that the path along which the ions prefer to move is off center from the channel's central axis [191]. For these studies, the channel formed by the AmB and cholesterol molecules was immersed into a uniform membrane, which was modeled as a low dielectric slab. The studies combined the free energy computations using the Poisson equation with a continuum solvent model. In the same work [191], Monte Carlo molecular simulations established that sodium and chloride ions can pass even together through the pore.

The model of the AmB channel (treated explicit), immersed in lipid membrane (treated implicit as a slab of low dielectric) was also used to calculate distribution of molecular electrostatic potential for AmB–cholesterol and AmB–ergosterol channels (A. Tereszczyn M.Sc. thesis – Gdansk University of Technology, Poland). The structures of both the channels were taken from MD simulations (see next paragraph). The distribution of molecular electrostatic potential was calculated using Poisson–Boltzmann methods (CEM methods). It was found that size of the pore is important for the potential distribution. Comparing AmB–cholesterol

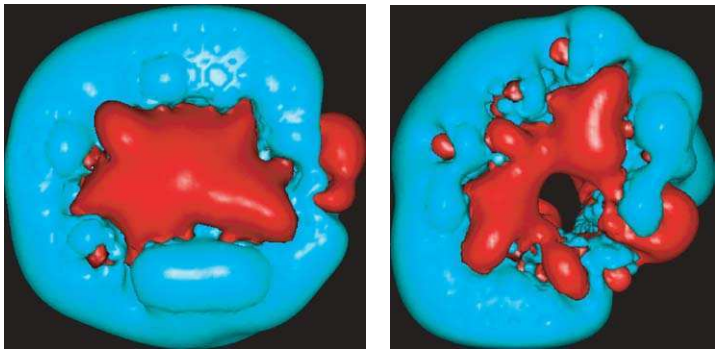

(a) (b)

Fig. 7. Distribution of molecular electrostatic potential presented on equipotential surfaces for AmB–cholesterol (a) and AmB–ergosterol (b) channels. Negative potential of -1 kcal mol^{-1} is red, positive potential of $+1$ kcal mol^{-1} is blue.

and AmB–ergosterol channels the former one generates more negative potential at the entrance of the pore where polar heads of AmB molecules are present (Fig. 7). This region of negative potential at the mouth of the channel (extracellular side of membrane) forms a potential well, which can be regarded as a trap for cations passing through the channel. These calculations agree with the previous results of the electrostatic studies of AmB–cholesterol channel [186] showing potential barrier for cations going through the pore. More extensive and deeper potential well observed in the case of AmB–cholesterol channel (Fig. 7) can also be responsible for lower ion conductance of these channels compared to AmB–ergosterol channels. Lower ability to conduct ions by AmB–cholesterol than AmB–ergosterol channels might quantitatively contribute to more selective action of AmB molecules toward ergosterol-containing membranes.

Only recent studies of AmB ionic channels and interactions between the antibiotic molecules and model phospholipid membranes take into account more elaborated models in which lipid molecules are treated explicit. These studies include interactions of AmB with the surface of phospholipid bilayer as well as studies of ionic channels formed by molecules of AmB in the lipid bilayer. In particular, MD studies were performed to analyze molecular properties of ionic channels built from AmB molecules and sterols (cholesterol or ergosterol) [37,61]. Models of these channels are presented in Fig. 8. Both type of channels contained eight AmB, eight sterol molecules, and 34 DMPC lipid molecules (17 in each layer). Comparative MD studies of both channels brought interesting data concerning molecular properties of AmB ionic membrane channels. First of all, it was found that ergosterol and cholesterol molecules interact slightly in a different way with AmB molecules inside the channel. Ergosterol molecules are more rigid, less prone to rotate around its long axis, and tightly interact with AmB molecules. Probably due to this fact, the chain of intermolecular hydrogen bonds between

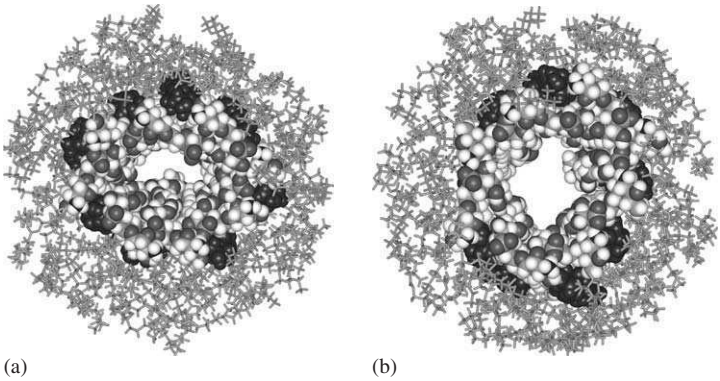

Fig. 8. Snapshots of AmB–cholesterol (a) and AmB–ergosterol (b) membrane channels from MD studies [37]. AmB molecules are presented as a gray-scale space filling models. Sterols are represented as dark space filling models. DMPC molecules are represented as stick models.

polar groups of neighbor AmB molecules is more stable. This chain of hydrogen bonds is formed between amino groups and carboxyl groups of neighbor AmB molecules. The chain can be formed only when AmB molecules take ''open'' conformation within its ''polar-head.'' This ''open'' conformation of AmB was more frequently encountered in the AmB–ergosterol than AmB–cholesterol channel. The important feature, which was also observed in MD studies, was the diameter of the pore. The lumen of AmB–ergosterol channel was bigger than for AmB–cholesterol channel. The size of the pore determines conductivity of the channel and, as it was calculated by Bonilla-Marin *et al*. [186], influences the height of electrostatic barrier for ions passing through the AmB channel. Too small diameter of the pore might be responsible for the break of ion passage. Tight AmB–cholesterol channels agree with the idea that there are open (functional) and closed (non-functional) AmB channels [327].

Studies of interactions between AmB and model phospholipid membranes also covered the interaction of single AmB molecule with the surface of lipid membrane [330] and interaction of AmB monomer and dimer with phospholipids inside the membrane [328]. The studies were performed to answer the question if a single AmB molecule exhibits a propensity to enter the membrane and if AmB dimers are stable structures inside the membrane. Answers to these questions may help to understand the mechanism of AmB channel formation. MD simulation lasting for more than 1 ns was performed with AmB–lipid systems. The lipid membrane contained 100 DMPC molecules in each layer and a proper number of water molecules to cover the surface of the membrane. The model of lipid membrane used in our studies was based on MD studies of DMPC model membrane performed by Zubrzycki *et al*. [329].

MD simulation of interaction between AmB and a surface of the lipid membrane revealed that AmB molecule takes perpendicular orientation to the surface (at the

starting point AmB lain horizontally on a surface). The AmB molecule, *via* carboxyl group, strongly interacts with amino group of DMPC molecules. These interactions are not random and AmB molecule together with one DMPC molecule tends to diffuse laterally. This means that single AmB molecule very unlikely is able to enter the membrane. Such an observation agrees both with the ability of AmB molecules to form monolayers at the phase border (for instance air/water interface) [109–112] and with the previous observations that AmB molecules can interact with DMPC molecules in a very specific way as it was found in MD simulations of AmB membrane channels [37,61].

MD simulation of AmB monomer and AmB dimer inside the membrane [328] revealed that AmB molecules like to interact with polar heads of DMPC molecules. The carboxyl group of AmB interacts with amino group from choline moiety and the amino group of AmB interacts with phosphate group of DMPC. However, the antibiotic molecules in the AmB dimer prefer to interaction with each other than with the DMPC molecules. This interaction enables to cover polar parts of AmB molecule and drift the dimer up and down in the membrane. Single AmB molecule, on the other hand, tends to stick to the membrane surface by its polar head. This observation may suggest that position of single AmB molecule in the lipid membrane is less favorable than dimer. The latter one is suggested to be a building bloc (intermediate) of the channel. MD simulations also showed that AmB molecules order acyl chains of the surrounding DMPC molecules. This observation may suggest that AmB molecules can form domains, which can be more ordered. Such behavior of AmB may be regarded as an important step to channel formation. Further studies concerning derivatives of AmB will also help to understand how modified polar heads of AmB influence behavior of the antibiotic molecules in the membrane.

5. CONCLUSIONS

Due to the chemotherapeutic value of PMAs the studies on their mechanism of action have been continued since this group of compounds was discovered. The important part of this mechanism comprises interaction of PMAs with cell membranes. Through years, different models of lipid membranes were applied for studies of PMA mechanism of action. Recently, *in silico* models for computational studies and monolayers for SFM were introduced. Evolution of models of lipid membranes as well as development of methodology enable to get better insight into molecular level of PMA–membrane interactions.

Data collected from studies on monolayers (including SFM techniques) suggest two type of AmB behavior. AmB molecules oriented perpendicularly to the plane of lipid layer form hydrophilic pores in the hydrophobic core of the membrane ($\sim$6 Å internal diameter; 6–8 molecules). AmB molecules oriented in the plane of the layer influence the membrane structure *via* creation of a network of hydrogen bonds between lipids and AmB.

The studies applying liposomes revealed many interesting features concerning structural and permeability effects caused by PMAs. It was confirmed that membranes containing ergosterol are more prone to permeability than those containing cholesterol and that mechanisms of membrane permeabilization by PMAs are different in ergosterol when compared to cholesterol-containing membranes. Due to these differences new AmB derivatives with remarkable selective toxicity have been synthesized. This finding encouraged to continue efforts to obtain new less-toxic generations of this drug. Important role of antibiotic state in aqueous media in ergosterol/cholesterol selectivity has also been established. However, the most important finding coming from recent studies on liposomes was PMA-induced permeabilization of sterol-free membranes, evidencing the existence of an alternative membrane damage mechanism apart from the widely accepted sterol-pore model. The studies on vesicles brought also a new interpretation of the action of filipin. Precluding any disruptive effect, inducement of permeability of filipin would result from the intrinsic permeability of the interfacial region at the boundaries of the gel-like domains corresponding to the filipin–phospholipid aggregates. Permeabilizing mechanism of filipin is the same in the absence and presence of cholesterol.

Studies utilizing *in silico* models of lipid membranes, first of all, enabled to determine molecular properties of AmB membrane channels as well as AmB monomer and dimer embedded in the membrane at atomic level. The analysis of results coming from these studies revealed differences between AmB–ergosterol and AmB–cholesterol channels. As it was found that these differences can influence the conductance and ion passage of such channels, what may contribute to selectivity of action of AmB and its derivatives against ergosterol- *versus* cholesterol-containing cell membranes. Moreover, the studies at molecular level using molecular modeling methods give a hope that further elements of AmB–membrane interactions can be analyzed in details by such approach. This includes studies on the mechanism of AmB (or its derivatives) channel formation, on the properties of different supramolecular structures formed by the antibiotic molecules inside membranes (both containing and sterol-free), and interaction of studied polyene macrolides with the membrane surface.

ACKNOWLEDGMENTS

MB and BC would like to acknowledge financial support from the State Committee for Scientific Research of Poland, grant no 3 P05F 012 25 and Gdansk University of Technology. WIG wishes to thank the State Committee for Scientific Research of Poland, grant no3 P05F01225 for financial support and his coworkers Monika Herec, Mariusz Gagos, and Peter Kernen for friendly collaboration and stimulating discussions.

REFERENCES

[1] E.L. Hazen, R. Brown, Fungicidin, an antibiotic produced by a soil actinomycete, Proc. Soc. Exptl. Biol. Med. 76 (1951) 93–97.
[2] D.R. Worthen, M. Jay, P.M. Bummer, Methods for the recovery and purification of polyene antifungals, Drug Dev. Ind. Pharm. 27 (2001) 277–286.
[3] S. Omura, H. Tanaka, Production, structure, and antifungal activity of polyene macrolides, in: S. Omura, (Ed.), Macrolide Antibiotics, Academic Press, Orlando, 1984, pp. 351–404.
[4] E.F. Gale, Mode of action and resistance mechanisms of polyene macrolides, in: S. Omura, (Ed.), Macrolide Antibiotics, Academic Press, Orlando, 1984, pp. 425–455.
[5] C.P. Schaffner, Polyene macrolides in clinical practice: pharmacology and adverse and other effects, in: S. Omura, (Ed.), Macrolide Antibiotics, Academic Press, Orlando, 1984, pp. 457–507.
[6] J. Bolard, How do the polyene macrolide antibiotics affect the cellular membrane properties? Biochim. Biophys. Acta 864 (1986) 257–304.
[7] D. Kerridge, Mode of action of clinically important antifungal drugs, Adv. Microb. Physiol. 27 (1986) 1–72.
[8] V. Joly, J. Bolard, P. Yeni, In vitro model for studying toxicity of antifungal agents, Antimicrob. Agents Chemother. 36 (1992) 1799–1804.
[9] S.B. Zotchev, Polyene macrolide antibiotics and their applications in human therapy, Curr. Med. Chem. 10 (2003) 211–223.
[10] D. Ellis, Amphotericin B: spectrum and resistance, J. Antimicrob. Chemother. 49 (2002) 7–10.
[11] T.M. Sternberg, E.T. Wright, M. Oura, A new antifungal antibiotic, amphotericin B, Antibiot. Ann. (1956) 566–573.
[12] W. Gold, H.A. Stout, J.F. Pagano, R. Donovick, Amphotericins A and B, antifungal antibiotics produced by a Streptomycete. I. In vitro studies, Antibiot. Ann. (1956) 579–585.
[13] J. Brajtburg, W.G. Powderly, G.S. Kobayashi, G. Medoff, Amphotericin B: current understanding of mechanisms of action, Antimicrob. Agents Chemother. 34 (1990) 183–188.
[14] H.A. Gallis, R.H. Drew, W.W. Pickard, Amphotericin B: 30 years of clinical experience, Rev. Infect. Dis. 12 (1990) 308–329.
[15] D.W. Warnock, Amphotericin B: an introduction, J. Antimicrob. Chemother. 28 (Suppl. B) (1991) 27–38.
[16] S.C. Hartsel, C. Hatch, W. Ayenew, How does amphotericin B work? Studies on model membrane systems, J. Liposome Res. 3 (1993) 377–408.
[17] S. Hartsel, J. Bolard, Amphotericin B: new life for an old drug, Trends Pharmacol. Sci. 17 (1996) 445–449.
[18] D. Gottlieb, H.E. Carter, J.H. Sloneker, A. Ammann, Protection of fungi against polyene antibiotics by sterols, Science 128 (1958) 361.
[19] J.O. Lampen, Interference by polyenic antifungal antibiotics (especially nystatin and filipin) with specific membrane functions, Symp. Soc. Gen. Microbiol. 16 (1966) 111–130.
[20] T.E. Andreoli, V.W. Dennis, A.M. Weigl, The effect of amphotericin B on the water and nonelectrolyte permeability of thin lipid membranes, J. Gen. Physiol. 53 (1969) 33–154.
[21] R. Holz, A. Finkelstein, The water and nonelectrolyte permeability induced in thin lipid membranes by the polyene antibiotics nystatin and amphotericin B, J. Gen. Physiol. 125 (1970) 145.
[22] D.B. Archer, E.F. Gale, Antagonism by sterols of the action of amphotericin and filipin on the release of potassium ions from *Candida albicans* and *Mycoplasma mycoides* subsp. *capri*, J. Gen. Microbiol. 90 (1975) 187–190.

[23] G. Medoff, J. Brajtburg, G.S. Kobayashi, J. Bolard, Antifungal agents useful in therapy of systemic fungal infections, Annu. Rev. Pharmacol. Toxicol. 23 (1983) 303–330.
[24] E. Borowski, B. Cybulska, Potassiumless death of *Saccharomyces cerevisiae* cells treated with *N*-succinyl perimicin and reversal of fungicidal action of the antibiotic by potassium ions, Nature 211 (1967) 1034–1035.
[25] B. Malewicz, H.M. Jenkin, E. Borowski, Repair of membrane alterations induced in baby hamster kidney cells by polyene macrolide antibiotics, Antimicrob. Agents Chemother. 19 (1981) 238–247.
[26] B. Cybulska, J. Mazerski, E. Borowski, C.M. Gary-Bobo, Haemolytic activity of aromatic heptaenes. A group of polyene macrolide antifungal antibiotics, Biochem. Pharmacol. 33 (1984) 41–46.
[27] B. Cybulska, E. Borowski, C.M. Gary-Bobo, Relationship between ionophoric and haemolytic activities of perimicin A and vacidin A, two polyene macrolide antifungal antibiotics, Biochem. Pharmacol. 38 (1989) 1755–1762.
[28] B. Cybulska, O. Seksek, N. Henry Toulme, A. Czerwinski, J. Bolard, Polyene macrolide antibiotics: indirect stimulation of the Na^+/H^+ exchanger of BALB/c B lymphoid cell line, A20, Biochem. Pharmacol. 44 (1992) 539–545.
[29] B.E. Cohen, Amphotericin B toxicity and lethality: a tale of two channels, Int. J. Pharm. 162 (1998) 95–106.
[30] T.E. Andreoli, On the anatomy of amphotericin B–cholesterol pores in lipid bilayer membranes, Kidney Int. 4 (1973) 337–345.
[31] A. Finkelstein, R. Holz, Aqueous pores created in thin lipid membranes by the polyene antibiotics nystatin and amphotericin B, in: G. Eisenman, (Ed.), Membranes, Marcel Dekker, New York, 1973, pp. 377–408.
[32] J.M.T. Hammilton-Miller, Fungal sterols and the mode of action of the polyene antibiotics, Adv. Appl. Microbiol. 17 (1974) 109–134.
[33] J. Kotler-Brajtburg, H.D. Price, G. Medoff, D. Schlessinger, G.S. Kobayashi, Molecular basis for the selective toxicity of amphotericin B for yeast and filipin for animal cells, Antimicrob. Agents Chemother. 5 (1974) 377–382.
[34] T. Teerlink, B. De Kruijff, R.A. Demel, The action of pimaricin, etruscomycin and amphotericin B on liposomes with varying sterol content, Biochim. Biophys. Acta 599 (1980) 484–492.
[35] J. Bolard, P. Legrand, F. Heitz, B. Cybulska, One-side action of amphotericin B on cholesterol-containing membranes is determined by its self-association in the medium, Biochemistry 30 (1991) 5707–5715.
[36] J. Szlinder-Richert, J. Mazerski, B. Cybulska, J. Grzybowska, E. Borowski, MFAME, *N*-methyl-*N*-D-fructosyl amphotericin B methyl ester, a new amphotericin B derivative of low toxicity: relationship between self-association and effects on red blood cells, Biochim. Biophys. Acta 1528 (2001) 15–24.
[37] M. Baginski, H. Resat, E. Borowski, Comparative molecular dynamics simulations of amphotericin B–cholesterol/ergosterol membrane channels, Biochim. Biophys. Acta 1567 (2002) 63–78.
[38] M.N. Neely, M.A. Ghannoum, The exciting future of antifungal therapy, Eur. J. Clin. Microbiol. Infect. Dis. 19 (2000) 897–914.
[39] J.A. Maertens, M.A. Boogaerts, Fungal cell wall inhibitors: emphasis on clinical aspects, Curr. Pharm. Design 6 (2000) 225–239.
[40] J.S. Tkacz, B. DiDomenico, Antifungals: what's in the pipeline, Curr. Opin. Microbiol. 4 (2001) 540–545.
[41] D.W. Denning, Echinocandins: a new class of antifungal, J. Antimicrob. Chemother. 49 (2002) 889–891.
[42] J. Grzybowska, P. Sowinski, J. Gumieniak, T. Zieniawa, E. Borowski, *N*-methyl-*N*-D-fructopyranosylamphotericin B methyl ester, new amphotericin B derivative of low toxicity, J. Antibiot. 50 (1997) 709–711.

[43] E. Borowski, Novel approaches in the rational design of antifungal agents of low toxicity, Farmaco 55 (2000) 206–208.
[44] J. Adler-Moore, R.T. Proffitt, AmBisome: liposomal formulation, structure, mechanism of action and pre-clinical experience, J. Antimicrob. Chemother. 49 (2002) 21–30.
[45] B. Dupont, Overview of the lipid formulations of amphotericin B, J. Antimicrob. Chemother. 49 (2002) 31–36.
[46] J.F. Aparicio, P. Caffrey, J.A. Gil, S.B. Zotchev, Polyene antibiotic biosynthesis gene clusters, Appl. Microbiol. Biotechnol. 61 (2003) 179–188.
[47] W. Mechlinski, C.P. Schaffner, P. Ganis, G. Avitabile, Structure and absolute configuration of the polyene macrolide antibiotic amphotericin B, Tetrahedron Lett. 44 (1970) 3873–3876.
[48] P. Ganis, G. Avitabile, W. Mechlinski, C.P. Schaffner, Polyene macrolide antibiotic amphotericin B. Crystal structure of the *N*-iodoacetyl derivative, J. Am. Chem. Soc. 93 (1971) 4560–4564.
[49] P. Sowinski, P. Gariboldi, J.K. Pawlak, E. Borowski, The structure of vacidin A, an aromatic heptaene macrolide antibiotic. II. Stereochemistry of the antibiotic, J. Antibiot. 42 (1989) 1639–1642.
[50] P. Sowinski, J. Pawlak, E. Borowski, P. Gariboldi, Stereostructure of rimocidin, J. Antibiot. 48 (1995) 1288–1291.
[51] P. Sowinski, J. Pawlak, E. Borowski, P. Gariboldi, Stereostructure of gedamycin, Polish. J. Chem. 69 (1995) 213–217.
[52] P. Sowinski, T. Bieszczad, J. Pawlak, E. Borowski, Stereostructure of amphotericin A, J. Antibiot. 49 (1996) 1232–1235.
[53] P. Rochet, J.M. Lancelin, Revised H-1 and C-13 NMR assignments of the polyene antibiotic filipin III, Magn. Reson. Chem. 35 (1997) 538–542.
[54] L. Volpon, J.M. Lancelin, Solution NMR structure of five representative glycosylated polyene macrolide antibiotics with a sterol-dependent antifungal activity, Eur. J. Biochem. 269 (2002) 4533–4541.
[55] C.N. Chong, R.W. Rickards, Macrolide antibiotic studies. XVII. Cyclic hemiketal structures in nystatin, amphotericin B, pimaricin and lucensomycin, Tetrahedron Lett. 49 (1972) 5053–5056.
[56] H. Rinnert, B. Maigret, Conformational analysis of amphotericin B. I. Isolated molecule, Biochem. Biophys. Res. Commun. 101 (1981) 853–860.
[57] J. Berges, J. Caillet, J. Langlet, N. Gresh, M. Herve, C.M. Gary-Bobo, Conformational study of the polar head of the amphotericin B in the isolated state and in the presence of water molecules, Stud. Phys. Theoret. Chem. 71 (1990) 253–263.
[58] S. Meddeb, J. Berges, J. Caillet, J. Langlet, Comparative theoretical study of the conformations of amphotericin methyl ester and amphotericin-B polar heads in the presence of water, Biochim. Biophys. Acta 1112 (1992) 266–272.
[59] J. Mazerski, E. Borowski, Molecular dynamics of amphotericin B. I. Single molecule in vacuum and water, Biophys. Chem. 54 (1995) 49–60.
[60] M. Baginski, P. Gariboldi, P. Bruni, E. Borowski, Conformational analysis of amphotericin B, Biophys. Chem. 65 (1997) 91–100.
[61] M. Baginski, H. Resat, J.A. McCammon, Molecular properties of amphotericin B membrane channel: a molecular dynamics simulation, Mol. Pharmacol. 52 (1997) 560–570.
[62] H. Resat, F.A. Sungur, M. Baginski, E. Borowski, V. Aviyente, Conformational properties of amphotericin B amide derivatives – impact on selective toxicity, J. Comput. Aid. Mol. Design 14 (2000) 689–703.
[63] J. Kotler-Brajtburg, G. Medoff, G.S. Kobayashi, S. Boggs, D. Schlessinger, R.C. Pandey, K.L. Rinehart, Classification of polyene antibiotics according to chemical structure and biological effects, Antimicrob. Agents Chemother. 15 (1979) 716–722.

[64] B. Cybulska, T. Ziminski, E. Borowski, C.M. Gary-Bobo, The influence of electric charge of aromatic heptaene macrolide antibiotics on their activity on biological and lipidic model membranes, Mol. Pharmacol. 24 (1983) 270–276.
[65] M. Herve, J.C. Debouzy, E. Borowski, B. Cybulska, C.M. Gary-Bobo, The role of the carboxyl and amino groups of polyene macrolides in their interactions with sterols and their selective toxicity. A ^{31}P-NMR study, Biochim. Biophys. Acta 980 (1989) 261–272.
[66] J. Mazerski, J. Grzybowska, E. Borowski, Influence of net charge on the aggregation and solubility behaviour of amphotericin B and its derivatives in aqueous media, Eur. Biophys. J. 18 (1990) 159–164.
[67] B. Cybulska, J. Bolard, O. Seksek, A. Czerwinski, E. Borowski, Identification of the structural elements of amphotericin B and other polyene macrolide antibiotics of the heptane group influencing the ionic selectivity of the permeability pathways formed in the red cell membrane, Biochim. Biophys. Acta 1240 (1995) 167–178.
[68] M. Cheron, B. Cybulska, J. Mazerski, J. Grzybowska, A. Czerwinski, E. Borowski, Quantitative structure–activity relationships in amphotericin B derivatives, Biochem. Pharmacol. 37 (1988) 827–836.
[69] E.D. Etingov, G.V. Kholodova, A.I. Karnaushkina, Acid–base properties of amphotericin B, Antibiotiki 17 (1972) 296–305.
[70] W. Mechlinski, C.P. Schaffner, Polyene macrolide derivatives. I. *N*-acylation and esterification reactions with amphotericin B, J. Antibiot. 25 (1972) 256–258.
[71] L. Falkowski, A. Jarzebski, B. Stefanska, E. Bylec, E. Borowski, The synthesis of amides of polyene macrolide antibiotics, J. Antibiot. 33 (1980) 103–104.
[72] C.P. Schaffner, Amphotericin B derivatives, in: R.A. Fromtling, (Ed.), Recent Trends in the Discovery, Development and Evaluation of Antifungal Agents, L.R. Prous Science Publishers, S.A., Barcelona, 1987, pp. 595–632.
[73] B. Stefanska, J. Zielinski, E. Borowski, L. Falkowski, Enamine and amidine derivatives of polyene macrolide antibiotics, Acta Pol. Pharm. 45 (1988) 71–76.
[74] A. Czerwinski, T. Zieniawa, E. Borowski, L.G. Micossi, Amphotericin B 2-morpholinoethylamide diaspartate, a new water soluble derivative of the antibiotic. Synthesis and biological properties, J. Antibiot. 43 (1990) 680–683.
[75] A. Czerwinski, W.A. Konig, T. Zieniawa, P. Sowinski, V. Sinnwell, S. Milewski, E. Borowski, New *N*-alkyl derivatives of amphotericin B. Synthesis and biological properties, J. Antibiot. 44 (1991) 979–984.
[76] N. Yamaji, N. Matsumori, S. Matsuoka, T. Oishi, M. Murata, Amphotericin B dimers with bisamide linkage bearing powerful membrane-permeabilizing activity, Org. Lett. 4 (2002) 2087–2089.
[77] J. Mazerski, B. Cybulska, J. Bolard, E. Borowski, Structural features determining the haemolytic activity of vacidin A derivatives, Drugs Exp. Clin. Res. 12 (1986) 627–633.
[78] A. Czerwinski, W.A. Konig, P. Sowinski, E. Borowski, Amides of polyene macrolide aureofacin. Synthesis and biological properties, J. Antibiot. 40 (1987) 1023–1027.
[79] T. Bruzzese, C. Rimaroli, A. Bonabello, E. Ferrari, M. Signorini, Amide derivatives of partricin A with potent antifungal activity, Eur. J. Med. Chem. 31 (1996) 965–972.
[80] A.W. Taylor, B.J. Costello, P.A. Hunter, W.S. Maclachlan, C.T. Shanks, Synthesis and antifungal selectivity of new derivatives of amphotericin-B modified at the C-13 position, J. Antibiot. 46 (1993) 486–493.
[81] W.S. Maclachlan, S.A. Readshaw, Stereoselective synthesis of 13-dehydroxy-(14*S*)-hydroxyamphotericin B methyl ester, Tetrahedron Lett. 36 (1995) 1735–1738.
[82] M.J. Driver, A.R. Greenlees, W.S. Maclachlan, D.T. Macpherson, A.W. Taylor, Synthesis of 16-decarboxy-16-hydroxymethyl amphotericin B – a novel antifungal agent, Tetrahedron Lett. 33 (1992) 4357–4360.

[83] M. Baginski, E. Borowski, Distribution of electrostatic potential around amphotericin B and its membrane targets, Theochem. J. Mol. Struct. 389 (1997) 139–146.
[84] I. Gruda, P. Nadeau, J. Brajtburg, G. Medoff, Application of differential spectra in the ultraviolet–visible region to study the formation of amphotericin B–sterol complexes, Biochim. Biophys. Acta 602 (1980) 260–268.
[85] J. Mazerski, J. Bolard, E. Borowski, Self-association of some polyene macrolide antibiotics in aqueous media, Biochim. Biophys. Acta 719 (1982) 11–17.
[86] C. Ernst, J. Grange, H. Rinnert, G. Dupont, J. Lematre, Structure of amphotericin B aggregates as reveled by UV and CD spectroscopies, Biopolymers 20 (1981) 1575–1588.
[87] R.P. Hemenger, T. Kaplan, L.J. Gray, Structure of amphotericin B aggregates based on calculations of optical spectra, Biopolymers 22 (1983) 911–918.
[88] P. Millie, J. Langlet, J. Berges, J. Caillet, J.P. Demaret, Self-association of amphotericin B in water. Theoretical energy and spectroscopy studies, J. Phys. Chem. B 103 (1999) 10883–10891.
[89] J. Milhaud, V. Ponsinet, M. Takashi, B. Michels, Interactions of the drug amphotericin B with phospholipid membranes containing or not ergosterol: new insight, into them role of ergosterol, Biochim. Biophys. Acta 1558 (2002) 95–108.
[90] J. Barwicz, W.I. Gruszecki, I. Gruda, Spontaneous organization of amphotericin-B in aqueous medium, J. Coll. Interfac. Sci. 158 (1993) 71–76.
[91] W.I. Gruszecki, M. Gagos, M. Herec, Dimers of polyene antibiotic amphotericin B detected by means of fluorescence spectroscopy: molecular organization in solution and in lipid membranes, J. Photochem. Photobiol. B – Biol. 69 (2003) 49–57.
[92] A.R. Balakrishnan, K.R.K. Easwaran, CD and NMR studies on the aggregation of amphotericin-B in solution, Biochim. Biophys. Acta 1148 (1993) 269–277.
[93] J. Caillet, J. Berges, J. Langlet, Theoretical study of the self-association of amphotericin B, Biochim. Biophys. Acta 1240 (1995) 179–195.
[94] H. Rinnert, C. Thirion, G. Dupont, J. Lematre, Structural studies on aqueous and hydroalcoholic solutions of polyene antibiotic: amphotericin B, Biopolymers 16 (1977) 2419–2427.
[95] J. Bolard, M. Seigneurt, G. Boudet, Interaction between phospholipid bilayer membranes and the polyene antibiotic amphotericin B, Biochim. Biophys. Acta 599 (1980) 280–293.
[96] I. Gruda, N. Dussault, Effect of the aggregation state of amphotericin B on its interaction with ergosterol, Biochem. Cell Biol. 66 (1988) 177–183.
[97] M.T. Lamy-Freund, V.F.N. Ferreira, S. Schreier, Polydispersity of aggregates formed by the polyene antibiotic amphotericin B and deoxycholate. A spin label study, Biochim. Biophys. Acta 981 (1989) 207–212.
[98] P. Tancrede, J. Barwicz, S. Jutras, I. Gruda, The effect of surfactants on the aggregation state of amphotericin B, Biochim. Biophys. Acta 1030 (1990) 289–295.
[99] M.T. Lamy-Freund, S. Schreier, R.M. Peitzsch, W.F. Reed, Characterization and time dependence of amphotericin B: deoxycholate aggregation by quasielastic light scattering, J. Pharm. Sci. 80 (1991) 262–266.
[100] J. Barwicz, S. Christian, I. Gruda, Effects of the aggregation state of amphotericin B on its toxicity to mice, Antimicrob. Agents Chemother. 36 (1992) 2310–2315.
[101] H.G. Brittain, Circular dichroism studies of the self-association of amphotericin B, Chirality 6 (1994) 665–669.
[102] J. Mazerski, E. Borowski, Molecular dynamics of amphotericin B. II. Dimer in water, Biophys. Chem. 57 (1996) 205–217.
[103] Z. Shervani, H. Etori, K. Taga, T. Yoshida, H. Okabayashi, Aggregation of polyene antibiotics as studied by electronic absorption and circular dichroism spectroscopies, Coll. Surfac. B – Biointerfac. 7 (1996) 31–38.

[104] D. Romanini, G. Avalle, B. Nerli, G. Pico, Thermodynamic and spectroscopic features of the behavior of amphotericin B in aqueous medium, Biophys. Chem. 77 (1999) 69–77.
[105] H.E. Lambing, B.D. Wolf, S.C. Hartsel, Temperature effects on the aggregation state and activity of amphotericin-B, Biochim. Biophys. Acta 1152 (1993) 185–188.
[106] F. Gaboriau, M. Cheron, L. Leroy, J. Bolard, Physico-chemical properties of the heat-induced 'superaggregates' of amphotericin B, Biophys. Chem. 66 (1997) 1–12.
[107] J. Barwicz, P. Tancrede, The effect of aggregation state of amphotericin-B on its interactions with cholesterol- or ergosterol-containing phosphatidylcholine monolayers, Chem. Phys. Lipids 85 (1997) 145–155.
[108] F. Gaboriau, M. Cheron, C. Petit, J. Bolard, Heat-induced superaggregation of amphotericin B reduces its in vitro toxicity: a new way to improve its therapeutic index, Antimicrob. Agents Chemother. 41 (1997) 2345–2351.
[109] M. Saint Pierre Chazalet, C. Thomas, M. Dupeyrat, C.M. Gary-Bobo, Amphotericin B–sterol complex formation and competition with egg phosphatidylcholine: a monolayer study, Biochim. Biophys. Acta 944 (1988) 477–486.
[110] J.R. Seoane, N. Vila Romeu, J. Minones, O. Conde, P. Dynarowicz-Latka, M. Casas, The behaviour of amphotericin B monolayers at the air/water interface, Progr. Coll. Polym. Sci. 105 (1997) 173–179.
[111] J. Minones, C. Carrera, P. Dynarowicz-Latka, O. Conde, R. Seoane, J.M.R. Patino, Orientational changes of amphotericin B in Langmuir monolayers observed by Brewster angle microscopy, Langmuir 17 (2001) 1477–1482.
[112] W.I. Gruszecki, M. Gagos, P. Kernen, Polyene antibiotic amphotericin B in monomolecular layers: spectrophotometric and scanning force microscopic analysis, FEBS Lett. 524 (2002) 92–96.
[113] R. Seoane, J. Minones, O. Conde, M. Casas, E. Iribarnegaray, Molecular organisation of amphotericin B at the air–water interface in the presence of sterols: a monolayer study, Biochim. Biophys. Acta 1375 (1998) 73–83.
[114] Y. Saka, T. Mita, Interaction of amphotericin B with cholesterol in monolayers, aqueous solutions, and phospholipid bilayers, J. Biochem. Tokyo 123 (1998) 798–805.
[115] R. Seoane, J. Minones, O. Conde, E. Iribarnegaray, M. Casas, Interactions between amphotericin B and sterols in monolayers. Mixed films of amphotericin B–cholesterol, Langmuir 15 (1999) 5567–5573.
[116] R. Seoane, J. Minones, O. Conde, M. Casas, E. Iribarnegaray, Interaction between amphotericin B and sterols in monolayers. Mixed films of ergosterol–amphotericin B, Langmuir 15 (1999) 3570–3573.
[117] J. Minones, O. Conde, R. Seoane, P. Dynarowicz-Latka, Influence of a spreading method on the properties of amphotericin B–dipalmitoyl phosphatidic acid mixed films at the air/water interface, Langmuir 16 (2000) 5743–5748.
[118] J. Minones, J. Minones, O. Conde, J.M.R. Patino, P. Dynarowicz-Latka, Mixed monolayers of amphotericin B–dipalmitoyl phosphatidyl choline: study of complex formation, Langmuir 18 (2002) 2817–2827.
[119] J. Minones, O. Conde, J. Minones, J.M.R. Patino, R. Seoane, Amphotericin B–dipalmitoyl phosphatidyl glycerol interactions responsible for the reduced toxicity of liposomal formulations: a monolayer study, Langmuir 18 (2002) 8601–8608.
[120] M.A. Kol, A.N.C. vanLaak, D.T.S. Rijkers, J.A. Killian, A.I.P.M. deKroon, B. deKruijff, Phospholipid flop induced by transmembrane peptides in model membranes is modulated by lipid composition, Biochemistry 42 (2003) 231–237.
[121] J. Minones, P. Dynarowicz-Latka, O. Conde, J. Minones, E. Iribarnegaray, M. Casas, Interactions of amphotericin B with saturated and unsaturated phosphatidylcholines at the air/water interface, Coll. Surface B 29 (2003) 205–215.
[122] R. Bittman, S.A. Fischkoff, Fluorescence studies of the binding of polyene antibiotics filipin III, amphotericin B, nystatin and lagosin to cholesterol, Proc. Natl. Acad. Sci. USA 69 (1972) 3795–3799.

[123] M.A. Castanho, M.J. Prieto, Fluorescence study of the macrolide pentaene antibiotic filipin in aqueous solution and in a model system of membranes, Eur. J. Biochem. 207 (1992) 125–134.
[124] N.O. Petersen, Intramolecular fluorescence energy transfer in nitrobenzoxadiazole derivatives of polyene antibiotics, Can. J. Chem. 63 (1985) 77–85.
[125] N.O. Petersen, P.F. Henshaw, Separation of fluorescent impurities from amphotericin B, Can. J. Chem. 59 (1981) 3376–3378.
[126] W.I. Gruszecki, M. Herec, Dimers of polyene antibiotic amphotericin B, J. Photochem. Photobiol. B – Biol. 72 (2003) 103–105.
[127] W.I. Gruszecki, M. Gagos, M. Herec, P. Kernen, Organization of antibiotic amphotericin B in model lipid membranes. A mini review, Cell. Mol. Biol. Lett. 8 (2003) 161–170.
[128] B.A. Steinberg, W.P. Jambor, L.O. Suydam, Amphotericin A and B: two new antifungal antibiotics possessing high activity against deep-seated and superficial mycoses, Antibiot. Ann. (1956) 574–578.
[129] J. El On, G. Messer, C.L. Greenblatt, Growth inhibition of *Leishmania tropica* amastigotes in vitro by rifampicin combined with amphotericin B, Ann. Trop. Med. Parasitol. 78 (1984) 93–98.
[130] A.A. McColm, N. McHardy, Evaluation of a range of antimicrobial agents against the parasitic protozoa, *Plasmodium falciparum, Babesia rodhaini* and *Theileria parva in vitro*, Ann. Trop. Med. Parasitol. 78 (1984) 345–354.
[131] C.B. Panosian, M. Barza, F. Szoka, D.J. Wyler, Treatment of experimental cutaneous leishmaniasis with liposome-intercalated amphotericin B, Antimicrob. Agents Chemother. 25 (1984) 655–656.
[132] R. Dietze, E.P. Milan, J.D. Berman, M. Grogl, A. Falqueto, T.F. Feitosa, K.G. Luz, F.A.B. Suassuna, L.A.C. Marinho, G. Ksionski, Treatment of Brazilian Kala-Azar with a short course of Amphocil (amphotericin-B cholesterol dispersion), Clin. Infect. Dis. 17 (1993) 981–986.
[133] H. Ramos, E. Valdivieso, M. Gamargo, F. Dagger, B.E. Cohen, Amphotericin B kills unicellular leishmanias by forming aqueous pores permeable to small cations and anions, J. Membrane Biol. 152 (1996) 65–75.
[134] C.P. Schaffner, O.J. Plescia, D. Pontani, D. Sun, A. Thornton, R.C. Pandey, P.S. Sarin, Anti-viral activity of amphotericin B methyl ester: inhibition of HTLV-III replication in cell culture, Biochem. Pharmacol. 35 (1986) 4110–4113.
[135] D.R. Pontani, D. Sun, J.W. Brown, S.I. Shahied, O.J. Plescia, C.P. Schaffner, G. Lopez Berestein, P.S. Sarin, Inhibition of HIV replication by liposomal encapsulated amphotericin B, Antivir. Res. 11 (1989) 119–125.
[136] O. Pleskoff, M. Seman, M. Alizon, Amphotericin B derivative blocks human immunodeficiency virus type 1 entry after CD4 binding: effect on virus–cell fusion but not on cell–cell fusion, J. Virol. 69 (1995) 570–574.
[137] K. Konopka, L.S.S. Guo, N. Duzgunes, Anti-HIV activity of amphotericin B–cholesteryl sulfate colloidal dispersion in vitro, Antivir. Res. 42 (1999) 197–209.
[138] M. Pocchiari, S. Schmittinger, C. Masullo, Amphotericin B delays the incubation period of scrapie in intracerebrally inoculated hamsters, J. Gen. Virol. 68 (1987) 219–223.
[139] Y.G. Xi, L. Ingrosso, A. Ladogana, C. Masullo, M. Pocchiari, Amphotericin-B treatment dissociates in vivo replication of the scrapie agent from PrP accumulation, Nature 356 (1992) 598–601.
[140] R.V. Stanton, L.R. Little, K.M. Merz, Quantum free energy perturbation study within a PM3 MM coupled potential, J. Phys. Chem. 99 (1995) 483–486.
[141] K.T. Adjou, J.P. Deslys, R. Demaimay, D. Dormont, Probing the dynamics of prion diseases with amphotericin B, Trends Microbiol. 5 (1997) 27–31.
[142] S.C. Hartsel, T.R. Weiland, Amphotericin B binds to amyloid fibrils and delays their formation: a therapeutic mechanism? Biochemistry 42 (2003) 6228–6233.

[143] W.E.J. Hauser, J.S. Remington, Effect of amphotericin B on natural killer cell activity in vitro, J. Antimicrob. Chemother. 11 (1983) 257–262.
[144] F. Bistoni, A. Vecchiarelli, R. Mazzolla, P. Puccetti, P. Marconi, E. Garaci, Immunoadjuvant activity of amphotericin B as displayed in mice infected with *Candida albicans*, Antimicrob. Agents Chemother. 27 (1985) 625–631.
[145] J.R. Little, V. Shore, Modulation by lipoproteins of amphotericin B-induced immunostimulation, Cell Immunol. 93 (1985) 212–221.
[146] J.E. Wolf, S.H. Stein, K.D. Little, A.L. Abegg, J.R. Little, Amphotericin B selectively stimulates macrophages from high responder mouse strains, Immunopharmacol. Immunotoxicol. 13 (1991) 221–235.
[147] M.A. Carlson, R.E. Condon, Nephrotoxicity of amphotericin B, J. Am. Coll. Surgeons 179 (1994) 361–381.
[148] S. Harbarth, S.L. Pestotnik, J.F. Lloyd, J.P. Burke, M.H. Samore, The epidemiology of nephrotoxicity associated with conventional amphotericin B therapy, Am. J. Med. 111 (2001) 528–534.
[149] D.E. Varlam, M.M. Siddiq, L.A. Parton, H. Russmann, Apoptosis contributes to amphotericin B-induced nephrotoxicity, Antimicrob. Agents Chemother. 45 (2001) 679–685.
[150] G. Deray, Amphotericin B nephrotoxicity, J. Antimicrob. Chemother. 49 (2002) 37–41.
[151] G. Maschmeyer, New antifungal agents – treatment standards are beginning to grow old, J. Antimicrob. Chemother. 49 (2002) 239–241.
[152] J.T. Cheng, R.T. Witty, R.R. Robinson, W.E. Yarger, Amphotericin B nephrotoxicity: increased renal resistance and tubule permeability, Kidney Int. 22 (1982) 626–633.
[153] R.A. Zager, C.R. Bredl, B.A. Schimpf, Direct amphotericin B-mediated tubular toxicity: assessments of selected cytoprotective agents, Kidney Int. 41 (1992) 1588–1594.
[154] J. Barwicz, R. Gareau, A. Audet, A. Morisset, J. Villiard, I. Gruda, Inhibition of the interaction between lipoproteins and amphotericin B by some delivery systems, Biochem. Biophys. Res. Commun. 181 (1991) 722–728.
[155] K.M. Wasan, M.G. Rosenblum, L. Cheung, G. Lopezberestein, Influence of lipoproteins on renal cytotoxicity and antifungal activity of amphotericin B, Antimicrob. Agents Chemother. 38 (1994) 223–227.
[156] S.F. Hsu, R.R. Burnette, Characterization of the effects of amphotericin B on ion channels in MDCK cells using the patch-clamp technique, Biochim. Biophys. Acta 1329 (1997) 26–38.
[157] J. Barwicz, I. Dumont, C. Ouellet, I. Gruda, Amphotericin B toxicity as related to the formation of oxidatively modified low-density lipoproteins, Biospectroscopy 4 (1998) 135–144.
[158] S.C. Hartsel, B. Baas, E. Bauer, L.T. Foree, K. Kindt, H. Preis, A. Scott, E.H. Kwong, M. Ramaswamy, K.M. Wasan, Heat-induced superaggregation of amphotericin B modifies its interaction with serum proteins and lipoproteins and stimulation of TNF-alpha, J. Pharm. Sci. 90 (2001) 124–133.
[159] W.G. Ellis, R.A. Sobel, S.L. Nielsen, Leukoencephalopathy in patients treated with amphotericin B methyl ester, J. Infect. Dis. 146 (1982) 125–137.
[160] W.G. Ellis, E. Bencken, R.A. LeCouteur, J.R. Barbano, B.M. Wolfe, M.B. Jennings, Neurotoxicity of amphotericin B methyl ester in dogs, Toxicol. Pathol. 16 (1988) 1–9.
[161] K.R. Reuhl, M. Vapiwala, M.T. Ryzlak, C.P. Schaffner, Comparative neurotoxicities of amphotericin-B and its mono-methyl ester derivative in rats, Antimicrob. Agents Chemother. 37 (1993) 419–428.
[162] J.P. Adler Moore, R.T. Proffitt, Development, characterization, efficacy and mode of action of Abisome, a unilamellar liposomal formulation of amphotericin B, J. Liposome Res. 3 (1993) 429–450.
[163] M. Gulati, S. Bajad, S. Singh, A.J. Ferdous, M. Singh, Development of liposomal amphotericin B formulation, J. Microencapsul. 15 (1998) 137–151.

[164] S. Arikan, J.H. Rex, Lipid-based antifungal agents: current status, Curr. Pharm. Design 7 (2001) 393–415.
[165] T.J. Walsh, R.W. Finberg, C. Arndt, J. Hiemenz, C. Schwartz, D. Bodensteiner, P.G. Pappas, N. Seibel, R.N. Greenberg, S. Dummer, S. Schuster, J.S. Holcenberg, Liposomal amphotericin B for empirical therapy in patients with persistent fever and neutropenia, New Engl. J. Med. 340 (1999) 764–771.
[166] J. Ritter, Amphotericin B and its lipid formulations, Mycoses 45 (2002) 34–38.
[167] L. OstroskyZeichner, K.A. Marr, J.H. Rex, S.H. Cohen, Amphotericin B: time for a new ''gold standard'', Clin. Infect. Dis. 37 (2003) 415–425.
[168] A. Lavasanifar, J. Samuel, G.S. Kwon, Micelles self-assembled from poly(ethylene oxide)-block-poly(*N*-hexyl stearate L-aspartamide) by a solvent evaporation method: effect on the solubilization and haemolytic activity of amphotericin B, J. Control. Release 77 (2001) 155–160.
[169] A. Lavasanifar, J. Samuel, S. Sattari, G.S. Kwon, Block copolymer micelles for the encapsulation and delivery of amphotericin B, Pharmaceut. Res. 19 (2002) 418–422.
[170] M.L. Adams, D.R. Andes, G.S. Kwon, Amphotericin B encapsulated in micelles based on poly(ethylene oxide)-block-poly(L-amino acid) derivatives exerts reduced in vitro hemolysis but maintains potent in vivo antifungal activity, Biomacromolecules 4 (2003) 750–757.
[171] R.R. New, M.L. Chance, S. Heath, Antileishmanial activity of amphotericin and other antifungal agents entrapped in liposomes, J. Antimicrob. Chemother. 8 (1981) 371–381.
[172] J.R. Graybill, P.C. Craven, R.L. Taylor, D.M. Williams, W.E. Magee, Treatment of murine cryptococcosis with liposome-associated amphotericin B, J. Infect. Dis. 145 (1982) 748–752.
[173] R.L. Taylor, D.M. Williams, P.C. Craven, J.R. Graybill, D.J. Drutz, W.E. Magee, Amphotericin B in liposomes: a novel therapy for histoplasmosis, Am. Rev. Respir. Dis. 125 (1982) 610–611.
[174] R. van Gool, The cost of treating systemic fungal infections, Drugs 61 (2001) 49–56.
[175] A. Cass, A. Finkelstein, V. Krespi, The ion permeability induced in thin lipid membranes by the polyene antibiotics nystatin and amphotericin B, J. Gen. Physiol. 56 (1970) 100–145.
[176] J. Brajtburg, S. Elberg, J. Medoff, G.S. Kobayashi, D. Schlessinger, G. Medoff, Stimulatory, permeabilizing, and toxic effects of amphotericin B on L cells, Antimicrob. Agents Chemother. 26 (1984) 892–897.
[177] J. Brajtburg, S. Elberg, D.R. Schwartz, A. Vertut-Croquin, D. Schlessinger, G.S. Kobayashi, G. Medoff, Involvement of oxidative damage in erythrocyte lysis induced by amphotericin B, Antimicrob. Agents Chemother. 27 (1985) 172–176.
[178] M.L. Sokol Anderson, J. Brajtburg, G. Medoff, Amphotericin B-induced oxidative damage and killing of *Candida albicans*, J. Infect. Dis. 154 (1986) 76–83.
[179] B. De Kruijff, R.A. Demel, Polyene antibiotic–sterol interactions in membranes of acholeplasma laidlawii cells and lecithin liposomes. III. Molecular structure of the polyene antibiotic–cholesterol complexes, Biochim. Biophys. Acta 339 (1974) 57–70.
[180] A. Marty, A. Finkelstein, Pores formed in lipid bilayer membranes by nystatin. Differences in its one-sided and two-sided action, J. Gen. Physiol. 65 (1975) 515–526.
[181] P. Van Hoogevest, B. De Kruijff, Effect of amphotericin B on cholesterol-containing liposomes of egg phosphatidylcholine and didocosenoyl phosphatidylcholine. A refinement of the model for the formation of pores by amphotericin B in membranes, Biochim. Biophys. Acta 511 (1978) 397–407.
[182] M.E. Kleinberg, A. Finkelstein, Single-length and double-length channels formed by nystatin in lipid bilayer membranes, J. Membrane Biol. 80 (1984) 257–269.

[183] G. Fujii, J.E. Chang, T. Coley, B. Steere, The formation of amphotericin B ion channels in lipid bilayers, Biochemistry 36 (1997) 4959–4968.
[184] V.E. Khutorsky, A.A. Kamenchuk, Molecular model for ionic permeability and selectivity of the amphotericin B channel, Biol. Membr. 5 (1988) 173–180.
[185] V.E. Khutorsky, A.A. Kamenchuk, L.N. Ermishkin, Computer analysis of amphotericin B channel structure, Biofizika 33 (1988) 794–799.
[186] M. Bonilla-Marin, M. Moreno-Bello, I. Ortega-Blake, A microscopic electrostatic model for the amphotericin B channel, Biochim. Biophys. Acta 1061 (1991) 65–77.
[187] V.E. Khutorsky, Structures of amphotericin B–cholesterol complex, Biochim. Biophys. Acta 1108 (1992) 123–127.
[188] I.B. Golovanov, I.G. Tsygankova, Simulation of an Amphotericin B channel, Membrane Cell Biol. 9 (1995) 335–346.
[189] V. Khutorsky, Ion coordination in the amphotericin B channel, Biophys. J. 71 (1996) 2984–2995.
[190] A. Silberstein, Conformational analysis of amphotericin B–cholesterol channel complex, J. Membrane Biol. 162 (1998) 117–126.
[191] H. Resat, M. Baginski, Ion passage pathways and thermodynamics of the amphotericin B membrane channel, Eur. Biophys. J. Biophys. Lett. 31 (2002) 294–305.
[192] M.P. Borisova, R.A. Brutyan, L.N. Ermishkin, Mechanism of anion–cation selectivity of amphotericin B channels, J. Membrane Biol. 90 (1986) 13–20.
[193] S.C. Hartsel, S.K. Benz, W. Ayenew, J. Bolard, Na^+, K^+ and Cl^- selectivity of the permeability pathways induced through sterol-containing membrane vesicles by amphotericin B and other polyene antibiotics, Eur. Biophys. J. 23 (1994) 125–132.
[194] B.D. Wolf, S.C. Hartsel, Osmotic stress sensitizes sterol-free phospholipid bilayers to the action of amphotericin B, Biochim. Biophys. Acta 1238 (1995) 156–162.
[195] B.V. Cotero, S. RebolledoAntunez, I. Ortega-Blake, On the role of sterol in the formation of the amphotericin B channel, Biochim. Biophys. Acta 1375 (1998) 43–51.
[196] T. Ruckwardt, A. Scott, J. Scott, P. Mikulecky, S.C. Hartsel, Lipid and stress dependence of amphotericin B ion selective channels in sterol-free membranes, Biochim. Biophys. Acta 1372 (1998) 283–288.
[197] B. Venegas, J. GonzalezDamian, H. Celis, I. OrtegaBlake, Amphotericin B channels in the bacterial membrane: role of sterol and temperature, Biophys. J. 85 (2003) 2323–2332.
[198] C.L. Weakliem, G. Fujii, J.-E. Chang, A. Ben-Shaul, W.M. Gelbart, Effect of tension on pore formation in drug-containing vesicles, J. Am. Chem. Soc. 99 (1995) 7694–7697.
[199] E.J. Dufourc, J.C.P. Smith, H.D. Jarrell, Amphotericin and model membranes. The effect of amphotericin B on cholesterol-containing systems as viewed by ^{2}H-NMR, Biochim. Biophys. Acta 776 (1984) 317–329.
[200] M. Baginski, Studies of selected molecular properties of amphotericin B and its cellular targets by theoretical chemistry methods – doctoral thesis, Gdansk (Polish), Technical University of Gdansk, 1995.
[201] M. Baginski, A. Tempczyk, E. Borowski, Comparative conformational analysis of cholesterol and ergosterol by molecular mechanics, Eur. Biophys. J. 17 (1989) 159–166.
[202] S. Clejan, R. Bittman, Rates of amphotericin B and filipin association with sterols. A study of changes in sterol structure and phospholipid composition of vesicles, J. Biol. Chem. 260 (1985) 2884–2889.
[203] M. Baginski, P. Bruni, E. Borowski, Comparative analysis of the distribution of the molecular electrostatic potential for cholesterol and ergosterol, Theochem. J. Mol. Struct. 311 (1994) 285–296.
[204] M.A. Ghannoum, L.B. Rice, Antifungal agents: mode of action, mechanisms of resistance, and correlation of these mechanisms with bacterial resistance, Clin. Microbiol. Rev. 12 (1999) 501ff.

[205] D.E. Mickus, D.G. Levitt, S.D. Rychnovsky, Enantiomeric cholesterol as a probe of ion-channel structure, J. Am. Chem. Soc. 114 (1992) 359–360.
[206] R.K. Richter, D.E. Mickus, S.D. Rychnowski, T.F. Molinski, Differential modulation of the antifungal activity of amphotericin B by natural and ent-cholesterol, Bioorg. Med. Chem. Lett. 14 (2004) 115–118.
[207] S.J. Singer, G.L. Nicolson, The fluid mosaic model of the structure of cell membranes, Science 175 (1972) 720–731.
[208] D. Brown, Structure and function of membrane rafts, Int. J. Med. Microbiol. 291 (2002) 433–437.
[209] M. Edidin, The state of lipid rafts: from model membranes to cells, Annu. Rev. Biophys. Biomol. Struct. 32 (2003) 257–283.
[210] C. Bernsdorff, R. Winter, Differential properties of the sterols cholesterol, ergosterol, beta-sitosterol, *trans*-7-dehydrocholesterol, stigmasterol and lanosterol on DPPC bilayer order, J. Phys. Chem. B 107 (2003) 10658–10664.
[211] D. Chapman, Biological Membranes, Academic Press, New York, 1968.
[212] R.A. Demel, B. DeKruyff, The function of sterols in membranes, Biochim. Biophys. Acta 457 (1976) 109–132.
[213] K. Bloch, Sterol structure and membrane function, Curr. Top. Cell. Regul. 18 (1981) 289–299.
[214] A.C. Oehlschlager, P. Laks, Nitroxide spin-probe study of amphotericin B–ergosterol interaction in egg phosphatidylcholine multilayers, Can. J. Biochem. 58 (1980) 978–985.
[215] M.J. Paquet, I. Fournier, J. Barwicz, P. Tancrede, M. Auger, The effects of amphotericin B on pure and ergosterol- or cholesterol-containing dipalmitoylphosphatidylcholine bilayers as viewed by H-2 NMR, Chem. Phys. Lipids 119 (2002) 1–11.
[216] H.T.Tien, A.Ottova-Leitmannova (Eds.), Planar Lipid Bilayers (BLMs) and their Application, Amsterdam, Elsevier, 2003.
[217] S.V. Rudenko, Structural rearrangements induced by glycerol increase the permeability of bilayer lipid membranes for amphotericin (Russian), Biofizika 31 (1986) 59–63.
[218] E.K. Alekberli, V.P. Topaly, Permeability of bilayer lipid membranes to amphotericin B (Russian), Biofizika 29 (1984) 322–323.
[219] S.I. Alekseev, M.C. Ziskin, Millimeter microwave effect on ion transport across lipid bilayer membranes, Bioelectromagnetics 16 (1995) 124–131.
[220] P. Koufen, U. Zeidler, G. Stark, Photodynamic inactivation of ion channels formed by the polyene antibiotic amphotericin B in lipid membranes, J. Photochem. Photobiol. B – Biol. 38 (1997) 129–135.
[221] W.I. Gruszecki, B. Zelent, H.A. Tajmir-Riahi, G.M. Wang, T. Taleb, K. Veeranjaneyulu, R.M. Leblanc, Chlorophyll *a*–violaxanthin interactions in monolayers at air–water interface and in Langmuir–Blodgett films, Coll. Surfac. B – Biointerfac. 19 (2000) 117–125.
[222] J. Milanowska, A. Polit, Z. Wasylewski, W.I. Gruszecki, Interaction of isomeric forms of xanthophyll pigment zeaxanthin with dipalmitoylphosphatidylcholine studied in monomolecular layers, J. Photochem. Photobiol. B – Biol. 72 (2003) 1–9.
[223] D. Niedzwiedzki, W.I. Gruszecki, Interaction between chlorophyll *a* and violaxanthin in different steric conformations – model studies in monomolecular layers, Coll. Surfac. B – Biointerfac. 28 (2003) 27–38.
[224] M.R. Lance, C. Washington, S.S. Davis, Evidence for the formation of amphotericin B–phospholipid complexes in Langmuir monolayers, Pharmac. Res. 13 (1996) 1008–1014.
[225] K. Wojtowicz, W.I. Gruszecki, M. Walicka, J. Barwicz, Effect of amphotericin B on dipalmitoylphosphatidylcholine membranes: calorimetry, ultrasound absorption and monolayer technique studies, Biochim. Biophys. Acta 1373 (1998) 220–226.

[226] P. Dynarowicz-Latka, R. Seoane, J. Minones, M. Velo, J. Minones, Study of penetration of amphotericin B into cholesterol or ergosterol containing dipalmitoyl phosphatidylcholine Langmuir monolayers, Coll. Surface B 27 (2003) 249–263.
[227] I. ReyGomezSerranillos, P. Dynarowicz-Latka, J. Minones, R. Seoane, Desorption of amphotericin B from mixed monolayers with cholesterol at the air/water interface, J. Coll. Interfac. Sci. 234 (2001) 351–355.
[228] M. Kasha, Energy transfer mechanisms and the molecular excitation model for molecular aggregates, Radiat. Res. 20 (1963) 55–71.
[229] M. Kasha, H.R. Rawls, M. Ashraf El-Bayoumi, The excitation model in molecular spectroscopy, Pure Appl. Chem. 11 (1965) 371–392.
[230] J. Parkash, J.H. Robblee, J. Agnew, E. Gibbs, P. Collings, R.F. Pasternack, J.C. de Paula, Depolarized resonance light scattering by porphyrin and chlorophyll *a* aggregates, Biophys. J. 74 (1998) 2089–2099.
[231] A.D. Bangham, M.M. Standish, J.C. Watkins, Diffusion of univalent ions across the lamelle of swollen phospholipids, J. Mol. Biol. 13 (1965) 238–252.
[232] C. Huang, Studies on phosphatidylcholine vesicles. Formation and physical characteristics, Biochemistry 8 (1969) 344–352.
[233] F.J. Szoka, D. Papahadjopoulos, Comparative properties and methods of preparation of lipid vesicles, Annu. Rev. Biophys. Bioeng. 9 (1980) 467–508.
[234] J. Bolard, J. Milhaud, Interaction of the anti-candida amphotericin B (and other polyene antibiotics) with lipids, in: R. Prasad, M.A. Ghannoum (Eds.), Lipids of Pathogenic Fungi, CRC Press, New York, 1996, pp. 253–274.
[235] A. Coutinho, M. Prieto, Cooperative partition model of nystatin interaction with phospholipid vesicles, Biophys. J. 84 (2003) 3061–3078.
[236] T.D. Madden, A.S. Janoff, P.R. Cullis, Incorporation of amphotericin B into large unilamellar vesicles composed of phosphatidylcholine and phosphatidylglycerol, Chem. Phys. Lipids 52 (1990) 189–198.
[237] A.S. Janoff, L.T. Boni, M.C. Popescu, S.R. Minchey, P.R. Cullis, T.D. Madden, T. Taraschi, S.M. Gruner, E. Shyamsunder, M.W. Tate, R. Mendelsohn, D. Bonner, Unusual lipid structures selectively reduce the toxicity of amphotericin B, Proc. Natl. Acad. Sci. USA 85 (1988) 6122–6126.
[238] W.R. Perkins, S.R. Minchey, L.T. Boni, C.E. Swenson, M.C. Popescu, R.F. Pasternack, A.S. Janoff, Amphotericin B–phospholipid interactions responsible for reduced mammalian cell toxicity, Biochim. Biophys. Acta 1107 (1992) 271–282.
[239] P. Rojanapanthu, N. Sarisuta, K. Chaturon, K. Kraisintu, Physicochemical properties of amphotericin B liposomes prepared by reverse-phase evaporation method, Drug Develop. Ind. Pharm. 29 (2003) 31–37.
[240] J. Milhaud, B. Michels, Binding of nystatin and amphotericin B with sterol-free L-dilauroylphosphatidylcholine bilayers resulting in the formation of dichroic lipid superstructures, Chem. Phys. Lipids 101 (1999) 223–235.
[241] N.M. Witzke, R. Bittman, Dissociation kinetics and equilibrium binding properties of polyene antibiotic complexes with phosphatidylcholine/sterol vesicles, Biochemistry 23 (1984) 1668–1674.
[242] J. Bolard, A. Vertut-Croquin, B. Cybulska, C.M. Gary-Bobo, Transfer of the polyene antibiotic amphotericin B between single-walled vesicles of dipalmitoylphosphatidylcholine and egg-yolk phosphatidylcholine, Biochim. Biophys. Acta 647 (1981) 241–248.
[243] I. Fournier, J. Barwicz, P. Tancrede, The structuring effects of amphotericin B on pure and ergosterol- or cholesterol-containing dipalmitoylphosphatidylcholine bilayers: a differential scanning calorimetry study, Biochim. Biophys. Acta 1373 (1998) 76–86.
[244] S. Jullien, A. Vertut-Croquin, J. Brajtburg, J. Bolard, Circular dichroism for the determination of amphotericin B binding to liposomes, Anal. Biochem. 172 (1988) 197–202.

[245] J. Milhaud, J. Berrehar, J.M. Lancelin, B. Michels, G. Raffard, E.J. Dufourc, Association of polyene antibiotics with sterol-free lipid membranes. 2. Hydrophobic binding of nystatin to dilauroylphosphatidylcholine bilayers, Biochim. Biophys. Acta 1326 (1997) 54–66.
[246] P. Legrand, M. Cheron, L. Leroy, J. Bolard, Release of amphotericin B from delivery systems and its action against fungal and mammalian cells, J. Drug Target. 4 (1997) 311–319.
[247] R. Strom, W.E. Blumberg, R.E. Dale, C. Crifo, The interaction of the polyene antibiotic lucensomycin with cholesterol in erythrocyte membranes and in model systems, Biophys. J. 16 (1976) 1297–1314.
[248] L.M.S. Loura, A.R.B. Castanho, A. Fedorov, M. Prieto, A photophysical study of the polyene antibiotic filipin self-aggregation and filipin–ergosterol interaction, Biochim. Biophys. Acta 1510 (2001) 125–135.
[249] N.O. Petersen, R. Gratton, E.M. Pisters, Fluorescence properties of polyene antibiotics in phospholipid bilayer membranes, Can. J. Chem. 65 (1987) 238–244.
[250] A. Coutinho, M. Prieto, Self-association of the polyene antibiotic nystatin in dipalmitoylphosphatidylcholine vesicles: a time-resolved fluorescence study, Biophys. J. 69 (1995) 2541–2557.
[251] N.O. Petersen, A new fluorescent derivative of amphotericin B: synthesis, characterization and application in fluorescence photobleaching, Spectrosc. Int. J. 2 (1983) 408–414.
[252] L.J. O'Neil, J.G. Miller, N.O. Petersen, Evidence for nystatin micelles in L-cell membranes from fluorescence photobleaching measurements of diffusion, Biochemistry 25 (1986) 177–181.
[253] N. Henry Toulme, M. Seman, J. Bolard, Interaction of amphotericin B and its *N*-fructosyl derivative with murine thymocytes: a comparative study using fluorescent membrane probes, Biochim. Biophys. Acta 982 (1989) 245–252.
[254] G. Strauss, The interaction of amphotericin B with lipid bilayer vesicles: determination of binding constants by absorption and fluorescence spectroscopy, Can. J. Spectrosc. 26 (1981) 95–102.
[255] K.S. Hamilton, K.R. Barber, J.H. Davis, K. Neil, C.W. Grant, Phase behaviour of amphotericin B multilamellar vesicles, Biochim. Biophys. Acta 1062 (1991) 220–226.
[256] J. Milhaud, J.M. Lancelin, B. Michels, A. Blume, Association of polyene antibiotics with sterol-free lipid membranes: I. Hydrophobic binding of filipin to dimyristoylphosphatidylcholine bilayers, Biochim. Biophys. Acta 1278 (1996) 223–232.
[257] J. Milhaud, J. Mazerski, J. Bolard, E.J. Dufourc, Interaction of filipin with dimyristoylphosphatidylcholine membranes studied by ^{2}H-NMR, circular dichroism, electronic absorption and fluorescence, Eur. Biophys. J. 17 (1989) 151–158.
[258] E.J. Dufourc, I.C.P. Smith, ^{2}H NMR evidence for antibiotic-induced cholesterol immobilization in biological model membranes, Biochemistry 24 (1985) 2420–2424.
[259] J. Milhaud, J. Mazerski, J. Bolard, Competition between cholesterol and phospholipids for binding to phospholipids, Biochim. Biophys. Acta 987 (1989) 193–198.
[260] E.J. Dufourc, J.C.P. Smith, H.D. Jarrell, Interaction of amphotericin B with membrane lipids as viewed by ^{2}H-NMR, Biochim. Biophys. Acta 778 (1984) 435–442.
[261] B.S. Whyte, R.P. Peterson, S.C. Hartsel, Amphotericin B and nystatin show different activities on sterol-free vesicles, Biochem. Biophys. Res. Commun. 164 (1989) 609–614.
[262] J. Milhaud, Permeabilizing action of filipin III on model membranes through a filipin–phospholipid binding, Biochim. Biophys. Acta 1105 (1992) 307–318.
[263] H. Ramos, A. Attias de Murciano, B.E. Cohen, J. Bolard, The polyene antibiotic amphotericin B acts as a Ca^{2+} ionophore in sterol-containing liposomes, Biochim. Biophys. Acta 982 (1989) 303–306.

[264] M. Herve, B. Cybulska, C.M. Gary-Bobo, Cation permeability induced by valinomycin, gramicidin D and amphotericin B in large lipidic unilamellar vesicles studied by ^{31}P-NMR, Eur. Biophys. J. 12 (1985) 121–128.
[265] B. Cybulska, M. Herve, E. Borowski, C.M. Gary-Bobo, Effect of the polar head structure of polyene macrolide antifungal antibiotics on the mode of permeabilization of ergosterol- and cholesterol-containing lipidic vesicles studied by ^{31}P-NMR, Mol. Pharmacol. 29 (1986) 293–298.
[266] S. Matsuoka, M. Murata, Cholesterol markedly reduces ion permeability induced by membrane-bound amphotericin B, Biochim. Biophys. Acta 1564 (2002) 429–434.
[267] Y. Aracava, S. Schreier, R. Phadke, R. Deslauriers, I.C.P. Smith, Effects of amphotericin B on membrane permeability-kinetics of spin probe reduction, Biophys. Chem. 14 (1981) 325–332.
[268] S.C. Hartsel, W.R. Perkins, G.J. McGarvey, D.S. Cafiso, A selective cholesterol-dependent induction of H^+/OH^- currents in phospholipid vesicles by amphotericin B, Biochemistry 27 (1988) 2656–2660.
[269] B.E. Cohen, A sequential mechanism for the formation of aqueous channels by amphotericin B in liposomes. The effect of sterols and phospholipid composition, Biochim. Biophys. Acta 1108 (1992) 49–58.
[270] K. Merz, B. Roux (Eds.), Biological Membranes. A Molecular Perspective from Computation and Experiment, Birkhauser, Boston, 1996.
[271] K.M. Merz, Molecular dynamics simulations of lipid bilayers, Curr. Opin. Struct. Biol. 7 (1997) 511–517.
[272] L.R. Forrest, M.S.P. Sansom, Membrane simulations: bigger and better? Curr. Opin. Struct. Biol. 10 (2000) 174–181.
[273] S.E. Feller, Molecular dynamics simulations of lipid bilayers, Curr. Opin. Coll. Interfac. Sci. 5 (2000) 217–223.
[274] H.L. Scott, Modeling the lipid component of membranes, Curr. Opin. Struct. Biol. 12 (2002) 495–502.
[275] D.P. Tieleman, S.J. Marrink, H.J.C. Berendsen, A computer perspective of membranes: molecular dynamics studies of lipid bilayer systems, Biochim. Biophys. Acta 1331 (1997) 235–270.
[276] T. Heimburg, Monte Carlo simulations of lipid bilayers and lipid protein interactions in the light of recent experiments, Curr. Opin. Coll. Interfac. Sci. 5 (2000) 224–231.
[277] D. Bassolinoklimas, H.E. Alper, T.R. Stouch, Solute diffusion in lipid bilayer membranes – an atomic level study by molecular dynamics simulation, Biochemistry 32 (1993) 12624–12637.
[278] P. Huang, E. Bertaccini, G.H. Loew, Molecular dynamics simulation of anesthetic–phospholipid bilayer interactions, J. Biomol. Struct. Dyn. 12 (1995) 725–754.
[279] B. Jin, A.J. Hopfinger, Characterization of lipid membrane dynamics by simulation. 3. Probing molecular transport across the phospholipid bilayer, Pharmaceut. Res. 13 (1996) 1786–1794.
[280] J.J.L. Cascales, J.G.H. Cifre, J.G. Delatorre, Anaesthetic mechanism on a model biological membrane: a molecular dynamics simulation study, J. Phys. Chem. B 102 (1998) 625–631.
[281] M.X. Fernandes, M.L. Huertas, M.A.R.B. Castanho, J.G. Delatorre, Simulation of the distribution and diffusion of a rigid amphipathic particle embedded in a model membrane, Biophys. Chem. 79 (1999) 41–53.
[282] M. Pasenkiewicz-Gierula, T. Rog, J. Grochowski, P. Serda, R. Czarnecki, T. Librowski, S. Lochynski, Effects of a carane derivative local anesthetic on a phospholipid bilayer studied by molecular dynamics simulation, Biophys. J. 85 (2003) 1248–1258.
[283] M.S.P. Sansom, D.P. Tieleman, L.R. Forrest, H.J.C. Berendsen, Molecular dynamics simulations of membranes with embedded proteins and peptides: porin, alamethicin and influenza virus M2, Biochem. Soc. Trans. 26 (1998) 438–443.

[284] W. Im, S. Seefeld, B. Roux, A grand canonical Monte Carlo–Brownian dynamics algorithm for simulating ion channels, Biophys. J. 79 (2000) 788–801.
[285] W. Im, B. Roux, Brownian dynamics simulations of ions channels: a general treatment of electrostatic reaction fields for molecular pores of arbitrary geometry, J. Chem. Phys. 115 (2001) 4850–4861.
[286] M.S.P. Sansom, I.H. Shrivastava, J.N. Bright, J. Tate, C.E. Capener, P.C. Biggin, Potassium channels: structures, models, simulations, Biochim. Biophys. Acta 1565 (2002) 294–307.
[287] B. Roux, Theoretical and computational models of ion channels, Curr. Opin. Struct. Biol. 12 (2002) 182–189.
[288] W.B. Fischer, M.S.P. Sansom, Viral ion channels: structure and function, Biochim. Biophys. Acta 1561 (2002) 27–45.
[289] C.E. Capener, H.J. Kim, Y. Arinaminpathy, M.S.P. Sansom, Ion channels: structural bioinformatics and modelling, Hum. Mol. Genet. 11 (2002) 2425–2433.
[290] O. Miyashita, J.N. Onuchic, M.Y. Okamura, Continuum electrostatic model for the binding of cytochrome *c*(2) to the photosynthetic reaction center from *Rhodobacter sphaeroides*, Biochemistry 42 (2003) 11651–11660.
[291] R.M. Peitzsch, M. Eisenberg, K.A. Sharp, S. Mclaughlin, Calculations of the electrostatic potential adjacent to model phospholipid bilayers, Biophys. J. 68 (1995) 729–738.
[292] D.J. Tobias, Electrostatics calculations: recent methodological advances and applications to membranes, Curr. Opin. Struct. Biol. 11 (2001) 253–261.
[293] J.H. Lin, N.A. Baker, J.A. McCammon, Bridging implicit and explicit solvent approaches for membrane electrostatics, Biophys. J. 83 (2002) 1374–1379.
[294] N. BenTal, B. Honig, C. Miller, S. Mclaughlin, Electrostatic binding of proteins to membranes. Theoretical predictions and experimental results with charybdotoxin and phospholipid vesicles, Biophys. J. 73 (1997) 1717–1727.
[295] A. Kessel, B. Musafia, N. BenTal, Continuum solvent model studies of the interactions of an anticonvulsant drug with a lipid bilayer, Biophys. J. 80 (2001) 2536–2545.
[296] W. Cheng, C.X. Wang, W.Z. Chen, Y.W. Xu, Y.Y. Shi, Investigating the dielectric effects of channel pore water on the electrostatic barriers of the permeation ion by the finite difference Poisson–Boltzmann method, Eur. Biophys. J. Biophys. Lett. 27 (1998) 105–112.
[297] G. Moy, B. Corry, S. Kuyucak, S.H. Chung, Tests of continuum theories as models of ion channels. I. Poisson–Boltzmann theory versus Brownian dynamics, Biophys. J. 78 (2000) 2349–2363.
[298] W. Im, B. Roux, Ion permeation and selectivity of OmpF porin: a theoretical study based on molecular dynamics, Brownian dynamics, and continuum electrodiffusion theory, J. Mol. Biol. 322 (2002) 851–869.
[299] S. Berneche, B. Roux, A microscopic view of ion conduction through the K^+ channel, Proc. Nat. Acad. Sci. USA 100 (2003) 8644–8648.
[300] P.B. Moore, C.F. Lopez, M.L. Klein, Dynamical properties of a hydrated lipid bilayer from a multinanosecond molecular dynamics simulation, Biophys. J. 81 (2001) 2484–2494.
[301] R.W. Pastor, R.M. Venable, S.E. Feller, Lipid bilayers, NMR relaxation, and computer simulations, Account. Chem. Res. 35 (2002) 438–446.
[302] C. Anezo, A.H. Devries, H.D. Holtje, D.P. Tieleman, S.J. Marrink, Methodological issues in lipid bilayer simulations, J. Phys. Chem. B 107 (2003) 9424–9433.
[303] M. Schlenkrich, J. Brickmann, A.D. Mackerell, M. Karplus, An empirical potential energy function for phospholipids: criteria for parameter optimization and applications, in: K. Merz, B. Roux (Eds.), Biological Membranes. A Molecular Perspective from Computation and Experiment, Birkhauser, Boston, 1996, pp. 31–81.
[304] T. Sintes, A. Baumgartner, Y.K. Levine, Coarse-grained continuum model for molecular diffusion in a lipid monolayer, J. Mol. Liq. 84 (2000) 77–88.

[305] C.F. Lopez, P.B. Moore, J.C. Shelley, M.Y. Shelley, M.L. Klein, Computer simulation studies of biomembranes using a coarse grain model, Comput. Phys. Commun. 147 (2002) 1–6.
[306] L. Saiz, M.L. Klein, Computer simulation studies of model biological membranes, Account. Chem. Res. 35 (2002) 482–489.
[307] K.V. Damodaran, K.M. Merz, Computer simulation of lipid systems, in: K.B. Lipkowitz, D.B. Boyd (Eds.), Reviews in Computational Chemistry, Vol. V, VCH Publishers, New York, 1994, pp. 269–298.
[308] L. Saiz, M.L. Klein, Structural properties of a highly polyunsaturated lipid bilayer from molecular dynamics simulations, Biophys. J. 81 (2001) 204–216.
[309] S.A. Pandit, D. Bostick, M.L. Berkowitz, Mixed bilayer containing dipalmitoylphosphatidylcholine and dipalmitoylphosphatidylserine: lipid complexation, ion binding, and electrostatics, Biophys. J. 85 (2003) 3120–3131.
[310] A.J. Robinson, W.G. Richards, P.J. Thomas, M.M. Hann, Behavior of cholesterol and its effect on head group and chain conformations in lipid bilayers: a molecular dynamics study, Biophys. J. 68 (1995) 164–170.
[311] R.R. Gabdoulline, G. Vanderkooi, C. Zheng, Comparison of the structures of dimyristoylphosphatidylcholine in the presence and absence of cholesterol by molecular dynamics simulations, J. Phys. Chem. 100 (1996) 15942–15946.
[312] K.C. Tu, M.L. Klein, D.J. Tobias, Constant-pressure molecular dynamics investigation of cholesterol effects in a dipalmitoylphosphatidylcholine bilayer, Biophys. J. 75 (1998) 2147–2156.
[313] A.M. Smondyrev, M.L. Berkowitz, Structure of dipalmitoylphosphatidylcholine/cholesterol bilayer at low and high cholesterol concentrations: molecular dynamics simulation, Biophys. J. 77 (1999) 2075–2089.
[314] M. Pasenkiewicz-Gierula, T. Rog, K. Kitamura, A. Kusumi, Cholesterol effects on the phosphatidylcholine bilayer polar region: a molecular simulation study, Biophys. J. 78 (2000) 1376–1389.
[315] A.M. Smondyrev, M.L. Berkowitz, Molecular dynamics simulation of the structure of dimyristoylphosphatidylcholine bilayers with cholesterol, ergosterol, and lanosterol, Biophys. J. 80 (2001) 1649–1658.
[316] T. Rog, M. Pasenkiewicz-Gierula, Cholesterol effects on the phosphatidylcholine bilayer nonpolar region: a molecular simulation study, Biophys. J. 81 (2001) 2190–2202.
[317] T. Rog, M. Pasenkiewicz-Gierula, Cholesterol effects on the phospholipid condensation and packing in the bilayer: a molecular simulation study, FEBS Lett. 502 (2001) 68–71.
[318] S.W. Chiu, E. Jakobsson, H.L. Scott, Combined Monte Carlo and molecular dynamics simulation of hydrated dipalmitoyl-phosphatidylcholine–cholesterol lipid bilayers, J. Chem. Phys. 114 (2001) 5435–5443.
[319] S.W. Chiu, E. Jakobsson, R.J. Mashl, H.L. Scott, Cholesterol-induced modifications in lipid bilayers: a simulation study, Biophys. J. 83 (2002) 1842–1853.
[320] T. Rog, M. Pasenkiewicz-Gierula, Effects of epicholesterol on the phosphatidylcholine bilayer: a molecular simulation study, Biophys. J. 84 (2003) 1818–1826.
[321] A.M. Smondyrev, M.L. Berkowitz, United atom force field for phospholipid membranes: constant pressure molecular dynamics simulation of dipalmitoylphosphatidicholine/water system, J. Comput. Chem. 20 (1999) 531–545.
[322] E.A. Dolan, R.M. Venable, R.W. Pastor, B.R. Brooks, Simulations of membranes and other interfacial systems using P2(1) and pc periodic boundary conditions, Biophys. J. 82 (2002) 2317–2325.
[323] R.B. Anachi, M. Bansal, K.R.K. Easwaran, K. Namboodri, B.P. Gaber, Molecular modeling studies on amphotericin B and its complex with phospholipid, J. Biomol. Struct. Dyn. 12 (1995) 957–970.
[324] M. Baginski, P. Gariboldi, E. Borowski, The role of amphotericin B amine group basicity in its antifungal action – a theoretical approach, Biophys. Chem. 49 (1994) 241–250.

[325] J. Langlet, J. Berges, J. Caillet, J.P. Demaret, Theoretical study of the complexation of amphotericin B with sterols, Biochim. Biophys. Acta 1191 (1994) 79–93.
[326] M. Baran, J. Mazerski, Molecular modelling of amphotericin B–ergosterol primary complex in water, Biophys. Chem. 95 (2002) 125–133.
[327] L.N. Ermishkin, K.M. Kasumov, V.M. Potseluyev, Properties of amphotericin B channels in a lipid bilayer, Biochim. Biophys. Acta 470 (1977) 357–367.
[328] J. Czub, M. Baginski, Interaction of amphotericin B with phospholipids in the model membrane – molecular dynamics study, Biophys. J. 86 (1) (2004) 2163-Pos.
[329] I.Z. Zubrzycki, Y. Xu, M. Madrid, P. Tang, Molecular dynamics simulations of a fully hydrated dimyristoylphosphatidylcholine membrane in liquid-crystalline phase, J. Chem. Phys. 112 (2000) 3437–3441.
[330] K. Sternal, J. Czub, M. Baginski, Molecular aspects of the interaction between amphotericin B and a phospholipid bilayer: molecular dynamics studies, J. Mol. Model. 10 (2004) 223–232.
[331] M. Herec, H. Dziubinska, K. Trebacz, J. Morzycki, W.I. Gruszecki, An effect of antibiotic Amphotericin B on ion transport across model lipid membranes and tonoplast membranes, Biochem. Pharmacol. 70 (2005) 668–675.

This page intentionally left blank

CHAPTER 10

On the Use of Impedance Spectroscopy for Studying Bilayer Lipid Membranes

A.E. Vallejo[1] and C.A. Gervasi[1,2,*]

[1]*Laboratorio de Ingeniería de Corrosión y Tecnología Electroquímica, LICTE, Facultad de Ingeniería, UNLP, 1 y 47, (1900), La Plata, Argentina*
[2]*Instituto de Investigaciones Fisicoquímicas Teóricas y Aplicadas, INIFTA, C.C. 16, Suc. 4, (1900) La Plata, Argentina*

Contents

Abstract

Different methods for supporting lipid bilayers onto conductive electrodes have proved useful to model biological membrane processes. The methods arousing greatest interest involve covalent attachment on gold substrates and noncovalent self-organization on metallic supports and semiconductor electrodes. Impedance spectroscopy (IS) applied to study these supported lipid bilayers was critically analyzed.

In this chapter, we have described the established ways to apply IS in structural characterization studies of supported lipid bilayers, with a particular focus on the strengths of the method as well as on its weaknesses. A word of caution was expressed concerning the use of equivalent circuit modeling under certain experimental conditions.

Full capabilities of IS were demonstrated in relation to ion permeation studies. The use of identifiability and distinguishability concepts was stressed, since this analysis provides a way to select experimental methods according to the structural properties of theoretical models. Accordingly, impedance experiments should be designed so as to allow discrimination between various postulated mechanisms. An example of a globally identifiable mechanism was introduced and this mechanism was used to derive rate parameters of the system from impedance data. Equations for the impedance and for the steady-state polarization curves can be satisfactorily fitted to the experimental results in order to generate the set of kinetic parameters that best describe the experiments.

*Corresponding author. Fax: +54-221-4254642; E-mail: gervasi@inifta.unlp.edu.ar

ADVANCES IN PLANAR LIPID BILAYERS AND LIPOSOMES, VOLUME 3
ISSN 1554-4516 DOI: 10.1016/S1554-4516(05)03010-3

1. INTRODUCTION

A biological membrane represents the most important electrified interface in living systems and provides the environmental matrix for proteins and other molecules, whose functions are of an electrical character. The same is true for experimental models of biomembranes as simple convenient systems that exhibit membrane mimetic behavior [1]. This is the reason why, along with spectroscopic methods, different electrochemical techniques were widely used to study biomembrane models.

The potential applied across the membrane in electrochemical experiments gives rise to a detectable charge flow directly related to the rates of various charge transfer processes. This serves not only to elucidate the nature of these processes but also to reveal structural features of the membrane.

Among the different electrochemical relaxation techniques, impedance spectroscopy (IS) is the most powerful one. The principle of this method is to apply a small AC potential perturbation to an electrochemical cell, which drives the system away from its steady state and then to measure the relation between the AC current response and the applied AC potential. In this way information can be gained about processes, such as the charging of the interface and conduction of electrical carriers (electrons and ions). Moreover, the use of IS allows to uncouple elementary phenomena that constitute the charge transfer processes [2].

The current availability of powerful commercial instruments, namely frequency response analyzers, explains its growing acceptance among researchers in the field of bioelectrochemistry. Present equipments operate under computer control covering a wide frequency range (<1 mHz to >100 kHz), which is well suited for bioelectrochemical impedance measurements. However, if a large number of elementary phenomena are involved in the process under study, data analysis can become rather difficult [3].

Different strategies were implemented to overcome the drawbacks of conventional black (bilayer) lipid membranes. This research effort resulted in the development of supported lipid membranes (s-BLMs) having a number of advantages: (i) ease and reproducibility of preparation, (ii) long-term stability, (iii) formation in the absence of solvent and finally (iv) formation on electrically conductive supports [4–6]. Consequently, s-BLMs as model systems for the study of biomembranes are conducive to electrochemical experimental analysis, from which, both structural and dynamical parameters, characterizing the electrical behavior of the membrane structure, can be derived.

This chapter does not intend to represent a comprehensive survey of the available literature but rather an appropriate selection of important contributions that illustrate the most frequently reported ways to apply IS in the field of bilayer lipid membranes (BLMs). Basic ideas and usual assumptions involved in mathematical derivations of the corresponding impedance expressions will be outlined.

2. STRUCTURAL CHARACTERIZATION OF SUPPORTED LIPID MEMBRANES

The realization of biomembrane models of improved quality, like s-BLMs, is one of the current challenges in fundamental studies of biological membranes and biosensor technology. Our ability to reach that goal, in turn, is critically dependent on the successful application of IS and other experimental methods that enable an accurate characterization of the resulting membrane system.

Electrical impedance measurements disclose information on the dielectric properties of materials [7]. Thus, capacitance and conductance measurements are routinely performed in order to reveal basic structural features of s-BLMs [4,8–11]. Characterization is primarily focused on kinetics of formation, packing efficiency, degree of coverage of the metal substrate and long-term stability.

2.1. Biomembrane models covalently attached to metallic supports

Self-assembled monolayers (SAMs) of alkanethiols covalently attached to gold surfaces provide a hydrophobic surface on top of which a phospholipid monolayer can be deposited *via* vesicle fusion. The analysis reported by Plant [4] of the structural features of this bilayer assembly represents a good example of the use of IS. Impedance measurements were used to monitor bilayer formation in the presence of vesicles. The process can be considered complete when the electrical parameters reach stable values. Capacitances of alkanethiol monolayers and phospholipid/alkanethiol bilayers were determined from impedance data recorded in the 10 Hz–63 kHz frequency range. Experimental data were fitted to a simple model for an equivalent circuit consisting of a resistor representing the electrolyte solution, in series with a capacitor, describing the electrode membrane (Fig. 1a). Within the studied frequency range, the contribution of the membrane resistance to the total impedance can be neglected (compare circuit in Fig. 1b). Recorded data exhibit a good fit to the model, at least when plotted in terms of the variation of the impedance modulus $|Z|$ with frequency. A plot of the inverse capacitance *versus* alkanethiol chain length (expressed as the number of CH_2 units) for alkanethiol monolayers and bilayers formed by vesicle fusion renders reasonably linear dependencies. Capacitance values for the phospholipid half-bilayer ($C_{\text{m-PL}}$) were estimated from capacitances for the alkanethiol monolayer ($C_{\text{m-monolayer}}$) and the phospholipid/alkanethiol bilayer ($C_{\text{m-bilayer}}$) using the following expression:

$$\frac{1}{C_{\text{m-PL}}} = \frac{1}{C_{\text{m-bilayer}}} - \frac{1}{C_{\text{m-monolayer}}} \tag{1}$$

that corresponds to a series combination of the two capacitors in the bilayer membrane.

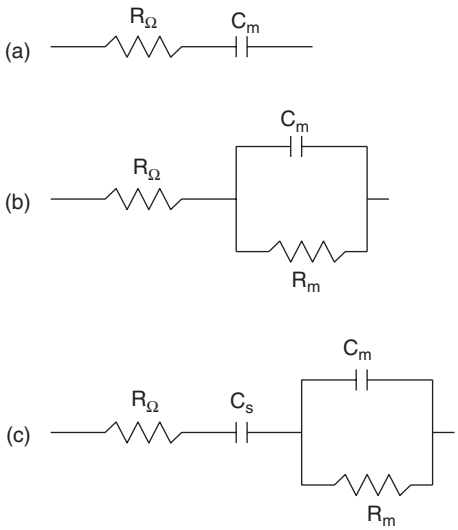

Fig. 1(a–c). Different equivalent circuit models used to represent sBLMs (see text for definitions of each element).

Moreover, it has been proposed that phospholipid monolayers can be modeled as a large capacitor (the polar headgroup region penetrated by water) in series with a smaller capacitor (the alkane chains) [12]. Consequently, the hydrocarbon portion is the only relevant contribution in $C_{m\text{-}PL}$. Capacitance data were considered in order to assess the effect of the solvent used to prepare the vesicles. Half-bilayer capacitance values for bilayers obtained in the absence of solvent (i.e. from vesicles prepared by the extrusion method) are smaller than those values resulting from the use of vesicles prepared by injection, while both sets of capacitance values are larger than values reported for BLMs. On the other hand, capacitance of the bilayer system is greatly reduced upon fusion of solvent-containing vesicles, indicating a bilayer with enhanced dielectric character. This can be understood in terms of a smaller chain tilt, and therefore larger hydrocarbon thickness compared to bilayers without solvent. Capacitance normalized by surface area takes the simple form:

$$C_m = \frac{\varepsilon_o \kappa}{d} \tag{2}$$

where ε_o is the permittivity of free space, κ the dielectric constant of the membrane material and d the membrane thickness. Unfortunately, both κ and d change according to changes in membrane composition and neither of these parameters can be known unambiguously to explain the inconsistency of these results.

This highlights the fact that film characterization with multiple techniques is crucial to understanding s-BLMs. For example, ellipsometry and infrared

spectroscopy were used in addition to electrochemical measurements to characterize phospholipid/alkanethiol bilayers [13]. A decrease in capacitance values was observed when changing from SAMs to bilayers. This result is consistent with the corresponding spectroscopic data and reflects an increase in film thickness. While capacitance determination by IS yielded similar results to those in the literature, the use of cyclic voltammetry consistently resulted in higher capacitance values.

Alkanethiol/phospholipid-coated gold electrodes were also studied combining four different techniques, namely, IS, quartz crystal microbalance (QCM), atomic force microscopy and ellipsometry, so that a consistent picture could emerge [14]. Impedance measurements were performed to follow dynamic changes accompanying the initial deposition of a monolayer of DOPG (dioleoylphosphatidylglycerol) on the modified gold surface and the formation, at longer times and in the presence of electrolyte and buffer, of a further DOPG bilayer on top of the lipid monolayer. Impedance data were analyzed assuming a simple *RC* series circuit (Fig. 1a) to convert changes in the impedance Z measured at a single frequency f (90 Hz) into changes in the apparent resistance and capacitance, according to:

$$Z = R_{\Omega} - \frac{j}{2\pi f C_{\mathrm{m}}} \tag{3}$$

where R_{Ω} represents the resistive limit of Z at $\omega \to \infty$, $j = \sqrt{-1}$, and f is the alternating voltage signal frequency.

C_{m} values change as a function of time in a fashion consistent with the timescales of the biphasic formation process detected in the QCM experiments. However, the authors conclude that the simple theoretical model assumed to interpret their impedance data is not entirely suitable for differentiating between monolayer and multilayer coverage of the electrode, due to the presence of pinholes and defects in the deposited lipid films.

The low flexibility and fluidity of the chemisorbed alkanethiol monolayer makes the metal-supported alkanethiol/phospholipid bilayers unsuitable for the incorporation of integral proteins [1]. In an attempt to overcome this limitation, alternative methods to support lipid bilayers were devised, that still retain the property of self-assembly of thiols onto clean gold surfaces.

One such possibility is to initially coat the solid support with a self-assembled charged monolayer and in a second step a bilayer of a charged lipid, having the opposite charge, is spontaneously spread onto the first monolayer.

An impedance analysis of this system was reported by. Steinem *et al*. [9]. The equivalent circuit in Fig. 1c was used to represent the electrical properties of the s-BLMs. The circuit contains an additional capacitance C_{s} in series with the membrane impedance to account for the presence of the charged monolayer on gold. Impedance data can be used to observe the fusion process. A tenfold decrease in capacitance values was measured after deposition of a bilayer on the charged monolayer. The use of mixed vesicles containing a mixture of a charged

lipid and a zwitterionic lipid yielded better results concerning the final capacitance, i.e. lower C_m values, in contrast to bilayers composed of the pure ionic lipid.

IS characterization of bilayers deposited on self-assembled charged monolayers was also performed by Stelzle *et al*. [5]. The authors propose to apply impedance analysis as a quality control tool for this system. Since defect sites strongly bind proteins, the preparation of defect-free lipid/protein layers is a prerequisite for biosensor design. With this aim, an impedance model based on an equivalent circuit was introduced and the fractional coverage of substrates was determined. The degree of coverage of the imperfect layer can be estimated by assuming the presence of two parallel capacitors. The measured capacitance C_m, for a covered area fraction θ is given by

$$C_m = \theta C_{mo} + (1 - \theta) C_{dl} \tag{4}$$

where C_{mo} corresponds to that part of the electrode, which is covered by a perfectly tight layer, and C_{dl} accounts for the capacitance at the membrane/electrolyte interface in flawed areas.

The resistance of the perfectly tight areas, being much larger than the resistance of the imperfect areas, cannot be determined. Consequently, the measured resistance R is determined by defects in the area fraction $(1 - \theta)$ according to:

$$R = \frac{R_o}{(1 - \theta)} \tag{5}$$

The authors showed that a simple model, like that in Fig. 1b, fails to describe s-BLMs containing numerous defect sites, probably resulting from a rough electrode surface. In order to obtain a better agreement between theory and experiment, additional circuit elements were incorporated in the equivalent circuit to represent the defects in the bilayer. However, concern can be expressed about the danger of using multicomponent models to fully describe impedance spectra, since it becomes increasingly difficult to prove the utility and interpretation of the various parameters [15].

A second alternative to the metal-supported alkanethiol/phospholipid bilayer is to replace the alkanethiol monolayer by a thiolipid monolayer and then to deposit a second phospholipid monolayer on top [10,16]. The thiolipid molecule consists of a phospholipid with the polar head covalently linked to a hydrophilic spacer terminated with an anchoring sulfydryl o disulfide group. Thus, the lipid bilayer results separated from the gold surface by the hydrophilic spacer that provides the space and water required for the incorporation of integral proteins.

In the work from reference [10], an impedance analysis of these systems was reported. Experimental impedance spectra were interpreted in terms of the model in Fig. 1b. Capacitance values for the top monolayer were calculated using an expression equivalent to that of equation (1), where the two series capacitances

correspond to the measured capacitance of a thiolipid monolayer and the measured capacitance of the whole bilayer. The calculated values, in turn, were used to deliver the thickness *d* of the lipid hydrocarbon chains in the frame of equation (2). Comparison of the resulting *d* values with those expected for a fully stretched chain indicates the degree of tilt with respect to the normal of the gold support. Moreover, contrasting capacitance data for the first monolayer with data for the bilayer, it is possible to envisage the structural mutual interaction, increasing or decreasing the chain order.

Interrupting the thiolipid chemisorption process after a short time an imperfect monolayer results. In a second step, the addition of a conventional lipid completes the imperfect monolayer besides forming a second monolayer on top, to generate a final bilayer arrangement. Thus, a fraction of the total sample surface remains free and therefore accessible for possible incorporation of proteins. The degree of coverage was calculated according to equation (4) with $C_{dl} = 27\,\mu Fcm^{-2}$, i.e. the capacitance of the Helmholtz layer on bare gold and C_{mo} are equal to the value calculated for a pure thiolipid monolayer.

Recently, novel synthetic lipids were used to tether a bilayer membrane (t-BLM) onto gold supports. The lipid molecule provides, additionally, a well-defined ionic reservoir between the gold electrode and the bilayer membrane [15]. A hydrophobic portion of the reservoir lipid incorporates into the bilayer and a hydrophilic portion, of varying lengths, is attached to gold *via* gold–sulfur interactions. Further, control of the lateral spacing between reservoir lipids can be obtained through adsorption of small hydrophilic disulfide-containing molecules. Impedance characterization of the t-BLMs was performed as described above, making use of equations (2) and (3). IS was also used to correlate membrane conduction characteristics to the ion reservoir capacity (see also [17]). Characteristic features develop in the experimental spectra upon addition of valinomycin, i.e. upon changing from a non-conducting to a conducting membrane. An inflexion in $\log|Z|$ *versus* $\log f$ plot appears between two straight lines of slope equal to -1. Over the same frequency range a phase (ϕ) minimum can be observed in the ϕ *versus* $\log f$ plot. The electrical analog model shown in Fig. 1c was selected to interpret these experiments. C_s represents here the effective Helmholtz capacitance due to the ionic double layer next to the gold surface. In the absence of valinomycin the bilayer resistance R_m is very large, and this results in a dependence of the impedance modulus $|Z|$ on *f* governed solely by C_m ($|Z| = 1/2\pi f C_m$) in the whole studied frequency range. In the presence of valinomycin in the bilayer and K^+ ions in the electrolyte, R_m decreases markedly giving rise to the distinctive features of the impedance spectra in the intermediate frequency range. In the low-frequency range, $|Z|$ approaches $1/2\pi f C_s$ according to a slope of -1 in the second linear portion of the $\log|Z|$ *versus* $\log f$ plot. The conductance of the ionophore ($1/R_m$) can be seen as a transition between the two capacitances and was calculated as the admittance for which ϕ goes through a minimum.

Increasing the reservoir volume, by increasing the reservoir lipid length or its lateral spacing, results in higher conductances. Moreover, the effect of having a restrictive reservoir, in terms of its volume, can be evidenced by varying the DC bias voltage. A gradual depletion of K^+ ions in the submembrane space results after the application of increasingly positive DC potentials, until R_m reaches the value corresponding to a non-conducting t-BLM. Larger reservoirs are less prone to restrict conductance at positive potentials.

2.2. Noncovalent self-organized bilayers on metallic supports

A simple different approach to realize a biomembrane model involves the noncovalent self-organization of a phospholipid monolayer on freshly formed surfaces of hydrophilic metals like, for example, Pt and Ag [18,19]. Polar heads of this first monolayer are spontaneously directed to the hydrophilic metal, while a second lipid monolayer is deposited on top of it, with the hydrocarbon tails in contact with those of the inner monolayer and the polar heads turned toward the aqueous solution. This procedure was followed by F. Bordi *et al*. [20] to obtain s-BLMs on the tip of a silver wire electrode. A proper cathodic potential was applied during membrane formation to avoid oxidation of the substrate and to favor a higher coverage by the membrane. In order to interpret the experimental data, a model based on an equivalent circuit was proposed. The equivalent circuit results from a parallel connection of a resistive element of the uncovered electrode regions and a sub-circuit that describes the impedance of the membrane-covered areas. The elements in this sub-circuit are two parallel connections *RC*, connected in series, and related to the lipid layer and to the ionic layer at the lipid-electrolyte interface, respectively. The fitting procedure according to this model also yields the covered area fraction θ.

2.3. Supported lipid membranes supported on semiconductor electrodes

Biomembrane models supported on semiconductor surfaces have a large potential for its application in biosensor devices. The use of IS to study these systems is focused on finding experimental conditions, that allow to discriminate between the capacitance of the semiconductor material and the capacitance and conductivity of the lipid membrane [21–23]. This is a difficult task since the capacitance of the semiconductor is normally too small. The use of Ti/Ti oxide electrodes was proposed as an alternative support to silicon/silicon dioxide electrodes [22]. A much higher dielectric constant of the former electrode material leads to capacitance values that are 15 times larger.

When using Si/SiO_2 electrodes, doping level and oxide thickness can be varied to obtain ideal properties of the bulk silicon material [23]. Moreover, under sufficiently negative bias potentials (for *p*-type Si), leading to the formation of an

inversion layer, or under sufficiently positive bias potentials for an accumulation layer to appear, the space-charge capacitance, becomes large in comparison with the oxide capacitance. This condition renders a final capacitance of the Si/SiO_2 electrode that is markedly increased. The electrical properties of the semiconductor/lipid bilayer system can be analyzed in terms of an equivalent circuit containing two parallel connections *RC*, connected in series, and related to the semiconductor material and the deposited lipid bilayer.

2.4. Some difficulties with the use of capacitance measurements

It has already been established that simple models like those in Fig. 1(a–c), although useful to describe the electrical features of s-BLMs, are unable to fully describe the impedance response. This fact is clearly evident from a poor fit in the phase spectra of a Bode plot [15,17]. Otherwise, a plot of $\log|Z|$ *versus* $\log f$ results much less sensitive to this effect.

One may be tempted to use multicomponent equivalent circuits in order to obtain a better agreement between theory and experiment. However, good agreement between the measured impedance and that calculated from the modeling circuit does not necessarily mean that the model used is the best representation, and it is often difficult to find an explanation for the different circuit components on a phenomenological basis.

A possible reason for the lack of full agreement is that, for example, the membrane capacitance does not, in general, behave as a pure capacitance, but rather as an impedance displaying a frequency-independent phase angle different from 90°. So, a second approach to improve the quality of the fit might be to replace the ideal capacitance C_m by a constant-phase element (CPE) in the model circuit [6]. Formally, this means that the classical representation of the impedance for a defect-free membrane (equation (3)) has to be replaced by an expression of the form:

$$Z = R_\Omega + (j\omega)^{-\delta} Y_o^{-1} \tag{6}$$

where Y_o is a constant expressed in $\Omega^{-1}\,cm^{-2}\,s^{\delta}$ and δ a dimensionless parameter. This expression is valid, when only the capacitance value is distributed along the interface. Accordingly, if the electrode behavior is complicated by the presence of a distributed capacitance but capacitance values are determined from the imaginary part of the impedance $\mathrm{Im}(Z)$ at a single frequency according to $C_m = -1/\omega\ \mathrm{Im}(Z)$ (see equation (3)), calculations yield C_m values that depend on the applied frequency, and are therefore of limited significance. Thus, if a distribution model is adopted, it is more appropriate to calculate C_m from equation (7) [24]:

$$C_m = \left[Y_o R_\Omega^{(1-\delta)} \right]^{1/\delta} \tag{7}$$

It should be emphasized that C_m depends on R_Ω and cannot be simply replaced by the fit parameter Y_o, as is frequently found in the literature. Finally, if the system is mathematically described in terms of a more complex branched network, Y_o is coupled not only to R_Ω but also to other circuit elements.

Another aspect, related to equivalent circuit modeling, deserves detailed consideration.

The whole charge density experienced by the diffuse layer ions in solution (q_s) equals the sum (q_m) of the charge density on the metal, the charge density of any charged groups buried well inside the polar head region and the charge density of any ionized groups directly exposed to the aqueous phase [1]. In this way, the two capacitances, C_m and C_s, of the electrode/membrane/electrolyte system are given by

$$\frac{dq_m}{dV_m} = C_m \tag{8}$$

$$\frac{dq_s}{dV_s} = C_s \tag{9}$$

where dV is the differential voltage change across each double layer.

It has often been proposed in the literature to describe this system in terms of an equivalent circuit containing two parallel *RC* connections, connected in series, as depicted in Fig. 2. Inspection of equations (8) and (9) yields

$$\frac{dV_s}{dV_m} = \frac{C_m}{C_s} \tag{10}$$

According to the model in Fig. 2, under steady-state conditions, we have

$$\frac{dV_s}{dV_m} = \frac{IR_s}{IR_m} \tag{11}$$

where the steady-state current I flowing through each resistor is the same. Thus, comparing equations (10) and (11), it is possible to show that, for the proposed model, the following relationship holds

$$C_m R_m = C_s R_s \tag{12}$$

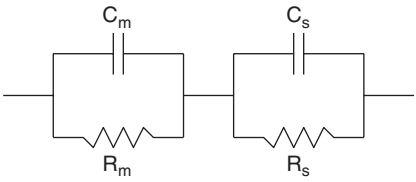

Fig. 2. Equivalent circuit used to represent the impedance response of sBLMs in the presence of a hydrophobic space between the support and the bilayer (see text for definitions of each element).

Equation (12) indicates that the model in Fig. 2 is unsuitable to represent the dynamic features of the two processes involved, i.e. DC current flow and charge accumulation in the membrane phase and in the aqueous phase, exhibiting distinctive time constants.

3. ION TRANSPORT THROUGH LIPID BILAYERS

3.1. Ion-carrier-mediated transport

Ion transport is most conveniently measured in terms of electrical properties and the dependence of these properties on chemical and physical parameters (e.g. concentration and time) [25]. Consequently, IS is well suited for studying ion permeation in BLMs.

The hydrophobic barrier imposed by lipid bilayers to ion permeation can be penetrated in different ways. One such way involves mediation by ion-carriers, like valinomycin, incorporated in the bilayer. In the previous section, we analyzed the use of valinomycin in the presence of K^+ ions as a test for impedance studies on t-BLMs. This test is based on a model, in which the transport of K^+ ions is represented by a resistor [15,17]. This description, although useful as a simple test, represents an oversimplification, from which relevant kinetic information cannot be obtained [26].

De Levie developed a full mathematical treatment yielding the impedance of ion transport mediated by ion-carrier complexes through lipid bilayers [25]. A lipid membrane can be conceived as a thin homogeneous macroscopic phase (continuum model) or as an interfacial barrier (single-barrier model). Considering its thickness, a biomembrane model lies in between these two extremes, as a result both the limiting approaches were analyzed. According to the continuum model, the Poisson equation is introduced in the continuity equation. Subsequent integration with respect to distance yields an expression for the total (ionic plus displacement) current due to diffusion and migration. Boundary conditions must be considered in addition to these equations describing permeation through the membrane phase. Boundary conditions reflect interfacial stoichiometries and aqueous diffusion as the transport-limiting process outside the membrane. The constant-field approximation was used to derive the admittance. The admittance equation was written out in a fractional form that facilitates to express it in terms of an equivalent circuit. Thus, in this treatment, the equivalent circuit is a derivation from the mathematical model. The equivalent circuit is also representative of the equation derived according to the single-barrier model with the same boundary conditions, but different definitions result for the circuit components, in terms of microscopic parameters. For example, the membrane resistance is interpreted in terms of a diffusion coefficient in the continuum approach, but as a rate constant in the single-barrier formalism. The single-barrier approach is briefly

described below in relation to a transport mechanism based on the presence of ion channels in the membrane. Thus, the experimentally measured admittance can be analyzed according to the dependence of the individual circuit elements on concentration, temperature, etc. Each element is related to a single physical phenomenon (dielectric charge displacement, ion transport across the membrane, ion transport across the interface, diffusion through the aqueous phase or adsorption at each side of the interface). However, prior to deriving specific rate parameters a choice between the two models must be made.

Impedance data obtained for valinomycin-mediated transport of Na^+ and K^+ ions through s-BLMs were analyzed in terms of a model [16] that incorporates some of the theoretical derivations of de Levie's. Specifically, data evaluation was performed by using the equivalent circuit depicted in Fig. 1c, assuming that R_m corresponds to a series connecting two resistive elements, namely, the membrane resistance R and the resistance of ion transport across the membrane/water interface R_{pt}. Definitions of R and R_{pt} in terms of physicochemical parameters correspond to de Levie's mathematical treatment for the continuum approach, where both parameters are dependent on the reciprocal cation concentration in solution c_w^+. The membrane conductance was found to increase significantly in the presence of K^+ ions, while only a slight increase was observed in the presence of Na^+ ions. The expected linear dependence of the conductance on c_w^+ was confirmed.

3.2. Ion transport through channels incorporated in a lipid bilayer

Participation of channels incorporated in s-BLMs represents another mechanism for ion permeation. Gramicidin is one of the best characterized and most extensively studied pore-forming molecular structures. In its active form, this antibiotic builds a dimeric helical structure long enough to span the bilayer. Recently, we reported impedance measurements applied to study ion transport through gramicidin channels [27,28]. A (SAM) of a short-chain mercaptocarboxylic acid can form on gold electrodes. On top of the charged monolayer fusion of lipid vesicles prepared from a positively charged lipid-containing gramicidin D, lead to electrostatic fixation of a gramicidin-doped bilayer. The presence of a hydrophilic space between the gold surface and the bilayer, as indicated by increased conductance in presence of gramicidin, is related to the numerous defects in a SAM of short chain length.

In its most general form the mechanism, proposed to describe ion permeation through gramicidin channels, comprises the following series of steps: (i) transport of cations through aqueous phase according to planar diffusion, (ii) adsorption onto the membrane at a surface site determined by an active G-channel and incorporation into it at the interface, and finally (iii) permeation through the membrane.

Interfacial transfer kinetics is of first order, while permeation inside the channel is characterized by a simple activation energy barrier (single-barrier approach).

The application of an external voltage varies the barrier height but the position of the potential-energy maximum along the reaction coordinate remains unaltered.

The reaction mechanism can be formally written as:

$$M^+ \underset{k_{-1}}{\overset{k_1}{\rightleftarrows}} M^+_{in} \tag{13}$$

$$M^+_{in} \xrightarrow{k_2} M^+_{out} \tag{14}$$

where M^+_{in} corresponds to the ion at the side where it partitions into the membrane and M^+_{out} denotes the ion at the other side, from where it leaves the membrane.

The potential (E) dependence of the rate constants can be expressed by an exponential law:

$$k_i = k_i^o \exp(b_i E) \tag{15}$$

$$k_{-i} = k_{-i}^o \exp(b_{-i} E) \tag{16}$$

where $b_i = -\alpha F/RT$ and $b_{-i} = (1-\alpha)F/RT$, k_i^o and k_{-i}^o are constants independent of E, α is the transfer coefficient and F the Faraday constant.

The maximum number of sites per unit surface, which can be occupied by the species M^+, is characterized by the coefficient β and the fraction of sites actually occupied by θ ($0<\theta<1$). As a consequence, the number of free electroactive sites is given by $\beta(1-\theta)$.

For a symmetrical membrane and identical surrounding aqueous solutions, analysis is simplest at the open circuit potential, in which case the backward reaction (anodic) results in the same impedance as that for the forward reaction and both impedances are connected in series in the global mechanism. In this way there is no need to consider the anodic reaction separately [25]. The net faradic current I_{net} results from the difference between cathodic and anodic partial currents.

Mathematical modeling of experimental input/output data in the field of electrochemistry is not an easy task, mainly because of the complexity and nonlinearity of the systems involved. Two major difficulties are encountered in modeling kinetic functions. Firstly, one has to make a proper selection of physicochemical parameters influencing the kinetics, in order to incorporate them in the model. Secondly, it is required to choose an appropriate analytical description for each kinetic process. The procedure leads to a set of nonlinear differential equations involving a family of parameters [29].

A clear distinction has to be made between basic parameters and those parameters that are determinable by an experiment (observational parameters). The latter may be functions of the basic kinetic parameters. When the observational parameters are not functions of a particular basic parameter, that parameter can be changed without affecting the observations. In the experiment this is an insensible parameter. However, if a basic parameter is sensible by the experiment,

it may be identifiable or nonidentifiable. For instance, multicomponent equivalent circuits used as a convenient, shorthand notation for experimentally observed behavior, often derive from the introduction of insensible parameters that cannot be interpreted in terms of physical phenomena.

Before estimating the unknown parameters by using mathematical methods, a theoretical identifiability analysis must be performed. Indeed, if the unknown parameters are not identifiable, the numerical values obtained have no significance, since these values are not necessarily unique.

It should be emphasized that the concepts of identifiability and distinguishability are of great practical relevance, even though they have been only recently introduced in the field of electrochemistry [30–33].

Before proceeding with the analysis of identifiability and distinguishability of the proposed permeation model, a few notes on basic concepts might be appropriate.

The various types of *(*a priori*)* identifiability are defined below:

(a) Local identifiability: If the observation function for an experiment determines a finite number of values for a parameter, the parameter is locally identifiable. Additional information may be needed to decide which one of the values is appropriate for the system. Local identifiability includes cases of symmetry in models in which two or more parameters play equivalent roles, so their values can be interchanged.
(b) Global identifiability: If the observation function determines exactly one solution value for a parameter in the entire parameter space, that parameter is globally identifiable for that experiment.
(c) Model identifiability: If for an experiment, all of the parameters of a model are globally identifiable, the experiment model is globally identifiable.

Let the process be replaced by a model $M^*(p^*)$ that describes the experimental data, where noise-free data are assumed. The expression $M^*(p^*) \equiv M^\wedge(p^\wedge)$ denotes that the model, with structure $M^*(\cdot)$ and parameters p^*, has the same input-output behavior as the model with structure $M^\wedge(\cdot)$ and parameters $p^\wedge$, for any input and time. Any given model structure $M(\cdot)$ will then be *uniquely identifiable* (*or globally identifiable*) if for almost any p^*, there is a unique solution for p of $M(p) \equiv M(p^*)$, which is $p = p^*$. In other words, if $M(\cdot)$ is not uniquely identifiable, then there are several parameter vectors that correspond to exactly the same input-output behavior, and it is impossible to eliminate any of them from the data alone. Moreover, each parameter vector corresponds to a different evolution of some state variables that are not measured directly.

Likewise, $M^*(\cdot)$ will be *distinguishable* from $M^\wedge(\cdot)$, if and only if, for almost any $p^\wedge$ there is no p^*, such that $M^*(P^*) \equiv M^\wedge(P^\wedge)$. This indicates that there is no other parameter vector that gives the same output for a given input. Expressing the idea in the opposite way, it can be said that $M^*(\cdot)$ is not distinguishable from $M^\wedge(\cdot)$ if it can reproduce experimental results in a strictly identical manner [34].

The set of differential equations (state and observation equations) describing the kinetics of the proposed mechanism for ion permeation through gramicidin-doped bilayers, is given by the mass and charge balances

$$\beta \frac{\mathrm{d}\theta}{\mathrm{d}t} = k_1(1-\theta)c - k_{-1}\theta - k_2\theta \equiv g(E, c, \theta) \tag{17}$$

$$I = FA[k_1(1-\theta)c - k_{-1}\theta + k_2\theta] \equiv I(E, c, \theta) \tag{18}$$

Two types of experiments will be considered for the structural identifiability analysis of the unknown parameters of the system: steady-state studies, where a constant input $E(t)$ takes various constant values, and IS, with small deviations around a constant input, where $E(t)$ takes the form of a small amplitude sinusoidal wave.

3.2.1. Steady-state analysis

When the steady state is reached ($\mathrm{d}\theta/\mathrm{d}t = 0$), the fractional coverage can be expressed as:

$$\theta^{ss} = \frac{k_1 c}{k_1 c + k_{-1} + k_2} \tag{19}$$

and the forward faradic current as:

$$I^{ss} = 2FA_e \frac{k_1 c k_2}{k_1 c + k_{-1} + k_2} \tag{20}$$

where A_e represents the electrode area and c the concentration of the diffusing species. The final fitting procedure to the model equations shows that the concentration gradient in solution is null, what indicates that the kinetics of the global process is solely controlled by the membrane processes. For the present identifiability analysis this condition is considered to be valid. However, in order to keep the theoretical treatment as general as possible, the condition will be relaxed upon deriving the transfer function for the electrode impedance.

If a single value of c is used, it is clear that $k_1 c$ and k_2 in equation (20) are interchangeable, therefore there are two sets of parameters p^* and $p\hat{}$ that have the same input-output behavior and the parameters are only locally identifiable from this steady-state study. This ambiguity may be removed by carrying out experiments with different concentrations c.

3.2.2. Impedance spectroscopy analysis

Since steady-state studies, in general, do not lead to global identifiability of the system, an additional study by IS might be required.

In order to derive an expression for the reaction impedance, equations (17) and (18), describing the rate of accumulation of incorporated ions $g(E, c, \theta)$ and the current $I(E, c, \theta)$, respectively, should be linearized, according to Taylor series expansion retaining only terms with first-order derivatives, to give

$$\beta \frac{\mathrm{d}\Delta\theta}{\mathrm{d}t} = \left(\frac{\partial g}{\partial E}\right)\Delta E + \left(\frac{\partial g}{\partial \theta}\right)\Delta\theta + \left(\frac{\partial g}{\partial c}\right)\Delta c \tag{21}$$

$$\Delta I = \left(\frac{\partial I}{\partial E}\right)\Delta E + \left(\frac{\partial I}{\partial \theta}\right)\Delta\theta + \left(\frac{\partial I}{\partial c}\right)\Delta c \tag{22}$$

Partial derivatives in equations (21) and (22) correspond to stationary conditions. Considering the application of a small AC perturbation signal $\Delta E = \tilde{E}\exp(j\omega t)$ and the resulting sinusoidal responses of ΔI, concentration Δc and fraction of occupied sites $\Delta\theta$, equations (21) and (22) can be rewritten as:

$$\beta j\omega \frac{\Delta\theta}{\Delta E} = \left(\frac{\partial g}{\partial E}\right) + \left(\frac{\partial g}{\partial \theta}\right)\frac{\Delta\theta}{\Delta E} + \left(\frac{\partial g}{\partial c}\right)\frac{\Delta c}{\Delta I}\left(-\frac{1}{Z}\right) \tag{23}$$

$$-\frac{1}{Z} = \frac{\Delta I}{\Delta E} = \left(\frac{\partial I}{\partial E}\right) + \left(\frac{\partial I}{\partial \theta}\right)\frac{\Delta\theta}{\Delta E} + \left(\frac{\partial I}{\partial c}\right)\frac{\Delta c}{\Delta I}\left(-\frac{1}{Z}\right) \tag{24}$$

where $Z = -\Delta E/\Delta I$ is the faradic impedance (the negative sign arises from the assumed convention in which the cathodic current is positive).

Since species M^+ diffuses toward the surface, one has:

$$\frac{\Delta c}{\Delta I} = -\frac{N(\omega)}{FA_\mathrm{e}} \tag{25}$$

where $N(\omega) = +\frac{1}{\sqrt{j\omega D}}$ for semi-infinite linear diffusion [35].

From equations (23) and (24), applying Cramer's rule Z can be calculated:

$$Z = \frac{\begin{vmatrix} 1 - \partial I/\partial c(-N(\omega)/FA_\mathrm{e}) & \partial I/\partial\theta \\ -\partial g/\partial c(-N(\omega)/FA_\mathrm{e}) & -\beta j\omega + \partial g/\partial\theta \end{vmatrix}}{\begin{vmatrix} -\partial I/\partial E & \partial I/\partial\theta \\ -\partial g/\partial E & -\beta j\omega + \partial g/\partial\theta \end{vmatrix}} \tag{26}$$

where

$$\frac{\partial I}{\partial c} = FA_e \cdot k_1(1-\theta)$$
$$\frac{\partial I}{\partial \theta} = FA_e(-k_1 c - k_{-1} + k_2)$$
$$\frac{\partial g}{\partial c} = k_1(1-\theta)$$
$$\frac{\partial g}{\partial \theta} = -k_1 c - k_{-1} - k_2$$
$$\frac{\partial I}{\partial E} = FA_e[(1-\theta)ck_1 b_1 - k_{-1}b_{-1}\theta + k_2 b_2 \theta]$$
$$\frac{\partial g}{\partial E} = k_1 b_1(1-\theta)c - k_{-1}b_{-1}\theta - k_2 b_2 \theta$$

After evaluating the derivatives in equation (26) with $\alpha = 0.5$ and replacing θ by its steady-state value, the final expression for the impedance can be obtained as:

$$Z = \frac{j\varpi + \dfrac{Q}{\beta} + PNj\varpi + 2PN\dfrac{k_2}{\beta}}{M\left(j\varpi cP + 2cP\dfrac{k_2}{\beta}\right)} \tag{27}$$

where $P = \frac{k_1(k_{-1}+k_2)}{k_1 c + k_{-1} + k_2}$, $Q = k_1 c + k_{-1} + k_2$ and $M = \frac{F^2 A_e}{RT}$.

It can be shown, using the same approach as that used for the steady-state equation, that the system has a single solution $p^* = p\hat{}$ and thus the proposed model is globally identifiable by IS. However, this approach is rather cumbersome for equation (27). Moreover, such approach does not confirm that a given mechanism is distinguishable from all other possible mechanisms. In this sense, the use of the similarity transformation method, allows to check whether a given mechanism is globally or locally identifiable, as well as to find all the possible mechanisms having the same input/output model representation [36,37].

Using matrix notation mass and charge balances can be expressed as:

$$\frac{\mathrm{d}\theta}{\mathrm{d}t} = A(E,\theta)\theta(t) \tag{28}$$

$$i(t) = C(E;\theta)\theta(t) \tag{29}$$

where

$$\theta(t) = \begin{bmatrix} \theta_0(t) \\ \theta_1(t) \\ . \\ . \\ \theta_n(t) \end{bmatrix} \quad \theta_i \text{ for } i = 0, 1, \ldots, n$$

represents a generic fractional coverage and $\theta_0 = 1 - (\theta_1 + ... + \theta_n)$ is the fractional coverage of free sites. $A(E,\theta)$ and $C(E,\theta)$are the squared matrix and row vector of length $(n+1)$, respectively, $i(t)$ is proportional to the measured current $I(t)$.

Consequently, according to this notation the equations for the proposed mechanism can be written in this form:

$$\theta = \begin{bmatrix} (1-\theta_1) \\ \theta_1 \end{bmatrix} \quad A = \begin{bmatrix} -k_1 c & (k_{-1}+k_2) \\ k_1 c & -(k_{-1}+k_2) \end{bmatrix} \quad C = \begin{bmatrix} k_1 c & (k_2 - k_{-1}) \end{bmatrix}$$

These expressions can be used, according to the similarity transformation, to obtain all mechanisms with the same input/output descriptions.

The similarity transformation method considers a compartmental system for which the coefficient matrix A has been subjected to a similarity transformation to give a system with a coefficient matrix $T^{-1}AT$, where T is any of the nonsingular squared matrix, whose columns are vectors that belong to the standard orthonormal basis of dimension $n+1$ without repetitions. Recall that under a similarity transformation, the eigenvalues do not change. Impose on $T^{-1}AT$ all the structural constraints on A and require that the response function of the system with matrix $T^{-1}AT$ be the same as that of the system with matrix A. If the only T that satisfies these requirements is the identity matrix I, all parameters are globally identifiable. If a $T \neq I$ satisfies the requirements, one can work out which parameters are identifiable and which are not [29].

Using the transformation T a new state vector $\tilde{\theta}$ can be obtained in the following way, $\tilde{\theta} = T^{-1}\theta$ with $\theta = T\tilde{\theta}$. Then, the transformed system holds:

$$\frac{\mathrm{d}\tilde{\theta}}{\mathrm{d}t} = T^{-1}AT\tilde{\theta} = \tilde{A}\tilde{\theta} \tag{30}$$

$$i = CT\tilde{\theta} = \tilde{C}\tilde{\theta} \tag{31}$$

For the system considered $n = 1$, then, the possible transformations of dimension $n + 1 = 2$ are:

$$T_1 = \begin{bmatrix} 1 & 0 \\ 0 & 1 \end{bmatrix} \quad \text{and} \quad T_2 = \begin{bmatrix} 0 & 1 \\ 1 & 0 \end{bmatrix}$$

Let us apply transformation T_2 to the original system (applying transformation T_1 is trivial)

$$\tilde{A}_2 = \begin{bmatrix} -(k_{-1}+k_2) & k_1 c \\ (k_{-1}+k_2) & -k_1 c) \end{bmatrix} \quad \tilde{C}_2 = \begin{bmatrix} (k_2 - k_{-1}), & k_1 c \end{bmatrix}$$

In this way, the two transformed mechanisms are:

(a) $\mathrm{M}^+ \underset{k_{-1}}{\overset{k_1}{\rightleftarrows}} \mathrm{M}^+_{\mathrm{in}} \xrightarrow{k_2} \mathrm{M}^+_{\mathrm{out}}$

(b) $\mathrm{M}^+ \underset{k_{-1}}{\overset{k_2}{\rightleftarrows}} \mathrm{M}^+_{\mathrm{in}} \xrightarrow{k_1} \mathrm{M}^+_{\mathrm{out}}$

Mechanism (b) obtained through transformation T_2 is electrochemically incoherent. Consequently, it can be concluded that there are neither mechanisms with the same structure but with different parameters sets nor mechanisms with different structure. The system is globally identifiable and distinguishable from any other one.

Following this structural study, which can be considered as the qualitative part of the experiment, the problem of how to estimate the parameter set must be addressed [38].

Classical estimators used in electrochemistry proceed by a minimizing least-square criterion, according to local iterative methods, such as the Levenberg–Marquardt, quasi-Newton or conjugate gradients algorithms. In the case of non-globally identifiable models, these methods yield several solutions for the parameters and the results depend heavily on the initial value given to the parameter vector. Recently, global identification procedures based on interval analysis have been proposed [37,39] that allow to find one of the possible solutions, by minimization of the cost function. With this particular solution and the structural analysis, all other possible solutions can be derived. The procedure results in a reduction of search range and computational time demanded.

Results of parameter estimation, based on the minimization of the impedance error function, are presented in Figs. 3 and 4 (unpublished results). A single set of fit parameters were derived, showing a good agreement between the model and experimental data obtained by both steady-state and impedance measurements.

A procedure different from that above was carried out in our previous work [27,28]. Thus, analyzing estimations of macroscopic parameters in an equivalent circuit derived from equation (27), we succeeded in confirming the accepted sequence of conductivity for different cations in solution, as well as, ion transport dependences on Na^+ ion concentration and temperature. However, this procedure is usually unsuitable for estimating microscopic parameters, such as rate constants.

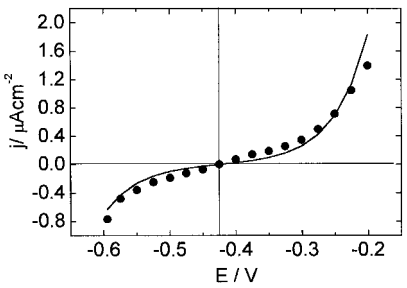

Fig. 3. Experimental (○) and simulated (—) steady-state polarization curve (j *versus* E, with $j = I_{net}/A_e$) for a phospholipid bilayer with added gramicidin in 0.1 M NaCl. Parameters used for the simulated curve: $k_1^o = 1.2 \times 10^{-1}$ cm $\cdot$ s^{-1}, $k_{-1}^o = 6.5 \times 10^5$ mol cm^{-2} s^{-1}, $k_2^o = 2.0 \times 10^6$ mol cm^{-2} s^{-1} and $\beta = 8.2 \times 10^{-14}$ mol cm^{-2}.

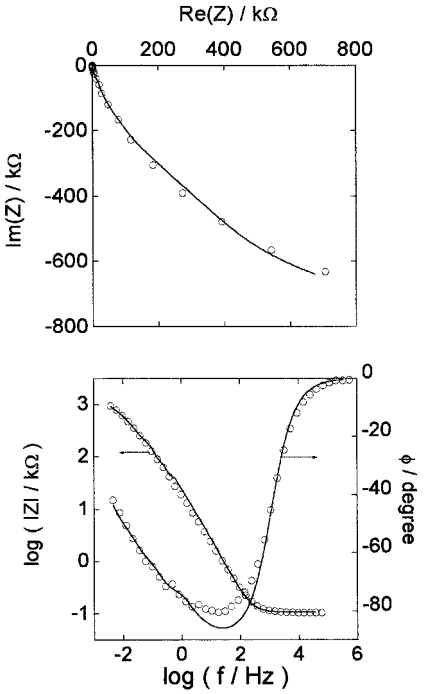

Fig. 4. Nyquist and Bode plots for a phospholipid bilayer with added gramicidin in 0.1 M NaCl. Experimental data (○) and simulated curves (—) according to faradic impedance from equation (27). Parameters used for the simulated curves as in Fig. 3.

In summary, we first advocate writing out of the differential equations of the system in the frame of a proposed model. Next, output equations, according to this model, should be derived, followed by identifiability and distinguishability analysis, in order to decide whether or not IS is suitable as an experimental technique. Finally, fitting of experimental data should be carried out to an impedance function involving microscopic parameters.

4. CONCLUSIONS

In this chapter, we have described the established ways to apply IS in structural characterization studies of sBLMs, with a particular focus on the strengths of the method as well as on its weaknesses. A word of caution was expressed concerning the use of equivalent circuit modeling under certain experimental conditions.

Full capabilities of IS were demonstrated in relation to ion permeation studies. The use of identifiability and distinguishability concepts was stressed, since this analysis provides a way to select experimental methods according to the structural properties of theoretical models. Accordingly, impedance experiments

should be designed so as to allow discrimination between various postulated mechanisms. An example of a globally identifiable mechanism was introduced and this mechanism was used to derive rate parameters of the system from impedance data.

ACKNOWLEDGMENTS

The authors gratefully acknowledge support from the Comisión de Investigaciones Científicas BA, as members of the research staff of this institution.

REFERENCES

[1] R. Guidelli, G. Aloisi, L. Becucci, A. Dolfi, M.R. Moncelli, F. Tadini Buonsegni, Bioelectrochemistry at metal l water interfaces, J. Electroanal. Chem. 504 (2001) 1–28.
[2] M. Rueda, Applications of the impedance method in organic electrode kinetics, in: R.G. Compton and G. Hancock (Eds.), Research in Chemical Kinetics, Vol. 4, Blackwell Science Ltd., New York, 1997, pp. 31–95.
[3] A. Lasia, Electrochemical impedance spectroscopy and its applications, in: B.E. Conway, J.O'M. Bockris, R.E. White (Eds.), Modern Aspects of Electrochemistry, Vol. 32, Plenum, New York, 1999, pp. 143–248, chapter 2.
[4] A.L. Plant, Self-assembled phospholipid/alkanethiol biomimetic bilayers on gold, Langmuir 9 (1993) 2764–2767.
[5] M. Stelzle, G. Weissmüller, E. Sackmann, On the application of supported bilayers as receptive layers for biosensors with electrical detection, J. Phys. Chem. 97 (1993) 2974–2981.
[6] S. Terrettaz, T. Stora, C. Duschl, H. Vogel, Protein binding to supported lipid membranes: investigation of the cholera toxin-ganglioside interaction by simultaneous impedance spectroscopy and surface plasmon resonance, Langmuir 9 (1993) 1361–1369.
[7] J.R. Macdonald, Fundamentals of impedance spectroscopy, in: J.R. Macdonald, (Ed.), Impedance Spectroscopy, Emphasizing Solid Materials and Systems, Wiley, New York, 1987, p. 13.
[8] C. Miller, P. Cuendet, M. Gratzel, K^+ sensitive bilayer supporting electrodes, J. Electroanal. Chem. 278 (1990) 175–192.
[9] C. Steinem, A. Janshoff, W.P. Ulrich, M. Sieber, H.J. Galla, Impedance analysis of supported lipid bilayer membranes: a scrutiny of different preparation techniques, Biochim. Biophys. Acta 1279 (1996) 169–180.
[10] H. Lang, C. Duschl, H. Vogel, A new class of thiolipids for the attachment of lipid bilayers on gold surfaces, Langmuir 10 (1992) 197–210.
[11] J. Li, L. Ding, E. Wang, S. Dong, The ion selectivity of monensin incorporated phospholipid/alkanethiol bilayers, J. Electroanal. Chem. 414 (1996) 17–21.
[12] R. Benz, O. Frohlich, P. Lauger, M. Montal, Electrical capacity of black lipid films and of lipid bilayers made from monolayers, Biochim. Biophys. Acta 394 (1975) 323–334.
[13] J. Ha, C.S. Henry, I. Fritsch, Formation and characterization of supported hexadecanethiol/dimyristoyl phosphatidylcholine hybrid bilayers containing Gramicidin D, Langmuir 14 (1998) 5850–5857.
[14] P.N. Bartlett, K. Brace, E.J. Calvo, R. Etchenique, In situ characterization of phospholipid coated electrodes, J. Mat. Chem. 10 (2000) 149–156.
[15] B. Raguse, V. Braach-Maksvytis, B.A. Cornell, L.G. King, P.D. Osman, R.J. Pace, L. Wieczorek, Tethered lipid bilayer membranes: formation and ionic reservoir characterization, Langmuir 14 (1998) 648–659.

[16] C. Steinem, A. Janshoff, K. von dem Bruch, K. Reihs, J. Goossens, H.-J. Galla, Valinomycin-mediated transport of alkali cations through solid supported membranes, Bioelectrochem. Bioenerg. 45 (1998) 17–26.
[17] C. Peggion, F. Formaggio, C. Toniolo, L. Becucci, M.R. Moncelli, R. Guidelli, A peptide-tethered lipid bilayer on mercury as a biomimetic system, Langmuir 17 (2001) 6585–6592.
[18] A. Wardak, H.T. Tien, Cyclic voltammetry studies of bilayer lipid membranes deposited on platinum by self assembly, Bioelectrochem. Bioenerg. 24 (1990) 1–11.
[19] T. Martynski, H.T. Tien, Spontaneous assembly of bilayer membranes on a solid surface, Bioelectrochem. Bioenerg. 25 (1991) 317–324.
[20] F. Bordi, C. Cametti, A. Gliozzi, Impedance measurements of self-assembled lipid bilayer membranes on the tip of an electrode, Bioelectrochemistry 57 (2002) 39–46.
[21] S. Gritsch, P. Nollert, F. Jähnig, E. Sackmann, Impedance spectroscopy of porin and gramicidin pores reconstituted into supported lipid bilayers on indium-tin oxide electrodes, Langmuir 14 (1998) 3118–3125.
[22] A. Sinner, A. Offenhäusser, The electrical characterization of supported phospholipid bilayers using titanium/titanium oxide microelectrodes, Thin Solid Films 327–329 (1998) 758–761.
[23] O. Purrucker, H. Hillebrandt, K. Adlkofer, M. Tanaka, Deposition of highly resistive lipid bilayer on silicon–silicon dioxide electrode and incorporation of gramicidin studied by ac impedance spectroscopy, Electrochim. Acta 47 (2001) 791–798.
[24] G.J. Brug, A.L.G. Van den Eeden, M. Sluyters-Rehbach, J.H. Sluyters, The analysis of electrode impedances complicated by the presence of a constant phase element, J. Electroanal. Chem. 176 (1984) 275–295.
[25] R. de Levie, Mathematical modeling of transport of lipid-soluble ions and ion-carrier complexes through lipid bilayer membranes, Adv. Chem. Phys. 37 (1978) 99–137.
[26] R. Naumann, D. Walz, S.M. Schiller, W. Knoll, Kinetics of valinomycin-mediated K^+ ion transport through tethered bilayer lipid membranes, J. Electroanal. Chem. 550–551 (2003) 241–252.
[27] A.E. Vallejo, C.A. Gervasi, Impedance analysis of ion transport through gramicidin channels in supported lipid bilayers, Bioelectrochemistry 57 (2002) 1–7.
[28] C.A. Gervasi, A.E. Vallejo, Sodium ion transport through gramicidin-doped bilayers. Influences of temperature and ionic concentration, Electrochim. Acta 47 (2002) 2259–2264.
[29] J.A. Jacquez, Design of experiments, J. Franklin Inst. 3358 (1998) 259–279.
[30] F. Berthier, J.P. Diard, L. Pronzato, E. Walter, Identifiability and distinguishability concepts in electrochemistry, Automatica 32 (1996) 973–984.
[31] F. Berthier, J.P. Diard, C. Montella, L. Pronzato, E. Walter, Choice of experimental method induced by structural properties of mechanisms, J. Electroanal. Chem. 399 (1995) 1–6.
[32] F. Berthier, J.P. Diard, P. Landaud, C. Montella, Steady-state investigation and electrochemical impedance spectroscopy: identifiability and distinguishability of metal dissolution and passivation mechanisms, J. Electroanal. Chem. 362 (1993) 13–20.
[33] M.J. Chappell, Structural identifiability of models characterizing saturable binding: comparison of pseudo-steady-state and non-pseudo-steady-state model formulations, Math. Biosci. 133 (1996) 1–20.
[34] E. Walter, L. Pronzato, On the identifiability and distinguishability of nonlinear parametric models, Math. Comput. Simul. 42 (1996) 125–134.
[35] C. Gabrielli, in: Identification of electrochemical processes by frequency response analysis, Technical Report No 004, Solartron, Hampshire, UK, 1984.
[36] R.H. Milocco, Structural identifiability of adsorption and electron transfer processes in metal dissolution and passivation mechanisms, J. Electroanal. Chem. 471 (1999) 1–8.

[37] R.H. Milocco, E.B. Castro, S.G. Real, Parameter identification and model validation of adsorption and electron transfer processes using impedance, Electrochim. Acta 47 (2002) 2035–2041.
[38] E. Walter, L. Pronzato, Qualitative and quantitative experiment design for phenomenological models – a survey, Automatica 26 (1990) 195–213.
[39] I. Braems, F. Berthier, L. Jaulin, M. Kieffer, E. Walter, Guaranteed estimation of electrochemical parameters by set inversion using interval analysis, J. Electroanal. Chem. 495 (2000) 1–9.

This page intentionally left blank

SUBJECT INDEX

D

E

F